EVAPORATING DROPS AND SPRAYS IN TURBULENT AIR STREAMS

A thesis presented for the
degree of Doctor of Philosophy in Chemical Engineering
in the University of Canterbury,
Christchurch, New Zealand.

by

W.J. Brehaut

1969

ACKNOWLEDGMENTS

This research was carried out under the direction and supervision of Drs R.B. Keey and W.B. Earl and the staff of the Chemical Engineering department, under Professor A.M. Kennedy, to all of whom I express my sincere thanks.

I gratefully acknowledge the personal receipt of a New Zealand University Grants Committee Postgraduate Scholarship and also their Research Grant 66/36 which financed the equipment necessary for the research.

Finally, I thank my wife for her encouragement and patience and the assistance given in all aspects of this work.

CONTENTS

continued

SUMMARY

The evaporation rates of single drops and whole sprays in turbulent air streams have been investigated using a pilot-scale cocurrent spray drier. The six basic parameters of the turbulent air flow, the mean velocity, the relative intensity, the micro- and integral scales, the energy spectrum and the dissipation spectrum of turbulent energy, were measured using techniques developed for a single hot-wire probe without the need for expensive correlating or recording equipment.

The evaporation rate of supported evaporating droplets was found to depend strongly on both the intensity and integral scale of turbulence as well as the droplet Reynolds number. An optimum value of the integral scale to droplet diameter ratio was found and is believed to result from resonance between the energy containing eddies and the shedding frequency of the drop. The existence of the optimum value of the ratio was previously suggested for heat-transfer from a cylinder and the present results are believed to be the first showing a similar optimum for held spheres or drops. The optimum ratio explains the seeming discrepancies found in the literature concerning the effect of turbulence intensity and scale on heat-transfer for spheres.

Drag coefficient data was obtained for free falling and cocurrently entrained, evaporating water droplets. All drops experienced the same drag as solid spheres moving in steady flow conditions and no separate effect of the scale or intensity of the entraining air was discerned. The standard drag curve by Smith (1970) is recommended. Further,

the reduction in drag due to the intensive mass-transfer effect of the vapour efflux from the evaporating droplet surface can be accounted for using corrected driving forces (incorporating the Mass-Transfer number B) with the boundary-layer theory.

An attempted study of turbulence effects on the evaporation rates of sprays was abandoned when a necessary basic assumption was found to be invalid. A spray momentum and entrainment effect in the nozzle zone is reported and significant drying air temperature and humidity radial profiles were found to exist at even the lowest spraying rates. The uncertain knowledge of droplet trajectories during the spray process means that a sound theoretical basis for spray drier design is still some distance away and experimental studies must be relied on for accurate design data. Many aspects of the spray evaporation process still require investigation, particularly those concerned with the spray momentum-transfer and entrainment effects as well as the turbulence aspect of the system. While a significant turbulence effect has been found for fixed evaporating droplets, the influence of turbulence on the evaporation rates of sprays is still an open question.

1. INTRODUCTION

The economy of New Zealand depends primarily on the export of agricultural and pastoral produce (136). Of the mass-transfer processes occurring in the food-processing industries of this country (dairy industry, food-preservation industry, meat industry and vegetable-extraction industry), drying is often the last process step. In the drying of fluids, Spray-Driers, with both jet and rotary atomisers have been introduced offering the advantage of extremely rapid drying of heat-sensitive products, a product particle size and density that are controllable within limits, and relatively low operating costs, especially in the case of high capacity driers (89).

The Department of Chemical Engineering of the University of Canterbury has for some time had studies of mass-transfer in dispersed phase systems as a major part of the research done on mass-transfer processes. In line with this and considering the national interest of the food-processing industries, the following study of the evaporation rates of drops and sprays in turbulent air streams was undertaken with the hope that the results may enable industry to better utilise spray-drying.

Although a beginning has been made on the rational design of Spray-Driers (31, 121, 161), incomplete knowledge about the spray drop size, the drop trajectories, the effect of the relative velocity between the drying gas and the drops and the effect of the turbulence of the drying gas on the evaporation rate of sprays (Appendix 1, 19, 142, 188) make it necessary to rely largely on experimental results for the design of spray-drying

equipment. A large number of problems will have to be resolved before such plant can be designed with the same accuracy as a distillation column.

Out of the wealth of unresolved problems a study of two particular aspects of heat- and mass-transfer for drops in forced convection has been undertaken for this present work. They are a study of the influence of the turbulence of the drying gas on the evaporation rate of sprays and an investigation of the effect of mass-transfer on the drag coefficient of evaporating droplets. The influence of turbulence on the evaporation rate of sprays was studied in two parts: evaporation rates for single droplets held on a glass fibre in a turbulent airstream; and evaporation rates for complete sprays of droplets moving cocurrently in a hot, turbulent airstream. It is hoped that the results of this study of these three separate, yet related aspects of spray evaporation will go some distance towards bridging the gap between the knowledge of fundamental processes and the design methods of spray-driers.

2. SPECIFICATION OF APPARATUS

For the present study and allowing for future research on Spray-Drier operations, a complete pilot-scale cocurrent spray drier was designed with an evaporative capacity of about 20 lbs of water per hour.

2(a) Design Considerations

A long, narrow drying chamber with a cocurrent gas-liquid flow pattern was chosen as against the conventional large diameter drying chamber and counterflow gas-liquid system usually found in industry. The reason for this is that the air and particles would then flow downward, parallel to the wall of the spray drier, giving a controllable air flow pattern, and still taking advantage of the cocurrent characteristic of higher allowable inlet temperatures. The average air velocity would generally be high (5 to 15 fps) which is necessary to minimise air turbulence close to the nozzle. The solutions to be dried would be atomised through a pressure nozzle. This method of atomisation was chosen because compared with pneumatic or two-fluid nozzles and spinning-disc atomisers, the pressure nozzle imposes the least disturbance on the main gas flow.

Placed at the top of the drying chamber which has an effective drying length of 12 feet is a variable flow straightener which will allow any gas pattern that is desired to be established inside the drying chamber. It was envisaged that a velocity distribution consisting of an annulus of high velocity gas about a centre core of

lower velocity would be set up for the drying gas in the nozzle and spray deceleration zone. Such a velocity pattern would help keep the spray drops from reaching the walls of the drying chamber.

Turbulence could be induced in the drying gas by placing grids immediately before the spray nozzle and the turbulence parameters would be measured by a hot-wire anemometer. Along the drying chamber a set of portholes would be positioned so that readings and samples could be taken and profiles of the changing conditions of the drying process established. The properties to be measured would be the temperature, humidity, velocity, turbulence intensity and scale of the drying gas and the temperature and size distribution of the spray droplets.

2(b) Design Details

The components of the experimental cocurrent spray drier are indicated in figure 2.1. As is suggested by the line diagram, the apparatus could easily be converted into a closed-circulation drier, as was done in some cases. The drying gas (air) at temperatures up to 300 F, was supplied to the drying chamber via the air heaters by a Roots-Connersville Rotary Blower of 250 cubic feet per minute capacity at a discharge pressure of 2 psig. Almost 20 kW of heat were available from the air heaters, consisting of 17 kW steam heat and 2.5 kW electric heat. The electric heater was supplied from a variable power source and the steam supply was manually controlled. Overall temperature control was achieved by a temperature-indicator-controller on the small bypass line around the air heaters. This controlled the addition of cold air

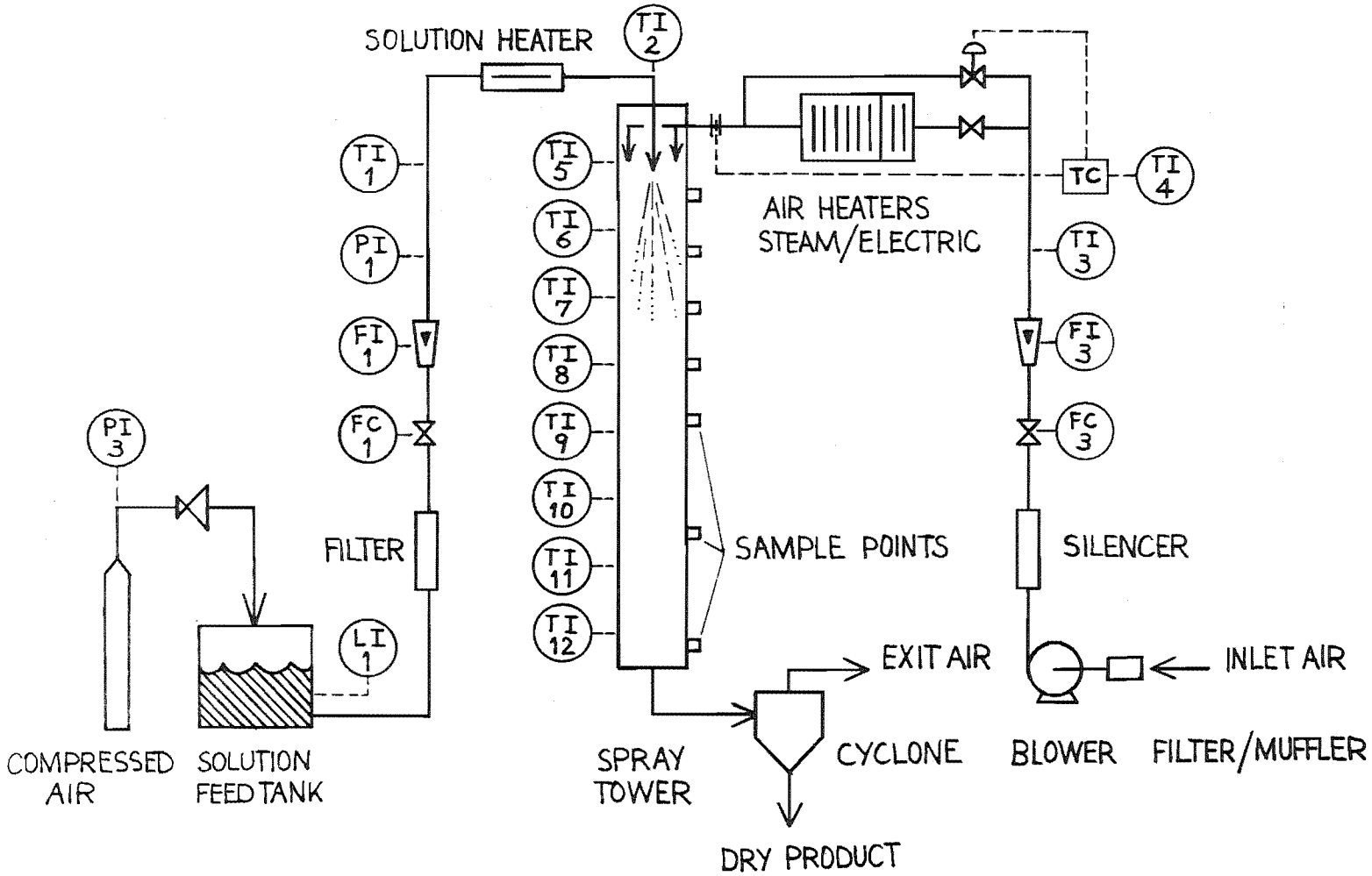

FIGURE 2.1 LINE DIAGRAM OF EXPERIMENTAL COCURRENT SPRAY-DRIER

into the hot gas leaving the heaters. The pressure drop through the heater section was deliberately made of the same order as that through the by-pass line by the setting of a butterfly valve in the main line to the heaters. The controlled injection of cold air by this method maintained the temperature of the air to the drying chamber to within ± 2 F for reasonable variations of the steam pressure with time.

At the head of the drying chamber an airflow straightener like that used by Baltas et al. (5) was used to generate the velocity profile required. The flow straightener consisted principally of a cylinder closed at the top and containing 34 uniformly spaced tubes attached to a tube sheet at the cylinder bottom only. To improve the profile symmetry even further, each of the 34 tubes was provided with a second, concentric tube, free to slide in the former. The vertical position of this second tube could be altered by means of a threaded shaft extending through the cylinder ceiling. By judicious selection of the secondary tube positions it was possible to reduce the maximum velocity discrepancy between points of equal radius to within a few percent. In the same manner it was possible to generate a variety of velocity profiles. Obviously, the greater the number of tubes, the greater would be the control over the profile.

The cocurrent drying chanber was 8 inches in diameter and well insulated with 1½ inches of pre-moulded fibreglass insulation. A total of 29 sampling portholes were placed at intervals of 5 or 10 inches in the upper and lower halves of the chamber respectively. Before covering

with the insulation, eight banks of temperature measuring copper/constantan thermocouples were recessed into the steel wall of the drying chamber at different levels down the column. These and other system temperatures were read out on a 12 point millivolt recorder and gave a clear indication of the attainment of steady-state conditions and any deviations from the desired operating conditions during the experiment. The internal contour of the drying chamber was maintained at all times by shaping blanks for each porthole and for any lighting or viewing porthole adaptors. For the latter, clear perspex was milled and then polished. The joints between sections of the steel column were also filled and sanded smooth. A cyclone was designed and built to separate the dried product (down to 10 microns) from the drying gas on exit from the chamber (Appendix 2).

The solution to be dried was atomised into the drying chamber through a spray nozzle. This nozzle had to provide the necessary atomisation and suit an 8 inch I.D. column. It was desirable that the back mixing phenomena in the region of the nozzle should be a minimum and that the evaporative load distribution would be over most of the column height. Such restrictions meant choosing a nozzle with a large Sauter-mean-diameter and two special F-80-N Monarch Co. pressure nozzles were selected which had narrow spray cone angles at flow rates of 1.0 and 1.75 gph at 100 psig. The liquid feed tank had a capacity of 6 gallons and the system was pressurised by compressed air. After the low flow rotameter, the liquid feed passed through a small heater of variable heat output. The nozzle support rod inside the top of the drying chamber consisted of a double jacket about the feed solution line. Cooling water

was passed through the jacket to counteract the effect of the hot drying air pre-heating the solution before atomisation occurred. A copper/constantan thermocouple was set inside the pressure nozzle to measure the temperature of the solution immediately before discharge from the atomiser.

Figure 2.2 is a photograph of the apparatus showing some of the described components and indicating their relative size. All valves, instruments and controls were mounted on a central control panel at the main working platform as shown in the photograph.

2(c) Air Humidity and Temperature Measurements

The small differences in the humidity of the drying air in the spray-drier required good accuracy in the measuring technique used to determine the air humidity. The conventional hygrometer, the dew-point method and wet- and dry-bulb thermometry all have respective inadequacies which include radiation effects, the drying out of the wet bulb, and the difficult precise determination of the dew point. Thermal conductivity measuring devices and conductance cells (LiCl type) suffer from the disadvantage of a narrow range of application and the necessity for frequent calibration. The volumetric method based on the measurement of the decrease in volume of an air sample due to the removal of water by an effective drying agent (14, 30, 117) has the disadvantage that because the decrease in volume is small any error is magnified in the calculation of the humidity. Such a method depends on the assumption that the volume of the drying agent does not change during the test. The need

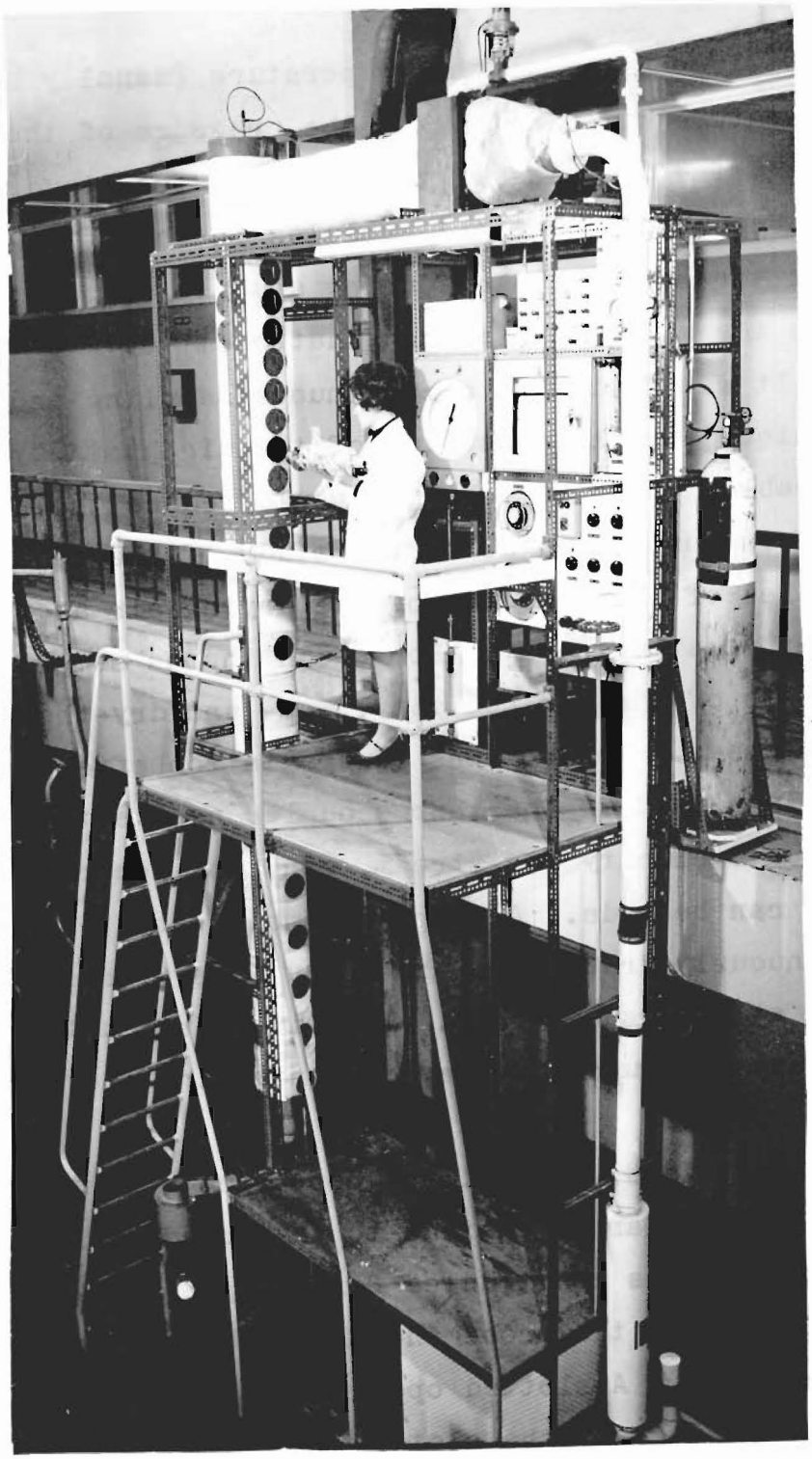

Figure 2.2 experimental cocurrent spray-drier.

for rigid control of the temperature (usually by a constant temperature water bath) and the pressure of the sample system, the slowness of the analysis technique and the requirement of air-tight capsules in which to keep the moist air samples taken during a spray evaporation test, makes the volumetric method unattractive.

It was felt that a continuous sampling and analysis technique for the measuring of the air humidity was desirable. Such a technique would reduce the experimental analysis burden and allow the study of the changing radial profiles of the humidity of the drying air as it meets the evaporating spray. For a continuous sampling and analysis of the air humidity, wet- and dry-thermocouples were chosen. Corrections for radiation effects can be calculated and if the thermocouples are kept wet in a constant velocity air stream, easy and accurate measurements can be made. A sample of moist air could be continuously drawn from the spray tower through a shielded probe at a measured rate. The air under suction would then pass through the chamber containing the wet- and dry-thermocouples.

A shielded, travelling, copper/constantan thermocouple probe of similar dimensions to that used by Hoffman and Gauvin (75) was constructed for the present work. An end cap was put on the probe and the probe was mounted horizontally. A slotted opening was cut on the underside of the probe head, the slot being below the midline of the probe body. The thermocouple measuring the drying air temperature was protected by the three shields. The outer

one was designed to prevent liquid-run-in which would tend to flood the thermocouple when operating near the nozzle. To increase the convective heat transfer coefficient at the thermocouple junction, the particle-free moist air was aspirated through the multifrontal orifices of the inner shields and over the thermocouple. The orifice openings were designed to provide approximetely equal flow on the outside and the inside on the inner shield. The volume rate of suction of the sample continuously removed from the drying column was 0.15% of the maximum air flow of 250 cfm. Hence the sampled air velocity at the probe was maintained well below the average terminal velocity of the drops and no separation problem was encountered.

On top of the probe another thermocouple was fixed inside the end of a fine hypodermic needle that was mounted clear of the probe head and inclined slightly to the horizontal. The drop temperature could be measured by this thermocouple for spray evaporation when the heat conduction effects along the hypodermic needle were small, as was the case when the temperature difference between the drying gas and the drops was small. The liquid drops accumulated at the tip of the needle and fell off under gravity, thus keeping the thermocouple junction at the spray temperature.

The sample of moist air was drawn under suction to the chamber containing the wet- and dry-thermocouples (Appendix 3, figure A3.1). The wet-thermocouple was cemented to a wet-bulb thermometer under the water-saturated wick. The chamber was airtight and constructed from clear perspex so that a visual check on the wetting of the wick was possible.

The air- and drop-temperature measuring thermocouples of the humidity probe were very carefully calibrated against

standard thermometers over a wide range of temperatures and the wet- and dry-thermocouples were checked against an existing calibrated wet- and dry-bulb thermocouple system that had been carefully designed and was operated under steady conditions. The wet-thermocouple and the wet-bulb thermometer of the humidity chamber both gave the same reading and when radiation corrections as per Appendix 3 had been made, the humidity results agreed closely with those of the calibrated system. The complete air-temperature and humidity measuring apparatus was compact and portable and profile measurements of the humidity and temperature of the drying air in the spray tower were easily made.

To mount the humidity sampling probe in the column and to facilitate radial positioning within the column a remotely-controlled, travelling probe carrier was built. The probe mounting plate was positioned by a ling screw driven by a small electric motor. A slide wire potentiometer was mounted alongside the screw thread and the position of the mounting plate (and so the probe) was indicated on a chart recorder. An almost linear relationship was obtained between the probe position in the drying column and the displacement of the chart recorder indicator. Figure 2.3(a) shows the probe carrier and the associated control box. The hot-wire probe support is shown fixed in the mounting plate. In figure 2.3(b), the probe carrier with the humidity probe mounted is shown fixed at a port-hole of the spray-drier column. A plastic sleeve entirely seals the opening of the traversing mounting plate while allowing full longitudinal movement. Also sealed is the opening about the tube through which the moist air sample was continuously being withdrawn to the measuring chamber.

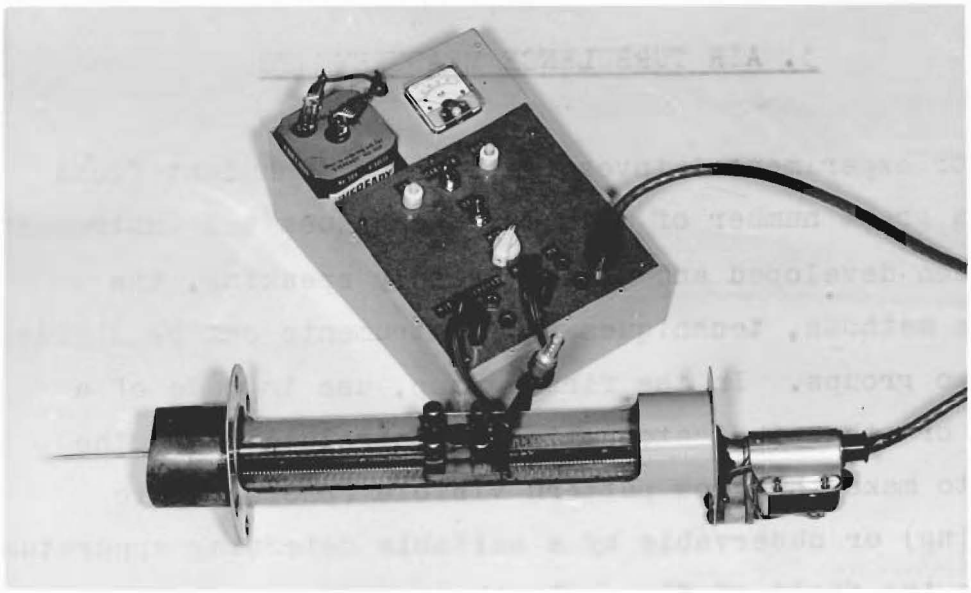

Figure 2.3a Remotely controlled, travelling probe carrier. Position of probe carrier was accurate to within ±3%.

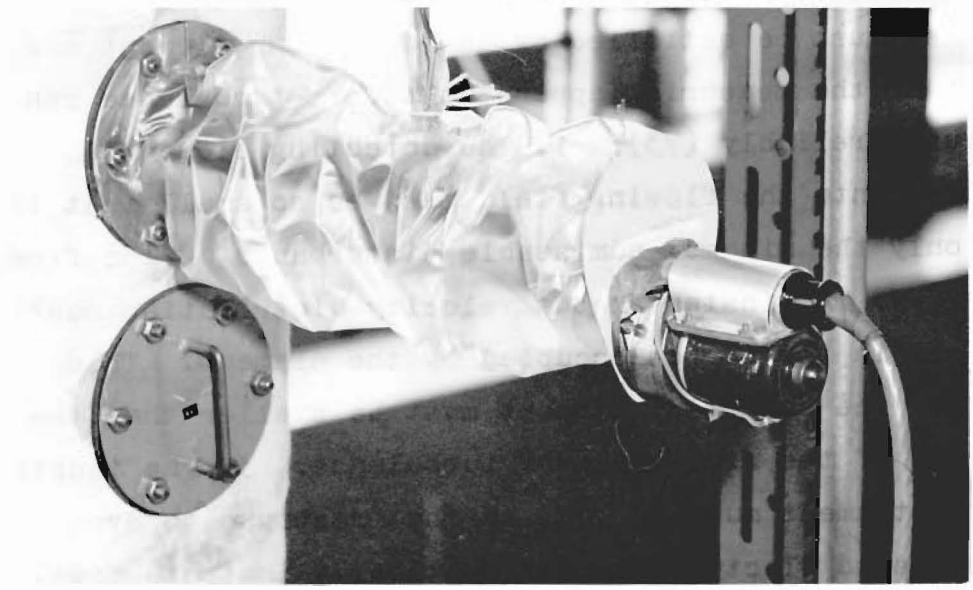

Figure 2.3b Probe carrier mounted on spray-drier column.

3. AIR TURBULENCE MEASUREMENTS

For experimental investigations of turbulent fluid flow, a great number of methods, techniques and instruments have been developed and used. Broadly speaking, the various methods, techniques and instruments can be divided into two groups. In the first group, use is made of a tracer or other indicator which is introduced into the fluid to make the flow pattern visible (photographic recording) or observable by a suitable detecting apparatus outside the field of flow. In the second group, a detecting element is introduced into the flowing fluid and the turbulence quantities are measured by the changes of a mechanical, physical, or chemical nature that occur in this element.

For the second group, there are a number of requirements that must be satisfied by the detecting element and the rest of the measuring apparatus before turbulence can be measured reliably (73): 1. The detecting element introduced into the flowing field must be so small that it causes only the minumum admissable disturbance of the flow pattern. 2. The instantaneous velocity distribution must be uniform in the region occupied by the element. This means that the detecting element must be smaller than the dimensions of the microscale of turbulence. 3. The inertia of the instrument must be low, so that response to even the most rapid fluctuations is practically instantaneous. 4. The instrument must be sufficiently sensitive to record small differences in the fluctuations; these differences are often only a few percent of the mean value. 5. The

instrument must be stable, so that no noticeable change in calibration occurs for at least one test run.
6. The instrument must be sufficiently strong and rigid to exclude vibrations or motions caused by the turbulent fluid flow.

There is one instrument whose development and application for measuring turbulent flow has far outstripped those of other instruments up till now, namely the hot-wire anemometer. Its popularity for making turbulence measurements will be easily understood if it is realised that this is the only instrument that reasonably satisfies all the aforementioned requirements, although it has its limitations.

Measurements of the parameters of a gas flow by means of hot-wire anemometry techniques have been known for a long time (23, 73, 100). More recently (93), the constant-temperature operation of the hot-wire anemometer has been shown to have particular advantages over the constant-current method. These advantages are: a much better compensation of the time constant of the hot wire, and consequently, a much wider band of transmitted frequencies; the danger of wire burnout is avoided; and particularly, instrument operation is greatly simplified.

Air turbulence measurements in the present experimental work were made with the DISA 55A01 Constant Temperature Anemometer (148). A large amount has been written on hot-wire anemometry techniques by many workers including Hinze (73), Corrsin (23) and Kovaszanay (98). In view or the wealth of this general literature the following discussion applies particularly to the DISA Constant Temperature Anemometer and its operation.

3(a) The Hot-Wire Anemometer

The derivation of the working equations for the hot-wire anemometer are given in the above mentioned works on anemometry. A block diagram of the DISA 55A01 constant temperature hot-wire anemometer is shown in figure 3.1 and the hot-wire probes used in the present study were 3mm in overall diameter with a platinum-coated tungsten wire of 5 microns diameter and 1.2mm in length, as the sensor. The resistance was approximately 3.5 ohms at room temperature (probe cold resistance, R_o) and velocities as high as 300 fps can be measured with these probes.

3(b) Static Probe Characteristics

The static characteristic of the DISA hot-wire anemometer - that is, the dependence of the bridge supply voltage on mean flow velocity - is described by King's law (94) which can be written

$$Q = L_w(T_w - T_g)(k_g + \sqrt{2\pi k_g \rho_g C_{p_g} d}\sqrt{U}) \qquad (3.1)$$

King's formula was derived as early as 1914 for the two dimensional heat-transfer from a cylinder in an incompressible potential flow.

For thermal-equilibrium conditions, the rate of heat loss from the wire must equal the heating power generated in the wire by the electric current. For a specific probe operated at a specific over-heating ratio in a specific fluid, King's formula takes the simple form:

$$\frac{R}{R-R_o} I^2 = V^2 = A + B\sqrt{U} \qquad (3.2)$$

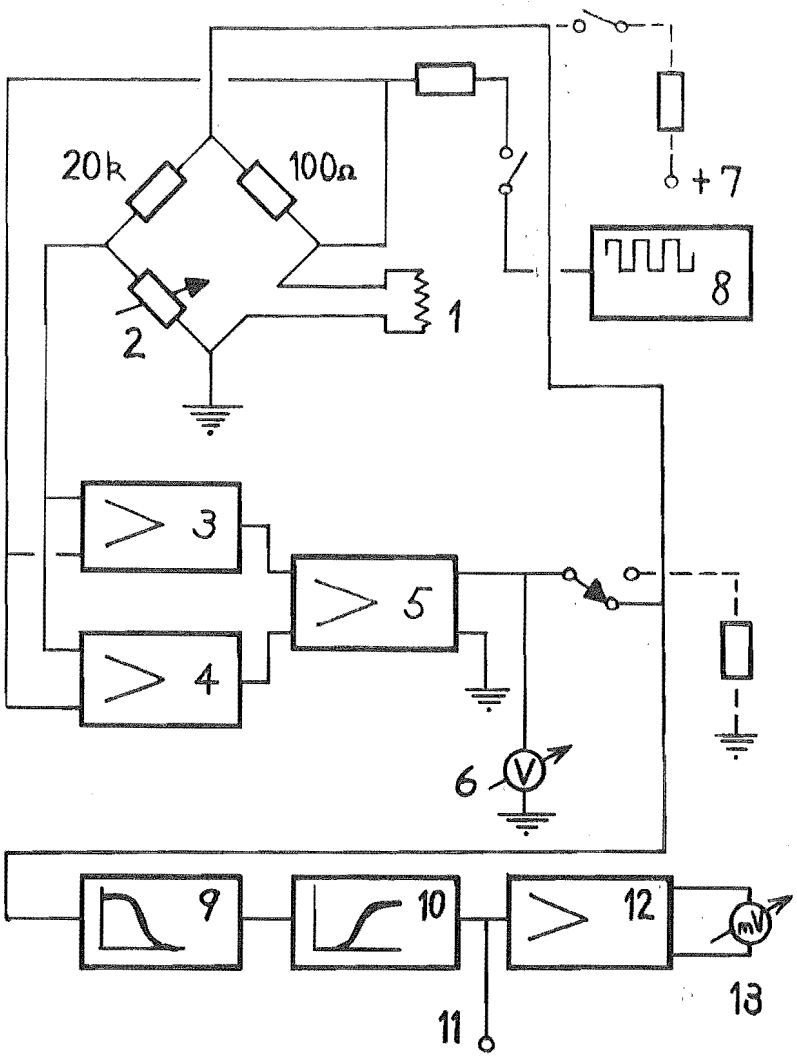

FIGURE 3.1 BLOCK DIAGRAM OF "DISA" CONSTANT TEMPERATURE ANEMOMETER. 1, HOT-WIRE PROBE; 2, DECADE RESISTOR; 3, D.C CHOPPER AMPLIFIER; 4, A.C AMPLIFIER; 5, D.C OUTPUT AMPLIFIER; 6, BRIDGE D.C VOLTMETER; 7, CONSTANT CURRENT SOURCE FOR PROBE RESISTANCE MEASUREMENT; 8, SQUARE WAVE GENERATOR; 9, LOW-PASS FILTER; 10, HIGH-PASS FILTER; 11, A.C OUTPUT; 12, A.C AMPLIFIER; 13, BRIDGE RMS METER.

The output of the anemometer is a bridge voltage V, and the squared voltage V^2 is linearly related to the heat loss of the wire at the velocity in question and at zero velocity respectively (see figure 3.3). King's law ($Q \propto U^{\frac{1}{2}}$) applies quite satisfactorily for a wire probe operated in atmospheric air at velocities down to 3 fps.

For the DISA hot-wire anemometer (compare with figure 3.1)

$$Q = \left(\frac{V}{100 + R_w}\right)^2 R_w \qquad (3.3)$$

but $R_w \ll 100\,\Omega$, so that

$$Q \backsim V^2 R_w \cdot 10^{-4} \qquad (3.4)$$

From this follows

$$V^2 = \frac{L_w(T_w - T_g)}{R_w \cdot 10^{-4}} \left(k_g + \sqrt{2\pi k_g \rho_g C_{p_g} d}\,\sqrt{U}\right) \qquad (3.5)$$

from which in turn follows, after comparing with equation (3.1)

$$A = \frac{L_w(T_w - T_g)}{R_w \cdot 10^{-4}}\, k_g \qquad (3.6)$$

and

$$B = \frac{L_w(T_w - T_g)}{R_w \cdot 10^{-4}}\, \sqrt{2\pi k_g \rho_g C_{p_g} d} \qquad (3.7)$$

Equations (3.6) and (3.7) show that the resultant characteristic of the hot-wire anemometer is noticeably

influenced by the wire length and temperature, the flow temperature and the wire operating resistance. The flow temperature also influences the physical properties of the flowing medium.

3(c) Dynamic Probe Characteristics

The empirical equation (3.2) between heat loss and velocity found by static calibration is used for the evaluation of the velocity fluctuations from the anemometer measurements. In order to describe the hot-wire response to fluctuating flow a term taking into account the thermal inertia of the wire must be added to the equation. Assuming a uniform temperature distribution along the wire then we can write

$$\frac{R}{R-R_o} I^2 = A + B\sqrt{U} + \frac{C}{R-R_o}\frac{dR}{dt} \qquad (3.8)$$

where C is the heat capacity of the wire. The instantaneous wire resistance and the flow velocity may be considered as the sum of a long-time average value and a fluctuating component.

$$R = \bar{R} + R' \qquad (3.9)$$

and $$U = \bar{U} + u' \qquad (3.10)$$

Then for equation (3.8) we have instead the following differential equation for the resistance variations:

$$\frac{dR'}{dt} + \frac{R_o(A+B\sqrt{\bar{U}})}{RC} R' = \frac{B^{\frac{1}{2}}(\bar{U})^{-\frac{1}{2}}(R-R_o).u'}{C} \qquad (3.11)$$

This first-order differential equation is characterised by the time constant:

$$\tau_w = \bar{R}C/R_o(A+B\sqrt{\bar{U}}) \qquad (3.12)$$

Note that the time constant is proportional to the heat capacitance and resistance ratio of the wire and decreases with increasing flow velocity. The upper frequency limit ($f = 1/2\pi\tau_w$) of a 5-micron tungsten wire is about 500 Hz when operated in atmospheric air at a resistance ratio of 1.8 and at 300 ft/sec. The frequency response decreases with decreasing mean air velocity but is in fact increased about a hundred times by the aid of the electronic accessories.

3(d) Other Probe Considerations

Accurate turbulence measurements will be obtained only after consideration of 3 external factors affecting the indicated hot-wire response to air velocity fluctuations. These factors are the accumulation of dirt on the hot wire, the heat loss through internal conduction to the wire end-supports and finally, the wall effects where heat is transferred between the wire and the surrounding enclosure by radiation.

Hot-wire probes should be periodically cleaned of dust by careful immersion in a solvent. The dust increases the aero-dynamic resistance of the wire and changes the calibration by altering the heat-transfer rate. Near zero velocity the heat-transfer rate is little affected or may actually be increased by the dirt accumulation (the increased surface area offsetting the insulation of the

dirt film) but at higher velocities the heat-transfer rate is always reduced.

For the majority of applications, the "end-effect" of heat loss to the wire support needles, does not change the form of the heat-transfer function substantially. Detailed analyses of end conduction effects are available (73, 99) and for steady flow the end correction is a function of the wire length to diameter ratio, the wire heating current and the heat transfer coefficient. The effect is an increase in the constants A and B in King's equation (3.2). This increase is automatically taken into account by an experimental calibration. These remarks apply equally well to unsteady constant temperature operation up to frequencies below the upper frequency limit.

Radiation transfer to the wire is proportional to the diameter of the wire and approximately proportional to the cube of the absolute temperature averaged between the wire and its surroundings. In contrast, the heat transferred by forced convection is proportional to the square root of the wire diameter. Therefore the very fine wires used in thermal anemometry suppress the effect of radiant heat transfer which is only significant for very high absolute temperatures or when the wire is placed so close to the wall that the thermal boundary layer about the wire extends to the wall.

3(e) Hot-wire anemometer operation and calibration

Doubts as to whether the delicate hot-wire probes are durable enough in operation are unfounded. With careful handling and proper vibration-free mounting the same probes have been used in the present study for more than a hundred

measurements with good results.

The hot-wire probes used in the experiment were calibrated over a wide temperature range from 50 to 300 F (maximum ambient temperature allowed). Measurements were made for each probe to determine the values of the probe cold resistance (R_o) and the zero-flow bridge D.C. voltage (V_o). The variation of R_o and V_o with changing ambient air temperature for a hot-wire probe operated at a constant overheating ratio of 1.6, is shown in figure 3.2. The overheating ratio is defined here as the ratio of the operating resistance to the cold resistance (R/R_o). A velocity calibration for the hot-wire probe was made by measuring the anemometer bridge D.C. voltage for variations of the air velocity. The air velocity was measured simultaneously with a standard pitot-static tube. The dynamic head indicated by the pitot-static tube was measured with a micro-manometer reading to 0.0002 inches of water. The resulting calibration curve is shown in figure 3.3. The "tailing" effect at lower velocities is the result of natural convection effects about the heated wire becoming significant compared with the heat loss by forced convection.

3(f) Intensity of Turbulence

The intensity of turbulence (or relative intensity) is defined as the ratio of the root-mean-square value of the fluctuating velocity component to the volume averaged free-stream velocity,

$$\tau = \frac{\sqrt{\overline{u_1}^2}}{U} \qquad (3.13)$$

Note: Mean square values referred to in the script should read as $\overline{u_1^2}$ rather than $\overline{u_1}^2$.

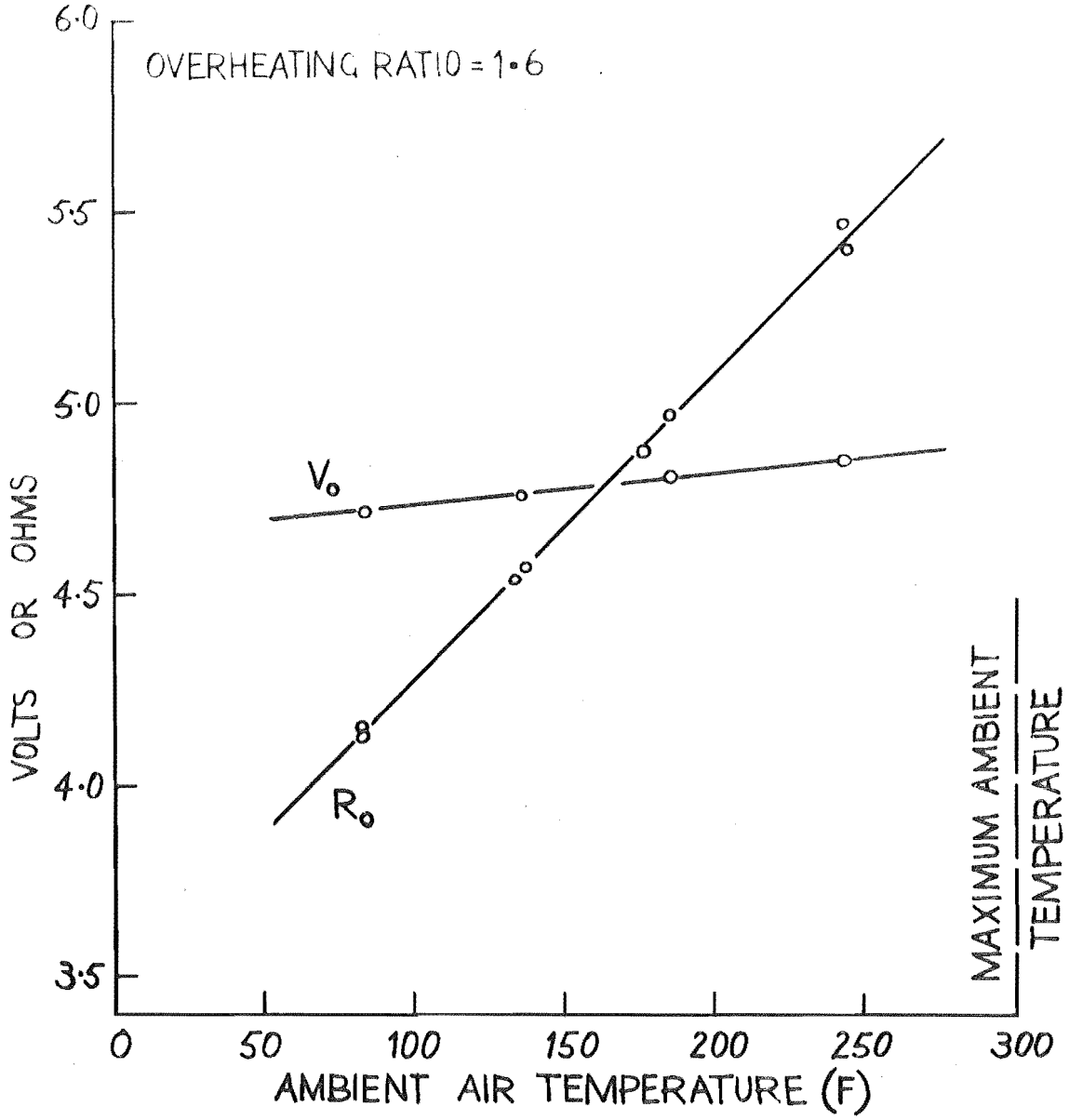

FIGURE 3.2 VARIATION OF V_o AND R_o WITH CHANGE OF AMBIENT AIR TEMPERATURE

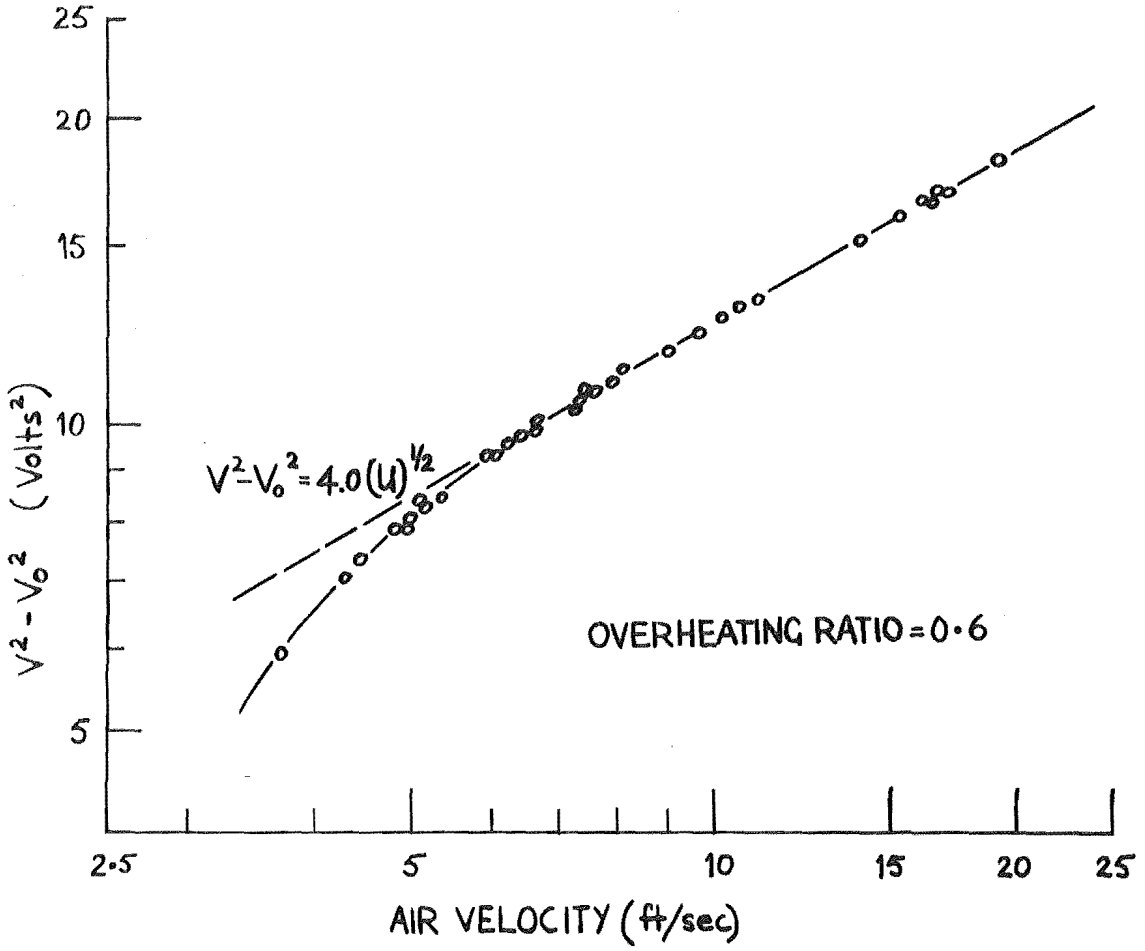

FIGURE 3.3 CALIBRATION OF HOT-WIRE PROBE IN ATMOSPHERIC AIR. (Temperature : 65-75 F Pressure : 990 - 1010 mb)

and can be calculated (28) from the formula

$$\tau\% = \frac{100 \cdot V_{RMS} \cdot 4V}{V^2 - V_o^2} \qquad (3.14)$$

where V_{RMS} is the A.C. output voltage rms. This formula is valid assuming that the coefficient in King's formula (3.2) is constant. This means

$$\frac{dB}{dV} = 0 \qquad (3.15)$$

Hence turbulence intensity measurements can be made without calibration of the probe for the average flow velocity, as a wire perpendicular to the mean flow direction will be sensitive to u_1 only, as long as u_1, u_2 and u_3 are small compared with $\bar{U}$ and u_2 and u_3 are not excessively greater than u_1.

The filters in the DISA hot-wire anemometer (low-pass and high-pass; see figure 3.1, no.9 and no.10), are used principally for improving the signal-to-noise ratio. They can also be used for approximate frequency analysis of the turbulence signal. More accurate frequency analysis of the turbulence signal may be performed by means of the electronic frequency analysers frequently employed in acoustics, and appropriate mathematical analysis methods are also available (100, 166). When measuring very small values of turbulence, allowance should be made for the level of the hot-wire anemometer self-noise, which depends on the width of the transmitted frequency band. The measured turbulence signal is the resultant of 1) actual turbulence, 2) induced interference, 3) the self-noise of the system, 4) the vibrations of the probe support, and 5) the macroscopic

pulses of the flow as caused by the blades of the air blower. It is therefore necessary to analyse the individual contribution of these factors to each measurement, for each given frequency band.

For the present experimental work, the analysis of the turbulence spectra was obtained by setting the high-pass filter at 1000 Hz and increasing the low-pass filter in steps from 2 up to 10 kHz which was approximately the upper frequency limit. Leaving the low-pass filter set on 10 kHz the high-pass filter was decreased from 1000 down to the lower limit of 5 Hz. Although the turbulence rms signal is shown as a millivolt reading, it is in fact measured by the anemometer as a power signal and represents the rms power required to keep the hot-wire probe at a constant temperature. Hence to evaluate the contribution to the frequency spectra that occurs over a given frequency range, the result must be the square root of the difference of the squares of the two signals at the two ends of the frequency range being considered.

Examples of the frequency spectra for the hot-wire rms millivolt output are shown in figure 3.4 as histograms. The drawing of a smoothed distribution curve through the histogram would not be valid unless the frequency range between readings was considerably reduced. The large contribution to the frequency spectra occurs in the low frequency range and probably comes mainly from the blower pulsations. Also included in the figure is the spectral plot of the self-noise of the system, indicating both the relative magnitude and the frequency range over which the self-noise contributes to the total rms turbulence signal.

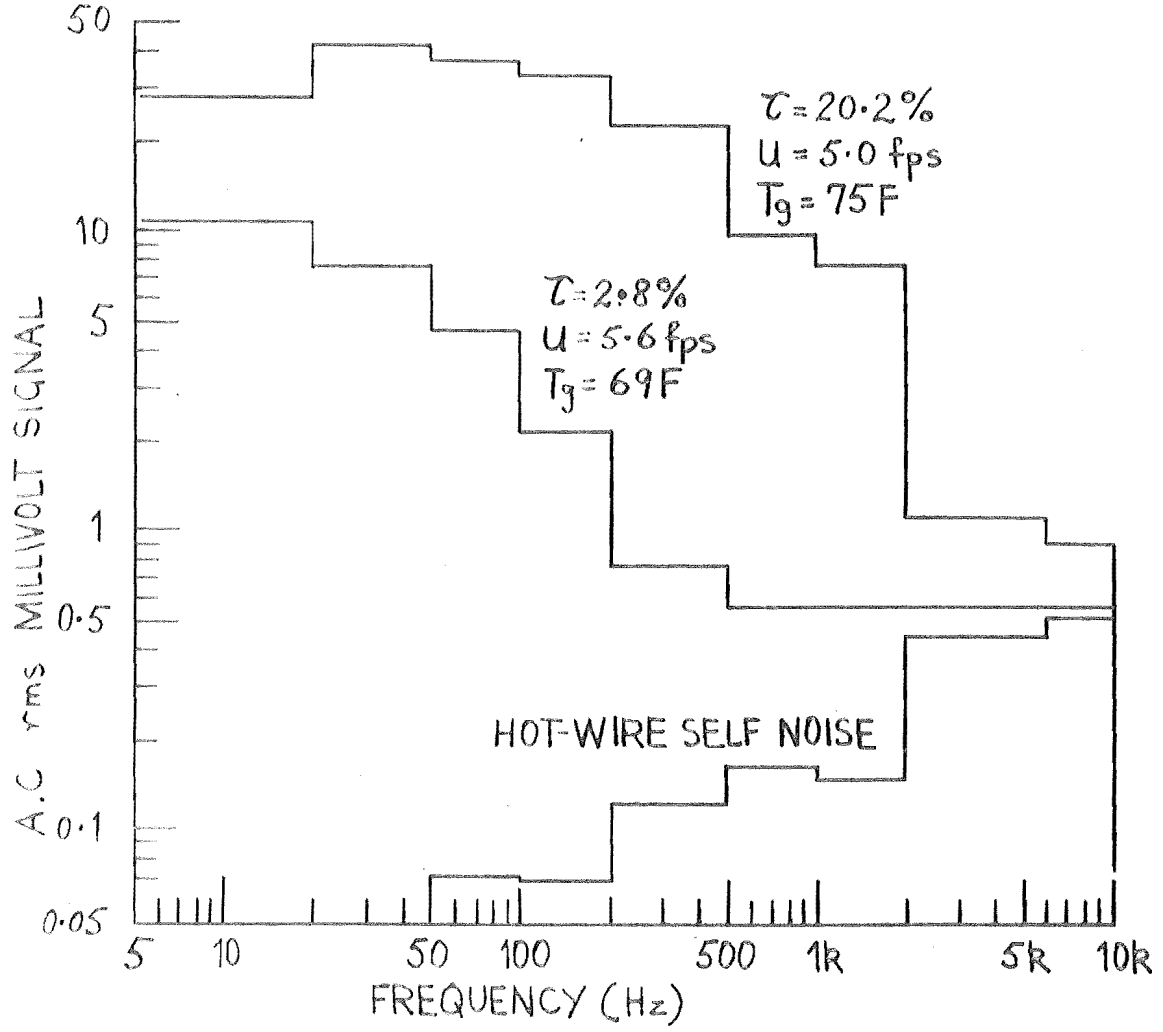

FIGURE 3·4 FREQUENCY SPECTRA AS MILLIVOLT HISTOGRAMS

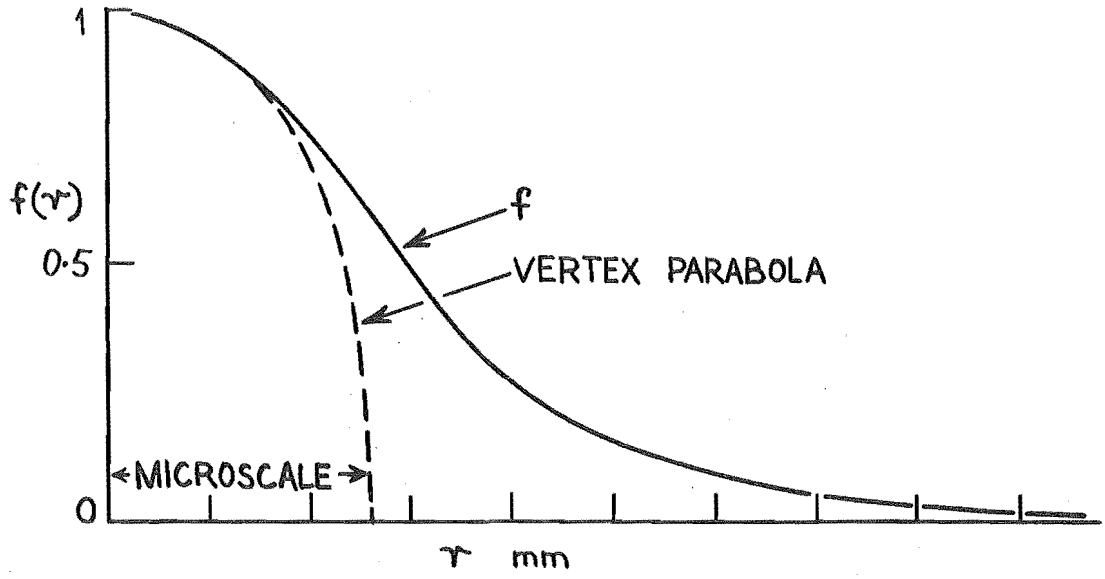

FIGURE 3.5 VARIATION OF LONGITUDINAL CORRELATION COEFFICIENT f(r), WITH DISTANCE BETWEEN CORRELATING POINTS

3(g) Scale of Turbulence

Turbulence is generated by the dissipation of energy and the way in which the velocity changes decay and so dissipate their energy, is known in detail only for isotropic and homogeneous turbulence. While the life span of the individual turbulent eddy cannot be traced, the relationship between velocity fluctuations at one point ($u_{1,x}$) and those fluctuations at a neighbouring point at distance r away ($u_{1,x+r}$) can be expressed as a correlation. The dimensionless ratio $\overline{u_{1,x}u_{1,x+r}}/(\overline{u_{1,x}})^2$ is known as the longitudinal correlation coefficient and represents the probability that a fluctuation at one point is matched by a fluctuation at another. For isotropic turbulence, this correlation coefficient f(r) wanes with distance r as shown in figure 3.5. The area under the curve ($= \int_0^\infty f(r)dr$) has the dimensions of length and may be regarded as the longitudinal integral scale of turbulence (Λ_f), the length over which an eddy preserves its identity before being swallowed up in the general flow.

The longitudinal microscale of turbulence (λ_f) can be determined from the intercept of the vertex parabola on the horizontal axis and represents the average dimension of the eddies that are mainly responsible for energy dissipation in the direction of the free-stream flow. The shape of the longitudinal velocity correlation coefficient curve and the longitudinal integral scale of turbulence can be obtained by using two hot-wire probes in the same plane of the air flow and separated by a variable distance r. The microscale can be determined from the vertex parabola provided that the shape of the correlation curve at its vertex is accurately known.

Measurement of the correlation coefficient when the correlation distance r becomes very small is not easy and Townsend (189) has succeeded in finding a fairly simple method for measuring the microscale λ_f (sometimes called Taylor's vorticity scale), using a single hot-wire probe. The method is quite direct when the turbulent field has a constant main velocity $\bar{U}$ which is high compared with the turbulence fluctuations. For this he made use of the relations

$$\frac{2}{\lambda_f^2} = -\left[\frac{\partial^2 f(r)}{\partial x_1^2}\right]_{x_1=0} = \frac{1}{u_1'^2}\left(\overline{\frac{\partial u_1}{\partial x_1}}\right)^2 = \frac{1}{\bar{U}^2 u_1'^2}\left(\overline{\frac{\partial u_1}{\partial t}}\right)^2 \qquad (3.16)$$

Laufer (104) and Liepmann (110) propose a method for determining λ_f from the average number of zeros of the u_1-fluctuations per unit time, N_o.

$$\frac{1}{\lambda_f} = \frac{\pi N_o}{\bar{U}\sqrt{2}} \qquad (3.17)$$

This relation can be proved in a simple way for the case in which u_1 is a pure harmonic.

$$u_1 = u_1^* \sin\frac{2\pi t}{T} \qquad (3.18)$$

where T is the period. The number N_o of zeros per unit time is $N_o = \frac{2}{T}$. It is possible to express T in terms of u_1 and du_1/dt but it is more convenient to express T in terms of $(\overline{u_1^2})^{\frac{1}{2}}$ and $(\overline{du_1/dt)^2}^{\frac{1}{2}}$, as then a simpler expression is obtained. Further, in real turbulence u_1 and du_1/dt are statistical quantities and the root-mean-square

values can be taken for the average values.

Because

$$\sqrt{\overline{u_1}^2} = \frac{u_1^*}{\sqrt{2}} \tag{3.19}$$

and

$$\sqrt{\overline{\left(\frac{du_1}{dt}\right)^2}} = \frac{2\pi u_1^*}{T\sqrt{2}} \tag{3.20}$$

then

$$N_o = \frac{2}{T} = \frac{\sqrt{\overline{(du_1/dt)^2}}}{\pi\sqrt{\overline{u_1}^2}} = \frac{\bar{U}\sqrt{\overline{(du_1/dx_1)^2}}}{\pi\sqrt{\overline{u_1}^2}} \tag{3.21}$$

Laufer and Liepmann have shown that exactly the same expression can be obtained for a real turbulence provided that both u_1 and du_1/dx_1 have a Gaussian probability-density distribution and that $\overline{u_1(du_1/dx_1)} = 0$. This latter condition is fulfilled in homogeneous turbulence and Townsend (189) has shown experimentally that the probability-density distribution of u_1 is practically Gaussian but that the distribution of du_1/dx_1 shows a slight but definite skew. For homogeneous turbulence

$$\frac{2}{\lambda_f^2} = \frac{\overline{(du_1/dx_1)^2}}{\overline{u_1}^2} \tag{3.22}$$

(compare with the 3rd term in equation (3.16)) and substitution of the relation (3.21) yields

$$\frac{1}{\lambda_f} = \frac{\pi N_o}{\bar{U}\sqrt{2}} \tag{3.23}$$

The measurement of the microscale of turbulence by this formula has an easy application to electronic counting, and although the result is only correct for those conditions

specified earlier, the method provides a quick, ready estimate of the micro-scale of turbulence that would be otherwise found only by a tedious and extended experimental program.

Laufer and Liepmann evaluated N_o by putting the turbulence signal on to an oscilloscope and blanking out the screen except for a narrow slit at the midscale of the trace. A photodiode with a very fast response time was placed in front of this slit and the signal from the photodiode was sent to an electronic counter. Each sweep of the oscilloscope trace past the slit triggered the photodiode and the corresponding pulses, equal to the number of zeros in the turbulence signal, were electronically counted.

In this present work, this technique has been improved upon, in that the turbulence signal from the anemometer was fed directly to a Phillips electronic pulse counter. It was found that in the frequency range of the turbulence signal in the experiment, the electronic counter would count the positive pulses of an alternating signal of sine-wave form if the pulses were more than 200 millivolts in amplitude. Since the A.C. output signal could be as small as 5 millivolts (rms) a small amplifier with a good frequency response was built (Appendix 4) to amplify the signal from the anemometer to the electronic pulse counter. The total number of zeros in the turbulence signal (N_o) was then equal to twice the actual number recorded by the electronic counter.

Hence, by measuring the average number of zeros of the turbulence signal per unit time and the bulk air velocity, a good estimate of the microscale can be made.

3(h) Turbulent Energy Spectra

The adoption of statistical correlations for the description of isotropic turbulence is at least partly due to the fact that they are relatively easy to measure. Another powerful method for describing a fluctuating field is to analyse it into Fourier components, that is, to adopt the spectral approach. The spectral theory and the correlation theory are intimately connected with each other by simple mathematical transformations and the former theory is often found to give a clearer description of the basic mechanism of turbulence. Conventionally, the turbulence spectra are represented in wavenumber rather than frequency notation.

For turbulent motion, if $\frac{1}{2}E_1(k_1)dk$ is the amount of kinetic energy per unit mass, associated with the longitudinal component of the velocity and lying in the range of wavenumbers $(k,k+dk)$, then $E_1(k)$ is related to the longitudinal correlation function $f(r)$ by the pair of Fourier transform relations:

$$\overline{u_1}^2 f(r) = \int_0^\infty E_1(k)\cos kr\,dk \qquad (3.24)$$

and

$$E_1(k) = \frac{2\overline{u_1}^2}{\pi}\int_0^\infty f(r)\cos kr\,dk \qquad (3.25)$$

It is clear from these quations that

$$\overline{u_1}^2 = \int_0^\infty E_1(k)\,dk \qquad (3.26)$$

where $E_1(k)$ is a distribution function and $\overline{u_1}^2$ is a constant average of u_1^2, which can be considered to consist of the sum of contributions of all the wavenumbers k. That is, $E_1(k)\,dk$

is the contribution to $\overline{u_1}^2$ of the wavenumbers between k and k+dk.

Taylor (186) made use of equations (3.24) and (3.25) to connect the observed time spectrum with the spatial correlation function by way of his assumption, that "the sequence of changes in u at the fixed point are simply due to the passage of an unchanging [frozen] pattern of turbulent motion over the point". The spatial distance r is replaced by $\overline{U}_1 t$ and the time frequency f is related to the wavenumber as $k_1 = 2\pi f/\overline{U}_1$. Then

$$\overline{u_1^2} f(r) = \int_0^\infty E_1(f) \cos \frac{2\pi f r}{\overline{U}_1} . df \qquad (3.27)$$

and

$$E_1(f) = \frac{4\overline{u_1^2}}{\overline{U}_1} \int_0^\infty f(r) \cos \frac{2\pi f r}{\overline{U}_1} . dr \qquad (3.28)$$

and also

$$E_1(k_1) = \frac{\overline{U}_1 E_1(f)}{2\pi} \qquad (3.29)$$

$E_1(f)$ is sometimes called Taylor's spectrum function and these relations are well verified both theoretically (112) and experimentally (177).

It should be noted that the wavenumber and frequency distribution functions $E_1(k_1)$ and $E_1(f)$ are one-dimensional sections of what is in fact the three-dimensional spectrum function, E(k). Figure 3.6 shows the general form of the energy spectrum for various wavenumber ranges. This three-dimensional spectrum function is a tensor of rank two and is not the same as the one-dimensional spectral tensor. The measured spectrum function is only exactly related for homogeneous and isotropic turbulence when it

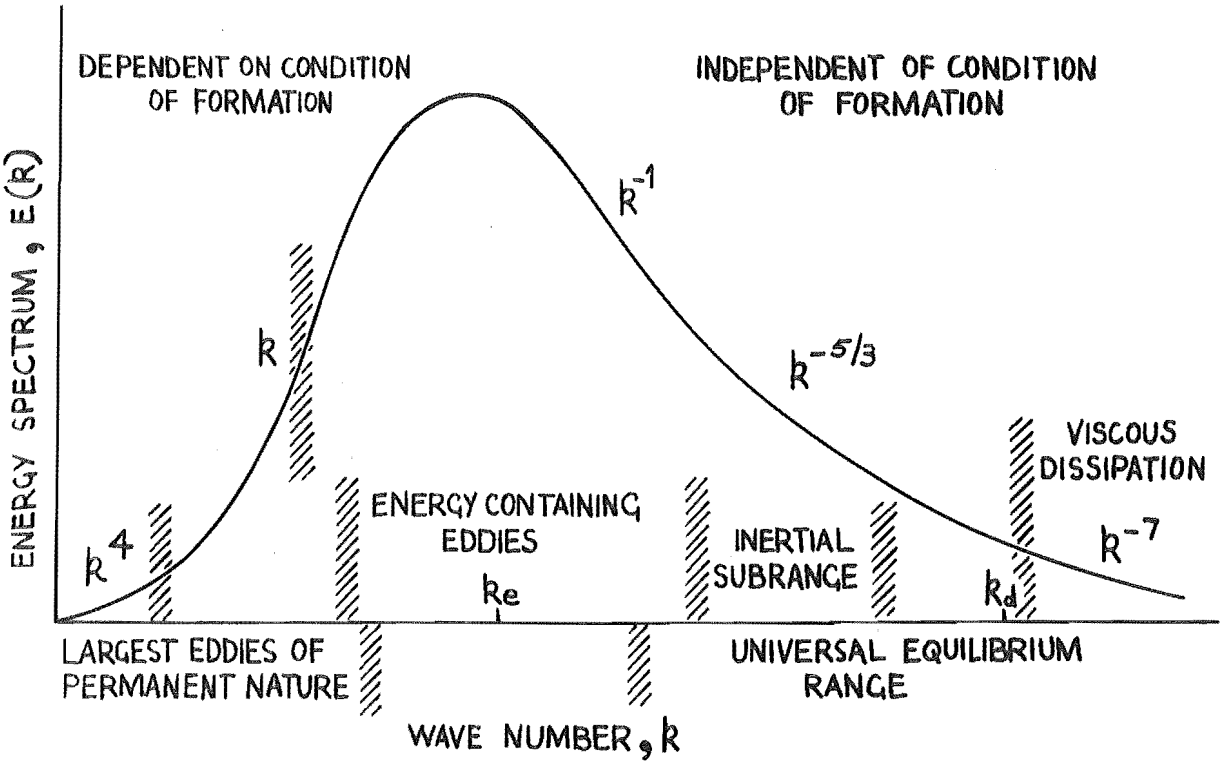

FIGURE 3.6 GENERAL SHAPE OF THE ENERGY SPECTRUM (ITS FOURIER TRANSFORM.(14))

can be shown (73) that

$$E(k) = 1/3 \left[k^2 E_1''(k) - kE_1'(k)\right] \qquad (3.30)$$

The dissipation spectrum of turbulent energy $\phi_1(k_1)$ is also shown to be determined as a function of the wave-number from

$$\phi_1(k) = k_1^2 E_1(k_1) \quad , \qquad (3.31)$$

the change of total kinetic energy of the turbulence being equal to the dissipation of energy into heat caused by viscous effects.

Since the energy and frequency spectra $E_1(k)$ and $E_1(f)$, and the longitudinal correlation coefficient $f(r)$ appear to be Fourier transforms, the first can be found from the other by an integrating process (equations 3.25 and 3.28) either graphically or analytically. The analytical solution is possible only if an explicit equation for the coefficient can be found. The development of some of the better known theories of turbulence such as those of Taylor (185) and Kolmogoroff (96) (the latter resulting in the Kolmogoroff spectra law where $E_1(k)$ is proportional to $k^{-5/3}$ - see figure 3.6) was the result of attempts to describe the form of the correlation coefficient curve and the turbulence spectra functions by approximate theoretical or empirical equations. Two such solutions are 1) the Von Karman interpolation formula (198) covering the range of wavenumbers between the k^4-range of the "permanent" largest eddies and the inertial

subrange and 2) the empirical relation by Liepmann (109) which is reported to apply over a wider wavenumber range than the Kolmogoroff 5/3 law.

$E_1(k)$ and consequently $E_1(f)$, can be measured experimentally with a single hot-wire probe, as from the definition in equation 3.26 (remembering that $\bar{u}_1^2$ is a constant average of u_1^2),

$$E_1(k) = \frac{\Delta \bar{u}_1^2}{\Delta k} \tag{3.32}$$

and putting $k = 2\pi f/\bar{U}$, then

$$E_1(f) = \frac{\bar{U}}{2\pi} \frac{\Delta \bar{u}_1^2}{\Delta f} \tag{3.33}$$

which compares with equation 3.29. Using the gating method described earlier in section 3(f), values of the change of $\Delta \bar{u}_1^2$ for the corresponding frequency or wavenumber range can be measured as

$$\Delta \bar{u}_1^2 = \bar{u}_1^2 \cdot \frac{\sqrt{\bar{V}^2_{t.s(k)} - \bar{V}^2_{t.s(k+\Delta k)}}}{\sqrt{\bar{V}^2_{t.s(total)}}} \tag{3.34}$$

where $\sqrt{\bar{V}^2_{t.s}}$ is the rms value of the amplified true signal corrected for the noise of the system.

$$\sqrt{\bar{V}}_{t.s} = \sqrt{\bar{V}^2_{\text{indicated}} - \bar{V}^2_{\text{noise}}} \tag{3.35}$$

Hence, using the definition of turbulence intensity (equation 3.13) the energy spectra function is written as

$$E_1(k) = \frac{\tau^2 \bar{U}^2}{\Delta k} \sqrt{\frac{\bar{V}^2_{t.s(k)} - \bar{V}^2_{t.s(k+\Delta k)}}{\bar{V}^2_{t.s(total)}}} \qquad (3.36)$$

The empirical relation by Liepmann can be written

$$E_1(k) = \frac{2}{\pi} \cdot \frac{\bar{u}_1^2 \Lambda_f}{1+\Lambda_f^2 k^2} \qquad (3.37)$$

and is the solution of equation 3.28 when the correlation curve is approximated by the exponential function $(-r/\Lambda_f)$. This appears to be a satisfactory approximation of the true shape of many f(r)-curves (73) and equation 3.37 approximates measured spectra curves satisfactorily except for that part of the energy spectra pertaining to high wavenumbers. When k approaches zero, equation 3.37 yields

$$\frac{2E_1(k)\pi}{\bar{u}_1^2 \Lambda_f} = \frac{\bar{U} E_1(f)}{\bar{u}_1^2 \Lambda_f} = 4 \qquad (3.38)$$

which is in good agreement with experimental data. Liepmann's equation 3.37 is a quadratic in Λ_f and by experimentally measuring $\bar{u}_1^2$ and $E_1(k)$ an estimate of the longitudinal integral scale of turbulence can be obtained.

In a similar manner, the energy spectra function solution obtained for the von Karman interpolation formula (73) can be used to estimate Λ_f. The interpolation formula yields

$$E_1(k) = \frac{2}{\sqrt{\pi}} \frac{\Gamma(5/6)}{\Gamma(1/3)} \frac{\bar{u}_1^2}{k_e} \left[1 + \left(\frac{k_1}{k_e}\right)^2\right]^{-5/6} \qquad (3.39)$$

where k_e is the wavenumber of the energy containing eddies (figure 3.6). The inverse of this wavenumber at which the

maximum occurs may be taken as a measure of the dissipation eddy scale. For isotropic turbulence, up to and including the wavenumber range of the energy containing eddies, $\Lambda_f \backsim 0.75/k_e$ (73). Using this approximation a solution for Λ_f can then be obtained from the modified von Karman interpolation formula.

3(i) Recapitulation

It may be useful to summarise the above-considered aspects of air turbulence measurements. The measuring techniques described above have all been for a single hot-wire probe, whereas most previous reported measurements of turbulence parameters in heat- and mass-transfer processes (146, 194) have used two probes at the same time to obtain experimental spatial correlation coefficient curves which can be integrated graphically to obtain a measure of Λ_f. The alternative method is to tape-record the observed time spectra (133) and relate it to the spatial correlation function in the manner used by Taylor (186). Both these methods require further additional electronic measuring equipment and considerably lengthen the time taken for an experimental investigation.

For a single hot-wire probe in a turbulent air stream, methods have been indicated above showing how measurements can be made of the bulk free-stream velocity $\bar{U}$, the intensity $\sqrt{\overline{u_1^2}}/\bar{U}$ and the microscale λ_f of turbulence. By way of the gating procedure, turbulence spectral analysis facilitates the measuring of the turbulence spectra function $E_1(k)$, which in turn allows the calculation of the frequency function $E_1(f)$ and the dissipation function $\phi_1(k)$. Solution of the proposed theoretical and empirical equations

describing the form of the energy spectra function, by using experimentally measured energy function values, then provides an estimate of the integral (or macro-) scale of turbulence. That is to say, measurements of the six basic parameters of turbulent flow $\bar{U}$, τ, λ_f, Λ_f, $E_1(k)$ and $\phi_1(k)$ are possible (each according to the respective constraints used in their derivation) from the operation of a single hot-wire probe in a turbulent air stream.

Finally, in the same manner that the turbulence output signal is sent to the electronic pulse counter for estimating λ_f, so the fluctuating signal can be observed on the screen of an oscilloscope. Such visual pictures are important for observing regular turbulent flow phenomena such as von Karman vortex streets.

4. EVAPORATION OF SUPPORTED DROPLETS

4.1 Introduction

Commercial applications of spray evaporation processes have existed for more than 100 years (Appendix 1). However, it is only in recent years that the subject of mass-transfer in dispersed phase systems has received close attention because of its fundamental significance in chemical engineering operations. In many items of process equipment, such as spray-driers, the rate determining step is that of mass transfer from a liquid drop in forced convection conditions. The main consideration in the prediction of design and performance is then the rate of mass-transfer.

The drying of droplets from atomisers in a spray-drier is a simultaneous heat and mass-transfer operation in which heat for evaporation is transferred by conduction and convection from hot gases to the drop surface and vapour is transferred by diffusion and convection back into the gas stream. The overall rate of drying is a function of the turbulence, temperature and transport properties of the drying gas; the diameter, temperature and relative velocity between the drop and its surroundings; and droplet oscillation circulation, deformation and surface phenomena which may be related to the nature of the solid material dissolved or suspended in the liquid (Appendix 1, 121). For the present, only the effect of the drying gas turbulence and the associated effect of the droplet relative velocity will be considered although the other aspects must be kept in mind when summarising particular results or extending the conclusions to other systems.

The first work on mass transfer from spherical particles was that of Maxwell (123), who solved analytically the case of radial molecular diffusion to obtain

$$k_g = \frac{2 D_v \rho_v}{D_p M} \qquad (4.1)$$

This was derived independently by Langmuir (102) many years later in 1918 who showed that for the case of natural convection (in dimensionless form)

$$Sh = Nu = 2.0 \qquad (4.2)$$

and estimated the stagnant film thickness to be about 4 mm, which is large in comparison with the diameter of the average spray-dried particle.

The forced convection case is not amenable to exact theoretical analysis except under the simplest conditions of potential flow. From boundary-layer theory it is known that the rate of evaporation is a maximum on the side of the drop facing the on-coming air stream, it decreases to a minimum value near the boundary-layer separation circle and increases to another, but lower, maximum rate on the trailing side, which experiences eddying and vortex velocities in the reverse direction.

Such a distribution of mass-transfer rates was reported in experiment by Frössling in 1938 for the sublimation of a naphthalene sphere. In his classical papers (48, 50) Frössling used the concept of the boundary-layer over a blunt-nosed body of revolution along with the variable factor suggested by Fuchs (52) (that the concentration of the diffusing vapour at an infinite

distance from the evaporating drop, be used as a variable factor) to propose the following empirical correlation for the rate of mass-transfer for spheres in a turbulent gas stream.

$$Sh = 2.0 + K_1 (Re)^m (Sc)^n \qquad (4.3)$$

then, drawing the analogy between heat and mass-transfer, he also proposed

$$Nu = 2.0 + K_2 (Re)^p (Pr)^q \qquad (4.4)$$

and indicated that the powers m, n, p and q were constant only for defined ranges of the values of the Reynolds and Schmidt or Prandtl numbers.

Frössling's boundary-layer equations for a blunt-nosed body of revolution combined with equations for heat and mass-transfer give a set of four partial differential equations which state mathematically how heat, mass and momentum are interchanged during the evaporation process. The equations, representing a heat-balance, a mass-balance for the diffusing component, a force-balance derived from the Navier Stokes equation and the required continuity equation, are all based on a boundary-layer defined as the region where the fluid velocities are less than those for potential flow because of the retarding effect of friction at the liquid interface. A general solution of the set of equations is not possible and such a solution is not justified in view of the numerous assumptions that must be made regarding the average physical properties across the transfer path and in view of the existence of drop rotation (84), drop vibration

and distortion (79), and unsteady-state phenomena (160).

However, the heat- and mass-transfer numbers $Nu = hD_p/k_f$ and $Sh = k_g D_p M/D_v \rho_v$ on the basis of dimensional analysis (147) can be shown to take the following theoretical forms.

$$Nu = f(Re, Pr) \qquad (4.5)$$

and $$Sh = f(Re, Sc.p_{BM}/P) \qquad (4.6)$$

The analogy between these equations comes from the fact that they are based on the boundary-layer equations which are mathematically equivalent and subject to the same boundary conditions. Hence, the dimensionless numbers for heat and mass-transfer should have exactly the same functional form, where Pr for heat-transfer is equivalent to $Sc.p_{BM}/P$ for mass-transfer. This conclusion is applicable for heat and mass-transfer, where the rate of transfer is controlled by the boundary-layer. p_{BM}/P represents the ratio of the average value of the vapour pressure of the non-diffusing species to the total pressure of the system (= 1/Drift factor) and is a measure of the enhancement of transfer due to the total flow in the direction of diffusion. As this ratio is nearly unity in most applications, the term is often omitted as a factor with the Schmidt number.

It should be noted that equations 4.5 and 4.6 hold only for small fluxes when cross-effects between the thermal and material processes are small. The mass-transfer flux is strictly a function of both the concentration and the temperature gradient and the more intensive the mass-transfer, the more the Transfer number B will be a dependent variable.

Most experimental results have been interpreted on the basis of the dimensional analysis of Ranz and Marshall (147) (equations 4.5 and 4.6) and many of the data have been correlated by a relationship of the form first used by Frössling (equations 4.3 and 4.4). For these latter equations the exponent on the Reynolds number is an index of the effect of convective velocity on mass-transfer and the Pr or Sc exponent is an index of the effect of the ratio of momentum and diffusion boundary-layer thicknesses on heat- and mass-transfer.

Boundary-layer theory predicts that the exponent of Re is $\frac{1}{2}$ in equations 4.3 and 4.4 (142) and many experimenters have found the Pr or Sc exponent of $\frac{1}{3}$ to fit their data best (142). The equations 4.3 and 4.4 can then be expressed in terms of normalised transport values.

$$Fs_m = Sh - 2.0/Re^{\frac{1}{2}}Sc^{\frac{1}{3}} \qquad (4.7)$$

and $$Fs_h = Nu - 2.0/Re^{\frac{1}{2}}Pr^{\frac{1}{3}} \qquad (4.8)$$

where Fs_m and Fs_h is the normalised transport ratio called the Frössling number of mass- and heat-transfer, respectively. When the molecular diffusivity term becomes negligible the modified Frössling numbers can be written

$$Fs_m' = Sh/Re^{\frac{1}{2}}Sc^{\frac{1}{3}} \qquad (4.9)$$

and $$Fs_h' = Nu/Re^{\frac{1}{2}}Pr^{\frac{1}{3}} \qquad (4.10)$$

The effect of the turbulence of the continuous phase on the rate of mass-transfer has generally been treated by

assuming that transfer by eddy diffusion is proportional to the concentration gradient (71, 107).

$$\frac{N}{A} = (D_v + E) \frac{dc}{dx} \qquad (4.11)$$

The eddy diffusivity E, can be thought of as the product of the mean length and the velocity of the eddy and semi-empirical relationships can be derived for this term based on postulated laws of turbulence decay (73).

Laminar boundary layer theory assumes a steady velocity outside the boundary layer, whereas in practice, for turbulent external fluid flow, the edge of the boundary-layer from the turbulent main stream would be expected to increase the mass-transfer rate. The greatest effect would be where the layer was thinnest as the eddies penetrating the layer temporarily steepen the concentration gradients about the disturbed region.

Another reason for presuming a turbulence effect is that droplets from pressure spray atomisers will have Reynolds numbers in the range 10 to 100. With wake formation reported Reynolds numbers as low as 17 (81), each droplet in the spray will have a following wake and while the vortex ring appears to be stable and self contained up to Re 450 (57), the analytical solution for viscous flow around a sphere using the steady-state Navier-Stokes equation of motion has been solved only for Re $<$100 (68, 81). Free stream turbulence might initiate vortex-shedding and unstable flows in the wake and resonance between the free-stream fluctuations and eddy shedding could then be expected. Experimental measurements of

local heat-transfer coefficients about a cylinder in cross-flow show a maximum effect of the intensity of turbulence at a certain scale (194). Data available for spheres (116, 146, 165, 196) suggest a similar effect may arise.

4.2 Previous Work

In recent years a number of reviews have been compiled from published results of heat- and mass-transfer for drops and spheres in forced convection (Appendix 1, 19, 57, 88, 142, 153). The outstanding conclusion of all reviews is the extreme range of values given for the exponent of the Reynolds number (as in equations 4.3 and 4.4). Variations in the value of the exponent for the Schmidt or Prandtl numbers were not as great although the recent trend towards high temperature studies of heat- and mass-transfer for spheres in molten salts or liquid metals (202) may produce more diverse results. Some transfer correlations have included both the natural and forced convection contributions (57, 160) but Skelland and Cornish (169) have shown that the effect of free convection on mass-transfer from drops is negligible above a drop Reynolds number of 15. In most commercial equipment the range of droplet Reynolds number encountered is 15 to 200, so for the present only forced convection effects will be considered.

Forced convection correlations for macroscopic transfer for spheres or drops are available for Reynolds numbers up to 10^6 (54). A comprehensive review by Keey and Glen (88) shows the inadequacy of equations 4.7 and 4.8 in that the Frössling number should increase with increasing Re if the exponents of Re, and Sc and Pr are taken as $\frac{1}{2}$ and $\frac{1}{3}$ respectively. This is attributed to the changing importance

of wake transfer with Re and is also due to the onset of turbulence in the boundary layer. While such a trend is apparent for heat- and mass-transfer for solid spheres, values of the Frössling number for the smaller Reynolds number range encountered for evaporating droplets, generally fall close to the experimentally measured values of Ranz and Marshall (147) ($Fs_m = 0.60$) and Frössling himself (48) ($Fs_m = 0.55$). At the same time however, the number of experimental values of overall transfer coefficients for drops that are available is rather smaller than the mass of correlations for transfer for solid spheres.

4.2(a) Drops in Forced Convection

For droplet evaporation in still air, it is assumed that the heat- and mass-transfer processes occur uniformly at all points on the drop surface. For airflow around the drop this condition of symmetry is destroyed and equations (4.7) and (4.8) may be thought of as averaging the non-uniform heat- and mass-transfer over the surface of a drop when there is relative motion between the drop and its surroundings. The reason for the transfer rates being variable over the surface of a drop which is moving, may be found in the boundary-layer theory. Qualitative explanations can be made with reference to figures (3.6) and (3.7) in Appendix 1. These figures show the variable nature of the evaporation around a drop in relative motion and the averaging that is evidently included in the correlations for heat- and mass-transfer for evaporating drops.

The first accurate measurements of the rate of evaporation of drops suspended in an air-stream were those

of Frössling (48) whose extremely careful work has served as a model for subsequent studies in this field. Drops of water, aniline and nitrobenzene were suspended on glass fibres or fine thermocouples and the rate of evaporation was determined by photographing the drop at regular intervals. His accurate analysis also included consideration of the drop sphericity, air turbulence, compressibility of the air, possibility of impurities in the liquids, the Kelvin convection (droplet curvature - vapour pressure effect), non-ideality and the Stefan flow, and he showed that their effect was within the experimental error. A value of $Fs_{m,h} = 0.55$ was obtained and the rather large scatter of experimental points for the evaporation of water drops was ascibed to errors in determining the humidity of the air.

Ranz and Marshall (147) also performed fundamental experiments like those of Frössling but the water drops were suspended on a micro-burrette and were supplied continuously at such a rate that the size of the drops was constant. The rate of evaporation was then equal to the rate of supply of water. For heat-transfer $Fs_h = 0.60$ was recorded for the forced convection studies and a Nusselt number of 2.23 was found for Re = 0, the difference from the theoretical value of 2.0 being attributed to free-convection effects. Expressions for temperature and mass changes of evaporating drops of pure liquids and salt solutions have been derived by Schlünder (160), using this value of $Fs_h = 0.60$ and good experimental agreement was obtained especially for pure liquid drops.

The experimental technique of Ranz and Marshall where the drop diameter was maintained constant, was also used by Hsu, Sato and Sage (78) in the Re range 70 to 300. They

evaporated drops of heptane (Sc ≃ 2.1) and because of the large size of the drops and the low surface tension of the liquid, particular attention was paid to the influence of droplet shape (which was far from spherical) on the rate of evaporation. Their results indicated $Fs_m = 0.55$ like Frössling, but the correlation also included a term for the non-sphericity of the drops.

Evaporation rates for suspended drops of dibutyl phthalate and molten sulphur were reported by Johnstone and Eades (83) who determined the time of complete evaporation of the drop as a function of its initial radius. Their experimental results allow computation of the diffusivities of the vapours, but the temperature data needed to check correctness of these results is lacking. Results for water droplets suspended on glass fibres in a stream of superheated steam of various steam-air mixtures, were reported by Ryozo Toei et al. (150), who found $Fs_h = 0.65$ for droplet Reynolds numbers in the range 9 to 120.

Fuchs (51), in his booklet on droplet evaporation and growth reports a number of Russian works with Frössling numbers for mass-transfer in the range 0.20 to 0.58. The low values were recorded for low droplet Reynolds numbers and are thought to be due to an error in determining the drop temperature with a thermocouple.

Spray evaporation studies using Lignosol have produced $Fs_h = 0$ (29) for small droplets ($< 40\mu$), while for water spray evaporation with droplet Reynolds numbers in the range 1 to 20, $Fs_h = 0.60$ (117). Free fall experiments of evaporation rates for drops falling in a vertical tube were made by Vyrubov (199) with $Fs_m' = 0.52$,

while using an original method (the Rotameter principle) Kinzer and Gunn (95) found Fs_m to rise from zero to a maximum value of 0.92 as the droplet Reynolds number increased to 4, then Fs_m gradually decreased to a value of 0.45 at Re = 100. These last results (95) completely contradict the data of other workers, for whom $Fs_{h,m}$ has a value in this region equal to or less than the value of greater Reynolds numbers.

For evaporating liquid drops with low diffusion fluxes a simple model has been described (204) for drops containing surface impurities, while for a study of high diffusion flux effects Downing (33) suspended drops in a free jet of dry, vapour-free, high-temperature air. Rates of evaporation and wet-bulb temperature were corrected for the vapour efflux and for Re=24 to 325, the correction to the Nusselt number ranged up to 35%. Evaporation rates under intensive mass-transfer conditions were studied by Eisenklam et al. (39) who considered the three theories 1) Film theory, 2) Laminar boundary-layer theory, and 3) Slow Viscous Flow theory, and obtained the best equation for evaporating drops as (boundary-layer theory equation)

$$Nu(1 + B) = 2.0 + 1.6\ Re^{\frac{1}{2}} \qquad (4.12)$$

where $B = (Cp\ \Delta T/Hv)$. For the case of low vapour diffusion fluxes they found $Fs_h = 0.63$.

For completeness, mention should also be made of measurements of rates of evaporation from comparatively large spheres (up to 2 ins. dia.). Such porous or wetted spheres allow measurements for Reynolds numbers up to 5×10^5 (116). The supply of liquid is so regulated that the surface

is always wetted with liquid and surface temperatures can be measured with thermocouples. In this way Pasternak and Gauvin (138) found $Fs_m' = 0.692\ Re^{0.01}$ for an evaporating acetone film on a 1 cm dia. sphere with $500 < Re < 5,000$. For water films, Frössling numbers (Fs_m') of the order $0.36\ Re^{0.08}$ to $0.33\ Re^{0.10}$ are reported (40, 141, 203) for wetted spheres of 2 to 5 cms in dia. in the range $600 < Re < 40,000$, while for gauze spheres of less than 1 cm dia., van Krevelen and Hoftijen (195) report $Fs_m' = 0.50$.

Ingebo (80), for the evaporation of organic solvents from cork spheres at temperatures up to 500 C found a dependence on the thermal conductivity ratio with $Fs_m = 0.30\ Re^{0.10}\ Sc^{0.27}\ (k_g/k_v)$. Maisel and Sherwood (116) using spheres of calcuim silicate wetted with water or benzene in the Reynolds number range 2×10^3 to 5×10^4, found Sh proportional to $Re^{0.56}$. The ratio of Sh for benzene and water was less than that calculated from $Sh \propto Sc^{\frac{1}{3}}$ and the authors consider that the benzene evaporated so quickly that the surface of the sphere was never completely wetted. This apparently also upset Ingebo's results where it must be remembered that for intensive mass-transfer conditions occurring at high temperatures or with volatile solvents, interaction between diffusion and heat-transfer in the boundary-layer must be considered.

4.2(b) Drops in Turbulent Air-streams

The effect of free-stream turbulence on the transport processes of an evaporating drop is dependent on the nature and thickness of the boundary-layer about the drop. As

long as the turbulence intensity of the free-stream is relatively small compared with the relative intensity of the turbulent boundary-layer itself, the effect may be expected to remain restricted to the outermost regions of the boundary-layer. But with increasing intensity of the free-stream turbulence, its effect may penetrate deeper into the boundary layer and enhance the turbulent transport process accordingly.

The effects of turbulent free-stream flow around the drop may be threefold: 1) Usually, the upstream part of the boundary layer is not yet turbulent and the transition into turbulence occurs at some point downstream from the forward separation point. Turbulence in the free stream may not only influence the location of the transition point but may also cause disturbances in the laminar part of the boundary layer and so affect the transport processes through it. 2) The free-stream turbulence may affect the turbulent part of the boundary-layer along the drop, as noted above. 3) If the flow past the body generates a wake, the free stream turbulence may interact with the wake flow. It is known from local heat-transfer measurements on spheres (147) that a maximum rate occurs at the forward stagnation point and in the wake region of the sphere, with a minimum at the separation ring. Hence, the effect of free-stream turbulence on heat-transfer can be expected to be greatest at the frontal and wake regions of the drop and that these separate effects should result in an increase in the overall transfer rate.

It has long been recognised that the application of the Statistical Theory of Turbulence to the problem of predicting mass-transfer rates in turbulent flows requires a knowledge of velocity, density and composition

fluctuations and their correlations (77). The mathematical complexity of problems involving anisotropic turbulence (which includes the majority of practical cases) usually precludes the application of the statistical theory, and transfer studies usually treat turbulent mass-transfer by means of a suitable eddy transfer coefficient or diffusivity (equation 4.11).

Liu (113) and Soo (174) presented theoretical studies of the forces acting on a simple system of single spherical particles suspended in a turbulent gas stream and their results indicated that the eddy diffusivity of the particle and the gas were almost equal at low intensities of turbulence for small particles. This implies that such small drops should evaporate at a rate corresponding to zero relative velocity conditions. Whether or not a droplet will exhibit Stokesian behaviour at very low Reynolds numbers will depend on the size of the drop in relation to the small domains of viscous motion in the turbulent field.

The theory of eddy diffusion developed by Taylor (182) has been confirmed by experiments in a turbulent water stream and can be adapted for transfer to gases (85). The scale of turbulence was found to enter directly into the eddy diffusion relationship, indicating that this quantity should be measured or estimated if diffusion in turbulent fluids is to be predicted accurately. It must be remembered however, that turbulence may be more important in mass-transfer in liquids than in gases, even though the concentration layer is closer to the interface. For liquids the diffusivity is 10^4 lower than for gases and it will take 10^4 times as long to establish steady-state concentration gradients following an upset such as an eddy sweeping into

the boundary layer.

In a theoretical study of three dimensional vorticity on heat-transfer, Sutera et al. (179) calculated that for an increase of 5% in shear stress due to vorticity, the increase in heat-transfer was 26% and was the result of amplification or "stretching" of the vorticity component in the cross-stream direction, which is absent in the case of streamwise oscillation. More recently Sutera (180) found that a vorticity input which increases the shear rate at a boundary by less than 3% is capable of increasing the heat-transfer rate by as much as 40%. These results are in accord with experimental observations that free-stream turbulence has a greater effect on heat- and mass-transfer than on momentum transfer (188). They also explain why turbulence has a significant effect on transfer rates in the diverging flow (pressure gradient) around the front of a buff body.

In his study of momentum-transfer in a two-phase system consisting of particles carried by the continuous phase, Soo (174) applied the statistical theory of turbulence and showed that the correlation, scale and intensity of turbulence of one phase could be calculated from those of the other phase. Assumptions made in this derivation included that the relative velocity between the entrained particle and the main stream be such that the particle Reynolds Number be less than unity, that the turbulence be isotropic and non-decaying and that there be no interaction between particles. The fundamental properties affecting momentum transfer between the two phases were found to be the turbulent Reynolds number Re_T, the ratio of the particle diameter to integral scale of turbulence, and the ratio of

the densities of the dispersed and continuous phases.

Soo also reported that where the gravity effect on the particles was significant, their turbulent motion was anisotropic even though the continuous phase was isotropic. Levich(107) has shown that when the phase densities are substantially different, particles whose dimensions are substantially less than the scale of turbulence will move as though under gravity. Some success in predicting mass-transfer rates for freely moving particles under such turbulent conditions was obtained by Harriott(70) who used the particle terminal velocity to evaluate the Reynolds number in the Ranz and Marshall correlation. In general, Soo found the scale of turbulence of the particles was greater than that of the gas stream, the intensity of the particle less than that of the gas stream, and the diffusivity of the particles greater than the eddy diffusivity of the stream, but tending to the latter when the entrained particle diameter was small.

The relative independence of the transfer processes in turbulent streams on the Schmidt number is a result of disruption of the boundary-layer by the turbulent eddies. The exponent of the diffusivity in mass-transfer relationships changes with the magnitude of the Schmidt number of the system (154). The magnitude of Sc is a measure of the thickness and nature of the diffusion boundary-layer and so determines the relative importance of diffusion in mass-transfer processes.

By extending Harriott's (69) concepts of a perturbed boundary-layer, Galloway and Sage (54) derived a semi-theoretical expression for the mean Frössling number Fs'_m

based on relating the eddy diffusivity to the Reynolds stresses $\overline{\rho u'_x u'_y}$. The solution involving a free-stream turbulence intensity term is valid only over the front half of a sphere and by considering the local motion in the wake region to be independent of the level of turbulence an overall (surface-mean) Frössling number was obtained as the sum of the forward and wake region contributions to the transfer process.

$$Fs'_m = A + B\tau(\tau+C) + DRe^{1/2}Sc^{1/6} \qquad (4.13)$$

Friedlander (46) comsidered heat- and mass-transfer for the dispersed phase as related to the relative velocity between the particle and the gas stream, and the eddy diffusion. The rms relative velocity between the particle and the continuous phase is assumed to represent the characteristic value for transfer calculations, as the velocity past the drops is not constant but varies with time and postion for each particle. If values of this parameter were available the mean particle Reynolds number could be established and the corresponding Nusselt number obtained. A method of estimating the rms relative velocity of a homogeneous turbulent fluid containing a large number of small, rigid, non-interacting spheres is given and the relative velocity effect on the drops calculated accordingly is shown in figure 6.2 of Appendix 1.

For particles larger than about 10 microns in diameter "slip" is reported to occur (46) and the mean relative velocity becomes significant. Friedlander points out that the assumption sometimes made, that the Nusselt number has a constant value of two (stagnant continuous phase) for

drops in a turbulent fluid, may be in error. The degree to which free droplets in a turbulent air-stream follow the general motion, will depend on the density difference between the two phases and on the droplet size. When the scale of turbulence is much larger than the droplet diameter, the droplet may be considered to be completely entrained and so feel only a steady motion. The degree of entrainment rises with increasing ratio of integral scale of turbulence to the time of mechanical relaxation of the drop (51), while the energy of the turbulent eddies falls as their period decreases. It is apparent that the effect of turbulence on the rate of evaporation must increase rapidly with the size of the drop.

In experiments with fixed drops the conditions change sharply, since all the turbulent eddies are effective in this case. The results of such experiments, while giving some insight to turbulent transfer processes, can only be applied to the evaporation of free drops in a turbulent air-stream for the case when the drops are so large that their entrainment is effectively zero.

The established works such as Frössling (50) and Ranz and Marshall (147) were performed in aerodynamic tubes where the natural turbulence would be 1 to 3%, but no attempt was made to vary the level of turbulence in the experiment. The only reported experiments for held drops where the turbulence level was deliberately varied are those of Richardson (149) who evaporated drops of butanol, methyl salicylate, aniline and nitrobenzene, suspended from a thermistor. The Reynolds number range for the held drops was 0 to 100 and turbulence generating grids of 30 and 10 mesh were placed in the aerodynamic tube 5 cms in front of

the drop. The turbulence intensity levels were 4% and 8% respecively though no scale of turbulence measurements were made. The evaporating rates were 10% and 15% greater than the grid-free evaporation results and considering that the air-stream in Frössling's experiments would have a similar natural turbulence to Richardson's grid-free results, the conclusion was that the small scale eddies had a greater effect on the rate of evaporation than did the large scale eddies, even in the complete absence of entrainment.

The only other evaporation studies available are by Maisel and Sherwood (116) and Fledderman and Hanson(43). The former studied the effects of large free-stream intensities on the evaporation rate of water from a 1.3 cm porous sphere, for a Reynolds Number range from 1000 to 20,000 and for turbulence intensities up to 24%. The high intensities are suspect because they were obtained close to a grid, and the velocity fluctuations may have been periodic. Increasing intensities caused a continual increase in the ratio of the actual mass-transfer coefficient to the value of the coefficient at zero turbulence. Instead of the rate of increase decreasing with the higher turbulence levels it was actually steeper in the region above 15-20%. An extremely interesting tendency can be observed in the data, indicated by an upward break in the curve for the results in the vicinity of Re = 5000, which occurs at an intensity of approximately 12%. Up to this level, the mass-transfer coefficient ratio had remained approximately constant and in the region above 15% the rise is a very gradual one. The combination of intensity and Reynolds Number for this break falls on the extension of the critical Reynolds Number curve given by Torobin and Gauvin

(188) (Re_c, by convention, is the point at which the characteristic steeply-sloped part of the drag coefficient curve intersects the C_D value of 0.3), and the discontinuity may well have resulted from a boundary layer transition on the sphere surface. Maisel and Sherwood also measured the scale of their turbulence and found that their results were unaffected by a two-fold variation of the scale.

Fledderman and Hanson (43) studied the effect of the turbulence and windspeed on the rate of evaporation of a fuel spray. They measured both the intensity and the scale of turbulence and found that an increase in turbulence intensity increased the evaporation rate of the spray and although not able to separate the scale from the intensity effects, they concluded a similar effect of increasing evaporation rate with scale.

Brown, Sato and Sage (16) studied the effects of turbulence intensity on mass-transfer from a sphere to turbulence levels of 15%. Unfortunately, the turbulence levels were not measured directly, but were obtained from measurements made previously in a somewhat similar system. At Re less than 1000, the turbulance intensity had little effect on the transfer rate, but at high Reynolds Numbers there was a marked increase at the higher intensities. Comparison of these results with those of Maisel and Sherwood (116) at the same turbulence level shows little agreement. This may be due to the fact that the scale of turbulence was excluded from the correlations (90), although it is still not certain that this effect is significant for reasonable variations in the scale or turbulence.

Local mass-transfer rates over the frontal half of spheres were measured by Short, Brown and Sage (165) for

turbulence intensity variations from 1 to 15% and for Reynolds Numbers up to 3,600. At the low turbulence level, the local heat-transfer coefficient varied from the front to rear poles about the sphere, by a factor of eight, while for the high turbulence level, at the same Reynolds Number the overall transfer rate had increased by 20% and the local variation factor was five. More recently Brown and Sage (17) found that an encrease in the turbulence level of the airstream decreased the relative transport over the front hemisphere of a porous sphere but increased transport on the rear half. In addition, the presence of mass-transfer was found to enhance the actual heat-transfer process resulting in an increase in the local Nusselt number, for the Reynolds number range of 950 to 3,700 and for turbulence intensities in the range of 1 to 14%.

As part of an extensive experimental and theoretical work on material transport in turbulent gas streams Galloway and Sage (54) correlated results for overall-transfer from spheres by

$$Fs_m = 0.562 + 0.1807\, D_p^{\frac{1}{2}} + 0.0672\,\tau(\tau+0.05)\, Re^{\frac{1}{2}} \quad (4.14)$$

The equation indicates that the Frössling number depends on the sphere diameter as well as the turbulence intensity of the free-stream. For D_p = 1 mm, τ = 2% and Re = 200 (typical conditions for Ranz and Marshall (147)), Fs_m = 0.65 and the turbulence contribution is only 0.2% of this. The correlation equation (4.14) represents the regression of a large amount of data for drops, and spheres up to 1 ft in diameter and, although cumbersome to use, holds over a wide range of values of D_p and τ. In a later work, Galloway and

Sage (55) studied local and macroscopic transport from a 1.5 inch diameter cylinder in a turbulent air-stream. For Reynolds numbers in the range 2,600 to 86,000, the turbulence intensity was varied from 1 to 25% and the integral scale of turbulence was estimated to be 0.3 to 0.5 inches. They found that the development of the separation circle varied with the turbulent Reynolds number Re_T and that the Frössling number for heat-transfer was a complicated function of the separation angle measured from the front pole, the Reynolds number, the free-stream turbulence and perhaps the integral scale of turbulence as well as depending on the molecular physical properties of the fluid. From semi-theoretical stochastic considerations of the effects of eddy transport induced in the laminar boundary-layer by external turbulent free-stream perturbations, they derived an empirical expression for either local or overall transport of the form shown in equation 4.13. The existence of such perturbations in the laminar boundary-layer has been reported by Armstead and Keyes (3) who used a hot-film sensor to study laminar to turbulent boundary layer transition and found that free stream turbulence induced heat-transfer fluctuations and thermal stresses in the boundary layer. The frequency of the heat-transfer fluctuations was found to be a function of the Reynolds number and a moderately high level of turbulence was measured in the laminar sublayer.

Other transfer results for held spheres that reflect a turbulence effect include the data of Garner and Suckling (56) for benzoic spheres in water where the coefficients for slightly turbulent flow (gauzes placed upstream of the sphere) were 1.5 times those coefficients

for laminar incident flow. Glen and Keey (62) have shown that heat- and mass-transfer rates from the front pole of a sphere are very sensitive to free-stream disturbances in the Reynolds number range 5×10^2 to 3×10^4. Even small-scale disturbances produced by straightening vanes appear to be sufficient to influence significantly the transfer rates from the leading area of a sphere.

Because of the paucity of data available on turbulence effects for evaporating droplets, in previewing considerations of possible turbulence effects on the transfer processes it is necessary to refer to heat-transfer results obtained for held solid spheres in turbulent gas-streams.

Heat-transfer from a $1\frac{1}{4}$" solid sphere was studied by Lavender and Pei (106) who reported having established that the Turbulent Reynolds number was a single important variable in turbulent heat- and mass-transfer and that the scale was of minor significance. They give upper and lower limits for the rate of heat-transfer from spheres in turbulent air-streams and define a value of Re_T above which there will be a marked increase in the Nusselt number. A solid, heated sphere was also used by Raithby and Eckert (146) who measured the turbulence intensity and scale behind grids placed before the held sphere with either a following- or cross-support. The latter arrangement gave results 10% higher than the former and for low turbulence levels (natural) they found $Fs_h = 0.21\ Re^{0.106}$. An increase in the intensity from 0 to 5% increased the Nusselt number by 8 to 18% for Reynolds numbers in the range 3.6×10^3 to 5.2×10^4. At low Re the most pronounced increase was with turbulence levels below 2%. The sphere diameter to integral scale of turbulence ratio, was varied from 0 to 12 and the Nusselt number was

found to increase with increasing values of the ratio. The ratio effect was large at high turbulence levels and high Reynolds numbers, though no maximum was found.

Heat- and mass-transfer data for solid cylinders show a conflict of results with some works reporting no definite trends and others clear trends with the most significant increase in transfer rates occurring for low turbulence levels from 2 to 4% (20, 61, 162, 172, 206).

One particular study of the effect of scale and intensity of turbulence on heat-transfer from a heated cylinder has done much towards helping explain the seeming discrepancies and even the contradictions found in the literature. Van der Hegge Zijnen (194) has systematically studied the rate of heat-transfer from cylinders to a turbulent airflow for a Reynolds number range of 600 to 25,800, with an intensity range from 2 to 13% and with ratios of the integral scale of turbulence to cylinder diameter varying from 0.31 to 240. However, results were also taken at Reynolds numbers of 60 and 580 and these showed no turbulence effect up to intensity levels of 13%. For the higher Reynolds number data he found that the rate of heat-transfer was effected and that the increase was a function of Re, $\sqrt{\overline{u^2}}/U$, and Λ_f/D_p. He then proposed that the first two parameters be combined into their product, the Turbulent Reynolds number. This reasoning may not be correct since it pre-supposes that the functional form of both parameters will be identical, which is not the case, at least with momentum transfer, since the critical behaviour for laminar to turbulent transition is very definitely a function of the Reynolds number. Van der Hegge Zijnen has correlated his data as a function of

($D_p\sqrt{\overline{u'^2}}/\mu$) and ($\Lambda_f/D_p$), but the success which he does have may be due to the ranges of intensities and Reynolds numbers which characterise his system (188). At a Reynolds number of almost 10,000 he obtained by interpolation a family of curves as shown in figure 6.1 of Appendix 1. Although his actual data are scattered about the curves, the effect of the integral scale of turbulence is significant. Below a Λ_f/D_p ratio of 1.6, the effect of increasing the scale would be to increase the effectiveness of the turbulence whereas the Taylor theory which considers the magnitude of the velocities of the pressure fluctuations which accompany the free-stream turbulence predicts the opposite and the data of Dryden (35) would seem to confirm this at Λ_f/D_p ratios below unity. The optimum value for heat-transfer for cylinders at that Reynolds number (10,000) occurs at a ratio value of 1.6 and seems to point to some resonance frequency between the turbulent flow and the shedding frequency of the eddies in the wake of the cylinder. This resonacne apparently reinforces the oscillations in the wake and van der Hegge Zijnen's hypothesis is supported by the results of Fand and Cheng (41) who studied the influence of acoustic vibration on convective heat-transfer from a cylinder.

4.3 Apparatus

The experimental cocurrent spray-drier described in Section 2 figure 2.1, was used as a vertical wind tunnel. The direction of the airflow was reversed so that the air moved up the drying chamber and a large capacitance vessel (an empty 44 gallon drum) was placed in line between the blower and the base of the drying chamber, to damp out pulsations of the air coming from the rotary blower. A

flush fitting, turbulence generating grid was placed in the column 10 feet away from the entrance. The grid was a perforated plate of 0.128" dia. holes on a 3/16" triangular pitch and had a solidarity of 0.594.

The drops of distilled water were supported on fine glass fibres made by drawing borosilicate glass rod ($k = 0.63$ Btu/ft.hr ^{o}F). The glass fibres were carefully selected for uniform diameter over their whole length and were mounted in cork ($k = 0.025$) attached to a hypodermic needle fitting. The glass fibre was held in the column by an assembly inserted in a porthole at the required distance behind the turbulence generating grid. The internal profile of the column was maintained by contouring the assembly and conduction effects were minimised by using polyethylene tubing ($k = 0.19$) for the main support arm (see figure 4.1). To evaluate the effect of the supporting glass fibre diameter on the evaporating rate of the drops, four sizes of glass fibres were used. Each fibre had the drop supporting end carefully ground flat and the sides of the fibres were lightly spray-coated with polytetrafluoro-ethylene (ptfe) to prevent the water drops climbing up the side of the glass fibre as a surface tension effect. The water drops were placed on the glass fibres in position in the column, using a fine hypodermic needle which was also spray-coated with ptfe as this reduced the difficulty of transferring the drop from the needle to the glass fibre.

4.4 Experimental

The calculation of the mass-transfer rates and the evaluation of the dimensionless Frössling number

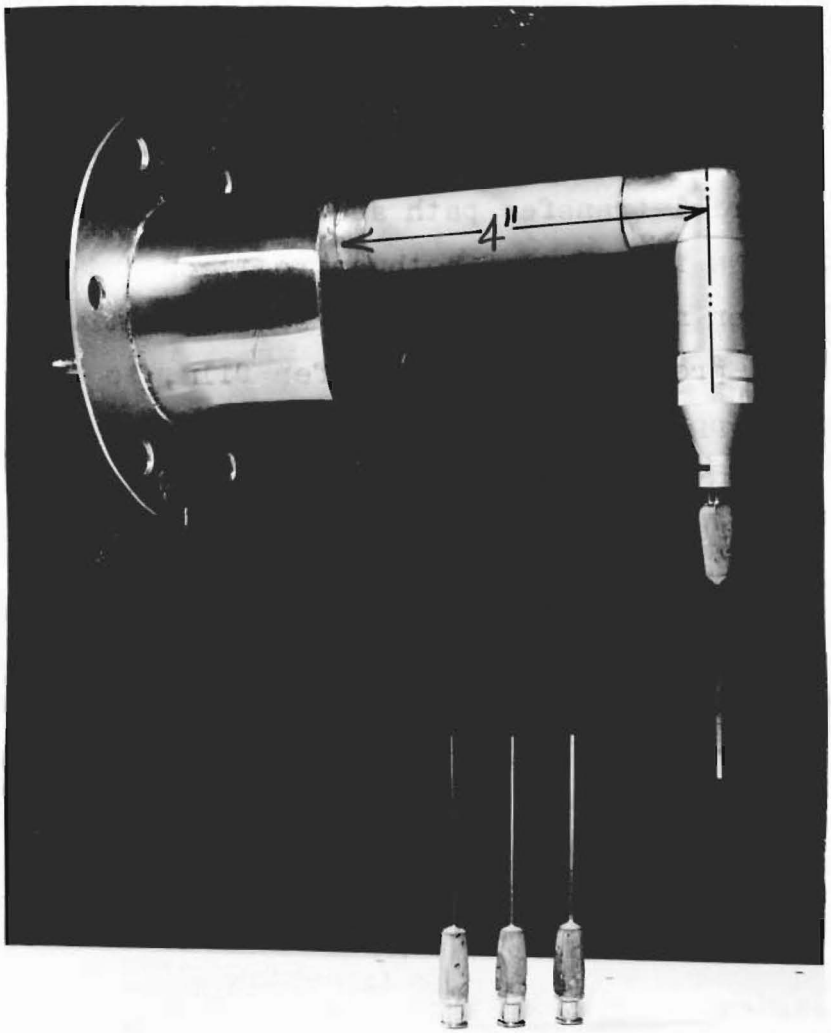

Figure 4.1 The 4 sizes of glass fibres used to support the evaporating droplets and the assembly for mounting the fibres in the column against an upflowing stream of air.

correlations which describe the evaporation processes are very dependent on the transport properties of the system. The correlations imply that the physical properties within the material transfer path are constant, whereas they are actually a function of both composition and temperature. It is then necessary to define some effective average physical property of the transfer film, to be evaluated at some appropriate composition and temperature. Many workers (39, 147, 156, 161) have taken mean conditions for evaporating drops to be the arithmetic mean between 100% vapour at the drop surface and temperature, and the surrounding gas at its approach conditions and temperature. This implies that the transfer film is thin compared with the diameter of the evaporating droplet. Downing (33) defines a volume-average film temperature as

$$T_f \propto \frac{1}{(D_{p_1}^3 - D_{p_2}^3)} \int_{D_{p_2}}^{D_{p_1}} T(D_p) D_p^2 dD_p \qquad (4.15)$$

and showed

$$T_f - T_d / T_g - T_d = m = 0.60 \qquad (4.16)$$

This definition attempts to account for the radial profile of the temperature and concentration of the diffusing vapour in the spherical transfer shell about a drop and the average film property is then weighted slightly more in favour of the approach or free stream conditions (as against arithmetic mean, where m = 0.50).

For this present work the film properties (temperature concentration, viscosity and thermal conductivity) are

evaluated at the column-mean film temperature and composition with m = 0.60. The specific heat property of the transfer film is a measure of the sensible heat gained by the vapour as it diffuses or is convected from the drop surface into the free stream $((C_{p_v} T)_d - (C_{p_v} T)_g)$ and is not a mean value for the film but a difference in properties at two limits. However, for convenience the specific heat is also evaluated under the same conditions as the other transport properties, as in studies where there is not intensive mass-transfer, the difference when the specific heat is calculated for m = o.6o is small and in the present study approximately $2\frac{1}{2}\%$.

The properties relating to the drop are evaluated at the drop temperature. A uniform temperature through the drop is assumed and this temperature is taken to be the wet-bulb temperature of the drying air. A number of reports (48, 147, 156) have shown that this is a good approximation to reality even considering that internal circulation within the drop is reduced.

Transport properties used for the calculations were cited from the following references.

Viscosity - air: Handbook of Physics and Chemistry (74), vapour: Chemical Engineer's Handbook (140), mixed gas: Herning and Zipperer formula (140).

Thermal conductivity - air: Chemical Engineers' Handbook (140), vapour: Chemical Engineering (24), mixed gas: Friend and Adler formula (140).

Heat capacity - air: Heat Exchanger Design (45), vapour: Tables of Physical and Chemistry Constants (86), mixed gas: Weighted mean of molar fractions.

Latent heat of Vaporisation - Handbook of Physics and Chemistry (74).

A computer program (HTCOEF) (see Appendix 7) was written to calculate the relevant physical properties of the system using as input data the humidity, vapour pressure and temperature of the drying gas, the temperature of evaporating drop (wet-bulb temperature of the air), and the total pressure of the system. The wet- and dry-bulb temperatures of the continuous sample of drying gas removed from the column, were measured using the humidity probe described earlier in section 2. A large pyschrometric chart readable to 0.1 F (144) was used to evaluate the true column wet-bulb temperature, humidity and vapour pressure of the air. The total pressure of the system was the sum of the column guage pressure and the atmospheric pressure, the former often negligible in terms of the latter.

The air velocity and turbulence parameters were measured before and after the evaporation of a held droplet at the same distance as the drop behind the grid. These measurements were all done under steady-state conditions in the same position within the column. The turbulence frequency and energy spectra were calculated by computer (see Appendix 7) as described earlier in section 3 and estimates of the macroscale of turbulence were obtained by solving the equations approximating the turbulence spectra. The frequency and energy spectra histograms as calculated directly from the experimental results were approximated by smooth curves and these were also plotted by the computer. (An example of the computer output is also given in Appendix 7).

To measure the evaporation rate of the held droplets, a photographic technique similar to that used by Frössling

(48), Ranz and Marshall (147) and Ryozo Toei et al. (156) was adopted. The evaporation rate of the droplet was determined by measuring the volume change of the droplet from photographs taken at measured time intervals. A camera with extension tube and lens was mounted in a port-hole at the same level as the supported droplet and the porthole at 90° to the camera (and in the same plane) was used for access to the glass fibre for depositing the liquid drop. The drop was illuminated by a photographic flash-lamp positioned at a porthole below the camera and an exposure time of 1/50th of a second was used. A solid naphthalene sphere was mounted in place of the drops and after a number of trials the best background on which to photograph the drops was found to consist of a black matt surface with a silver line ($\frac{1}{2}$ to 1" wide) running vertically down the column in line with the drop and its supporting fibre. (A single test run of the sublimation of the solid naphthalene sphere is reported in Appendix 8. Although not directly related to the liquid droplet studies, the variation of the local transfer rate over the surface of the sphere may be of interest to future workers in this field.) Figure 4.2 shows photographs of a held water droplet as the evaporation process proceeded. At the end of each droplet evaporation test, a microscope graticule was photographed under the same conditions as the droplet. This photograph was processed in the same manner as the evaporating drop photographs so that the absolute and relative sizes of the evaporating drops were accurately known.

Since the drops were not completely spherical (see figure 4.2), rather than use a mean droplet diameter

(147, 156), the volume of each droplet was determined by a graphical integration method. From each photograph, the droplet diameter was measured at equal intervals along the vertical axis from the front pole of the drop. Each diameter was then taken in turn as the upper and lower diameter of a frustrum of a right cone and the total surface area and volume of the drop are determined as the sums of the surface area and volume of the frustrums approximating the droplet.

To further improve the accuracy of the method, the Lagrange Interpolation formula (Appendix 5) was used in the form of a 2nd order polynomial fitting the measured values, and from which intermediate diameters were then calculated. Planimeter measurements of the vertical cross-sectional area of a held droplet (as photographed) showed much less than 1% difference compared with the graphically integrated area. The curved surface area and volume of the evaporating droplet were then taken to be accurate to at least 1%.

From each photograph measurements of the drop diameters at intervals along the vertical axis, allowed the calculation by computer (Appendix 7) of the droplet volume, surface area, maximum and average diameters as well as the droplet length. The variation of these parameters with time is illustrated in figure 4.3 which plots the calculated parameters against time for the evaporation of a held droplet. The curves fitted to the data were obtained using a computer library subroutine (POLFIT) which fits a polynomial to a given set of data points. 1st and 2nd order polynomials were fitted as part of the main computer program and the best fitting polynomial expression describing the change in droplet

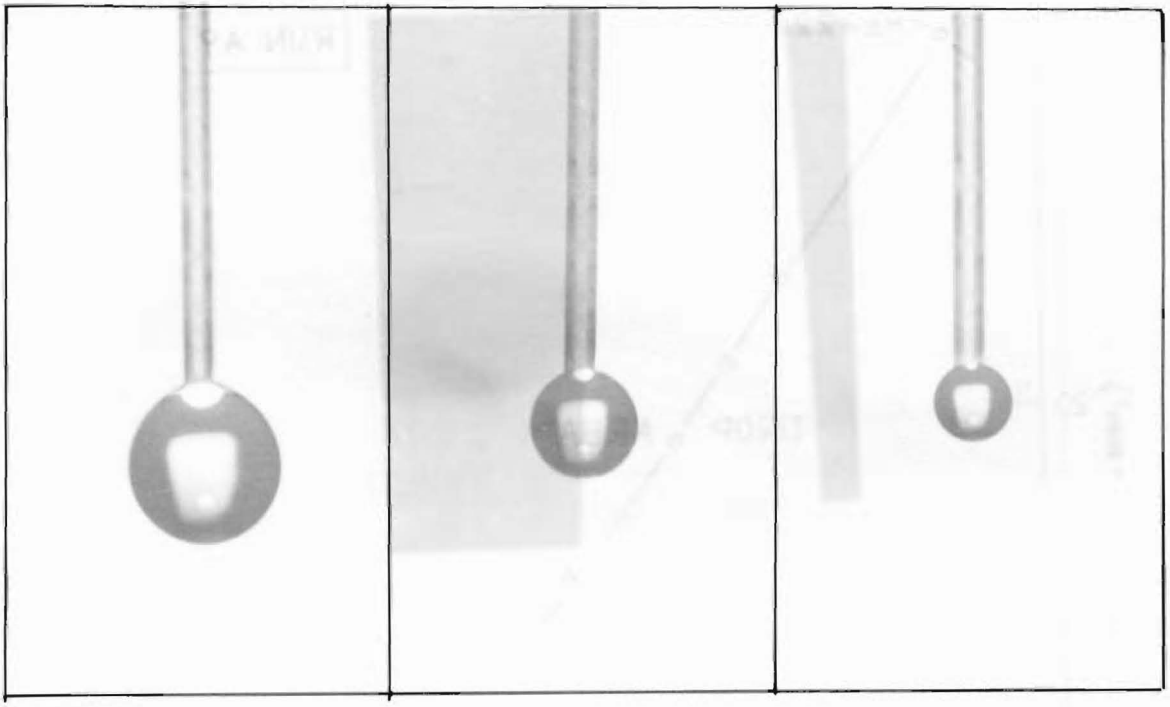

Figure 4.2 Progressive evaporation of a supported water droplet. Initial diameter=1.597mm. Final diameter=0.826mm. Times of photographs were 0, 6 and 12 minutes. T_g=65.9F, V_g=3.49fps and the supporting glass rod diameter=0.334mm.

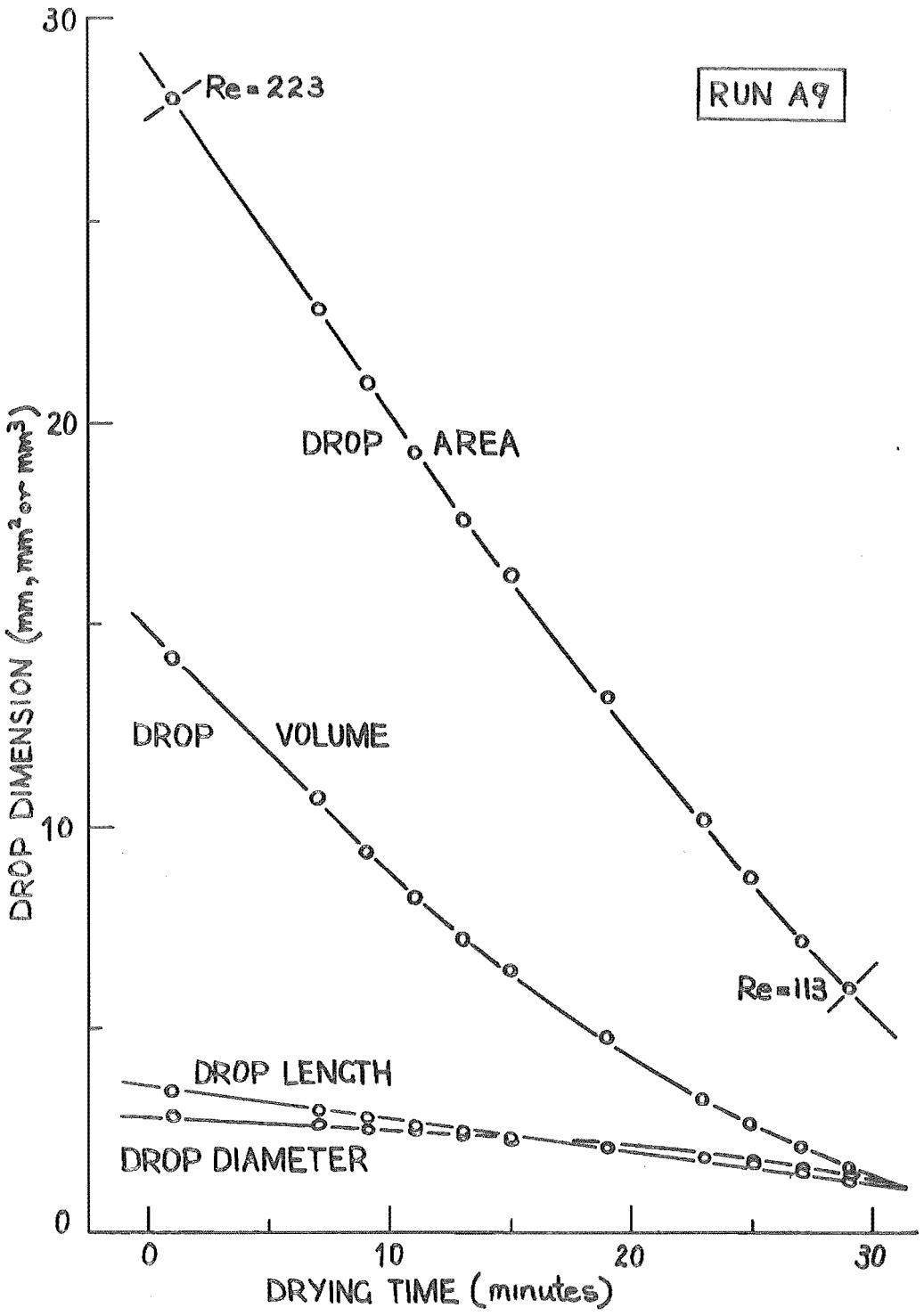

FIGURE 4.3 EVAPORATION OF A HELD WATER DROP. o = EXPERIMENTAL VALUES, — — = COMPUTER FITTED CURVES. SELECTED DROP REYNOLD'S NUMBERS WERE 225, 200, 175, 150, 125.

volume with time was differentiated analytically to provide an expression for the droplet volume rate of change and so the droplet evaporation rate. The majority of data consisted of from 5 to 15 points and higher-order polynomials fitted to them confirmed that a 2nd-order curve was good enough as shown in figure 4.3.

The experimental droplet Reynolds number range was calculated based on the maximum droplet diameter exposed to the upflowing air at the beginning and the end of the evaporation study. The Reynolds number range was rounded up or down into a range covering only multiples of 25 and a trial and error method was used in the computer program to find the drying time at which these calculated Reynolds numbers (multiples of 25) occurred. The analytical expressions for the computer fitted curves were then solved by extrapolation or interpolation at each drying time, to provide values of the parameters of the droplet volume rate, surface area, diameter and length.

Neglecting the temperature distribution in the drop, the heat balance for the evaporating held droplet is written

$$- \rho_d \frac{dV}{dt} H_v = Q_{total} = Q_{con} + Q_{rod} + Q_{rdn} \qquad (4.17)$$

and $$Q_{con} = Q_{total} - Q_{rod} - Q_{rdn} = h_c A(T_g - T_d) \qquad (4.18)$$

Equations 4.17 and 4.18 combine to give

$$h_c = \frac{- \rho_d \frac{dV}{dt} H_v - Q_{rod} - Q_{rdn}}{A (T_g - T_d)} \qquad (4.19)$$

and so $$Nu = \frac{h_c D_p}{k_f} = \frac{D_p \left(- \rho_d \frac{dV}{dt} H_v - Q_{rod} - Q_{rdn}\right)}{A k_f (T_g - T_d)} \qquad (4.20)$$

The correction for the sensible heat gained by the evaporated water vapour as it is transported through the transfer film can be approximated by

$$h_c' = h_c/\gamma \qquad (4.21)$$

where h_c' is the heat-transfer coefficient in the absence of mass-transfer and γ is the Ackermann correction (1)

$$\gamma = \frac{\log_e(C_{pf}(T_g-T_d)/H_v+1)}{C_{pf}(T_g-T_d)/H_v} \qquad (4.22)$$

When the effect of simultaneous mass-transfer on the convective heat-transfer coefficient is small, the correction can be written

$$h_c' = h_c/(1-B/2) \qquad (4.23)$$

where $B = C_{pf}(T_g-T_d)/H_v$ and is known as the Transfer number, representing the ratio of the sensible to latent heat gained by the vapour during the evaporation process. Equation 4.23 indicates that the heat-transfer coefficient in the absence of mass-transfer is larger than the convection evaporation heat-transfer coefficient. For the present study of held droplets evaporation under conditions of low mass-transfer rates, the Transfer number B took values from 0.33 to 0.62%. The effect of mass-transfer on the heat-transfer coefficient was therefore negligible and no correction was made.

Radiative heat transfer to the drop Q_{rdn}, was described by the usual equation

$$Q_{rdn} = \sigma F_A F_B \left\{ \left(\frac{T_A + 459.4}{100} \right)^4 - \left(\frac{T_B + 459.4}{100} \right)^4 \right\} \qquad (4.24)$$

In the experiment T_A was the measured wall temperature (see Section 2) and T_B was the drop temperature equal to the wet-bulb temperature of the drying air. Because the drop was entirely enclosed by the walls of the column, F_A was equal to unity and since the surface area of the held droplet was far smaller than the area of the enclosing wall, F_B was estimated to be the emissivity of water, 0.96. Equation 4.24 then reduced to

$$Q_{rdn} = 0.1642 \left\{ \left(\frac{T_{wall} + 459.4}{100} \right)^4 - \left(\frac{T_d + 459.4}{100} \right)^4 \right\} \qquad (4.25)$$

The rate of conductive heat-transfer to the supported droplet from the fine glass rod Q_{rod}, was estimated by assuming the fine rod to be an insulated fin with heat flowing to the droplet at the end (x=0). The quantity of heat flowing to the droplet is then

$$Q_{rod} = -k_{rod} A_{rod} (dT/dx)_{x=0} \qquad (4.26)$$

Solving for (dT/dx) at x=0, the approximate solution is

$$Q_{rod} = \frac{\pi}{2} \sqrt{k_{rod}\, h_{rod}\, D^3_{rod}} \cdot (T_g - T_d) \qquad (4.27)$$

Equation 4.27 shows Q_{rod} to be independent of the size of drop supported from the fine glass rod. The coefficient h_{rod} is constant over the whole length of the glass rod and is a combined radiation and convection coefficient for the rod from the surrounding air flowing vertically upwards

and parallel to the rod. The value of h_{rod} was estimated using equations described in Appendix 6 which also gives the derivation of equation 4.27 and describes a more correct analysis of this problem which as yet cannot be solved.

The solution of the equation for the evaporating drop Nusselt number (eq. 4.20), the evaluation of the relevant physical properties of the system, and the calculation of the drying gas turbulence parameters, were all obtained from the computer program (HTCOEF) which was a combination of the various smaller programs and subroutines. Details of the program usage and the required input data are given in Appendix 7, along with a listing of the program. A computed output is also given showing the solutions to the subprograms calculating the system physical properties, the air velocity and turbulence parameters, the frequency and energy spectra graph plots, the graphical integration of the surface area and volume of the droplet, the drying rate curve fitting procedure, the conductive heat-transfer from the supporting glass fibre and finally, the values of the drop Nusselt numbers calculated at drop Reynolds numbers that are multiples of 25.

4.5 Results

As the first of a three part study of the evaporation of single drops and sprays, the study of the evaporation rates for supported droplets serves a dual purpose. Firstly, the method of application of the proposed turbulence measuring technique was developed and experimental measurements of the turbulence parameters obtained were compared with previously published results. Secondly,

the influence of the turbulence parameters on the evaporation rate of supported water droplets was investigated for low-temperature (ambient) conditions where the influende of mass-transfer on heat-transfer was negligible. These latter results would provide an insight to the behaviour of evaporating sprays of droplets falling cocurrently with the hot drying air under conditions of intense heat- and mass-transfer.

The evaporation study of supported droplets deals with evaporating droplets held behind the turbulence generating grid which was placed in the column and with droplets held in the column with no grid present, or with the grid a very long distance away from the droplet (grid at base of column). For the former case turbulence was expected to be nearly isotropic and the turbulence parameters would be expected to follow the decay laws, while for the latter case, natural turbulence would exist and these conditions approach those found in industrial applications of spray processes.

4.5(a) Turbulence Results

The turbulence intensity measurements obtained using the DISA constant temperature hot-wire anemometer are shown in figure 4.4. The turbulence intensity is seen to decrease with increasing air velocity in agreement with van der Hegge Zijnen (193) and contrary to the results of Raithby and Eckert (146). The air velocity variation across the column at a distance of 5 inches behind the grid ($X/M \backsim 40$) was not more than 5%.

If the measured turbulence intensities are to be correct, it is necessary that the length of the hot-wire be much smaller than the integral scale of turbulence. This

condition was not always fulfilled in the present measurements. The effect of wire length on the measured longitudinal spectra $E_1(k)$ has been analysed by Uberoi and Kovasznay (192) with the assumption of uniform wire heating. The correction for a wire length of 1 mm was found to be negligible for wavenumbers less than 500 ft^{-1} and approaches 24% as k nears 1000 ft^{-1}. For a wire of 1.2mm in length as used in the present study, the wire correction was found to be negligible in almost every case.

Frenkiel (47) has postulated that far downstream from a grid the turbulence intensity should decay proportionally to $(X/M)^{-5/7}$. Considering that the plotted results in figure 4.4 were obtained for slightly different velocities, the measurements show this to be approximately true when compared with the line with slope -5/7 for values of X/M greater than 30 (See footnote).

Equations of the form

$$\tau = A\left(\frac{X}{M} - \frac{Xo}{M}\right)^{-n} \qquad (4.28)$$

FOOTNOTE: When the decay of fully developed isotropic turbulence is to be investigated, all data obtained closer to the grids than a certain minimum distance are to be discarded (because of streaming effects). Some authors take this minimum distance as 20M (193) while others use the limit of 50M (146); in fact it is a complicated function of many variables such as the mesh and solidarity of the grid and the air velocity. Many more experiments are needed to ascertain where fully developed isotropic turbulence is established.

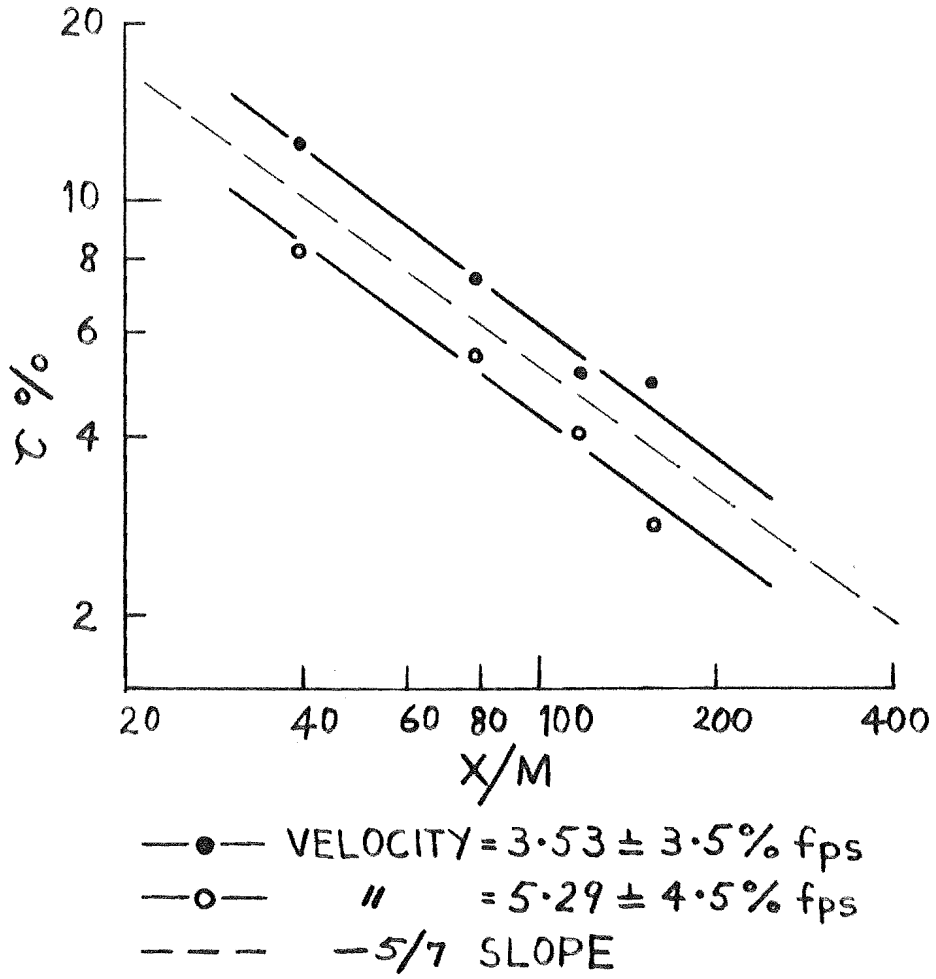

FIGURE 4.4 TURBULENCE INTENSITY MEASUREMENTS DOWNSTREAM FROM THE GRID ($\sigma = 0.594$)

fit the data reasonably well over the limited range of X/M covered by the results. The constants required for the data are n = 0.73, A = 1.51 and $X_o/M = 16$ for the low velocity results and n = 0.73, A = 0.64 and $X_o/M = 48$ for the high velocity data. The method of calculating X_o was to plot $1/\tau$ as a function of x and extrapolate back to $1/\tau = 0$. As van der Hegge Zijnen (193) points out, the procedure is more or less arbitrary and yields only a rough estimate of X_o, but no more accurate method could be found. A review of turbulence in air downstream of grids (193) reports values of A from 0.19 to 1.0 and the range of n from 0.55 to 0.74. These data were for grids of solidarity rather less than that used in the present study and as the intensity will depend strongly on the solidarity and geometry of the grid, reasonable agreement is found.

In figure 4.5 experimental measurements of the micro- and integral scale of turbulence are shown plotted against the dimensionless distance downstream of the grid (X/M). The microscale of turbulence λ_f, was obtained using the technique described earlier in section 3(g) and the integral or macro-scale of turbulence Λ_f was calculated (Appendix 7) using the Liepmann empirical formula as described in section 3(g). Whereas the turbulence intensity results show good agreement with existing data, the turbulence microscale measurements do not.

The integral scale Λ_f was calculated by solving the Liepmann formula using wavenumber and energy distribution function values that were calculated from the turbulence

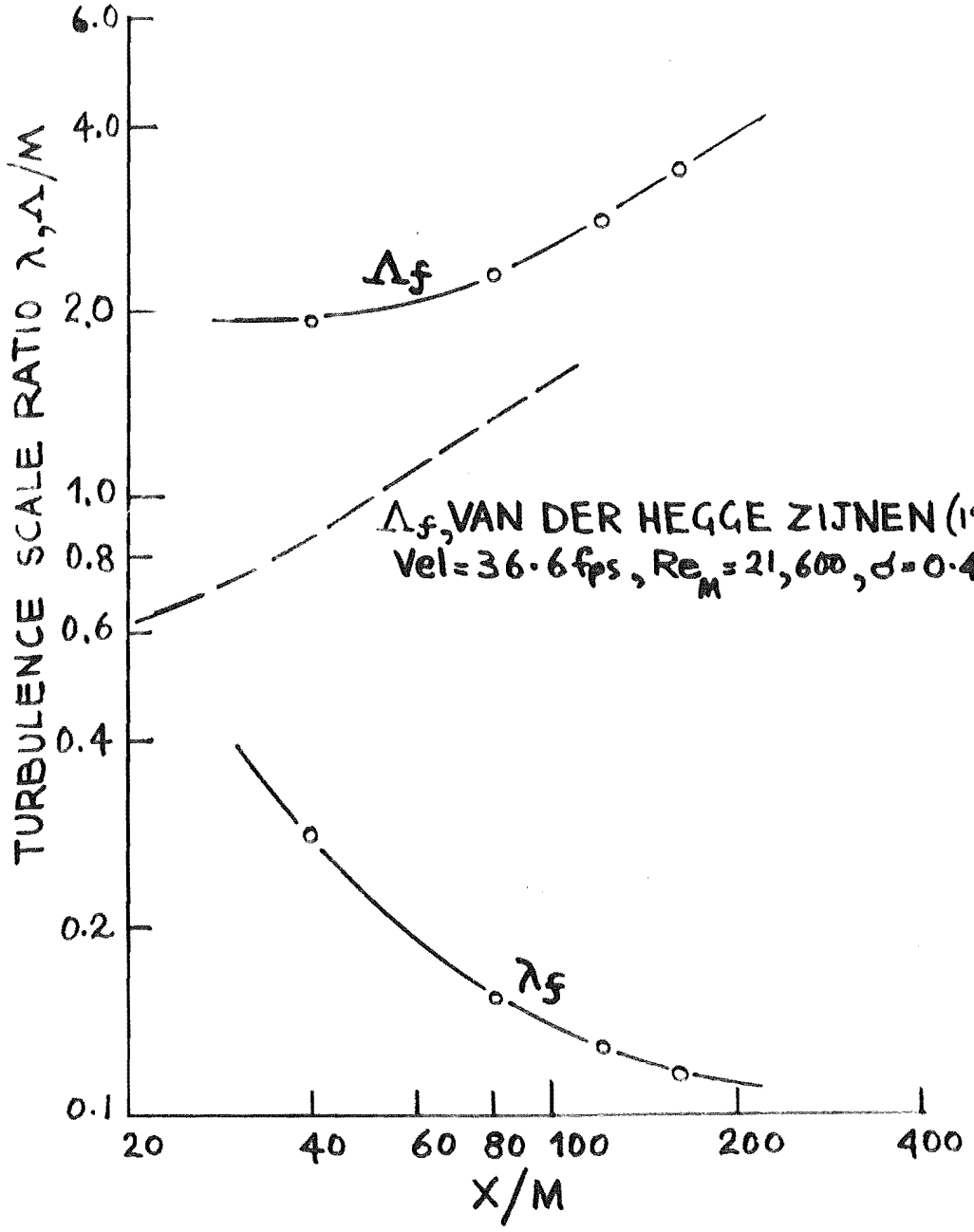

FIGURE 4.5 TURBULENCE MICRO- AND INTEGRAL SCALE MEASUREMENTS DOWNSTREAM FROM THE GRID. (Vel=5·3 fps, Re_M=350, σ=0·59)

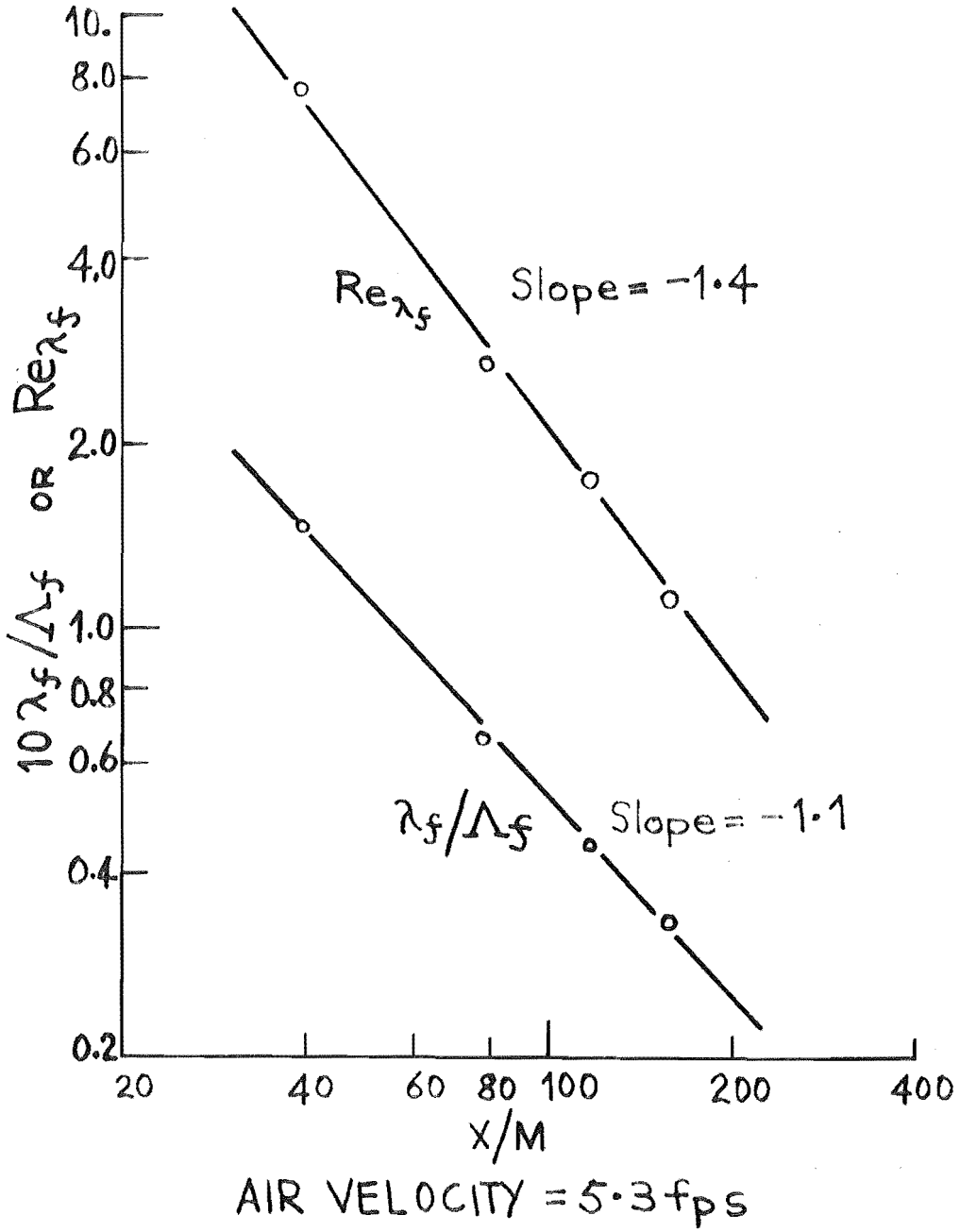

FIGURE 4.6 TURBULENCE SCALE RATIOS AND REYNOLDS NUMBERS DOWNSTREAM FROM THE GRID

intensity spectra. The curve for Λ_f is much the same as that recorded by van der Hegge Zijnen (193) and also Baines and Peterson (4), although tending to larger values than reported by these and other workers (146). The integral scale is of the order of size of the turbulence generator which is consistent with grid generated turbulence (191).

From the theories developed by Taylor (183, 186) and von Karman and Howarth (197), λ_f is expected to be related to the distance and velocity in the form

$$\lambda_f \propto \sqrt{X/MU} \qquad (4.29)$$

Measurements of the longitudinal and lateral microscales λ_f and λ_g by van der Hegge Zijnen (193), Batchelor and Townsend (9) and Stewart and Townsend (177) show this relationship to hold for grid or mesh-Reynolds numbers ($Re_m = UM/\nu_g$) of the order of 10^4. The opposite trend as shown in figure 4.5 has only been reported (177) for the case where X/M is very small (close to the turbulence generating grid). However, Batchelor and Townsend (9) also made measurements with a low mesh-Reynolds number $Re_m = 650$. For this case they found that the decay period where λ_f takes the form described in equation (4.29) was only obtained for values of X/M greater than 600. In the present study Re_m took values of 225 and 350 and large deviations from the decay laws can then be expected. The turbulence microscale as shown in figure 4.5 is seen to begin to increase with distance from the grid at $X/M \backsim 200$, suggesting that up to this point isotropic turbulence has not yet been fully developed but exists some distance further downstream.

Further evidence to support this conclusion is provided

in figure 4.6 where the ratio of the turbulence micro- to integral scale (λ_f/Λ_f) and the Reynolds number of (longitudinal) turbulence ($Re_{\lambda_f} = \sqrt{\overline{u'^2}}\,\lambda_f/\nu_g$) are plotted against the dimensionless distance X/M. As in all fluid flows, the Reynolds number is an important parameter and the character of turbulence varies appreciably whether Re_λ is large or small (73). In the initial period, decay is determined predominantly by the decay of the energy-containing eddies, Re is large and constant and λ_f/Λ_f will vary with distance downstream of the grid. In the final period of decay the viscous effects predominate over the inertial effects, Re is small and varies as the $-\frac{3}{4}$ power of the distance, and the scale ratio is constant. In figure 4.6 neither set of conditions for Re_λ and the scale ratio is seen to apply, supporting the conclusion that isotropic turbulence was not fully established for the range of X/M investigated. However, the behaviour of the relative intensity of turbulence and the various scales are not in themselves an accurate measure of the actual behaviour of the details of turbulence, these being reflected more in the precise shape of the energy sprectrum, for instance (73).

The turbulence energy spectra were obtained in the form of frequency histograms which were the result of spectral analysis of the turbulence intensity signal by the gating procedure described before in sections 3(f) and 3(h). An example of the calculation steps made to convert the frequency/mV signal results into a wave number/energy spectrum histogram is shown in Appendix 7, along with the results presented as the computer output. As was said in section 3(f), the drawing of a continuous curve describing

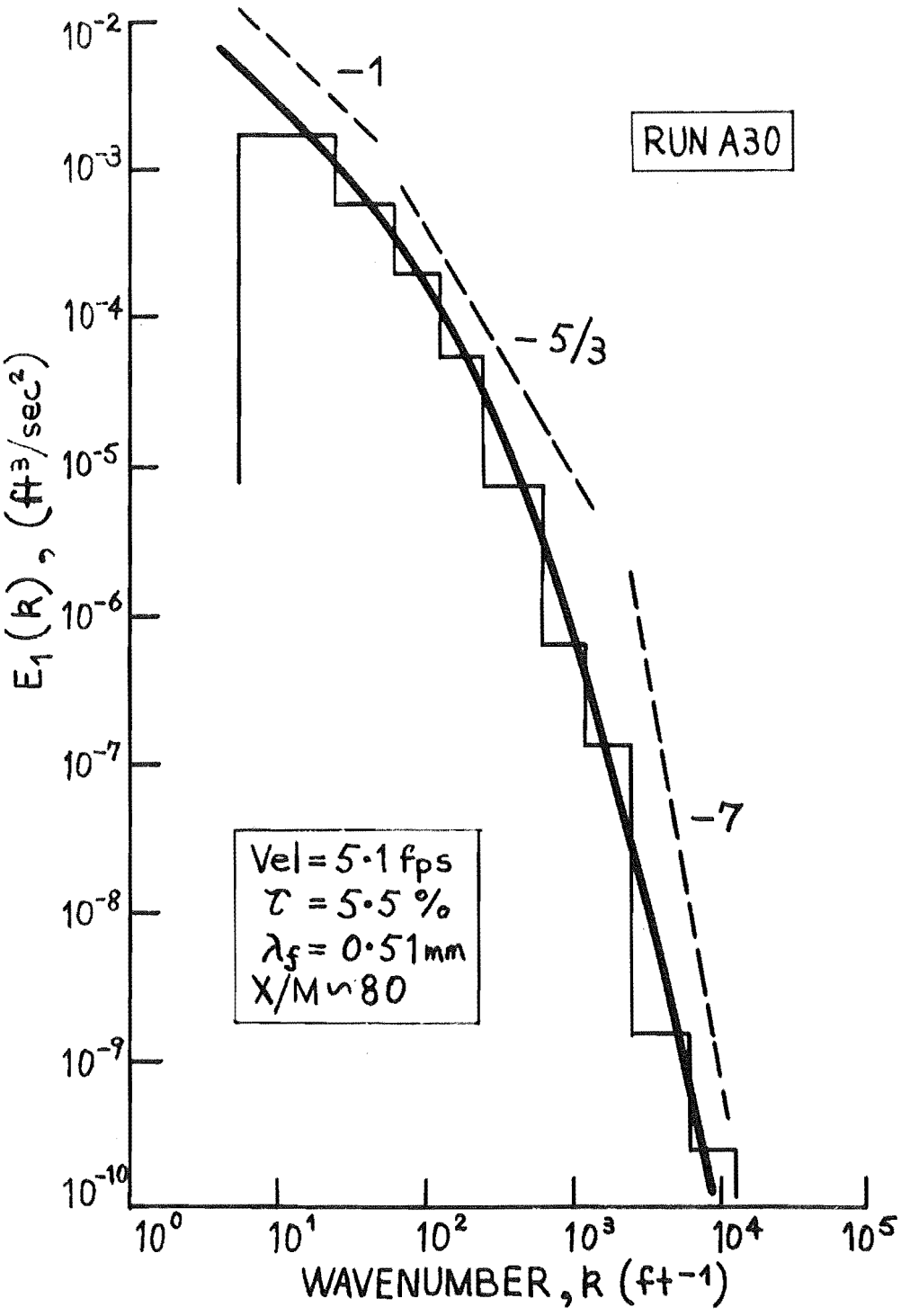

FIGURE 4.7 ONE-DIMENSIONAL TURBULENCE SPECTRUM FUNCTION $E_1(k)$ HISTOGRAM AND SMOOTHED CURVE.

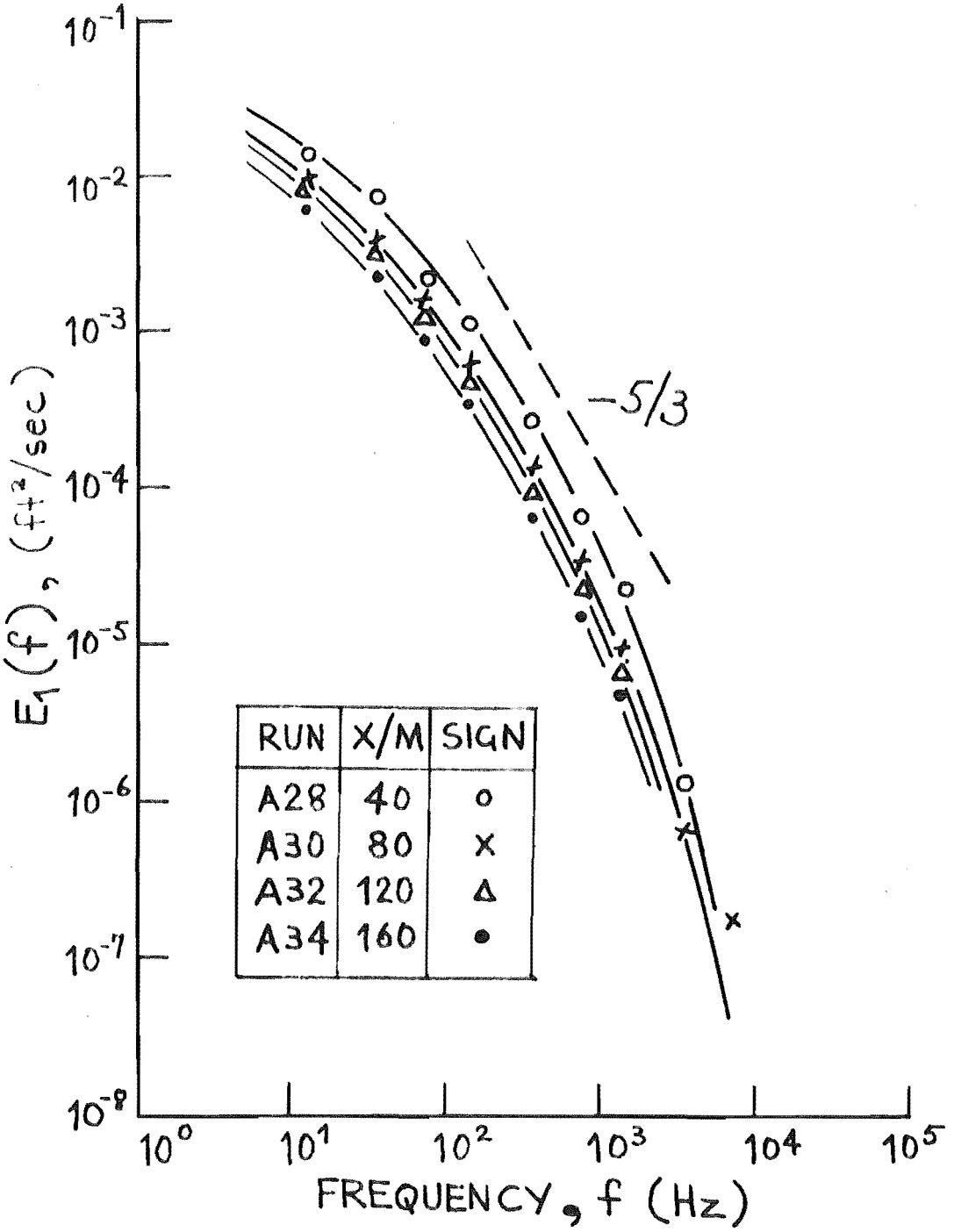

FIGURE 4.8 ENERGY FREQUENCY SPECTRA DOWNSTREAM OF A GRID (Vel = 5·3 f_{ps}, Re_M = 350)

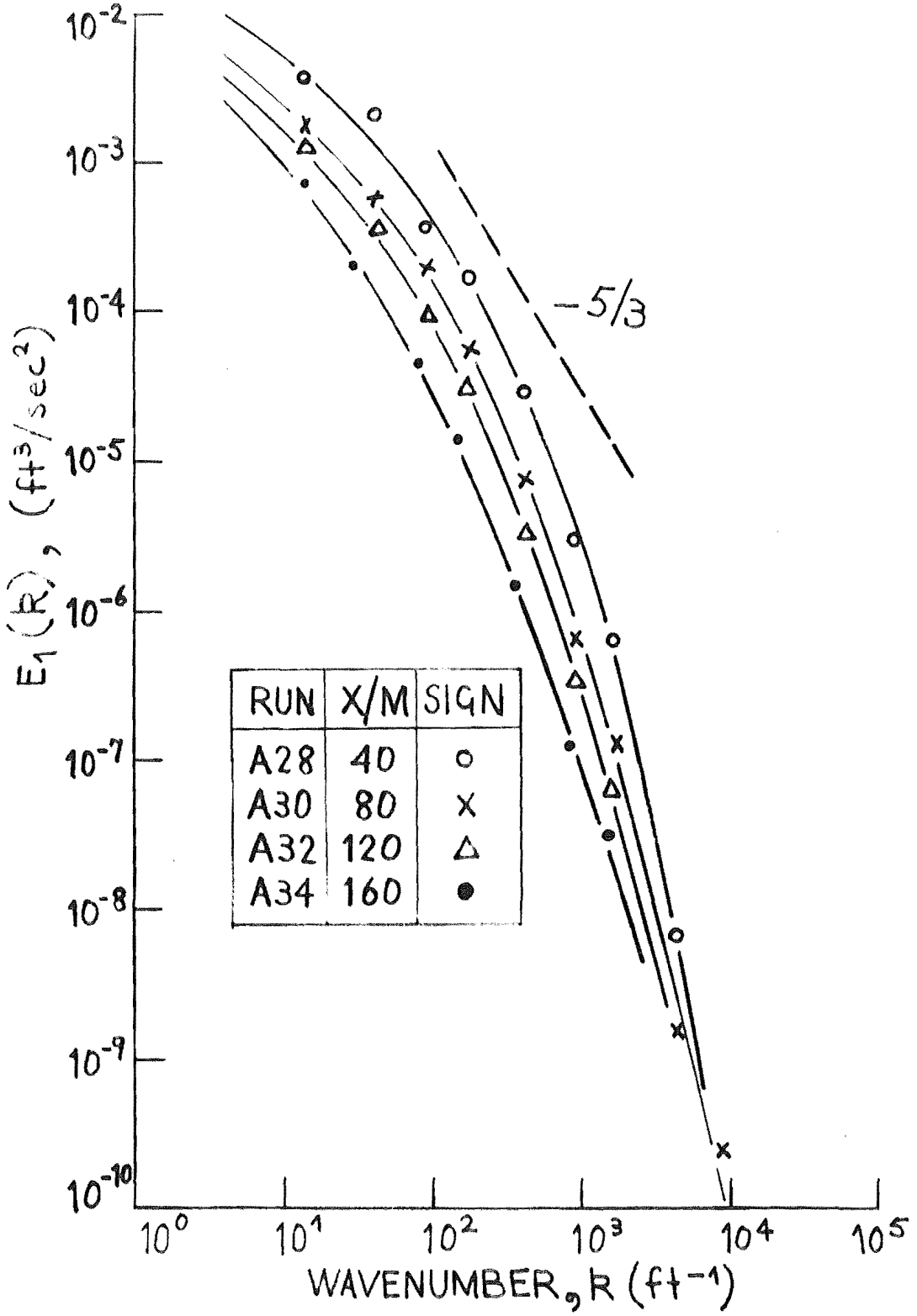

FIGURE 4.9 SPECTRUM FUNCTIONS DOWNSTREAM OF A GRID (Vel = 5·3 fps, $Re_M = 350$)

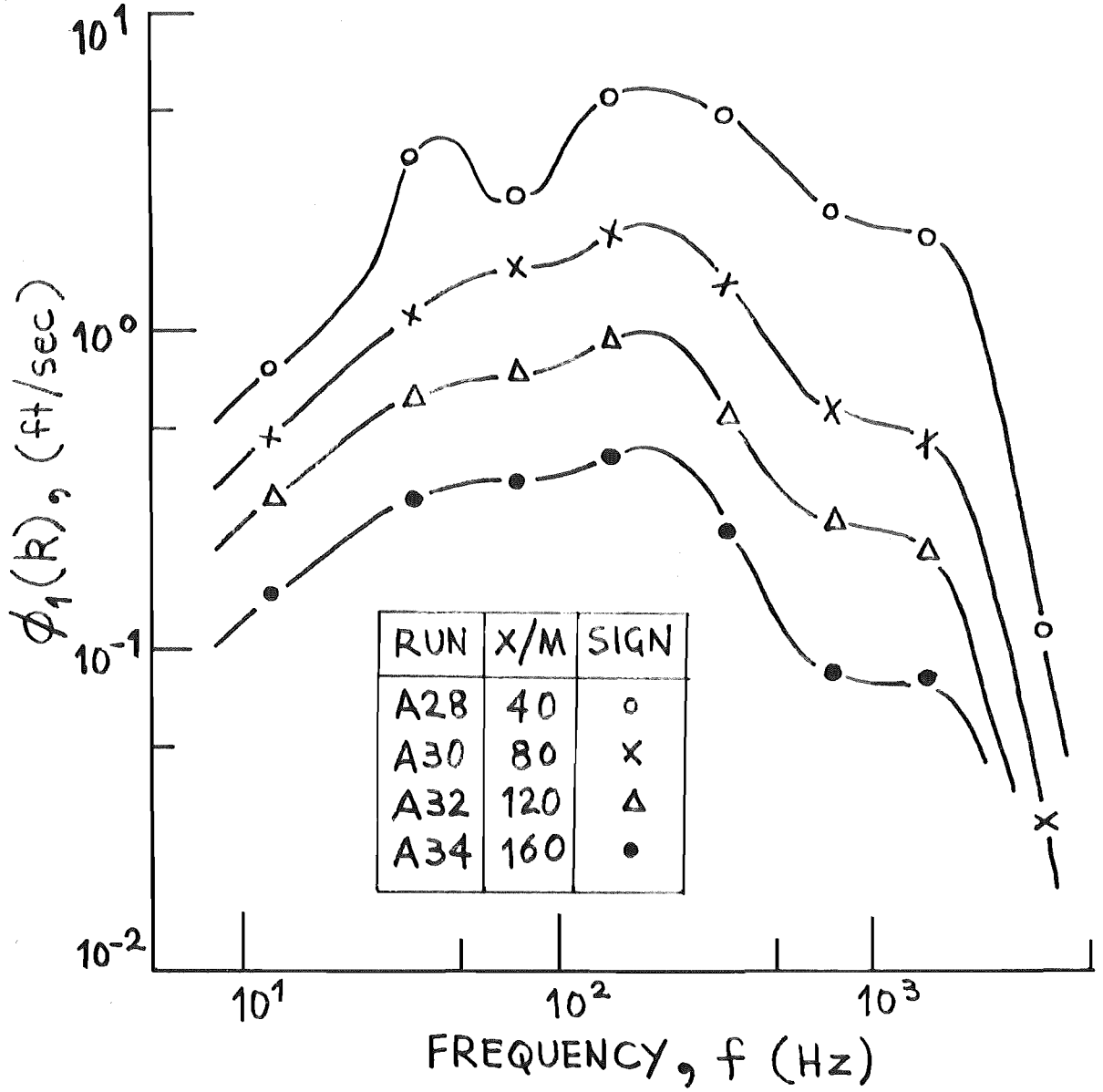

FIGURE 4.10 ENERGY DISSIPATION SPECTRA DOWNSTREAM OF A GRID (Vel = 5·3 fps, Re_M = 350)

the turbulence energy distribution function $E_1(k)$ through the mid-points of the histogram values, is not strictly correct as the frequency interval over which the measured spectrum result is taken to apply is rather large (9 intervals over a frequency range from 5Hz to10kHz).

As an approximate indication of the shapes of the energy spectra however, the smoothed curves have the advantage of allowing easy comparison with other experimental results as well as with energy spectra curves published in the literature. An example of an energy spectrum histogram and the smooth curve spectrum distribution assumed is shown in figure 4.7. Also drawn in the figure are dashed lines of slopes -1, -5/3 and -7 and reference to figure 3.6 shows that the present spectrum measurements cover that wavenumber range above k_e in the inertial and viscous dissipation ranges.

Energy frequency and wavenumber spectra functions measured at distances downstream from the turbulence generating grid are shown in figures 4.8 and 4.9. The line of slope -5/3 representing the Kolmogoroff (96) 5/3 spectra law region is also shown on each graph. With increasing distance downstream from the grid, the energy function decreases and slope increases slightly as more of the turbulence energy is expended by viscous dissipation further downstream.

Energy dissipation spectra $\phi_1(k)$ determined at various distances downstream from the grid are shown in figure 4.10. The spectra show a primary peak at 200 Hz and this is due to the eddies responsible for the dissipation and decreases with distance from the turbulence generating grid. The dissipation energy peak at $f \sim 50$ to 60 Hz for X/M = 40 is thought to be due to the turbulence generating frequency of the air blower.

That this peak exists (even with the large capacitance vessel in the discharge line from the blower) is further evidence that Re_m was too low for isotropic turbulence to be established within the measured range of X/M. The effect is however damped out by the viscous effects of the small eddies of turbulence acting on the large periodic fluctuations from the blower and has disappeared at X/M = 80. A measure of the smallest eddies can be found from the maximum of the dissipation spectra. The inverse of the wavenumber at which the maximum occurs may be taken as a measure of the dissipation eddy scale or the lateral microscale, λ_g. In figure 4.10 the maximum occurs at f$\backsim$200 Hz so that $\lambda_g \backsim 1.3$ mm and then $\lambda_f = 1.8$mm (assuming isotropy where $\lambda_f = \sqrt{2}\,\lambda_g$) which is in contrast to the measured values of the order of 0.9 to 0.4 mm.

From previously published results it was expected that the integral scale would be 2 to 5 times the microscale (133, 193). Such a relation holds between the scales of turbulence for Λ_f calculated using the Liepmann empirical relation and λ_f calculated for the maximum of the dissipation function (figure 4.10). The relation is not obtained using values of λ_f calculated from the technique described in section 3(g) (after Laufer (104) and Liepmann (110)). The microscale of turbulence calculated using this method was much smaller than that obtained using energy spectra results and it was felt that this was the result of the bias of the zero counting procedure by the periodic fluctuations of the air supply from the blower. That this periodic component was present is shown in the dissipation spectra in figure 4.10 for X/M = 40 and under these conditions the method of zero

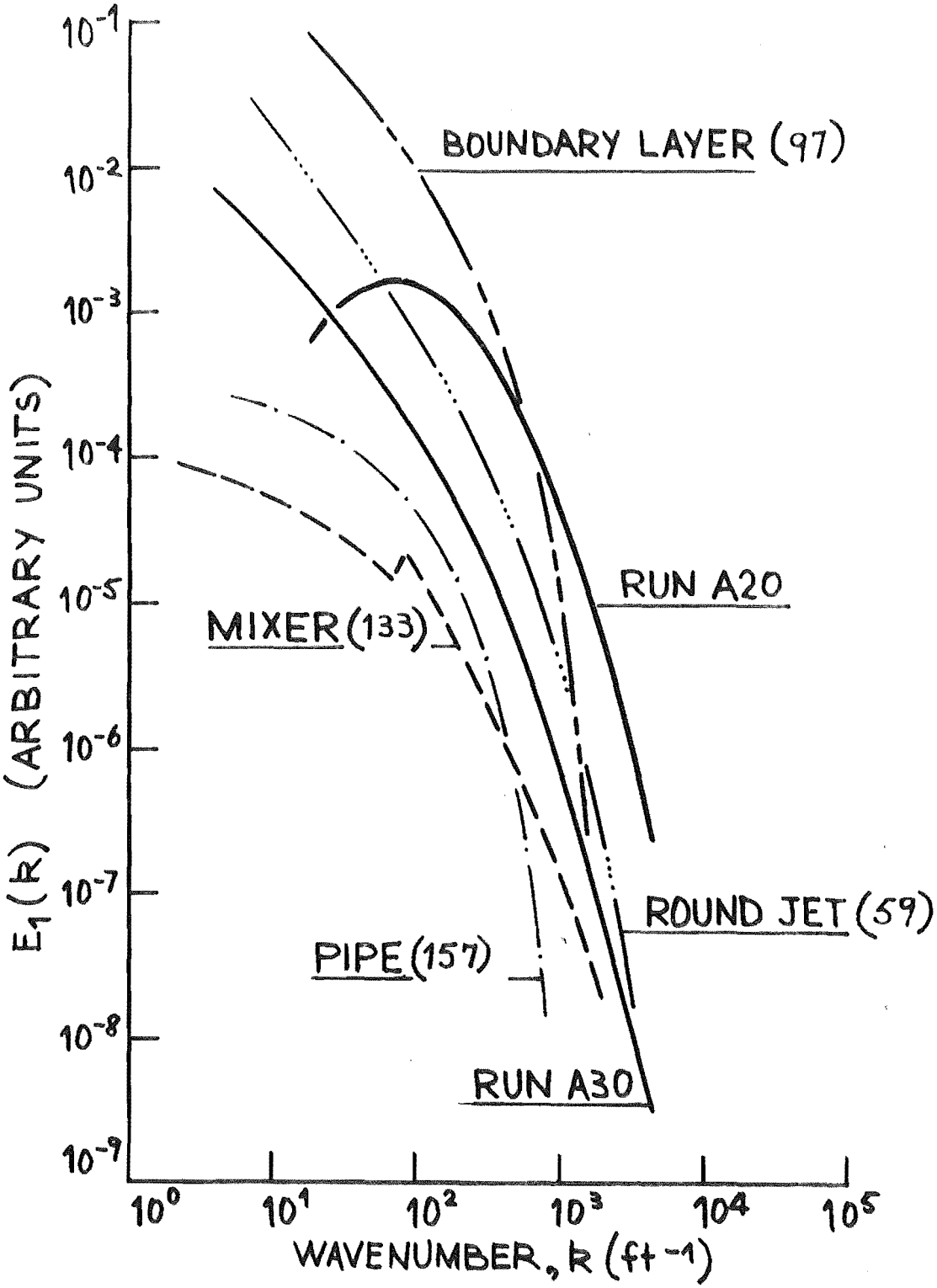

FIGURE 4.11 TURBULENT ENERGY SPECTRA MEASUREMENTS FOR VARIOUS SYSTEMS

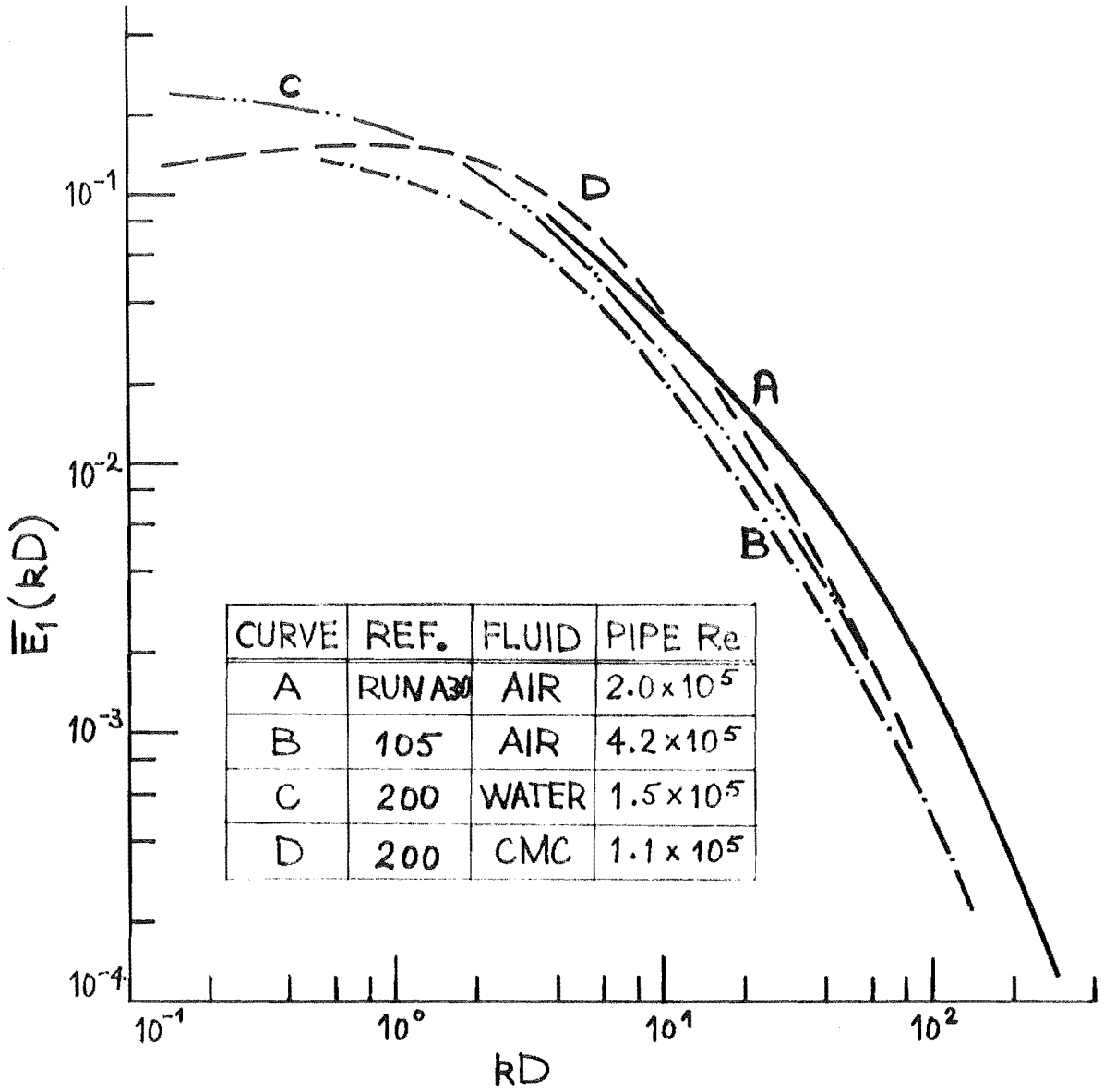

CURVE	REF.	FLUID	PIPE Re
A	RUN A30	AIR	2.0×10^5
B	105	AIR	4.2×10^5
C	200	WATER	1.5×10^5
D	200	CMC	1.1×10^5

FIGURE 4.12 DIMENSIONLESS WAVENUMBER SPECTRA FOR VARIOUS FLUIDS IN PIPE FLOW

counting proved to be unreliable.

A comparison of one-dimensional energy spectra for a number of different systems (all using air as the turbulent medium) is made in figure 4.11. The curves cover the same wavenumber range and are plotted with values of $E_1(k)$ in arbitrary units. The present study results (Runs A20 and A30) and the spectrum of turbulence in a round jet (59) have the energy units ft^3/sec^2. The boundary layer (97) and stirred tank mixer (133) spectra have arbitrary units and the latter curve exhibits a spectrum peak at the turbulence generating frequency of the moving impeller, characteristic of mixer spectra. The pipe flow data is that of Sandborn (157) for air flowing in a pipe for $Re = 5 \times 10^4$. All spectra have much the same shape in the -5/3 and -7 slope regions.

By dividing the spectrum component by the mean-square fluctuating velocity and the pipe diameter, and at the same time multiplying the wavenumber by the pipe diameter, dimensionless energy spectra can be obtained (200) which are then directly comparable with other published results. Figure 4.12 is a plot of dimensionless wavenumber spectra for various fluids in pipe flow. The data of Wells et al. (200) for water and CMC (sodium carboxymethylcellulose) flowing in a 0.76 inch dia. pipe at $Re \backsim 1.1 \times 10^5$ and the results of Laufer (105) for air in a 9 inch pipe at $Re \backsim 4 \times 10^5$ are compared with one spectrum from the present study for air in the 8 inch column at $Re \backsim 2 \times 10^5$. In general the spectra contain their significant energy at about the same range of dimensionless wavenumber kD, and the gross shape of the curves are the same.

To conclude this section of turbulence results, a

tentative summary will be made of the turbulence measuring techniques and their results. This summary will be more fully discussed later in section 4.6 and is only included at this stage to facilitate evaluation of the droplet evaporation results which follow.

The turbulence intensity ($\mathcal{T}$) measurements made using the customary technique for a constant-temperature hot-wire anemometer, follow the reported trend and are satisfactory. Turbulence energy ($E_1(k)$) and dissipation ($\phi_1(k)$) spectra obtained from the intensity measurements by the gating procedure are also like reported spectra and can be assumed reliable even considering the approximation of the histograms into smooth curves. Estimates of the integral scale of turbulence Λ_f, obtained by solving the Liepmann empirical equation using values of the energy spectra are also reasonable. The modified von Karman interpolation formula estimates of Λ_f only agree with the Liepmann estimates when values of the wavenumber of the energy containing eddies (k_e) are available (such as could be obtained from RUN A20 shown in figure 4.11). Calculated values of the microscale of turbulence λ_f by the zero-count method are unreliable because of the presence of large periodic fluctuations in the air supply to the column. However, an estimate of the order of size of λ_f can be obtained from the maximum exhibited by the dissipation spectra. It was unfortunate that low values of the grid Reynolds number (Re_m) were used in the grid turbulence study but such values were required for the droplet evaporation studies so measurements were continued in this low velocity range.

4.5(b) Supported Droplet Results

To evaluate the results of the evaporation rates of supported droplets, the influence of the supporting fibre on the evaporation process must be known. A measure of this effect was obtained for evaporating droplets supported on glass fibres of 4 different diameters, in the same turbulent air stream conditions. Glass fibres of 1.134, 0.897, 0.527 and 0.334 mm in diameter (see figure 4.1) were prepared as described in section 4.3. To approach the conditions of an evaporating free droplet, the fibres must be as fine as possible, but the restraint imposed is the condition of equilibrium between the maximum supported mass of the droplet and the surface tension forces:

$$2\pi D_{rod}\sigma' \mathrm{Cos}\theta = \pi D_{p_{max}}^{3}/6 \qquad (4.30)$$

where σ' is the surface tension of the liquid and θ is the angle of contact between the drop and the fibre. The bouyancy drag of the upward flowing air must also be considered, but equation 4.30 was found to hold approximately (estimated by equation 4.30, $D_{pmax} \sim 3.3$ mm, actual $D_p \sim 2.8$ mm). The equation shows that rod diameter imcreases much more rapidly than the drop diameter.

Using the analysis technique described earlier (section 4.4 and Appendix 7), Frössling numbers (Fs_h) for the evaporating drops were calculated and are plotted against the ratio of the diameters of the drop to supporting fibre, as curve A in figure 4.13. Although a trend was apparent for diameters less than 2, there is a large scatter among the asymptotic values for values of the diameter ratio larger than 2. The results were obtained for a variety of

shapes of water drops, as with fine fibres the drops were pendant-shaped and on wider fibres tended to truncated spheres. The scatter of the asymptotic values of Fs_h was attributed to the variation in drop shape and the correction of Hsu, Sato and Sage (78) was made by defining a modified Frössling number Fs_h^*, as

$$Fs_h^* = \frac{Nu/\infty - 2.0}{Re^{\frac{1}{2}} Pr^{\frac{1}{3}}} \qquad (4.31)$$

(cf. $Fs_h = Nu-2.0/Re^{\frac{1}{2}}Pr^{\frac{1}{3}}$). α is the correction obtained by Hsu et al. and depends on both the drop sphericity ($\mu = 6V/S\ D_p$) and the drop length to diameter ratio (ϕ).

$$\alpha = \left[1 + 1.147(1-\mu)\right]\left[1 - 0.037(1-\phi)\right] \qquad (4.32)$$

Curve B in figure 4.13 shows a much reduced scatter of results and the decreasing trend of Fs_h^* with increasing drop Reynolds number for diameter ratios less than 2 is more readily apparent. (α took values from 0.852 to 0.977). The heavy curve suggests that evaporation results for supported droplets should only be evaluated at drop to rod diameter ratios greater than 2 and if diameter ratios less than this value are to be used the drop Reynolds number should be greater than 200.

If values of Nu are taken from the results of figure 4.13 where the diameter ratio is greater than 2, when plotted against the product $Re^{\frac{1}{2}}Pr^{\frac{1}{3}}$ a straight line is obtained as shown in figure 4.14. This indicates that the results follow the usual definition of the Frössling number by being proportional to the square root of the drop Reynolds number. The dashed line in the figure represents

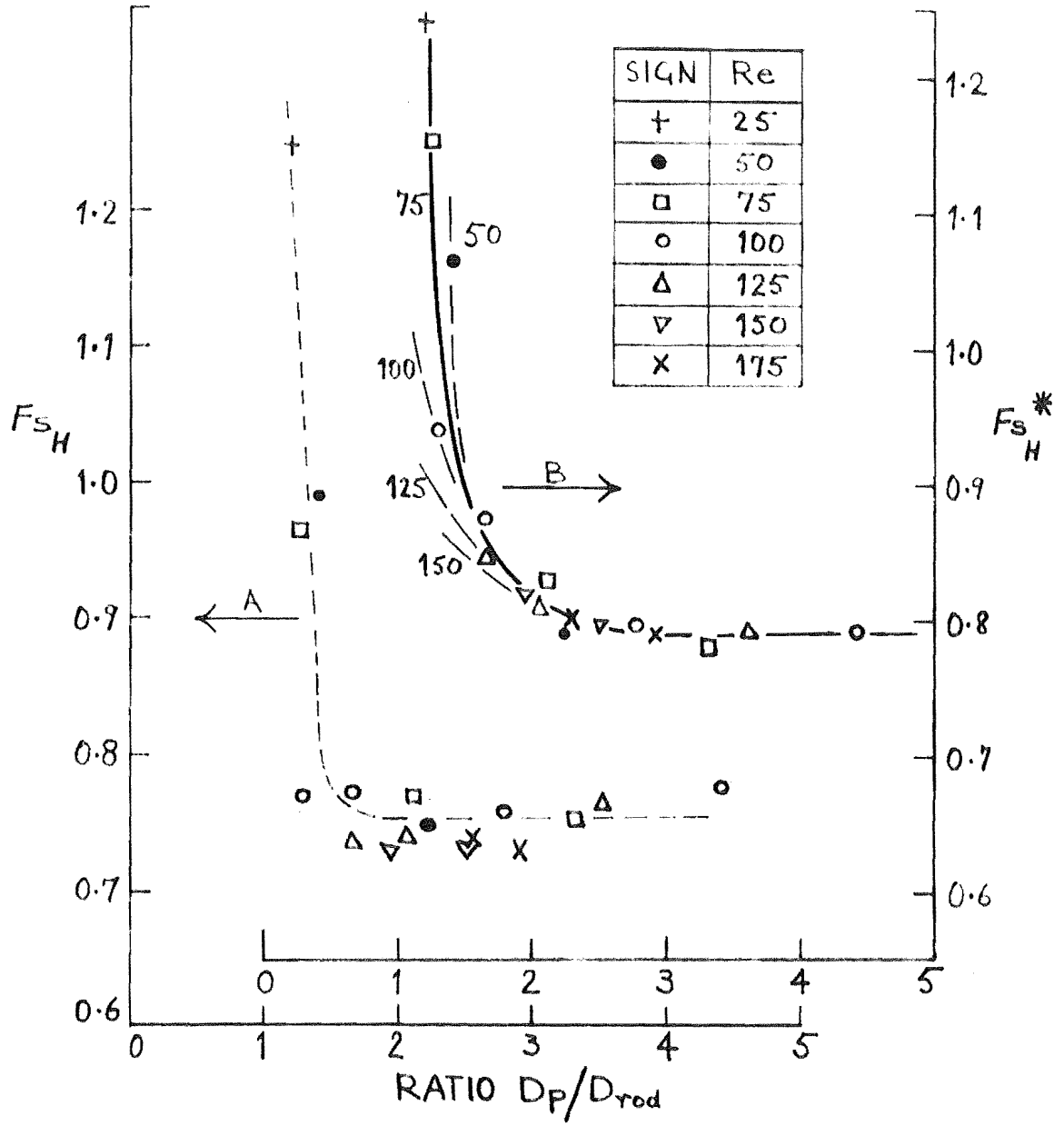

FIGURE 4.13 VARIATION OF FRÖSSLING NUMBERS WITH INCREASING DIAMETER RATIO. ($\tau \sim 12\%$; $X/M \sim 40$; Vel, λ_f, Δ_f and T_g CONSTANT)

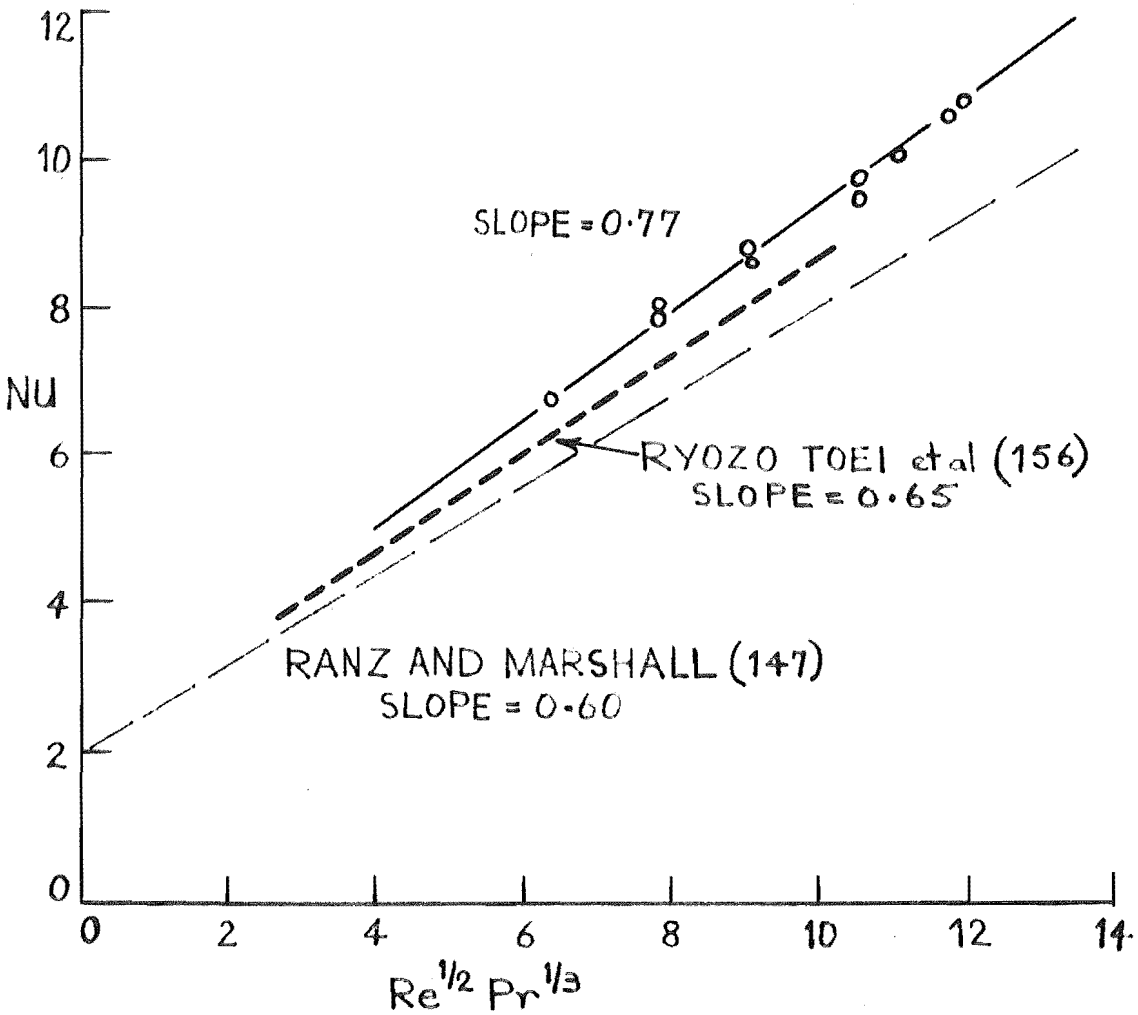

FIGURE 4.14 HEAT TRANSFER TO SUPPORTED DROPLETS
(C ≈ 12%; X/M ≈ 40; Vel, λ_f, Λ_f and T_g CONSTANT)

the smoothed data of Ranz and Marshall (147) ($Fs_h = 0.60$) and shows the present results to be greater by approximately 20%. The only variable over the Re range is the ratio of the scale of turbulence to drop diameter (Λ_f/D_p). The slope of the line (0.77) is close to the asymptotic value indicated for Fs_h^* in figure 4.13 and this agreement may be an indication of the independence of the Nusselt number on the ratio Λ_f/D_p, at least for the ranges of Reynolds numbers and scale to drop diameter ratios plotted in figure 4.14.

With due consideration to the limiting ratio of D_p/D_{rod} as indicated in figure 4.13, graphs were drawn of the experimental Frössling numbers obtained for different levels of turbulence intensity. The results are presented in 3 sections and are shown in figure 4.15 for: (A) supported droplets held close behind the turbulence generating grid ($40 < X/M < 160$); (B) evaporating droplets held in the column a large distance from the grid ($X/M \sim 850$); and (C) droplets held in the empty column and so evaporating under free or natural turbulence conditions. The results show no distinct trend and the value of the Frössling number may increase or decrease with increasing Reynolds number ($150 < Re < 250$) at any one value of turbulence intensity. This suggests that at least one other free stream parameter should be considered in analysing the results.

This parameter must be the integral scale of turbulence, since turbulent flow is described by this parameter, along with the relative intensity of turbulence and the free stream Reynolds number. For the experimental conditions A, B and C (described above), plots of Fs_h as a function of the ratio of the integral scale of turbulence to drop diameter ratio (Λ_f/D_p) with the relative intensity of turbulence as a

parameter (after van der Hegge Zijnen (194)), are presented in figures 4.16, 4.17 and 4.18. By drawing partial contour plots through the available experimental data, the results suggest an optimum for Fs_h at some value of the ratio Λ_f/D_p between 1 and 2. It could be suggested that instead of contour plotting for a maximum at some value of the ratio Λ_f/D_p, the trend of the results could be considered in the form shown in figure 4.19. Indeed, most of the 12 graphs could be finished in such a manner, but consideration of the plots for Reynolds numbers of 150 and 175 in figure 4.16 indcate that if Fs_h is to vary continuously over the range of Λ_f/D_p, then there must be a maximum at some value of the scale to drop diameter ratio. For values of $\tau \sim 8\%$ and 12%, the plots in figure 4.16 for Re=150 and Re=175 show that Fs_h can only be continuous with increasing Λ_f/D_p if a maximum for this ratio extists.

Contour plots for each Reynolds number suggested the existence of a maximum value of Fs_h for each value of τ. The grid turbulence results (for real X/M, figures 4.16 and 4.17) are practically the same, while the natural turbulence results show values of Fs_h which are slightly above those former values. This could be the result of anisotropic flow conditions that occur in pipe flow (139) and would be produced for the grid-free column results. The value of the maxima of Fs_h for different turbulence intensities can not be determined from the limited data obtained but the position of the optimum moves to smaller values of the ratio Λ_f/D_p as the Reynolds number increases.

4.6 Discussion

The experimental results for the turbulence

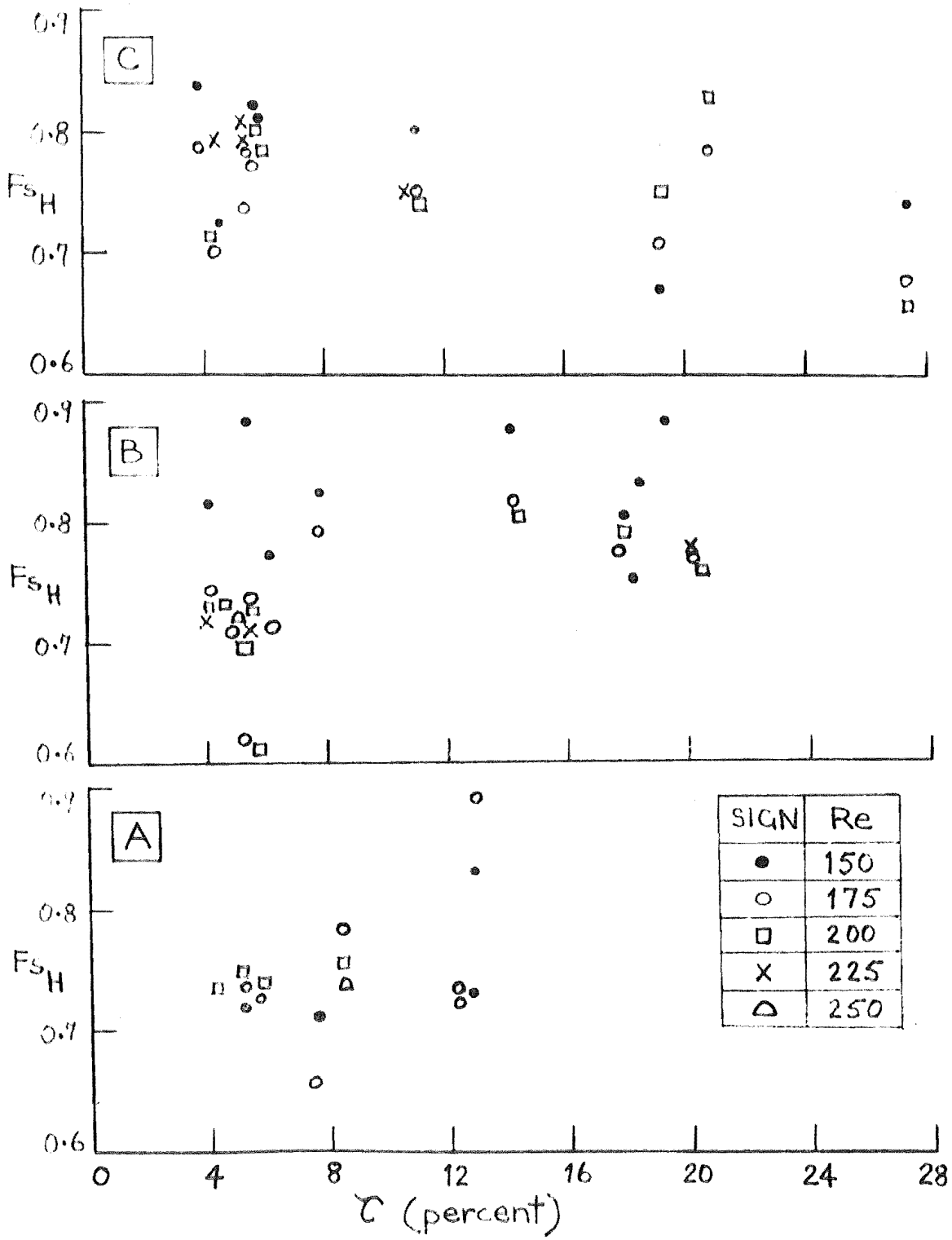

FIGURE 4.15 DEPENDENCE OF THE AVERAGE FRÖSSLING NUMBER ON THE INTENSITY OF TURBULENCE

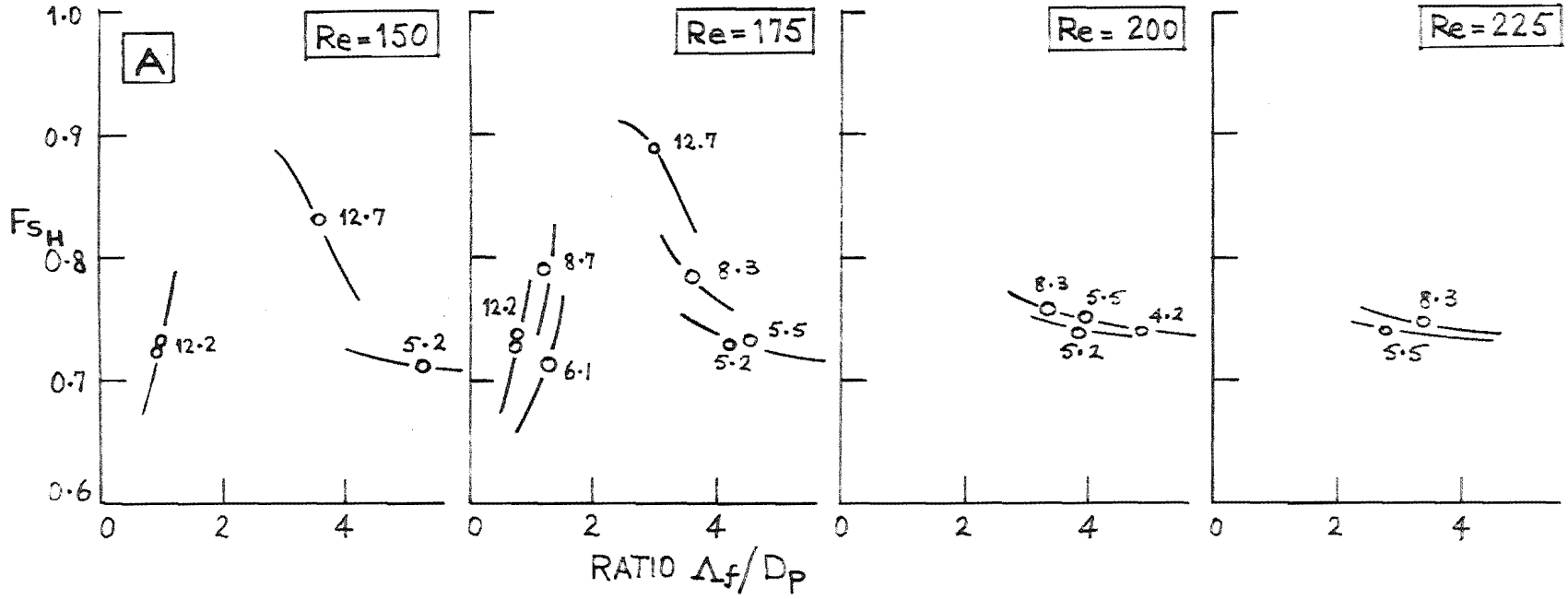

FIGURE 4.16 EFFECT OF INTENSITY AND SCALE OF FREE-STREAM TURBULENCE ON THE AVERAGE FRÖSSLING NUMBER FOR VARIOUS REYNOLDS NUMBERS (PLOTTED VARIABLE = PERCENT TURBULENCE)

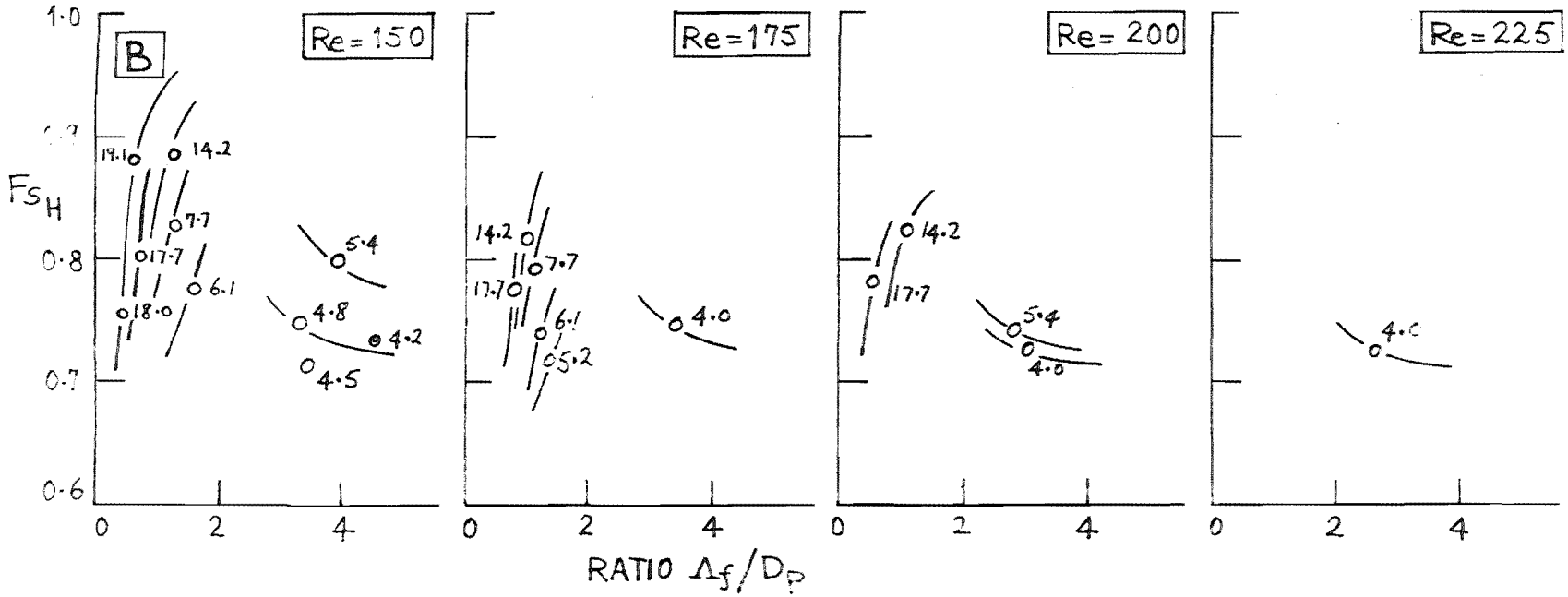

FIGURE 4.17 EFFECT OF INTENSITY AND SCALE OF FREE-STREAM TURBULENCE ON THE AVERAGE FRÖSSLING NUMBER FOR VARIOUS REYNOLDS NUMBERS
(PLOTTED VARIABLE = PERCENT TURBULENCE)

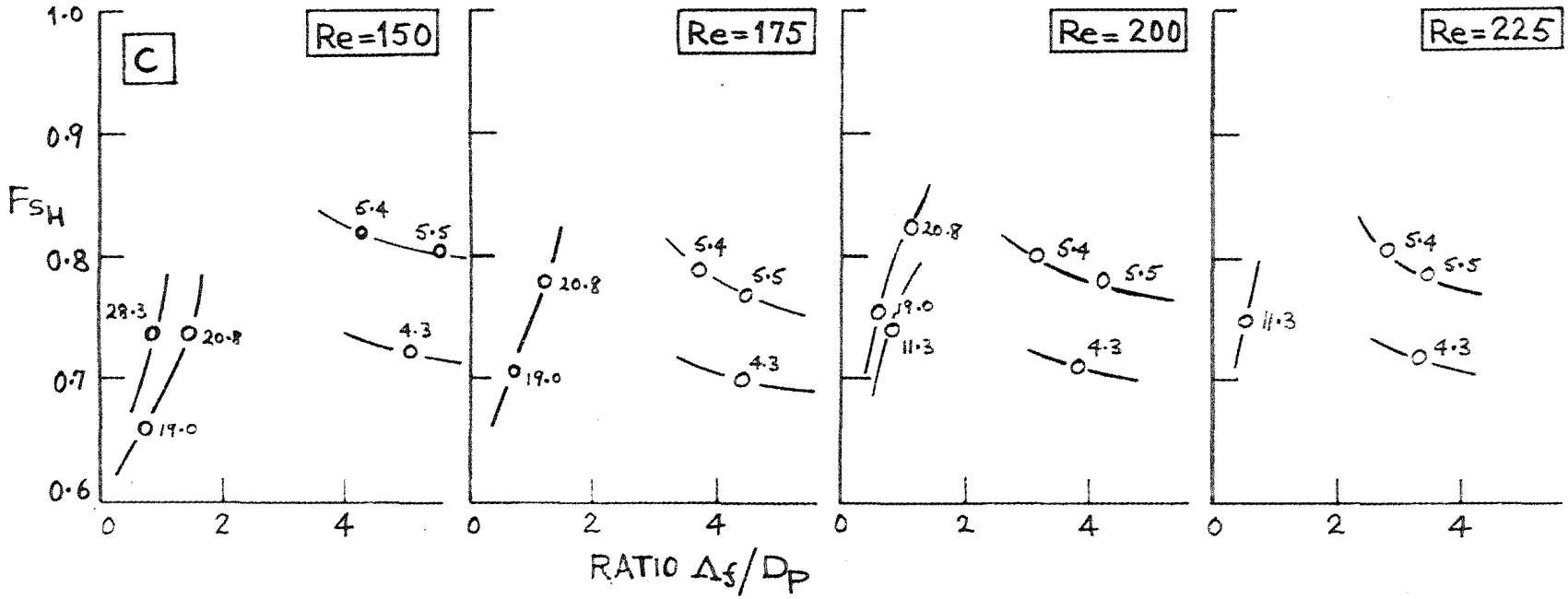

FIGURE 4.18 EFFECT OF INTENSITY AND SCALE OF FREE-STREAM TURBULENCE ON THE AVERAGE FRÖSSLING NUMBER FOR VARIOUS REYNOLDS NUMBERS
(PLOTTED VARIABLE = PERCENT TURBULENCE)

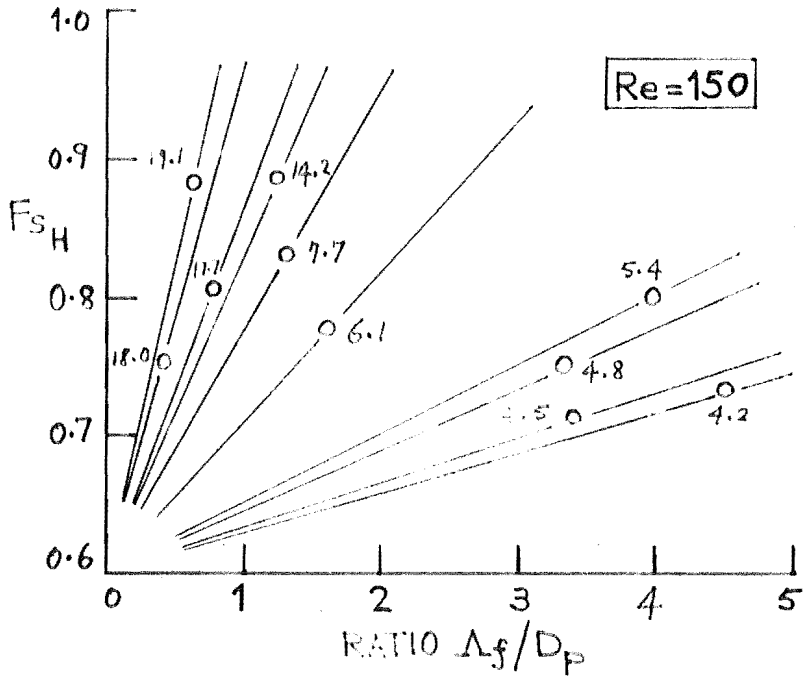

FIGURE 4.19 AN APPROXIMATION TO THE EFFECT OF THE FREE-STREAM TURBULENCE ON Fs_H (PLOTTED VARIABLE = PERCENT TURBULENCE)

parameters obtained using a single hot-wire probe, indicate that the technique is satisfactory for obtaining reasonable estimates of the turbulence intensity, integral scale and energy spectrum. Reliable measurements of the micro-scale of turbulence can be obtained provided certain flow conditions are present.

The relative intensity of turbulence measurements are in good agreement with reported works (4,7,102,193). The results follow postulated relationships by Frenkiel (47), in that behind the grid the intensity decay is proportioal to $(X/M)^{-5/7}$. The intensity is seen to decrease with increasing air velocity (and Re_m). This behaviour is in agreement with van der Hegge Zijnen (193) and Baines and Peterson (4) but contrary to the results of others who report an increase with velocity (7,66) while still others (35) report no velocity or Re_m effect. For accurate turbulence intensity measurements, the ratio of the integral scale to the length of the hot-wire must be large. For the present study the ratio varied from more than 10 down to occaisional values approaching unity. For the very few instances where the ratio was not large, the correction for the wire length was made assuming local isotropy.

The turbulenc parameters of a turbulent fluid downstream from a turbulence generating grid, depend on the grid dimensions and solidarity and no data could be found for grids similar to that used in the present study. The magnitude of the turbulence intensity as measured depends also on the free or natural turbulence of the system. A correction for the free-stream natural turbulence based on the difference between the squares of the measured and free-stream natural intensities (66) would be suitable if

both turbulent motions retained their individual character in the downstream direction. This is not the case however as Dryden (36) shows the free-stream natural turbulence to increase the measured value. Consequently, all measured intensities of turbulence involve the free-stream natural turbulence which would be more perceptible when the turbulence decays to low values.

The microscale of turbulence λ_f measured by the zero count method does not follow the usual reported trend (9, 177,193) described by equation 4.29, where λ_f increases as the square root of the distance downstream from the grid. The converse result determined experimentally is thought to be the result of the combined effect of the two flow conditions that arose during the experiment. First, isotropic turbulence is reported not to exist for values of X/M close to the grid when Re_m takes values as used in the experiment (9). A decrease in λ_f with distance from the grid is then found (9) and isotropic turbulence has not yet been fully developed but exists some further distance downstream ($X/M > 200$). Secondly, the zero counting method is strongly biased by periodic fluctuations of the airstream, such as those due to the rotary blower supplying air to the column. This periodic influence has been reported by Mujumder et al. (133) where large periodic fluctuations were produced by the passage of the turbine blades in a stirred-tank mixer. The zero count method applies for a turbulent field that has a mean velocity U which is high compared with the turbulence fluctuations u_1' , where u_1' and du_1'/dx_1 both have Gaussian probability-density distributions and where $\overline{u_1'(du_1'/dx_1)}=0$. It is expected that for isotropic turbulence ($u_1' \ll U$) the zero count method would be reliable, although even here

differences between the values of λ_f measured by the zero counting procedure and other methods are reported to exist (108).

The two possible flow effects of non-isotropic flow and periodic bias, invalidate the use of the zero count method for measuring λ_f. However, an estimate of the order of size of λ_f can be obtained from the maxima exhibited by the dissipation spectra (figure 4.10). The spectra show a primary peak at about 200 Hz and this is due to the eddies responsible for the dissipation of the turbulent energy. The inverse of the wavenumbers at which the maxima occur may be taken as a measure of the dissipation eddy scale or conventionally, the lateral microscale λ_g and assuming isotropy, $\lambda_f = \sqrt{2}\lambda_g$. The dissipation spectra show the presence of the periodic effect due to the turbulence generating frequency of the airblower and although damped out as X/M increases, the effect is to bias the dissipation maximum towards lower frequencies. The values of λ_f suggested from figure 4.10 are approximately constant (whereas the zero count values were not) and as Λ_f increases downstream, then the ratio λ_f/Λ_f decreases and $Re_{\lambda f}$ (~ 45) remains constant with increasing distance behind the grid. The trend of these values of λ_f/Λ_f and $Re_{\lambda f}$ indicate that turbulence decay is in the initial range and this contrasts with the results of figure 4.6 (based on zero count method values of λ_f), showing no agreement with the conditions for either the initial or final decay ranges. This further confirms the bias of the zero count method and for the present experimental conditions the dissipation spectra maxima estimates of λ_f are considered more reliable.

The turbulence energy spectra obtained by the gating procedure using a single hot-wire probe are shown to agree well with reported spectra from a variety of systems. The approximation of the experimental histograms to a continuous distribution curve allows easier manipulation of the function $E_1(k)$ and provides a more comprehensible visual picture. The use of frequency spectra or wave analysers would eliminate any uncertainty that exists with the present gating technique. The technique was applied over rather wide frequency intervals and the more subtle changes of the energy spectra would only be found by a continuous analysis such as with a wave analyser. Length corrections were not made to the spectra even though the possibility of anisotropy exists, since they were obtained in pipe flow (139). This further complicates the use of a length correction usually derived for local isotropic conditions. Approximate length corrections (10, 192) show the corrections to apply only at the highest frequencies and these raise the spectra only a small amount.

The energy frequency and wavenumber spectra functions cover the range of slopes -1, -5/3 and -7, the second of these being the inertial subrange resulting from Kolmogoroff's similarity hypothesis (96) which is the same as Heisenberg's transfer theory (72). The latter theory applies only to very high values of wavenumber slope of -7. Only for large values of turbulence ($\tau \backsim 20\%$) was the maximum of the energy spectra obtained (Run A20, figure 4.11). In these cases the value of wavenumber at which the maximum occurred k_e, could be ascertained and the slope of +1 for wavenumbers less than k_e was approximated. The change of the energy spectra with distance behind the grid (figure 4.9) follows that variation

reported by Stewart and Townsend (177) for the shape of spectra at different stages of decay.

For the present study results ($Re_{\lambda_f} \backsim 45$), the Kolmogoroff 5/3 spectra law approximates the measured one-dimensional spectra only in a very narrow wavenumber range. Sato (159) concluded that for $Re_{\lambda_g} \backsim 60$, the -5/3 range hardly existed and this result has also been reported by other workers (109, 133). Streamwise and cross-stream spectra functions that were well fitted by the -5/3 power law have been reported (59, 60) for Re_λ from 500 to 800, but more generally, large grid Reynolds numbers ($Re_m \backsim 10^5$) are required before a better agreement with the Kolmogoroff spectra law is obtained in the higher part of the measured wavenumber range. Stewart and Townsend (177) have shown that for the -5/3 inertial subrange to exist, Re_m should be at least of the order of 10^6 and $Re_\lambda > 1{,}500$.

The dimensionless wavenumber spectra (200) compared with the other published pipe flow results, show very good agreement for a variety of materials. This good agreement is significant since the pipe diameters differ by a factor of 12. The spectra all contain their significant energy at about the same range of dimensionless wavenumber, kD. Since these spectral measurements were made for wavenumbers ranging up to the energy containing maxima at k_e, the successful use of the diameter to reduce the data for different pipe sizes suggests that the energy containing eddies occur over a unique range of kD. Wells et al. (200) show that for turbulent boundary layers most of the energy ($\backsim 90\%$) is contained below frequencies given by

$$f = 2\, u_{local} / \delta \qquad (4.33)$$

where δ is the boundary-layer thickness. If this is extended to pipe flow, substitutingthe pipe radius as the boundary-layer thickness and assuming that the eddies propagate with the local mean velocity, then most of the energy would be in the wavenumber range below kD = 8, which provides justifiaction for normalising k with the pipe diameter. The validity of the normalisation is seen in the spectra comparison made in figure 4.12. Remembering that for isotropic turbulence, Batchelor (8) reports the energy spectrum peak to occur at values of k given by

$$k_e \backsim 1/M \qquad (4.34)$$

then it appears that most of the turbulence energy is contained in wavenumbers of the order of 1) the mesh size for grid produced turbulence, 2) the boundary-layer thickness for boundary-layer flow, and 3) the pipe radius for pipe flow. This is a gross effect and does not necessarily imply anything about the detailed shape of the spectrum.

The integral scale of turbulence Λ_f was calculated using the energy spectra data. Three estimates of Λ_f were obtained by considering expressions derived to approximate three separate regions of the energy spectrum. First, for isotropic flow conditions, $\Lambda_f \backsim 0.75/k_e$ (73). For those turbulence results of high relative intensity, the <u>maximum</u> of the energy spectrum was observed and the wavenumber of the energy containing eddies k_e could be obtained. In practice, values of Λ_f using this relationship were calculated for each wavenumber used in

the energy spectra plot and the estimate at k_e (if it occurred) was in reasonable agreement with the other values of Λ_f calculated by the second and third methods. The second method was to solve the Liepmann empirical correlation (109) which describes the energy spectra in the -5/3 region, by using experimental values of $E_1(k)$. This quadratic has two solutions but only one gives sensible solutions for Λ_f. The third method for solving for Λ_f was using the modified von Karman interpolation formula (198) derived for the -7 region, again by substituting values of $E_1(k)$. This formula depends on a value of k_e and the isotropic approximation between Λ_f and k_e was made. The Liepmann correlation uses the approximation of the correlation coefficient curve by the exponential function $\exp(-x_1/\ _f)$ and like the von Karman formula, applies only to large Reynolds numbers where the inertial subrange ($k^{-5/3}$ law) exists and viscosity effects are negligible (no k^{-7} region). The first and third methods are soluble only if k_e can be found, when the first will provide only a single estimate of Λ_f at the one value k_e, while the third method will provide a series of estimates of Λ_f for each wavenumber of the energy spectra providing the von Karman formula applies.

Experimentally, it was shown that the -5/3 law existed only for a very restricted wavenumber range and consequently the solutions obtained by the second and third methods were sensible only at one or two values of $E_1(k)$ which approached the -5/3 or -7 slopes. These sensible values of Λ_f did occur where the energy spectra best approximated the -5/3 slope. For the complete wavenumber range of any one spectrum, the sensible Λ_f occurred as a

minimum value among the other solutions, indicating the same deviation from the -5/3 law on either side of the wavenumber range for which the law held. This is shown in figures 4.7, 4.8 and 4.9 where the experimental curves are less than the -5/3 law for the wavenumbers above and below the Kolmogoroff range. (See also the calculated results in Appendix 7).

The calculated values of the integral scale agree reasonably with other reported values (4,193), although tending to somewhat higher values than reported for grids of less solidarity. However, Raithby and Eckert (146) showed Λ_f to increase with increasing grid solidarity and the present estimates appear reasonable in order of size and by increasing with distance downstream from the grid. The size of Λ_f was of the same order of the grid mesh for measurements behind the grid and took larger values for turbulence in the grid-free column. This is in agreement with the conclusion obtained from the results of the dimensionless wavenumber spectra, where it was shown that most of the energy would be in the wavenumber range below $k=8\pi/D_{pipe}$ (as shown by RunA20, figure 4.11). Martin and Johnson(122) integrated their autocorrelationcurves to obtain integral scales for water flowing in the centre of a 6 inch pipe, as

$$\Lambda_f = 0.846\times10^{-2} D_{pipe} (Re \times 10^{-3})^{0.51} \qquad (4.35)$$

The value of Λ_f obtained from this equation (in feet) are larger than the experimental values and Patterson and Zakin (139) report that the product $(U^{0.5} D_{pipe}^{1.5})$ did not correlate their data. These workers suggest that the diameter effect is too large and the velocity term may be

too small.

The computer fitted curves for the decrease with time of evaporation of the drop area, volume, length and maximum diameter follow closely the experimental values obtained from the photographs of the evaporating droplets (see figure 4.3). Because of this good agreement (sum of the squares of the deviations of the experimental data from the computer fitted curve was very small), the evaporation rate obtained as the tangent to the volume curve by the first-order differentiation of the computer equation, is considered to be reliably estimated.

The study of the variation of the Frössling number with increasing diameter ratio D_p/D_{rod} (figure 4.13) resulted in the important conclusion of the significance of this ratio for the evaporation of supported droplets. The conclusion was that evaporation results for supported droplets should only be evaluated for drop to rod diameters greater than 2 and if diameter ratios less than this value are used then the drop Reynolds number should be greater than 200. Consideration of the sphericity of drop was also shown to be important when comparing the results for drops of different shapes and sizes supported from fibres of different diameters. The drop shape influence on the evaporation rate was well corrected for by the Hsu, Sato and Sage (78) correction and the results for Fs_h^* in figure 4.13 show the decreasing effect of the drop to rod diameter ratio as the drop Reynolds number increases. Most previous workers (Frössling, 48, Ranz and Marshall, 147, Ryozo Toei et al. 156) have experimented for values of the ratio of the order of 10. The results of Hsu, Sato and Sage (78) for Re range 30 to 700, were obtained with

diameter ratios from 10 down to unity and the results for these low ratios at low Reynolds numbers are to be questioned. Even for relatively large Reynolds numbers 10^3 to 10^5, the sphere to support stem diameter ratio effect has been reported (146) and this effect should be considered not only for supported droplets but also for fixed spheres in high velocity flows.

Experimental values of the drop Nusselt number when plotted against the product $Re^{\frac{1}{2}}Pr^{\frac{1}{3}}$ for the same intensity of turbulence, showed a linear relation with slope of 0.77. The experimental line in figure 4.14 tends to the same limiting value of Nu = 2.0 (Re$\rightarrow$0) in agreement with most other works. The slope of the line (Fs_h = 0.77) was for a relative intensity of 12% and is higher than the values reported by Frössling (Fs_h = 0.55), Ranz and Marshall (Fs_h = 0.60) and Ryozo Toei et al. (Fs_h = 0.65). However, these latter results were obtained under conditions of low turbulence ($\mathcal{T} \backsim 1$ to 2%) and this may account for the variation. The result is of course dependent on the estimation of the amount of heat flowing to the drop via the supporting fibre (Q_{rod}). This heat rate depends on the estimation of h_{rod} and as mentioned in Appendix 6, the only other estimate of h_{rod} is reported by Ryozo et al. (156). Such a value would only decrease the present value of Fs_h by only a few percent since Q_{rod} itself was usually only of the order of 10% of the total heat transferred by the evaporating vapour.

The dependence of the Frössling number on the longitudinal level of turbulence shows no distinct trend in contrast to the results of Raithby and Eckert (146) and the conclusions of the extensive review of turbulence effects

by Galloway and Sage (54). These workers reported an increasing trend of Fs_h with increasing turbulence intensity and Reynolds number. However, Raithby and Eckert did report a reduction in the scatter of their results when the integral scale of turbulence was considered as a correlating parameter. The use of the ratio of the integral scale of turbulence to the drop diameter Λ_f/D_p, did indeed bring order to the experimental results as was shown in figures 4.16, 4.17, and 4.18. These graphs suggest that for a given Reynolds number there is a value of the ratio Λ_f/D_p where the effect of the level of turbulence on the Frössling number is a maximum and that the optimum value of Λ_f/D_p decreases with increasing Re.

Of the investigators of the analogy between turbulent fluid friction and heat transfer by turbulence, Taylor (184) was the first to show that the drag of a body of revolution is affected by both the intensity and scale of turbulence. Theoretically he showed the critical Reynolds number for spheres to depend on the relative intensity of turbulence and the ratio Λ_f/D_p. Experimental confirmation of this theory was provided by Dryden et al. (35) and the conclusion follows that the transfer of heat and mass from curved surfaces to turbulent flow will be affected also by the combined action of intensity and scale of turbulence. The only report showing this combined effect is the comprehensive study of heat-transfer from a cylinder by van der Hegge Zijnen (194) who obtained the empirical correlation

$$Nu = Nu_o(1 + \varphi(\tau Re)\psi(\Lambda_f/D_p)) \qquad (4.36)$$

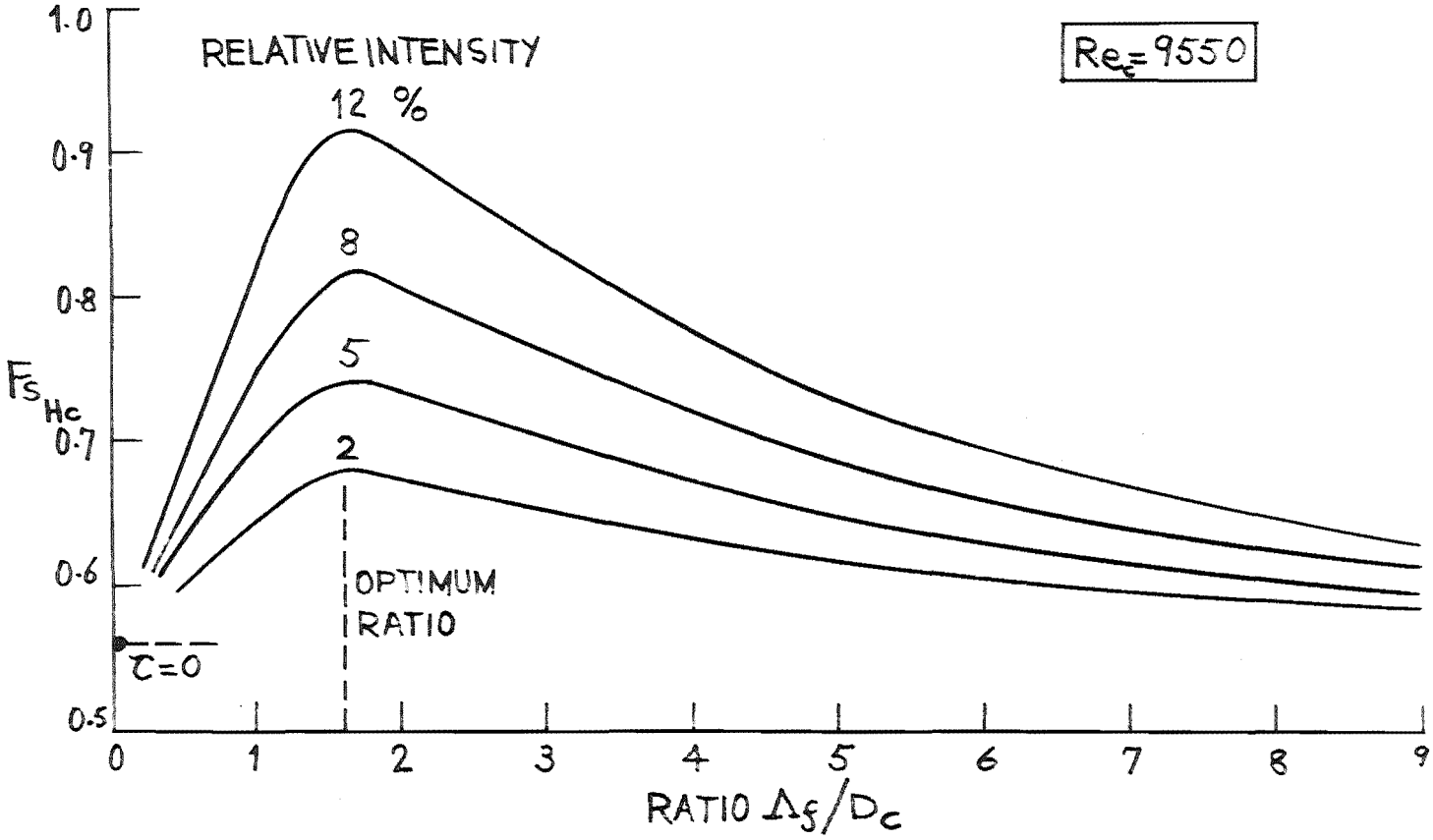

FIGURE 4.20 EFFECT OF INTENSITY AND SCALE OF FREE-STREAM TURBULENCE ON HEAT TRANSFER FROM A CYLINDER (REDRAWN FROM FIGURE 6·1 OF APPENDIX 1)

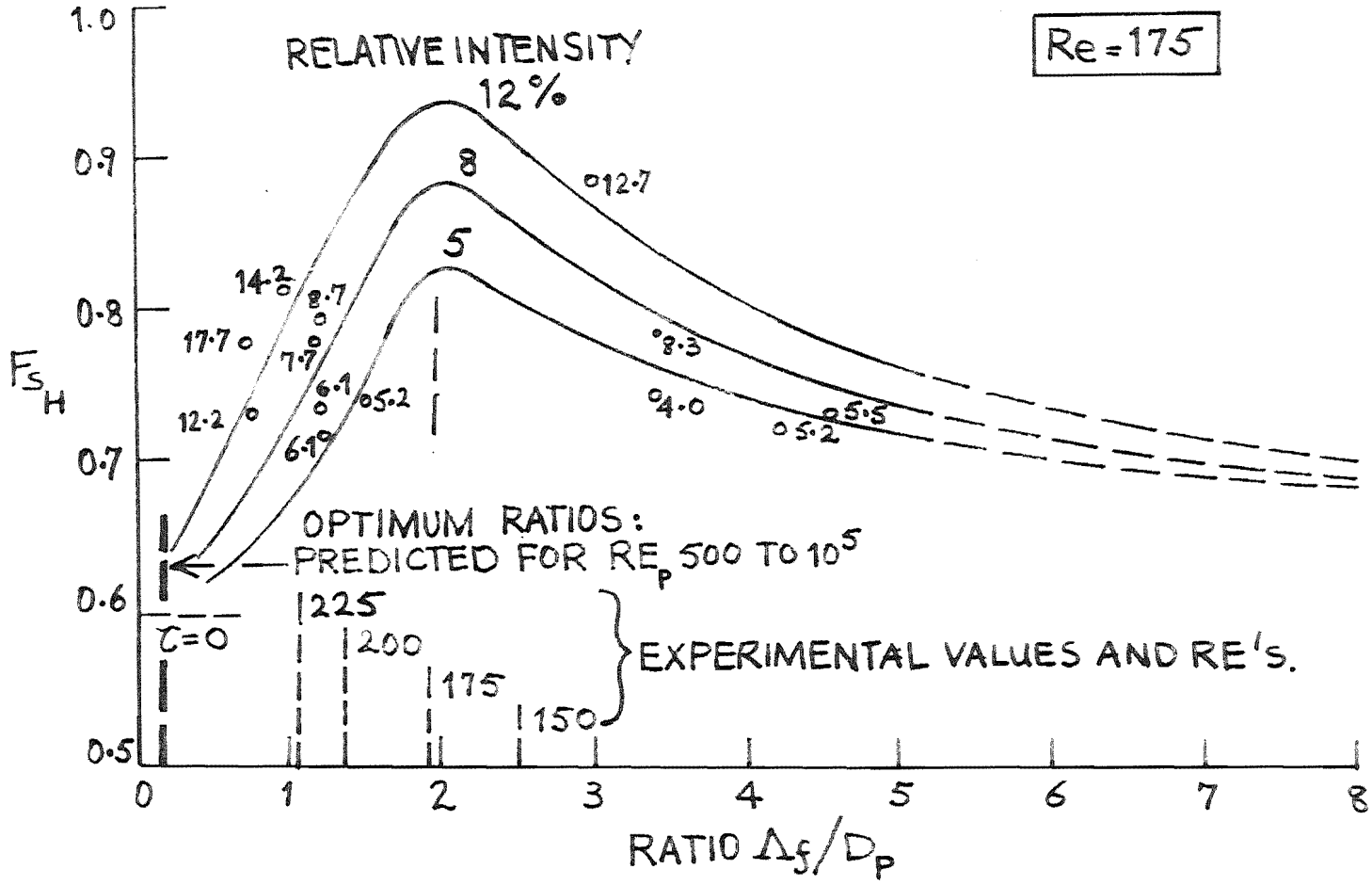

FIGURE 4.21 EFFECT OF τ AND Λ_f ON AVERAGE F_{S_H} AND THE SHIFT OF OPTIMUM Λ_f/D_p WITH INCREASING REYNOLDS NO. OF THE HELD EVAPORATING WATER DROPLET.

(Nu_o is the Nusselt number for zero turbulence intensity conditions). For a given Reynolds number, Nu is expected to be a function of both $\mathcal{T}$ and Λ_f/D_p and this relationship is shown for van der Hegge Zijnen's results in figure 6.1 of Appendix 1. Using McAdams' (124) recommended correlation for heat-transfer from cylinders in turbulence-free cross-flow conditions

$$Nu = 0.35 + 0.56Re^{0.52}Pr^{\frac{1}{3}} \qquad (4.37)$$

the results of van der Hegge Zijnen were recalculated in terms of the average Frössling number notation used in the present study and are presented in figure 4.20. The occurrence of the maximum Fs_h at an optimum value of the ratio Λ_f/D_p points toward some resonance between a mean frequency of the turbulent flow and the shedding frequency of the vortex eddies in wake of the cylinder. The experimental results of the present study for spherical drops are summarised in figure 4.21 for Re = 175 and also show the same optimum profile which is independent of the level of turbulence.

For a cylinder, Hinze (73) showed analytically that there would be resonance between the energy-containing eddies and the shedding frequency of the cylinder, when Λ_f/D_p is 1.2. The Strouhal number ($Sl = f_sD/U$) for cylinders is about 0.19 for $500 < Re_c < 10^5$ (108). Assuming resonance with the energy-containing eddies of the turbulent flow, the shedding frequency f_s should be twice the frequency f_e of the vortex eddies: that is,

$$f_s = Sl.\frac{U}{D_c} = 0.19\frac{U}{D_c} = 2x\frac{k_e U}{2\pi} \qquad (4.38)$$

where k_e is the wavenumber of these eddies ($k_e = 2\pi f_e/U$). For isotropic turbulence, $\Lambda_f \sim 0.75/k_e$ (73), whence one obtains $\Lambda_f/D_c \sim 1.25$ which is of the same order of magnitude as the value 1.6 obtained experimentally by van der Hegge Zijnen.

For a sphere, the shedding frequency is approximately 10 times that for a cylinder (130) and using Hinze's method one obtains a value of Λ_f/D_p equal to 0.125 as the condition for resonance. This optimum value is rather less than those values obtained experimentally and indicated in figure 4.21. The reason for this difference is that the frequency of vortex shedding as computed from the Strouhal number, is a function of the Reynolds number and for cylinders is constant only for the range $500 < Re < 10^5$ (108). For Reynolds numbers less than 500, the Strouhal number decreases with decreasing Re until $Re \sim 40$ when vortices are difficult to detect. The periodicity of the vortex street of a cylinder is most marked over the range $40 < Re < 1000$ where the Strouhal number can be described (12) by

$$Sl = 0.19\ (1-20/Re) \qquad (4.39)$$

For Reynolds numbers the same as those obtained in the present study, the optimum ratio Λ_f/D_c for a cylinder is seen to increase with decreasing Re according to the resonance frequency given by equation 4.22 along with the variation of the optimum ratio for held, evaporating droplets obtained in the experiment. The shift is away from the limiting value which holds for Reynolds numbers between 500 and 10^5. The more significant shift of the

evaporating droplet results is a reflection of the difference between two and three dimensional flow patterns as occur for cylinders and spheres. For spheres in three dimensional flow, one cannot have the simple alternate shedding of vortices, but rather there is formed a vortex loop which is inclined to the direction of motion. The deviation of the optimum ratio Λ_f/D_p from the limiting value as shown in figure 4.22, is then due to the difference between a sphere and a cylinder having distinctly different behaviour patterns of vortices in 2 or 3 dimensions.

It must be pointed out that the available data for values of the Strouhal number for spheres is very limited and is based on results that were not very consistent. As used in the above derivation, Möller (130) reports a value for the Strouhal number of 1.9 (10 times that for a cylinder) but Winny (201) suggests that the shedding frequency of a sphere is 1.5 times that for a cylinder (Sl = 0.25). However, the limited experimental data indicate that like a cylinder in crossflow, the limiting value of the optimum ratio Λ_f/D_p would be reached at a Reynolds number of 500, for either value of the Strouhal number and that that this result would then apply up to Re 10^5. Above Re $\sim 4 \times 10^5$ the Strouhal number increases rapidly and the vortices are then weak and aperiodic(176).

The experimental results presented as a graphical summary in figure 4.21 can then be considered to present an accurate qualatative description of the influence of the relative intensity and scale of turbulence on the transfer processes of a held sphere or droplet. While the values of

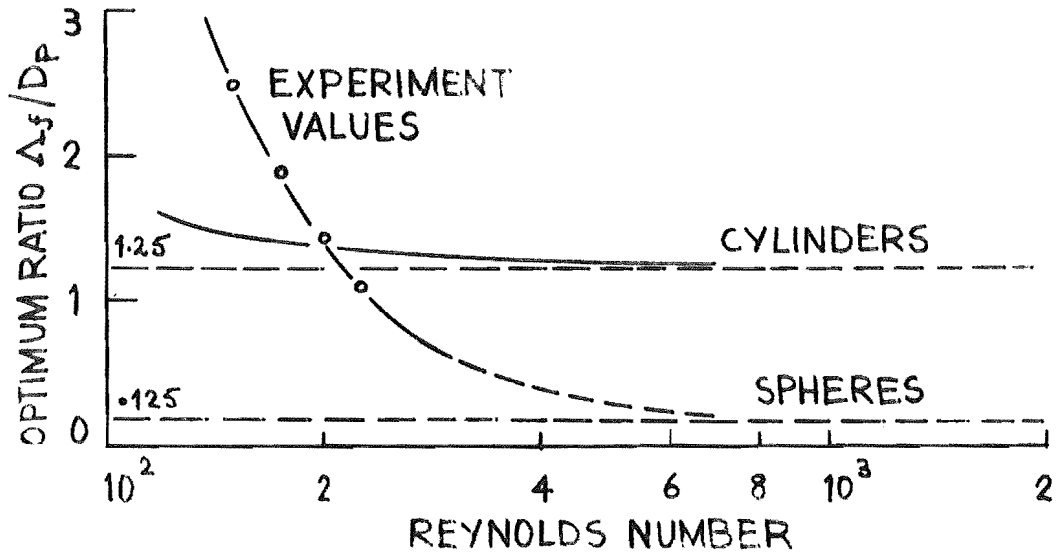

FIGURE 4.22 DECREASE OF OPTIMUM RATIO Λ_f/D_p TOWARDS LIMITING VALUE AS THE REYNOLDS NUMBER INCREASES.

Fs_h are considered to be reasonably accurate ($\sim 7\%$) (major source of error being the estimation of Q_{rod}), the estimation of the optimum value of the integral scale to the drop diameter can only be considered to be qualitative. The values of the maximum Frössling numbers at the optimum ratio are at present unknown. Λ_f was determined by approximating the measured spectrum curve with theoretical and semi-empirical equations and the spectra themselves will contain some error (as will the measured intensity of turbulence) because of the interaction of the grid produced turbulence with the rather high natural turbulence that existed in the system.

From the general trend indicated in figure 4.21, the following conclusions can be drawn: 1) Fs_h increases as the product $Re.\gamma$ increases. Hence (a) when Re is constant, the heat transfer to the evaporating droplet increases continuously with the intensity of turbulence, (b) when the intensity of turbulence is kept constant, Fs_h increases with the Reynolds number.

2) The rate of increase of Fs_h with the product $Re.\gamma$ is highest in the region of a low product of the Reynolds number and the intensity of turbulence.

3) When Re and γ are kept constant, the heat transfer rate either increases or decreases with increasing scale to drop diameter ratio; the maximum occurring at the optimum ratio Λ_f/D_p of 0.125 for $Re > 500$. The value of the optimum increases with decreasing Re below 500.

4) Any variation in the intensity of turbulence and in the scale ratio is more

effective the higher Re is.

These conclusions help explain the differences and even contradictions reported by various workers concerning the influence of turbulence on the transport processes for cylinders and spheres. The apparent independence of the drop Nusselt numbers on the integral scale of turbulence for a constant relative intensity, as suggested by the good fit of the line of slope $Fs_h = 0.77$ in figure 4.14, is now seen to result from measurements made where the ratio Λ_f/D_p was large and the effect of changing Λ_f is small.

As the level of turbulence is reduced the maximum for the Fs_h curve diminishes until at $\mathcal{T} = 0$, the Frössling number for forced convection in a turbulence-free stream is attained. Curves in figures 4.16, 4.17, 4.18 and 4.21 all tend to the value obtained for almost turbulence-free conditions by Ranz and Marshall (147) ($Fs_h = 0.60$, $\mathcal{T} = 0$).

The only work reporting both an effect of the level and integral scale of turbulence on heat transfer from spheres is that of Raithby and Eckert (146) who worked with values of $\mathcal{T}$ up to 7% and Λ_f/D_p from 0.14 up to 2. They reported an increase in the Nusselt number with increasing turbulence intensity and Reynolds number and a <u>decrease</u> of Nu with increasing ratio Λ_f/D_p for the same $\mathcal{T}$ and Re. This latter result suggests that the results were obtained for values of the scale to sphere diameter ratio beyond the optimum. Since their Reynolds numbers were between 10^3 and 10^4, the optimum ratio would be 0.125 as shown earlier and as their results were for Λ_f/D_p greater than 0.14 they failed to find a maximum value of Nu. From the occasional measurements made with low values

of $\mathcal{T}$ (0 to 2%) they report a sharp increase in the Nusselt number over this range. This same effect was recorded by van der Hegge Zijnen (194) but was not encountered in the present study as no measurements were made for intensity levels below 2%.

Lavendar and Pei (106) reported measurements on the investigation of the effect of the intensity and scale of turbulence on the average Nusselt number for a sphere. The Nusselt number was found to increase with the parameter $Re.\mathcal{T}$ and the ratio Λ_f/D_p exhibited some significance, but the magnitude of this influence was not specified.

The extensive review of the effect of turbulence intensity on transport processes for spheres by Galloway and Sage (54) reports a continuing increase in the Frössling number with increasing turbulence and Reynolds number. This expression does not adequately describe the scale effect but incorporates a sphere diameter influence which may be a hint of the ratio Λ_f/D_p effect.

4.7 Conclusion

A technique for measuring the intensity, integral and microscale of turbulence and the energy spectrum functions of a turbulent air stream, using a single hot-wire probe has been developed and shown to provide reliable measurements of these turbulence parameters. The technique differs from other single wire methods used to calculate the scale of turbulence (133, 189) which require the measurement of the correlation duration between velocity fluctuations in space as a correlation in time and can only be made using expensive correlators and recording apparatus. The new approach is to measure the one-

dimensional energy spectrum function and obtain estimates of the integral scale by approximating the measured curve by theoretical and semi-empirical equations which are functions of the integral scale.

The zero count method used to estimate the microscale of turbulence was shown to be heavily biased by the periodic fluctuations of the air blower supplying air to the column, but could be expected to produce reasonable results for flows free of periodic fluctuations.

The measured decay of turbulence behind a grid of solidarity 0.594, followed the same trends as reported in the literature. Further testing of the measuring technique for estimating the integral scale is needed to confirm the reliability of the results as determined from the energy spectrum functions.

Measurements were made of the evaporation rate in turbulent air streams for held droplets supported from fine glass fibres. The Frössling number for held droplets was found to depend on the relative intensity and the integral scale of turbulence, and the Reynolds number of the turbulent air flow. The Reynolds number range was limited from 150 to 225, the intensity of turbulence from 2% to 20% and the integral scale to drop diameter ratio from 0.2 to 5.0.

The results show the Frössling number to increase with increasing level of turbulence for constant Reynolds number and scale to drop diameter ratio. For a constant level of turbulence and Reynolds number, the Frössling number experiences a maximum value as the scale to drop diameter ratio increases from zero. This optimum is believed to result from resonance between the energy-

containing eddies and the shedding frequency of the spherical drop and can be shown theoretically to take a value of the scale to drop diameter ratio equal to 0.125, for the Reynolds number range 500 to 10^5. Although the present results are for Reynolds numbers less than this range, the trend with increasing Reynolds number is towards this limiting value of 0.125 and the value of the optimum ratio decreases with increasing Reynolds number below 500 (figure 4.21).

The existence of the optimum value of the scale to drop diameter ratio was suggested from results for heat-transfer from a cylinder (194) and the present results are believed to be the first results indicating a similar optimum ratio for spheres or drops. The optimum ratio of the scale to drop diameter as found in the present study, explains the seeming discrepancies found in the literature concerning the effect of the intensity and scale of turbulence on heat transfer for spheres (54, 146).

It is evident that there remains considerable work still to be completed. The effect of the sphere to support diameter ratio and results at higher Reynolds numbers need to be evaluated. The nature of the vortex behind a sphere and the frequency of shedding should be investigated to clarify the interaction and resonance of the shed vortices with the energy-containing eddies of the turbulent air stream. Although the experimental results are considered to accurately show the qualitative effect of the intensity and integral scale of turbulence on the transport processes for a sphere, a quantitative estimate of the optimum ratio value could only be considered after the measuring technique for the integral scale has been better proved.

Finally, the results presented have been obtained with

held droplets and to complete the study of the effect of the level of turbulence and the integral scale on evaporating drops, the results for free droplets must by obtained. In this case not all the turbulent eddies will be effective since small droplets may be completely entrained when the scale of turbulence is large. The following sections are studies of the effects of the turbulence parameters with free-falling and cocurrently entrained droplets as they are influenced by a reduction in the drag force on a single droplet (section 5) and the presence of other drops in a spray cloud evaporating under high mass-transfer rate conditions (section 6).

5. DRAG COEFFICIENTS FOR MOVING DROPS

5.1 Introduction

An exact analysis of the momentum transfer from a decelerating spray of droplets to the surrounding air stream requires detailed knowledge of the nature of the flow fields around each drop and the manner in which the interacting zones in the spray drier affect the movement of the drops. To predict evaporating droplet behaviour, the drop velocity, the drag forces acting on the drop and the air turbulence parameters need to be accurately defined.

In the preceding section, a significant effect of the air turbulence intensity and integral scale on the transfer rates for held evaporating droplets was reported. The turbulent velocity fluctuations penetrate the boundary layer around the droplet and resonance with the vortices of the wake occurs. Such disturbances change the material and momentum transfer profiles. If a similar effect is recorded for freely moving, evaporating drops then the altered flow profile could be expected to alter the skin friction and form drag of the moving droplet. The former is caused by the viscous resistance of the gas at the drop surface and the latter is caused by the shape of the droplet, which produces the back eddies in the wake owing to the separation of the boundary layer.

The movement of particles through fluids requires that a density difference exist between the particles and the fluid. Also, an external force (usually gravitational or centrifugal) is needed to impart motion

to the particle relative to the fluid. Three forces act on a particle moving through a fluid:

1) the external force, F_e, gravitational (or centrifugal);
2) the bouyancy force, F_b, which acts parallel with the external force but in the opposite direction; and
3) the drag force, F_D, which appears whenever there is relative motion between the particle and the fluid. The drag force acts to oppose the motion and is parallel with, but in the opposite direction to, the particle motion.

Under the force of gravity, a drop falls in air at a certain velocity U. During the motion, the liquid drop attains a velocity v' while the gaseous medium surrounding the drop attains a velocity v. Since U = v'-v, a force balance can be written

$$V\rho_p \frac{dv'}{dt} - V\rho_g \frac{dv}{dt} = \frac{m}{g}\frac{dU}{dt} = F_e - F_b - F_D \qquad (5.1)$$

By expressing the three forces according to their component masses and accelerations, and defining a drag coefficient C_D as the ratio of the drag force to the kinetic energy of the moving drop

$$C_D = F_D/(U^2\rho_g A/2g) \qquad (5.2)$$

(as obtained from dimensional analysis of the resistance of a spherical particle in a fluid), then the right-hand side of equation 5.1 becomes

$$\frac{dU}{dt} = \frac{g(\rho_p - \rho)}{\rho_p} - \frac{C_D U^2 \rho_g A}{2m} \qquad (5.3)$$

For gravitational settling, the drop quickly reaches

a constant velocity which is the maximum attainable under the conditions and is called the terminal velocity, U_t. For this steady drop motion dU/dt, dv'/dt and dv/dt are all equal to zero and from equation 5.3, the expression for U_t is obtained.

$$U_t = \sqrt{\frac{2g(\rho_p - \rho_g)m}{A \rho_p C_D \rho_g}} \qquad (5.4)$$

If an instantaneous terminal velocity is measured and substituted in equation 5.4 using for the projected area the great circle area of the drop ($\pi D_p^2/4$) based on the instantaneous drop diameter, a value of the drop drag coefficient C_D can be obtained and recorded for the corresponding value of the drop Reynolds number also based on the drop diameter and terminal velocity.

The drag coefficient as defined by equation 5.2 is analogous to the friction factor for pipe flow and must be found experimentally by solving equation 5.4 using experimental values of the terminal velocity. The drag coefficient can be estimated theoretically for rigid spheres at low Reynolds numbers from Stokes' law (178), although some numerical solutions of the equations of motion exist up to $Re_p \sim 100$ (68, 81).

This section is the second part of a program investigation the effect of the air turbulence parameters on heat-, mass- and momentum-transfer for evaporating droplets and describes an experiment conducted to determine whether changes in the longitudinal level of turbulence show up in changes of the value of drag coefficient. The effect of mass-transfer on heat-transfer is considered as an effect of the momentum of the vapour on the flow field about the

evaporating droplets.

5.2 Previous Work

A number of experimental investigations have been made to determine how the value of the drag coefficient varies with the particle Reynolds number. Figure 3.6 of Appendix 1 shows the type of correlation usually reported for the drag coefficient of spheres. The region up to Re $\sim$ 1 is generally designated as the Stokes' Law region (178) and the curve for this case has the equation

$$C_D = 24/Re_p \qquad (5.5)$$

The region from Re equals 1 to 10^3 is termed the intermediate or transition region. Beyond Re $\sim 10^3$, C_D is virtually constant up to Reynolds numbers of the order of 5×10^5 and this region is termed the Newton's Law region (134).

The motion of droplets in spray driers is confined entirely to the first two regions and in many instances to the Stokes' Law region alone. However, when droplets are first formed at the atomiser, they are undoubtedly well into the intermediate region but decelerate very quickly to lower Reynolds numbers. The intially formed drops undergo distortion due to violent oscillations and experience a variable condition of drag as the drop shape changes.

The study of liquid drop velocities and drag coefficients cover a wide range of sizes of drops. Experimental results are available for drop Reynolds numbers as low as 10^{-4} as reported for Millikan's condenser experiments (129) and up to values as large as

10^3 for drops with included solid powders as reported by Lihou (111).

Two of the more notable early works for drag coefficients of spheres are those by Shakespear (163) and Davies (26). Early in 1914, Shakespear used hollow spheres of different masses falling a distance of 125 feet. He found the drag force to be proportional to the frontal area of the sphere and the square of the velocity. In 1945 Davies produced equations for drag coefficients over the ranges $0 < Re < 4$ and $3 < Re < 10^5$. These equations were given as especially suitable for airborne particles and were obtained by fitting curves to the experimental data. His own experiments were with spheres of paraffin wax and small drops which were shown to fall like rigid spheres if not too large. He also gave an equation for the correction for particle slip in gases to be applied in the Stokes' law region.

Studies of droplet terminal velocities are limited and many workers have used Davies' (26) report and assumed the drops to behave as solid spheres. For single drops, Sjenitzer (168) reported values of measured terminal velocities and showed the smooth curve results to follow the C_D values for solid spheres. Lihou (111), in his study of the effect of small amounts of powders on the shape and terminal velocity of large water drops in air, found the velocity to be less for drops containing solids. The difference was attributed to distortion and the absence of circulation. His results, which have a large scatter were for the limited range, $1 \times 10^3 < Re < 4 \times 10^3$.

Terminal velocity correlations based on smoothed drag data for freely-falling solid spheres and recommended as suitable for drops in air in the Stokes' and transition

region, have been given by Schlünder (161), Grassmann and Reinhart (64), Lapple and Shepherd (103), Hughes and Gilliland (79) and Smith (170). Schlünder (161) gives equations for the terminal velocity of drops for the range $0.6 < Re < 2{,}500$. The formulae are built up from Frössling's equations (49),

$$\frac{1}{U_t} = \frac{1}{U_{t_{Stokes}}} + \frac{1}{U_{t_{Newton}}} \qquad (5.6)$$

and neglect buoyancy since the density difference between water and air is large. The equations are presented for the Reynolds number ranges 0.6 to 8, 8 to 300, and 300 to 2,500. By introducing a dimensionless velocity and a dimensionless diameter, an expression for U_t independent of the nature of the material, is derived. It is then possible to present the terminal velocity as a function of the drop diameter for a given temperature and mixture of the two phases, by a single curve.

Grassmann and Reinhart (64) published a method for evaluating steady rising or falling velocities of spheres using the terms $(ReFr)^{\frac{1}{3}}$ and $(Re^2/Fr)^{\frac{1}{2}}$, where Fr is the Froude number of the drop which was observed to behave as a solid sphere. Equations for calculating the paths taken by bodies undergoing accelerated motion, taking into account the effect of fluid friction, have been presented by Lapple and Shepherd (103). They also produced C_D values for spheres as a standard curve based on the smoothed data of 17 workers. This standard curve has become widely accepted and is referred to in textbooks (140, 125).

Several important aspects of the motion of drops

including the effects of acceleration and deceleration on the drag coefficient, the factors influencing distortion, and the internal circulation within drops, have been reviewed by Highes and Gilliland (79). They collected the drag coefficient data of previous workers and presented their results in terms of a Terminal Velocity group and a Gravitational group. They included data for drops in gases but this was mainly for large drops.

The reference curve obtained from smoothed drag data for free-falling solid spheres by Smith (170), has the equation

$$C_D = \frac{1}{\Psi} + \frac{2.69}{\Psi^{0.390}} + \frac{\Psi^{0.36}}{(1.8\Psi^{0.36}+77)} \qquad (5.7)$$

where Ψ is the drag coefficient group $C_D(Re_p/24)^2$. Equations 5.7 represents the better data with a standard deviation of $\pm$ 2.3%. The attraction of the equation is that each term dominates the expression in turn. These terms describe the influence of viscous drag ($\Psi < 0.05$), of the circulating wake ($0.1 < \Psi < 10^3$), and of turbulence within the boundary layer ($\Psi > 10^3$).

An extensive review dealing with fundamental aspects of solids-gas flow has been presented by Torobin and Gauvin (188). Pertinent comments, as to the inability of standard drag curves to predict the motion of decelerating droplets and the treating with caution of published drag coefficients for cocurrent flow systems, are made. They suggest that it may be necessary to correlate unsteady state drag coefficient data as a function of a time parameter to relate to the total time allowed for the buildup of the boundary layer and the wake of the drop. In their discussion of the effect of

fluid turbulence on the drag coefficient, they define a critical Reynolds number (Re_{crit}) as the point at which the characteristic steeply sloped curve intersects the drag coefficient value of 0.3. For a standard curve: Re_{crit} $2x10^5$, π_{crit} $3x10^7$ (170). Their warning on the use of occurrent drag coefficient data is that such results are complicated by variables which at times obscure even qualitative interpretation of results. It is reported that flow disturbances in some cases increased and in others, decreased the drag coefficients.

From their own experimental work Torobin and Gauvin (188) found that it would be unlikely for any turbulence effect on the drag coefficient to be noticed for drop Reynolds numbers less than 400, unless turbulence intensities greater than 40% were present. However, non-random vortices of a suitable type may cause a change at Re as low as 30 (2). In general, the multiparticle results reviewed by Torobin and Gauvin show a tendency to be lower than the standard curve and this could be due to an intensity of turbulence effect.

The estimation of C_D to two significant figures for a given situation in the transition region is not advised, since the phenomenon is not well fixed and a variation in results does not necessarily reflect an error in observation. Even the use of a standard drag curve for estimating drag to the second figure for bodies moving freely at a steady rate in a laminar fluid outside the Stokesian region is not valid. Recent measurements (6) have shown as much as 30% scattering about the average curve which cannot be attributed to instrumentation errors.

Drag coefficients for droplets injected from rest into

a moving air stream were obtained by Ingebo (80). His data were correlated by the straight line relationship

$$C_D = 27/Re^{0.84} \qquad (5.8)$$

The results are unique for several reasons as they show a decrease in C_D whereas other workers report an increase for similar conditions and also his results show an increasing departure from the standard curve as the Reynolds number increases. This latter result may have been the influence of an unknown amount of free-stream turbulence which would have effected the droplet mass-transfer rate.

Buzzard and Nedderman (18) found the drag coefficients of accelerating droplets to be the same as those for drops moving at constant velocity. They experienced a big scatter of results and the lack of reproducibility of the drag coefficients was considered to indicate some random variation. Minute quantities of surface active agents were found to affect the results significantly. This influence of surfactants is noteworthy, as even distilled water may contain impurities with surfactant properties that will inhibit droplet circulation. Pritchard and Biswas (142) in their review of mass-transfer from drops in forced convection remind the reader that droplet circulation causes renewing of the drop surface and an increase in the overall drying rate. For large drops, Downing (33) reported that under free fall conditions, a helical rather than straight-line flight path was observed, and this may be initiated by surfactant influences and supported by vortex shedding in the wake.

For a spray of droplets in air, the relative turbulence intensity will be affected by changes in the drop discharge

velocity, the absolute air velocity and possibly the droplet spray concentration. The air turbulence intensity would also be expected to decrease as the distance of the drops from the nozzle increases. The effects of the presence of other particles for dispersions of high concentrations may be treated as two factors: the viscosity and the density differences. The first is not usual in sprays of drops in gases but the second may be important when considering the presence of large drops near others. It is generally accepted that for volumetric concentrations below 0.2% the particles will behave as individuals (140).

Only one work has been found for drag coefficients of drops falling as a spray in air. For spray droplets both entrained and accelerating in air streams, Fledderman and Hanson (43) showed the drag coefficients to depend on the air velocity. The C_D values were found to be reasonably low, at times representing a decrease of 1,000% below the standard drag curve. This decrease was attributed to an evaporation mass-transfer effect but other evaporating droplet drag coefficient studies, such as Ingebo's (80) have not reported decreases of this magnitude. The droplet velocity estimation may have been in error though, as this was derived by correlating their heat- and mass-transfer results with Frössling's equation (48). The small size and the small relative velocity of the air-borne drops meant that values of the drop Reynolds numbers did not approach Re_{crit}, where the level of air turbulence intensity influences C_D. Accordingly, Fledderman and Hanson did not consider turbulence when calculating drag coefficient values from the mass-transfer

data even though a dependence of C_D on the air velocity was apparent.

Evaporation from a drop is likely to reduce the film drag due to a thickening of the boundary-layer with the momentum of the effusing vapour. The properties of the evaporating material should have an effect on C_D owing to the coupling effect between heat-, mass- and momentum-transfer(150). Further possible effects are the alteration of the position of boundary-layer separation and the creation of steep variations in properties due to the large temperature and concentration gradients associated with intense mass-transfer (55,175). Muggia (132) derived an expression for the drag of an evaporating droplet by considering Oseen's approximation for slow flow around a sphere (137). For Reynolds numbers up to 500, Hamilec et al. (67) showed the drag coefficient to be reduced for large mass-transfer rates. They used a numerical method and attributed the reduction in C_D to the alteration of the flow field about the drop because of the radial mass efflux and found the vorticies in the wake were also extended.

For Reynolds numbers up to 2×10^3, the laminar boundary-layer theory has been used to obtain an expression for the effect of mass-transfer on heat-transfer for droplets evaporating under intense mass-transfer conditions (39). Assuming that the effect of mass-transfer on the drag coefficient can be expressed as the ratio of the coefficient with and without mass-transfer, it is possible to obtain some idea of the effect on viscous drag by analogy with the effect of heat-transfer. Eisenklam, Arunachalam and Weston (39) found the boundary-layer theory results for evaporating drops to be

$$Nu^*(1+B) = 2 + 1.6Re^{\frac{1}{2}} \qquad (5.9)$$

and $C_D^* (1+B) = C_D$ (5.10)

where * indicates intensive transfer conditions and B is the mass-transfer number ($B = C_p \Delta T / H_v$). C_D^* is then the drag coefficient corrected for evaporative effects. Equation 5.10 was reported to reasonably describe the data for intensive evaporation of droplets up to Re $\sim$ 10 under approach temperatures between 400 and 1100 F which cover and exceed the normal temperatures found in intensive spray-drying.

For freely falling spheres impregnated with sulphur dioxide, Clamen and Gauvin (19) found mass-transfer to decrease the drag on a sphere and reduce the influence of the free stream turbulence. They found that the drag coefficient was not altered significantly by mass-transfer if the concentration of the vapour at the surface was small. This condition they defined as

$$\Delta C_D / C_D < 0.28\ C_s / Sc^{\frac{1}{3}} \qquad (5.11)$$

for $(C_s / Sc^{\frac{2}{3}}) < 0.1$ and $Sc \gg 1$. C_s is the mass fraction of the diffusing vapour present at the sphere surface. It is suggested that when these conditions are satisfied other factors such as the free-stream turbulence will have a dominating influence.

Rabin et al. (145) studied the displacement and shattering of propellant droplets and obtained an almost constant value of C_D for evaporating droplets. For the Reynolds number range 100 to 10,000 C_D took the approximate value of 0.9 and this result crosses the standard drag curve for solid spheres.

5.3 Apparatus

An experiment was designed to provide data for evaluating the instantaneous value of the drag coefficient of evaporating droplets. The experimental cocurrent spray-drier described in section 2 and figure 2.1 was used as a vertical wind tunnel, the droplets and the drying air moving cocurrently down the column. The droplets were formed by atomising distilled water through the pressure nozzle at the head of the column. For the nozzle, considerably reduced flow rates were used over a range of pressures (10 to 100 psig) to produce a wide range of droplet sizes and also to keep the droplet spray concentration very low (less than 0.002%). The turbulence intensity and scale of the cocurrent airstream could be varied either by changing the volume flowrate of air down the column or by fitting different turbulence generating grids at the head of the column and immediately before the pressure nozzle. The instantaneous velocity of the droplets was obtained by photographing the drops during their steady fall at a distance of 12 feet below their point of formation.

The velocity of a moving drop can be obtained using "still"-camera photographic techniques in one of two ways. Either the camera shutter speed can be controlled to record an image of the moving drop on the exposed film for a known time of opening of the camera shutter, or a double exposure of the same drop onto the same film can be obtained using a delayed, double-flash technique. The first method was tried successfully

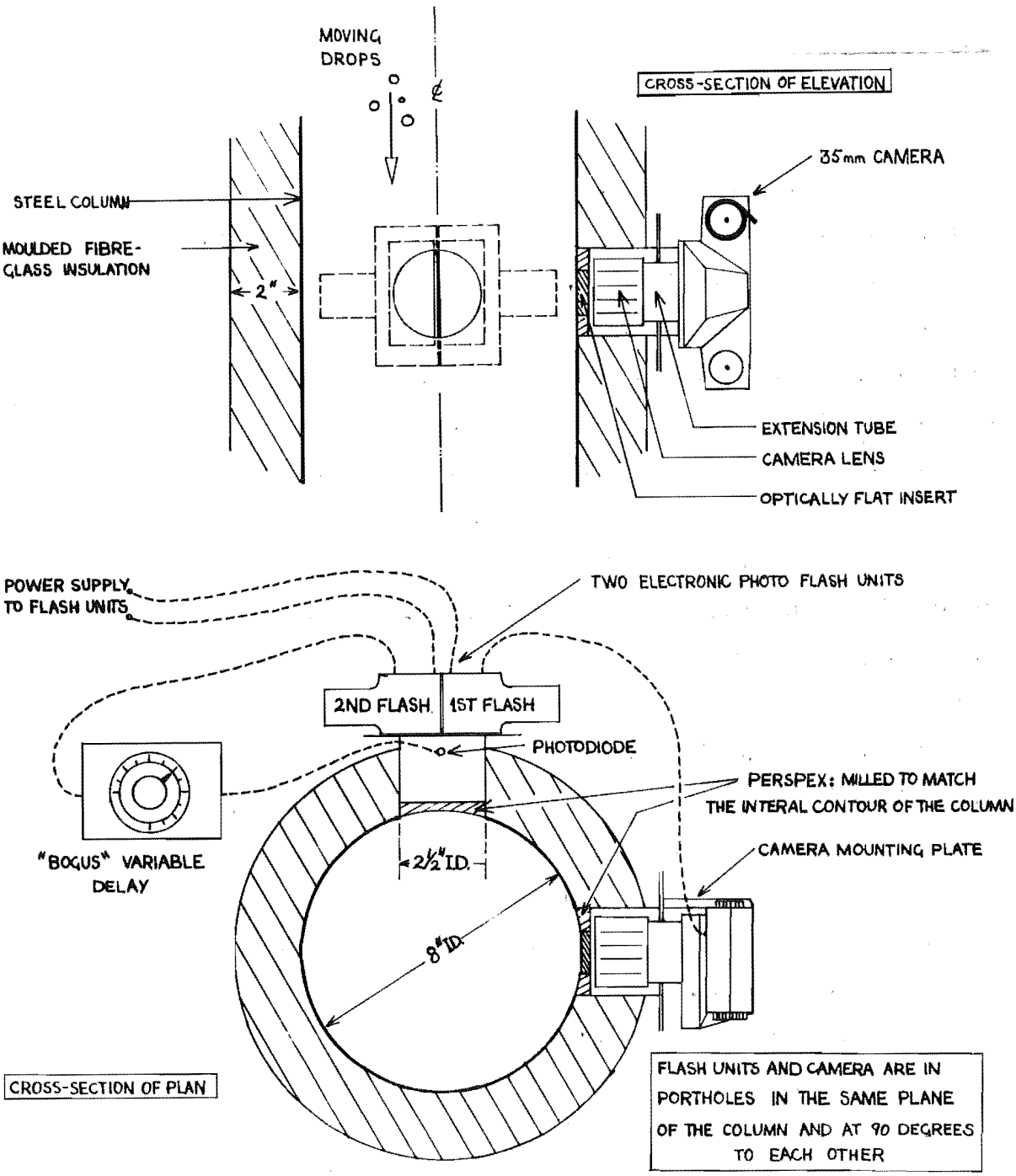

FIGURE 5.1 ARRANGEMENT FOR PHOTOGRAPHING MOVING DROPS.

using a 1000 watt quartz-iodine flood-lamp as a constant light source with camera exposure times of 1/125th and 1/500th of a second on a focal plane shutter camera. However, the method proved unsatisfactory because the camera shutter speed, and hence the exposure time of the drop image on the film, could not be guaranteed to better than 15%.

The alternative method of a delayed double-flash exposure of the same drop was then developed successfully and proved much more reliable. The double exposure was obtained by side lighting the moving drop using two electronic flash units with flash duration times of the order of one or two milliseconds. The delay between the two flashes was controlled by an electronic circuit variable from less than one-half a millisecond up to two or three seconds. The experimental arrangement of the two flash units, the variable delay and the camera, is shown in figure 5.1 approximately to scale.

The distilled water droplets moved cocurrently with the drying air down the column past the camera and the two flash units. The camera lens system was chosen for a small depth of field and a suitable focal length. A 35mm camera was used with a 35mm wide-angle lens and a 1 inch extension tube. This gave a magnification on the film of $1\frac{1}{4}$ times and some photographs in each experimental run were taken taken with a lens doubler placed between the extension tube and the camera so increasing the magnification twofold. Fine grain film was used and the exposures were taken at f16 without the lens doubler and at f8 when the doubler was used. The electronic flash units were operated on half power.

Figure 5.1 shows how the opening of camera shutter triggered the first electronic flash unit in the usual manner. This flash of light was sensed by a photodiode which started the variable delay timer of the "Bogus" delay unit (description and calibration curve given in Appendix 9). After the time delay the "Bogus" delay unit then fired the second flash unit so double exposing the image of a drop on the same negative. The camera shutter was held open for about 1 second while the double flash occurred.

5.4 Experimental

The experimental study was conducted in three stages. These stages were the evaluation of drag coefficients for water droplets 1) falling in still, cold air conditions, 2) cocurrently entrained in cold air, and 3) cocurrently entrained in hot air. In the first and second stages, droplet evaporation was expected to be minimal while for the third stage, the evaporation rate for the droplets was considered to approach intense mass-transfer conditions.

For the first stage the spray drier tower was sealed at the base and still air conditions existed. The spray of distilled water droplets was introduced and allowed to continue for some time until constant humidity (saturation) conditions were approximated. Droplet evaporation was then minimal and falling droplet photographs were taken while the pressure nozzle operating pressure and flow rate were varied. This produced a wide range of droplet sizes. The air temperature and humidity were recorded continuously

while the photographs were taken.

For the second and third stages with cocurrently entrained droplets, the desired air operating temperature was chosen and preset on the automatic controller. The experimental spray drier was operated without the spray present, until steady conditions were obtained by the automatic control of the air heaters. The air velocity, humidity and turbulence parameters were then measured in the absence of the spray of droplets. These measurements were made using the pitotstatic tube, the humidity sampler and the hot-wire anemometer methods as described in earlier sections. The camera was then placed in the porthole used for the air turbulence measurements and the spray of water droplets introduced to the air moving down the column. A wide range of droplet sizes was again produced and the air temperature and humidity were recorded while the drop photographs were taken. After the spray had stopped the air velocity profile was re-checked.

Two films of about 30 exposures each were taken for the two camera lens systems used (with and without the lens doubler). A scale rule was photographed under the same conditions for use as a reference length and the exposed films were developed and projected onto a screen. Droplet sizes and distances of fall were measured from these projected negative pictures. In this way, drops were tracked in the size range from 80 to 300 microns, falling in still, or cocurrently moving air at instantaneous mean velocities of 0.6 to 13 fps.

An example of the photographs of moving droplets taken using the double flash method is shown in figure 5.2.

This method gave two stark silhouettes with a well defined leading edge and separated in time by between $\frac{1}{2}$ millisec and 1 sec, as shown in the photograph. Note that the drops are moving downwards and that the second image is more bright than the first. The rise time of the electronic flash units was very short whereas the decay in light intensity of the flash tended to be exponential and so the brightness of the drop image decreases as the drop falls. The difference in brightness between the two images of one drop was attributed to internal reflection of the drop and external reflection from the surrounding droplets and the column walls. Also of course, the first flash partly sensitised the film for when the image of the second flash was recorded.

The drops were photographed under side-lighting conditions and the reflection of the flash light from the two sides of the droplet as seen in the focal plane of the camera is either direct reflection or internal reflection. As the drop image moves across the film so the bright spots trace out continuous lines. Other photographs of slower moving droplets obtained during the experiment showed this effect with an image of a drop clearly seen between two streaks representing the diameter of the drop. Only images clearly in focus were measured and the time delay between the flashes was known accurately according to the time delay setting. The depth of the focal plane of the camera-lens system was measured and found to be less than $\frac{1}{8}$ inch. All photographs indicated that at the test level of the column all droplets were falling vertically through the focal plane.

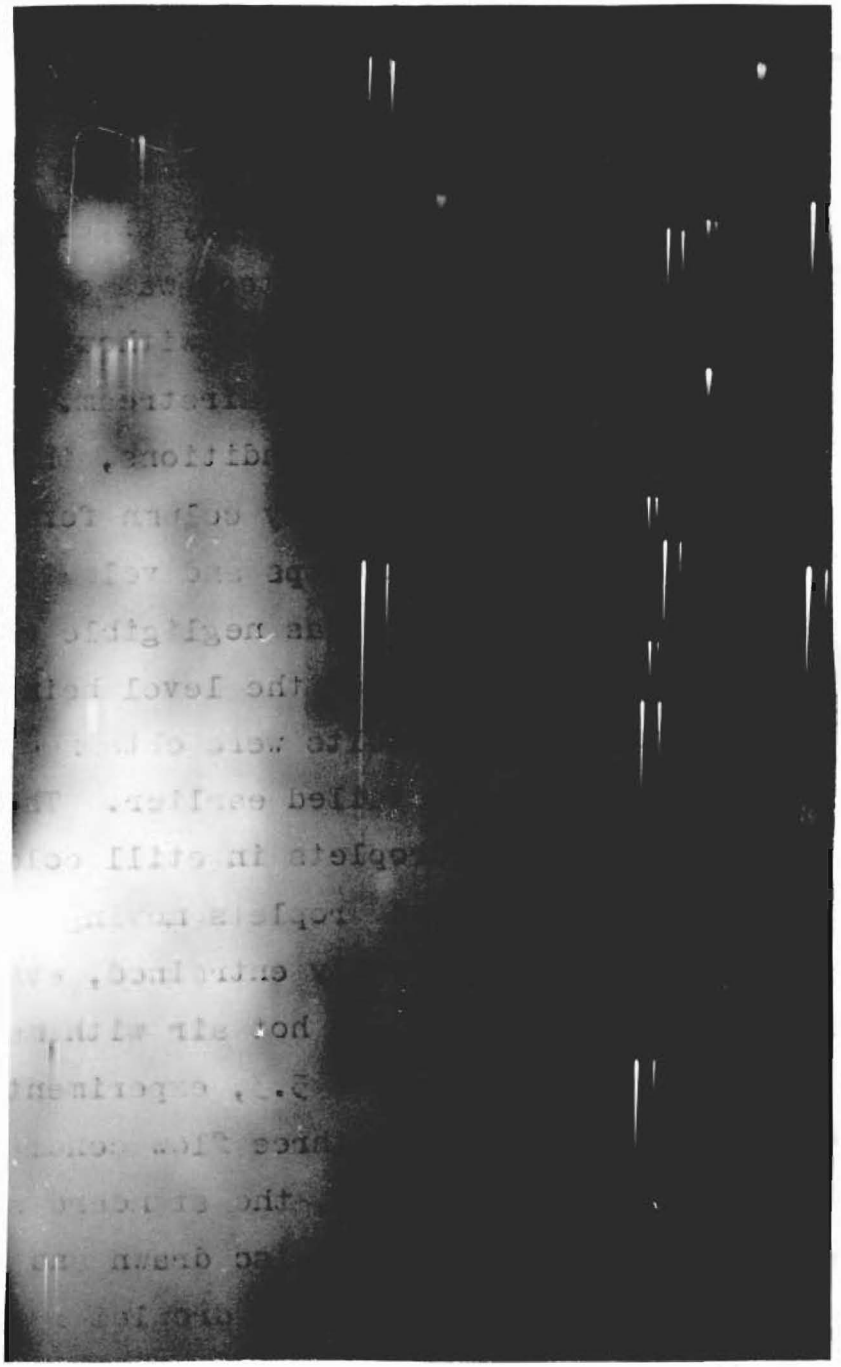

Figure 5.2 Double flash photograph of free-falling droplets. Delay = 4.57 millisecs. Drop diameters from 140 to 500 μ. Drop velocities from 2 to 7 fps.

5.5 Results

Although the spray droplet concentration was never more than 0.002% (100 times less than the recommended concentration above which drops may experience "hindered settling" conditions (140)), a test was conducted to measure the air velocity with and without the spray droplets present in the moving airstream. For the low spray droplet concentration conditions, the pitotstatic tube could be used in the spray column for some minutes before being flooded with drops and velocity measurements indicated that there was negligible change in the profile across the column at the level being sampled.

The experimental results were obtained for the three flow regimes as detailed earlier. These regimes were 1) free falling droplets in still cold air, 2) cocurrently entrained droplets moving downwards in cold air, and 3) cocurrently entrained, evaporating droplets moving downwards in hot air with mass-transfer numbers, $B \backsim 0.04$. In figure 5.3, experimental terminal velocity examples of these three flow conditions are shown. For each set of data, the standard solid sphere drag curve of Smith (170) is also drawn and is used as a reference with which evaporating droplet results may be compared.

The accuracy of the reported results depended primarily on the following measurements: the delay time between flashes ($\pm$ 2%), the measurement of the air velocity ($\pm$ 4%), and the measurement of the drop diameter. The accuracy of this last measurement

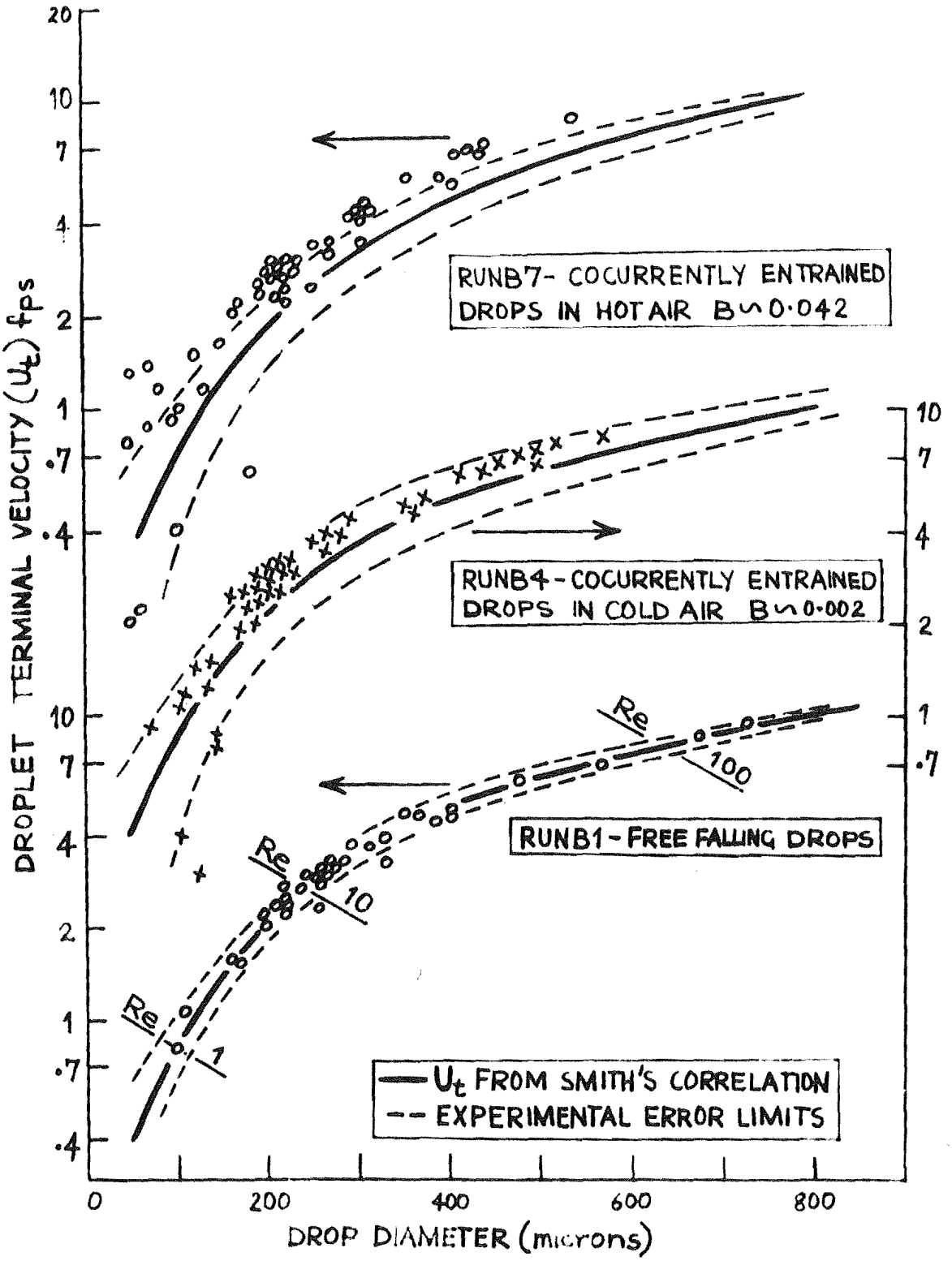

FIGURE 5.3 TERMINAL VELOCITIES OF WATER DROPS MOVING IN AIR.

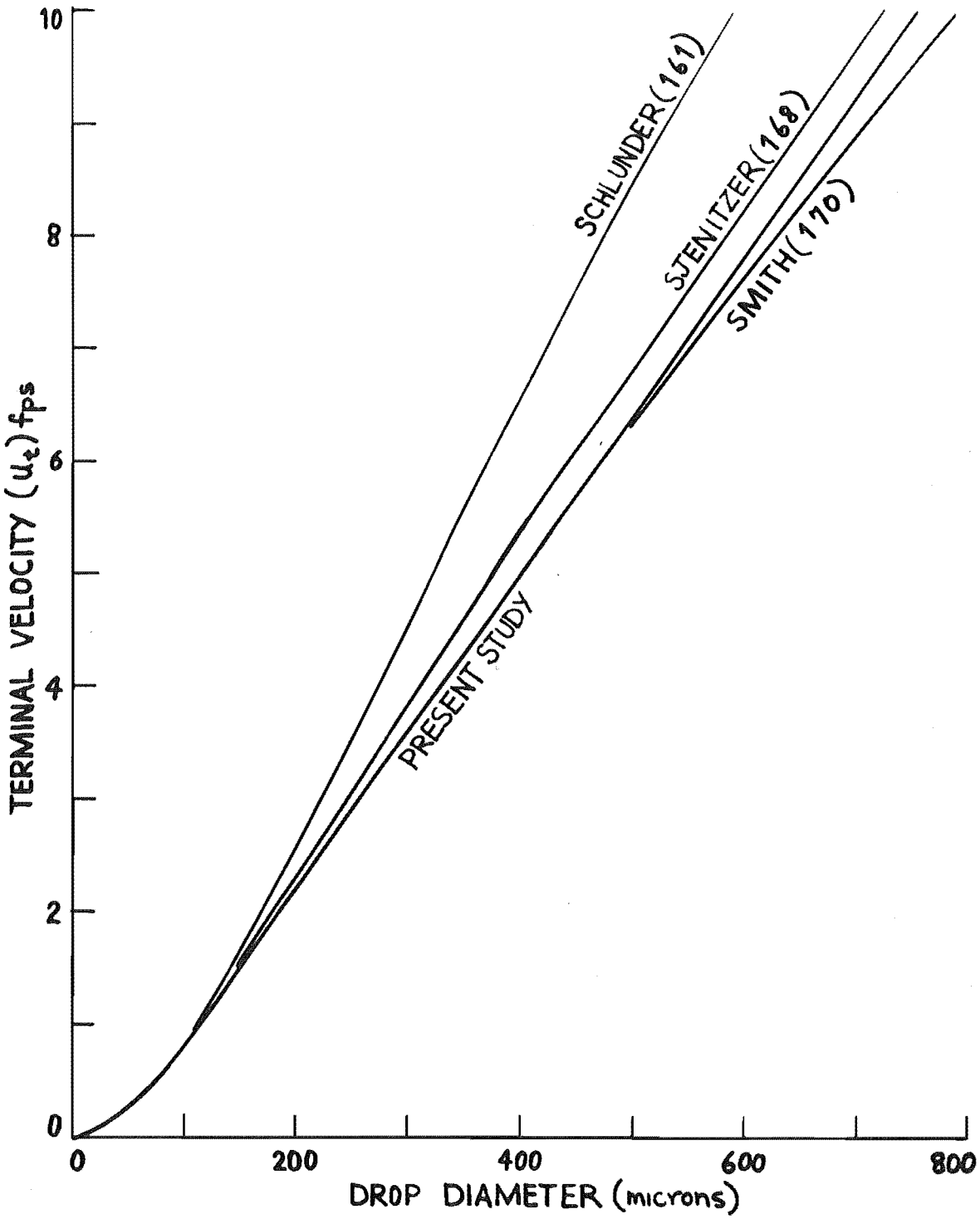

FIGURE 5.4 COMPARISON OF TERMINAL VELOCITIES OF FREE-FALLING WATER DROPLETS.

varied with the size of the drop (assumed spherical) and for Re $\sim$ 100 was $\pm$ 3%, for Re $\sim$ 10 was $\pm$ 7% and for Re $\sim$ 1 was $\pm$ 10%. Hence, in figure 5.3, for free falling droplets at Re $\sim$ 100, the error will be $\pm$ 5% and for Re $\sim$ 1 will be $\pm$ 12%. For the cocurrently entrained droplets, the error limits will be $\pm$ 9% and $\pm$ 16% respectively.

In figure 5.4 the terminal velocity results for water droplets falling freely in still cold air are compared with other reported data for free-falling drops. Sjenitzer's data (168) were obtained from free-fall experiments at a higher air temperature ($T_g \sim 182$ F) and the curves of Schlünder (161) and Smith (170) were calculated using the physical properties of the actual experiment run B1($T_g \sim 65$ F). The curve representing the present study results was obtained by fitting a polynomial to the data using the computer program DROPVEL described in Appendix 10. The program fitted 1st, 2nd, 3rd and 4th order polynomials to the terminal velocity results then used the smoothed curve equations to calculate values of the drop Re, C_D*, C_D and π for drop diameters increasing in multiples of 50μ up to 750μ. While agreeing with Snedecor (171) that graphical representation of the data is sufficient and that the smoothed curves do not necessarily represent the true relationship, the use of the smoothed drag coefficient curves does allow easier comparison with the standard curve by Smith. This may be of value in evaluating the shift of the C_D results with a change in the turbulence intensity or scale of the entraining air, or an increase in the Mass-Transfer number B.

The drag coefficient results for the free falling drops are plotted in figure 5.5 as a function of the drag

coefficient group $\Pi = C_D(Re/24)^2$ and in figures 5.6 and 5.7 similar curves are plotted for examples of the results obtained for cocurrently entrained droplets moving in cold and hot air. In each of these figures the experimental error limits about the standard drag curve by Smith are drawn to indicate the extent of the difference between the drag experienced by water drops and that by solid spheres. The results shown in figure 5.7 are values of the experimental drag coefficient C_D^* not corrected for the mass efflux of the vaporising water. Using the boundary layer theory solution of Eisenklam et al (39), $C_D = C_D^*(1+B)$, the corrected values of C_D are shown as the computer smoothed curve in figure 5.8 where C_D is now the drag coefficient uncorrected for evaporative effects. The corrected values of C_D are larger by 4.2% and so closer to the standard curve by Smith.

Also in figure 5.8, the computer smoothed curves are drawn for the examples of free falling (curve A) and cocurrently entrained (curve B) droplets, moving in cold air. The free falling droplet results lie on the standard curve by Smith and the curve for drops cocurrently entrained in cold air falls within the lower experimental error limit about the standard curve. The curve for cocurrently entrained droplets moving in hot air lies practically on the lower error limit about the standard solid sphere curve. So far, these results have been presented without regard to the air turbulence parameters and the lowering of the drag curve for cold entrained drops below the free fall curve suggests a turbulence effect.

As seen in figures 5.6 and 5.7, the experimental results show a large scatter and comparison of the drag

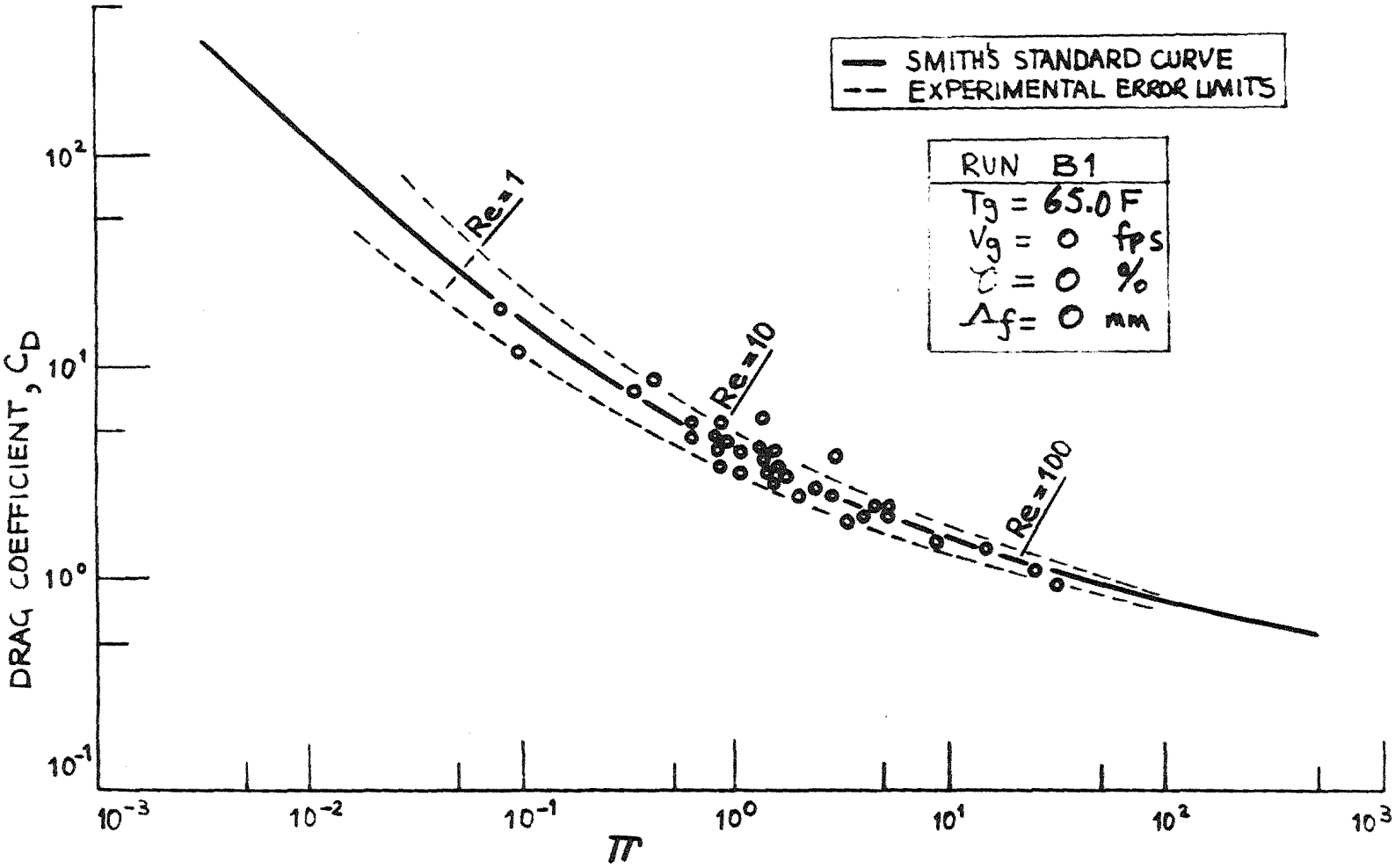

FIGURE 5.5 DRAG COEFFICIENTS FOR FREE FALLING WATER DROPS IN COLD STILL AIR.

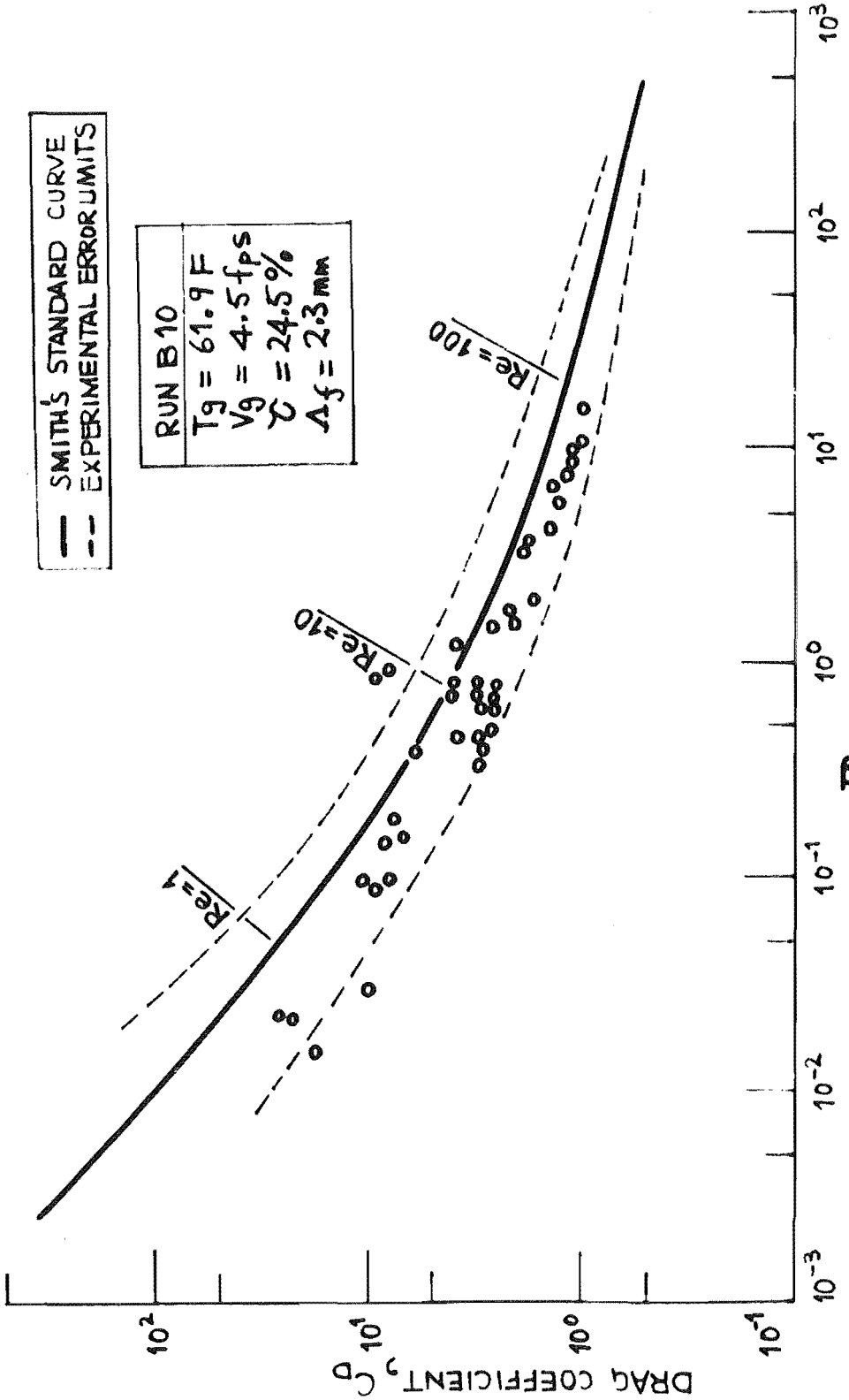

FIGURE 5.6 DRAG COEFFICIENTS FOR COCURRENTLY ENTRAINED WATER DROPS MOVING IN COLD AIR.

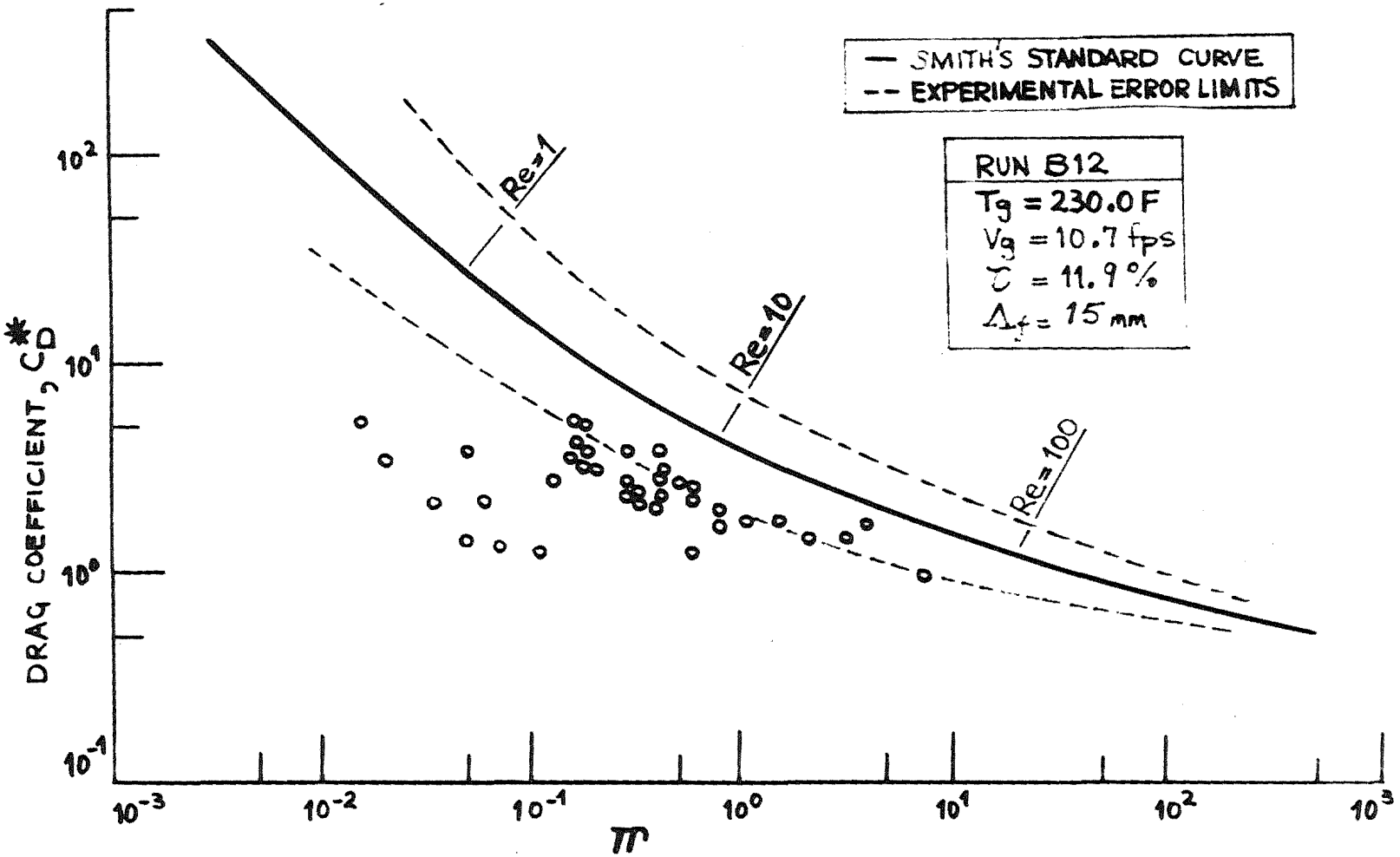

FIGURE 5.7 DRAG COEFFICIENTS FOR COCURRENTLY ENTRAINED WATER DROPS MOVING IN HOT AIR. ($T_g \sim 230F$, $B \sim 0.042$)

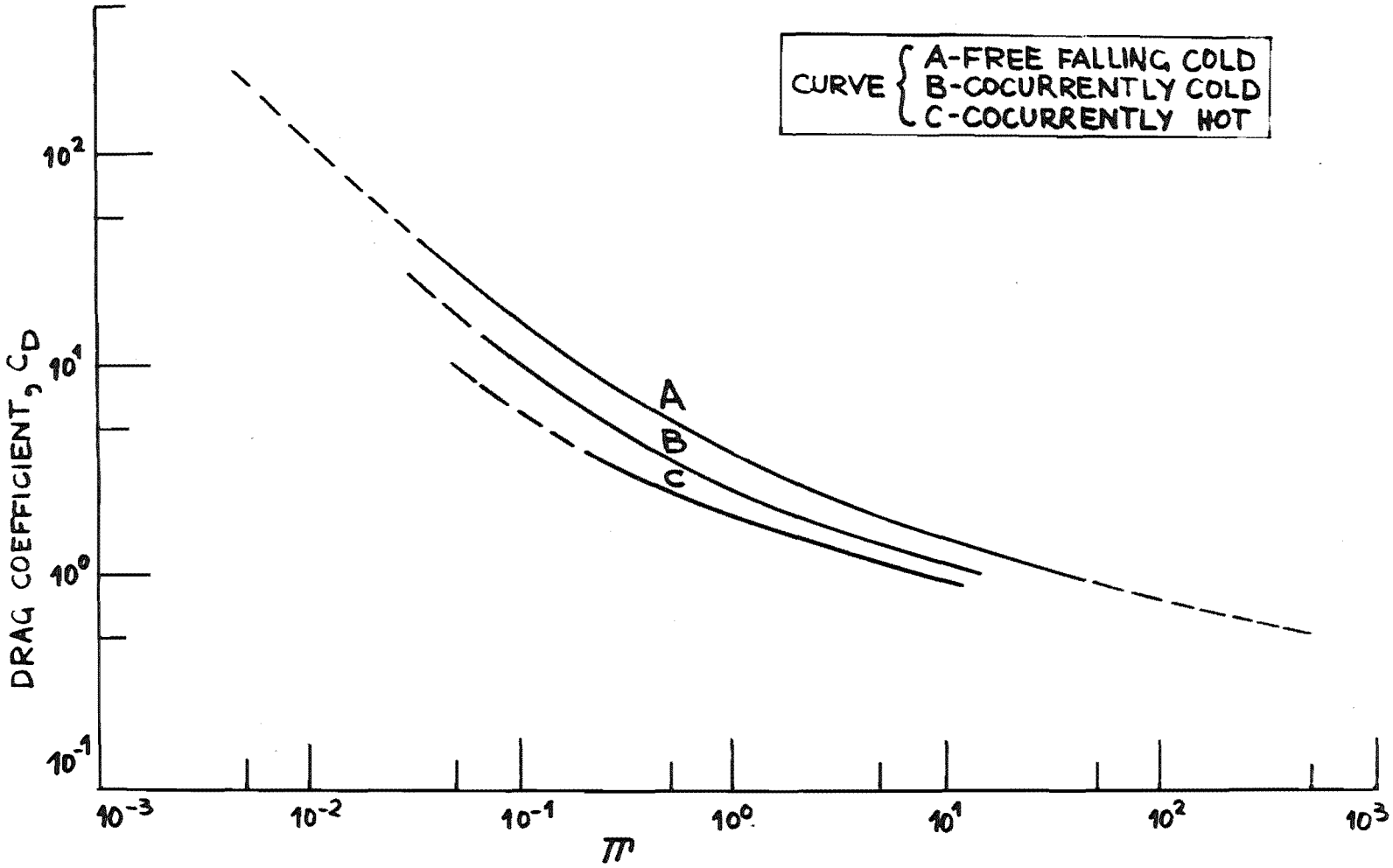

FIGURE 5.8 DRAG COEFFICIENTS FOR WATER DROPS MOVING IN AIR. APPROXIMATE SMOOTHED CURVES FOR THE THREE FLOW CONDITIONS STUDIED.

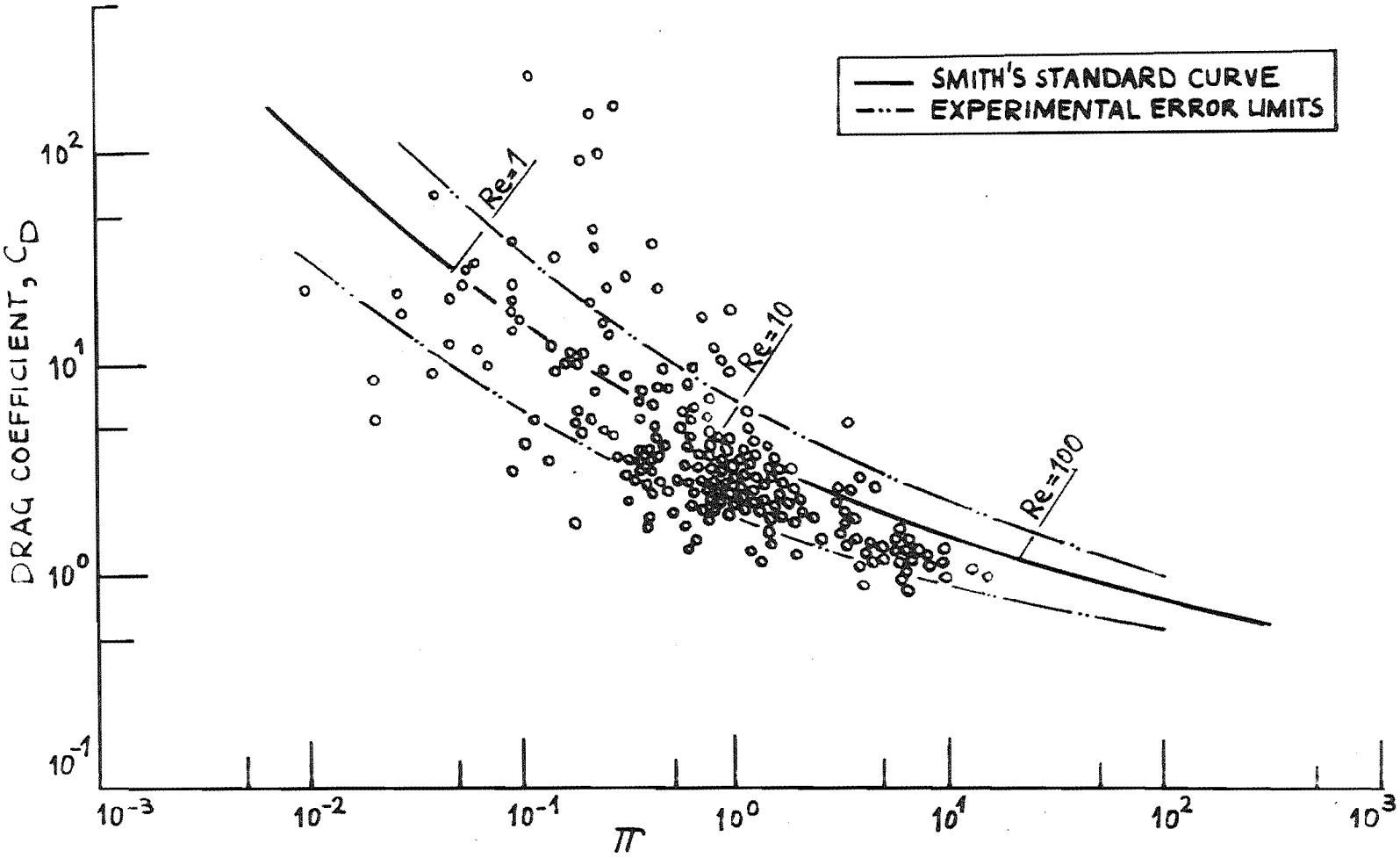

FIGURE 5.9 DRAG COEFFICIENTS FOR WATER DROPS MOVING COCURRENTLY WITH COLD AIR. ALL EXPERIMENTAL RESULTS SHOWN FOR $7 < \tau < 24\%$, $2 < \Lambda_f < 20$ mm.

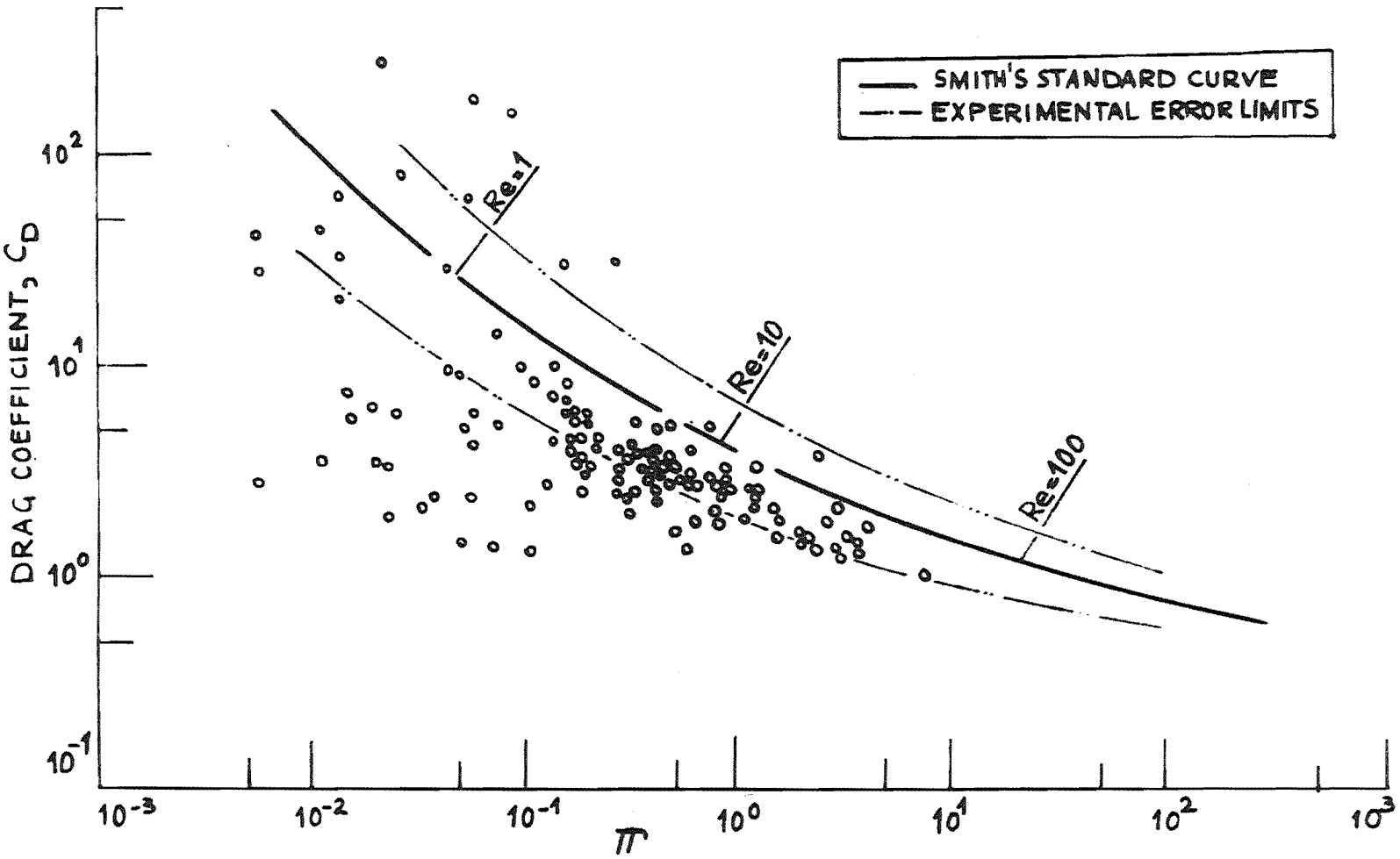

FIGURE 5.10 DRAG COEFFICIENTS FOR EVAPORATING WATER DROPS MOVING COCURRENTLY WITH HOT AIR. ALL EXPERIMENTAL RESULTS SHOWN FOR $6 < \tau < 12\%$, $2 < \Lambda_f < 20$ mm. $B \sim 0.04$ FOR $C_D = (1+B)\, C_D^*$

coefficients for different air turbulence conditions was best made by comparing the computer smoothed curves. For water drops cocurrently entrained in both cold and hot air, no discernible trend in the value of the drag coefficient was observed either with changing level of longitudinal turbulence or integral scale. These parameters were varied from 6 to 24% and from 2 to 20 mm respectively. However, the indicated trend shown by the result examples in figure 5.8 continued for all experimental results and for this reason all measured values of the drag coefficient are shown in figures 5.9 and 5.10. From these two figures the mean of the computer smoothed curves was obtained without regard to the intensity and scale of turbulence and a summary of the drag coefficient results is presented in figure 5.11.

This figure (5.11) shows the free falling droplets to take drag coefficient values identical with the standard solid sphere curve values. The drag coefficients for cold air take values less than the standard curve values and for drops entrained in hot air the drag coefficients are still further reduced. This is the same pattern as indicated in figure 5.8 but in figure 5.11 all the experimental smoothed curve results (corrected for mass-transfer effects) are within the experimental error limits about the standard curve.

5.6 Discussion

The terminal velocities and drag coefficients for free-falling droplets moving in still air were shown to be identical with the values reported for solid spheres over the Reynolds number range from 1 to 100 (droplet diameters

from 100 to 700μ). This same result was reported by Eisenklam et al. (39) for small water droplets under room-temperature conditions where the standard curve was reproduced to an accuracy of ± 10%. Sjenitzer (168) also found that drops falling in warm airdid so like solid spheres (B∿ 0.027). A dependence of the value of the drag coefficient on the Surface Tension group ($Su = g\sigma D_p \rho_g / \mu_d^2$) was reported by Meisse (126). He found the drag coefficient to increase above the standard solid sphere curve according to the value of Su but this effect was not realised for Reynolds numbers less than 100. For large water drops, Lihou (111) found the drag coefficient to agree with the solid sphere curve for cold, free-falling drops at $Re \backsim 10^3$, but the value of the coefficient increased above the solid sphere curve for increasing Re thereafter. This is in agreement with Meisse's results and the increase in the drag coefficient is attributed to changing drag due to drop distortion. The Surface Tension group is a measure of the surface tension force preventing distortion and large drops tend to adopt a fying saucer shape and C_D then takes values close to those for discs which are higher than those for spheres.

The standard solid sphere drag curve by Smith (170) compares well with the more commonly used curve by Lapple and Shepherd (103) and has the advantage of being easily expressed mathematically. The drag coefficient group $\Pi = C_D(Re/24)^2$ is a function of the cube of the drop diameter only, while the drag coefficient C_D is proportional to the drop diameter and inversly proportional to the square of the terminal velocity. The good agreement of the present study free-falling drop results with the

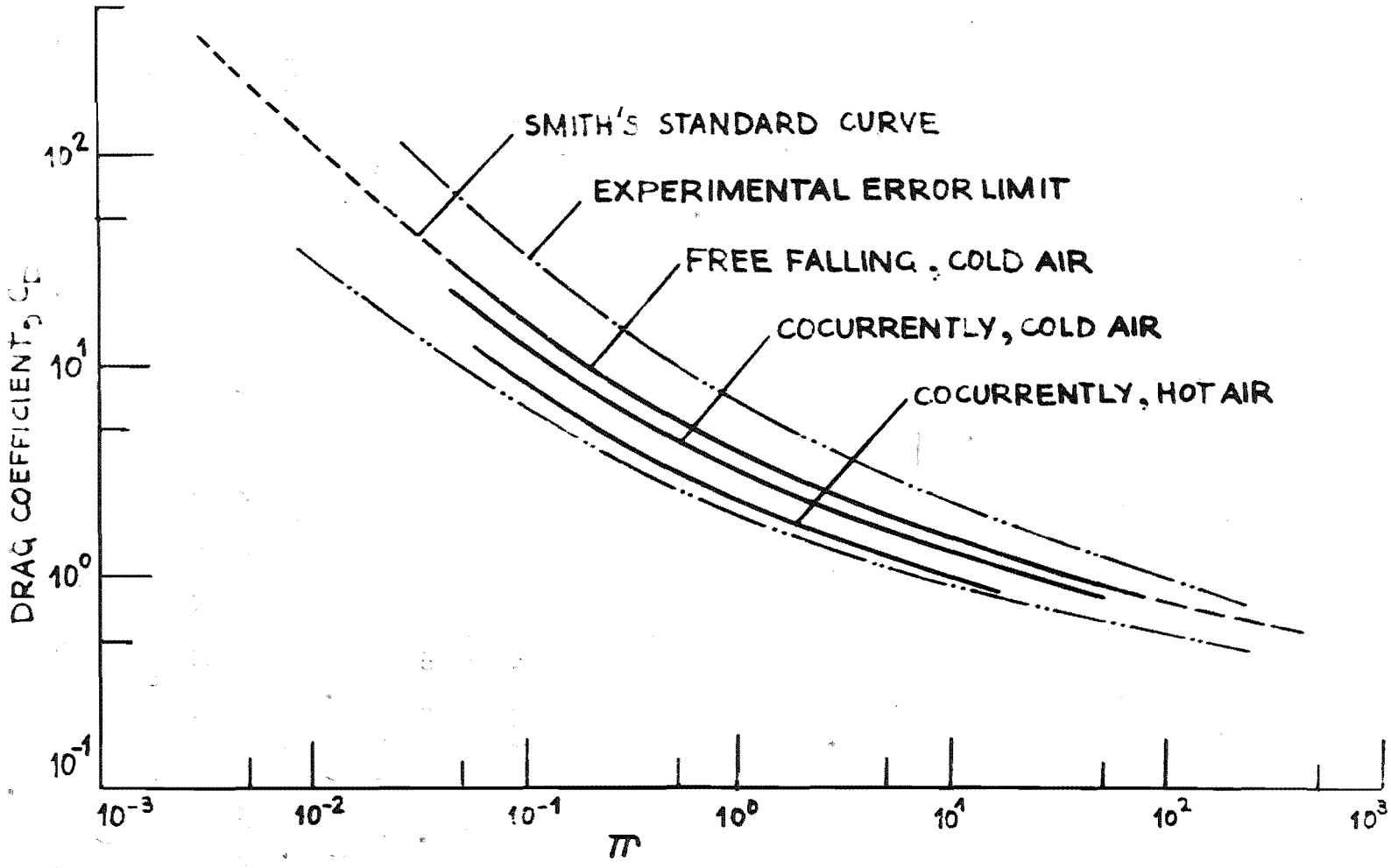

FIGURE 5.11 DRAG COEFFICIENTS FOR WATER DROPS MOVING IN AIR.

standard curve was shown in figure 5.5 where the terminal velocities according to the different equations were compared. The poor agreement shown by the expression for terminal velocity given by Schlunder (161) presumably results because he uses an expression combining the results from the Stokes' and Newton's law regimes. His expression could be used for Reynolds numbers less than 10 say and may give better agreement for much larger values in the Newton's law region for $Re > 10^3$.

All three graphs showing <u>all</u> experimental drag coefficient results for the respective flow conditions (cold-free falling, cold-cocurrent and hot-cocurrent) indicate some values outside the experimental error limits, even when these limits are drawn about the computer smoothed curve rather than the solid sphere drag curve. It was thought that this could be a deceleration effect and the maximum discharge velocity at the nozzle was calculated which could be permitted for a drop of 300 μ and still allow the drop to attain a quasi-steady terminal velocity at the point of photography, 12 feet below the nozzle. The calculations were based on the various empirical formulae and graphical methods given by Sjenitzer (167), Lapple and Shepherd (103) and Marshall (121). The results indicated that even with the maximum cocurrent airflow down the column (15 fps) the residence time of the drop in the column would be sufficient for the attainment of the terminal velocity relative to the air. (This was assuming a constant drop diameter.) The residence times were calculated for $B \sim 0.05$ to be between 0.5 and 1.2 seconds with, for example, an allowable discharge velocity at the nozzle of 800 fps if gravity was neglected. For the pressure nozzle the discharge

velocity was calculated to be between 90 and 160 fps (181). It was concluded that at the point of photography the drops should have reached their quasi-steady terminal velocity relative to the moving airsteam.

Comparison of the results for the drag coefficients of the examples of the free falling and cocurrently entrained droplets, both moving in cold air(figures 5.5 and 5.6), showed the latter results to take drag coefficient values slightly less than the solid sphere standard curve. This suggested an effect due to the cocurrently entraining airflow and was presumed to be a turbulence effect. However for the range of turbulence intensities and integral scales measured, no distinguishable effect of either turbulence parameter could be discerned. The integral scale to drop diameter ratios were large and far bigger than the optimum ratio required for resonance between the energy-containing eddies and the shedding frequency of the mean drop as described in section 4. At the same time, the longitudinal level of turbulence intensity was never less than 7% and yet the depression of the drag coefficient below the solid sphere standard curve persisted even when all drag coefficients were plotted as shown in figure 5.9. The fact that for cocurrently entrained drops in cold air, the computer smoothed curves took nearly identical values below the standard curve, suggests that there is a turbulence effect but that it occurs at a lower level of intensity (less than 7%). This pattern of behaviour follows that reported for heat-transfer for cylinders (194) and spheres (146), where the significant rate of increase of the Nusselt number (for the same Re) due to increasing turbulence intensity occurred for the range 0 to 2%. The rate of increase was less sharp

for intensities greater than this level.

No reports on the effect of free stream turbulence on the drag of droplets moving cocurrently in a turbulent airstream are available, although drag coefficient results obtained for such systems are available (39, 80, 145). For single solid spheres a moderate turbulence intensity is reported to cause a relatively small increase in the drag values and at sufficiently high disturbances there is a sharp drop in the momentum transfer and then an increase up to values which lie below the standard curve (188). The sharp decrease occurs at the critical Reynolds number and Torobin and Gauvin (188) have theoretically shown this number to decrease with increasing free stream turbulence intensity. They also confirmed the result experimentally and showed that at a drop Reynolds number of 400 for example, intensities in excess of 40% would be required to precipitate a reduction in the drag coefficient. Although Torobin and Gauvin conclude that such reductions are not likely to occur at Reynolds numbers below 200, non-random vorticities of a suitable type may cause a reduction in drag to occur at Reynolds numbers as low as 30 (2).

In cocurrent flow systems, the boundary-layer and wake of an entrained particle can be subjected to very high relative turbulence intensities even if the free stream level is a moderate one. Consider the terminal velocity results of Run B4 shown in figure 5.3. The cocurrent air velocity was 6.73 fps and the turbulence intensity 12%. For water drops of 100, 400 and 800μ in diameter, the terminal velocities were 0.7, 5 and 10 fps. Assuming that its inertia is such that it does not have a

fluctuating motion, the boundary layer and wake of the drop will be generated by the relative movement equal to the drop terminal velocity, and the relative disturbance to this flow will amount to intensities of the order of 100, 17 and 8% respectively. In fact because of the large amount of kinetic energy associated with this fluctuating component, compared with the kinetic energy of the mean relative motion, it would no longer be proper to consider the former as being merely a disturbance which is superimposed on the latter. Very high relative intensities introduce a new complication because their action would cause particles of small inertia to have a fluctuating motion of their own. This motion can be described by an acceleration modulus ($\mathring{U}_p D_p / U_p^2$) and the total drag coefficient has been shown to increase with increasing values of the modulus (25).

The indicated decrease in drag for cocurrently entrained drops could then be the result of high relative intensities producing a low value of the critical Reynolds number and so a reduction in the total drag on the drop. At the same time, the fluctuating motion of a drop described by the acceleration modulus probably occurs and so increases the drag coefficient. For the experimental drop Reynolds number range from 1 to 100. and for turbulence intensities from 7 to 24%, the combined result of these two proposed flow effects is a slight overall reductioh (10 to 15%) in the drag coefficient for cocurrently entrained drops.

The drag coefficient result examples shown in figure 5.5, 5.6 and 5.7 and summarised in figure 5.8 suggested that in addition to a decrease in C_D below the standard curve because of a turbulence effect, these was a further reduction due to a mass-transfer effect. The drag coefficients shown in

figure 5.7 were the measured values C_D^* corrected for the mass efflux from the surface of the evaporating droplet. The uncorrected values were approximately 4% higher and so closer to the standard drag curve but still falling below the values for cocurrently entrained drops moving in cold air. Again, as with the cold cocurrent air case, no discernible trend with either turbulence parameter was observed although the depression of the coefficient below the standard curve persisted when all drag results for evaporating drops ($B \sim 0.04$) were considered as shown in figure 5.10.

Such a reduction in the drag coefficient due to thinning of the boundary-layer by the vapour efflux associated with intense mass-transfer conditions was reported by Eisenklam et al. (39) for evaporating droplets. They found the Mass Transfer number B to be a good criterion for assessing the effect of mass-transfer on heat-transfer and the boundary-layer correction to the momentum coefficient $C_D = C_D^*(1+B)$ best correlated their results. From this agreement with theory they concluded that the bulk of the drag reduction was due to the momentum of the effusing vapour and that the streamline flow around the drop is not altered much even at high transfer rates. Clamen and Gauvin (19) used fairly large cellite spheres impregnated with liquid sulphur dioxide and injected cocurrently into the airstream. They found an effect of mass-transfer on the drag coefficient and concluded that besides the coupling effect of momentum-, heat- and mass-transfer, the vapour efflux reduced the drag by two possible means. Firstly, by reducing the skin friction of the turbulent boundary-layer

on the sphere and secondly, by increasing the pressure in the wake behind the sphere presumably because of mass accumulation. This latter effect is probably not as significant in the present study Reynolds number range as it was in their study about $Re \sim 10^4$.

Figure 5.11 was an approximate summary of all the present study results and showed the average values of the drag coefficients for the three flow regimes to fall within the experimental error limits about the standard drag curve for solid spheres. The evaporating drop coefficients were still slightly less than the cold cocurrently entrained drop values even when the former were uncorrected for the mass efflux effect. The correction was about 4% for the results of 4 runs and one other run with a Mass Transfer number of 0.01 was completed and these results lay between the cold cocurrent and the hot cocurrent ($B \sim 0.04$) results. This suggested that qualitatively the Mass Transfer number correction (1+B) is correct. It must be remembered that the definition includes a <u>mean</u> film property C_{pf} and the present study results follow Downing (33) in assessing the physical properties of the film at the volume average film temperature and composition between the drop surface and the free stream flow. Eisenklam et al. (39) used the arithmetic mean and for the present study this would give larger values of B (5 to 6%) and so the uncorrected drag coefficients C_D for evaporating drops would be closer to the standard curve.

A comparison of the approximate smoothed curves representing present study results with reported drag coefficient values for drops and evaporating spheres is shown in figure 5.12. The data of Eisenklam et al. (39)

for free falling evaporating drops, Buzzard and Nedderman (18) for accelerating drops in cold air, Ingebo (80) for accelerating spheres and drops in cold and hot air, Rabin et al. (145) for accelerating evaporating droplets, Fledderman and Hanson (43) for evaporating cocurrently entrained sprays of drops, Clamen and Gauvin (19) for cocurrently entrained evaporating spheres and Lihou (111) for large free falling water drops in cold air, are compared with the standard solid sphere drag curve of Smith (170), Stokes' Law (178) for the creeping flow region, and the results of the present study.

Evaporation rates and drag coefficients for evaporating drops falling freely in hot air were obtained by Eisenklam et al. (39) for drops in the Reynolds number range 0.01 to 40. Most of their experiments were carried out in the unsteady portion of the drop flight but the maximum acceleration experienced by the drop was small enough for the effect on drag and mass-transfer to be neglected (188). Their results, uncorrected for mass transfer ($B \backsim 0.09$ for water to $B \backsim 3.0$ for volatile organic solvents), fall about the standard curve for Reynolds numbers above 10.

The curve of Lihou (111) agrees with the standard drag values at $Re \backsim 10^3$ and tends to larger values as the Reynolds number increases. This is in agreement with Meisse (126) and the deviation is described by the Surface Tension group Su.

Ingebo (80) reported data for the acceleration of small droplets and solid spheres injected as a cloud into an airstream moving with velocities of 100 to 180 fps with temperatures from 40 to 700 F. The particles had

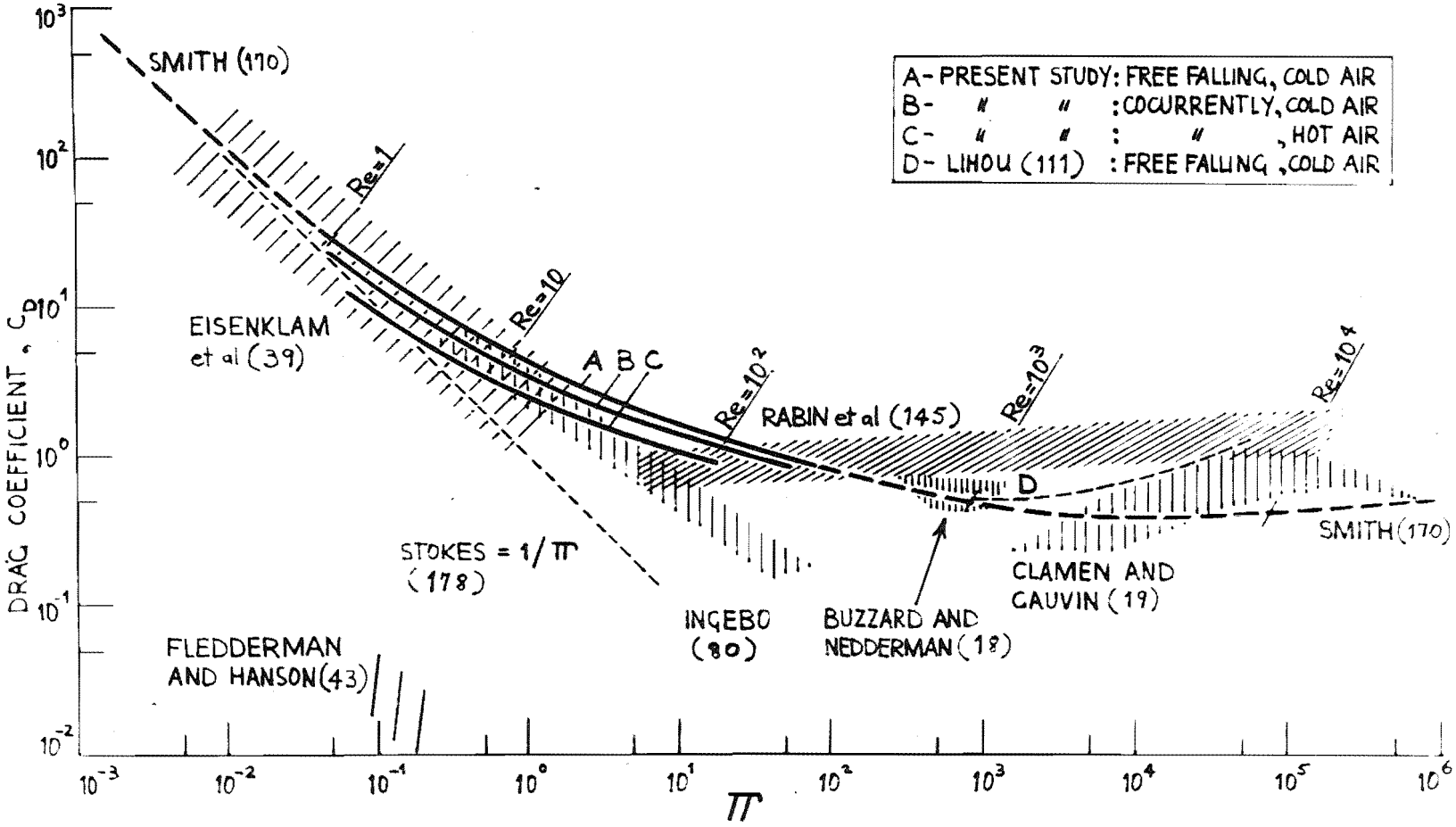

FIGURE 5.12 DRAG COEFFICIENTS FOR DROPS AND SPHERES MOVING IN AIR. REPORTED DATA FOR THE C_D GROUP Π OVER THE RANGE $10^{-2} < \Pi < 10^6$.

large accelerations and their velocities were measured at fixed stations downstream from the injection point. Surprisingly all data, regardless of the acceleration magnitude, the evaporation mass-transfer effect or whether they were obtained for solid or liquid particles, fell on the single line given by the equation $C_D = 27/Re^{0.84}$, for the entire Reynolds number range from 6 to 500. The particle drag was not affected by the presence of other particles since a ten-fold increase in their concentration did not bring about any significant alteration of their velocities.

A similar investigation was carried out by Fledderman and Hanson (43) using a photographic technique to observe evaporating spray droplets entrained and accelerating in airstreams moving from 50 to 70 fps. The droplets had Reynolds number from 20 to 100 and their data shown in figure 5.12 indicated a clear dependence on the air velocity unlike those given by Ingebo. The results are surprisingly low, at times representing a decrease of 1,000% from the standard drag coefficient curve. Fledderman and Hanson felt that this was due to evaporation occurring at the droplet surface, but this is doubtful when Ingebo's work and other data shown in figure 5.12 are considered. The droplet velocity data may have been in error since they were not obtained directly but were derived from Frössling's mass-transfer equation (48).

The large difference between the data of Ingebo and those of Fledderman and Hanson remains to be explained, as well as the complete contradiction between these results which indicate a reduction in drag as compared with the increase caused by acceleration reported in other works,

such as Rabin et al. (145) and Buzzard and Nedderman (18) shown in figure 5.12. Ingebo's data are complicated by the presence of an unspecified amount of free stream turbulence and by some uncertainty as to the accuracy of the fluid velocity determinations. The fluid turbulence intensity in Fledderman and Hanson's test section was of the order of 2% (measured in absence of droplets) and it may be that the disagreement between the two works reflects a reaction to varying relative intensities and scales of turbulence which become significant when cocurrently entrained drops move in air streams of high velocity.

The picture is further complicated by a reanalysis of Ingebo's work by Mercier (128), according to which the coefficients A and B of Ingebo's equation $C_D = A/Re^B$ are not equal to 27 and 0.84 respectively as reported by Ingebo but vary widely, A having values ranging from 16 to 75 and B ranging from 0.5 to 2. Although Mercier's analysis seems to fit Ingebo's results it may be that the results are subject to systematic errors (as was suggested by Ingebo himself) and secondary effects such as acceleration.

Buzzard and Nedderman (18) obtained results for drag coefficients of liquid droplets accelerating through air. They discussed acceleration, deformation and internal circulation effects on the drag of a droplet and found the drag coefficient of accelerating spheres not to differ significantly from non-accelerating spheres. They therefore concluded that the drag coefficients for accelerating droplets would equal those for droplets moving at constant velocities. In figure 5.12 their results lie about the standard drag curve and they also reported that the drag coefficient was very sensitive to minute quantities of

surface active agents.

The sensitivity of the drag coefficient to surface active agents in the liquid droplets is related to the reduction in skin drag that occurs when the drop is circulating. Velocities in drops measured by dark field particle trace photography (76) show a slow decay and change in circulatory pattern with the accumulation of minute quantities of surface active agents. These tend to migrate to the rear of the drop and form a mono-molecular cap.

Investigating the displacement and shattering of propellant droplets, Rabin et al. (145) found the drag coefficients for accelerating drops to be greater than the standard drag curve values for Reynolds numbers above 200. Their results cover a wide range of Reynolds numbers and they report a decrease in the drag with increasing mass transfer rate.

Clamen and Gauvin's results (19) are shown in figure 5.12 as a crescent which crosses the standard drag curve. They found mass transfer to decrease the drag on a sphere and also to reduce the influence of the free stream turbulence. No effect of the acceleration rate or the scale of turbulence was discerned. Their results were for the turbulence intensity range from 5 to 30% and for sphere Reynolds numbers from 2×10^3 to 3×10^4. The upper boundary of the crescent shown in figure 5.12 represents the turbulence level of 30% while the lower boundary is for 5% intensity. For large mass transfer rates they report a modification of the critical Reynolds number but conclude that the general shape of the drag curve for evaporating spheres is similar to that for non-evaporating particles

indicating that the same overall mechanism governs the transition process for both cases.

The reduction in drag by mass-transfer for small vapour concentrations at the drop surface, is given by Clamen and Gauvin (19) as $\Delta C_D/C_D = -0.28\ C_s/Sc^{\frac{2}{3}}$ where C_s is the mass fraction of vapour at the surface. The relation is defined for the boundary conditions $C_s/Sc^{\frac{2}{3}} < 0.1$ and $Sc \geq 1$. For $Sc \backsim 1$ and $C_s \backsim 0.1$ the reduction in C_D is about 3% which is not significant and is of the same order as the correction obtained using the Mass Transfer number relation $C_D^* = C_D(1+B)$. These workers suggested as a fundamental variable the mass-transfer parameter $(U_w/U)Re^{\frac{1}{2}}$ used to describe the effect of the "blowing velocity" of the effusing vapour normal to and at the surface of the sphere, on the boundary layer about the sphere. $U_w = \dot{m}/\rho_w A_p$. A similar "blowing velocity" effect was discussed by Galloway and Sage (55) where smaller temperature and concentration gradients resulted because of the increased boundary layer thickness. At very high blowing rates the boundary layer separates from the surface and gives rise to pressure gradients normal to the surface. In the present study the drag reduction due to mass-transfer was not expected to be large as values of the "blowing velocity" were small.

In figures 5.12, the three curves from the present study overlap many of the previously reported data. These data each show a considerable range of scatter as indicated by the shaded limits in the figure. The present results also have large experimental error limits which increase at lower values of the drag coefficient group Ψ. It will be noted however, that some results for cocurrently entrained

droplets are reported with drag coefficients far outside the error limits. Variations of at least an order in the coefficient are discernible at Re ~1. Now the turbulence is a root-mean-square measure of the velocity fluctuations and the peak velocity will be $\sqrt{2}$ times this. At low Reynolds numbers this fluctuation is of the same order as the relative velocity of the cocurrently entrained drop itself. That is, it experiences a relative turbulence intensity of the order of 100%. This results in a large scatter of drag coefficients measured by the double-flash technique, for there is a range of possible coefficients depending on the relative fluctuating velocity at the moment of photography. As the relative velocity increases, the range of possible coefficients decreases until at Re ~ 100, the data are well correlated by a single curve within the experimental error limits.

It is for this reason, that in spite of highly sophisticated particle-tracking techniques (19, 39) results are still reported with scatter which cannot be attributed to instrumentation errors (6, 18). Recent work on droplet behaviour close to a hollow cone pressure nozzle (127) has shown how unpredictable the behaviour of very small droplets is ($D_p < 120\mu$). While larger drops on fragmentation approach the liquid-sheet velocity, smaller drops may fall at any velocity between that of the sheet and that of the cocurrent airstream. The smaller drops are ejected in many directions but the larger droplets tend to move in the sheet direction. In a spray, it is the small droplets that evaporate with intense mass transfer conditions and such drops are now being credited with indeterminate flight trajectories. This is an effect which has not been

considered in spray evaporation studies before.

In reviewing all the data presented in figure 5.12 it is apparent that for drops cocurrently entrained in cold or hot air, most results for Reynolds numbers less than 100 give drag coefficient below the stnadard curve and for Reynolds numbers greater than 100, values above the standard curve. The present study results indicate that there is some turbulence effect and some mass-transfer effect, and that the latter is reasonably allowed for by the boundary-layer mass-transfer correlation. The uncertain effect of high relative turbulence intensity effects occurring for drops cocurrently entrained in high velocity airstream is a complicating factor and for general use the standard drag curve for solid spheres can be considered to adequately represent the behaviour of liquid droplets, at least for values of the drag coefficient group up to 10^3. The warning by Torobin and Gauvin (188) about the inadvisable use of published drag coefficients for cocurrent flow systems and the unwarranted estimation of drag coefficients to a second figure for a given situation in the transition region, is obviously well founded.

5.7 Conclusion

Drag coefficient data for free falling droplets and droplets cocurrently entrained in cold and hot air were obtained for distilled water drops moving at quasi-steady terminal velocities. Drop sizes and velocity data were obtained using a double-flash photographic technique which was developed and reliably calibrated.

Free-falling water drops moving in still cold air were found to experience the same drag as solid spheres. The

solid sphere curve used to describe this behaviour was correlated by Smith (170) and is a function of the drag coefficient group, $\Pi = C_D(Re/24)^2$. The standard curve equation is

$$C_D = \frac{1}{\Pi} + \frac{2.69}{\Pi^{0.310}} + \frac{\Pi^{0.36}}{(1.8\,\Pi^{0.36}+77)} \qquad (5.12)$$

Cocurrently entrained drops moving in cold turbulent airstreams have drag coefficients only slightly below the standary drag curve for turbulence intensities from 7 to 24% over drop Reynolds number range from 1 to 100. For cocurrent entrainment in hot air, with intense mass-transfer, the drag coefficients were still further reduced, but the use of the mass-transfer correction based on the boundary-layer theory by Eisenklam et al. (39) reduces the deviation from the standard curve. All cocurrent drag data could be correlated without reference to the scale and intensity of turbulence and the decrease of the drag coefficients below standard drag curve values, both as a turbulence and a mass-transfer effect, can only be described qualitatively and for the present study was small.

For a general description of the behaviour of moving liquid droplets, the standard drag curve for solid spheres can be considered adequate and it is recommended that this curve be used for spray evaporation studies and on spray-drier design methods. For Reynolds numbers of the order of 100 and less, turbulence effects on the drag coefficient do not appear significant and the intensive mass-transfer effect of the vapour efflux from the evaporating drop surface can be resolved with the correction based on the

boundary-layer theory (39).

Results for the cocurrently entrained drops, with and without intensive mass-transfer, showed scatter beyond the experimental error limits. This was concluded to be the result of the generation of high relative turbulence intensities which are peculiar to cocurrent gas-particle systems. Because of the large scatter in the present results and also in previously reported drag studies, the comments of Torobin and Gauvin (188) are considered to be well founded.

> " ... that experimental observations will have to be relied on for any useable information on drag coefficients in cocurrent systems and that the estimation of the coefficient to two significant figures for a given situation in the transition region would not be warranted since the phenomenon is not well fixed, and a variation in results does not necessarily reflect an error in observation. Even the use of the standard drag curve for drag estimation to the second figure for bodies moving freely at steady state in a laminar fluid outside the Stokesian region is not valid."

When high relative turbulence intensities exist in a cocurrent gas-particle system, a great number of experimental measurements must be made, as many data will not be recorded at the mean fluctuating particle velocity. The measurement of this mean velocity is then a question of probability and the use of the standard drag curve by Smith (170) is recommended to avoid tedious experimental studies that may

not be of much value when concluded.

6. EVAPORATION OF SPRAYS

6.1 Introduction

The most important problem in spray drying is the mechanism of the evaporation of sprays. This mechanism is affected by the boundary conditions such as the turbulence and high temperature of the drying gas, and the mechanics of the falling drops. In the earlier sections, a turbulence intensity and scale effect on the evaporation of a held droplet was reported and a minor influence on the drag coefficient for moving drops due to both the turbulence and the vapour efflux from the surface of the evaporating droplet, was found. To complete this study of the effect of turbulence on the evaporation rates of drops and sprays, the influence of turbulence on the evaporation of whole sprays was investigated, making use of the results from the preceding sections.

The theoretical and experimental studies of transfer to drops have generally been attempted for drops falling freely in a still atmosphere or fixed in position, usually behind grids generating nearly isotropic turbulence in the moving airstream. The majority of practical applications include polydisperse sprays of drops entrained in a turbulent fluid and the fluid-dynamic conditions are rather different from those for free-falling and held droplets. To predict the behaviour of an evaporating drop, the drop velocity and the drag forces acting on the drop (as determined by the magnitude of the mass-transfer rate and the turbulence parameters of the entraining airstream) need to be accurately defined. To predict the behaviour of an evaporating poly-disperse spray, the additional effects of droplet interaction

at moderate spray concentrations, the spray/continuous phase interaction and the range of sizes of the droplets of the dispersion, must also be considered. It is this last effect which greatly complicates the application of single drop evaporation results to evaporating spray systems and has made it necessary to rely largely on experimental results from pilot-scale equipment for spray drier design.

In a spray drier the atomiser produces a spectrum or distribution of drop sizes and consequently the drops evaporate at varying rates depending on their initial diameter. The small droplets evaporate first and any exceedingly large drops will require drying times much greater than average. These large drops then constitute the controlling time in the drying process. The influence of turbulence appears to be greatest when the scale to drop diameter ratio is less than unity. When the scale of turbulence is much larger than the drop size the drop should feel only a steady motion but this depends in part on the relative intensity of turbulence especially for cocurrent spray systems. Because of the distribution of drop sizes in the spray some drops may have scale to diameter ratios less than unity and so will experience a significant turbulence effect, while other drops with much smaller or much greater than average diameters will experience little or no turbulence influence. In fact, as the drops evaporate and their diameters change with time, the turbulence effect may become significant over some part of the total drying path.

The problem of estimating the total evaporation time for a spectrum of drops is complicated then, by the

different drying paths taken by drops of different initial diameter. Information on the drop-size distribution created by the atomiser is therefore important and is also the property most difficult to predict theoretically and determine experimentally. Most correlations for heat-transfer in the evaporation of sprays are based on either a mean drop size or evaluated by a "step" method for a series of drop size ranges. It is therefore important that the size distribution of a spray be determined as accurately and simply as possible.

6.2 Previous Work

Although heat- and mass-transfer for each individual drop in a spray is similar to that of a moving single drop, it is very difficult to provide a correlation for the whole spray because of the variation of drop sizes in the spray. The drop-size distribution of sprays produced by atomisation may be concisely represented mathematically by a distribution function and two parameters, one of which is a mean diameter of some kind and the other a measure of the dispersion of the spray, or the deviation from the mean. In some instances it may prove convenient to introduce other parameters, such as maximum and minimum drop sizes (121).

Various kinds of mean diameters with different physical meanings and applications have been reported (121, 143) and Mugele and Evans (131) have tabulated the various types of mean diameters which may be required for different applications. Theoretically, all the various mean diameters may be computed from the expression for the frequency-distribution curve of the spray, if a suitable function can be established. The mean diameters can also be determined directly from experimental data where it should be noted

that certain methods of particle-size analysis automatically give certain types of average diameters directly: microscopic counts usually furnish number averages, sedimentation and impaction methods give volume or mass averages, and light-absorption methods give surface averages.

The average or median diameter of a spray is that diameter which divides the spray into two equal portions either by number, surface area, or volume or mass. Median diameters are usually established from the 50% point on the cumulative plot although they can be calculated if the mathematical expression of the frequency-distribution curve of the spray is known. Bevans (11), Mugele and Evans (131) and Thomas (187) have presented discussions of mean diameters, distribution functions and variance as applied to droplet statistics and Marshall (121) has produced a comprehensive review of reported distributions for spinning disc, pneumatic and pressure nozzle atomisers. The principal conclusion of all these studies appears to be that spray-droplet size distributions should be presented in each case by the best empirical representation obtainable. Until atomisation mechanism can be suitably related to one or more distribution functions, there seems to be no theoretical justification for expecting that one function should be generally superior to another.

In spray evaporation studies the drying process is usually described as a change in the average or median drop-size of the spray and this value is obtained either from the experimentally determined drop size distribution or from a mathematical function describing distributions

found for the same type of atomiser. The available data on the evaporation of sprays of drops can be grouped into three classes. First, there are purely analytical approaches, second are the experimental investigations for the case of no relative motion between the drops and the drying gas, and finally there are correlations presented for the case where there is relative motion between the evaporating droplet and the gas.

6.2(a) Theoretical Correlations

Ruckenstein (155) has developed equations for evaluating the mass-transfer coefficient in the continuous phase from a bubble or drop in a group of drops. She provides solutions for the two cases of the drop Reynolds number greater or less than unity. The effect of interaction between particles in a group or cloud is shown in that the Sherwood number is dependent in part on the volume fraction of the continuous phase. In spray drying, this voidage effect is generally negligible (46, 140).

A series of equations for calculating the paths taken by particles undergoing accelerated motion, taking into account the fluid friction, have been developed by Lapple and Shepherd (103). The results predicted by the equations showed good agreement with the experimental results of their short study on spray crystallisation.

An example of the cocurrent spray drying of a solution was given by Meisse (126) in his theoretical study of the ballistics of evaporating droplets. An allowance for the remaining spherical shell of crystallised residue was made and for low evaporation rates an equation relating the evaporation process to the initial droplet diameter was determined. Probert (143) made a mathematical analysis

of the variation of the size distribution in a fuel spray which was assumed to follow the Rosin-Rammler distribution function (152). Assuming no relative motion, the simple expression for the heat-transfer coefficient was used and equations for the variation of the mass median diameter with time under various conditions of spray uniformity were derived. From his calculations he concluded that a spray with a narrow size distribution and a small mass median diameter would evaporate completely in a shorter time than would a spray with a wide size range and a large mass median diameter.

A theoretical method for calculating the complete evaporation history of a spray of liquid which was injected into a stream of gas was presented by Sjentizer (167, 168). The size and location of the droplets can be found at any moment during the entire evaporation process using values of the gas velocity, pressure and temperature and the initial drop size distribution. The formulae are based on Frössling's (50) evaporation equation and the drag coefficient data of Ingebo (88). Examples are given showing the calculation of the time of evaporation, the path length and the critical Reynolds numbers for the drop size range of the spray, both during the period when drops accelerate immediately after formation at the atomiser and also during the second period when the drops fall at a constant velocity.

Marshall (120) has proposed a step-by-step method for calculating the time of evaporation of a pure liquid spray of a known size distribution. The procedure consists of calculating the change in mean drop diameter of selected mass fraction increments of the spray over short intervals

of time on the assumption that all drops evaporate under the same constant temperature conditions for the same time interval. This approach has been confirmed experimentally by Dlouhy and Gauvin (30) for the drying of "lignasol" solutions under cocurrent conditions. For the evaporation of a spray with no relative motion, Marshall showed the mass mean diameter of the spray to increase with time because the very small drops evaporated much more rapidly than the larger drops. This shows that sprays with large drops will not dry completely in small towers and emphasises the need to design a drier for the largest drops in the spray. The step-by-step method has the disadvantage that, for reasonable accuracy, a lengthy set of calculations have to be carried out, although modern computing techniques reduce this burden somewhat.

Gluckert (63) has proposed an alternative method of calculation based on the maximumdrop size and he has applied it fairly successfully to the drying of sodium sulphate solutions in well-mixed (stirred) systems where uniform drying conditions are obtained throughout the drying chamber. His correlation makes use of the many studies of the individual factors involved in the process of spray drying (Appendix 1) and assumes a Nusselt number of two. In the spray drying of solutions, a constant drop diameter is used on the assumption that a surface shell of crystallised product forms (38,147). The rate of heat-transfer to sprays is given for the three main types of atomisers as a function of the maximum drop diameter which is defined as being three times the Sauter mean drop diameter. Gluckert's approach suffers from the disadvantage that it is difficult to estimate the "true" maximum drop size of a spray (65).

After reviewing the basic principles underlying the evaporation of liquid drops with a solids content, a simplified method of calculation was proposed by Dombrowski and Johns (31) for determining the overall preformance of cocurrent and well-stirred spray driers. They assume that the droplets move with the velocity of the gas stream and found their calculated drying times to compare favourably with the limited experimental data available in the literature. The mean spray droplet diameter chosen is the linear–volume diameter and they show that this mean diameter remains approximately constant during most of the evaporation process. The time taken for the first 90% of the liquid mass of the spray to evaporate is shown to be small compared with the total time taken for complete evaporation and the drying time of a spray is also shown to be directly proportional to the square of the mean drop size. It is then essential to know, with some accuracy, the dropsize distribution of the spray to be dried in the drying chamber.

6.2(b) Experimental Correlations With No Relative Motion

Dlhoughy and Gauvin (30) studied the evaporation of a spray of water drops in a cocurrent spray drier. They commented that the high relative velocities between the drops and the air (as reported in nozzle zone spray evaporation rate studies (117) and for fuel atomiser nozzles (13)), masked the effects due to air turbulence so that the results could not readily be applied to the main evaporation zone of a spray drier.

The rate of evaporation was calculated directly either from a heat- or material-balance for the evaporating drops. For accurate calculation of the

instantaneous heat-transfer coefficients an equation was derived on a differential basis because of the continuous variation in the values of the variables involved in the system. From this and other equations, the instantaneous values of the heat-transfer coefficient could be readily calculated. The results were calculated using arithmetic film properties and indicated that the rate of evaporation during spray drying could be safely calculated by assuming the individual droplets of the spray to evaporate at a rate corresponding to stagnant conditions.

A similar result was obtained by Kessler (91) who showed for drops in the same diameter range as Dloughy and Gauvin, that the effective relative velocity between the drops and the drying gas was practically zero. The rate of evaporation could then be calculated using a value of two for the Nusselt number.

In an investigation of the atomisation of liquid sulphur as a means of introducing the feed material to burners, Conroy and Johnstone (21) studied the time required for at least 99.9% of the spray to evaporate. The transfer rate equation based on a value of the Nusselt number equal to two, was integrated in a stepwise method with all quantities evaluated at the drop temperature except the thermal conductivity of the gas film, which was based on an average film temperature. The time of evaporation of a sulphur spray was described by a simple equation relating the initial mean drop size and the temperature of the gas, and good experimental agreement was obtained.

A computational study of the evaporation rates of sprays of pure liquids was completed by Dickinson and Marshall (27). Their study was in two parts: 1) for drops

having negiligble velocity with respect to the air, and 2) for drop velocities large enough to affect the evaporation rate. The principal parameters considered were the mean diameter and the initial drop-size distribution of the spray, the initial temperature difference and mean drop velocity, the ratio of the air to spray and the air velocity.

For sprays with low or negligible velocities Dickinson and Marshall found those with less uniform drop size distributions to evaporate more rapidly in the initial period than more uniform sprays with the same mean diameter, because of the many small drops which evaporate at higher rates. However, the less uniform sprays took much longer for complete evaporation since there were more large drops which evaporate slowly. Because of the different evaporation times required for sprays with different distributions but with the same Sauter mean diameter, they consider that no mean diameter can adequately characterise a non-uniform spray and a distribution or dispersion parameter must be taken into account. Such a dispersion or spray uniformity coefficient changes during evaporation. A general tendency for the average diameter of the remaining drops to increase in non-uniform sprays and to decrease in more uniform sprays as evaporation proceeds was reported. At the same time, the temperature of the drying gas falls and the evaporation rate decreases unless the air rate is infinitely great.

6.2(c) Experimental Correlations With Relative Motion

In determining the rate of heat- and mass-transfer for a spray in a cocurrent drier, Bose and Pei (14) reported that the relative motion of the drops was

significant. This work was the result of an attempt by these workers to extend the work of Kessler (91) and Dloughy and Gauvin (30) in evaluating the heat- and mass-transfer coefficients for drops in a spray drier when the droplet sizes compare with those used in some industrial applications. Their results showed the evaporation rate to follow the Ranz and Marshall (147) correlation and also indicated no turbulence effect.

Manning and Gauvin (117) investigated rates of heat- and mass-transfer in the nozzle zone of water sprays. Using the results of York and Stubbs (205) which showed that the drop velocity depended on the radial position of the drop in the spray chamber, they found the Nusselt number to be correlated by the Ranz and Marshall (147) equation. A step-by-step method like that of Marshall (120) was used and took into account the changing drop size and velocity. A marked effect on the evaporation rate by increasing the feed temperature was reported. They suggested that an increase in turbulence intensity might result in an increase in the heat-transfer rate, but found the effect to be small for the range of droplet Reynolds numbers encountered.

Spray evaporation in a high temperature environment was studied by Hoffman and Gauvin (75) who discussed the applicability of the Ranz and Marshall (147) equation and the modifying factors to be used for intense mass-transfer conditions. Feder (42) has prepared a series of charts predicting the rates of evaporating using the empirical relationship between droplet diameter, liquid spray residence time and the fraction of spray unevaporated, plus the four operating variables of the spray boiling point, the velocity

of the drying air, the air temperature and the air pressure.

In the second part of their computational study on spray evaporation, Dickinson and Marshall (27) compare the evaporation of sprays with appreciable relative velocity to the results for zero velocity sprays. They found that the distance travelled by the spray to achieve a given degree of evaporation was much greater and for a given high initial velocity, the relative error in neglecting the drop velocity effect is greatest for small drops. These smaller drops decelerate for a considerable part of their total evaporation path. For small drops produced by the more common atomisers, the usual assumption that they will reach terminal velocity almost instantly is then not generally valid. The study was limited to pure liquid drops remaining at a constant drop temperature and the velocity effect was more significant at higher initial velocities and with higher temperature differentials.

An experimental study of the effect of turbulence and air velocity on the rate of evaporation of a fuel spray was reported by Fledderman and Hanson (43). They assumed a Nukiyama-Tanasawa distribution function for the spray (135) and measured the velocity, and intensity and scale of turbulence with a hot-wire anemometer. The form of the Ranz and Marshall (147) equation was reported to be correct but for sprays of highly volatile liquids they suggest that a different value be given to the empirical constant term. Fledderman and Hanson concluded that an increase in turbulence intensity increased the spray evaporation rate and that this effect did not appear to work through the Reynolds number but was due rather to an increase in the diffusing coefficient. Although they

could not separate the scale from the intensity effects they considered that there was the same trend of increasing evaporation with turbulence scale. The turbulence of the entraining air tended to broaden or increase the drop-size distribution uniformity coefficient and a strong dependence of the evaporation rate on the air velocity was noted, as shown in their drag coefficient results in figure 5.12.

Schlünder (161) has presented an extensive study on the drying of held single drops and falling spray clouds. He considers the drying process of falling single drops under constant air conditions as well as the drying process of falling spray clouds under constant and variable air conditions. This latter theoretical study uses the particle size distribution data of other workers and he provides for an induction region and a coalescence zone close to the nozzle. For spray drying under varying air conditions, a solution is possible if the variations of the air conditions are expressed in a form which is related to the distance of fall of the sprayed drops in a cocurrent drier.

One of the few equations found in the literature on heat-transfer in spray driers is that of Luikov (114) who defined a volumetric heat-transfer coefficient by the equation

$$h = 1.58 \times 10^{-3} \left(\frac{kw}{\rho_s \bar{A}}\right) \left(\frac{1}{\bar{D}p}\right)^{1.6} \left(\frac{1}{U+U_t}\right)^{0.8} \qquad (6.1)$$

where W is the mass flow rate of the spray and $\bar{A}$ is the cross-sectional area of the drying chamber. Turba and Németh (190) in studying the spray drying of paste-like materials, found $h = 13.8$ Kcal/m^3hr ^oC for a heat flow of 4090 Kcal/hr. From these values, according to Luikov's expression, they could

expect the volume of the drier to be 4.1 m^3 for a temperature difference of about 70 C. This value did not agree with the 0.7 m^3 volume of the drier used in the experiment, but Luikov's semi-empirical equation was probably not considered for the drying of pastes. It does however predict the trend of the volumetric heat-transfer coefficient and Turba and Németh suggest that for thick pastes a different numerical constant be used with the equation.

Another study of the volumetric mass-transfer coefficient was presented by Ki (92) who presented equations for the design of spray drier equipment based on the volumetric coefficient rather than the surface area coefficient. The mass-transfer volumetric coefficient was considered for two regions depending on the value of the Reynolds number and equations were given for each region.

6.3 Apparatus

The experimental cocurrent spray drier described in section 2 was used to evaporate sprays of distilled water droplets. The spray was atomised by the pressure nozzle and evaporated in cocurrently entraining hot air. The air velocity, turbulence parameters, temperature and humidity were measured using the techniques described in earlier sections.

To measure the drop size distribution of the spray the Sampling Cell method was used (14, 30, 181). Drops were collected and held in an immiscible solvent in the cell. This and other methods of sampling sprays were discussed by Marshall (121) and although no one method is

entirely satisfactory for the capture and measuring of drops, the immersion cell technique has been successfully tried in research and industry. A mechanical sampling device introduces an inevitable bias and this bias will be large for large samplers in dispersions of small drops. For this reason the multiple immersion cell drop catcher used in the present study was made as small as possible.

In figure 6.1 drawings are shown of the plan, elevation and cross-section of the multicell drop catcher used in the present study. The principle was the same as previous sampling cell techniques with a sliding cover over the sampling cells. For the present study the single cell method was extended to a multi-cell collection of drops across the complete diameter of the spray tower. The cross-section (twice scale size) drawing of the drop catcher shows the main components: A) the sliding cover above the cells, B) the holder for the immersion cells, and C) the support arm for holding the assembly in position in the spray tower.

The brass collection cells were $\frac{1}{4}$" I.D. and glued onto the bottom of the perspex channel B. The perspex surface of the base of the channel and the bottom surface of each cell were carefully polished so that the water drops held in suspension in the oil in each cell could be photographed from below. In the plan view, the spring-loaded handle of the sliding cover is shown pulled back to expose the collecting cells to the falling drops, while the elevation view shows the handle released and the sliding cover shielding the cells from the spray. The support arm C has cooling-water tubes along the bottom edge through which cold water circulated and so kept the complete assembly at a reasonable temperature when the drop catcher was put into

the hot atmosphere of the evaporating spray.

The collection cells in section B were deliberately not spaced symmetrically about the centre of the spray tower. This meant that a more continuous distribution of drop sizes and number was obtainable. Two collections through port-holes at right angles to each other were usually made and section B was easily detached from the assembly by releasing two spring clips. It was then placed on the table of a microscope and micro-photographs taken of the drops suspended just below the surface of the immiscible solvent in each of the eleven cells. The photographic technique, immersion solvent and sampling cell method was the same as that used by Robertson (151) and also by Son (173) who used a multi-cell sampler designed after that used in the present study.

6.4 Experimental

The inevitable bias with physical sampling to determine drop size distributions, results from the deflection of flow lines around the sampler. This bias is reduced to manageable proportions if the size of the sampler is reduced to the order of magnitude of the small droplets, but such a sampler is incapable of capturing and removing drops for leisurely study. If all suspended droplets maintained their position in the flow lines during this deflection, none would be intercepted by the sampler. If the droplets all had sufficient inertia to leave their flow lines and to continue in a straight path, the drop catcher would intercept all drops with paths projecting into it. Actual operation of the sampler lies between these extremes; larger droplets are intercepted and smaller droplets tend

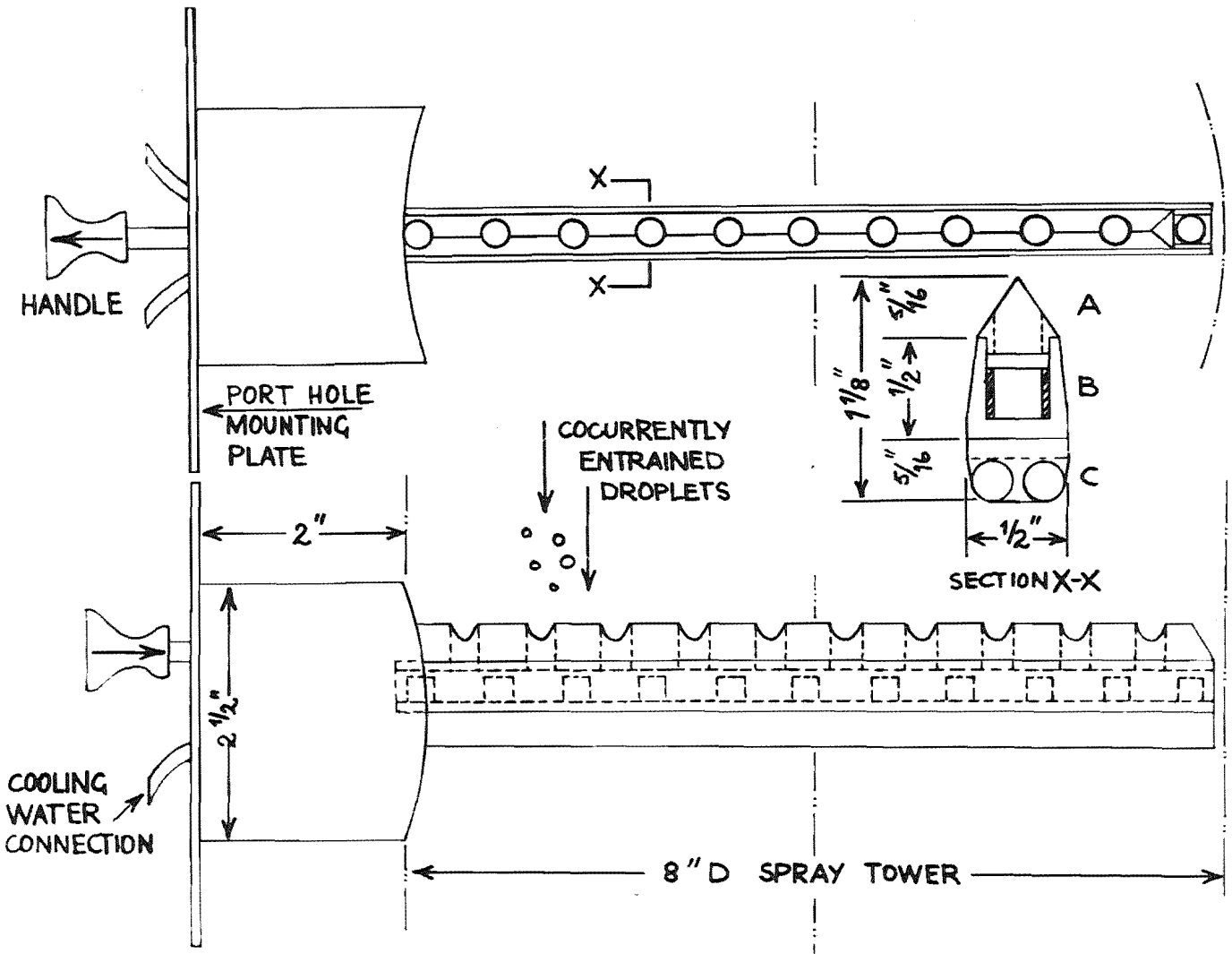

FIGURE 6.1 MULTI-CELL DROP CATCHER. PLAN AND ELEVATION TO SCALE; CROSS-SECTION TWICE SCALE SIZE.

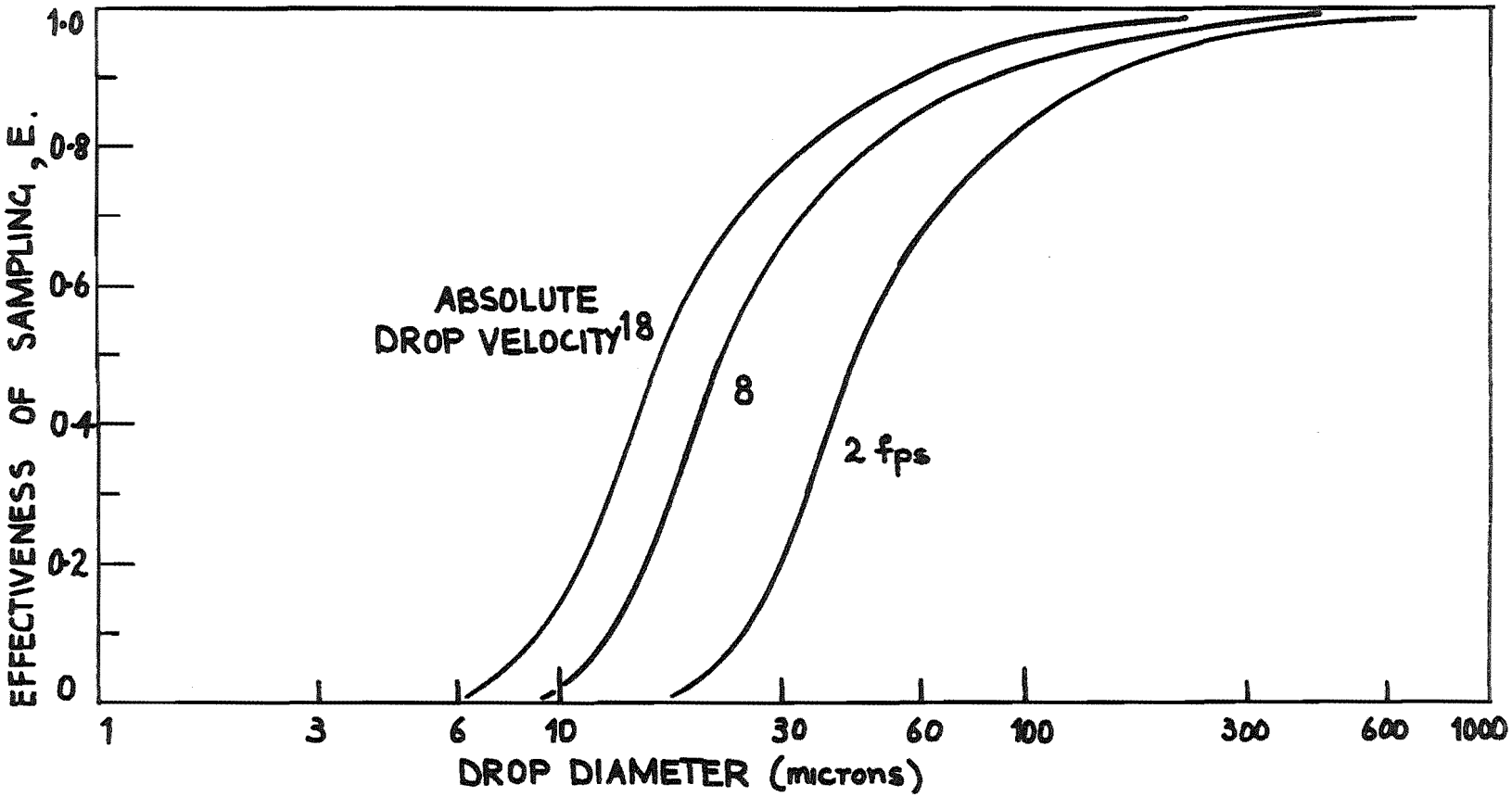

FIGURE 6.2 DROP COLLECTION EFFECTIVENESS OF MULTI-CELL SAMPLER FOR WATER DROPS IN AIR AT 70F and 740 mmHg.

to follow the flow lines around the sampler.

The effectiveness of sampling is defined as the ratio of the number of droplets intercepted by the sampler to the number that would be intercepted if none were deflected around the sampler. Generally, higher velocities, smaller samplers, and larger droplets give higher values of effectiveness. Although there is disagreement in the quantitative results of effectiveness calculations (review by Geist et al. (58)), there is sufficient qualitative agreement to estimate some limitations of spray sampling devices. Based on the method of Langmuir and Blodgett (101) the effectiveness of the sampler described above and shown in figure 6.1, was calculated for water drops moving in air at 70 F and 740 mm Hg pressure. The results are presented in figure 6.2 and indicate that data on size distributions obtained with large samplers without regard to the collection effectiveness of the sampler, are to be questioned for droplet sizes smaller than 50 microns.

The sampling bias resulting from the lack of interception of small droplets was corrected for by multiplying the actual number of collected small droplets by the reciprocal of the sampler effectiveness. The air velocity at the sampler was measured and the drop terminal velocity determined from the drag coefficient curve according to Smith (170). Corrected for the mass-transfer effect (1+B), the drag coefficient depends on the drag coefficient group Π, which is a function only of the cube of the drop diameter. Adding the air velocity and terminal velocity, the effectiveness of the sampler based on the absolute drop velocity could be determined. For each drop size, the corrected number of drops that should have been intercepted was

calculated and the true spray median and distribution evaluated.

The drop sampler collected drops in 11 cells spaced across the diameter of the spray tower. A photograph was taken of the drops in each cell and drop-size measurements made from the photograph prints. In this manner, a radial drop number distribution was obtained. However, the drops shown in each photograph represented the droplet concentration per unit area of the annulus swept out by the collecting cell when rotated about the centre axis of the spray tower. By dividing this annulus area by the area of the cell covered by the photograph, a weighting number was obtained for each cell and the observed number of drops in each photograph was multiplied by this number. Finally then, a weighted radial drop number distribution was obtained, corrected for the radial location of each cell as well as the effectiveness of the sampler.

In Appendix 11, the computer program DROPS is shown and this program was used to compute the corrected distributions from the measured drops in each cell photo. From the measured number and sizes of the drops in each cell, the radial location of each cell and the air velocity past the sampler, the computer program scans all drops for sizes within a small diameter range and so calculates the corrected number that should have been collected in each cell, as well as the droplet concentration per unit area across the spray tower radius. From the corrected data, the spray mean diameters (number, surface area, volume and sauter) and the spray non-uniformity coefficient (β) are evaluated. From the radial droplet/area concentration profile, the total number of drops passing through the

spray tower cross-section during the time of sampling can be calculated using a graphical integration method. The spray non-uniformity coefficient is defined as the ratio of the total number of droplets counted to the number of droplets that would be obtained if all were of the same uniform size equal to the Sauter mean diameter. In figure 6.3, examples of the radial drop number distributions are shown for the results 1) as measured, 2) when corrected for the sampler effectiveness only, and 3) when corrected for both the sampler effectiveness and the weighting factor according to the radial position of each cell in the spray tower. Also shown in the figure is the percentage distribution of all the droplets in the whole spray as obtained from the radial droplet/area concentration profile.

The drop number distributions shown in figure 6.3 are typical of sprays from hollow-cone pressure nozzles. The measured number of drops decreased from 290 at column radius equal to 0, towards 60 collected near the wall of the drying tower. More large drops are found at the centre of the tower and close to the wall, while at intermediate radii there are more small drops. This trend is reflected when the radial number distribution is corrected for sampler effectiveness. The effectiveness correction is more for small droplets about the column radii from 1.5 to 3 inches. Multiplying by the weighting factor further amplifies this correction with the weighting factors ranging from 6 at the centre of the column ($r = 0$) to a factor of nearly 400 for the sampling cell closest to the tower wall. For this example, the measured number of drops was 1.61×10^{3}, the corrected number total was 5.78×10^{5} and the grand total of drops per second passing through the plane of sampling in the drying tower

was calculated as 5.26×10^7. This means that the average overall correction factor was approximately 360 and it must be emphasised that for reliable estimates of drop size distributions, large samples must be counted particularly when the measured results are to be significantly corrected. The sauter mean diameter of the spray was 87.3 microns and the spray non-uniformity coefficient was 2.78 (mono-disperse spray coefficient equals unity). The radial cumulative percentage curve indicates that more than 90% of the whole spray was within the centre three-quarters of the column cross-sectional area at the level of sampling.

By taking spray samples at various distances down-stream from the atomiser, the average rate of evaporation can be measured as the decrease in the mean diameter of spray droplets and the change in the spray non-uniformity coefficient. Because of the continuous variation in the system variables down the spray tower, the overall heat-transfer coefficient for the evaporating spray was evaluated on a differential basis (after Dloughy and Gauvin (29)). Considering a height dx in the column, the heat balance over this interval can be written as

$$-G(1+H)\, C_{p_g}\, dT_g = G\, dH(H_v + C_{p_f}(T_g - T_d)) \qquad (6.2)$$

while the rate of heat-transfer to the drops in the differential volume of column height dx, is given by

$$G\, dH.H_v = h(T_g - T_d)dA \qquad (6.3)$$

dA is the surface area of the droplets and can be obtained

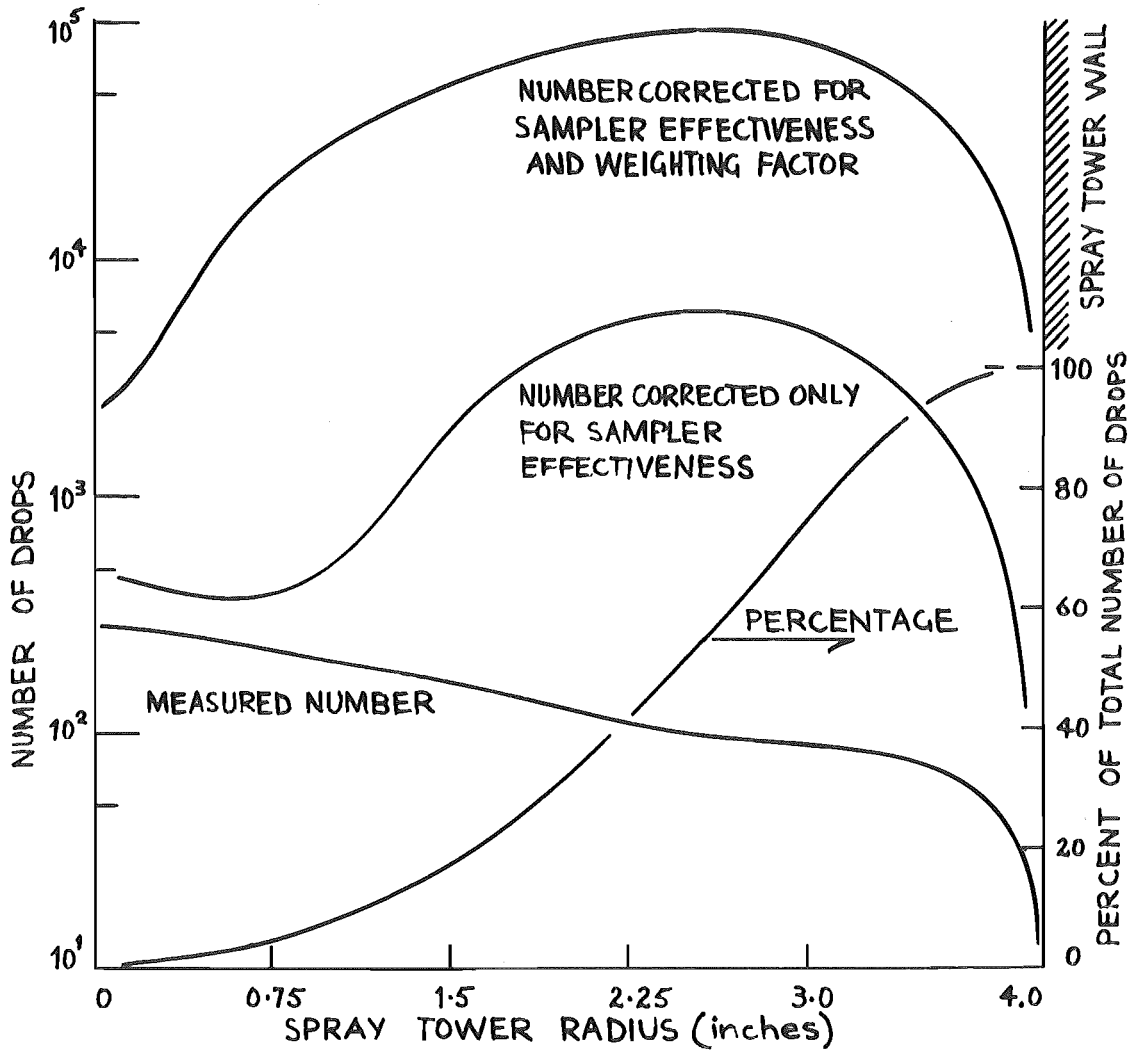

FIGURE 6.3 RADIAL DROP NUMBER DISTRIBUTIONS. MEASURED NUMBER = 1.61×10^3. TOTAL CORRECTED NUMBER = 5.8×10^5

from the specific area of the spray, (S = ft^2 area/lb of water) from the equation

$$dA = (SL/(U_g+U_t))dx \tag{6.4}$$

where L is the lbs of unevaporated spray drops per hour passing through the cross-section of the column at the level about dx. The specific area of the spray is defined as

$$S = 6 \Sigma niD_{p_i}^{\ 2} / \rho_d \Sigma niD_{p_i}^{\ 3} \tag{6.5}$$

which is the same as

$$S = 6/\rho_d D_{p_{vs}} \tag{6.6}$$

Combining equations 6.2 and 6.3 and substituting for equations 6.4 and 6.6, one obtains

$$h = -\frac{dT_g}{dx}\left[\frac{G_T(1+H)C_{p_g}\rho_d D_{p_{vs}}(U_g+U_t)}{6L(T_g-T_d)(1+B)}\right] \tag{6.7}$$

where B is the Transfer number. Hence, by knowing dT_g/dx, L and $D_{p_{vs}}$ one can find the heat-transfer coefficient and so calculate the Nusselt number for the spray ($Nu=hD_{p_{vs}}/k_f$). The liquid rate L(lb/hr) can be obtained knowing the spray volume mean diameter and the total number of drops per unit time passing through the column cross-section where the measurements are made. dT_g/dx is the value of the tangent to the mean temperature profile of the drying air

down the column.

The operating procedure for an experimental run made to determine the rate of evaporation of the spray under various air turbulence conditions, was as follows. After selecting the proper air temperature and air rate, the system was allowed to reach steady state conditions. No liquid feed was introduced to the nozzle at this stage and the temperature, humidity and velocity and turbulence profiles of the drying air were measured in a number of portholes at various levels down the spray tower.

Water was then introduced at the nozzle and once again time was allowed for steady state to be reached. Special precautions were taken at this stage to ensure that the spray did not impinge on the chamber walls as shown by observation of the wall temperatures and physical inspection of the walls with proper lighting. The impingement of the spray on the column walls could be prevented either by "pinching" the spray in an annulus of high velocity air about a slower moving, central core (achieved by suitable arrangement of the air flow straightener tubes) or by operating the pressure nozzle at a reduced pressure so that the full spray cone angle was not developed. For the present study, an initial uniform air velocity profile in the drying chamber was required and so the latter method was used to control any spray droplet impingement. The feed and drying air conditions and rates were noted and the temperature and humidity distributions across and along the drying chamber were determined as described previously. Droplet size distributions were also obtained at the selected distances from the nozzle greater than 1.5 feet below the nozzle. The reason for not working close to the

nozzle zone is because of the suspected existence of a droplet coalescence zone within which the spray non-uniformity coefficient would change markedly (151, 161, 173).

6.5 Results

Atomisation with a swirl-type, hollow cone pressure nozzle as used in the present study, is produced by liquid turbulence and by the attenuation effect of the tangential velocity component of the liquid. The exact mechanism of breakup is not completely understood and considerable discrepancies exist among the reported data with an obvious omission, in most cases, of any correlation of the spray non-uniformity coefficient (121). Drop size analysis by the count method of samples taken from sprays which follow infinite distribution functions (e.g. normal, log-normal, root-normal), indicate the existence of a maximum size by the usual methods of calculation. Interest in the concept of the maximum size for drop size distributions has increased because of the improved manner in which experimental data have been fitted by an Upper-limit equation (131). However, Gwyn et al. (65) have shown how the capture of the maximum size of drop is a probability relation and even when a large number of drops are counted, significant statistical errors still occur, especially at the "tails" of the distributions. For example, they show that with a sample size of 700 the probability of the largest drop in the spray having been captured is 99.9% and for a sample of 4,000 the probability is 99.99%.

In figures 6.4 and 6.5 cumulative log-normal and

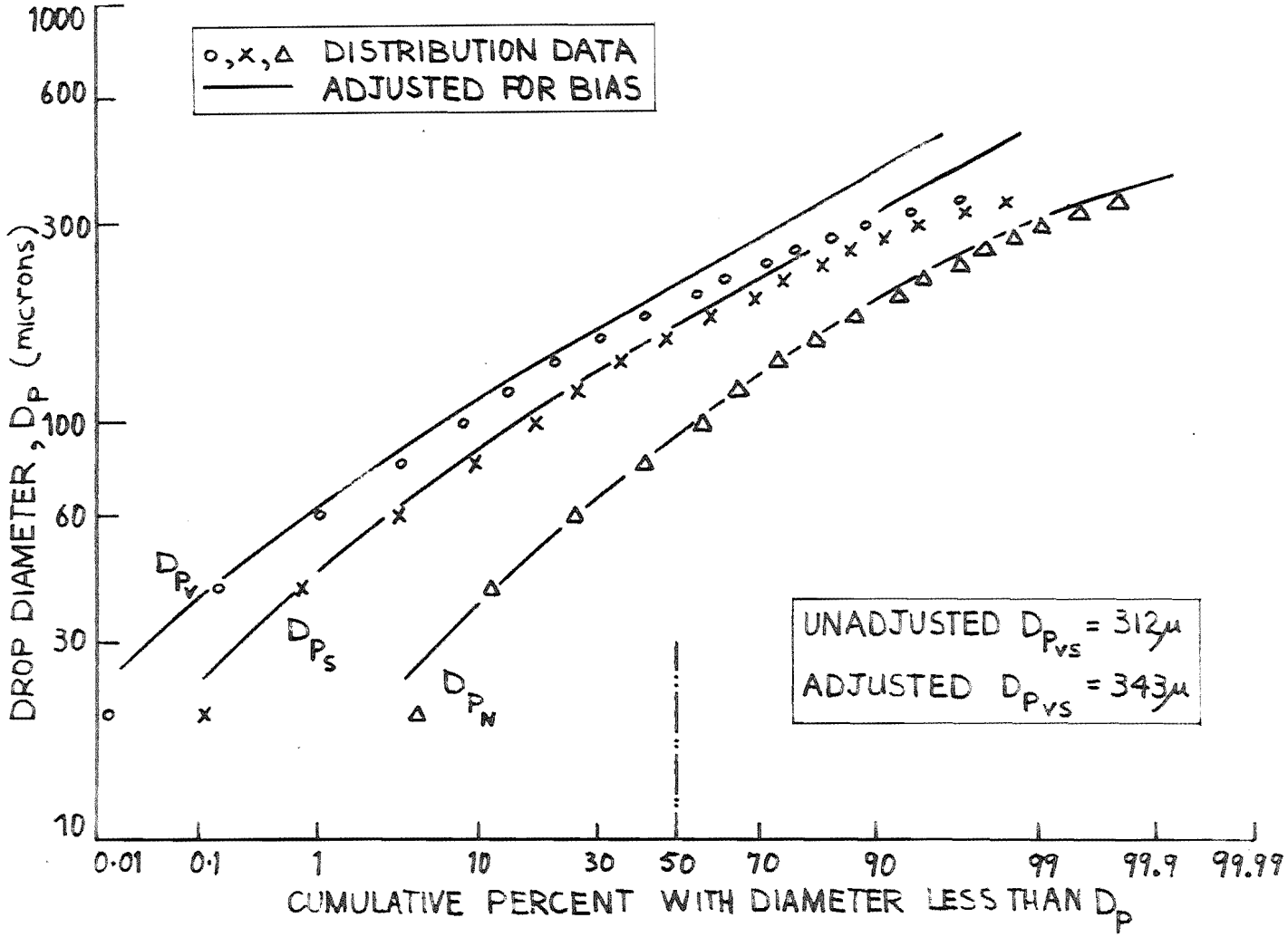

FIGURE 6.4 LOG-NORMAL PLOT OF PRESSURE NOZZLE DROP SIZE DISTRIBUTION

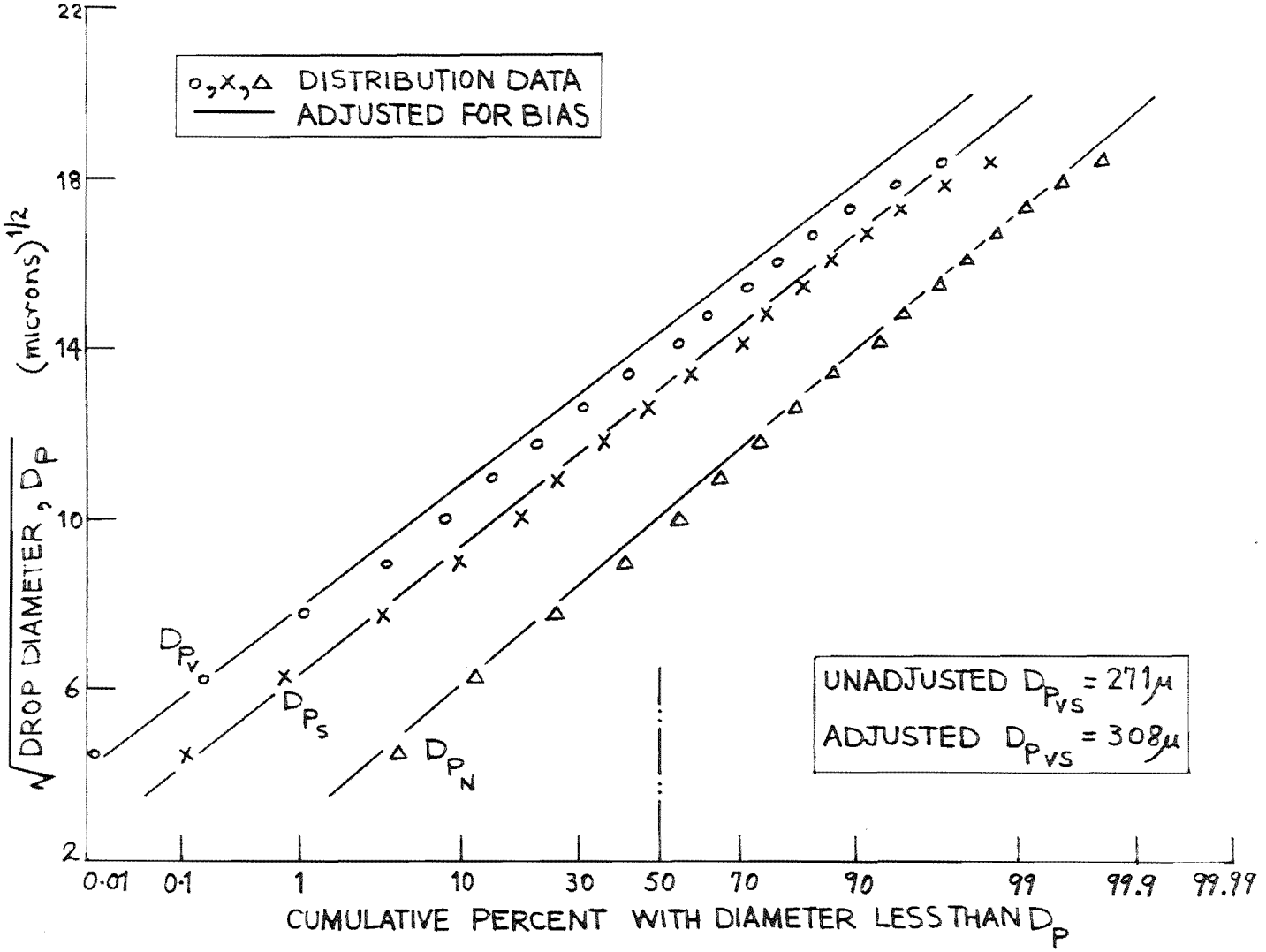

FIGURE 6.5 ROOT-NORMAL PLOT OF PRESSURE NOZZLE DROP SIZE DISTRIBUTION

root-normal distributions obtained for sprays from the pressure nozzle are shown.* The experimental data were corrected for bias according to the equations given by Gwyn et al. and show how significant is the probability function of the maximum drop size. The adjusted drop size distributions show that the root-normal distribution is the best as demonstrated by the fact that the plots of the cumulative distributions of number, area and volume are parallel. This agrees with previous results for this type of nozzle (151, 173, 181). The sauter mean diameter obtained from the computer solution of the drop size data was 315 microns.

Because measurements cannot be taken with a hot-wire anemometer in a droplet-laden airstream, one must rely on the assumption that the air turbulence and velocity profiles with and without the spray present, remain the same. The basis for this assumption is that if the volume concentration of the liquid spray is kept very small, then as discrete particles in a continuous flow of large volume-rate, the drops should not change the velocity and turbulence profiles. Experimental reports have shown that voidage fractions up to 0.1% can be tolerated before there is need to account for droplet interaction as it affects the droplet motion (80, 140). For the present study, the maximum droplet concentration was 0.005%. In the study of drag coefficients of evaporating cocurrently entrained drops in section 5, the velocity profile was measured to be the same if the spray concentration was low. However, these results were obtained far from the nozzle and in regions close to the nozzle, the turbulent drying gas may experience a spray momentum effect (32).

* sampling level = 130", liquid flow = 3.8 lb/h, nozzle pressure = 90 lb/in^2.

To approximate the effect of the spray momentum on the drying gas, air was forced through the pressure nozzle to simulate the liquid spray. In this manner, the air turbulent parameters could still be measured and the spray momentum effect observed. This approach is only approximate as the motion of a poly-disperse spray would be particulate whereas the air from the nozzle will produce a continuous flow effect. For a pressure nozzle spray it can be shown that the momentum energy is much greater than the surface energy, so that most of the energy is imparted to the droplets as momentum. (There would be a little heat also). To simulate the spray momentum effect then, the test should be for equal momentum conditions. However the physical limitations of the available air pressure and supply did not enable equal conditions to be attained, but the test was completed for the maximum air flow through the nozzle that could be maintained.

Figure 6.6 shows the simulated momentum test results and records an effect of the momentum on the drying gas velocity and turbulence parameters. There is a substantial increase in the turbulence intensity and the longitudinal microscale λ_f for both the maximum and the minimum drying gas flow rates. The increase in τ and λ_f results partly from the increased air flow rate in the column due to the additional volume of atomised air, and partly from the impact of the atomised air on the drying gas.--The spray momentum effect. For maximum air flow conditions the increase in turbulence intensity was nearly 20% (from 3.8 to 4.8%) and for minimum airflow the increase was 15% (from 15.2 to 18.0%). A similar order of increase was observed for the turbulence microscale. It was thought

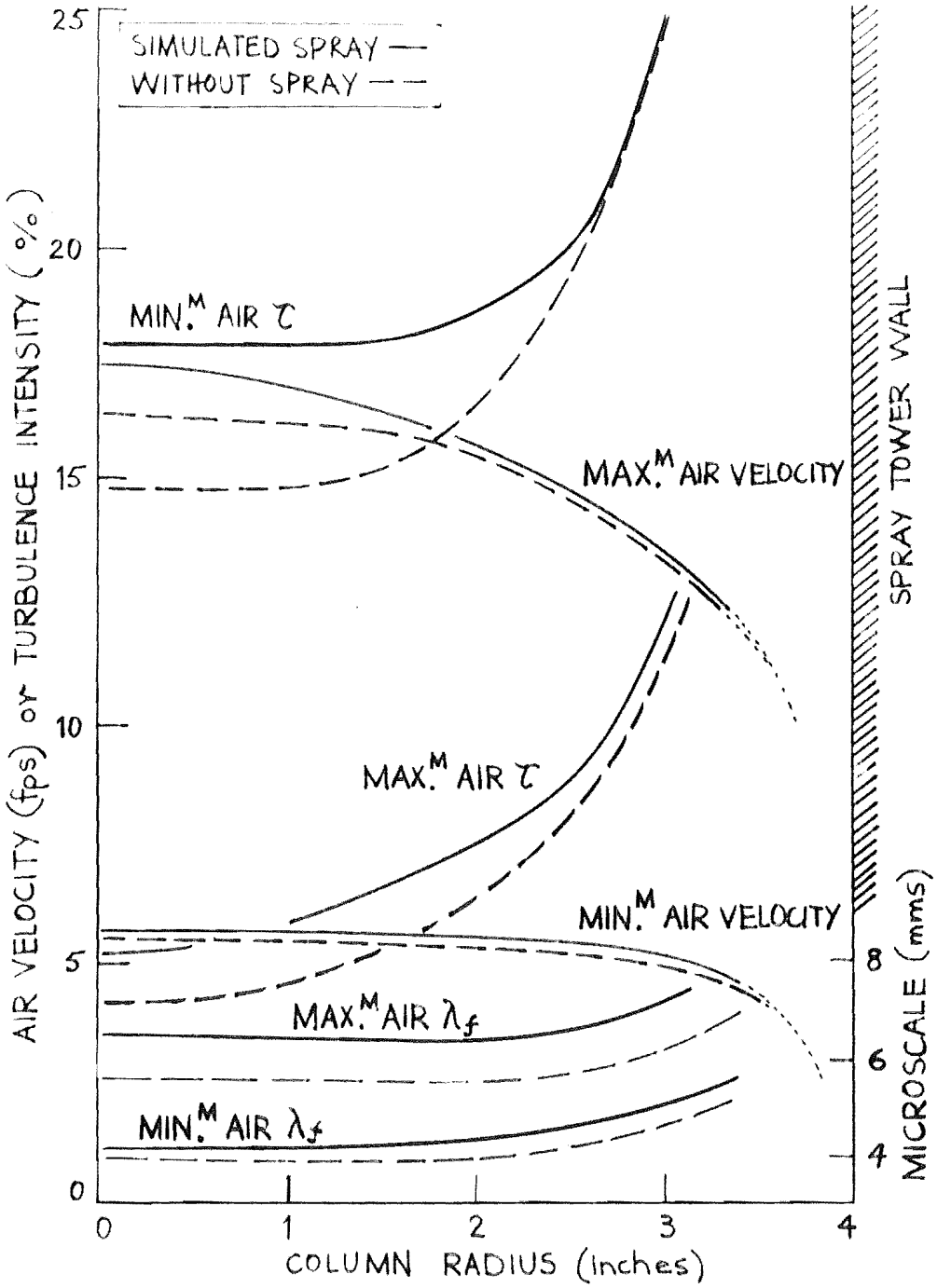

FIGURE 6.6 SIMULATED SPRAY MOMENTUM EFFECT ON AIR AIR VELOCITY AND TURBULENCE PARAMETERS FOR MAXIMUM AND MINIMUM AIRFLOW DOWN THE TOWER

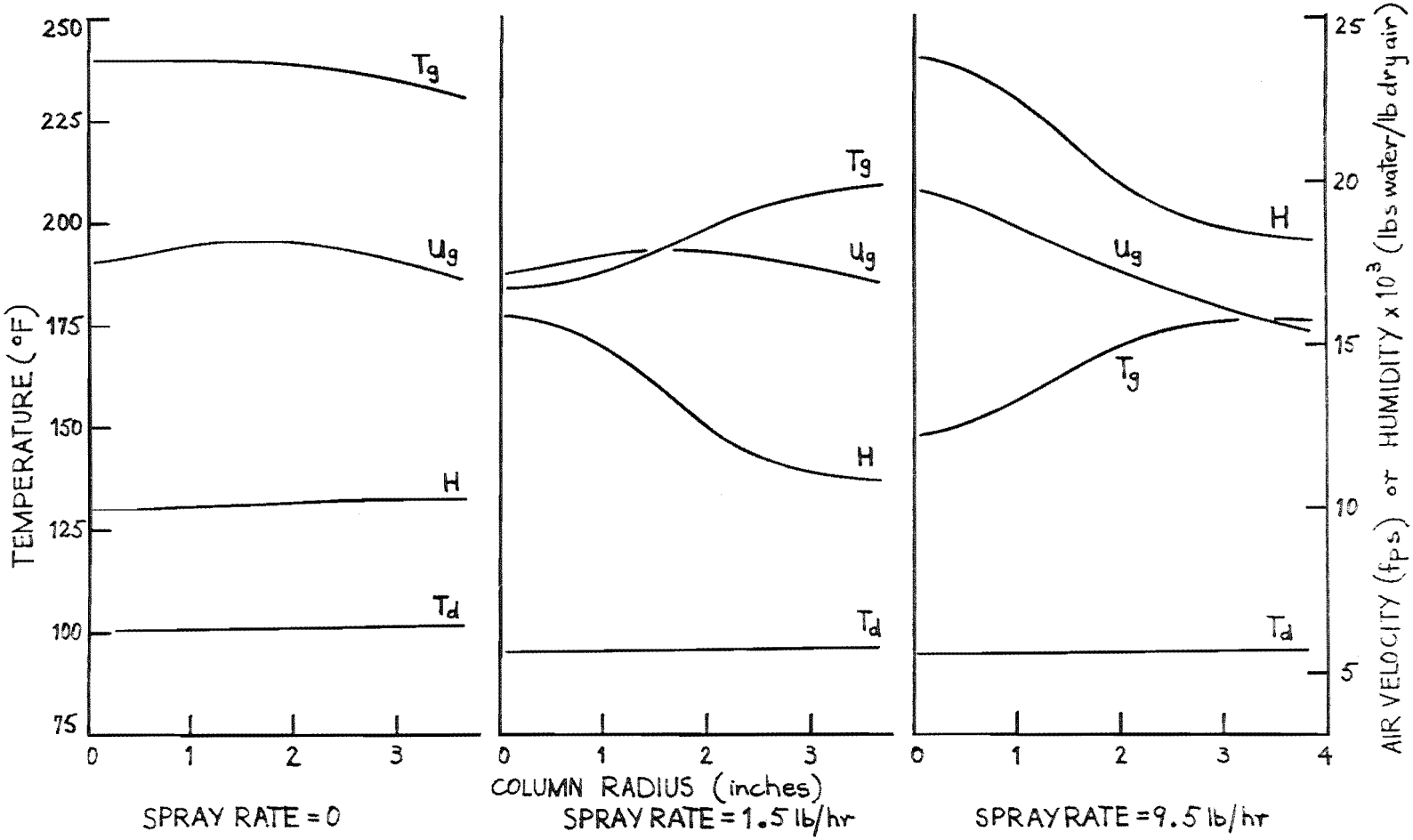

FIGURE 6.7 EFFECT OF SPRAYING RATE ON AIR TEMPERATURE, HUMIDITY AND VELOCITY RADIAL PROFILES. DISTANCE FROM NOZZLE = 36 ins.

that the volume fraction of air forced through the pressure nozzle would be of no consequence (32) in that equal momentum conditions would be the criterion for simulating the spray momentum effect. However, the results presented in figure 6.6 show an increase in air velocity due to the volume fraction of the air admitted through the nozzle and this would partly increase the turbulence parameters. This effect may decrease with distance from the nozzle and with increased volume flow of the drying gas.

Because the spray momentum tests indicated a possible influence of droplet momentum on the velocity and turbulence profiles of the drying gas, further investigation of the change in velocity profile when high spraying rates are used was considered necessary. The drag coefficient study had shown that the velocity profile of the drying air, with and without the spray present, would be the same provided the spraying rate was kept reasonably low. The first test then, was to measure the drying air temperature, velocity and humidity with and without the spray present for high and low spraying rates and to compare the results. Figure 6.7 shows the results for spraying rates of 0, 1.5 and 9.5 lbs/hr at a distance of 36 inches below the nozzle. The air velocity was the maximum possible so as to reduce as far as possible any spray momentum effect. The spraying rate of 9.5 lbs/hr was close to the maximum capacity of the pressure nozzle (1 gph at 100 psig.).

In figure 6.7 significant air temperature and humidity profiles are shown for both spraying rates, and a velocity profile change is noted for the maximum spraying rate. The humidity and temperature profiles show changes of the order of 25% across the radius of the drying tower. The low

spraying rate was the lowest at which a full hollow cone spray was still produced at the same nozzle pressure. In this case, the air velocity remains nearly the same as for the no spray case, but the temperature and humidity profile changes still exist. The change in these two profiles means that the density and viscosity of the drying gas are different from those values taken when the air turbulence parameters were measured, even if the air velocity has remained the same. It is interesting to note that the combined effect of an increasing air temperature proflie and a decreasing air humidity profile across the column radius, results in a near constant drop temperature (air wet-bulb temperature.).

By repeating the profile mapping procedure at different levels down the column the change in the air temperature and humidity was recorded as shown in figure 6.8 for an intermediate spraying rate of 5.3 lbs/hr. The curves shown in the figure are volume-mean values of the radial profiles and were obtained by fitting a polynomial curve to the measured radial profile and integrating the curve about the column axis to obtain the total enclosed volume and finally dividing this volume by the column cross-sectional area. The result was the mean value in the column at the particular radius considered. A small computer program was written to do this calculation and the volume enclosed by the air temperature or humidity profile when revolved about the column axis, was obtained using a graphical integration method. Figure 6.8 shows the significant temperature decrease which occurred within the first 20 inches of the nozzle and also the similar humidity increase. Of particular interest is the temperature profile along the axis of

NOTE: The original tabulated data for Figs 6.7 & 6.8 are deposited in the Dept. Chemical Engineering, Univ. of Canterbury.

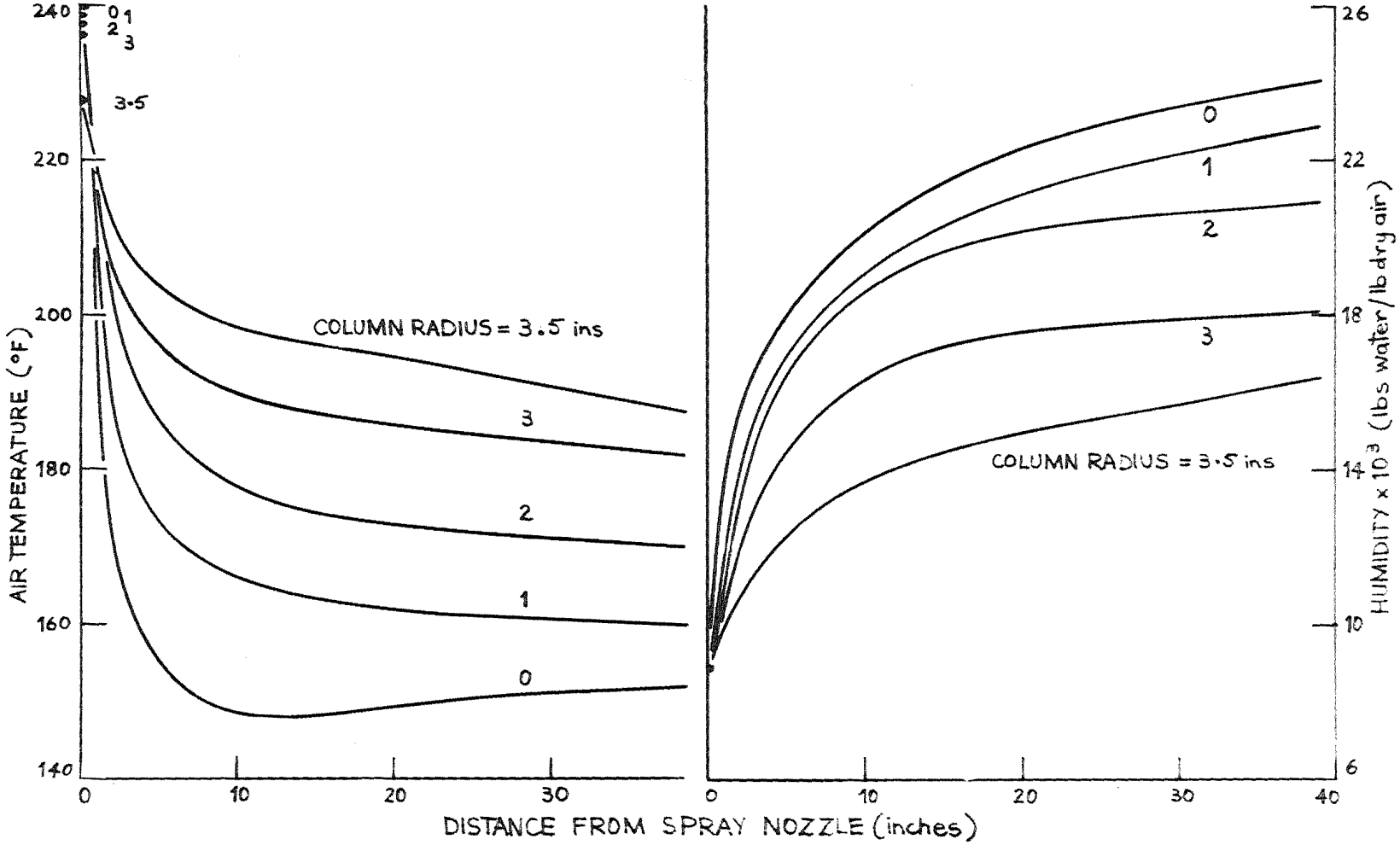

FIGURE 6.8 VARIATION IN DRYING AIR TEMPERATURE AND HUMIDITY DOWN THE DRYING TOWER. SPRAYING RATE = 5.3 lb/hr., AIR VELOCITY ≈ 16 fps.

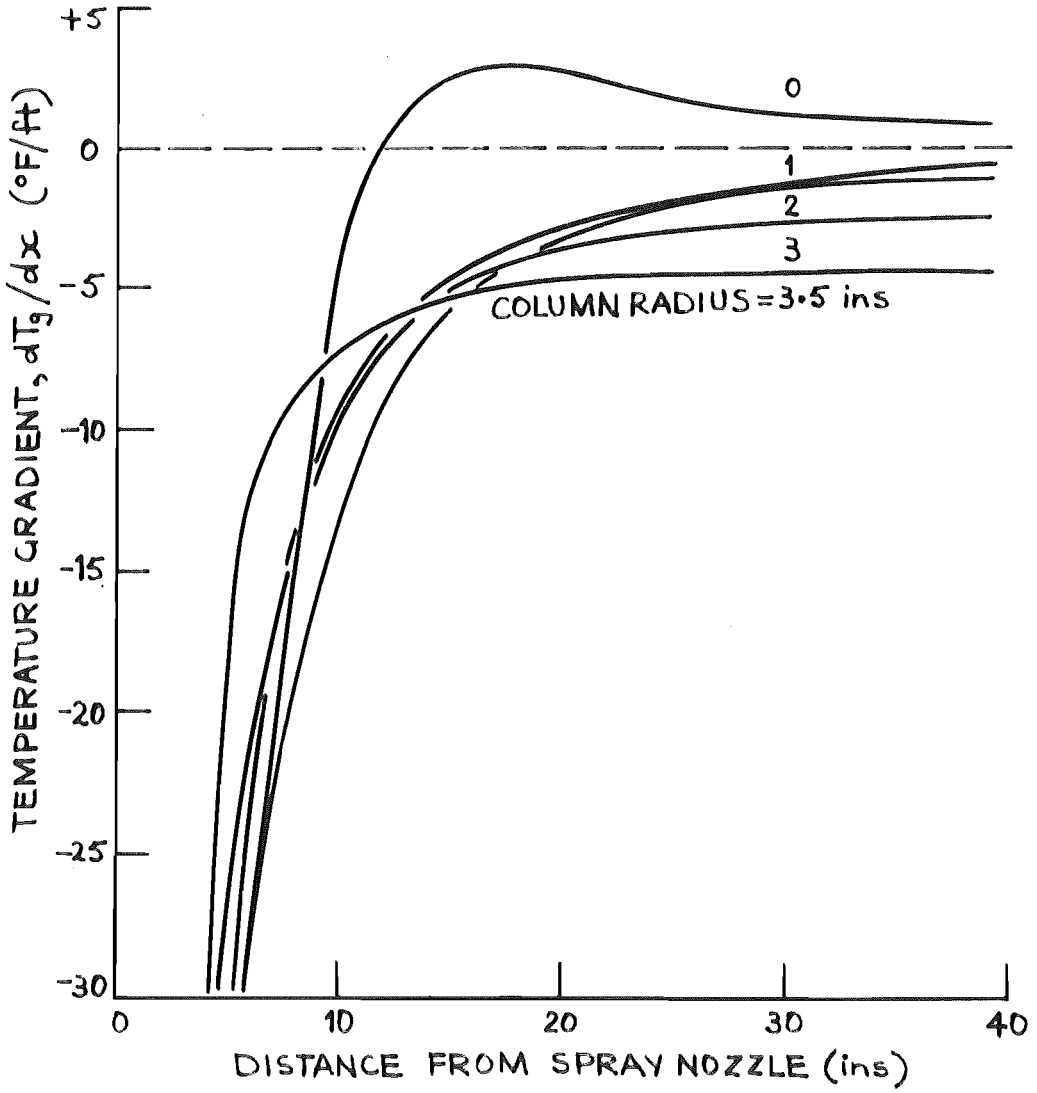

FIGURE 6.9 VARIATION OF TEMPERATURE GRADIENT dT_g/dx FOR VARIOUS RADII WITH DISTANCE DOWN THE DRYING TOWER. (FROM FIGURE 6.8 RESULTS)

the drying tower (column radius = 0), where the temperature passes through a minimum about 12 inches from the nozzle. The temperature and humidity profiles along the drying tower suggest that the significant radial profiles will exist for some considerable distance downstream from the nozzle in the cocurrent spray drier. The air velocity for the results of figure 6.8 was approximately 16 fps and showed a slight net increase with distance downstream, probably due to the increase in gas volume as the liquid spray evaporates.

The method of evaluating the overall heat-transfer coefficient of an evaporating spray in a cocurrent drier was based on a differential approach (equation 6.7) and the solution depends on the specific heat C_{pg}, temperature T_g and total flowrate G, of the drying gas as well as the temperature gradient dT_g/dx at each sampling point down the column. The results presented in figures 6.7 and 6.8 suggest some difficulty may be experienced in selecting the proper values of C_{pg} and T_g and the estimation of dT_g/dx is complicated by results like those in figure 6.8 where for column radius = 0, dT_g/dx becomes positive. In figure 6.9, the temperature gradients dT_g/dx at various distances downstream from the nozzle are plotted from the results shown in figure 6.8. Significant gradients occur for distances less than 10 inches from the nozzle and the temperature gradient along the axis is seen to become positive at the 10 inch level, attain a maximum at about 15 inches and then reduces tending to the value $dT_g/dx = 0$. At other column radii the gradients are all negative (as

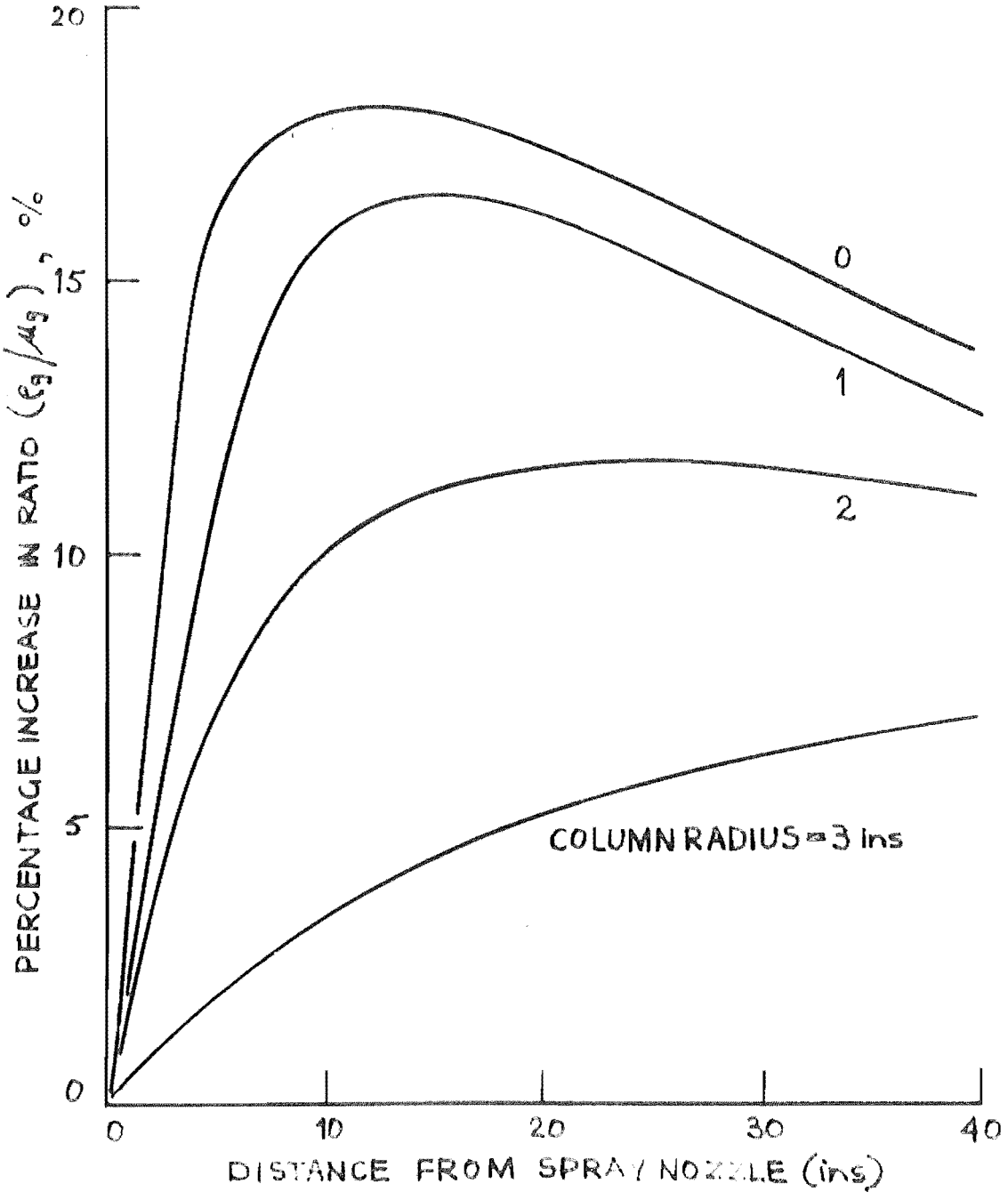

FIGURE 6.10 INCREASE DRYING GAS DENSITY/VISCOSITY RATIO WITH DISTANCE DOWN THE COLUMN.

required for solving equation 6.7) although close to the axis of the column, the values of the gradients are small for distances greater than 30 inches from the nozzle. Since the values of dT_g/dx vary widely with radial position and distance down the column, the <u>average</u> value for use in equation 6.7 will have to be selected after considering the radial distribution of the spray droplet/area concentration numbers.

Operating with the lowest liquid spraying rate, it was possible to show the air velocity with and without the spray to remain the same (see figure 6.7). However, the air temperature and humidity profiles still exist and are significant. The change in the air temperature and the increase in humidity means a change in the value of the physical properties of the drying air (ρ_g, μ_g) and it could be expected that this would change the air turbulence parameters due to a different viscous damping rate of the turbulent fluctuations. The decay of turbulence also depends on the turbulence stresses (sometimes called Reynolds stresses) which depend on the viscosity and density of the turbulent fluid.

In figure 6.10, for the nozzle spraying at the lowest rate, the percentage increase in the ratio (ρ_g/μ_g) is shown for different column radii at distances downstream from the nozzle. For the same velocity, the percentage increase in the ratio ρ_g/μ_g is also the increase in air Reynolds number down the column. The changing increase in the ratio of the two physical properties of the drying gas, even though the velocity profile remains the same, means that the turbulence parameters of the drying air with and without the spray present, will not be the same.

At this point, it is necessary to review the results so far recorded, to indicate the complexity of the problem of measuring the evaporation rates of sprays cocurrently entrained in hot turbulent air streams. The basic assumption made in analysing this problem was that the drying air velocity and turbulence profiles would not change when the spray was introduced into the drying tower. The proviso was that the volume concentration of the spray droplets be kept low, at least below 0.1%. Also, any change in the physical properties of the drying air must be small and uniform over the diameter of the drying tower.

The results obtained for the cocurrent spray drier so far, have indicated: 1) that there is most probably a spray momentum effect which, when simulated by forcing air through the nozzle, indicates a change in the air turbulence intensity and microscale. The results from the momentum transfer between the spray and the cocurrently entraining air in a region close to the nozzle (nozzle zone) and may be less significant further downstream from the nozzle;

2) that the air velocity profile of the drying air only remains the same with and without the spray present, if very low spraying rates are maintained. These rates are at the lower limit of the pressure nozzle operating range. At higher spraying rates, the velocity profile changes, partly as a result of the increase in gas volume in the drying tower as the drops evaporate and partly as a momentum transfer effect;

3) that significant temperature and humidity profiles exist for all spraying rates and the increases of these profiles above those for no spray conditions, are not at all uniform;

4) that because of the changing increase in the drying air density/viscosity ratio when the spray is present, it is unlikely that the turbulence parameters will not be altered from those measured for no spray conditions. The change in viscosity and density of the drying air during spray evaporation will create different viscous damping and turbulence stress rates in the turbulent air stream.

Because of the complex manner in which the drying air parameters vary with different air velocities and liquid spraying rates, and the failure of the basic assumption (that the air turbulence and velocity profiles would remain the same both with and without the spray present), the experimental investigation of the evaporation rates of sprays cocurrently entrained in hot turbulent airstreams was abandoned.

6.6 Discussion

The experimental results obtained for a cocurrent spray drier indicate that it is not possible to measure the turbulence intensity and scale profiles in the drying tower before introducing the liquid spray and then assume the same profiles exist when spray evaporation takes place. It is apparent that only with very low liquid flow rates (relative to the total drying gas flow) can the air velocity be assumed to remain the same with and without the spray present. Under such conditions, the mean liquid drop size from a pressure nozzle of the type used in the present study, becomes large and control of the liquid flow rate difficult. However, significant humidity and temperature profiles still exist which must change the turbulence profile. That the velocity is the same must be the result of a change in the

humidity and a decrease in the air temperature so that the total dynamic head measured by the pitotstatic tube, remained the same.

Only very close to the spray nozzle could the velocity and turbulence profiles be expected to be relatively unaffected, if the liquid spraying rate was kept low to minimise the collapsing effect of the hot drying air as it is suddenly cooled. However, it is in this nozzle zone that the significant peak values of the drying gas properties (ρ_g / μ_g) occur and below this region there is a net increase in the air velocity as the volume change of the drops from the liquid to vapour phase takes place. The main reason for not working close to the nozzle zone where dT_g/dx is very large, is that there is some evidence (151, 173) to support the claim (161) that within the nozzle zone there is coalescence and redistribution of the drop size spectrum accompanied by a change in the spray non-uniformity coefficient β.

Spray evaporation analysis depends on the size and velocity of the droplets, the spray nozzle type and operating characteristics, and the state of the drying gas into which the droplets are sprayed. In general the evaporation of whole sprays has recieved little attention and most work has been related to fundamental principles rather than practical conditions. The pattern of fall of each drop in a given type of drier appears haphazard and many relationships developed for held drops do not apply.

The simulation of the spray momentum effect suggests that this may have an important effect on the initial droplet trajectories. The flow fields around all but the very smallest drops are more or less unknown, and experimental

data specific to each problem have little to offer in way of generalisation. The spray momentum transfer results in an entraining effect with flow into the boundaries of the spray cone creating turbulent mixing. This probably heightens the severe temperature gradients existing in the nozzle zone and peculiarities of the flow pattern around the drops must be considered as well as the gross motion of the drops through the drying gas (115).

The unpredictable behaviour reported for small droplets from pressure nozzles (127) probably results from varying degrees of entrainment into the liquid spray. In a detailed study of the nozzle zone, Manning and Gauvin (117) claim that little spray evaporation occurs in this region even though the forced convection transfer rate is high. The drops may have a high velocity on discharge from the nozzle but their residence time in the nozzle zone is too small to contribute any large amount of evaporation to the total process. This is in contrast with the report by Briffa and Dombrowski (15) who studied the entrainment of air into a liquid spray and found the initial nozzle zone played a large part in the mixing of the spray droplets with the drying gas. The system variables were the density, velocity, size and distribution of the spray, the spraying rate and the density, temperature and volume rate of the drying gas.

As the spray moves through the gas it experiences aerodynamic drag and because momentum is conserved within the system, the reduction in drop velocity is accompanied by an increase in the local gas velocity. With this forward displacement of the gas, an equivalent mass of drying gas is entrained into the spray. At the same time as this momentum transfer occurs, the hot air reaching the spray is cooled by

evaporation. The surrounding air rushes to fill the void left by the collapsing air volume and probably creates a turbulent zone. The degree of turbulence created will be a function of the gas rate near the spray nozzle and the spray evaporation rate. It is apparent, that an exact analysis of the momentum transfer and air entrainment for whole sprays of evaporating droplets requires a detailed knowledge of the nature of the flow fields around each drop and the manner in which interacting fields affect the movement of the droplets.

The effect of momentum transfer and particularly the entrainment of air into the spray, results in a change in the drop size spectrum of the spray. This coalescence zone has been reported by Shapiro and Erikson (164) as a change in spectrum of droplet clouds during evaporation and was caused by turbulence during the initial spray period. A correction procedure for this change in drop-size distribution is available (22) by extrapolation to zero volume of spray liquid in the drying gas.

The significant radial temperature, humidity and velocity profiles found in this experiment, have not been reported previously. Experimental results obtained using rigidly standardised procedures with special precautions for accurate estimation of proper heat balances for evaporating sprays, are reported (14, 30) based only on single values of T_g, H, T_d and the drying gas velocity taken at an unreported radial location. Bose and Pei (14) measured the radial air velocity and turbulence profiles and also the radial drop size distribution, but did not allow for a change in these profiles with and without the spray present.

An examination of the spray behaviour in the turbulent drying gas stream by considering a slender annulus down the column would not be valid because of the complicated droplet flow pattern in the nozzle zone and the resulting cross flow of droplets and drying gas. Only at distances greater than say 40" from the nozzle could such a study be made, but then dT_g/dx is very small. It must be emphasised that the existence of these profiles, preceded by the turbulence effects in the nozzle air entrainment zone and the spray momentum transfer region, makes the analysis of spray evaporation in hot turbulent air streams a problem which at present cannot be solved.

One could measure the turbulence intensity before the spray was introduced and then plot the velocity and humidity profiles when the spray was present. An attempt to predict the change in level of intensity and scale of turbulence to that existing in the spray tower with the spray present could then be made with due consideration to the change in the viscous damping rate and the Reynolds shear stresses both radially and longitudinally in the column. To do so the velocity and turbulence profiles from the nozzle down to the column level considered would have to be plotted both with and without the spray present. Because of the three-dimensional change in the profiles down the column, the prediction of the turbulence change would have to be attempted using a numerical step-by-step method assuming isotropic and homogeneous turbulence for each step. This is a problem of some considerable magnitude and lends itself to solution by computer techniques. If the air turbulence were not considered isotropic and homogeneous for each iteration in the calculation, the problem would seem insoluble.

The analysis of heat transfer by convection in spray drying is obviously exceedingly difficult because of the complicated hydrodynamics involved and any solution must be based on simplifying assumptions which at best, are valid only within certain close limits. Dickinson and Marshall (27) conclude their study of spray evaporation for the two cases of sprays with and without significant relative velocity, by pointing out that in practice the situation is more complex than they analysed and includes solids in drops, back mixing of the air, interference between drops and transverse behaviour during and immediately after drop formation. It does appear that the droplet dynamics in the nozzle zone may be rather more important than some workers suggest (117) and Marsh and Heideger's (118) results emphasise the need for further consideration of the nozzle zone contribution to the total evaporation process. These workers found that for mass-transfer from free drops, 30% of the transfer occurred during the droplet formation and another 30% during the first second after formation.

It is conceded that the general form of the Ranz and Marshall (147) or Frössling (48) equations do appear to describe the overall process reasonably well. For drops of small mean diameter ($<100\mu$) there seems to be no velocity or turbulence effect (91, 113, 174) and as Dloughy and Gauvin (29) found, the Nusselt number can be considered to take the value of two. For drops in turbulent air streams with Nu = 2, it may be that the high molecular diffusivity of the volatile solvent reduces the transient effects (Biot modulus, $D_v t/D_p^2$ is large) and the eddy diffusion of the drops and the gas are nearly equal. This

is supported by evidence from a report for a cocurrent drier which showed the liquid spraying rate and the air temperature to have practically no influence on the longitudinal mixing of the gas phase (44). In spray drying with small droplets, the effect of wake flow and turbulence intensity will only be completely negligible when the droplet Reynolds number is very small (53).

Sprays of large mean drop diameters must be corrected for relative velocity effects, although there are indications that there may still be no turbulence effect (14). However, Fledderman and Hanson (43) do report a turbulence intensity effect and further suggest that there may be a turbulence scale effect as well. From the results of the limited studies of spray evaporation processes, no voidage or spray interaction effects occurred, at least for the spray concentrations reported. However, there has been some uncertainty shown in the use of the Ranz and Marshall equation for small diameter particles moving in more dense clouds (82) and this may be a problem in industrial operations where much larger liquid spraying rates occur.

The results of the present experimental study of spray evaporation in a turbulent air stream have been obtained with a hollow cone pressure nozzle and for investigating the air entrainment effect a full cone spray may produce slightly different results, at least in terms of the radial distribution of the spray evaporative load. The present study joins other attempts to correlate the turbulent behaviour of particles as a function of the continuous phase turbulence and as Torobin and Gauvin show (188), these researches have uncovered such difficulties that experimental observations will have to be relied on for any useable

information. The present preliminary results suggest that the equations used to describe the overall evaporation process do not take full account of the various forces acting on the spray droplets and one cannot agree with Dloughy and Gauvin (30) who predicted that a solution to the problem of spray drier design on a sound theoretical basis would soon be possible. The effect of turbulence on an evaporating spray of droplets is still an open question.

6.7 Conclusion

The attempted study of turbulence effects on the evaporation rates of sprays of droplets was abandoned when the assumption, that a low liquid spray volume concentration in the drying gas would ensure that the air velocity, temperature and turbulence profiles would remain effectively the same, was shown to be invalid. Significant drying air temperature and humidity profiles exist at even the lowest spraying rates and the corresponding changes in the physical properties of the air means that the turbulence profiles must be different with and without the spray present.

A spray momentum and entrainment effect in the nozzle zone of a cocurrent drier suggests that a local field of turbulence may be created in this region which would result in indeterminate droplet trajectories and extreme cross-flow of both droplets and drying air. The possibility of the droplet spectrum changing in a coalescence zone is suggested and supports previous work on this aspect (151, 173).

The limited number of previous cocurrent drier studies of spray evaporation rates in turbulent air

streams, make no mention of the existence of the significant radial profiles of the drying air temperature, humidity and velocity found in the present study. It is generally agreed that the Ranz and Marshall (147) equation describes the overall spray evaporation process reasonably well, but the contribution to the Nusselt number by the relative velocity effect and especially the air turbulence effect, is still uncertain. The contribution to the ovarall evaporation process for the decelerating spray in the nozzle zone may be of more importance than is thought at present (14, 30) and further investigation of this zone is needed. For accurate information on the spray evaporation process in a particular system, experimental observations will have to be relied on for some time to come.

7. SPRAY DRIER DESIGN

By surveying existing literature and presenting new data, this thesis has shown the evaporation rates of drops and sprays to be controlled by the motion of the drying gas. The evaporation rate for a held droplet has been shown to depend amongst other parameters on both the relative intensity and the scale of turbulence of the drying gas. For sprays, the moving droplets have been observed to experience the same drag as solid spheres but the influence of turbulence on the evaporation rate remains inconclusive. The exact prediction from first principles of spray drying rates in turbulent air streams has not been achieved but this new work will enable a better assessment of previous design methods for spray driers.

Momentum-, heat- and mass-transfer in a cocurrent spray drier are affected by the longitudinal and radial patterns of the velocity and physical properties of the drying gas, by the physical properties and size distribution of the sprayed drops, and by the location of the evaporative load within the drying tower. Until recently, spray drying chambers have been designed solely on empirical lines because of the lack of quantitative data on the inter-relations between these variables. However, over the last decade, a considerable number of experimental and theoretical investigations have been carried out in order to elucidate the principles involved and to put spray drier design on a sound theoretical basis. At the same time, these researches along with the present study have uncovered such difficulties that experimental observations will have to be relied on for any useable and accurate information.

An added problem is that small-scale experimental results may not represent the operating conditions of large commercial spray driers.

In table 7.1 are listed most of the design methods given for calculating the time of evaporation of a pure liquid spray. Because of the complex motion of the spray in the drying gas, any solution must be based on simplifying assumptions which at best are valid only within certain close limits. The assumptions used in each design procedure are listed in the table and the design methods fall into the two categories of being either iterative or analytical solutions. For reasonable accuracy with an iterative method a lengthy set of calculations have to be completed, but with fast, modern computing techniques this is no longer a problem. However, because of the complex profiles in a spray drier (except perhaps in well-mixed drying chambers), lengthy iterative procedures are probably not worthwhile and the approximate analytical methods may prove adequate. In general, the methods of Marshall (120), Dombrowski and Johns (31) and Schlünder (161) appear to be the most flexible. Schlünder's approach extends to large drop sizes and includes the forced convection effect, although his equations for the droplet terminal velocity may be in error in the intermediate Reynolds number region. Use of Smith's (170) standard drag curve may prove this method to be the best for future spray drier correlation studies.

The data for the design correlations given in table 7.1 are drawn in most cases from a fairly limited range of operating conditions, and experimental tests in conjunction with the use of a proven design method for a similar drier

TABLE 7.1

Design Method	Author(s)	Assumptions
Iterative	Marshall (120)	Nu=2.0; Measured drop size distribution; changing D_p; C_D=intermediate region; T_g=constant
	Sjenitzer (167, 168)	$Nu = 2.0+0.55Re^{\frac{1}{2}}Pr^{\frac{1}{3}}$; C_D = Ingebo's (80); D_p constant or variable
	Meisse (126)	like Sjenitzer; C_D 1/Re; U_g varies linearly down the drying tower; constant D_p.
	Manning and Gauvin (117)	Marshall's method; changing D_p and U_g.
Analytical	Probert (143)	Nu = 2.0; T_g constant; Rosin-Rammler (185) drop size distribution.
	Gluckert (63)	Nu = 2.0; T_g constant; based on biggest drop size; Nukiyame-Tanasawa (196) distribution
	Dombrowski and Johns (31)	Nu = 2.0; mathematical drop size distribution; T_g and D_p constant
	Marshall and Seltzer (119)	Nu = 2.0; C_D = Stoke's; constant average T_g.
	Duffie and Marshall (38)	$Nu = 2.0+0.60\ Re^{\frac{1}{2}}Pr^{\frac{1}{3}}$; average T_g; C_D = intermediate region
	Johnstone and Eads (83)	$Nu = 2.0+0.55\ Re^{\frac{1}{2}}Pr^{\frac{1}{3}}$; constant drop velocity; constant T_g.
	Schlünder (161)	$Nu = 2.0+0.60\ Re^{\frac{1}{2}}Pr^{\frac{1}{3}}$ Empirical drag; any drop size distribution; constant or variable drying conditions and D_p

and fluid, is advised. The final operating characteristics depend on the spray-drier type and constuction, and qualitative descriptions of flow patterns in a number of different types of driers are given by Kessler (91) and Marshall (121). In commercial applications, with high drying gas inlet rates, correction should be made for intense mass-transfer effects on the design values of the droplet drag coefficients and Nusselt numbers.

The present investigation was for evaporating sprays of pure water drops in a cocurrent drier and most design methods listed in table 7.1 are also for pure sprays. Some methods are available for sprays of drops containing dissolved or suspended solids and these are reviewed in Appendix 1, which also discusses the concept of transfer units in spray drying processes. This concept appears favourable because of the need for an overall concept of the spray evaporation process if local droplet trajectory peculiarities are to be neglected.

A sound theoretical basis for spray drier design is still some distance away and experimental studies must be relied on for accurate design data. Many aspects of the spray evaporation process still require investigation, particularly those concerned with the spray momentum-transfer and entrainment effects as well as the turbulence aspect of the system.

... ...

TABLE 7.1 contd.

Graphical	Feder (42)	Series of charts predicting evaporation rates using empirical relationships

8. NOMENCLATURE

ROMAN LETTERS

A	Area for heat- or mass-transfer, ft^2, also equation constant.
B	Equation constant.
C	Equation constant; also modified heat capacity of hot wire, Btu/lb^oF.
c_p	Heat capacity at constant pressure, Btu/lb^oF.
c_s	Mass fraction of diffusing species.
D	Equation constant.
D_p	Diameter of particle or droplet, ft; D_{pN}, D_{pA}, D_{pv} and D_{psv} are number, area, volume and surface-volume or sauter mean diameters, ft.
d	Diameter, ft; also notation for differential operator.
E	Eddy diffusivity, ft^2/hr.
E(k)	Three-dimensional energy function, ft^3/sec^2.
$E_1(k)$	One dimensional energy function, ft^3/sec^2.
$E_1(f)$	One-dimensional frequency spectrum function, ft^2/sec.
F_A, F_B	Radiation view factors.
F_b, F_d, F_e	Bouyant, drag and external forces acting on a falling droplet.
f	Frequency of oscillation, sec^{-1}.
f(r)	Longitudinal correlation coefficient.
G	Gas flow rate, lb/hr.
g	Gravitational acceleration constant, ft/sec^2.
H	Humidity, lbs water vapour/lb dry air.
H_v	Latent heat of vaporisation, Btu/lb.
h	Heat-transfer coefficient, Btu/ft^2hr^oF.
$\bar{h}$	Volumetric heat-transfer coefficient, Btu/ft^3hr^oF.

I	Current, amps.
K_1, K_2	Equation constants.
k	Thermal conductivity, Btu-hr/ft^{2}hr$^\circ$F; also wave number, ft^{-1}; also mass-transfer coefficient, lb moles/ft^{2}hr/mole fraction.
k_e	Wave number of the energy-containing eddies, ft^{-1}.
L	Unevaporated liquid spray rate, lbs/hr; also length, ft.
M	Molecular weight; also grid mesh size, ft.
m	Mass of droplet, lbs.
N	Molal flux, lb moles/hr.
N_o	Number of zeros/unit time for hot-wire signal, sec^{-1}
P	Total pressure, atmos.
p_{BM}	Bulk mean partial pressure of non-diffusing species, atmos.
Q	Heat-transfer rate, Btu/hr.
R	Resistance, ohms; also universal gas constant, ft lb force/lb mole $^\circ$K.
r	Correlating distance between two hot-wires, ft.
rms	Root-mean-square value.
S	Specific area of spray, ft^2/lb.
T	Temperature, $^\circ$F; also harmonic period, sec.
t	Time, hrs.
U	Velocity, ft/sec; (slip) U_t terminal velocity, ft/sec.
u_1'	Turbulent eddy velocity, ft/sec.
V	Volume, ft^3; also voltage, volts.
v	Gas velocity, ft/sec; v' drop velocity, ft/sec.
X	Longitudinal distance behind grid, ft.

GREEK LETTERS

α Drop sphericity correction function.

β Spray non-uniformity coefficient.

γ Ackermann correction - see dimensionless numbers.

δ Boundary layer thickness, ft.

$\mathcal{D}_v$ Diffusivity, ft^2/hr

λ_f Longitudinal micro-scale of turbulence, ft.

λ_g Lateral micro-scale of turbulence, ft.

Δ_f Longitudinal integral scale of turbulence, ft.

μ Viscosity, lb/ft hr; also drop sphericity, V/SD_p.

ν Kinematic viscosity, ft^2/hr

ρ Density, lb/ft^3.

σ Surface tension, lb force/ft; also stefan-Boltzman radiation constant, $Btu/ft^2hr^oR^4$.

τ Relative intensity of turbulence $u_1'^2/U$, %.

τ_w Time constant of hot-wire, sec.

ϕ Droplet length to maximum diameter ratio, l/D_p.

$\phi_1(k)$ One-dimensional dissipation spectrum, ft/sec^2.

DIMENSIONLESS NUMBERS

γ Ackermann number, $(\log_e(1+B)/B)$

B Mass-Transfer number, $(c_{pf}\Delta T/H_v)$; sometimes called Spaldings Transfer number.

C_D Drag coefficient, $(2gF_d/U^2 \rho_g A_p)$

C_D^* Drag coefficient corrected for intense mass-transfer effect, $(C_D/(1+B))$.

Fs_h Frössling number for heat-transfer, $(Nu-2.0)/Re^{\frac{1}{2}}Pr^{\frac{1}{3}}$

Fs_m Frössling number for mass-transfer, $(Sh-2.0)/Re^{\frac{1}{2}}Sc^{\frac{1}{3}}$

Fs_m', Fs_h' Frössling numbers modified for no natural convection effect, e.g. $(Nu/Re^{\frac{1}{2}}Pr^{\frac{1}{3}})$.

Fs_h^* Frössling number modified for droplet sphericity effects.

Nu Nusselt number, (hD_p/k_f).

Nu* Nusselt number corrected for intense mass-transfer effect, $(Nu/(1+B))$.

Pr Prandtl number, $(C_p\mu/k)$.

Sc Schmidt number, $(D_v\rho/\mu)$.

Sh Sherwood number, (kD_p/D_v).

Sl Strouhal number, (fD_p/U).

Su Surface tension group, $(g\sigma D_p \rho_g/u_d^2)$.

Re Reynolds number, $(\rho_g UD_p/\mu_g)$.

Re_λ Turbulent Reynolds number, $(\rho_g u_1' \lambda/u_g)$.

Π Drag coefficient group, $(C_D(Re/24)^2)$.

SUBSCIPTS

d Droplet or dispersed phase.

f Film property value.

g Gas phase.

max Maximum value.

p Particle or droplet.

o Zero or initial value.

t Terminal value.

v Vapour phase.

w Hot-wire.

SUPERSCRIPTS

$\bar{}$ Time smooth value

' Transfer in turbulent conditions.

' '' First and second differentials.

* Intense mass-transfer conditions.

9. BIBLIOGRAPHY

1. Ackermann, G. Forschungsh.Ver.dtsch.Ing.,pg 382 (1937).
2. Ahlborn, F. Zt.Fur.Technsihe.Physik, 12, 10 (1931).
3. Annistead. R.A. and Keyes, J.J. Trans.A.S.M.E. 90c, 13, (1968).
4. Baines, W. D. and Peterson, E.G. Trans. A.S.M.E. 73A, 467 (1951).
5. Baltas, L., Clamer, A. and Marchider, E.K. Brit. Chem.Eng., 9, 852 (1965).
6. Barker, D.H. Ph.D.Thesis, Univ. of Utah, (1951).
7. Batchelor, G.K. and Townsed, A.A. Proc.Roy.Soc., A193, 545 (1948).
8. Batchelor, G.K. "Theory of Homegeneous Turbulence", Cambridge Univ.Press, Cambridge (1960).
9. Batchelor, G.K. and Townsend, A.A. Proc.Roy.Soc. London, A194, 538 (1948).
10. Betchov, R.J. J.Fluid Mech., 3, 205 (1957).
11. Bevans, R.S. Conference on Fuel Sprays, Univ. of Mich., (1949).
12. Birkhoff, G. and Zarantonello, E.H. "Jets, Wakes and Cavities", Academic Press, N.Y. (1957).
13. Bond, W.N. and Newton, D.A. Phil.Mag., 5, 794 (1928).
14. Bose, A.K. and Pei, D.C. Canad.J.Chem.Eng. 42, 259 (1962).
15. Briffa, F.E.J. and Dombrowski, N. A.I.Ch.E.Journal, 12, 708 (1966).
16. Brown, R.A.S. Sato,K. and Sage, B.H. I.E.C.and Eng Series, 3, 263 (1958).
17. Brown, R.A.S. and Sage, B.H. J.Chem.Eng.Data, 6, 355 (1961).

18. Buzzard, J.L. and Nedderman, R.M.,Chem.Eng.Sci., 22, 1577 (1967).

19. Clamen, A. and Gauvin, W.H.G.,Canad.J.Chem.Eng., 46, 73 (1968).

20. Comings, E.W., Clapp, J.T. and Taylor, J.F.,I.E.C.,40, 1076 (1948).

21. Conroy, E.H. and Johnstone, H.F.,I.E.C.,41, 2741 (1949).

22. Consiglio, J. and Sliepcevich, T.,A.I. Ch.E. Journal, 3, 418 (1957).

23. Corrsin, S.,N.A.C.A.Tech.Note, 1864 (1949).

24. Coulson, J.M. and Richardson, E.G. "Chemical Engineering", McGraw-Hill, New York (1955).

25. Crooke, R.C. Beach Erosion Board Tech.Mem., 71, (1955).

26. Davies, C.N. Proc.Phys.Soc., 57, 259 (1945).

27. Dickinson, D.R. and Marshall, W.R., A.I.Ch.E.Journal, 14, 541 (1968).

28. DISA Electronik A/S, Denmark. Instruction manual for 55A01 H.W.anemometer.

29. Dloughy,J. and Gauvin, W.H., Canad.J.Chem.Eng.,38, 113 (1960).

30. Dloughy, J. and Gauvin, W.H., A.I.Ch.E.Journal, 6, 29 (1960).

31. Dombrowski, N. and Johns, W.R., Dept.Chem.Eng.,Imperial College, London.

32. Dombrowski,N. Private Comm.

33. Downing, G.C., A.I.Ch.E.Journal, 12, 760 (1966).

34. Dryden, H.L., J.Washington Acad.Sci., 25, 101 (1935).

35. Dryden. H.L., N.A.C.A.Tech.Rep., 581 (1937).

36. Dryden, H.L., Quart.Appl.Math.,1, 7 (1943).

37. Dryden, H.L., I.E.C.,31, 416 (1939).

38. Duffie, J. A. and Marshall, W.R., C.E.P. ,49, 417, 480 (1953).

39. Eisenklam, P., Arunachalam, A. and Weston, J.A., 11th Symp. (Int.) Combustion, Pitts., Penns., (1967).

40. Evnochides, S. and Thodos, G., A.I.Ch.E.Journal, 7, 78 (1961).

41. Fand, R.M. and Chang, P., Int.J.Heat Mass Transfer, 6, 571 (1963).

42. Feder, A., Chem.Eng., 66, 159 (1959).

43. Fleddermann, R.G. and Hanson, A.R., Univ.of Mich.Eng. Res.Inst.,Rept no CM667 (1951).

44. Fokin, A.P., Planovskii, A.N. and Akopyar, L.A., Inzhenerofizicheskii Zhurnal, 8, 116 (1965).

45. Fraas, A.P. and Ozisiki, M.N., "Heat Exchanger Design", J.Wiley & Sons, N.Y. (1965).

46. Friedlander, S.K., A.I.Ch.E.Journal, 3, 381 (1957).

47. Frenkiel, F.N., Trans.A.S.M.E., 70, 311 (1948).

48. Frössling, N., Gerlands Beitri.Geophys., 52, 170 (1938).

49. Frössling, N., Z.Bl.Mech., 6, 373 (1938).

50. Frössling, N., Lunds Univ.Arsskr., 36, (4) (1940).

51. Fuchs, N.A. "Evaporation and Droplet Growth in Gaseous Media", Permagon Press, London (1959).

52. Fuchs, N.A. Phys.Z.Sowjet, 6, 244 (1934).

53. Galloway, T.R., Provate Comm.

54. Galloway, T.R. and Sage, B.H., Int.J.Heat Mass Transfer, 7, 283 (1964).

55. Galloway, T.R. and Sage, B.H., A.I.Ch.E.Journal, 13, 563 (1967).

56. Garner, F.H. and Suckling, R.D., A.I.Ch.E.Journal, 4, 114 (1958).

57. Garner, F.J. and Grafton, R.W., Proc.Roy.Soc., A224, 64, (1954).

58. Geist, J.M., York, J.L. and Brown, G.G., I.E.C., 43, 1371 (1951).

59. Gibson, M.M., J.Fluid Mech., 15, 161 (1963).

60. Gibson, C.H. and Schwartz, W.H., J.Fluid Mech., 16, 365, (1963).

61. Giedt, W.H., J.Aeroneut.Sci., 18, 725 (1951).

62. Glen, J.B. and Keey, R.B., Chem.Eng.Sci., 20, 444 (1965).

63. Gluckert, F.A., A.I.Ch.E.Journal, 8, 461 (1962).

64. Grassmann, P. and Reinhart, A., Chemie.Ingn.Tech., 33, 348 (1961).

65. Gwyn, J.E., Crosby, E.J. and Marshall, W.R., I.E.C. Fundamentals, 2, 204 (1965)

66. Hall, A.A., Aero.Res.Comm.Rep.and Mem., 1842, 135 (1938).

67. Hamielec, A.E., Hoffman, T.W. and Ross, L.L., Symp. Fund.Res.Fluid Mech., 58th Ann.A.I.Ch.E.Meeting, Phil., (1965).

68. Hamielec, A.E., Hoffmann, T.W. and Ross, L.L., A.I.Ch.E.Journal, 13, 212 (1967).

69. Harriott, P., Chem.Eng.Sci., 17, 149 (1962).

70. Harriott, P., A.I.Ch.E.Journal, 8, 93 (1962).

71. Harriott, P., Canad.J.Chem.Engr., 42, 60 (1962).

72. Heisenberg, W., Z.Physik, 124, 628 (1948).

73. Hinze, J.O., "Turbulence", McGraw-Hill Co., N.Y. (1959)

74. Hodgman, C.D. (Editor) "Handbook of Chamistry and Physics", Chemical Rubber Co., Ohio (1959).

75. Hoffman, T.W. and Gauvin, W.H., Canad.J.Chem.Eng., 40, 110 (1962).

76. Horton, T.J., Fritsch, T.R. and Kintner, R.C., Canad.J. Chem.Eng., 43, 143 (1965).

77. Howe, N.M. and Shipmen, C.W., A.I.Ch.E.Journal, 9, 85 (1963).

78. Hsu, N.T., Sato, K. and Sage, B.H., I.E.C., 46, 870 (1954).

79. Hughes, R.R. and Gilliland, E.R., Chem.Eng.Progr., 48, 497 (1952).

80. Ingebo, R.D., N.A.C.A.Tech.note, 3762 (1953).

80. Ingebo, R.D., Chem.Eng.Prog., 48, 403 (1952).

81. Jenson,V.G., Proc.Roy.Soc.,A249,346 (1950).

82. Johnstone,H.F.,Pigford,R.L. and Chapin,J.H., Trans. A.I.Ch.E.,37,95 (1941)

83. Johnstone, H.F. and Eades, D.K., I.E.C.,42,2293 (1950)

84. Jones,S.R and Smith, W., "Symp. Interaction Fluids and Particles", Instn Chem. Engrs, London (1962).

85. Kalinske, A.A. and Pien, C.L., I.E.C.,36,220 (1944).

86. Kaye, G.W.C. and Laby, T.H., "Tables of Physical and Chemistry Constants", Longmans-Green & Co, London (1966).

87. Kayes, W.M., "Convective Heat and Mass Transfer", pg 220, McGraw-Hill Co, N.Y. (1966).

88. Keey, R.B. and Glen, J.B., Canad.J.Chem.Eng., 42, 227 (1964).

89. Keey, R.B. "Mass-Transfer Operations in N.Z.", Dept. Chem.Eng., Univ.Canterbury (1965).

90. Kestin, J. and Maeder, P., N.A.C.A.Tech.note 4018 (1957).

91. Kessler, H.C., Chemi.Ing.Tech., 36, 479 (1964).

92. Ki, Man Kim, Int.Chem.Eng., 6, 57 (1966).

93. Kidrow, I., "Measurement of Dynamic Flow", DISA publication, DISA Electronik.

94. King, L.V., Phil.Trans.Roy.Soc.London, 214A, 373 (1914).

95. Kinzer, G.D., and Gunn, R.J., J.Meteor., 8, 71 (1951).

96. Kolmogoroff, A.N., Acad.Sci.U.R.S.S., 30, 301 (1941), 32, 16 (1941).

97. Kovasznay, L.G., N.A.C.A.Tech.note 2839 (1953).

98. Kovasznay, L.G., N.A.C.A.Tech.note 1209 (1954), memo 1130 (1947).

99. Kronauer, R.E., "Survey of Hot-Wire Theory and Techniques", P.and W.Res.Rept. 137 Harvard Univ., (1953).

100. Ladenburg, R.W., "Physical Measurements in Gas Dynamics and Combustion", Princeton (1954).

101. Langmuir, I. and Blodgett, K.B., U.S.A.A.F.Tech.Rept, 5418 (1946).

102. Langmuir, I., Phys.Rev., 12,368 (1918).

103. Lapple, C.E. and Shepherd, C.B., I.E.C.,35,605 (1940).

104. Laufer, J., Ph.D. Thesis, Cal.Inst.Tech.,Pasadena (1948).

105. Laufer,J., N.A.C.A. Rept, 1174 (1954).

106. Lavender, W.J. and Pei, D.C.T., Int.J.Heat Mass Transfer 10,528 (1967).

107. Levich, V.G., "Physiochemical Hydrodynamics", Prentice-Hall, N.Y. (1962).

108. Liepmann, H.W. and Robinson, M.S., N.A.C.A. tech.note 3037 (1953).

109. Liepmann, H.W., N.A.C.A. Tech.note 2473 (1951).

110. Liepmann, H.W., Helv.Phys.Acta, 2, 119 (1949).

111. Lihou, D.A., Birmingham Univ.Chem.Engr, 17, 1 (1966).

112. Lin, C.C., Quart.Appl.Math., 10, 295 (1953).

113. Liu, V., Dept U.S.A.F.proj.2160 (1955).

114. Luikov, M.V., Szuska Rasp.,Mos.,Pischepromizdat (1955).

115. Magarvey, R.H. and Maclatchey, C.S., A.I.Ch.E.Journal, 14, 260 (1968).

116. Maisel, D.S. and Sherwook, T.R., Chem.Eng.Prog., 46, 131 (1950).

117. Manning, C. and Gauvin, W.H., A.I.Ch.E.Journal, 6, 184 (1960).

118. Marsh, B.D. and Heideger, W.J., I.E.C.Fundamentals, 4, 129 (1965).

119. Marshall, W.R. and Seltzer, E., Chem.Eng.Progr., 46, 501, 575 (1950).

120. Marshall, W.R., Trans.A.S.M.E., 77, 1377 (1955).

121. Marshall, W.R., "Atomisation and Spray Drying", Chem.Eng.Prog,momograph, 50 (1954).

122. Martin, G.Q. and Johnson, L.N., A.I.Ch.E.Journal, 11, 30 (1965).

123. Maxwell, J.C., Collected Scientific Papers, Cambridge, 11, 625 (1890).

124. McAdams, N.H., "Heat Transfer", pg 259, 3rd Ed., McGraw-Hill Co., N.Y. (1942).

125. McCabe, W.L. and Smith, J.C., "Unit Operations of Chemical Engineering", McGraw-Hill Co., N.Y. (1956)

126. Meisse, C.C., Jet Propulsion, 24, 237 (1954).

127. Meller, R., Sheffield Univ., Private Comm.

128. Mercier, R., Compt.Rend, 246, 698 (1958).

129. Millikan, R.A., Phys,Rev., 2, 122 (1913).

130. Möller, W., Phys.Zeits., 39, 57 (1938).

131. Mugele, R.A. and Evans, H.D., I.E.C.,43,1317 (1951).

132. Muggia, A., Aerotecnia Roma,36,127 (1956).

133. Mujumdar, A.S. et al., "Turbulence Parameters in a Stirred Tank", to be published, Univ. McGill.

134. Newton, I.,Phil.Nat.Primo.Math.,2,7 (1719).

135. Nukiyama, S. and Tanasawa, Y.,Trans.Soc.Mech.Eng. (Japan),4,86,138 (1938);5,63,68,(1939);6,II-7, II-8 (1940).

136. "New Zealand Official Yearbook", pg 562, Dept Statistics, N.Z. (1968).

137. Oseen. W., Arkiv för Mat.Astr.Fys., 6, 29 (1910), F.Neother, Zeits.Math.Phys., 62, 1 (1011), "Hydrodyamik", Leipzig (1927).

138. Pasternak, I.S. and Gauvin, W.H., A.I.Ch.E.Journal, 7, 254 (1961).

139. Patterson, G.K. and Zakin, J.L., A.I.Ch.E.Journal, 13, 513 (1967).

140. Perry, J.H. (Editor). "Handbook of Chemical Engineers", 4th Ed., McGraw-Hill Co., N.Y. (1963).

141. Powell, R.W., Trans.Instn Chem.Engrs, 18, 36 (1940).

142. Pritchard, C.L. and Biswas, S.K., Brit.Chem.Eng., 12, 288 (1967).

143. Probert, R.P., Phil.Mag., 37, 94 (1946).

144. "Psychrometric Chart". Prep. from Instn Heat Ventilating Engrs Hygrometric Tables, Edward Arnold Co., London, (1942).

145. Rabin, E., Schallenmuller, A.R. and Lawhead, P.B., TR-60-75, (1960), A.F.O.Sci.Res., Rocketdyne, Calif.

146. Raithby, G.D. and Eckert, E.R., Int.J.Heat Mass Transfer, 11, 1233 (1968).

147. Ranz, W.E. and Marshall, W.R., Chem.Eng.Progr., 48, 141 (1952).

148. Rasmussen, C.G. "DISA Constant Temp. Anemometer", DISA Electronik A/S, Herlev, Denmark

149. Richardson, E.G., Gen.Discuss.Heat Transfer, Instn Mech. Engrs, 66, (1951).

150. Romanenko, P.N. and Kharchenko, V.N., Int.J.Heat Mass Transfer, 6, 727 (1963).

151. Robertson, G.R., B.E.Rept, Univ.Canterbury (1967)

152. Rosin, P. and Rammler, E., J.Inst.Fuel,7,29 (1933).

153. Rowe, P.N., Claxton, K.T. and Lewis, J.,Trans.Instn Chem.Engrs,43,T14 (1965).

154. Ruckenstein, E., Chem.Eng.Sci.,18,233 (1963).

155. Ruckenstein, E., Chem.Eng.Sci.,19,131 (1964).

156. Ryozo Toei, Morio Okazaki and Katsuyuki Kuboia, Mem.Faculty Engng, Kyoto Univ., 28, 413 (1966).

157. Sandborn, V.A., N.A.C.A.Tech.note, 3266 (1955).

158. Sano, Y. and Nishikawa, S., Chem.Eng.Japan, 28, 275 (1964).

159. Sato, H., J.Phys.Soc.Japan, 6, 387 (1951). 7, 392, (1952).

160. Schlunder, E.U., Int.J.Heat Mass Transfer, 7, 49 (1964).

161. Schlunder, E.U., "Drying of Held Drops and Falling Sprays", Dissertation, T.H.Darmstadt (1962).

162. Seban, R.A., Trans.A.S.M.E., 82C, 101 (1960).

163. Shakespear, G.A., Phil.Mag., 28, 728 (1914).

164. Shapiro, A.H. and Erickson, A.J.,Trans.A.S.M.E.,79, 775 (1957).

165. Short, W.W., Brown, R.A.S. and Sage, B.H., J.Appl. Mech.,27E,393 (1960).

166. Simmons, L.F.G. and Salter, C.,Proc.Roy.Soc.,A165, (1938).

167. Sjenitzer, F., Cehm.Eng.Sci.,1,101 (1952).

168. Sjenitzer, F., Chem.Eng.Sci.,17,309 (1962).

169. Skelland, A.H.P. and Cornish, A.R.H., A.I.Ch.E. Journal,9,73 (1963).

170. Smith, S.C.T.,unpublished,Chem.Eng.Dept.,Univ.of Canterbury.

171. Snedecor, G.W., "Statistical Methods", 5th Ed.,

Iowa State Col. Press,Ames,Iowa (1956).

172. Sogan, H.H. and Subramanian, V.S.,Trans.A.S.M.E.,83C, 483 (1961).

173. Son, Nygen.T., B.E.Report, Univ.Canterbury (1968).

174. Soo, S.L., Chem.Eng.Sci.,5,57 (1956).

175. Spalding, D.B., Proc.Roy.Soc.,221A,78 (1954).

176. Steidel, A., J.Appl.Mech.,23,649 (1956).

177. Stewart, R.W. and Townsend, A.A., Phil.Trans.,A243, 359 (1951).

178. Stokes, G.G.,Phil.Mag.,32,343 (1848).

179. Sutera, S.P.,Maeder, P.F. and Kestin,J.,J.Fluid Mech., 16,497 (1963).

180. Sutera, S.P.,J.Fluid Mech.,21,513 (1965).

181. Tate, R.W. and Marshall, W.R.,Chem.Eng.Prog.,49,162, 226 (1953).

182. Taylor, G.I.,Proc.London Math.Soc.,20,196 (1921).

183. Taylor, G.I.,Proc.Roy.Soc.London,A151,421 (1935).

184. Taylor, G.I.,Proc.Roy.Soc.London,A156,307 (1936).

185. Taylor, G.I. and von Kármán, Th.,J.Roy.Aeronaut.Soc., 41,1109 (1937).

186. Taylor, G.I.,Proc.Roy.Soc.London,164A,476 (1938).

187. Thomas, R.E.,Confr.Atomisation,Sprays and Drops, Northwest.Univ. (1953).

188. Torobin, L.B. and Gauvin, W.H.,Canad.J.Chem.Eng., 37,129,167,224 (1954); 38,142,189 (1960); 39,113 (1961).

189. Townsend, A.A.,Proc.Cambridge Phil.Soc.,43,560 (1947).

190. Turba, J. and Němeth, J.,Brit.Chem.Eng,9,457 (1964).

191. Uberoi, M.S. and Corrsin, S.,N.A.C.A.,Rept 1142 (1953).

192. Uberoi,M.S. and Kovasznay, L.S.G., Quart.Appl.Math., 10,375 (1953).

193. van der Hegge Zijnen, B.G., Appl.Sci.Res., A7, 149 (1957).

194. van der Hegge Zijnen, B.G., Appl.Sci.Res., A7, 205 (1957).

195. van Krevelen, D.W. and Hoftijzer, P.J., J.Soc.Chem. Ind., 68, 59 (1049).

196. Venezian, E., Crespo, M.J. and Sage, B. H., A.I.Ch. E.Journal, 8, 383 (1962).

197. von Karman, Th. and Howarth, L., Proc.Roy.Soc.London A164, 192 (1938).

198. von Karman, Th., Proc.Natl.Acad.Sci., 34, 530 (1948).

199. Vyrubov, D.N., "Mechanism of Internal Combustion Engine", Mashgiz, (1946).

200. Wells, C.S., Harkness, J. and Meyer, W.A., A.I.A.A. Journal, 6, 250 (1968).

201. Winny, H.F., Aero.Res.Counc.London, Rept 1531 (1932).

202. Witte, L.C., Trans.A.S.M.E. 90C, 1 (1968).

203. Yen, Y.C. and Thodos, G., A.I.Ch.E.Journal, 8, 34 (1962).

204. Yen-Ping Shhi and Goughanowr, D.R., A.I.Ch.E.Journal, 14, 502 (1968).

205. York, J.L. and Stubbs, H.E., Trans.A.S.M.E., 74, 1157 (1952).

206. Zapp. G.M., M.Sc.Thesis, Oregon State Coll., (1950)

10. APPENDICES

APPENDIX 1

THE EVAPORATION OF LIQUID DROPS AND SPRAYS

By

W.J. Brehaut

University of Canterbury
Chemical Engineering Department

August 1966

SUMMARY.

The process of spray drying offers the advantage of extremely rapid drying of heat-sensitive products, a product particle size and density which are controllable within limits and relatively low operating costs, especially in the case of large capacity driers.

Spray driers are used for a wide variety of products, including such diverse materials as organic and inorganic chemicals, pharmaceuticals, as well as soap and detergent products. Although a beginning has been made on the rational design of such driers, incomplete knowledge concerning drop size, drop trajectories, relative velocity of gas and drop, and rates of drying make it necessary to rely largely on experimental results for spray drier design.

This review of the literature dealing with heat- and mass-transfer in spray driers considers the basic problem of the transfer processes in the evaporation of single, held or free falling drops and considers the modification of such results for their application to the case of drying of sprayed solutions. The mechanism of the evaporation of sprays, which is the most important problem in spray drying, is discussed in detail as it is affected by the boundary conditions such as the turbulence and high temperature of the drying gas, and the mechanics or ballistics of the falling drops.

Considerable scope for further research with respect to these and other effects on the evaporation of sprays is apparent. Not only do the results obtained for spray driers need to be understood in terms of the hydrodynamics of the evaporating droplets, but opportunity exists for the design or modification of techniques associated with the overall process of spray drying.

CONTENTS

1. INTRODUCTION.

The drying of droplets from an atomiser in a spray drier is a simultaneous heat- and mass-transfer operation in which the heat of evaporation is transferred by conduction and convection and in some cases by radiation from the hot gases to the drop surface. At the same time, the solvent vapour is transferred by diffusion and convection back into the gas stream. The overall rate of drying is a function of the temperature, humidity and turbulent properties of the drying gas; the diameter, temperature and size relationship between the drop and its surroundings; and the nature of the solid material dissolved or suspended in the liquid.

In spray drying, the main resistance to heat- and mass-transfer is in the gas film, and the properties of the evaporating material are relatively unimportant except as regards their influence on the particle temperature and surface condition. Also, since the time of drying in such equipment is so very small and dynamic equilibrium probably not attained, then their importance is almost negligible. The very short drying time (of the order of seconds) in spray drying processes, permits the drying of highly heat-sensitive materials. The desired consistency, bulk density, appearance and flow properties of some products such as foods or synthetic detergents, may be difficult to obtain in any other type of drier.

Spray drying is distinct from other drying methods because of the magnitude of the evaporation rate. Whereas the initial or constant rate of evaporation

from the surface of the bulk of the solution before atomisation may be up to 1 lb water / ft^2.hr, the surface rate of evaporation from a single droplet may range from 100 to 1,000 times this value, depending on the diameter of the drop. This contrast between the evaporation rate for a bulk mass of liquid before and after atomisation shows the evaporation rate to be increased nearly a millionfold. This is because the increase in surface area produced by atomisation varies inversely with the diameter of the drops, while the coefficients of the transfer processes also increase inversely as the drop diameter. Consequently, since the rate is proportional to the product of a transfer coefficient multiplied by the area of transfer, it will be proportional to the reciprocal of the square of the drop diameter. The heat transfer coefficients obtained in spray driers for very small droplets can exceed 30,000 BTU / ft^2.hr.^oF. This is due to the large increase in surface area on dispersion and also to the fact that transfer is by direct contact between the hot gas and the dispersed droplets.

Spray drying involves the three fundamental unit processes: (1) Liquid atomisation, (2) Gas-Droplet mixing, and (3) Drying of liquid droplets. The following review considers in detail the last of these unit operations referring to the drying of droplets either singly or in sprays. The first and second unit processes are also referred to as they influence the spectrum of droplets introduced to the drying chamber, and affect the hydrodynamic conditions about the evaporating drops, respectively.

2. HISTORICAL BACKGROUND.

The commercial application of the process of spray evaporation has a long history. Indeed, more than a century ago (1865) the patent of a process for the production of spray-dried egg powder (114) was registered. However, little work on the mechanism of droplet or spray evaporation was carried out until nearly fifty years later.

In 1910, Morse (157) obtained experimental data on the sublimation of iodine beads and showed that the rate of evaporation from a stationary sphere in a gas was proportional to the diameter of the drop and not to the surface area. The number of molecules escaping from unit surface in unit time is not constant, then, but increases rapidly as the radius diminishes.

Five years later Lord Rayliegh (175) (1916), in a pioneering study, investigated the mechanism of atomisation by observing the collapse of a liquid jet at low velocities, when disturbed symmetrically to the axis of the jet. He found that a symmetrical disturbance would cause the jet or ligament to break up when the amplitude of the disturbance grew to one half of the diameter of the undisturbed jet or column of liquid. He also derived the equations of motion for an oscillating liquid sphere moving under gravity in a fluid.

The basic relationships for the evaporation of spherical liquid drops in quiescent air were set forth by Langmuir (118) (1918), who analysed the results of Morse and presented the following theoretical equation:

$$-\frac{dm}{d\theta} = s\int D_v d\rho_v \quad , \tag{2.1}$$

where the factor 's' accounted for the thickness of the film surrounding the drop, through which diffusion of the vapour occurred and was defined as

$$s = \frac{2\pi D_p D_f}{(D_f - D_p)} \quad . \tag{2.2}$$

This analysis of the evaporation rate (which neglects the convection effect and attributes all transfer to conduction) was achieved by considering the evaporation of droplets to be analogous to the loss of heat from small wires. In comparing heat transfer by conduction with material transfer by diffusion, he showed that if the rate of flow was assumed to be arithmetically proportional to the area of flow and the driving force, and inversely proportional to the distance across which the force acts, then the mathematical treatment in both cases was the same. While this treatment can be extended to give an approximate indication of what to expect for spheres, it does not take into account the hydrodynamic convection effect and is therefore less fundamental than the treatment by Lorenz (138) and Nusselt (161). From his analysis of radial diffusion from a sphere to an infinite stagnant medium, Langmuir showed

$$Sh = Nu = 2.0 \quad . \tag{2.3}$$

For the case of gases in natural convection, he estimated the stagnant film thickness to be about 4mm, which is large in comparison with the diameter of the average

spray-dried particle.

Whitman, long and Wang (218) (1926) made early studies of gas absorption by droplets and indicated that during the process of mass-transfer there are three distinct periods or stages in the lifetime of the drops. These stages were droplet formation, droplet acceleration after formation, and the period of transfer occurring when the drop is falling at constant velocity.

By application of Stefan's theory of diffusion (198), Topley and Whytlaw-Gray (208) (1927) showed that the rate of evaporation in a still atmosphere under isothermal conditions is given by

$$-\frac{dm}{d\theta} = \frac{2\pi MP}{(1/D_p - 1/D_f)} \log_e \frac{1}{(1-p/P)} \quad . \qquad (2.4)$$

This equation is similar to that of Langmuir and again shows that the rate of evaporation is not proportional to the surface area exposed, as is the case for a flat plate. Shortly afterwards Whytlaw-Gray and Patterson (219) (1932) were among the earliest workers to provide experimental proof of Langmuir's analysis by showing that for the evaporation of water drops

$$D_p \frac{dD_p}{d\theta} = \text{constant} \qquad (2.5)$$

and so

$$Nu = \frac{h D_p}{k_f} = \text{constant.} \qquad (2.6)$$

Their excellent experimental technique was to suspend

by an electrostatic field in dry air at 18°C, a small globule of water, and determine the rate of evaporation by measuring the rate of change of the droplet diameter. The rate of surface area change with time was found to be constant as

$$2\pi D_p \frac{dD_p}{d\theta} = 3.16 \times 10^5 cm^2/sec \ . \qquad (2.7)$$

The temperature of the drop was not measured but estimated within narrow limits from psychrometric charts.

The work of Langmuir was further extended by Fuchs (55) (1934) to include the behaviour of much smaller drops. He suggested that the concentration of the diffusing vapour at an infinite distance from the evaporating drop, be used as a variable factor. This was the result of his investigation of a number of factors related to the evaporation of drops, which till that time had been neglected.

In his paper on heat-transfer to small particles by natural convection, Meyer (154) (1937) pointed out that with small particles the difference between the forced and free convection was not sharp, and that the smaller the particle, the less was the difference between the velocities of the particle and the air stream. He suggested that the smaller the particle, the more would the mechanism of heat exchange tend to become that of natural convection. As heat-transfer by forced convection is a function of the Reynolds number (and so a function of the diameter), and natural convection is a function of the Grashof number (and so a function of the cube of the diameter), this observation is of doubtful significance. Indeed, Meyer himself

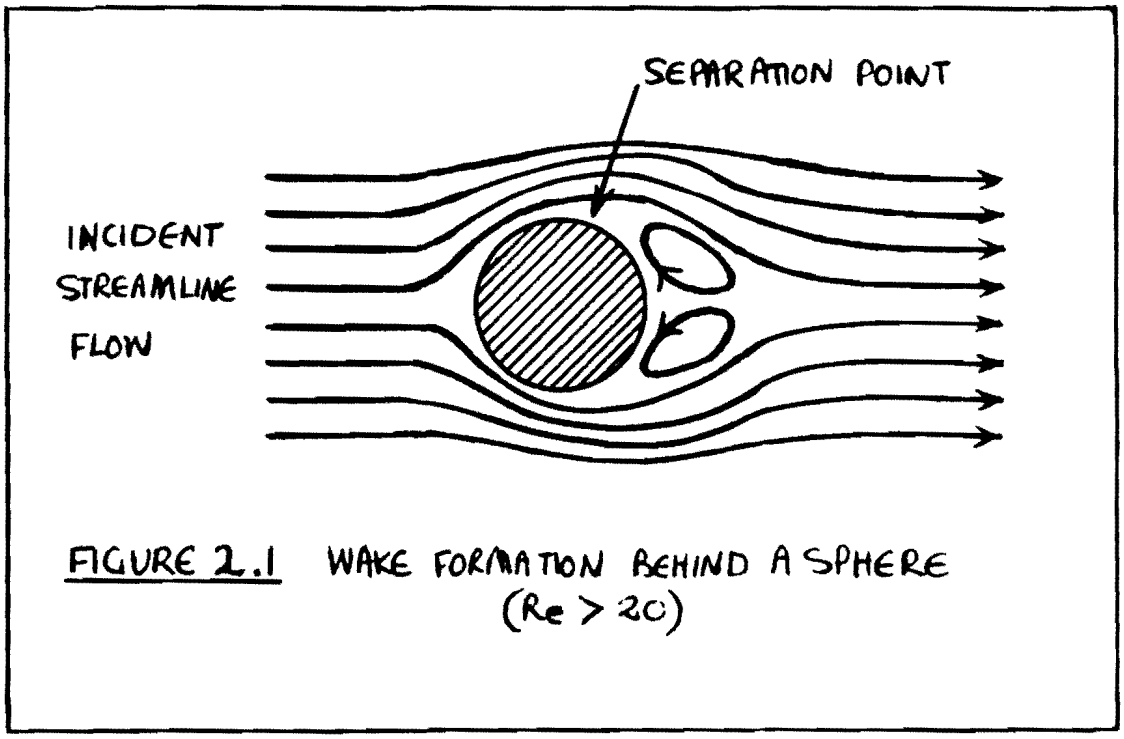

FIGURE 2.1 WAKE FORMATION BEHIND A SPHERE
(Re > 20)

found that in practice the effect of turbulence was not entirely absent and that the rate of heat transfer found by treating the heat exchange as by natural convection only, was on the low side.

Frössling (53,54) (1938), in his classical papers, used the concept of the boundary layer over a blunt-nosed body of revolution along with the variable factor suggested by Fuchs to propose the following empirical correlation for the rate of mass-transfer for spheres in a turbulent gas stream.

$$Sh = 2.0 + K_1(Re)^m(Sc)^n \quad . \qquad (2.8)$$

Then, drawing the analogy between heat- and mass-transfer, he also proposed

$$Nu = 2.0 + K_2(Re)^p(Pr)^q \quad , \qquad (2.9)$$

and indicated that the powers m, n, p and q were constant only for defined ranges of values of the Reynolds and Schmidt or Prandtl numbers. Equation (2.9) can be compared with equation (2.3) by Langmuir and shows that the Nusselt number has been increased by the amount $K_2(Re)^p(Sc)^q$, by creating a relative velocity between the drop and the gas.

For drop Reynolds numbers greater than twenty, the boundary layer theory predicts that the rate of transfer is a maximum on the upstream surface layer of the drop, decreases to a minimum value near the separation ring and increases to another but smaller maximum rate at the rear pole of the drop, where velocities in the reverse direction are experienced, as illustrated in figure 2.1.

Such a distribution of mass-transfer was shown by Frössling working with spheres of nitrobenzene, aniline, water drops and solid naphthalene, materials of low volatility so that the problem was essentially one of mass-transfer only. His work was with drops 0.2 to 2 mm in diameter and with relative air velocities from 0 to 7 metres per second. He estimated that for low flow rates the contribution of the upstream surface of the sphere (forward of the separation zone of the boundary layer) was 80% of the total transfer rate.

The effect of convection currents present in the wake of a drop falling through a gas was commented on by Johnstone and Williams (94) (1939). In addition, they pointed out that falling drops do not follow the Gravitational law or that of Stokes over the entire distance of fall, nor do they remain perfect spheres. Saito (181) (1913) had shown mathematically that for water droplets in air, the forces acting on the drops tend to deform them into spheroids, oblate normal to the direction of motion, while for mercury drops, the deformation forms the drops into prolate spheroids. Later work (46) has shown that the terminal velocity of drops is much less than predicted by Stokes' law.

The above brief chronological survey serves as an introduction to the following critical review of the literature dealing with heat- and mass-transfer in the process of spray evaporation. It covers the period from 1900 till about 1940, when spray drying was in its infancy. From 1950 on, the published work on this subject has increased rapidly and is at present a field of intense activity. Undoubtedly, much of the change of emphasis which occurred after the second World War can be attributed

to the fact that much spray drier type equipment was pressed into war service during the war years with no basis of design or operation other than trial and error. The opportunity for coordinated theoretical and experimental research that became available in the 1950's has led to the publication of much data in this field.

3. EVAPORATION FROM PURE LIQUID DROPS.

The process of heat- and mass-transfer for a single evaporating pure liquid drop in still air underlines the fundamental principle for the evaporation of liquid drops, either pure or as solutions, singly or in sprays, in still or moving gas streams. Heat- and mass-transfer during the evaporation from a surface with free moisture can be expressed in the following ways:

for Heat-Transfer $$\frac{dm}{d\theta} = \frac{h\, A_h\, \Delta T}{H_v} \quad , \qquad (3.1)$$

and for Mass-Transfer $$\frac{dm}{d\theta} = k_G A_m \Delta p \, . \qquad (3.2)$$

3.1 THEORETICAL CORRELATIONS FOR EVAPORATING DROPS.

In a mathematical study of the evaporation of a single droplet in still air, Langstroth and Luchak (120) and Langstroth et.al. (119) assumed a drop to be suspended in a spherical chamber maintaining zero vapour concentration at its walls. They extended the method of Fuchs (55) (who considered the drop diameter to be constant with time), and established an equation that differed by less than 1% from that of Fuchs, suggesting that no serious error would be produced if the change in drop size is neglected in spray drier calculations.

The same problem has been treated by Langmuir (118), Frössling (53) and Ranz and Marshall (173), who established for a spherical liquid drop of diameter D_p in still air, the eqation for the rate of evaporation as

$$\frac{dm}{d\theta} = \frac{2\pi D_v D_p \rho_d}{p_{BM}} (p_s - p_g) \, . \qquad (3.3)$$

This equation (3.3) is a specific expression of the general equation (3.2) for the rate of mass-transfer from the drop. The equation (3.3) assumes no relative motion between the drop and its surroundings and also assumes isothermal conditions and the attainment of a steady state at each infinitesimal stage of the evaporation process. It also assumes infinite surroundings.

It can be seen from the equation (3.3) that for the evaporating drop, the rate of change of the surface area is constant. This is readily shown, as for the droplet

$$m = \frac{\rho_d \pi D_p^3}{6} \quad \text{so that} \quad \frac{dm}{d\theta} = \frac{\rho_d \pi D_p^2}{2} \cdot \frac{dD_p}{d\theta} \qquad (3.4)$$

$$\text{and so} \quad \frac{\rho_d \pi D_p^2}{2} \cdot \frac{dD_p}{d\theta} = \frac{2\pi D_p D_v \rho_d}{p_{BM}} (p_s - p_g) \cdot \qquad (3.5)$$

$$\text{whence} \quad \frac{d(D_p^2)}{d\theta} = \frac{8D_v(p_s - p_g)}{p_{BM}} = \text{constant.} \qquad (3.6)$$

From this last equation, it can be seen that the total lifetime of a pure liquid droplet evaporating in still air, is proportional to the square of the original drop diameter.

The more general problem of droplet evaporation is when the drop is moving with a relative velocity with respect to the drying gas. Vapour removal is then promoted because of the decrease in size of the film around the drop, and because of the more rapid removal of the diffusing vapour.

The first of these effects decreases the resistance to diffusion and the second increases the rate of diffusion, since the partial pressure gradient is increased and

no longer approaches zero at infinite time as in the case of the stationary drop.

For the evaporation of a liquid drop in an airstream, Frössling (53) developed boundary layer equations which when combined with the equations for heat- and mass-transfer, give a set of four partial differential equations which state mathematically how heat, mass and momentum are interchanged during the evaporation process. The equations, representing a heat-balance, a mass-balance for the diffusing component, a force-balance derived from the Navier Stokes equation and the required continuity equation, are all based on a boundary layer defined as the region where the fluid velocities are less than those for potential flow because of the retarding effect of friction at a solid or liquid interface. A general solution of the set of equations is not possible and such a solution is not justified in view of the numerous assumptions that must be made regarding the average physical properties across the transfer path and in view of the existence of drop rotation (95), drop vibration and distortion (86), and unsteady state phenomena (184).

However, the dimensionless Numbers for heat- and mass-transfer can be shown to take the form

$$Nu = Nu\left[Re(Re,Pr)\right] \qquad (3.7)$$

and

$$Sh = Sh\left[Re\left(Re,Sc.\frac{p_{BM}}{P}\right)\right] \quad . \qquad (3.8)$$

The analogy between these equations comes from the fact that the equations are based on the boundary layer equations which are mathematically equivalent and subject to the same boundary conditions. Hence, the dimensionless numbers for heat- and mass-transfer should have exactly

the same functional form, where (Pr) for heat-transfer is equivalent to $\left(Sc.\frac{p_{BM}}{P}\right)$ for mass-transfer. This conclusion is applicable for heat- and mass-transfer, where the rate of transfer is controlled by the boundary layer. Since $\frac{p_{BM}}{P}$, representing the ratio of the average value of the vapour pressure of the non-diffusing species to the total pressure of the system, is nearly unity in most applications, the term is often omitted as a factor with the Schimdt number.

Johnstone, Pigford and Chapin (93), developed a solution for the equation (3.7) on the assumption that the ratio of the velocity component parallel to the drop interface and the velocity of the main stream were equal to unity and that there was no perpendicular velocity component of flow. Kronig and Bruijsten (111) obtained a solution using a perturbation method and found, that in the Stokes' law region where the velocity pattern is symetrical about the centre of the spherical particle and the boundary layer does not break away from the surface, the theoretical expression is given by

$$Nu = 2 + \tfrac{1}{2}(Pr)(Re) + \frac{581}{1920}(Pr^2.Re^2) + \ldots \quad (3.9)$$

This equation suggests that the extrapolation of experimental data to zero velocity by plotting the Nusselt number against the square root of the Reynolds number may not be correct, as was the case reported by Kramers (109).

In a study of mass-transfer with a change of interfacial area, Beek and Kramers (75) give the equation

$$\frac{dm}{d\theta} = 2C\sqrt{\left(\frac{D_v}{\pi}\right)\left(\frac{2V_s}{3D_p}\right)\left(\frac{\pi D_p^2}{2}\right)} \quad (3.10)$$

where C is the drop concentration and V_s is the interfacial velocity at a stream incident angle of 90°. The equation is derived assuming; creeping flow and a mobile interface; small penetration of the concentration layer of the drop compared to the diameter of the drop and a ratio of the interfacial to falling velocity of the drop of not more than 0,2 .

At relatively low interfacial velocities (high values of the density ratio $\rho d/\rho c$), the gradient of the tangential velocity in the surrounding continuous phase may not be neglected, but it has been shown (7) that equation (3.10) still holds for interfacial velocities up to one-fifth of the falling velocity of the drop.

Ruckenstein (179) , presented an equation for the mass-transfer coefficient of a single spherical drop in the continuous phase, valid for a whole range ofvalues of the tangential component of the velocity at the interface. Results for the particle Reynolds number greater or less than unity were obtained using a simple interpolation method and were compared with similar results obtained by the integral method.

A method of computing the transition to the steady-state for evaporating drops in the initial heating-up period is given by Buikov and Dukhin (23), who present a diffusional and thermal relaxation method of solution. The problem of the evaporation of unsteady-state stationary droplets in a constant temperature atmosphere is reduced to the solution of the equation for the surface temperature of the drop. Such a solution is given by the authors for the case when the degree of un-saturation is small.

Sjenitzer (192) described the evaporation of liquid

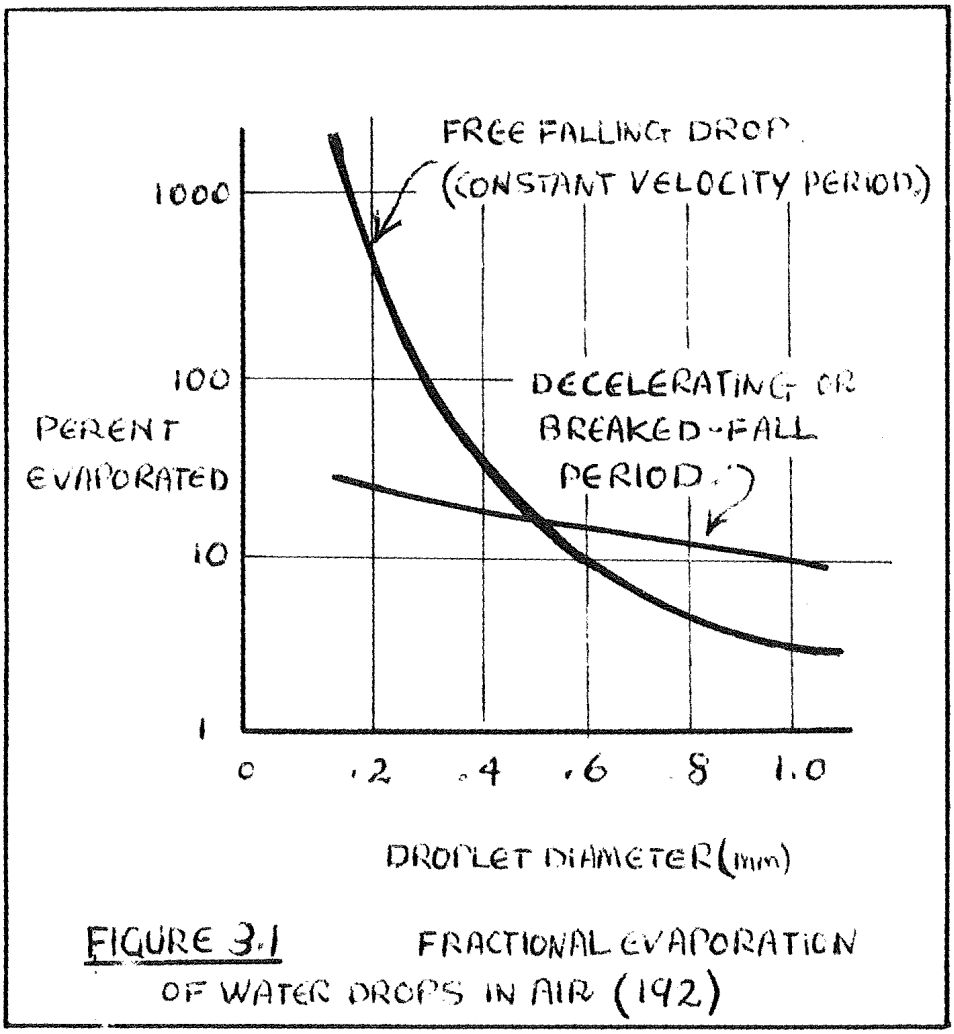

FIGURE 3.1 FRACTIONAL EVAPORATION OF WATER DROPS IN AIR (192)

drops as occuring at two rates. First there was the rate of evaporation for the period during which the drop was being decelerated to its terminal velocity, and a second rate was described for when the drop fell under conditions of free fall. He assumed the drop diameter to be constant and used Frösslings equation to develope expressions for the addtional rate of evaporation (above that for quiescent conditions) which occurred during the decelerating and free fall regions. The fractional evaporation occurring in these two different regions is shown in figure 3.1.

At zero relative velocity, if heat-transfer is by simple conduction and mass-transfer is by molecular diffusion, then the theoretical equations predict

$$Nu = Sh = 2.0 \qquad (3.11)$$

In the practical case however, a density difference exists across the transfer path and a fluid velocity caused by free convection contributes to the transfer rate. To allow for this effect Ranz and Marshall (173) proposed that the velocity term in the Reynolds number of their equation be taken as the vector sum of the velocity due to free convection and the relative velocity between the air and the droplet. Then, for zero relative velocity they proposed

$$Nu = 2.0 + K_1(Pr)^{\frac{1}{3}}(Gr)^{\frac{1}{4}} \qquad (3.12)$$

and

$$Sh = 2.0 + K_2(Sc)^{\frac{1}{3}}(Gr)^{\frac{1}{4}} \quad , \qquad (3.13)$$

which is consistent with the standard empirical correlations for transfer with free convection conditions (141), at least insofar as the form of the Grashof number is concerned.

Lorenz (138) and Nusselt (161) had developed from hydrodynamic reasoning, the relationship for heat-transfer by free convection as

$$\bar{Nu} = f_1(Pr)\, f_2(\bar{Gr}) \quad , \qquad (3.14)$$

where the Nusselt number ($\bar{Nu}$) and the Grashof number ($\bar{Gr}$) are based on the length dimension L. For most gases, the Prandtl number is equal to unity and the Nusselt number can be regarded simply as a function of the Grashof number only.

$$\bar{Nu} = f(\bar{Gr}) \qquad (3.15)$$

The form of this function needs to be determined experimentally and results obtained (105) for large values of the Grashof number showed

$$\bar{Nu} \propto (\bar{Gr})^{\frac{1}{3}} \qquad (3.16)$$

whence, the dimension L can be cancelled from both sides of the equation and no longer influences the heat-transfer process. At low values of the Grashof number the Nusselt number tends to a limiting value of 0.5.(154). This limiting value can be compared to the value of 2 for the Nusselt number based on the dimension of the drop diameter and for this case $L=D_p/4$. Meyer (154), in his study of heat-transfer to small particles by free convection proposed that the dimension L be given by the equation

$$\frac{1}{L} = \frac{1}{L_x} + \frac{1}{L_y} \qquad (3.17)$$

for irregular particles falling in a fluid.

3.2 EVAPORATION OF PURE DROPS IN STILL AIR.

Since the physical situation in finely dispersed systems is such that the droplet Reynolds number becomes vanishingly small, the limiting case for a drop evaporating in still air is of practical importance. Many studies have been made of heat-transfer to single spheres in still air conditions, while less studies have been made of the evaporation of drops in still air.

Significant among these evaporation studies are the works of Füchs (55), Langmuir (118), Frössling (53), Ranz and Marshall (173), and Langstroth et. al. (119). From all these studies for both heat- and mass-transfer, it has been well verified that the rate of mass-transfer for still air conditions can be expressed by equation (3.3).

A similar relationship to that expressed by equation (3.3) may be written for heat-transfer to spherical drops. Thus, the rate of heat-transfer is defined by the equation

$$q = h A_h \Delta T. \tag{3.18}$$

By substituting from equation (3.3) for h in equation (3.1), then

$$q = (\pi D_p^2) \frac{(2 k_f)}{D_p} \Delta T \tag{3.19}$$

or $$q = 2\pi D_p . k_f \Delta T . \tag{3.20}$$

By equating equations (3.2) and (3.18), one obtains the expression for the wet bulb temperature of the evaporating drop.

To account for the effect of the surroundings of a system of finite dimensions Füchs (55) multiplied the rate of evaporation in infinite surroundings, equation (3.3), by the term $1/(1-D_p/D_1)$, where D_1 was the diameter of a finite spherical enclosure. Langstroth et. al. (119) observed the effect of the size of a finite surrounding vessel on the evaporation of drops in still air and concluded that for vessel to drop diameter ratios

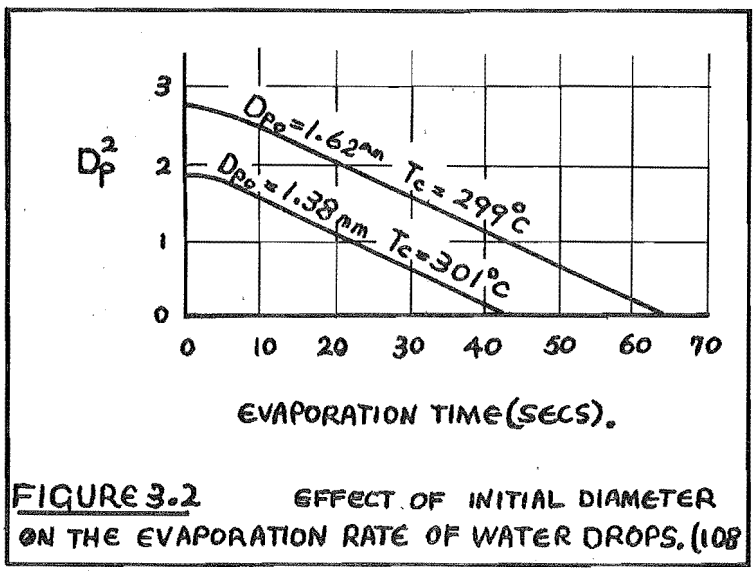

FIGURE 3.2 EFFECT OF INITIAL DIAMETER ON THE EVAPORATION RATE OF WATER DROPS. (108

greater than about 35 the free convection effects contributed to increase the drying rate. These workers also reported a difference between the drop surface temperature and the internal drop temperature. However, only the internal temperature was measured, the surface temperature being calculated from experimental rate data which, of necessity, involved the transport properties not accurately known. Their findings do not agree with those of Ranz and Marshall (173) and Johnson (91), who measured drop temperatures substantially equal to the temperature of the drop surface, which was computed to be the wet-bulb temperature for the humidity conditions prevailing.

Luchak and Langstroth (120) and Fuchs (55), considered the problem of the unsteady-state rate of an evaporating drop and showed that the steady-state rate of evaporation for liquids of low volatility in humid air was achieved very quickly.

The variation of droplet diameter as evaporation proceeds has been shown (64,173) to follow the equation

$$D_p^2 = D_{p_o}^2 - \lambda\theta \ , \qquad (3.21)$$

where λ is the evaporation parameter. This experimental relationship is in agreement with equation (3.6) and the assumptions, that the rate of change of surface area of the droplet is constant and that the total lifetime of such a drop is proportional to the original drop diameter, have been verified experimentally by a number of workers (82,118). A similar result was reported by Kobayasi (108) in his study of the evaporation of held droplets and his results are shown in figure (3.2).

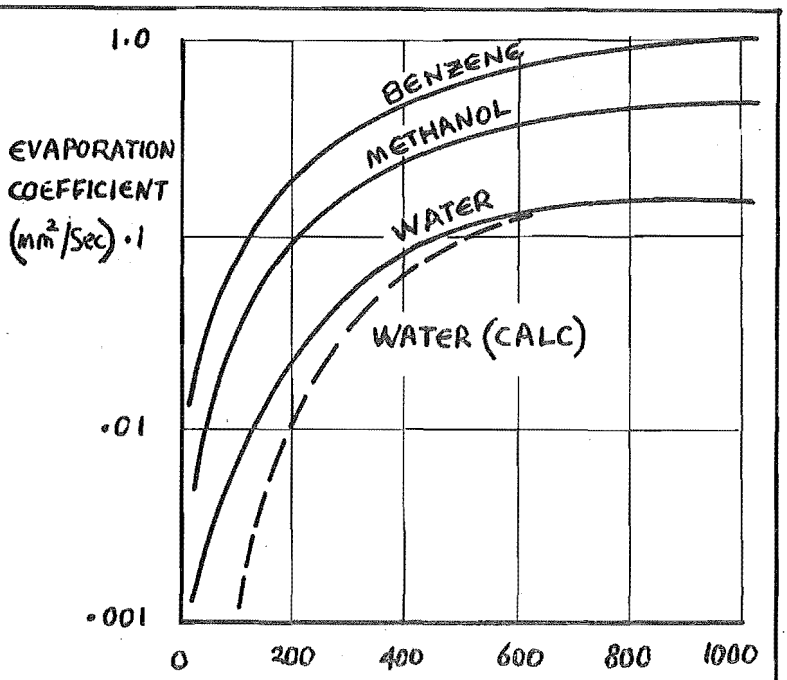

FIGURE 3.3 COMPARISON OF MEASURED AND CALCULATED EVAPORATION COEFFICIENTS (108)

He showed that the total time of evaporation of a drop could be expressed as

$$\theta = \theta_1 + \theta_2 = \frac{D_{po}^2}{4k_f}(E_1 + E_2) \quad , \qquad (3.22)$$

where E_1 and E_2 are calculable constants for given drying conditions. The evaporation coefficients for various liquids were obtained by photographic methods and are shown in figure (3.3). The solid and dotted lines represent theoretical values of the coefficient calculated assuming measured and actual boiling point temperatures respectively, as the drop surface temperature. The former values show a better agreement even in the low temperature range of the drying air.

3.3 EVAPORATION OF PURE DROPS IN FORCED CONVECTION.

In the previous sections, droplet evaporation in still air was expressed in terms of the rates of heat- and mass-transfer by the simple relationships given by equations (3.2) and (3.18). when relative motion occurs between the drop and its surroundings, the correlations for the heat- and mass-transfer coefficients must take account of this relative velocity. Frössling (54) and Ranz and Marshall (173) showed that for held and free falling drops, the transfer coefficients can be represented over a wide range of conditions by equations of the form

$$\frac{k_G M D_p p_{BM}}{D_v \rho_c} = 2.0 + K_1 (Sc)^m (Re)^n \qquad (3.23)$$

for mass-transfer and

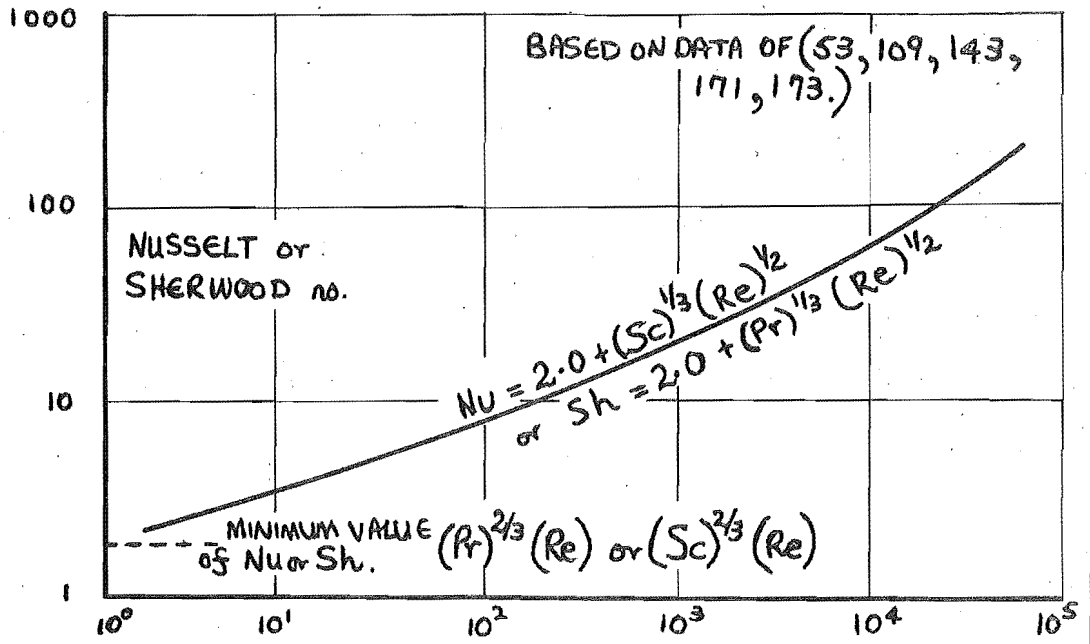

FIGURE 3.4 RANGE OVER WHICH THE RANZ & MARSHALL EQUATIONS HAVE BEEN FOUND TO HOLD FOR BOTH HEAT- AND MASS-TRANSFER.

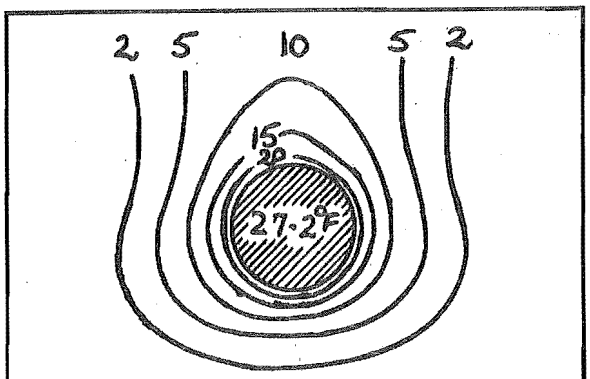

FIGURE 3.5 TEMPERATURE GRADIENTS AROUND AN EVAPORATING WATER DROP SHOWING LINES OF CONSTANT ΔT. $D_p = 1mm$, $Re = 8.4$, $T_e = 68.6$ DRY AIR (173)

$$\frac{hD_p}{k_f} = 2.0 + K_2(Pr)^p(Re)^q \qquad (3.24)$$

for heat-transfer rates. The best correlations of this type for transfer at steady state conditions appear to be the following, due to Ranz and Marshall

$$Nu = 2.0 + 0.6(Pr)^{\frac{1}{3}}(Re)^{\frac{1}{2}} \qquad (3.25)$$

and $$Sh = 2.0 + 0.6(Sc)^{\frac{1}{3}}(Re)^{\frac{1}{2}} \ . \qquad (3.26)$$

Equation (3.26), as shown in figure (3.4), is essentially the same as the correlation that was developed by Frössling (54), except that he reported for mass-transfer a value of only 0.52 instead of 0.6. Ranz and Marshall (173) studied heat- and mass-transfer in droplet evaporation for the range of droplet Reynolds number from 0 to 200. From an experimental exploration of the temperature profile around the drop, they determined the form of the boundary layer and gave the positions of the maximum transfer rates. Their results shown in figure (3.5) indicate that the greatest transfer rate occurs at the front surface of the drop where the isotherms are closest together. It is also evident that the boundary layer is of the order of one drop diameter and since the drop is continually decreasing in size, any rigorous analysis of the rate of evaporation must include the variation of the size of the boundary layer.

For droplet evaporation in still air, it is assumed that the heat- and mass-transfer processes occur uniformly at all points on the drop surface. For air flow around the drop this condition of symmetry is destroyed and equations (3.23) and (3.24) may be thought of as averaging the nonuniform heat- and mass-transfer over the surface

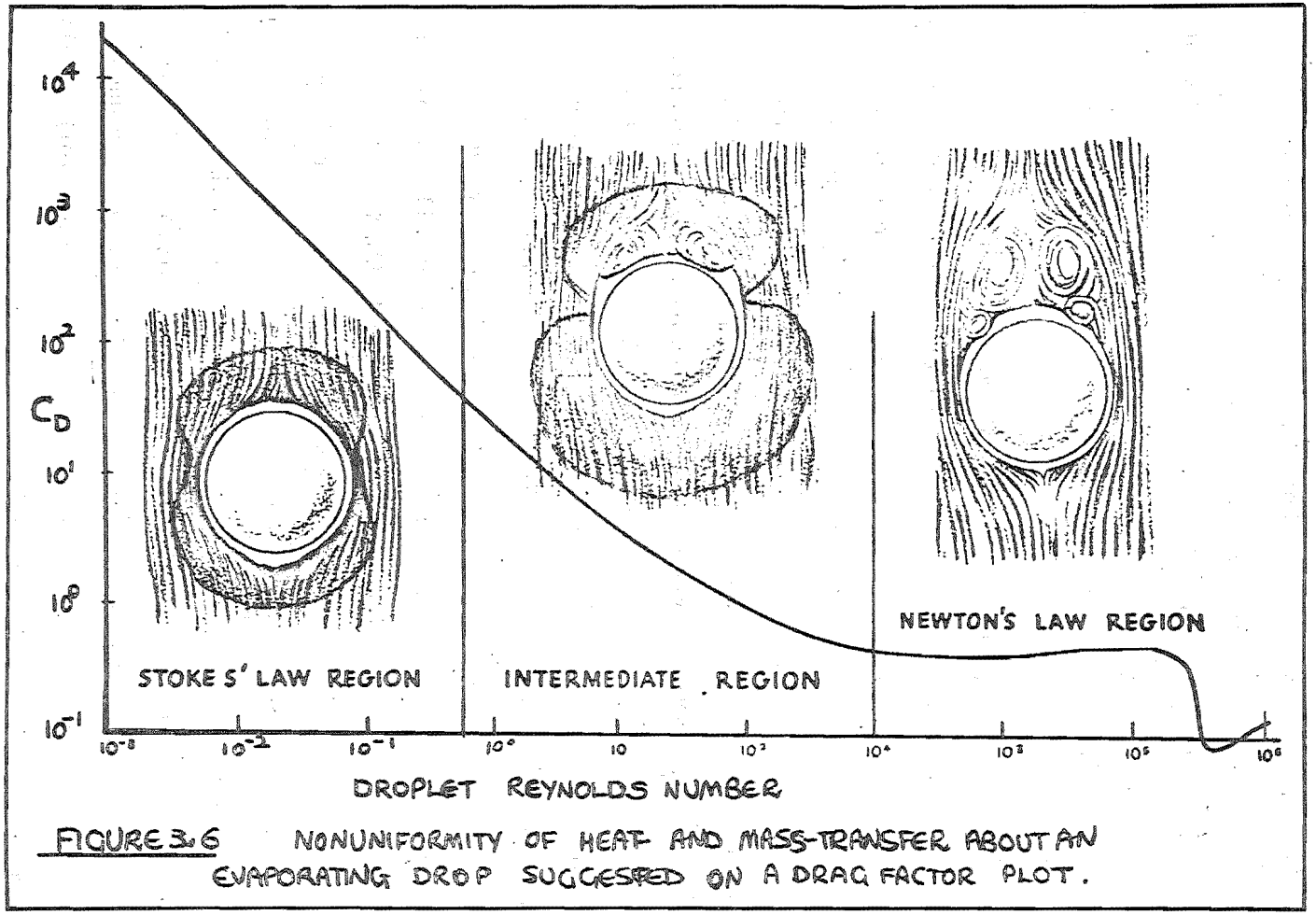

FIGURE 3.6 NONUNIFORMITY OF HEAT AND MASS-TRANSFER ABOUT AN EVAPORATING DROP SUGGESTED ON A DRAG FACTOR PLOT.

of a drop when relative motion between the drop and its surroundings occurs. This may be shown by rewriting these equations as

$$(k_g)_{av} = (k_g)_{\text{still air}} \left[1 + 0.30(Sc)^{\frac{1}{3}}(Re)^{\frac{1}{2}}\right] \quad (3.27)$$

and $$(h)_{av} = (h)_{\text{still air}} \left[1 + 0.30(Pr)^{\frac{1}{3}}(Re)^{\frac{1}{2}}\right]. \quad (3.28)$$

The reasons for the transfer coefficients being variable over the surface of a drop which is in relative motion with its surroundings may be found in the boundary layer theory. Qualitative explanations can be made with reference to figure (3.6), showing the flow patterns around droplets in the various regions. These sketches indicate how the boundary layer varies from the front to the rear of the drop. Also shown, superimposed on the flow patterns, is a shaded portion to represent the magnitude of the Nusselt number at various positions around the drop. This variation, from a maximum value at the front to a minimum value at the sides and then to another smaller maximum value at the rear, is shown more quantitatively in figure (3.7) where values of the Nusselt number around the drop have been plotted for various values of the Reynolds number for the evaporation of a naphthalene sphere. This shows the variable nature of the evaporation around a drop in relative motion and the averaging that is evidently included in the correlations for the heat- and mass-transfer coefficients.

Since the majority of drying operations deals with the air-water vapour system, specific values of the dimensionless numbers for this system can be evaluated for equation (3.25), to give the following relationships.

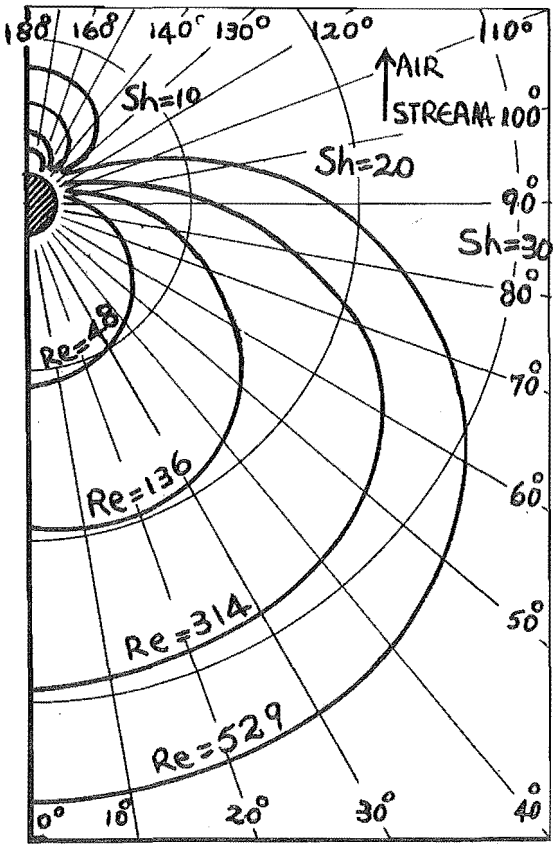

FIGURE 3.7 EVAPORATION RATES AROUND THE SURFACE OF A NAPHTHALENE SPHERE. (FROM DATA OF FRÖSSLING.)

For heat-transfer with no relative velocity

$$h = \frac{0.028}{D_p} \quad BTU/ft^2hr\ ^oF \quad , \tag{3.29}$$

and for evaporation with a finite velocity

$$h = \frac{0.028}{D_p}\left(1 + 0.27(Re)^{\frac{1}{2}}\right) . \tag{3.30}$$

These equations have been evaluated for water drops from 1 to 100 microns in diameter and as shown in figure (3.8), the heat-transfer coefficients can vary from 85 to 30,000 $BTU/ft^2hr\ ^oF$ depending on the droplet size and Reynolds number.

Rowe et. al. (178) have presented a review of the published data on heat- and mass-transfer to spheres in the range $10 < Re < 10^4$, pointing out that although the literature on the subject is extensive, the evidence is inadequate to establish the relationship between the transfer number and the Reynolds number. They refer to additional theoretical justification (18) of the use of the equations (3.23) and (3.24), and point out that for an exact correspondance between heat- and mass-transfer, the constants K_1, K_2, m, n, p and q should be common, so that

$$\frac{Nu-2}{(Pr)^m} = \frac{Sh-2}{(Sc)^m} = K(Re)^n \tag{3.31}$$

In fact, there appears to be some latitude in varying the terms of the equation, but in spray-drying applications with droplet Reynolds numbers of a limited range, these appear to be fixed. Some of the reported values they reviewed are given in table (3.1).

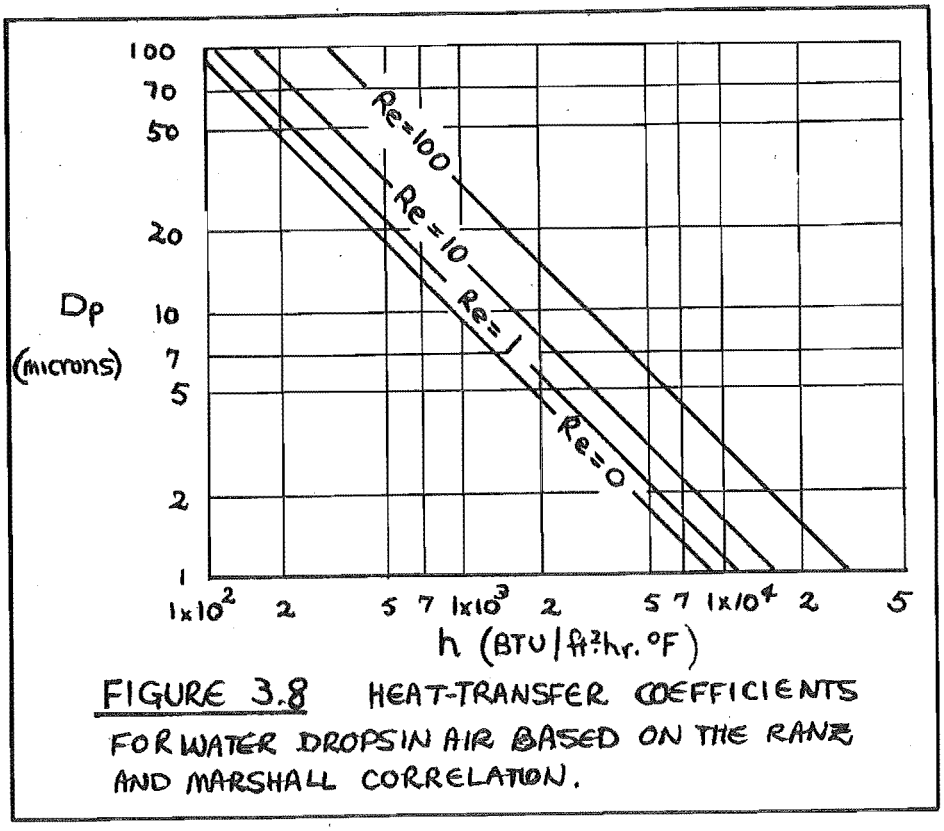

FIGURE 3.8 HEAT-TRANSFER COEFFICIENTS FOR WATER DROPS IN AIR BASED ON THE RANZ AND MARSHALL CORRELATION.

TABLE 3.1

AUTHORS	SYSTEM	B	Re RANGE
RANZ & MARSHALL (173)	MASS-TRANSFER TO AIR	.60	2 → 200
FRÖSSLING (54)	MASS-TRANSFER TO AIR	.552	1 → 1300
MAXWELL & STERRAN (150)	MASS-TRANSFER TO AIR	.552	1 → 1000
TIUBONCHI & SATO (207)	HEAT-TRANSFER TO AIR	.50	.1 → 1000
YUGE (223)	HEAT-TRANSFER TO AIR	.493	10 → 1800
KUDRYASHEV & IPATCAKO (112)	HEAT-TRANSFER TO AIR	.326	0 → 300

Theoretical approaches to the problem of estimating the mass-transfer rate fron single spheres were reviewed by Kinard et. al. (104), and a semi-empirical equation, based on the linear addition of the contributions of radial diffusion, natural convection and forced convection (189), was developed from their summary. The radial diffusion contribution to the mass-transfer rate always exists and can only be isolated when the Reynolds number and Grashof number are both equal to zero, as for the case of a suspended sphere in a stagnant fluid. The overall mass-transfer process can be correlated by the equation

$$Sh = Sh\ (\ Re,\ Sc,\ Gr\ ) \qquad (3.32)$$

and transfer under natural convection is defined as occurring for $Gr > 0$ and under forced convection as for $Re > 0$. Colburn (27) proposed that the Sherwood number would vary as the one third power of the Schmidt number and this has been accepted and justified by a number of workers (53, 173, 63, 56).

The contribution to the transfer process occurring over the rear surface behind the separation ring is due to turbulent transfer through the wake. Unfortunately, this transfer is not amendable to a rigorous theoretical treatment. White and Churchill (217) suggested that this contribution in the turbulent wake be proportional to the Reynolds number of the particle, so giving a correlation of the form

$$Sh = K_1\ (Re)^{\frac{1}{2}}\ (Sc)^{\frac{1}{3}} + K_2\ (Re)\ (Sc)^{\frac{1}{3}} \qquad (3.33)$$

which combines the individual contributions of the front and rear surfaces. Frössling (54) had established that at low flow rates, the contribution of the front surface of the sphere was about 80% of the total transfer, so that K_2 can be given the value

$$K_2 = 0.80 \times 0.552 = 0.45.$$

By linearly adding the diffusional resistances (189, 1, 199), a correlation of the form

$$Sh = 2.0 + (Sh)_n + 0.45(Re)^{\frac{1}{2}}(Sc)^{\frac{1}{3}} + 0.00484(Re)(Sc)^{\frac{1}{3}}, \quad (3.34)$$

was obtained from the selected data of a number of workers (6, 31, 123, 227). Kinard et. al. (104) reported that this correlation with the separate term describing mass-transfer from the rear surface of the sphere gave a significant improvement over the correlation of Frössling (54).

Jones and Smith (95) studied mass-transfer from solid particles freely suspended in a stream of air. This work is an intermediate step between the studies of transfer of held solid spheres or drops and those studies, such as by Garner and Lane (57) of transfer to freely suspended liquid drops. The mass-transfer rate for single spheres was measured and the relationship to the state of turbulence in the gas stream was noted. The solid spheres were observed to rotate at high speed and to fluctuate about a mean position, but mass-transfer rates no higher than those for held solid particles were recorded. The Sherwood number was found to be correlated to the one-quarter power of the tube Reynolds

number. The authors found

$$Sh = 2 + 25 \left(Re.Sc.Re_t^{\frac{1}{2}} \right)^{\frac{1}{3}} \qquad (3.35)$$

for transfer in the laminar flow region, and

$$Sh = 2 + 0.055 \left(Re.Sc.Re_t^{\frac{1}{2}} \right)^{\frac{1}{2}} \qquad (3.36)$$

for transfer in the turbulent range. Their results covered the particle Reynolds number range from 10^1 to 10^7 and they reported that the onset of turbulence as it affects the mass-transfer rate, took place over a wide range of the Reynolds number. They also correlated data from other studies of held drops and spheres using the tube Reynolds number correlation with good success.

Ingebo (89) has presented correlations for heat- and mass-transfer to spheres which differ in several respects from the equations (3.25) and (3.26). In his intensive study of the subject of drop evaporation, he considered the types of bimolecular collisions possible between the air and the diffusing vapour, and derived a dimensionless correlation involving the ratio of the thermal conductivity of the gas phase to the thermal conductivity of the vapour phase.

$$Sh = 2 + 0.303 \left(Re.Sc \right)^{0.6} \left(\frac{k_c}{k_v} \right)^{\frac{1}{2}} \qquad (3.37)$$

In a later paper he considered momentum-, heat- and mass-transfer on a molecular and a macroscopic scale and derived the relationship

$$Sh = f\left[\left(\frac{k_c}{k_v}\right)^{\frac{1}{2}}(Re.Sc)^{0.6}\left(\frac{g\bar{l}}{\bar{c}^2}\right)^{n}\right] \qquad (3.38)$$

where $\bar{l}$ is the mean free path of the molecules and $\bar{c}$ is the root-mean-square velocity. Experimentally he found the coefficients and gave the correlation as

$$Sh = 2.0 + 2.58 \times 10^{6}\left[\left(\frac{k_c}{k_v}\right)^{\frac{1}{2}}(Re.Sc)^{0.6}\left(\frac{g\bar{l}}{\bar{c}^2}\right)^{0.6}\right] \qquad (3.39)$$

A study of the evaporation phenomena for drops of pure liquids and salt solutions was presented by Schlunder (184). His microphotography study of held droplets covered the quasi-stationary thermal equilibrium period of evaporation and also the intial induction period. For mass-transfer from a drop to a gas at constant temperature and conditions, he showed theoretically and experimentally,

$$Nu = \frac{h\,l}{k_f} = \Upsilon + 0.6\,(Pr)^{\frac{1}{3}}(Re^{*})^{\frac{1}{2}} \qquad (3.40)$$

and

$$Sh\,\rho_m = \frac{k_G l}{Dv} = \Upsilon + 0.6\,(Sc)^{\frac{1}{3}}(Re^{*})^{\frac{1}{2}} \quad . \qquad (3.41)$$

for the equations, $l = \Pi\frac{D_p}{2}$ = the characteristic length,

$$\rho_m = \frac{p_{BM}}{P} = \frac{1}{\text{drift factor}}$$

and $$Re^{*} = Re + \tfrac{1}{2}(Gr)^{\frac{1}{2}} \quad .$$

The derivation of this modified Reynolds equation is based on

$$\underline{V}^{*} = \underline{V}_{\substack{\text{forced}\\\text{convection}}} \quad \underline{V}_{\substack{\text{free}\\\text{convection}}} \qquad (3.42)$$

The equations (3.40) and (3.41) were shown to hold

for the range of small Reynolds numbers to high Nusselt numbers and the expression Nu = π shown to be valid for Re* < 0.1, where no convective transfer can be detected. Equation (3.40) can be compared with the Ranz and Marshall (173) correlation by replacing l by $\frac{\pi D_p}{2}$. Their equation is then of the form

$$Nu = \pi + 0.75\ (Re)^{\frac{1}{2}}\ (Pr)^{\frac{1}{3}} \qquad (3.43)$$

and differs from the equation by Schlünder in that the value of the coefficient is 0.75 instead of 0.60 and that the latter's equation is based on a modified Reynolds number continuing the velocity effect of free as well as forced convection. From equations (3.40) and (3.41), the ratio of the Nusselt and Sherwood numbers for heat- and mass-transfer is given by

$$\frac{Nu}{Sh} = \frac{h\ l}{k_f} \cdot \frac{D_v \rho m}{k_G\ l} \qquad (3.44)$$

and the ratio of the transfer coefficients given by

$$\frac{h}{k_G} = \left[\frac{\pi/\sqrt{Re^*} + 0.60\ (Pr)^{\frac{1}{3}}}{\pi/\sqrt{Re^*} + 0.60\ (Pr')^{\frac{1}{3}}}\right] \cdot \frac{k_f}{D_v \rho m} \cdot \qquad (3.45)$$

From this last equation, when $(Re^*)^{\frac{1}{2}} \ll \pi$ or $(Re^*)^{\frac{1}{2}} \gg \pi$, then the ratio of the coefficients is independent of the drop size. Under such conditions, for water vapour-air systems,

$$\frac{h}{k_G} = \frac{k_f}{D_v \cdot \rho m} \qquad (3.46)$$

and so it follows that the water drop temperature remains constant throughout the evaporation process.

Experimentally, he found the time of evaporation of a water drop to be almost unaffected by the initial drop temperature and under conditions of thermal equilibrium (where the vapour pressure at the drop surface is dependent only on the drop temperature, there is no radiation from the gaseous heat-transfer medium, and $Pr/Sc \backsim 1$) the drop surface to change linearly only with time for $Re^* \ll \pi^2$. For the Re* range from 1 to 3, Nu and $Sh\,\rho_m$ were found to have an invariant value of 3.5 over the temperature fange from 200 to 700 F and this value is just above the minimum value of π valid for pure molecular transport. The arithmetic mean of the air temperature and the drop temperature was used as the temperature at which to evaluate physical properties of the vapour film about the drop. He also integrated the differential equation describing the thermal induction for the drop on the understanding that the drop radius changes to only a small extent, during this period. This assumption is verified, since the thermal induction period itself exists for only a small fraction of the whole evaporation time under extreme cases.

The various attempts by different authors to take into account the free convection or "bouyancy effect" can be compared with the study of evaporation with high mass-transfer rates for the Reynolds number range of 5.5 to 570 at turbulence intensities less than 1%, as reported by Pei et. al. (165). They found that for pure natural convection, the effect of the bouyancy forces could not be accounted for by the Grashof number alone, but by a parameter involving the radial velocity of the vapour at the surface of the drop. The forced

convection and natural convection effects were shown to be non-additive and the transition from one mechanism to another was gradual. Their system was found to be best described by the parameter (Gr/Re^2).

3.4 EVAPORATION LIFETIMES OF LIQUID DROPS.

Marshall and Seltzer (147) presented a solution for the drying time of pure liquid drops assuming the drops to be at their terminal velocities in the Stokes' law region.

A heat balance about an evaporating drop gives the time of evaporation as

$$\theta = \frac{\rho_d H_v}{2\Delta T}\int_{D_{p_1}}^{D_{p_o}} \frac{dD_p}{h_c} \quad . \tag{3.47}$$

For a drop evaporating in still air conditions, the time for complete evaporation is then

$$\theta = \frac{\rho_d H_v D_{p_o}^2}{8k_f \Delta T} \quad . \tag{3.48}$$

Using the correlation developed by Frössling (54) for the rate of heat-transfer to the drop, we can substitute for h_c in equation (3.47) to show

$$\theta = \frac{\rho_d H_v}{4k_f \Delta T}\int_{D_{p_1}}^{D_{p_o}} \frac{D_p dD_p}{\left[1+0.276(Re)^{\frac{1}{2}}(Pr)^{\frac{1}{3}}\right]} \quad . \tag{3.49}$$

The terminal velocity of the drop in the Stokes' law region is given by

$$V_t = \frac{g(\rho_d - \rho_c)D_p^2}{18\mu_c} \tag{3.50}$$

and this expression can be used in the Reynolds number term of equation (3.49) to give

$$\theta = \frac{\rho_d H_v D_{p_o}^2}{8k_f \Delta T}\left[1 - \frac{2}{D_{p_o}^2}\int_0^{D_{p_o}} \frac{B_1 D_p^{5/2} dD_p}{\left[1+B_1 D_p^{3/2}\right]}\right], \quad (3.51)$$

where

$$B_1 = 0.276\left(\frac{c_p \mu_c}{k_f}\right)^{\frac{1}{3}}\left[\frac{g(\rho_d - \rho_c)\rho_c}{18\mu_c}\right]^{\frac{1}{2}}. \quad (3.52)$$

Equation (3.51) can be integrated to give the total time of evaporation as

$$\theta = \frac{\rho_d H_v D_{p_o}^2}{8k_f \Delta T}\left[1 - \sum_{m=1}^{\infty}(-1)^{m-1}\frac{4}{(3m+4)} B_1^m D_{p_o}^{3m}\right], \quad (3.53)$$

the series converging if $D_{p_o}^{3/2} > 1/B_1$.

In commercial spray drier applications the droplet size range is such that the Reynolds number range is from 10^{-1} to 10^2. The Stokes' law region is generally accepted to be for Reynolds numbers less than 2. Consequently, sprayed particles in a spray drier will be for the most part in the Stokes' law region.

For the evaporation of spray droplets at higher Reynolds numbers than those in the Stokes' law range, Duffie and Marshall (42) have proposed that the evaporation time be given by an equation similar to that of Seltzer and Marshall (147), but based on the Ranz and Marshall correlation (173) rather than that of Frössling (54). Equation (3.49) then becomes

$$\theta = \frac{\rho_d H_v}{4k_f \Delta T}\int_{D_{p_1}}^{D_{p_o}} \frac{D_p dD_p}{\left[1+0.30(Re)^{\frac{1}{2}}(Pr)^{\frac{1}{3}}\right]}. \quad (3.54)$$

Using the relationship given by Perry (70) for the terminal velocity of a droplet in the transition or intermediate region, as

$$V_t = \frac{0.153\, D_p^{1.14} \left[g(\rho_d - \rho_c)\right]^{0.71}}{(\rho_c)^{0.29}(\mu_c)^{0.43}} \qquad (3.55)$$

then equation (3.54), when V_t is substituted in the Reynolds number, becomes

$$\theta = \frac{\rho_d H_v}{8k_f \Delta T} \int_{D_{p_1}}^{D_{p_o}} \frac{D_p\, dD_p}{(1+B_2 D_p^{1.07})}, \qquad (3.56)$$

where

$$B_2 = 0.3 \left[\frac{0.153\, g\, \rho_c (\rho_d - \rho_c)^{0.71}}{\mu_c^2}\right]^{\frac{1}{2}} \left[\frac{c_p \mu_c}{k_f}\right]^{\frac{1}{3}}. \qquad (3.57)$$

Equation (3.56) can be expressed as the sum of two drying times as follows.

$$\theta = \frac{\rho_d H_v}{8k_f \Delta T} \left[(D_{p_o}^2 - D_{p_1}^2) - 2 B_2 \int_{D_{p_1}}^{D_{p_o}} \frac{D_p^{2.07} dD_p}{(1+B_2 D_p^{1.07})}\right] \qquad (3.58)$$

Equation (3.58) can be expressed in a more convenient form by integrating the equation from an appropriate lower limit, below which the correction for the terminal velocity effect on the evaporation rate is negligible. for example, we can neglect the velocity effect for drops below one hundred microns in diameter. Sherwood and williams (190) and Ranz and Marshall (173) in their treatments of the evaporation lifetimes of pure liquid drops in still air and falling at terminal velocities in the Stokes law region, showed that corrections to the time

of evaporation in still air would be negligible for droplets less than one hundred microns in diameter moving in the Stokes' law region. Hence , we can add to equation (3.58) the time of evaporation from 100 to zero microns diameter as given by equation (3.48), to give

$$\theta = \frac{\rho_d H_v D_{p_o}^2}{8 k_f \Delta T}\left[1 - \frac{2B_2}{D_{p_o}^2}\int_{100}^{D_{p_o}} \frac{D_p^{2.07} dD_p}{(1+B_2 D_p^{1.07})}\right] \quad . \quad (3.59)$$

In this equation, the first term represents the time of evaporation of a drop at zero relative velocity conditions and the second term is the correction to account for the terminal velocity effect where the drop diameter is more than 100 microns.

Johnstone and Eads (92) used Frösslings equation (54) and assumed the temperature of the drop and so the vapour pressure about the drop, to be constant during the evaporation process. They also assumed the relative velocity of the drop to be constant with time. The time of evaporation of a pure drop was shown by them to be given by the equation

$$\theta = \frac{1}{\gamma}\left[\left(\frac{2}{3}\right) D_{p_o}^{3/2} - \left(\frac{2}{\epsilon^2}\right) D_{p_o} + \left(\frac{8}{\epsilon^3}\right) D_{p_o}^{\frac{1}{2}} - \left(\frac{16}{\epsilon^4}\right) \log_e\left[1 + \frac{\epsilon\left(D_{p_o}\right)^{\frac{1}{2}}}{2}\right]\right] \quad (3.60)$$

where $\epsilon = 0.552(Sc)^{\frac{1}{3}}\left[\frac{V \rho_c}{\mu_c}\right]^{\frac{1}{2}}$ = constant for constant relative velocity, (3.61)

and $\gamma = \frac{2 D_v P M \Delta p}{\rho_d \mathbb{R} T p_{BM}}$ = constant for constant vapour pressure. (3.62)

Hence they defined the general equation for the drying time as

$$\theta = \frac{f(D_{p_o}, \epsilon)}{\gamma} \quad . \tag{3.63}$$

For drying with zero relative velocity $\epsilon = 0$ and so

$$\theta = \frac{D_{p_o}^2}{4\gamma} \quad . \tag{3.64}$$

The evaporation rate of a falling drop can be calculated by means of a step-wise procedure regarding the velocity of fall as being constant for each increment of drop diameter change.

Equation (3.60) by Johnstone and Eads (92), was originally derived as a correlation based on the evaporation of small sulphur droplets. This was an extension of the work by Conroy and Johnstone (31) whose study of the burning of sulphur droplets gave an equation for the time of evaporation of such drops in a gas temperature range from 1250 to 1750 ^{o}K, as

$$\theta = D_{p_o}^2 (453.2 - 0.174\ T_g x\ 10^{-8}). \tag{3.65}$$

This equation was derived from equations for the rate of heat- and mass-transfer to evaporating drops as given by

$$\frac{dm}{d\theta} = (Nu)\pi k_f \left(\frac{6m}{\pi \rho_d}\right)^{\frac{1}{3}} \Delta T \tag{3.66}$$

and

$$-\frac{dm}{d\theta} = (Sh)\pi D_v \left(\frac{6m}{\pi \rho_d}\right)^{\frac{1}{3}} \frac{P\ M\ \Delta p}{R\ T\ p_{BM}} \ , \tag{3.67}$$

where Nu = Sh = 2.0

Sjenitzer (193) presents equations with graphical solutions for calculating the complete evaporation history of a spray of liquid drops. The equations are based on Frössling's correlation (54) for the evaporation of a spherical liquid drop and Ingebo's expression (88) for the

instantaneous, unsteady-state drag coefficient, given as

$$C_D = 27\ Re^{-0.84} \qquad (3.68)$$

for the particle Reynolds number range from 6 to 500. The method of solution involves the evaluation of the drying conditions for a special case of a droplet with Reynolds number of 500. In general, the initial droplet Reynolds number is less than 500 and the same graphical solution curves are used as for the case of the droplet with Re=500, but the evaporation of a ficticious droplet is studied such that the parameters intially chosen will during the latter part of the life of the droplet, produce evaporation conditions closely resembling those of the droplet to be investigated.

Meisse (152, 153) has also presented equations for the drying time and path length of evaporating droplets. His equations are similar to those of Sjenitzer (193), but he assumes that the drag coefficient of the evaporating droplet varies inversely with the drop Reynolds number and that the velocity of the surrounding gas varies linearly with the distance down the drying chamber.

4. EVAPORATION OF DROPS CONTAINING SOLIDS.

The complexity of the process of evaporation from a droplet having a velocity relative to the surrounding air is greatly increased by the presence of dissolved or suspended solids within the droplet.

In general, the concentration of solution is initially uniform within the droplet, but as soon as some evaporation has taken place from the droplet surface concentration gradients are set up and there is diffusion of the solute toward the drop centre. In addition, since the drop is necessarily decreasing in size, the solute in the surface layer is swept inward by the retreating interface.

For evaporation of the droplet with a relative velocity, boundary layer theory predicts and Frössling (54) has experimentally demonstrated, that the evaporation rate varies from a maximum at the point of impingement at the front of the drop, through a minimum at some latitude beyond the equator to a second but smaller maximum rate at the rear of the drop. As a result of this flow pattern about the drop, the diffusion has a tangential component toward the rear of the drop as well as a radial component and the concentration profiles within the drop are not simple. Superimposed on the flow owing to diffusion, may be the internal circulation from density gradients caused by temperature and concentration differences within the drop and by the viscous drag of the continuous phase. Generally, droplet rotation is sufficiently rapid and random to tend to restore the spherical symmetry of the drop, but if the particle has no initial rotational motion and its relative velocity is in the direction of gravity, then the maximum evaporation rate at the front of the droplet

TABLE. 4.1

AUTHORS	PRODUCT STATE	OPERATING VARIABLES
SMITH (194)	BULK DENSITY	A, B, C, E, F.
CROSBY & MARSHALL (33)	BULK DENSITY & SIZE	A, B, C, D.
CHU, STOUT & BUSCHE (96)	BULK DENSITY & MOISTURE CONTENT	A, B, C, G, H.
DUFFIE & MARSHALL (42)	BULK DENSITY	A, B, I.
CHALOUD, BAKER & MARTIN (24)	BULK DENSITY, MOISTURE CONTENT & DRYING RATE	A, C, D, I, K, L.
BUCKHAM & MOULTON (22)	INTIAL DROPLET TO FINAL DRY PARTICLE SIZE RATIO	A, C, D, H, J.
SELTZER & MARSHALL (147)	BULK DENSITY	A, C, E.
COSLETT (32)	BULK DENSITY & MOISTURE CONTENT	A, B, C, D, L.

OPERATING VARIABLE	SYMBOL	OPERATING VARIABLE	SYMBOL
DRYING AIR TEMPERATURE	A	SOLVENT IN LIQUID FEED	G
LIQUID FEED TEMPERATURE	B	TYPES OF ATOMISER	H
LIQUID FEED CONCENTRATION	C	PROPERTIES OF DRIED MAT'L.	I
SPRAY DROP SIZE	D	DRYING AIR FLOW RATE	J
SPRAY DROP SIZE DISTRIBUTION	E	HEIGHT OF DRYING CHAMBER	K
DRYING RATE	F	TURBULENE OF DRYING AIR	L

results in a high concentration of solute in that area. This creates a greater than average density at the front of the drop, a situation which should add to the stability of the drop against rotation.

Reported studies of the evaporation of sprayed solutions containing solids either dissolved or in suspension are few and usually refer to one of two particular aspects of spray droplet evaporation. The first aspect is the study of the overall effect on the final product obtained by varying the operating conditions of the spray drier. The second aspect is the study of single held droplets containing solids, evaporating under controlled conditions.

Studies of the overall effect on the evaporation of sprayed solutions have generally been carried out on commercial equipment. The effects on the product characteristics for a change in any one of a number of operating variables have been presented by a number of authers. Table 4.1 shows a list of some of these workers along with the properties investigated in terms of the various operating conditions. Perhaps one of the more extensive of these works is that of Crosby and Marshall (33), whose study of the effects of the drying conditions on the properties of the spray dried materials produced numerous curves of experimental data relating the various operating variables. The photomicrographs they produced explain in part why the density of spray dried particles varies with the final particle diameter. This explanation is based on the shape and thickness of the crystallised shell of the dried particle and on the final moisture content of the particle.

The drying of a single held droplet of a solution has been studied by a small number of workers, some of whom modified the correlations developed for the evaporation of pure drops and used these modified equations to evaluate the heat- and mass-transfer rates of the evaporating droplet. When a droplet contains dissolved materials which lower the normal vapour pressure of the liquid, the vapour pressure and temperature differences causing mass- and heat-transfer, respectively, are lowered and the evaporation rate is less than for pure liquid drops. For droplets of solutions with a negligible vapour-pressure lowering and for suspensions of inert solids, the evaporation rates in the initial stages can be treated in the same manner as for pure liquid drops of the same size.

In addition to the effect on the vapour pressure, the presence of solids introduces all the complications usually encountered in the falling rate period of the drying of solids. The evaporation and drying of drops in spray drying generally involves a period of evaporation comparable to the evaporation of pure liquid drops at a constant temperature, followed by a period in which the rate decreases rapidly, the drop temperature increases, and the temperature driving force decreases towards zero. The time of evaporation of the drop is then equal to the sum of the time for surface evaporation of the free moisture and the time for the subsurface evaporation of the held moisture.

Ranz and Marshall (173) showed that for the evaporation of drops containing a dissolved component, the drop evaporated as though it were saturated even though its average concentratio was well below saturation. This was explained on the basis

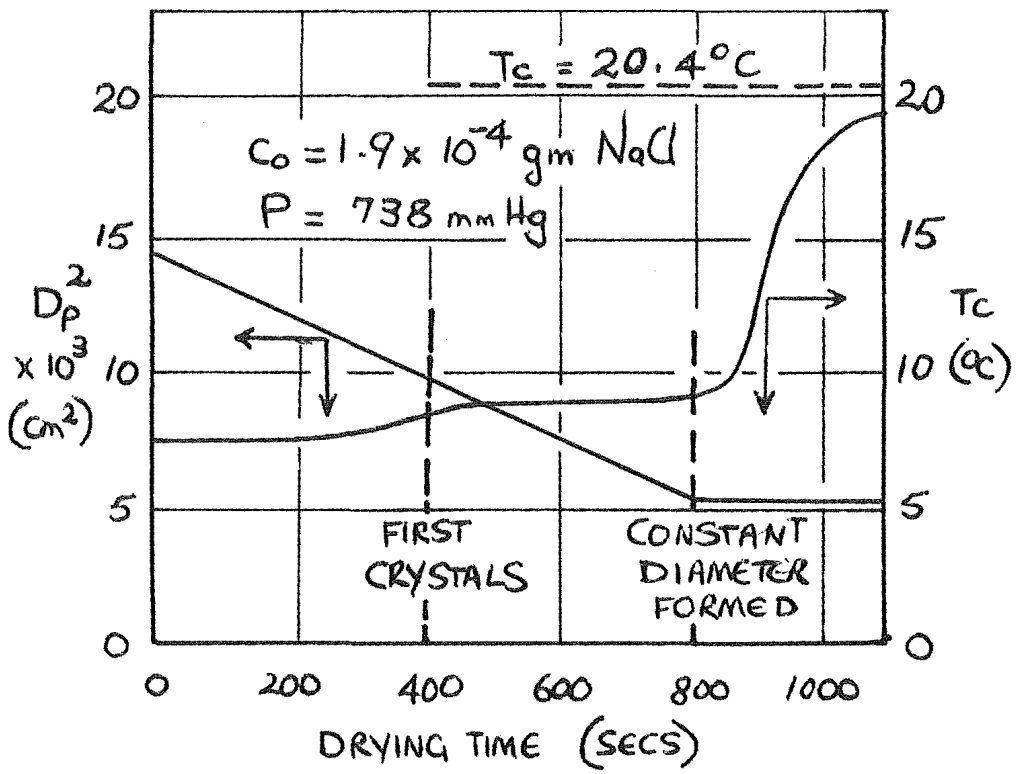

FIGURE 4.1 VARIATION OF DROP DIAMETER AND TEMPERATURE FOR THE DRYING OF A DROP OF SODIUM CHLORIDE SOLN. (173)

that the rate of diffusion of the dissolved material back into the drop was slow compared with the evaporation rate and hence the solids concentrated at the surface of evaporation faster than they could diffuse toward the centre of the drop. Experimental evidence of this was obtained with drops of ammonium nitrate solution. The results showed that regardless of the concentration in the drop, the evaporation rate was within 0.33% of the rate obtained assuming that the surface of the drop was completely saturated.

Charlesworth and Marshall (25) showed a result contrary to that of Ranz and Marshall (173), in that for certain soluble salts such as calcium chloride, the droplet of a less than saturated solution does not evaporate as though it were saturated.

When the drops containing the solids have been evaporated fractionally, then the heat of crystallisation and also super-saturation effects become significant. Although the drying time of a drop one millimeter in diameter at room temperature may be up to one thousand times greater than for the same drop in a spray drier, the life-history of such a held drop is of interest in predicting the phenomena which might occur in a spray drier. Figure (4.1) shows the time variation of diameter and temperature for an evaporating drop containing sodium chloride. So long as the drop presents a completely wetted surface to the drying air, then the rate of change of the square of the droplet diameter and the temperature difference driving force are a measure of the drying rate at any instant. Ranz and Marshall reported no supersaturation at the surface and the three zones of temperature exhibited in this case may be interpreted as a primary zone where the

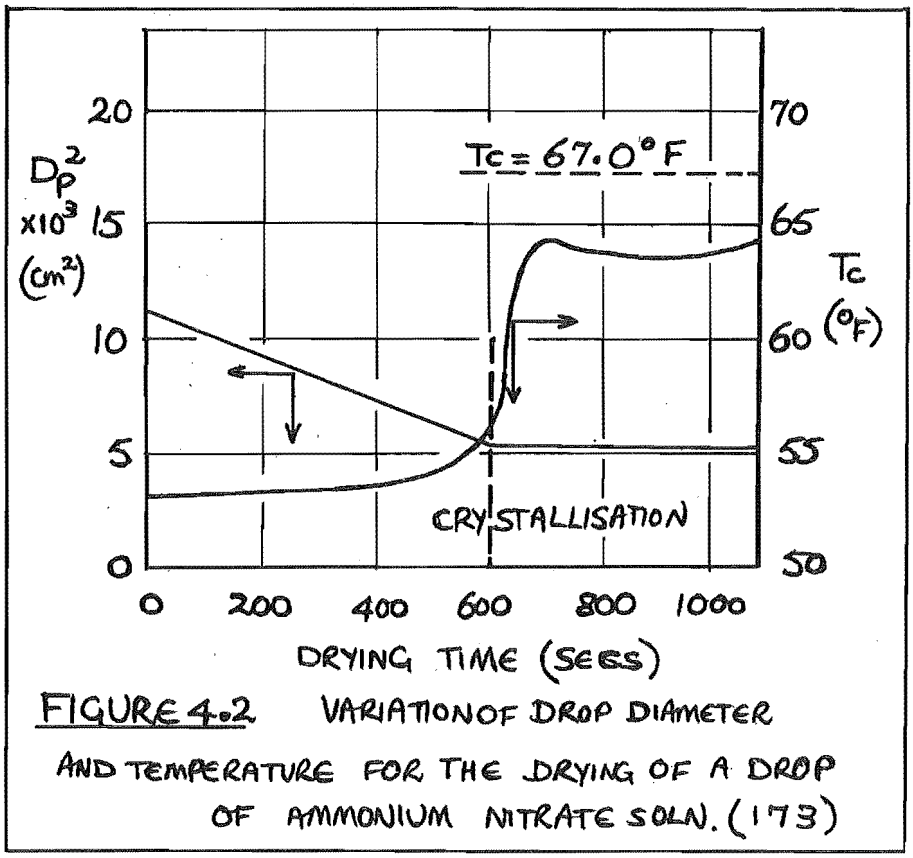

FIGURE 4.2 VARIATION OF DROP DIAMETER AND TEMPERATURE FOR THE DRYING OF A DROP OF AMMONIUM NITRATE SOLN. (173)

temperature of the drop increases slightly because of an increasing concentration at the surface of the drop, a constant zone of quasi-thermal equilibrium caused by the crystallisation process, and a final falling rate zone. For the evaporation of drops of ammonium nitrate solution, Supersaturation did occur since crystals of the solute were reported to have appeared suddenly covering the whole of the surface of the drop. Figure (4.2) illustrated that the effect of the heat of solution of the ammonium nitrate is appreciable in that the rapid increase in the drop temperature is due to the complete crystallisation and the evolution of the high heat of crystallisation.

Recently, Sano and Nishikawa (182) reported a study of the drying mechanism of drops of polymer solutions. Held droplets of high molecular weight polymer solution were dried in a special chamber. Temperature and concentration variations with time of drying were investigated and constant rate (I) and first (II) and second (III) falling rates measured. Good agreement between their theoretical predictions and the experimental results were obtained as shown in figure (4.3).

The relationship between the drop size before drying with that after drying for a detergent and a roasted-wheat extract were reported by Laster (122). For the former material, the following relationship was given:

$$D_{p_s} = 1.026\, D_{p_o}^{1.135} \qquad (4.1)$$

where D_{p_s} is the dry-particle diameter. For the

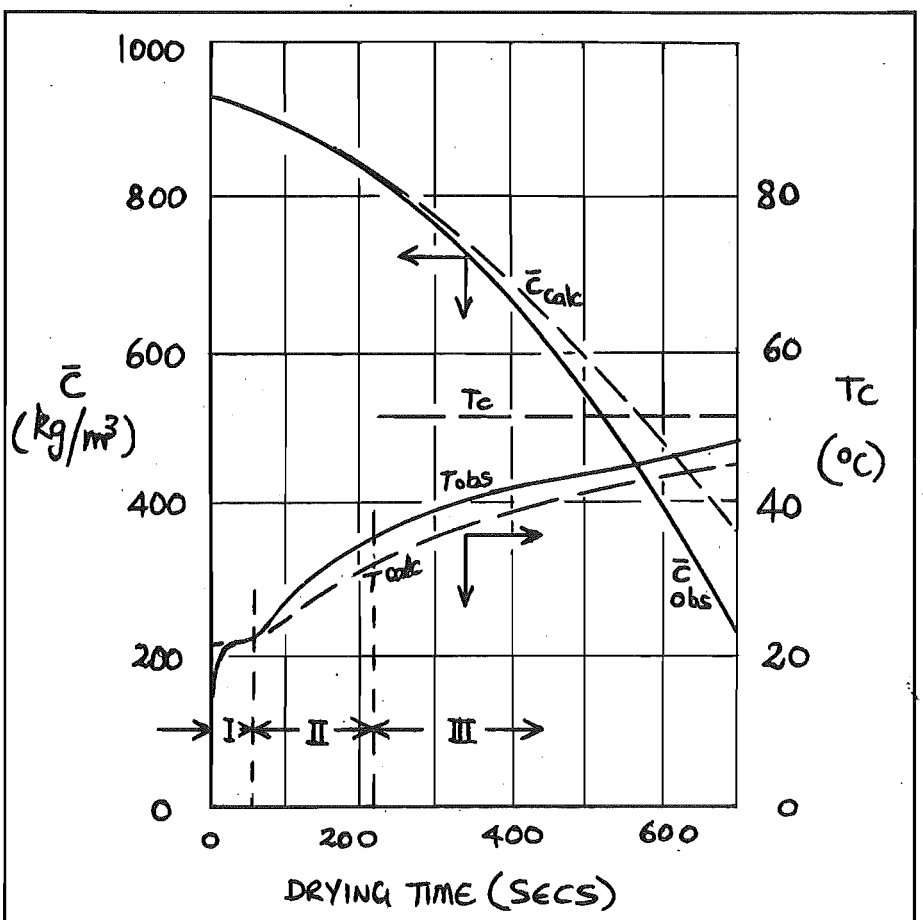

FIGURE 4.3 TEMPERATURE AND CONCENTRATION VARIATION FOR THE DRYING OF A DROP OF HIGH MOLECULAR WEIGHT POLYMER SOLUTION. (182)

extract he gave

$$D_{p_s} = 250 \log_{10} D_{p_o} - 425. \qquad (4.2)$$

Thus, the detergent increased in size and the dried extract was smaller than the original spray droplet. Kirschbaum (107) reported substantially no difference in the size of spray dried yeast particles from the original spray droplets.

Schlunder (184) proposed theoretical equations for the drying of salt solutions using quasi-stationary conditions within the gas, based on the assumption that the temperature rise within the drying droplet is relatively slow even though the vapour pressure about the drop decreases because of the increasing salt concentration at the drop surface. This slow change of drop temperature assumes of course that the heat of crystallisation is negligible. To calculate the extent of mass-transfer under such quasi-stationary conditions, the dependence of the salt concentration (as defined by the vapour pressure at the drop surface) on the mass-transfer rate must be known.

Two limiting cases are apparent. First, the case where there is complete mixing within the drop and so the surface concentration is always equal to the mean concentration which is readily calculated from the mass tramsferred. Secondly, there is the case where the salt left behind by the evaporating solvent is not dispersed into the bulk of the drop but exists as a concentration boundary at the surface of the drop. This surface concentration is always higher than the bulk mean concentration of the drop and the lowering of the vapour pressure because of this high

salt concentration, is significant in the evaporation of some salt solutions.

Evaporation tests by Schlunder (184), using lithium chloride solutions gave results that agreed well with the theoretical calculations for the variation of the evaporation rate as a function of the mean salt concentration. On the other hand his results for for the variation of the surface to bulk mean concentration ratio (which was measured indirectly) shows an ambiguity in that a significant retardation of the rate of salt back diffusion was observed for the drying of dilute solutions but not for the drying of concentrated solutions. One deduces that the surface layer of high concentration for the drop of low bulk concentration is then built up before the back diffusion of this surface concentration layer sets in.

The drying time of a drop containing solids is the sum of the individual drying periods. The first drying period ends when the liquid surface of the drop becomes solid. This may occur before conditions of uniform saturation throughout the drop are reached, and hence the final particle may have an unusual porosity. In order to estimate the time of the first drying period, some method must be established to predict critical moisture content, corresponding to the end of the first period. From values of the critical and final moisture content, the time in the falling-rate period can be estimated using the following equation by Ranz and Marshall (173).

$$\theta_f = \frac{H_v D_{p_c} \rho_s (W_c - W_1)}{6\, h_c \Delta T_{av}} \qquad (4.3)$$

θ_f is the falling-rate drying time and W_c is the critical

moisture content.

For a drop drying at a low Reynolds number and under conditions where there is negligible vapour-pressure lowering, an expression for the total drying time can be written as

$$\theta = \frac{H_v \rho_L (D_{p_o}^2 - D_{p_c}^2)}{8k_f(T_c - T_s)} + \frac{H_v(W_c - W_1)\rho_s D_{p_c}^2}{12k_f \Delta T_{av}} . \qquad (4.5)$$

To use this equation one must know or have available a method of determining the relationship between the moisture content and the drop temperature.

Equation (4.5) is a simplification of the actual condition in a spray drier where the air temperature changes markedly during the constant rate period. For this case, $(T_c - T_s)$ must be averaged over the constant rate period. From the equation it is evident that the evaporation time for the drying of drops with solids present may be somewhat greater than for pure liquid drops, the increase in drying time depending in part on the value of the critical moisture content. For those cases where the vapour pressure above the drop is lowered due to solids within the drop, the temperature driving force will be less and this will increase the drying time still more.

Because in actual spray driers the time of drying is extemely small, it is quite possible that the dynamic equilibrium for any one phase of the drying process may never be reached and the physical situation represented in the figures above will be smoothed into a continually changing form not amendable to analysis by methods employed so far.

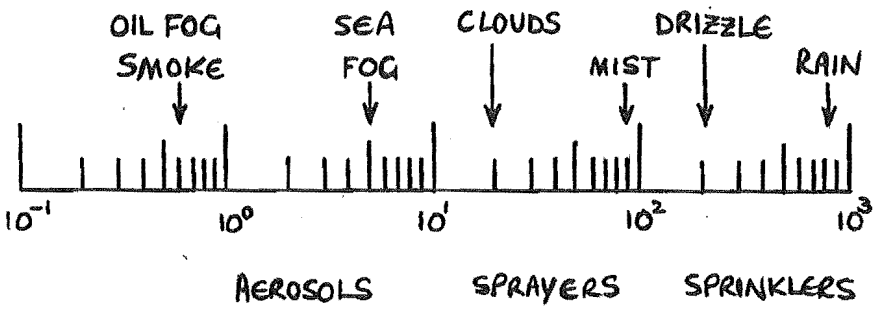

FIGURE 5.1 SPECTRUM OF DROP SIZES.
(DROP DIAMETERS IN MICRONS)

5. EVAPORATION OF SPRAYS.

Dispersions of liquids in gases are given a number of names intended to classify them, but a precise and exclusive definition is not conveyed by any of the terms in common use (166). The term "spray" generally implies the deliberate production by mechanical means of a dispersion of relatively large drop size. A spectrum of drop sizes is shown in figure (5.1) and the drop size of sprays usually implies drops with diameters within the range of 10 to 500 microns (51). By defining a spray as being composed of droplets then, we eliminate the macroscopic cases wher large drops, slugs or columns of liquid may exist and also the microscopic cases where the dispersion is of the order diameter of the component molecules (159).

In the process of spray drying, the requirement is to produce a large surface area for the evaporation process and achive a uniform specified droplet size. If in spray drying, drops of only one size could be produced, their drying rates and flow patterns would then be uniform and easily established. The drying chamber could then be accurately designed with the full knowledge of the mechanics and the heat- and mass-transfer requirements of the droplets. In practice however, a wide size range of droplets are produced and some difficulty in operating the drying chamber is experienced when this drop size range is to great(51). As the design of the dryer is based on the need to dry completely the largest drop formed by the atomiser, it is necessary to control the process by proper selection of the atomiser and the atomising conditions. A small reduction in the drop size of the largest drops will change significantly the rate of evaporation.

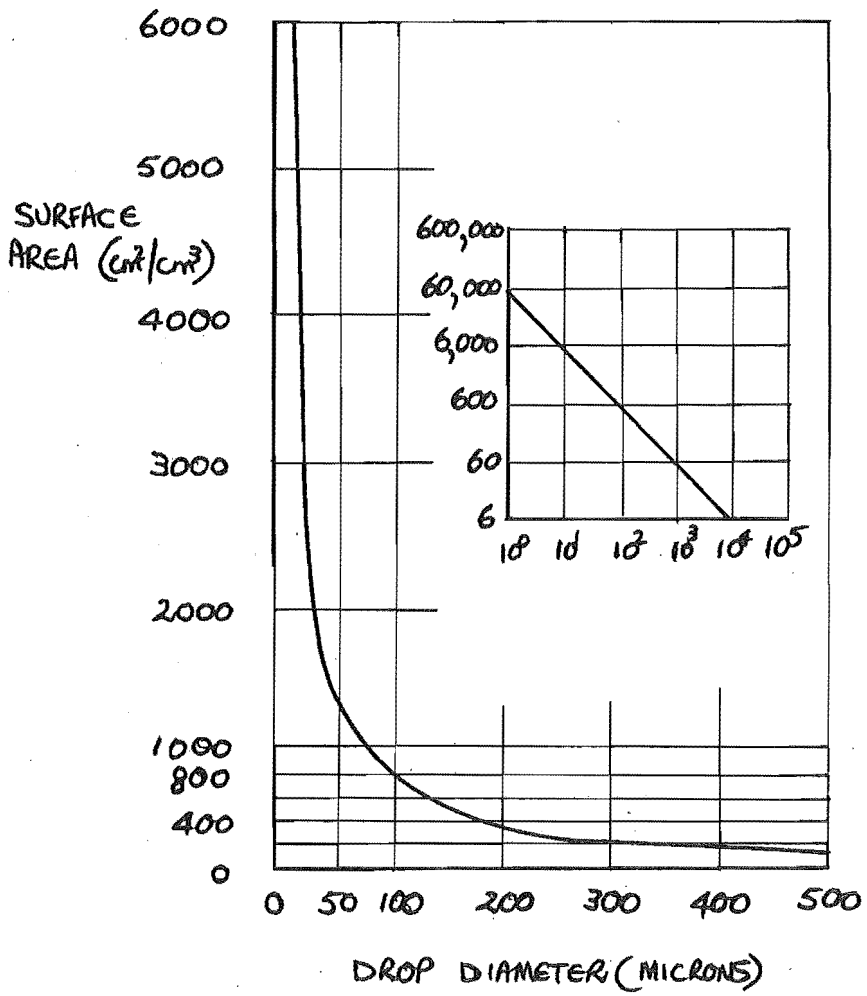

FIGURE 5.2 RATE OF INCREASE OF SPECIFIC AREA ON REDUCTION OF THE DROP DIAMETER (51)

5.1 ATOMISATION.

Recent expansion in the application of spray drying to industial uses has necessitated more attention being paid to the design of atomisers and atomisation techniques in general. The process of spray drying takes place in three stages. Intially the liquid feed must be atomised into the drying chamber, then the contacting of the spray with the hot gaseous drying medium takes place and finally the dried product is separated from the gas. That the atomisation stage holds the key to the successful application of spray evaporation is quite evident.

The purpose of atomisation is to provide a very large surface area from which evaporation can take place rapidly. This vast increase in surface area is shown in figure (5.2) where the equivalent surface area for one cubic centimeter of liquid is plotted against the drop diameter. The very great rate at which the surface area increaes below the drop size of 50 microns is also indicated in the much greater atomiser energy requirements to produce such small particles. The actual increase in surface area is from 250 to 1000 times in the atomising range providing drops from 20 to 500 microns in diameter (51).

Fraser and Eisenklam (50) presented an extensive survey of the field of atomisation and major spray applications of interest to Chemical Engineers. They showed the effect of the spraying atmosphere on atomisation to be marked, as an atmosphere at high pressures caused a shortening of the liquid sheet immediately before disintegration while an atmosphere at low pressure caused the products of a viscous material when atomised to be stringy and brittle. Two separate distinguishable effects were that of the sheet thickness of liquid and the mode of disintegration, and that of the

effect on the drops as they moved through the drying gas. Fraser, Dombrowski and Rowtley (49) have shown that the size of the drop on atomisation is a function of the thickness of the liquid sheet on impact with the air stream. Thin liquid sheets are then an essential pre-requisite of fine atomisation. They developed a semi-empirical relation correlating a mean drop size with the sheet thickness for a wide range of operating conditions.

The drop size distrbution of a spray from a nozzle can be shown to be dependent on the orifice diameter and the Reynolds, Weber and Froude numbers of the liquid at the nozzle (98). Consider the flow of liquid form a nozzle as it forms a spray of liquid drops. We can assume that the average size of the drops formed in the spray will be dependent on the physical and mechanical properties of the system as such;

$$D_p = f(\rho_d, \mu_d, \sigma, g, D_o, U) \quad , \qquad (5.1)$$

where D_o is the orifice diameter and U the discharge velocity of the liquid at the orifice. Then taking ρ_d, D_o and U as the primary quantities, we find by dimensionless analysis that

$$\frac{D_p}{D_o} = f(\mathrm{Re}, \mathrm{We}, \mathrm{Fr}). \qquad (5.2)$$

The three common types of atomisers found in industry are the Pressure Nozzle, the Pneumatic or Two-Fluid Nozzle and the Centrifugal Disc atomiser. In spite of much published data (166, 145, 149) the subject of the mechanism of atomisation still requires further study. The basic mechanism of atomisation can be summarised as the disintegration of a liquid sheet promoted by turbulence in the flow of the liquid from the orifice and the action of air forces, while at the same time being opposed by the viscosity and

surface tension forces of the liquid. Various relationships have been developed to give the mean diameters of the spray droplets for the different types of atomisers.

A correlation for general use with pressure nozzles is given by Lewis (127):

$$D_{p_s} = 157\left(\frac{\sigma}{P_n}\right)^{\frac{1}{2}} + 597\left[\left(\frac{\mu}{\sigma\rho_d}\right)^{0.45}\left(\frac{Q}{K_n D_o(\rho_c/\rho_d)^{\frac{1}{2}}}\right)^{1.5}\right] \quad (5.3)$$

and for pneumatic or two-fluid nozzles, one well known relation (160) is

$$D_{p_s} = \frac{1410}{V}\left(\frac{\sigma}{\rho_d}\right)^{\frac{1}{2}} + 191\left[\frac{\mu}{(\sigma\rho_d)^{\frac{1}{2}}}\right]^{0.45}\left[\frac{1000}{J}\right]^{1.5}. \quad (5.4)$$

A comparison between spray nozzles and atomising discs is rather difficult and involves the following considerations (147). (1) The atomisation capacity, expressed as square feet of surface created per pound of atomised liquid per minute.

(2) The atomisation efficiency expressed as power consumed per square foot of new surface area created.

(3) The drop size distribution at identical feed rates to both atomisers.

(4) The weight flow distribution.

Atomisation by disc is generally more flexible from the view if operating conditions. Both nozzles and discs will atomise low viscosity liquids with equal merit. In practice, one seldom has the choice between a nozzle or a disc atomiser as the design features of the drying chamber and the physical properties of the liquid to be sprayed, characterise the atomiser requirements. Standardisation of spray drying equipment is accordingly difficult

as each application must be considered on its own merits.

The initial drop size distribution of an atomiser can usually be expressed in the form of a simple mathematical probability function or as a mean value obtained from such equations as expressed above. In general, it is better to determine experimentally the distribution for a given nozzle under specific liquid feed rate and properties.

Masters (149) and Marshall (145) have both presented extensive reviews of the literature on the three types of atomisers mentioned and for each type of atomiser deal with the mechanism of drop formation and the drop size distributions obtained under various operating conditions.

5.2 DROP-SIZE DISTRIBUTIONS.

The drop-size distribution is the most fundamental characteristic and one of the more important features of sprays from atomisers. It is also the property most difficult to predict theoretically and to determine experimentally. Since most correlations for heat-transfer in the evaporation of sprays of droplets are based on either a mean drop size or evaluated by a "step" method for a series of drop size ranges, it is important that the size distribution of a spray be determined as acurately and simply as possible.

The analysis of the drop size distribution of an atomiser is usually done in three stages. First, a representative sample of the spray must be captured by one of the many methods available. Secondly, the drops of the sample must be measured and counted by visual or electronic techniques. Finally, the numerical results must be fitted to a mathematical distribution function which best describes the experimentally measured distribution of the spray.

5.2 (a) DROPLET SAMPLING TECHNIQUES.

Numerous papers on techniques for the capture of spray-droplet samples have been presented, with reference in particular to the following methods.

(i) Sampling Cell method of collecting drops and containing them in an immiscible solvent in a cell (2,15,61, 180,202,203).

(ii) Coated Slide method of impacting droplets on slides coated with a powder such as magnesium sulphate or soot (61,128,151,172,174).

(iii) Solidified Droplet method where frozen or solid drops of wax or suitable liquids are captured and measured (71,135,204).

(iv) Direct Photography method requiring a small sample size and separate calibration (213,220,222).

(v) Special Electronic methods (2,60).

The above methods of sampling sprays are discussed along with other less often used techniques by Marshall (145) in his monograph on Atomisation and Spray Drying. Pilcher and Thomas (168) report on some of the methods developed for capturing and measuring drops and conclude that although no one method is entirely satisfactory, the immersion cell technique has been sucessfully tried in research and industry. Analysis by manual or automatic counting equipment proved to be accurate enough for most purposes.

A number of investigators (5,116,186) have shown that mechanical sampling introduces an inevitable bias and that this bias may be very large for large samplers in dispersions of small particle size. The bias results from the deflection of the flow lines around the sampler. If all suspended particles maintain their postion in the flow lines during

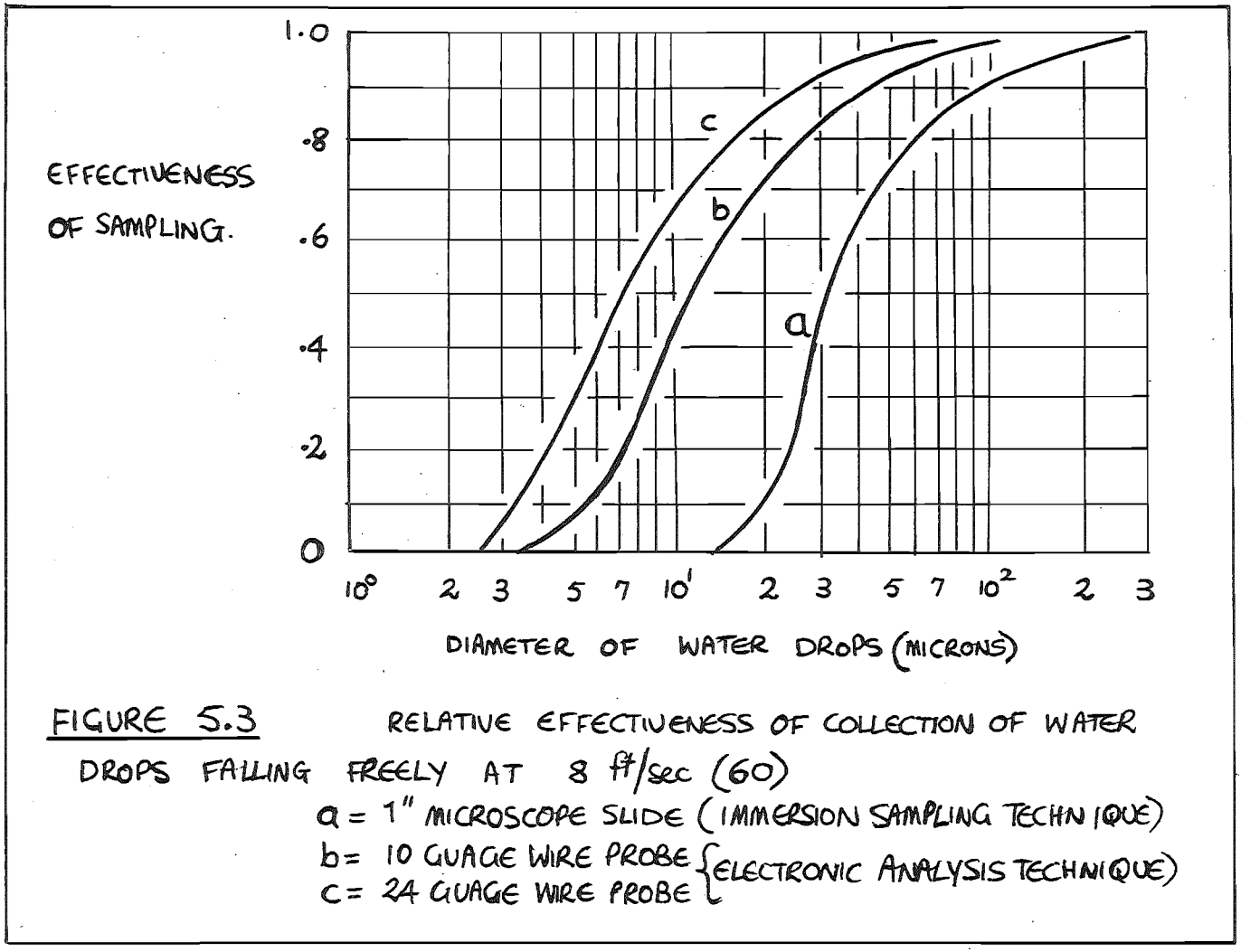

FIGURE 5.3 RELATIVE EFFECTIVENESS OF COLLECTION OF WATER DROPS FALLING FREELY AT 8 ft/sec (60)

a = 1" MICROSCOPE SLIDE (IMMERSION SAMPLING TECHNIQUE)
b = 10 GUAGE WIRE PROBE } ELECTRONIC ANALYSIS TECHNIQUE)
c = 24 GUAGE WIRE PROBE }

this deflection, none would be intercepted by the sampler. On the other hand, if the particles had sufficient inertia to leave their flow lines and continue in a straight path, the sampler would intercept all those whose paths project into the collection surface. In practice, the actual operation of samplers lies between these two extremes. The effectiveness of a sampler is defined as the ratio of the number of particles intercepted by the sampler to the actual number that would be collected if none were deflected around the sampler. The various workers show and agree, that higher velocities, smaller samplers and larger particles, give higher values of the effectiveness of sampling as shown in figure (5.3).

This result indicates that data on size distributions obtained with large samplers (such as the immersion cell type) are to be questioned for reported particle sizes less than 50 microns. Guyton (67) reported the developement of an analyser based on an electrically charged probe which produced an electrical pulse when droplets impinged on it. Such a sampling device is described by Geist et.al. (60) and used to study drop-size distributions of sprays.

5.2 (b) COUNTING AND MEASURING OF SPRAY SAMPLES.

Turner and Moulton (212) reported on a number of micrograph sample counters used to give drop size distribution data. The problem of determing the drop size distribution of a spray sample by counting and measuring drops in a sample has resulted in the developement of a number of special techniques. Rupe (180) reported the developement of an automatic counter in which drop images on a photographic negative were counted by a modified scanning technique. Pigford (167) used a scanning procedure which required the production of opaque drop images printed on a photographic film, as did Adler et.al.(2). Hillier (74) also used a

scanning procedure utilising a moving light spot as a profile counter and measuring device. Other methods based on optical and light adsorption methods are avaiable (166,145).

All these methods referred to are limited to an analysis of the images obtained from the photographs of samples of the spray collected on slides or in cells. A more direct sampling technique and counting device such as that described by Geist et.al. (60) appears to be much more desirable involving less work and time than the mechanical sampling methods.

5.2 (c) DROP-SIZE DISTRIBUTION.

The drop size distribution of a spray can usually be expressed as a simple mathematical probability function. Of the mathematical functions available for such distributions, the Rosin-Rammler equation (177), the Nukiyama and Tanasawa equation (160) and the Logarithmic-probability distribution equation are the most commonly used.

Mugele and Evans (159) present a review of the data on droplet distribution in sprays similar to that of Marshall (145) and clarify the definition of the terms "mean diameter" and "distribution parameter". They examined the three commonly used distribution functions with reference to the available spray data and found like Turner and Moulton (212) that none of these three distribution curves fitted the data satisfactorily. As a result, they produced a new distribution equation called the "Upper Limit Equation", to be used as a standard for describing droplet size distributions in sprays. It is based on the difference equation of the "normal" or Gaussian distribution and is dependent on the maximum stable diameter of the dispersed phase.

Because the drop size distribution and drop size are important in controlling the rate of evaporation of sprays, the need to evaluate these variables shows up the disparity

between available methods and results. Binark and Ranz (12) have proposed a standard test method for hollow cone sprays based on the relation between the stopping distance and the size of the drops when subject to a high velocity cross-flow of air. Theoretical equations for the predictions of the distribution resulting from the injection of a liquid into a high velocity air stream is given by Longwell and Weisse (137). The equations are based on the principles of turbulent diffusion and an allowance for the wall effects and changing boundary dimensions can be made. Another theoretical correlation is by Shapiro and Erickson (187) who added to the literature on sprays by presenting a paper on the changing size spectrum of particle clouds undergoing evaporation. They described a model for the process and gave evidence that although approximate in its representation the results obtained from the model compare favourably with the calculated results from more expensive computational methods. In a study of the flashing of liquid jets, Brown and York (21) found that this technique was effective in producing sprays with dropsize patterns similar to those produced by convectional types of atomisers.

A study by Weiss and Worsham (216) is of interest in that they obtained drop size distribution data for ten different hydraulic pressure nozzles spraying axially into large steady air streams and found that the drop size distribution observed for sprays in fast air streams bore little relation to the distributions obtained for the same nozzles and operating conditions in static tests.

5.3 CORRELATIONS FOR THE EVAPORATION OF SPRAYS.

Under the actual operating conditions of spray drying, an atomiser produces a spectrum or distribution of drop

sizes and consequently the drops evaporate or lose moisture at varying rates depending on their initial diameters. Furthermore, the smallest drops will lose their moisture first and so will be subject to overheating and possible degradation by prolonged exposure to the high temperature drying medium. The problem of estimating the total evaporation time for a spectrum of drops is so complicated, amongst other things, by the fact that information is required on the drop size distribution created by the atomiser. Only a limited number of attempts have been made to analyse this problem.

The available data on the evaporation of sprays of drops can be grouped into three classes. First, there are the purely analytical approaches, such as those of Meisse (152), Sjenitzer (192) and Probert (170). Then there are the experimental investigations for the case of no relative motion between the drop and the drying gas, such as the work of Marshall (146), Kessler (101) and Dlouhy and Gauvin (40). Finally, there are correlations presented for the case where there is relative motion between the evaporating droplet and the gas, such as the work by Luikov (139), Bose and Pei (15) and Manning and Gauvin (144).

5.3 (a) THEORETICAL CORRELATIONS.

Ruckenstein (179) has developed equations for evaluating the mass-transfer coefficient in the continuous phase from a bubble or drop in a group of drops. He provides solutions for the two cases of the particle Reynolds number greater or less than unity. The effect of interaction between particles in a group or cloud is shown in that the Sherwood number is dependent in part on a

quantity characterising the group of particles. For uniformly distributed particles in a group, this quantity is the volume fraction (e) occupied by the continuous phase. The Sherwood number then can be represented as

$$Sh = f(Re, Sc, \frac{u_o}{u}, e) \quad , \tag{5.5}$$

where u is the velocity of the drop and u_o the velocity of the continuous phase at the interface with respect to the centre of the drop. The effect of the concentration of the dispersed phase on the mass-transfer rate would appear to be rather small as Perry (166) suggests that for a dispersed phase volume fraction of less than 0.1%, the voidage effect is negligible. Indeed, Ingebo (88) found that a tenfold increase in the particle concentration produced no noticeable alteration to the drag coefficient of a single drop, so presumably drag data obtained for single drops can be used for multiparticle systems.

A series of equations for calculating the paths taken by particles undergoing accelerated motion, taking into account the fluid fraction, have been developed by Lapple and Shepherd (121). The results predicted by new equations show good agreement with the experimental results in their short study of spray crystallisation.

An example of the spray drying of a solution in a chamber with countercurrent air flow is given by Meisse (152) in his theoretical study of the ballistics of evaporating droplets. An allowance for the remaining spherical shell of crystallised residue is made and for low evaporation rates the equation relating the evaporation process to the initial droplet diameter is

$$D_{p_o}^2 = \left(\frac{\lambda L}{u_o}\right)\left(\frac{1+q}{2}\right) \quad (0.6)^q \quad , \tag{5.6}$$

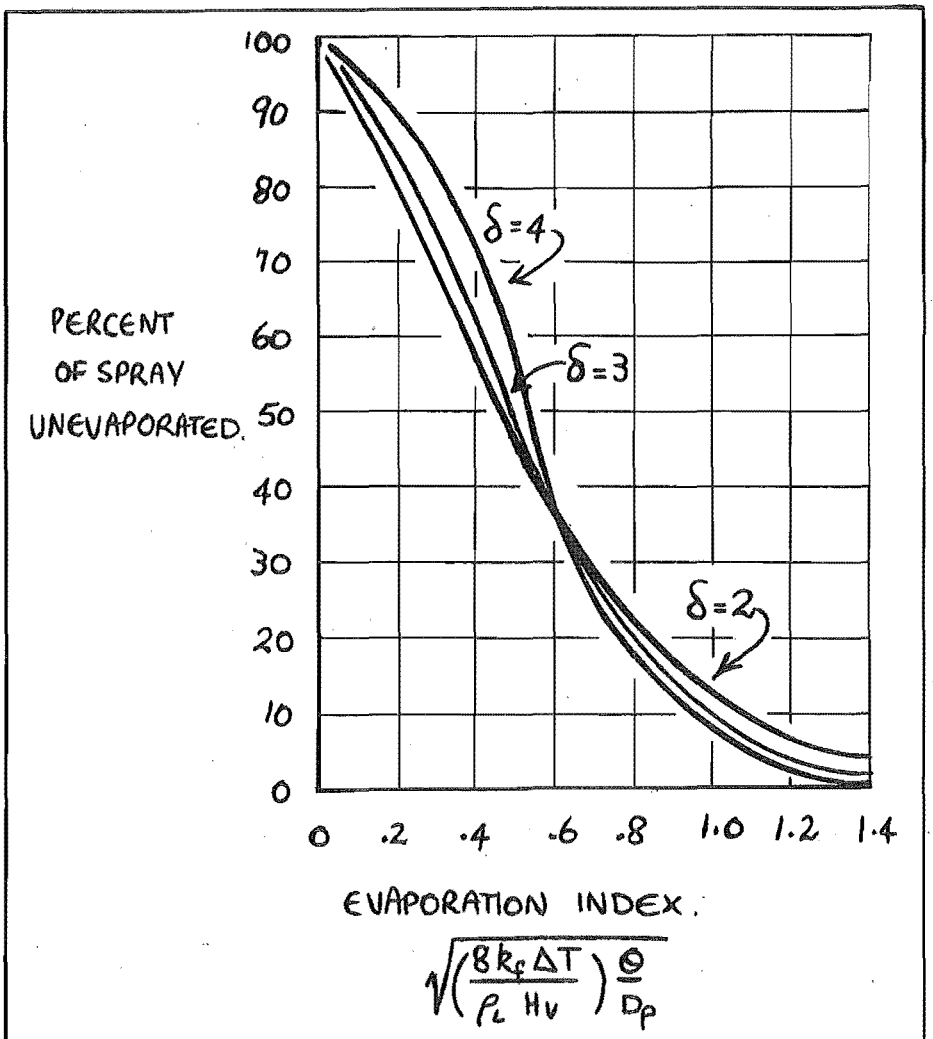

FIGURE 5.4 THE EFFECT OF THE SPRAY NON-UNIFORMITY PARAMETER (δ) ON THE PERCENTAGE OF SPRAY EVAPORATED WITH TIME (170)

which is a convenient formula for determining the proper relation between the governing variables. λ is the "evaporation" parameter (64, 173) and L is the length of path taken by the drop while it evaporates completely. Probert (170) made a mathematical analysis of the variation of the size distribution in a fuel spray which was assumed to follow the Rosin- Rammler distribution function. Assuming no relative motion, the simple expression for the heat-transfer coefficient was used and equations for the variation of the mass median diameter with time under various conditions of spray uniformity were derived. From his calculations, he concluded that a spray with a narrow size distribution and a small mass median diameter would evaporate completely in a shorter time than would a spray with a wide size range and a large mass median diameter. The results of his analysis are summarised in figure (5.4).

A theoretical study of a method of calculating the complete evaporation history of a spray of liquid which is injected into a stream of gas is presented by Sjenitzer (192, 193). The size and location of the droplets can be found at any moment during the entire process of evaporation using values of the gas velocity, pressure and temperature and the initial droplet size distribution. The formulae are based on Frössling's (54) equation for the evaporation of drops and the drag coefficient data of Ingebo (88) for liquid drops in the range of $6 < Re < 500$. A critical drop Reynolds number is defined according to a maximum Weber number of 13 (76). He presents examples showing the calculation of the time of evaporation, the path length and the critical Reynolds numbers for the drop size range of the spray, both during the first period immediately after the formation of the spray as the drops accelerate

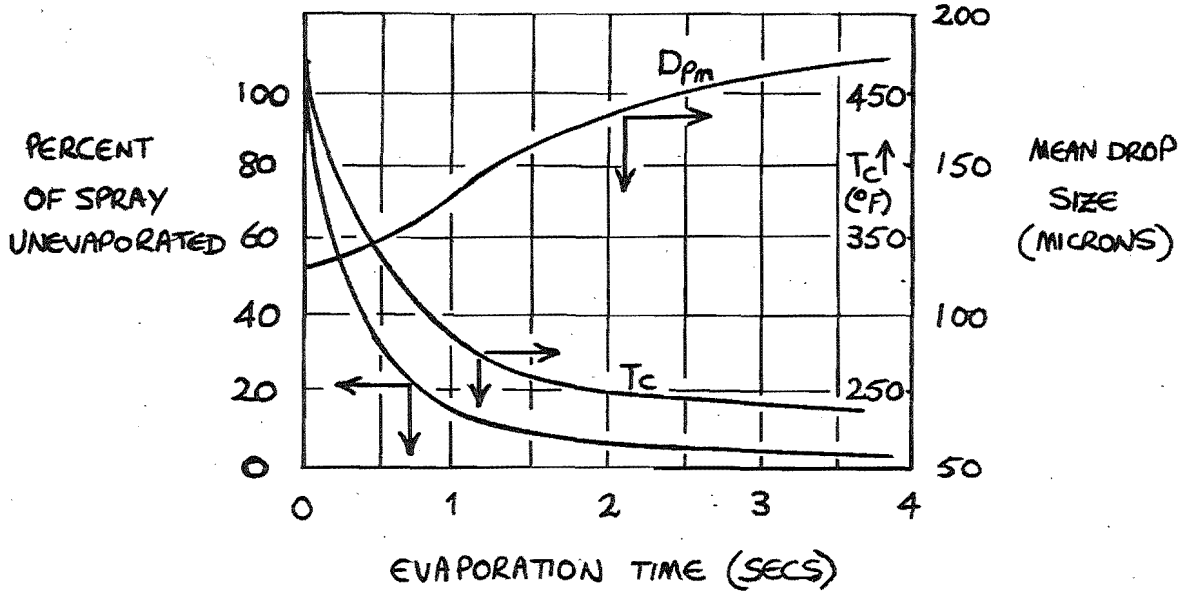

FIGURE 5.5 VARIATION OF AIR TEMPERATURE, MEAN DROP SIZE AND PERCENT OF SPRAY EVAPORATED WITH TIME (146).

and also during the second period when the drops fall at a constant rate. The calculations are based on the equation

$$\frac{d(y^2)}{d\theta^*} = -E_1 \left[1 + 0.30\,(Re)^{0.5}\,(zy)^{0.5}\right], \qquad (5.7)$$

where y is a reduced droplet diameter D_p/D_{p_o}, z is a reduced relative velocity $1-V/V_t$ and θ^* is a reduced time defined as

$$\theta^* = \left[\frac{9\mu_c}{\rho d D_{p_o}^2}\right]\theta \qquad (5.8)$$

Marshall (146) has given a procedure for the stepwise calculation of various mass fraction increments of drop size in the spray during the process of evaporation. The procedure consists of calculating the change in mean drop diameter of the selected increments over short intervals of time on the assumption that all the drops evaporate under the same constant temperature conditions for the same time interval. By selecting various mass fraction increments, the fraction of the spray remaining at various times as well as the variation of the air temperature with time, were obtained for a hypothetical spray for evaporation with no relative motion. His results, shown in figure (5.5), indicate that the evaporation is 90% complete in 1.5 seconds and that the air temperature has approached to within $30^{o}F$ of the final outlet value. Also plotted is the mass mean diameter of the spray as it varies with time and this mean size is seen to increase. This is because the very small drops evaporate completely much more rapidly than the larger drops. Figure (5.6) shows a plot of temperature difference against

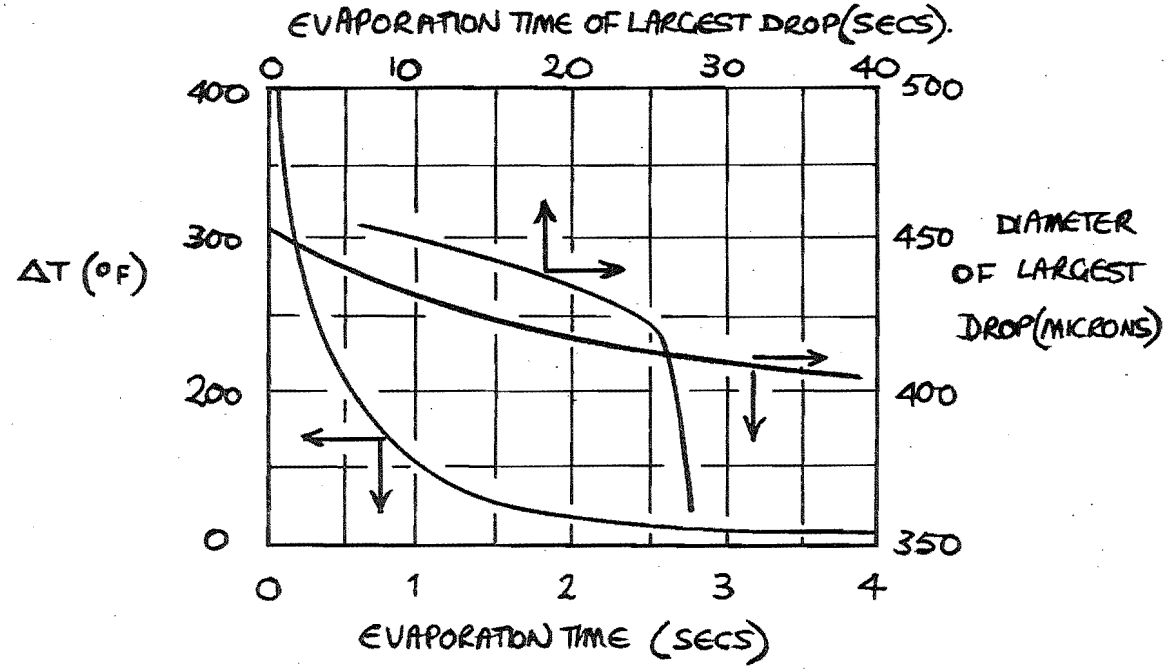

FIGURE 5.6 VARIATION OF THE LARGEST DROP SIZE, ITS EVAPORATION TIME AND THE TEMPERATURE DIFFERENCE WITH TIME. (146)

time, and the time required for the complete evaporation of the maximum drop size. This latter curve shows that the time of evaporation for the largest drop in the hypothetical spray increases from 8 to 26 seconds in 3.5 seconds because of the rapid decrease in the temperature difference between the drops and the drying gas. This shows that sprays with large drops will not dry completely in small towers and emphasises the need to design a drier for the largest drops in the spray.

5.3 (b) EXPERIMENTAL CORRELATIONS ASSUMING A DROPLET REYNOLDS NUMBER EQUAL TO ZERO.

Dlouhy and Gauvin (40) studied the evaporation of a spray of water drops in a cocurrent spray drier after commenting that the high relative velocities between the drop and the air (as reported in studies of the rate of evaporation in the nozzle zone of a spray drier (144) or fuel atomising nozzle (14)), masked the effects due to air turbulence so that the results could not readily be applied to the evaporation zone of a spray drier.

The rate of evaporation was calculated directly either for a heat balance or a material balance for the evaporating water drops. For the accurate calculation of the instantaneous heat-transfer coefficients however, an equation had to be derived on a differential basis because of the continuous variation in the values of the variables involved in the system. Considering a height dx in the drying chamber, the following heat balance can be written,

$$-mc_p dT = mdH \left[H_v + c_p(T_c - T_d)\right] , \qquad (5.9)$$

while the rate of heat-transfer to th drops located in the

differential volume is given by

$$mH_v.dH = h\ (T_c - T_d)\ dA \quad . \qquad (5.10)$$

dA, the surface area of the droplets, can be obtained from the specific area of the spray (in square feet per pound of sprayed liquid) by means of the equation

$$dA = \left[\frac{S.W}{V + V_t}\right] dx \quad . \qquad (5.11)$$

The authors considered that in general the terminal velocity of the droplets V_t was negligible compared with the absolute gas velocity in the drier and W, the pounds of unevaporated liquid droplets passing per hour through the cross-section of dx, was calculated from the liquid feed rate at the nozzle and a humidity balance. The specific area of the spray S, was obtained from the droplet count at the section in question by substitution into the equation

$$S = 6\Sigma n\ D_p^2 \,/\, \rho_d \Sigma n\ D_p^3 = 6\,/\,\rho_d D_{p_{vs}} \quad . \qquad (5.12)$$

From these equations, the instantaneous values of the heat-transfer coefficient could be readily calculated. These were the actual values from which the actual Nusselt numbers ($Nu = h\ D_{p_{vs}} / k_f$) were obtained and the latter were compared with the relationship of Ranz and Marshall as the drying air temperatures were low and the correction for high mass-transfer rates consequently negligible. Similar equations were used to give values of the instantaneous mass-transfer coefficient k_g and the Sherwood number for mass-transfer. The equations used mean values of the film properties

μ_f, ρ_f, and k_f, which were estimated at the arithmetical average temperature of the air and the surface of the droplet, or at the wet bulb temperature of the air.

Their results indicated conclusively that the rate of evaporation during spray drying could be safely calculated by assuming that the individual droplets of the spray evaporate at a rate corresponding to stagnant conditions. This result was also the conclusion of Kesler (101), who also showed that for drops in the same diameter range as in the study of Dlouhy and Gauvin, the effective relative velocity between the droplets and the airstream was practically zero and that the rate of evaporation could be calculated accurately by assuming a value of two for the Nusselt number.

In an investigation of the atomisation of liquid sulphur as a means of introducing the feed material to the burners, Conroy and Johnstone (31) studied the time required for at least 99.9% of the spray to evaporate. This is the time for the complete evaporation of a drop of diameter such that 0.1% of the total volume of the spray remaining consists of drops of a larger diameter. The transfer rate equation based on a value of the Nusselt number of two, was integrated in a stepwise method with all quantities evaluated at the drop temperature except the thermal conductivity of the gas film, which was based on an average temperature. The time of evaporation of a sulphur spray was described by equation (3.65), and good experimental agreement was obtained.

Gluckert (63) prepared an overall correlation of spray drier performance from which the design of a spray drier can be specified subject to the limitations of the correlating equations. In an attempt to facilitate

scale up and design from basic principles using a uniformity theory, the correlation makes use of the many studies of the individual factors involved in the process of spray drying. Using the correlation, the capacity heat-transfer or production rate based on the heat-transfer rate to the largest spray drop, can be calculated.

The correlation assumes a Nusselt number of two and that entrainment and recirculation of the hot gas within the drying chamber ensures that the process of evaporation occurs at a temperature effectively that of the gas outlet. In the spray drying of solutions, a constant drop diameter is used on the assumption that a surface shell of crystallised product forms (42, 173). The rate of heat-transfer to sprays is given in three equations for the three types of atomisers. For example, the equation of heat-transfer for a pressure nozzle spray is given as

$$q = \frac{10.98\ k_f V^{\frac{2}{3}} \Delta T}{(D_{p_{max}})^2} \cdot D_{p_o} \sqrt{\frac{\rho_c}{\rho_d}} \quad , \qquad (5.13)$$

where $D_{p_{max}}$ is the maximum drop size produced by the nozzle and is defined as being three times the surface per unit volume mean drop size.

5.3 (c) EXPERIMENTAL CORRELATIONS ASSUMING A DROPLET REYNOLDS NUMBER GREATER THAN ZERO.

That the relative motion between the droplets and the air stream was of significance in determining the rate of heat- and mass-transfer, was reported by Bose and Pei (15) in their study of the evaporation of pure water drops in a cocurrent spray drier. This conclusion resulted from

an attempt by these workers to extend the work of Kesler (101) and Dloughy and Gauvin (40) in evaluating the heat- and mass-transfer coefficients for drops in a spray drier with droplet sizes comparable with those used in some industrial applications. Their results showed the rate of evaporation to follow the correlation proposed by Ranz and Marshall (173) and also indicated that the turbulent eddies of the drying air stream had no direct effect on the evaporation rate of the spray.

Manning and Gauvin (144) investigated rates of heat- and mass-transfer in the nozzle zone of water sprays. Using the results of York and Stubbs (222), which showed that the velocity of the drops in the spray depended on the radial position of the drop in the chamber, they found the Nusselt number to be correlated by the Ranz and Marshall equation. They suggested that an increase in the intensity of the turbulence of the gas stream might result in an increase in the heat-transfer rate (215), but found the effect to be small for the range of droplet Reynolds numbers investigated. The effect of increasing the feed temperature on the evaporation was marked and could be explained in part as; (i) flashing of the sprayed liquid as the droplet temperature decreases to the wet bulb temperature corresponding to the surrounding gas, (ii) a decrease in the values of the surface tension and viscosity forces at the higher temperatures producing a decreased drop size distribution (203,212), (iii) an increase in the residence time of the drops and in the evaporation because of the lower values of drop velocity.

Using a step-by-step method similar to that proposed by Marshall (146), and taking into account the changing drop size and velocity, Manning and Gauvin calculated the evaporation rate in the nozzle region of the spray and found good agreement

between the experimental values and those given by the Ranz and Marshall equation.

Hoffman and Gauvin (80) in their study of spray evaporation in a high temperature enviroment discuss the applicability of the Ranz and Marshall equation and the modifying factors to be used to allow for high rates of mass-tramsfer. Feder (45) has drawn up a series of charts predicting the rates of evaporation using the empirical relationships between droplet diameter, liquid stay time and fraction of liquid evaporated, plus the four operating variables of the spray liquid boiling point, the velocity of the drying air, the air static pressure and temperature.

One of the few equations found in literature on heat-transfer in spray driers is that of Luikov (139) who defines a volumetric heat-transfer coefficient by the equation

$$\bar{h} = 1.58 \times 10^{-3} \left[\frac{k\ W}{\rho_s \bar{A}}\right] \left[\frac{1}{D_{p_s}}\right]^{1.6} \left[\frac{1}{V+V_t}\right]^{0.8} . \qquad (5.14)$$

Turba and Nèmeth(~~146~~ 211) in a study of the spray drying of paste like materials, found $\bar{h}$ = 13.8 Kcal/m^3hr^{o}C for a heat flow of 4090 Kcal/hr. From these values, according to Luikov's expression, they could expect the volume of the drier to be 4.1 m^3 for a temperature difference of about 70^{o}C. This value did not agree with the volume of the drier which was used in the experiment and was 0.7 m^3. Luikov's equation would then appear to give values for the drier volume almost an order of magnitude greater than that found necessary in the work described. However, the semi-empirical equation was not probably considered for the drying of thick pastes, but it does predict the trend of volumetric heat-transfer coefficients, and Turba and Nèmeth suggest that for thick

pastes, the equation could be used with a different numerical constant. Another study of the volumetric mass-transfer coefficient was presented by Ki (103). He presented equations for the design of spray drier equipment based on the volumetric coefficient rather than the surface area mass-transfer coefficient.

5.4 TRANSFER UNITS IN SPRAY DRYING.

In spite of the existence of much published data (15,40, 145.) an accurate and reliable method of designing spray driers has not yet been fully developed due to the lack of reliable heat- and mass-transfer relations. The application of the concept of transfer units to spray drying is an attempt to provide a rational evaluation of the process. Two notable attempts of this aspect have been by Fokin, Planovskii and Akopyan (48) and by Sjenitzer (192).

Engineering equipment is designed for either ideal mixing or unmixing (35), although in practice real equipment only approximates to one or other of these ideal cases.. The reduction of the harmful effect of mixing in spray driers can be achieved by logical control of the motion of the heating stream and the sprayed material (101).

In designing real equipment, it is necessary to know the nature of the mixing of the flows which determine the concentration field. Fokin, Planovskii and Akopyan express the concentration field in the drying chamber in terms of the "effective motive power", or the ratio of the motive power in the actual equipment to that in equipment with ideal unmixing.

$$E = \frac{\Delta M.P_{act}}{\Delta M.P_{ideal}} \qquad (515)$$

The effect of the motive power may be conveniently designated

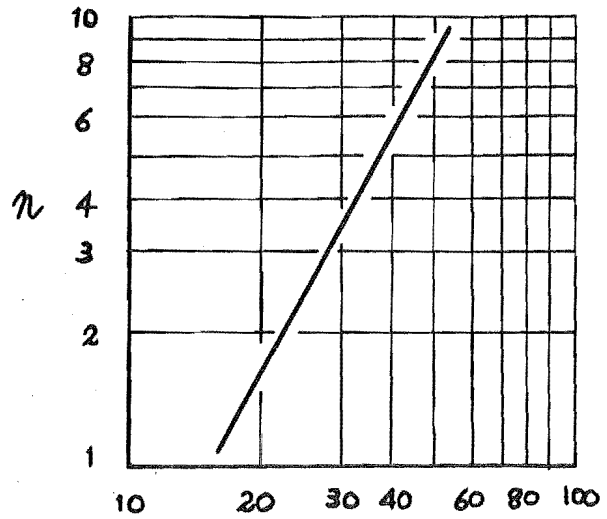

FIGURE 5.7 DEPENDENCE OF THE NUMBER OF PSEUDO-SECTIONS (n) ON THE FLOW RATE OF THE HEAT-TRANSFER AGENT PER UNIT CROSS-SECTIONAL AREA OF THE SPRAY DRYER CHAMBER. (48)

by the number of pseudo sections or transfer units which in turn depends on the hydrodynamic conditions in the drying chamber. For ideal mixing then, the number of sections (n) is equal to unity and for ideal un-mixing the number is infinite.

The authors show that once through equipment is close to the ideal un-mixing equipment, while the flow rate of the sprayed material and the temperature of the drying gas was found to effect the concentration field in the drying chamber as shown in figure (5.7). Since the flow rate of the drying gas in spray driers is seldom less than 200 lb/ft^2hr, the number of pseudo sections will be about 8 to 10 and hence the motive power of the process can be calculated assuming ideal un-mixing equipment.

Sjenitzer (192) in a theoretical study of the movement of liquid droplets in drying gases, applied the concept of transfer units as heat-transfer through an air film. The number of transfer units N_t was defined as

$$N_t = \int_1^2 \frac{dT}{\Delta T} \quad . \tag{5.16}$$

For evaporating drops of water in air when the surface temperature of the drops is the wet bulb temperature,

$$N_t = \int_2^4 \frac{dT}{\Delta T} = \int_2^4 \frac{dT}{(T - T_1)} = \log_e \left[\frac{T_4 - T_1}{T_2 - T_1}\right] \tag{5.17}$$

$$\text{or} \quad N_t = \log_e \frac{1}{(1 - \eta_t)} \qquad \text{whence} \quad \eta_t = 1 - e^{-N_t} \quad . \tag{5.18}$$

This relation between the efficiency ratio and the number of transfer units applies only for the adiabatic evaporation of a pure liquid. The result can be extended to the case for the drying of drops containing solids in suspension or in

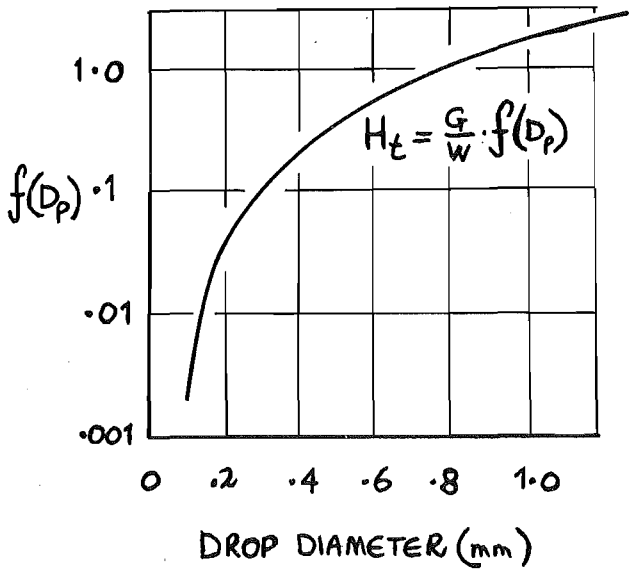

FIGURE 5.8 HEIGHT EQUIVALENT TO A TRANSFER UNIT FOR FREE FALLING WATER DROPS IN STILL AIR. (192) H_t IS DIRECTLY PROPORTIONAL TO THE GAS AND WATER FLOW RATE RATIO (G/W) AND THE SMALLER THE DROP SIZE THE MORE DIFFICULT IT BECOMES TO HUMIDIFY THE DRYING AIR BY THE SPRAY OF WATER DROPS.

solution.

The height of a transfer unit H_t for water drops evaporating in still air can be calculated starting with the equation for the fractional evaporation of the drops per unit fall in height. If the airflow through the drying chamber is G and the flow of liquid at any section dl is W, then the increase in humidity at this section is given by the following equation.

$$\frac{dH}{dl} = \frac{G}{W}.\frac{dW}{dl} \qquad (5.19)$$

and as

$$H_t = \frac{\text{lenght dl}}{\text{No. of units in lenght dl}} \qquad (5.20)$$

so

$$H_t = \frac{dl}{(N_t)dl} = \frac{dl}{dl/\Delta H} = \int(D).\frac{G}{W} \qquad (5.21)$$

Equation (5.21) as illustrated in figure (5.8), refers then to every moving drop of water in air and for drops falling at a constant velocity in stationary air, the height of the transfer unit being the same regardless of the solids content of the drops. This is because in the wetting of the air, the difference in vapour pressures for drops with and without solids content is accounted for in the defining concept of the number of transfer units N_t which is dependent on the humidity of the drying gas.

The transfer unit concept can be extended to any solvent with or without solids in suspension or solution and a rational evaluation of the spray drying process is suggested.

5.5 SPRAY DRIERS.

The operation of spray driers for the production of various heat sensitve materials has been discussed in a number of papers (10,34,47,126,147,194). These papers cover

the various aspects of control of the operating variables with reference both to the needs of the manufacturer and the product buyer. Crosby and Marshall (33) have designed an experimental spray drier for use for product developement studies on a number of materials. The effects of the drying gas conditions on the size and density of the spray dried particles as compared to the initial size of the spray drops has been investigated. Kiraly (106) has described the work carried out with a pressure atomiser spray drier of unconventional design. From the results of a study of the spray drying of pigment slurries in an experimental spray drier, he discusses the design of a large scale spray drier.

Marshall and Seltzer (147) have defined the efficiency of spray driers in two ways. First, there is an Overall Efficiency defined as

$$\eta_o = \left[\frac{T_1 - T_2}{T_1 - T_a}\right] x \frac{100}{1} \qquad (5.22)$$

and second, there is an Evaporative Efficiency defined by the equation

$$\eta_e = \left[\frac{T_1 - T_2}{T_1 - T_s}\right] x \frac{100}{1} \quad . \qquad (5.23)$$

The temperature difference $(T_1 - T_2)$ represents the drop in air temperature due to the drying process only (assuming no heat losses) and T_a and T_s are the drying gas atmospheric and adiabatic saturation temperatures corresponding to T_1. The Overall Efficiency indicates the fraction of the total heat input to the dryer that is used solely for drying and the Evaporative Efficiency indicates the degree of approach to the saturation of the drying air which is achieved during the drying process.

Place, Ridgway and Dankwerts (169) carried out an

investigation of the behaviour of air flowing through a large spray drier using a tracer technique and also with a model on 1/80 size scale using water as the continuous phase medium. The results showed clearly the swirling flow in the spray drier and in particular the zone of reversed flow which could be the main mechanism for the back mixing observed in spray driers. This mixing gives a more uniform temperature distrbution in the drying chamber which is said to be beneficial in the drying of detergents (34). The density of air at the top of the drier was found to be about 20% greater than that near the bottom, so causing instability of the gas flow. Visual observation of the drying process leads to the suggestion that the concentration of suspended particles is too low to have an appreciable effect on the flow pattern in the spray tower.

Kessler (101) also pesented a study of the gas flow in cocurrent spray driers and showed that poor gas flow in the drier is in many cases the cause of poorutilisation of the drying chamber. This fault can be eliminated entirely with an appropiate inlet for the gas stream in the drier and with a corresponding adjustment of the heating medium.

Marshall (145) discusses airflow in spray driers and the design and performance of such, in his extensive paper on atomisation and spray drying. The three basic types of flow in the drying chamber are discussed as well as the drying ability of the equipment as influenced by the various factors which determine the final properties of the spray dried products.

5.6 JET-SPRAY DRIERS.

A spray drier of rather unique design, the Jet-Spray drier features the introduction of the solution or suspension to be dried, directly into a hot, high-velocity gas stream. This arrangement results in extremely high rates of evaporation and

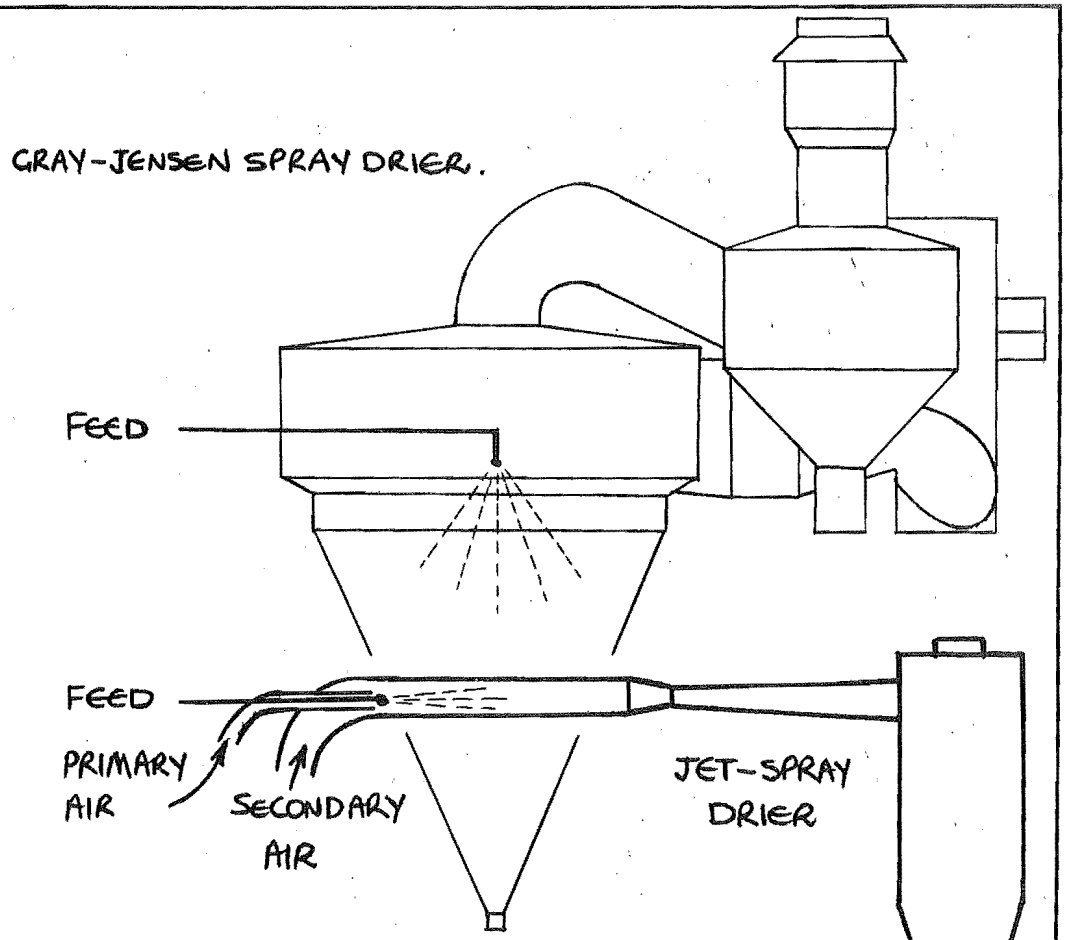

FIGURE 5.9 RELATIVE SIZES OF A JET-SPRAY DRIER AND A CONVENTIONAL SPRAY DRIER OF THE SAME CAPACITY. (30)

gives an inherently small particle size. Comings and Coldren (30) extended the work of Ashmus (6) and built such a jet-spray drier as described, in which the time that the drops were subjected to the elevated temperature of the drying medium and the size of the equipment required for a given drying capacity as compared with a conventional spray drier, were greatly reduced. The difference in size of equipment is illustrated in figure (5.9), which shows the relative sizes of a high-velocity spray drier and a conventional spray drier of the same capacity for the production of dried milk. M^{c}Lain, Comings and Meyers (142) used the jet-spray drier of Comings and Coldren, and working with solutions of sodium sulphate found the heat requirements to be larger than those of similar capacity conventional spray driers and the power requirements to be considerably higher. Bradford and Briggs (19) found the jet-spray drier easy to construct and operate. They also found that the drier required more power than other spray driers and presumed that because of the smaller size of the equipment the heat losses should be less and so the drying costs of the two types of spray drier comparable.

The drop size distribution in the jet-spray drier obtained by the impact method was found to follow the linear log-normal probability distribution function (142) and the product size to be less than 10 microns in diameter (19). A product of such small size made reconstitution difficult and wetting of the product in the collection chamber of the jet-spray drier was introduced to give a larger final product as an aggolmeration of fines.

6. THE EFFECT OF TURBULENCE ON EVAPORATION RATES.

The diffusion of heat- and mass in turbulent fluids is a problem of some importance in numerous chemical engineering processes. The effect of turbulence on the unsteady-state process of mass-transfer in a turbulent stream has generally been reported under one of the following headings. For the case of evaporating drops, these headings are the effect of the turbulence of the dispersed phase, of the continuous phase and at the interface between the two phases.

6.1 DISPERSED PHASE TURBULENCE.

Turbulence within the dispersed phase has not been reported as an observed fact but rather as a conclusion, in that circulating drops immediately after detachment from the spray nozzle are reported to have very high rates of circulation probably in turbulent flow. This very high rate of circulation within the drop is rapidly damped out by the viscous forces of the drop and although lasting for only a very short time as compared to the total time of fall of the drop results in momentary high rates of mass-transfer (57).

6.2 CONTINUOUS PHASE TURBULENCE.

The effect of the turbulence of the continuous phase on the rate of mass-transfer has generally been treated by assuming that transfer by eddy diffusion is proportional to the concentration gradient.

$$\frac{N}{A} = (D_v + E) \frac{dC}{dZ} \qquad (4.1)$$

Laminar boundary layer theory assumes a steady velocity outside the boundary layer, whereas in practice, for turbulent external fluid flow, the edge of the boundary layer will be irregular

and eddies penetrating the boundary from the main stream would be expected to increase the mass-transfer rate. For gases ($Sc \backsim 1$), the effect for normal turbulence intensities seems to be small, since data agree well with the theory of laminar flow (70). For turbulence intensities of about 10% the transfer rate may be 10 to 50% higher than normal depending on the geometry of the system and the scale of turbulence (77).

The theory of eddy diffusion developed by Taylor (205) has been confirmed by experiments in a turbulent water stream and can be adapted for transfer to gases (97). The scale of turbulence was found to enter directly into the eddy diffusion relationship, indicating that this quantity should be measured or estimated if diffusion in turbulent fluids is to be predicted accurately. Dryden (41), reporting on Taylor's theory and its verification, indicates the difference between momentum-, and heat- and mass-transfer, is that diffusion by momentum is affected by the pressure gradient whereas there is no corresponding factor occuring in the diffusional processes of heat- and mass-transfer. Hence the analogy between skin friction and heat-transfer(100) is invalid except for some special cases where the pressure gradient vanishes (43), or where the flow is one dimensional and Pr (or Sc) $\backsim 1$. The hydrodynamic and heat- (or mass-) transfer boundary layers are then nearly equal(99).

Liu (132) and Soo (195)presented theoretical studies of the forces acting on a simple system of single spherical particles suspended in a turbulent gas and their results indicated that the eddy diffusivity of the particle and the gas were almost equal at low intensities of turbulence for small particles. This implies that such small drops should evaporate at a rate corresponding to zero relative velocity conditions. Whether or not a particle will exhibit

Stokesian behaviour at very low Reynolds numbers will depend on the size of the particle in relation to the small domains of viscous motion in the turbulent field. Bose and Pei (15), Dlouhy and Gauvin (40) and others (100, 20), have reported experiments that indicated that turbulent eddies in the airstream had no direct effect on the evaporation rate of spray droplets.

On the other hand, reports of significant effects of turbulence on the transfer rates are just as numerous. Hsu and Sage (83) measured heat- and mass-transfer from single spheres in turbulent gas streams and predicted temperature and heat-flux profiles about the spheres. They recorded an effect of the level of turbulence but did not measure it. Garner and Suckling (59) reported on the mass-transfer from solid benzoic acid spheres into water and their data showed an increase in the dissolution transfer rate in turbulent streams. A significant increase in the heat- and mass-transfer rates of evaporating drops in gas streams of relatively high turbulent intensity was reported by Hoffman and Gauvin (80), who attributed some of the effect to a decrease in drag coefficient, the result of turbulent intensity in itself. They suggested that drops of mean Sauter diameter of 60μ or lass tend to follow the turbulence eddies. Maisel and Sherwood (143), in their study of the evaporation of liquids from the surface of porous spheres into turbulent gas streams, found that the effect of turbulent intensity was marked, but that of the scale of turbulence was of little consequence and Torobin and Gauvin (209) also showed the necessity of considering the effect of large turbulence intensities on momentum-transfer for cocurrent multiparticle systems.

Friedlander's calculations (52) show that the mass-transfer coefficient should be somewhat higher because of the velocity fluctuations in turbulent flow as compared with the transfer rates of drops in stagnant fluids.

In his book, Hinze (77) discusses the effect of free-stream turbulence on the transport processes in the boundary layer region. If the free stream outside the boundary layer of a body is itself turbulent, it will affect the turbulence transport processes through the boundary layer. As long as the turbulence intensity of the free stream is relatively small compared with the relative intensity of the turbulent boundary layer itself, the effect may be expected to remain restricted to the outermost regions of the boundary layer. But with increasing intensity of the free stream turbulence, its effect may penetrate deeper into the boundary layer and enhance the turbulent transport process accordingly.

For flow around the body, the effect of the free stream turbulence may be threefold:

(1) Usually, the upstream part of the boundary later is not yet turbulent and the transition into turbulence occurs at some point downstream from the forward stagnation point. Turbulence in the free stream may not only influence the location of the transition point but may also cause disturbances in the laminar part of the boundary layer and so affect the transport processes through it.

(2) The free stream turbulence may affect the turbulent part of the boundary layer along the body, as noted above.

(3) If the flow past the body generates a wake, the free-stream turbulence may interact with the wake flow.

It is known from local heat-transfer measurements

on spheres (173) that a maximum rate of heat-transfer occurs at the forward stagnation point and in the wake region of the body, with a minimum at the separation ring. Hence, the effect of free-stream turbulence on heat-transfer can be expected to be greatest at the frontal and wake regions of the body surface.

Early measurements made by Loitianskii and Schwab (134) showed that by increasing the relative intensity of free stream turbulence from 0.5 to 3% an increase in the Nusselt number of 30 to 35% resulted. They used heated spheres of 7 cm in diameter and Reynolds numbers from 5x104 to 10^5. Some workers (29, 39) have reported no further increase in the evaporation rate when the intensity is increased above the 5% level, but for the evaporation of water from wetted spheres and cylinders, Maisel and Sherwood (143) showed an ever-increasing rate of evaporation with increasing intensity of turbulence. The rate of this increase was found to increase as the particle Reynolds number increased. They found no effect of the scale of turbulence on the evaporation rate, but it is noted that the scales of turbulence used were comparable in size to the diameter of the spheres and cylinders.

From extensive measurements of the effect of scale and intensity of turbulence on heat-transfer from a heated cylinder, van der Hegge Zijnen (215) obtained an empirical correlation of the form

$$\frac{Nu'}{Nu_o} = 1 + f_1\left[\frac{u_1' D_c}{\nu_c}\right] \quad f_2\left[\frac{\Lambda_f}{D_c}\right] \quad , \qquad (4.2)$$

where Λ_f is the longitudinal integral scale of turbulence.

Figure (6.1) shows curves of the Nusselt number ratio Nu'/Nu_o as a function of Λ_f/D, with the relative intensity u_1'/u_1 as a parameter, according to the correlation. With this correlation it is possible to explain the seeming discrepancies and even the contradictions found in the literature concerning the effect of intensity and scale of turbulence on heat-transfer. The optimum value of Nusselt number ratio occurs at a value of Λ_f / D of 1.6 and seems to point to some resonance between the frequency of the turbulent flow and the shedding frequency of eddies in the wake of the cylinder.

There is little information available concerning the effect of the level of turbulence of the approach stream on the rate of evaporation of liquid drops. (129) Theoretical and experimental studies of transfer to spheres have generally dealt with fixed or free-falling drops in quiescent air. The majority of practical applications however, involve particles suspended or conveyed in a turbulent gas stream. Where turbulence effects have been studied, such as Pasternak and Gauvin's study of turbulence effect for mass-transfer from stationary particles, the direct effect of intensity of turbulence, varied independently of the gas velocity, has not been investigated. The apparent lack of effect of turbulence of the main stream on the evaporation of small drops, suggests that possibly the high molecular diffusivity makes the transient effects less important in gases than in liquids where the effect of turbulence on mass-transfer may become important (10).

Seban (185) has indicated that thermal transport across a turbulent boundary layer should be proportional to the Reynolds number to the power 0.8 and Friedlander

(52) and Soo (195) have discussed the diffusion process as being dependent on the relative motion between the particle and the main air stream.(136). In his study of momentum-transfer in a two phase system consisting of particles carried by the continuous phase, Soo applied the statistical theory of turbulence and showed that the correlation, scale and intensity of turbulence of one phase could be calculated from those of the other phase. Assumptions made in this derivation included that the turbulence be isotropic and non-decaying, that the relative velocity between the entrained particle and the main stream be such that the particle Reynolds number be less than unity, and that there be no interaction between particles. The fundamental properties affecting momentum transfer between the two phases were found to be

$$\left[\frac{D_p \sqrt{\overline{u}^2}\, \ell_c}{\mu_c}\right] , \left[\frac{D_p}{l_1}\right] \quad \text{and} \quad \left[\frac{\ell_d}{\ell_c}\right] . \qquad (6.3)$$

(l_1 being the Langrangian scale of turbulence of the gas stream.) It was also reported that where the gravity effect on the particles is significant, their turbulent motion was anisotropic even though the continuous phase was isotropic. In general the scale of turbulence of the particles was greater than that of the gas stream, the intensity of the particles less than that of the gas stream, and the diffusivity of the particles greater than the eddy diffusivity of the gas stream, but tending to the eddy diffusivity of the stream when the entrained particle diameter was small.

Friedlander (52) considered heat- and mass-transfer for the dispersed phase as related to the relative velocity

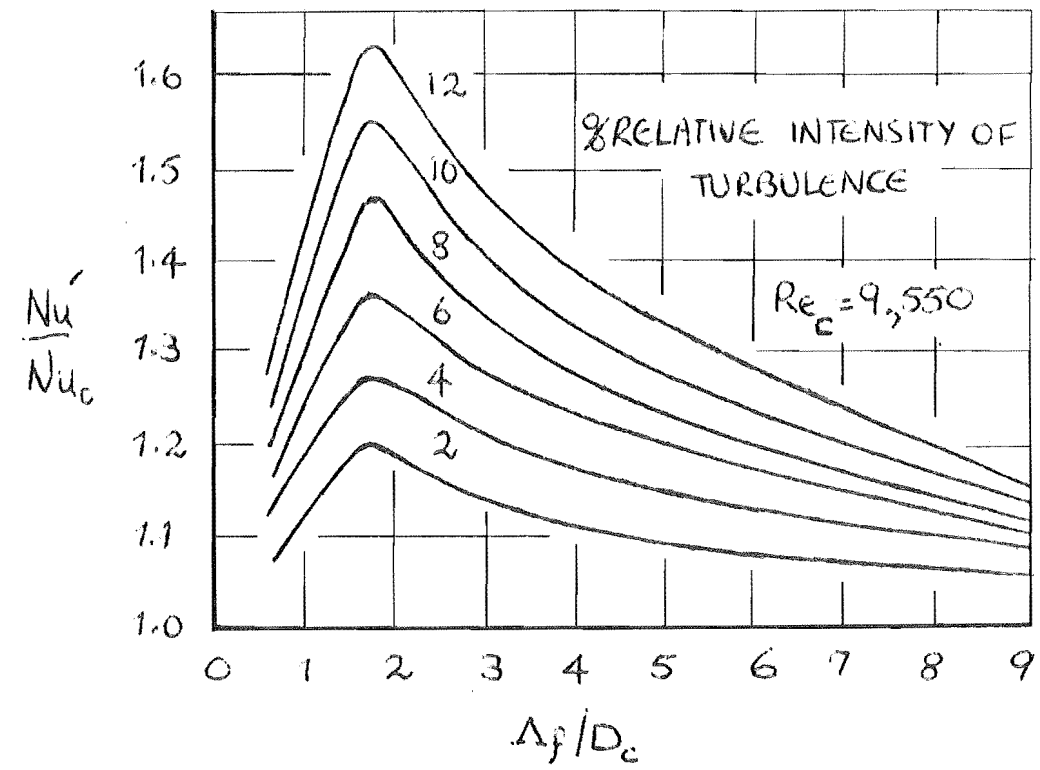

FIGURE 6.1 EFFECT OF INTENSITY AND SCALE OF FREE STREAM TURBULENE ON HEAT-TRANSFER FROM A CYLINDER (77)

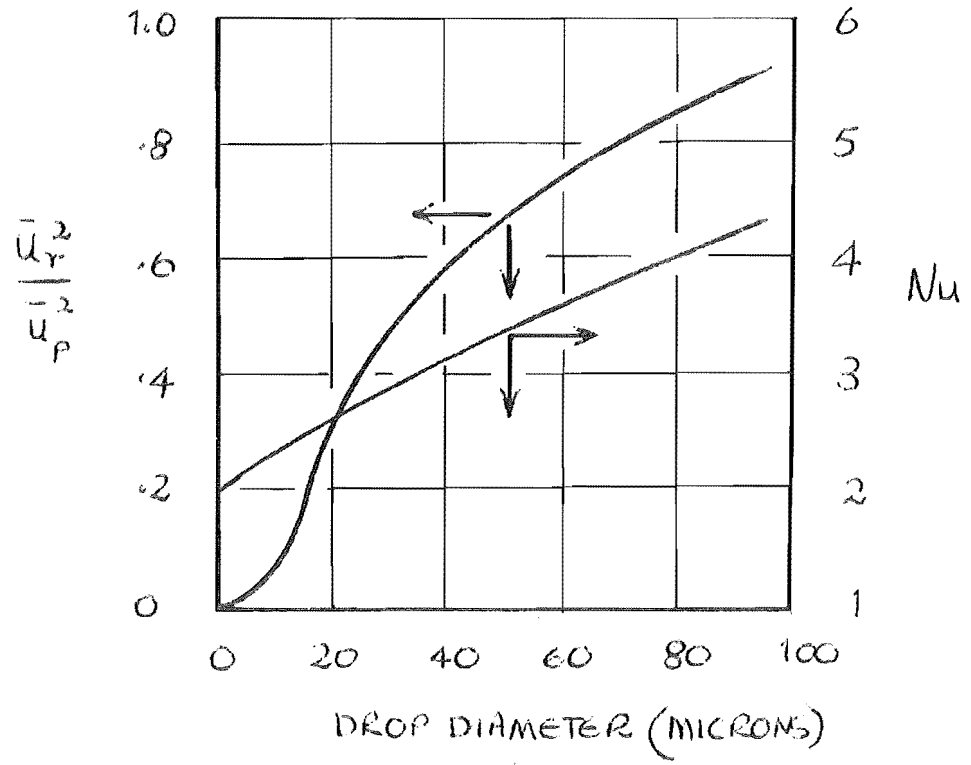

FIGURE 6.2 RELATIVE VELOCITY FUNCTION AND NUSSELT NUMBER VARIATION WITH LIQUID DROP SIZE FOR EVAPORATION IN AIR AT 20°C. (52)

between the particle and the gas stream, and the eddy diffusion described as the mean-square particle displacement. The root-mean-square relative velocity between the particle and the continuous phase is assumed to represent the characteristic value for transfer calculations, as the velocity past the drops is not constant but varies with time and postion for each particle. If values of this parameter were available the mean particle Reynolds number could be established and the corresponding Nusselt number obtained. A method of estimating the root-mean-square relative velocity of a homogenous turbulent fluid containing a large number of small, rigid, non-interacting spheres is given and the relative velocity effect on the drops calculated accordingly is shown in figure 6.2.

For particles larger than about 10 microns in diameter "slip" is reported to occur (52) and the mean relative velocity becomes significant. Friedlander points out that the assumption sometimes made, that the Nusselt number has a constant value of two (stagnant continuous phase conditions) for drops in a turbulent fluid, may be in error and he shows theoretically that the initial spreading of drops initially at rest should depend little on the correlation coefficient but very much on the intensity of the turbulence of the gas stream.

Sherwood and Woertz (191) in a study of the overall process of transfer from a liquid surface to a turbulent air stream found the eddy diffusivity to be essentially a constant value over the main central portion of the gas stream in fully turbulent flow. This observation needs to be related to the report by Torobin and Gauvin (210) who showed that the turbulence intensity in a particle free duct would vary from about 3% in the core to about 60% at the wall. The effect

of the presence in such a system, of particles whose Reynolds numbers are sufficiently high for them to have turbulent wakes requires further investigation. The boundary layer and wake structure of an entrained particle can be subjected to a very high relative turbulence intensity even though the free stream level of turbulence is only moderate. This can be illustrated by considering a particle moving at 90 ft/sec cocurrently with a gas stream which has a mean velocity of 100 ft/sec and an intensity of turbulence of 5%. Assuming that the inertia of the particle is such that it does not have a fluctuating motion, the boundary layer and wake of the particle will be generated by a relative velocity of 10 ft/sec and the relative disturbance of this flow will be to an intensity of 50%. In fact, because of the large amount of kinetic energy associated with this fluctuating component compared with the kinetic energy of the relative motion of the particle in the main, it would no longer be proper to consider the former as being merely a disturbance imposed on the latter.

For high Reynolds numbers in the range 10^3 to 10^5 the "j" factor dimensionless group j_D, where

$$j_D = \frac{k_c p_{BM} Sc^{\frac{2}{3}}}{U P} = \int (Re) \ , \qquad (6.4)$$

correlates the data for mass-transfer in turbulent flow for a number of cases (26, 188, 143) such as a cylinder shape, providing the friction factor represents only that portion of the total drag due to skin friction. Garner and Suckling (59) have recently provided data for the slow flow pattern about spheres in the Reynolds number range from 100 to 700.

A study of the effects of turbulence on the drag coefficients of spheres moving in both steady and accelerated

motion was reported by Torobin and Gauvin (210), who found that for a cocurrent solids-gas system, the relative intensity of turbulence was affected by changes in the particle relative velocity, the absolute fluid velocity and possibly by the solid particle concentration in the continuous phase. In the case of a spray, the system is further complicated in that the continuous phase intensity would be expected to decrease as the distance of the drop from the spray nozzle is increased or as evaporation takes place. Ingebo (88), in reporting on the drag coefficients of drops, showed the drop Reynolds number to decrease with increasing distance downstream from the nozzle, indicating an increasing relative intensity as would be expected from the decreasing relative velocity of the droplet as it decelerated relative to the continuous gas phase.

A common plot of available data on the drag coefficients for drops and particles moving in air streams of different intensities of turbulence (210) shows the completely divergent tendencies as reported by different investigators, who in some cases found increasing and in other cases decreasing drag forces with increasing particle Reynolds number for the same intensity of turbulence of the air stream. An explanation of the effects of the level of the free stream turbulence on the momentum-transfer of a two phase system, requires an understanding of the reasons and conditions for unstability of laminar flow and the resulting transition to the region of turbulent flow. Edwards and Fuber (44) have reported that heat-transfer was not significantly changed by turbulence in the main stream while the boundary layer was either wholly laminar or wholly turbulent, but strongly affected during the transition between these flow regimes.

The extent to which free-stream turbulence exerts an influence on the particle momentum-transfer would appear to

depend on the magnitude of the relative turbulence parameters and the particle Reynolds number. Intensity seems to be the predominant turbulence parameter with scale of minor importance. An increase in turbulence intensity causes regression of the transition region of the drag coefficient towards lower Reynolds numbers. Free-stream turbulence also diminishes the drag coefficient dependency on the acceleration of the particle as previously noted in laminar flow systems and this probably results from a decreased orderliness in the wake structure as a result of turbulence.

6.3 INTERFACIAL TURBULENCE.

The orgin of interfacial turbulence is explained as the long-known, though much neglected Marangoni effect (11), wherein the movement in an interface is caused by longitudinal variations of the interfacial tension. Reported at first for various combinations of liquids, the disturbances also occur at some liquid-gas interfaces. The clean surface of an ether-water drop twiches continuously as the drop evaporates in air. The phenomena involves gross fluid motions and so demands the concept of hydrodynamics for an explanation. It is well known that longitudinal variations of surface tension not only cause movement in a liquid surface, but also bring forces to bear on the underlying liquid setting it in motion.

Analysis shows that the conception of the Marangoni effect leads to an explanation of interfacial turbulence. the instabilty has been shown to be dependent also on the direction in which interfacial tension changes with solute concentration change (200). The intensity of the turbulence is dependent on the concentration profile near the surface, which is related to the initial difference of solute concentration between the phases, and the magnitude of the surface viscosity, which reflects the presence of highly surface-active

agents.

The practical significance of this interfacial agitation referred to as interfacial turbulence (a description which includes both highly irregular and more or less ordered flows originating in the interface) has not been fully realised. Such interfacial behaviour gives abnormally high transfer rates (38,129,130), though the effect is more often observed in laboratory scale experiments than in industrial processes. Laboratory experiment concentration differences are usually large and surfaces undisturbed as compared to industrial practice where small concentration differences and vigorous agitation are used.

Glen (62) reports that interfacial phenomena influence the overall mass-transfer process, but as yet, increases in the mass-transfer rates caused by interfacial turbulence remain unpredicted. He suggests that consistent fluid turbulence-controlled transfer data may best be obtained in the abscence of interfacial phenomena effects. A clean apparatus, purified materials and a stable liquid interface with mass-transfer, are apparently necessary. He suggests that the change in resistance to mass-transfer in the continuous phase film about a mobile interface, may be described by either of two mechanisms. The surface mobility may arise from the interfacial turbulence caused by surface tension gradients over the interface (the Marangoni effect) or from internal circulation of the droplet caused by the relative motion of the drop and the fluid.

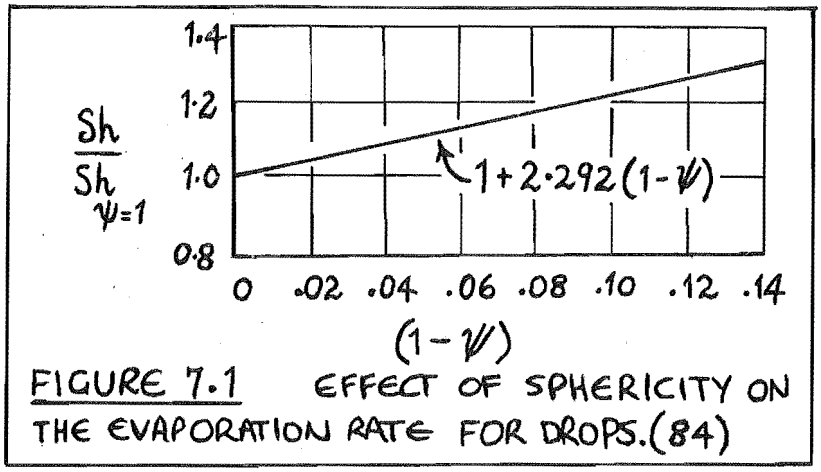

FIGURE 7.1 EFFECT OF SPHERICITY ON THE EVAPORATION RATE FOR DROPS.(84)

7. THE MECHANICS OF DROPS.

The extent of mass-transfer between drops and the surrounding continuous phase depends largely on the mechanics of the evaporating drops. Such factors as drop shape, drop oscillation and the rate of circulation within the drop, result in the ballistics and so the evaporation rate of the drop being very different from those of a solid sphere in the same continuous phase. From studies of the motion of drops, drop velocity, oscillation, circulation and breakup are seen to be functions of the shape of the drop, and the distortion of the drop to have a marked effect on the motion of the fluid particle. In addition, distortion of the drop effects the surface area and so the rate of heat- and mass-transfer to and from the drop.

7.1 DROP SHAPE.

Experimental verification of the effect of the shape of the drop on the rate of mass-transfer during evaporation was obtained by Hsu et. al. (84), who reported a marked increase in the Sherwood number with deviation from the spherical shape form. Under conditions of nearly potential flow, they presented the relative rate of evaporation for a held drop as the ratio of the Sherwood numbers of the actual drop shape to that of a spherical drop. The result as shown in figure (7.1) is reported as a defined trend rather than as a description of the actual influence of the height to diameter ratio and the sphericity of the drop on the evaporation rate.

The basic types of deformed shape of the drops are described by Hinze (76) as the "lenticular, cigar-shaped and bulgy" forms. The distortion itself can be one of two types; that of an equilibrium nature, or that of an oscillatory nature resulting from vibrations about this equilibrium

position. The shape of the distorted drop usually assumed is spherical with the minor axis in the direction of motion. Hughes and Gilliland (86) compare a theoretically derived distribution of the pressure and force over the surface of a drop with the photographic results of Laws (123) and Hendrickson (73), showing the assumption of a spheroid drop shape to be reasonable. Experimental investigation of drop distortion in terms of the pressure distribution about and in the drop has shown that the pressure exerted by the surrounding fluid on a moving drop is not uniform, whereas within the drop since the fluid motion is generally slight, the pressure is uniform except for the gravitational head.

Dealing with intermediate and high Reynolds numbers, Spilhaus (197) suggested that the force tending to separate the drop laterally could be considered as being proportional to the area over which it acts and to the kinetic head of the continuous phase. He introduced the dimensionless proportionality factor for the relationship as a Distortion Coefficient and assumed this to be constant. Hence, for a given distortion, drop Reynolds number and surface tension group, the Distortion Coefficient could be calculated.

Findlay (46) in his study of the shapes of drops of various liquids falling in air, found that the surface tension and liquid density along with the drop size, play a major part as to the extent of deformation of the drop that occurs. The following equation based on the Bond and Newton number (14) and combining the factors mentioned, was given by Davies (37) to define the condition which drops falling in gases must satisfy if they are to remain spherical.

$$\frac{\Delta\rho\, D_p^2\, g}{\sigma} < 0.4 \qquad (7.1)$$

In a study of mass-transfer to drops of liquid freely

suspended in an upwards flowing gas stream, Garner and Lane (57) observed the drops to oscillate, change shape and undergo internal circulation. Experimentally they found that the dimensionless group of equation (7.1), representing the ratio of the maximum hydrostatic head inside the drop to the surface tension forces tending to keep the drop spherical, gave a better correlation of the shape of the drops at their terminal velocity than when correlated using the Weber number. This dimensionless group,

$$We = \frac{\varrho_d D_p V^2}{\sigma} \qquad (7.2)$$

failed to correlate their results because drop distortion and oscillation altered the terminal velocity of the drops.

7.2 DROP BREAKUP.

Theoretical and experimental investigations into the bursting of drops in air and drop deformation of more recent date (76,117) add to the work which has been done in a field that has been studied from before 1904 when Lenard (124) published the results of his experiments.

In the previous section on the shapes of drops, values of the Weber number were given(37,46), below which drops could be expected to retain their sphericity. The larger the value of the Weber number, the greater will be the deformation of the drop, as the external deforming force will then be large compared with the interfacial tension force. At a critical or maximum value of the Weber number (We_{max}), breakup of the drop will occur.

For the ideal situation where the droplet is acted on only by the drag of the continuous phase medium, Mugele (158) equated the viscous drag force and the surface tension force and obtained a maximum stable droplet diameter and so a

maximum Weber number, defined as

$$We_{max} = \frac{D_p \rho_d V^2}{\sigma} = \frac{8}{C_D} \quad . \qquad (7.3)$$

He obtained correlations for droplet distribution in dispersiods and gave evidence to show that the maximum stable droplet diameter could be separately correlated for many dispersoids. Hinze (75) also reported on the criteria of droplet splitting and used the value of the initial Weber number after atomisation as being less than 13, if splitting were to be prevented. In a later paper (76), he defines a generalised Weber number as

$$We = \frac{\tau D_p}{\sigma} \qquad (7.4)$$

where τ is the force per unit surface area of the drop causing the deformation and is a function of time. In this definition, τ need not be the dynamic pressure force of the fluid flow. He also made use of the Viscosity Group,

$$V_i = \frac{\mu_d}{(\rho_d \sigma D_p)^{\frac{1}{2}}} \qquad (7.5)$$

which accounts for the effect of the viscosity of the dispersed phase.

The deformation process can be described in terms of these two dimensionless groups, and in general the maximum Weber number will be a function of the Viscosity Group. For this relation, Hinze found

$$We_{max} = K \left[1 + \phi\ (V_i)\right] \qquad (7.6)$$

where ϕ tends to zero as Vi becomes small. In this relation K and ϕ are still dependent on the external conditions, since is determined by the continuous phase flow conditions. The maximum Weber number for drop stability will be different then, for the three basic types of deformation described (76) and will also be dependent on the local flow pattern around the drop. Indeed, Hinze found that the maximum Weber number was appreciably smaller for breakup of drops according to the second type of deformation. The difference in density between the dispersed and continuous phase was also found to have an important effect on the way breakup occurred.

Sjenitzer (192) defined a maximum initial Reynolds number using the earlier data of Hinze, (that the Weber number be less than 13 to prevent drop splitting) and gave as the criteria for splitting to be prevented

$$Re_o < Re_{max} = \frac{1}{\nu_c}\ (13\ D_{p_o} \sigma \rho_c)^{\frac{1}{2}} \ . \qquad (7.7)$$

In this equation Re_o and D_{p_o} are the initial values after atomisation and ν_c is the dynamic viscosity in the gas phase.

In a study of the fall of single drops of liquid through water, Hu and Kintner (85) found most liquids to be correlated by the equation

$$K = \frac{3}{4} \frac{(Re)^4}{C_D (We)^3} \qquad (7.8)$$

where the Weber number is defined as in equation (7.2).

The maximum stable drop size was found to be dependent on the criteria

$$C_D \cdot We = \text{constant.} \qquad (7.9)$$

This relationship leads to an equation for estimating the maximum drop size for such a system from the density difference and the interfacial surface tension of the two liquids.

Equations for the behaviour of large drops and the criteria for the breakup of drops in laminar and turbulent flow are derived theoretically by Levich (125) whose expressions for the critical radius of the drop before breakup are in good agreement with reported experimental values (87,102).

Drops falling cocurrent with air of high velocity are flattened and at a critical air velocity, are blown out into the form of a hollow bag attached to the rim of liquid which breaks when the drop shatters. Measurements of the pressure distribution over a liquid sphere showed a positive pressure over the frontal area and a reduced pressure at the rear surface (65). It is then understandable that the liquid drop should become flattened and that the deformation be opposed by the surface tension forces.

With water drops of 0.5 to 5 mm in diameter, Lane (117) made measurements of the critical velocity of the air stream (U) required to shatter the drops and the velocity of the entrained drop (V) at the instant of breakup. He found that

$$(U - V)^2 D_p = 612. \qquad (7.10)$$

Such a relationship of the form $(U - V)^2 D_p$ equal to a constant would be expected, assuming that the liquid sphere placed in a steady stream of air would break when the force due to the variation of aerodynamic pressure over the drop exceeded that

due to the surface tension. Then,

$$\tfrac{1}{2}C_D \rho_c (U - V)^2 = \frac{46}{D_p} \qquad (7.11)$$

and for the range of Reynolds number in question, Lane assumed $C_D = 0.4$, so giving

$$(U - V)^2 = 1200 \ , \qquad (7.12)$$

which is twice the value obtained experimentally. An over-estimate would be expected since photographs showed that the drops did not remain spherical when moving, but approximated a disc shape before bursting. The drag on a disc is considerably less than that of a sphere and so a reduced value of the drag coefficient would decrease the value of the constant term of equation (7.12). If equation (7.10) holds over a wide range of drop sizes (there is as yet no experimental evidence to support such a proposition), then water droplets of 5 microns in diameter would just remain intact in air moving at sonic velocity relative to the drops.

For true shock exposure of the drop to the gas stream of high velocity, the maximum Weber number was found to be about one half of the value for a falling drop (76). Even when actual splitting of the drops did not occur, strong deformations of the liquid sphere were caused during the initial period when the drop Reynolds number was close to the critical value. Such deformations during that initial period will lead to an increased rate of evaporation which is difficult if not impossible to calculate.

7.3 DROP VELOCITY.

The distortion of a drop has been related to the pressure differential between the front and rear poles of the drop as it moves in a gaseous medium. Because of this change of shape

a distorted drop will not experience the same drag as a solid sphere in the same flow conditions and so their terminal velocities will be different. This was reported by Findlay (46), who found that because of drop distortion all drops with diameters greater than 2 mm fell at a velocity appreciably less than that of the equivalent solid sphere.

Theoretical equations relating the initial and final sizes of the drops, the physical properties of the liquid drop and the surrouding gas, and the distance through which the drop travels, were derived by Meisse (152), who presented a solution based on a number of assumptions. These included, that the drag coefficient varied inversely with the drop Reynolds number; that the velocity of the surrounding gas varied with time; that the surface area of the drop varied linearly with time and that the gas flow about the drop was laminar. From his experimental results he concluded that by making these simplifying assumptions, it was possible to define analytically the velocity profile of an evaporating droplet in a gas stream. A new theory for a simple method of calculating the terminal velocity of fluid particles in a media of either infinite or restricted extent, is presented by Harmathy (69). The result has good experimental verification for liquid drops in a liquid media but only approximate verification for drops in gases.

In their study of gas absorption by liquid droplets, Johnstone and Williams (94) calculated the resistance to mass-transfer allowing for droplet distortion. From work by Saito (181), they assumed spheroidal shapes for the drops and calculated the ratio of the distorted diameter to that of the original spherical diameter and used this result to determine the velocity and so the time of fall of the drops. An extension of this work was reported by Sjenitzer (193) whose study of the two simultaneous processes of the acceleration

and evaporation of liquid drops in air, produced data on the velocities and Reynold numbers of free falling water drops in air as shown in figure (7.2). The effect of small amounts of various powders on the shape and so the terminal velocity of water drops falling in air was investigated by Lihou (131), who showed that solids that were more dense than water sank to the front of the drop which becomes more flatter than usual. Complete evaporation then yeilds solid shapes ranging from flying saucers to truncated spheroids. The reason why the terminal velocity of drops containing solids was less than that for pure water drops was attributed to the distortion of of the former drop and also the absence of any internal circulation.

The problem of evaluating the velocity of fall of a liquid drop can be further complicated for the case of evaporation at high temperatures (146). The increase in volume and so drag of the drop due to thermal expansion during the heating up period affects the velocity of fall of the drop.

A complete derivation of the Rybczynski-Hadamard equation is given by Levich (125), showing that a change in the boundary conditions at the surface of the drop in the viscous flow region ($Re < 1$), leads to a significant change in the velocity of the falling drop. Saito (181) also showed this, when he extended the derivation of stokes for the drag on a sphere to a second approximation, whence the general equation of motion predicts distortion of the drop even in the creeping flow region.

The difference in values of the terminal velocities of a liquid drop and a solid sphere under the same flow conditions indicates that the drag experienced by the distorted drop is different from that of the solid sphere. Skin friction drag and form drag can be considered as the two components of the drag on a sphere. The skin friction drag is given by the

integral of the tangential shearing stress taken over the entire surface of the sphere. The form drag is given by the integral of the normal component of stress taken over the surface. Separation of the flow, with the formation of eddying and turbulent wake causes failure to achive the full pressure recovery over the rear half of the sphere and this contributes to the form drag. For solid spheres moving in a fluid, it has been shown that separation of the flow occurs between particle Reynold numbers of 15 to 20 and that instability of the wake arises at Reynolds numbers about 200.(64). Eddy rings form in the wake behind the sphere at Reynolds numbers of 500 or more and the "eddy street" effect is apparent when the Reynolds number is more than 1,000. Similar effects occur with liquid drops and gas bubbles, though not necessarily at the same values of the Reynolds numbers.

The first major work on flow around drops was done by Gunn (66) who found that water drops falling freely in still air underwent marked side slipping as they fell. In the course of their investigation of mass-transfer for droplets, Garner and Skelland (58), showed the flow separation to occur first at Reynolds numbers between 19 and 23, depending on the concentration of the drop. Further work is required to show whether drops can be considered as spheres for the purpose of predicting the flow patterns about them and also whether the "helical eddy" structure or the "eddy street" effect predominates in the wake structure. An attempt to understand this behaviour was made by Suckling (201) who studied the flow patterns around a model of various droplet shapes. A pellet modelled to drop shapes as recorded by photographs was mounted in a water stream and the flow pattern and separation points observed. Observations of the flow patterns showed similar results as obtained for spheres, but a different

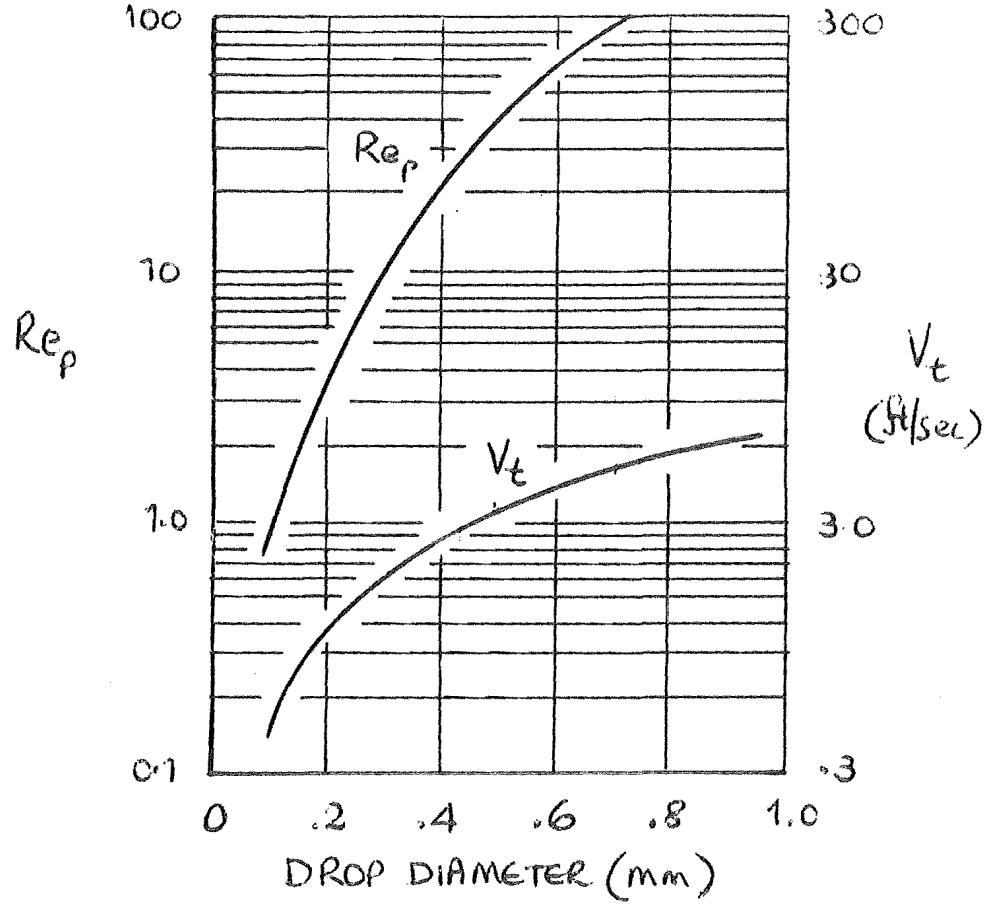

FIGURE 7.2 TERMINAL VELOCITY AND REYNOLDS NUMBER FOR FALLING WATER DROPS IN AIR (86)

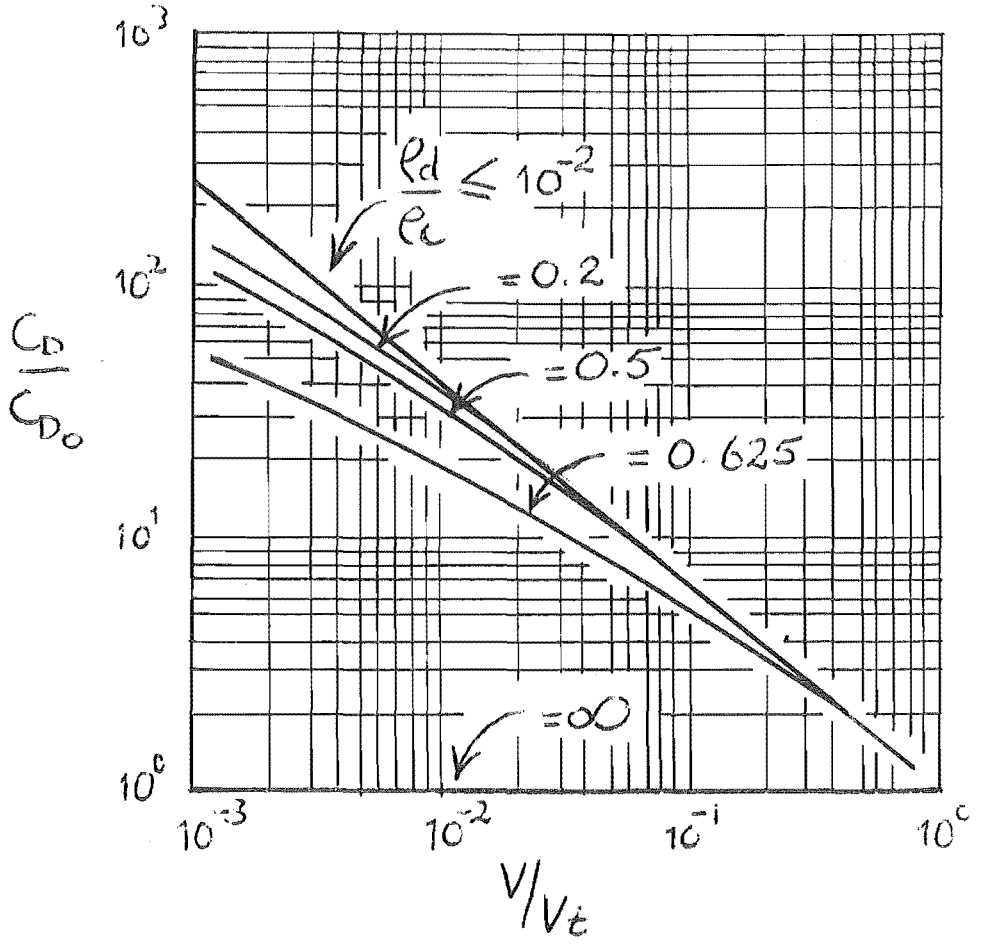

FIGURE 7.3 THE EFFECT OF ACCELERATION ON THE DRAG ON A SPHERE IN CREEPING FLOW. (86)

flow pattern was shown at low Reynolds numbers. Visible circulation occured at Re=90, oscillation at Re=210 and turbulence at Re=350.

From the equation of drag force for a sphere, the drag coefficient C_D can be defined as

$$C_D = \frac{\text{Drag Force}}{(\text{Frontal Area})} \times \frac{2g}{(\rho_d V^2)} \quad . \qquad (7.13)$$

Because of the undefined shape of the distorted drop, the geometry is usually assumed to be spherical and the value of the drag coefficient allowed to adjust to suit the actual situation. In considering the force balance for the vertical motion of a drop falling through an infinite stagnant continuous phase, Hughes and Gilliland (86) gave by dimensional analysis

$$C_D = \phi(Re, Su, Wt, Ac, \frac{\rho_c}{\rho_d}, \frac{\mu_c}{\mu_d}) \quad , \qquad (7.14)$$

indicating the complicated nature of the coefficient with its dependency not only on the drop Reynolds number but also on the Surface Tension, Gravitational and Accelerational groups as well as the physical properties of the two phases.

Reported values of the drag coefficient for liquid drops are rather different from those for solid spheres. For the drop Reynolds number range $0 < Re < 500$, Ingebo (88) found the unsteady state drag coefficient of evaporating droplets to be given by the equation

$$C_D = \frac{27}{(Re)^{0.84}} \qquad (7.15)$$

as compared to the relation for solid spheres in the same Reynolds number range, of

$$C_D = \frac{24}{Re} \quad . \qquad (7.16)$$

His investigation contained a number of accurate experiments including the injection of a liquid spray into an airstream of constant velocity.

Reliable drag coefficients have been evaluated only for bodies in steady motion with respect to turbulence free flows. To completely characterise a momentum transfer situation in a turbulent flowing fluid, the turbulence parameters must be measured, since the free stream vorticity can, under the proper conditions, cause profound changes in the particle boundary layer and wake structure. Consider the earlier example of an entrained particle moving at 90 ft/sec in a fluid which has a mean velocity of 100 ft/sec and a 5% intensity of turbulence. Since the particle boundary later and wake are generated by a relative velocity of 10 ft/sec, they are subject to a relative turbulence intensity of 50%. It has been shown (4) that high turbulence intensities can cause the laminar- turbulent transition of a sphere to occur at particle Reynolds numbers as low as 40.

Torobin and Gauvin (210), in a study of drag coefficients for solid spheres report that an increase of the free stream vorticity relative to the motion generating the particle boundary layer will cause at first a moderate increase, and then a sharp decrease in value of the particle drag coefficient. The moderate increase corresponds to the disruption of the wake system, while the sharp decrease is due to the laminar-turbulent transition in the attained boundary layer. Their results for smooth spheres at up to 100 ft/sec^2 and relative turbulence intensities of up to 45%, showed the drag coefficient to be a function of the particle Reynolds number and the relative intensity of turbulence, but not of acceleration

or the relative macro- and micro-scale variations. In an earlier work (209), again with solid particles, they supported the correlation of data by means of a total drag coefficient which appeared to be a function of the particle Reynolds number and of a reduced time parameter, which was related to the number of particle diameters traversed since the initiation of motion of the particle. Studies of the flow fields about blunt bodies revealed the extreme complexity of the phenomena during acceleration.

Because measurements of drag coefficients have been limited mainly to systems of steady flow, the effect of acceleration on the motion of liquid spheres has been overlooked. The mathematical solution for the case of very slow or creeping flow gives an indication of acceleration on drag. This solution for acceleration in creeping flow has long been established (8) and makes use of the terminal velocity as defined by Stokes law. The significant effect of acceleration is clearly seen in figure 7.3 from the longer time taken to reach the same velocity and is well illustrated when the ratio of the true drag coefficient to that for steady motion is plotted against the ratio of the actual velocity to the terminal velocity, for the case of zero initial velocity. This change in velocity under acceleration conditions is a result of the virtual weight effect. The apparent weight of the particle when accelerating is different from that under steady conditions. This acceleration effect on the mass of the particle can be allowed for by including the factor in the equation of momentum of the particle.

Reported measurements of the acceleration of drops and solid spheres at higher Reynolds numbers (up to 2,000)

have indicated that drag coefficients during the acceleration period are much larger than those for steady motion systems. Williams (220) calculated drag coefficients for accelerating water drops from the measurements made by Laws (123) and while the chief observed effect was an oscillation of the liquid drop referred to later, there was a significant decrease in velocity below about one half of the terminal velocity.

Accelerational drag does exist, then, and generally the ratio C_D/C_{Do} is larger in the turbulent flow region than in the creeping flow region.

A modified drag coefficient must also be used for the case of droplet evaporation with a high rate of mass-transfer. If the equations used to calculate the momentum-, heat- and mass-transfer rates are analogous with those used for low mass-transfer rates, then the drag coefficient of the evaporating drop must be modified. Bird, Stewart and Lightfoot (13) deal with this problem by using a correction factor, defined as

$$\theta_v = \frac{\dot{C}_D}{C_D} \qquad (7.17)$$

The superscript dot indicates that transfer conditions are dependent on the mass-transfer rate. This correction factor can be predicted for three simplified systems, by solving the equations of change for the evaporating drop allowing for the finite velocity due to high mass-transfer rate, at the film interface. In chronological order these are the Film theory, the Boundary Layer theory and the Penetration theory models (70). With accurate data, distortion of liquid drops can be calculated

from drag measurements on the assumption that the only difference between the drag on a solid sphere and that on a liquid drop is distortion, although such a method is not very convenient. Figure 7.4 compares the data of the references above and compares drag coefficients of liquid drops with those for solid spheres as calculated according to Stokes law.

Hughes and Gilliland (86) presented plots of terminal velocity with C_D, Re and Su replaced by

$$W_t = (C_D Re^2)^{\frac{1}{3}} \tag{7.18}$$

$$= D_p \left[4/3\ g \rho_c(\rho_d - \rho_c)/\mu_c^2\right]^{\frac{1}{3}} \tag{7.19}$$

$$T_v = \frac{Re}{W_t} = \left(\frac{Re}{C_D}\right)^{\frac{1}{3}} \tag{7.20}$$

$$= V_t \left[\tfrac{3}{4} \rho_c^2/g\mu_c(\rho_d - \rho_c)\right]^{\frac{1}{3}} \tag{7.21}$$

and

$$S_d = \frac{Su}{W_t} \tag{7.22}$$

$$= \left[\frac{g\sigma}{\mu_c}\right]\left[\tfrac{3}{4} \rho_c^2/g\mu_c(\rho_d - \rho_c)\right]^{\frac{1}{3}}. \tag{7.23}$$

The parameter Sd is independent of both the diameter and the velocity of the drop, and so is fixed for any given combination of phases, as shown in figure 7.5.

The relationships so far presented have dealt with the motion of particles present in relatively dilute concentrations and in surroundings of relatively large cross-sectional areas. When the dispersed phase concentration becomes high, the drops will be close enough to each other to exert a mutual retarding effect on their respective

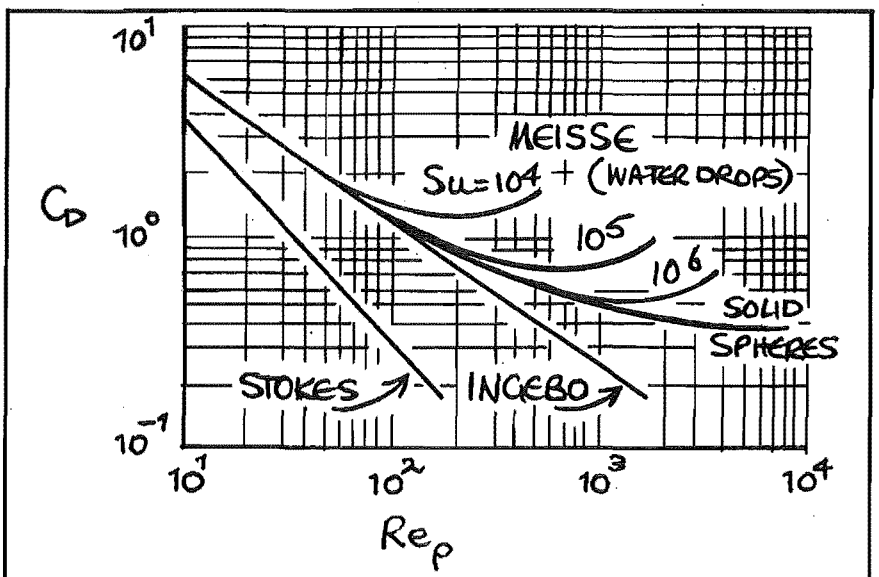

FIGURE 7.4 DRAG COEFFICIENTS FOR LIQUID DROPS IN GASES (86)

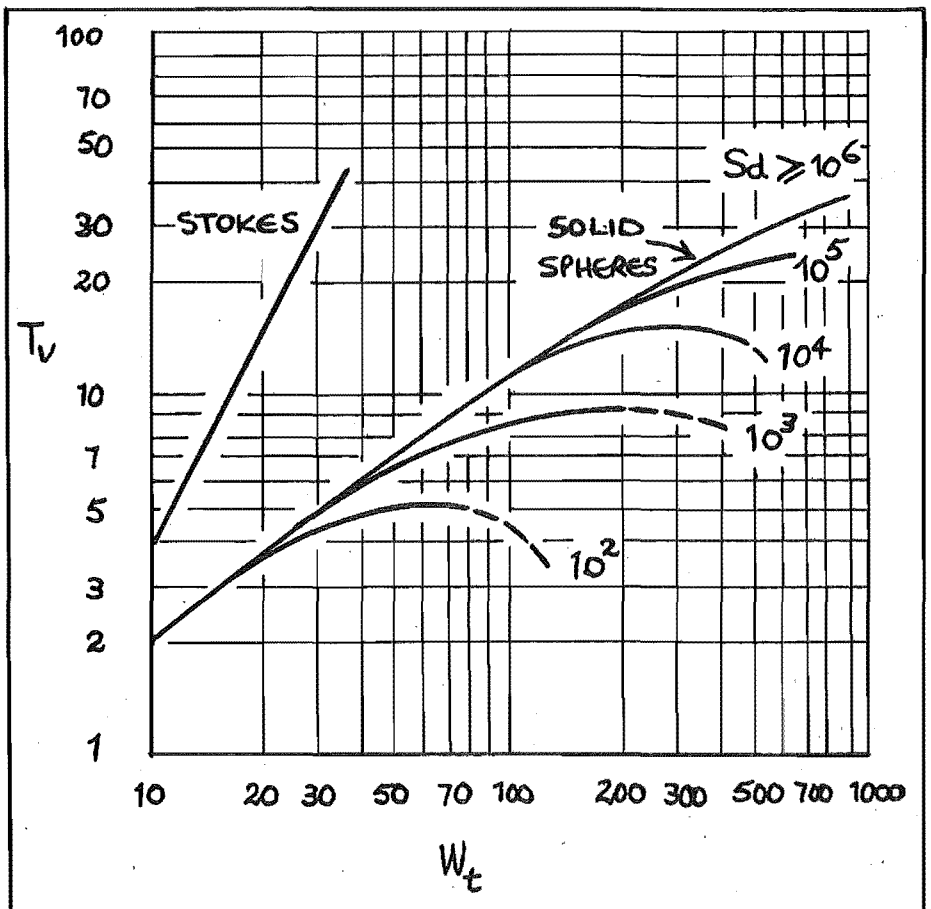

FIGURE 7.5 TERMINAL VELOCITIES OF DROPS AND SPHERES (86)

rates of fall and so attain the condition referred to as "hindered settling". This effect is not significant for volumetric concentrations below 0.1 per cent (166). The retarding effect on the rate of fall of drops due to the containing walls of the system will be negligible for commercial spray drying systems, as the diameter of the drops is not appreciable with respect to the diameter of the drying chamber. However, the effect could be significant in experiments with drops falling through a gas in a small bore tube.

7.4 DROP OSCILLATION.

The distortion correlated by various equations in the preceding sections is an average value about which the drop continually oscillates as it falls. Some of these oscillations are started by the elongation which occurs when the drop breaks loose from the nozzle tip. Others are the result of the motion of the surrounding fluid, particularly in the wake region where intermittant shedding of vortices probably occurs. In spite of evidence of the oscillation of falling drops (73, 220), the apparent success of the drag coefficient correlations based on the average value of distortion of the liquid drop, shows that the oscillations do not severely influence the mechanics of the drop. However, the effect on the internal motion of the drop could be quite large, so some consideration of the variables involved in drop oscillation is justified.

Rayleigh (175) calculated the oscillatory motion of a liquid sphere and Lamb (115) presented a complete derivation of this work, on the basis of no viscosity at the surface. The inviscid sphere solution appears to hold in real cases

of moderate values of viscosity. The equation of motion of an oscillating drop shows that the amplitude of oscillation of a 3 mm diameter water drop decreases to about one half of its original value in 0.35 seconds, or at a distance of fall in quiescent air of about 60 cm. The effect of eddies within the drop, if they existed, would be to increase the rate of energy dissipation and so increase the rate at which the amplitude of oscillation decreases

Drops have been observed to oscillate in three different ways.

(a) Prolate-oblate oscillation about an equilibrium shape,
(b) Oscillation about axes 90° apart in the horizontal plane,
(c) Eccentric rotation about the vertical axis while the horizontal axes remain constant. Type (a) is the usual reported form of oscillation, about the generally assumed equilibrium spheroid shape of the drop. The frequency of oscillation of this type has been calculated by Lamb (115), whose equation for drops falling in gases reduces to

$$f = \left[\frac{8\sigma}{3\pi M}\right]^{\frac{1}{2}} \qquad (7.24)$$

Garner and Lane (57) have confirmed that the frequency of prolate-oblate oscillation of drops falling in a gas agree with the frequency calculated from this equation. Oscillations of the type (b) are rare and Findlay (46) found that such oscillations were of small amplitude. Type (c) was found to occur for large drops of liquids having low values of viscosity and surface tension.

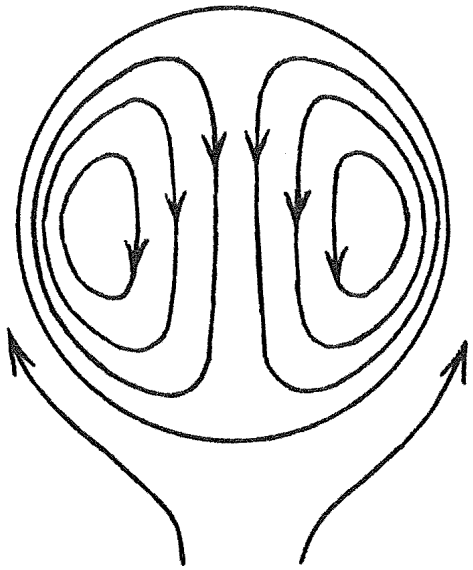

FIGURE 7.6 STREAMLINES FOR THE INTERNAL MOTION OF A LIQUID DROP. (EQUIDISTANT VALUE OF THE STREAM FUNCTION IMPLIED) (115).

7.5 DROP CIRCULATION.

Oscillatory distortion is a source of internal circulation and for the case of streamline flow of the surroundings, the flow pattern within the drop can be calculated and shown as in figure 7.6.

For drop circulation in creeping flow region with no surface tension, the streamlines show most of the motion to occur near the surface. The maximum circulating velocity occurring at the centre of vortex equal to $D_p/2\sqrt{2}$ has been calculated (86) for a water drop of 3 mm diameter, oscillating with a 5% amplitude for Reynolds number of 1100, and the velocity (or rather the amplitude of this velocity) found to be 37 cm/sec. With such a non-linear fluctuating flow of large amplitudes, eddies would undoubtedly form and tend to distribute the circulatory motion away from the surface to the interior of the drop.

Drops falling from a nozzle have a very high initial rate of circulation immediately after detaching from the nozzle tip. This could be caused by the mechanism of breakaway from the nozzle and the initial rapid circulation (probably in turbulent flow) would be rapidly damped out by viscous forces inside the drop and fall to the natural circulation rate caused by the falling drop motion.

Drop circulation has been widely reported and commented on. Increased gas absorption rates with circulation were reported by Garner and Lane (57) and the formation of vortices in fluid spheres was long ago postulated by Hadamard (68). Bond and Newton (14) in a mixed study of the transition region for circulation in drops, showed that drop circulation became appreciable when the skin friction was a major portion of the surface forces. They suggested that the initial radius of

the drop at which circulation is first detected is dependent on the dimensionless group of equation (7.1) which is primarily dependent on the interfacial tension. According to such a criterion, water drops falling freely in gases at a diameter of 5mm should just circulate.

The importance of surface active impurities in reducing the rate of mass-transfer by delaying the onset of vortex formation and sp circulation inside drops, has been increasingly realised in recent years and is discussed in some detail in section 9.2 . For drops with high surface tension, only a trace of impurity is needed to cause an appreciable gradient of surface tension. Drop circulation can also be retarded or even stopped by the formation of rigid films of insoluble surfactants or solid particles, that do not transmit the external shear to the fluid inside the drop.

It has been found that rapid circulation currents inside the drop do not increase the mass-transfer rate inside the drop by the extent that one would expect (70). The reason why there is only a 1.5 fold increase with rapid circulation is that the laminar flow stream-lines within the drop are closed loops and above a minimum velocity the transfer rate is independent of the circulation velocity. The increased transfer rate can be considered to come from the increased area of diffusional transfer, with solute diffusing out from the central region of the drop as well as from the surface of the drop.

The effect of internal circulation within a drop on the external transfer rate has received less attention, even though the effects are as important. It has been shown that the velocity boundary layer about a circulating drop is reduced by a factor $\sqrt{1 - k}$, where k is the ratio of the surface velocity to the velocity of potential flow of the continuous medium. For large drops with low internal

viscosity, the surface velocity approaches that of potential flow and the velocity gradient in the boundary layer vanishes.

8. EVAPORATION AT HIGH TEMPERATURES.

The evaporation of droplets in high temperature surroundings requires modifications of the assumptions used to solve the evaporation equations for droplets evaporating in an atmosphere, the temperature of which was only moderately higher than that of the droplets. Heat-transfer by radiation and mass-transfer must now be considered, as the assumption that all the heat transferred from the gas is used as latent heat of evaporation no longer holds. The sensible heat transferred to the vapours as they move out into the main gas stream must be supplied by the surrounding hot gas, and variations in the transport properties k, μ and C_p caused by temperature and concentration gradients in the gas film surrounding the drop must be taken into account.

In high temperature sorroundings, heat-transfer by mass-transfer and radiation may become significant (80). A large mass flow of cold vapour from the droplet surface to the surrounding gas acts exactly like a convective velocity in the positive radial direction. An overall mass and energy balance will show that the required sensible heat to warm the vapour may be considerable when compared with the latent heat requirements, particularly when the liquid is one of low latent heat. The heat supplied by radiation can normally be treated as coming directly from the surroundings to the droplet surface without intermediate absorption or radiation and can be incorporated in the heat-transfer equations as such. For intermediate absorption and radiation, a term representing the shielding effect and the heat generation within a drop must be introduced and the equations then become non-linear and the solution complex.

8.1 FREE CONVECTION.

The situation of no forced convection during the evaporation of droplets is a case of technical importance and mathematical solutions for the pseudo-stationary equations of such a system have been presented by Marshall (146), Ranz (171) and others. The solutions are similar and differ only in the definition of the rate of evaporation as to whether or not it includes the effect of radiation. Ranz in his solution has allowed for radiation effects (without intermediated absorption and radiation) whereas Marshall's equation can be considered valid only where the gas and the containing walls of the system are at the same temperature.

A heat balance over a differential spherical shell through which heat is passing inward toward the drop while mass is passing outward, as illustrated in figure 8.1, results in the following differential equation.

$$k\left[\frac{d^2T}{dr^2} + \frac{2}{r}\cdot\frac{dT}{dr}\right] = \frac{W\,C_p\,dT}{4\pi r^2\,dr} \qquad (8.1)$$

The terms on the left hand side of the equation represent the heat transferred by conduction, while those of the right hand side represent the mass flow of heat.

Assuming steady state conditions with no convection, Ranz showed that for heat-transfer by conduction only,

$$Nu = \frac{2E/r_o}{\left[\exp E\left(\frac{1}{r_o} - \frac{1}{r_f}\right) - 1\right]} = \frac{h_c\,To}{k_{av}} \qquad (8.2)$$

where $E = \dfrac{W\,C_{p_{av}}}{4\pi k_{av}}$, (8.3)

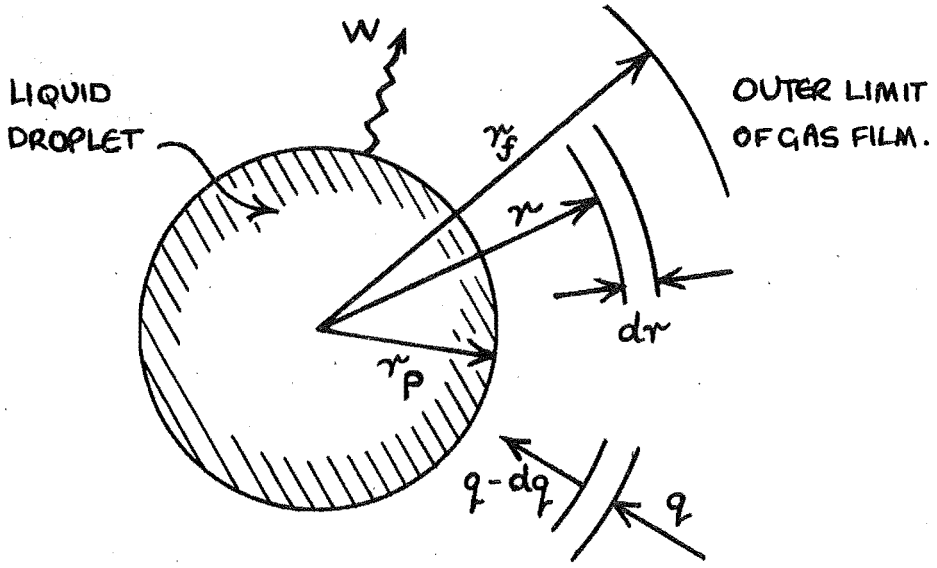

FIGURE 8.1 MODEL REPRESENTATION OF THE HEAT BALANCE ABOUT A DROPLET IN HIGH TEMPERATURES. (172).

$$\text{and } W = \frac{4\pi r_o^2}{H_v}\left[k_o\left(\frac{dT}{dr}\right)_{r=r_o} + \sigma_r(T_f-T_o)F_A F_e\right], \quad (8.4)$$

which is the rate of evaporation of the droplet and includes the effect of radiation.

From equation (8.2) it can be seen that as the evaporation rate increases (E becomes large) then the Nusselt number decreases and conversely, when the stagnant film thickness increases and the evaporation rate is low (E becomes small), then the Nusselt number equals 2.0 in accordance with the theory.

Hence, when E = 0 (no mass-transfer)

$$Nu_{E=0} = \frac{2/r_o}{(1/r_o - 1/r_f)} \quad (8.5)$$

and the ratio of the Nusselt numbers for heat-transfer by conduction with and without mass-transfer is shown to be

$$\frac{Nu}{Nu_{E=0}} = \frac{E(1/r_o - 1/r_f)}{[\exp E\,(1/r_o - 1/r_f) - 1]} \cdot \quad (8.6)$$

The demominator of the equation can be expanded and it will be seen that when the evaporation rate is large, the actual Nusselt number can be substantially less than that at low evaporation rates. This has been reported in experiments where mass-transfer controlled the heat-transfer and experimental values of the Nusselt number were only one quarter of the value predicted for heat-transfer alone.(64).

From equation (8.6), the actual and apparent heat-transfer coefficients based on heat-transfer with and without mass-transfer can be expressed as

$$h_{c_{act.}} = h_{c_{app.}}\left[\frac{a}{e^{a}-1}\right], \qquad (8.7)$$

where $$a = \frac{WCp_{av}}{4\pi k_{av}}\left(\frac{1}{r_o} - \frac{1}{r_f}\right) . \qquad (8.8)$$

This relationship between the two heat transfer coefficients is very similar to that derived by Colburn and Drew (28) for the condensation of mixed vapours.

To obtain a solution of equations (8.2), (8.6) and (8.7) Ranz made use of the average values of the thermal conductivity and heat capacity of the vapour film about the evaporating drop. Because the thermal conductivity of the vapour may vary several fold over a large temperature range, it was necessary to choose an unspecified average value to avoid non-linearity. A discussion on the validity of this "average" value and the Nusselt number based on such a conductivity and heat capacity follows in section 8.4 .

The inclusion of the effect of radiation on the evaporation rate in equation (8.4) would suggest that radiation effects could account for a significant fraction of the heat transferred to the droplet during evaporation.

It has been found (80) that although radiation accounts for a large fraction of the heat transferred from the walls of the drying chamber to the gas at relatively high temperatures, radiation plays only a minor part in the evaporation of droplets with diameters less than 100 microns. The effect of radiation often warrants the calculation of its order of magnitude (184), but rarely is it of great importance.

Williams (220) has reported that the extent of the influence of radiation is in part dependent on the internal reflection of the drop as the absorptivity varies appreciably according to the reflectivity of the drop.

Hoffman and Gauvin (79, 80) have reported studies of spray evaporation at high temperature employing falling spray and atomised suspension techniques. They predicted the evaporation rate of stationary droplets in high temperature surroundings using the equation

$$\frac{dm}{d\theta} = \log_e\left(1 + \frac{C_p \Delta T}{H'_v}\right) \Bigg/ \left(\frac{C_p}{4\pi k_f}\right)\left(\frac{1}{r_o} - \frac{1}{r_f}\right) \qquad (8.9)$$

where $$H'_v = \left[H_v - q_R \Big/ \left(\frac{dm}{d\theta}\right)\right] . \qquad (8.10)$$

This analysis attributes all transfer to conduction as did previous authors and the equation (8.9) shows the effect of the evaporation rate on the heat-transfer to the droplets to depend on the magnitude of Spalding's transfer number (196),

$$B' = \left(\frac{C_p \Delta T}{H'_v}\right) \qquad (8.11)$$

It has been shown theoretically that the "true" Nusselt number (Nu_T) for pure heat transfer with no evaporation should be modified to become an "actual" Nusselt number (Nu_A), such that

$$Nu_A = \log_e\left(\frac{1 + B'}{B'}\right) . Nu_T \qquad (8.12)$$

This equation can be compared with equation (8.7) for

actual and apparent heat-transfer coefficients. The "actual" Nusselt number then yields the actual heat-transfer that is available for evaporation at the droplet surface. Equation (8.12) has not been experimentally verified and the problem of selecting a proper temperature at which to evaluate the gas properties is as yet unsolved.

Because their results indicated that the Nusselt number was not dependent on the Grashof number, Hoffman and Gauvin concluded that the evaporation rate of stationary drops in high temperature environment was not governed by the rate of heat-transfer by natural convection. They found, however, however, that the evaporation rates could be predicted by the equation

$$B' \, Nu_A (Pr)^{-\frac{1}{3}} = 3.2 \, B^{0.97} \qquad (8.13)$$

This equation involves the total heat transferred (both by convection and radiation) rather than the individual transfer coefficients (or Nu or Nu') as in most previous correlations. Since the mass rate of vapour evolution depends on the evaporation rate, the above correlation then relates the vapour flow in the boundary layer to the system conditions expressed by Spaldings number B.

In extending this result to the evaporation of small droplets, it may well be that the existence of relative velocity resulting from the free fall of the drop, or turbulence effects, will affect the boundary layer phenomena and the droplet shape, and the resulting heat-transfer under such conditions may be less than predicted here, as indeed other studies have indicated (80, 146, 171).

8.2 FORCED CONVECTION.

The rate of evaporation of a drop in high temperature surroundings under forced convection conditions can only be approximated. The general method applied is to assume that the effective film thickness as specified by the Reynolds number remains unchanged for the same convective conditions. For appreciable mass-transfer in a forced convection field, the velocity around the surface of the drop may be of the same magnitude as the fluid velocity in the boundary layer. The momentum associated with this mass will have to be taken into account when a solution of the momentum equation is attempted and apart from the usual boundary conditions employed an additional condition

$$\rho_v W = D_v \frac{dc}{dT} \qquad (8.14)$$

$= 0$, must be considered.

For high mass transfer rates, with natural and forced convection effects both present and of comparable magnitude, Pei (164) has shown that the Ranz and Marshall equation predicts values which are too high. Pasterak and Gauvin (162) verified that an approximate allowance for the cooling effect of the evolved vapours at high mass-transfer rates can be made, by multiplying the right hand side of the Ranz and Marshall equation by the factor $\log_e (1+B)/B$. The modified equation which results can be compared with the equation (8.12).

8.3 HIGHLY INTENSIVE HEAT- AND MASS-TRANSFER.

In order to intensify heat- and mass-transfer, high temperatures and pressures are employed in modern engineering on an increasing scale. Under such extreme conditions the mechanism of transfer of matter and energy is considerably

modified. In addition to transfer by molecular processes, molar processes of a filtrational nature start to play an important part.

A theoretical investigation of transfer under such conditions has been reported by Mikhailov (153), who presents solutions for a system of differential equations for heat- and mass-transfer in dispersed medium.

8.4 THE DEFINITION OF THE NUSSELT NUMBER.

The evaporation of droplets with large mass-transfer rates in high temperature atmospheres has required solutions of the energy equations that account for the sensible heat transferred to the vapours moving radially away from the drop surface. This in turn, led to the defining of a modified Nusselt number and required the selection of a proper temperature at which to evaluate the gas properties k and C_p.

The Nusselt number has the following meaning according to Haussen (72),

$$Nu = \frac{hD_p}{k} = \frac{D_p}{k/h} \quad . \qquad (8.15)$$

The length k/h represents under certain conditions a thickness of the boundary layer and the Nusselt number can therefore be determined as the ratio of the diameter of the drop to a certain thickness k/h of its boundary layer.

Martinelli (148) defines the Nusselt number as the ratio of two temperature gradients and Jacob (90) introduces the concept of total heat transport and uses the Nusselt number as representing a ratio of diffusing heat quantities. In his investigation of the physical concept of the equation

$$Nu = C_1 (Re)^m (Pr)^n \qquad (8.16)$$

Bouroutis (17), refers to the above references (72,90,148) and concludes that the Nusselt number is a ratio of diffusions, as

$$Nu = \frac{\text{Total heat diffused normally to flow}}{\text{Heat diffused by conduction normal to flow}} \qquad (8.17)$$

The definition of the Nusselt number as given in equation (8.15) and used in the above sections, resulted in the ratio of the heat transferred to the edge of the vapour film surrounding the drop to that which actually reached the liquid surface, being of the order of four or more in some cases. Hence, various authors have introduced so-called "actual" Nusselt numbers and coefficients as related to "true" or "apparent" values for the same conditions of heat-transfer but with no mass-transfer.

The Nusselt number for an evaporating droplet as written by Ranz (171) was

$$Nu = \left[k_o \left(\frac{dT}{dr}\right)_{r=r_o}\right] 2r_o \,/(T_f - T_o)k_o \quad . \qquad (8.18)$$

Uyehara and Meyers (214) point out that the effect of heat-transfer to a drop differing by a factor of four or more does not occur when the Nusselt number was defined as in equation (8.18), with

$$dT^* = \frac{dT}{(T_f - T_o)} \qquad \text{and} \qquad dr^* = \frac{dr}{2r_o}$$

for $\left(\frac{dT^*}{dr^*}\right)_{r=r_o}$. Clearly then the temperature gradient will be different with and without mass-transfer.

This definition of the Nusselt number takes into account the effect of mass-transfer on heat-transfer and also makes it clear that the thermal conductivity should be evaluated at the drop surface $(r = r_o)$ and not taken as an average value between the liquid and gas temperatures.

Schlünder (184) in his extensive theoretical and experimental study of the evaporation phenomena of pure liquid and salt solution drops, used the arithmetic mean of the air and drop temperatures and showed that only through such a mean temperature value did a physically meaningful relationship arise from his experimental results.

There would appear to be some degree of flexibility in the definition of the Nusselt number. The reply by Ranz to the comments of Uyehara and Meyers sums up the situation when he says that the only rules for defining the Nusselt number, are that it be entirely composed of the quantities which are known or wanted and that it be clearly defined. The definition should not be restricted since the Nusselt number can be a generalised dimensionless heat-transfer rate which is related to the boundary conditions applying and fines many uses.

9. OTHER EFFECTS ON THE EVAPORATION RATE.

9.1 SONIC ENERGY EFFECT.

In furnaces where powdered fuel was being burnt, dramatic increases in the combustion rate and efficiency have been reported (176), under conditions of sonic resonance in the combustion chamber.

For a gas contacting system then, taking into consideration the limits imposed by the system as to the amount of turbulence which could be introduced by mechanical means, it would seem reasonable to assume that sonic energy might decrease the surface film resistance to mass-transfer, for the condition where the sound was added to the gas from an external source, rather than by producing it by the passage of the drying gas.

This reasoning was the basis of work done by Hodgins, Hoffman and Pei (78) who found that for a power input of 1 watt/cm^2 of cross-sectional area of the contacting chamber at 256 cps, air particles would vibrate with an amplitude of 5mm. This distance is as large (if not larger) than the diameter of spray droplets.

The thickness of the film at the interface between the gas and the droplets is a factor (among other things) of the degree of turbulence at the interface. Maisel and Sherwood (143) have examined this effect of the scale of turbulence on mass-transfer in turbulent air streams. In their experiments, turbulence was introduced by placing drilled plates in the air duct at various distances upstream of solid spheres from which the rate of evaporation of water was measured. The scale of turbulence was measured by a standard technique involving two separated wire probes and gave an indication of the size of the eddies in the air stream. Turbulence intensity, the measure of the velocity fluctuations at a given point, was recorded using a hot-wire

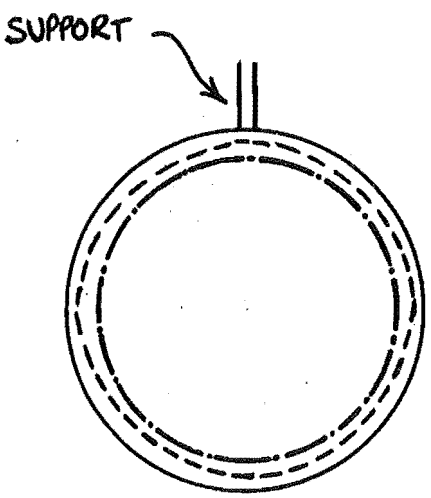

D_{p_o} = 0.313 ins
Re_p = 208
TIME = 300 mins
---- = QUIET RUN
—·— = 275 cps, 160 db

FIGURE 9.1 TYPICAL PROFILE OF A SINGLE HELD SPHERE OF NAPTHALENE SHOWING THE EFFECT OF SOUND ON THE EVAPORATION RATE (15).

anemometer providing a signal to an oscilloscope. In all their experiments the effect of the intensity of turbulence was marked, but that of the scale of turbulence, of little consequence. Since the mass-transfer enhancement was so very dependent on frequency (turbulence intensity), it was apparent that the movement of the air by the sound would have a much greater effect than that of the bulk velocity of the gas stream, as the velocity imparted by the sound to the gas was ten to twenty times greater than the superficial velocity of the air.

As is to be expected for turbulent flow past a spherical surface (where the mass-transfer coefficient is an inverse function of the sphere diameter), Hodgins, Hoffman and Pei (78) found the mass-transfer coefficient to decrease with increasing sphere diameter for constant sonic energy input and superficial air flow rate. The enhancement of mass-transfer as shown in figure 9.1 is quite marked. The interpretation of these effects in terms of normal turbulence phenomena is questionable, particularly because of the velocity difference and also because an increase in the superficial gas velocity for constant sonic power did not result in an increase in the mass-transfer rate.

Problems such as gas cleaning and defoaming have also been solved by the use of ultrasonic energy. It is a relatively inexpensive form of energy and the sonic generator can be electrically (electromagnetic vibrator) of mechanically (air-jet siren) powered.

Boucher (16) reports on the use of static sirens for accoustic of heatless drying of heat-sensitive materials. The rate of evaporation at a liquid-gas

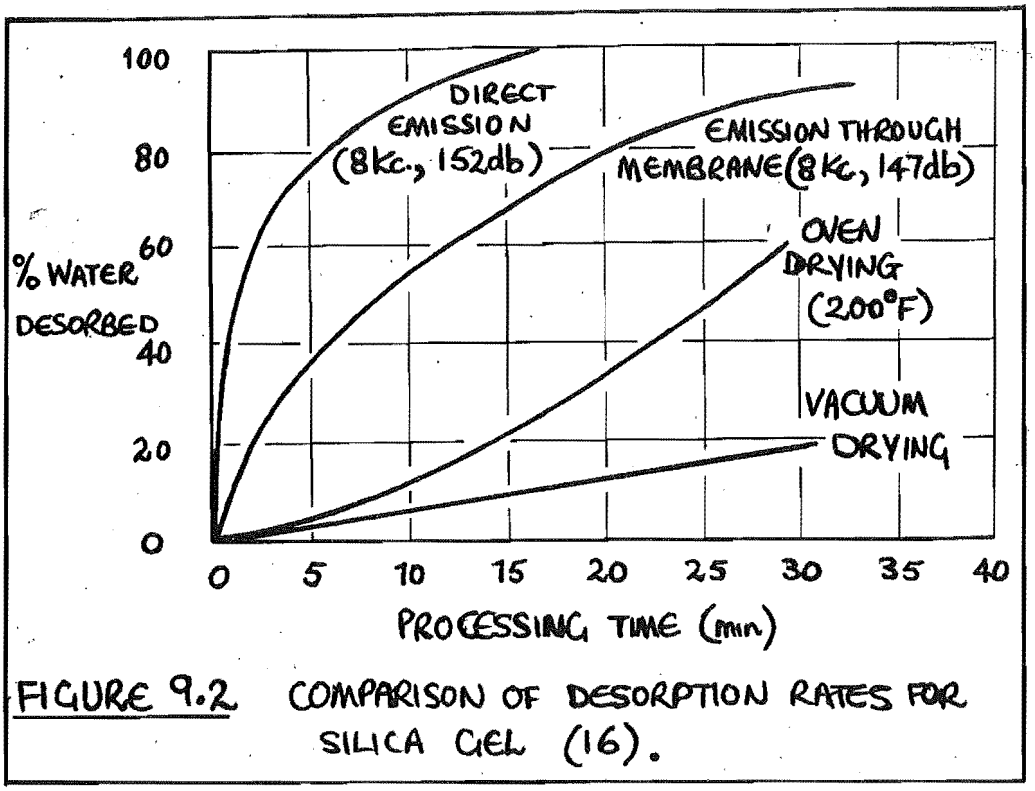

FIGURE 9.2 COMPARISON OF DESORPTION RATES FOR SILICA GEL (16).

TABLE 9.1

SCREEN MESH SIZE	SIEVE ANALYSIS OF PRODUCT	
	WITHOUT ULTRASONICS	WITH ULTRASONICS
25	0.5%	0.6%
40	1.9	9.0
60	31.9	49.8
100	60.7	39.6
ON PAN	5.7	1.0

interface is in part directly proportional to the gas turbulence above the interface and the surface area of the interface, and inversely proportional to the static gas pressure surrounding the liquid boundary. The production of a high-intensity accoustic field above a liquid surface creates a very strong field of turbulence and has a marked effect on the drying rate of the material, as shown in figure 9.2.

Spray driers appear to be an ideal situation for ultrasonics. Fine atomised wet globules can be held longer in suspension by an accoustic field and when the particles are vibrated, their surface is exposed to more drying air.

Another factor to consider is the agglomeration which occurs between smaller sprayed globules with a large oscillation amplitude and larger globules with a small oscillation amplitude. This leads to higher recovery rates and to a definite change in the size distribution of the product collected from the drier, as shown by the results given in table (9.1).

The results of improved drying under sonic energy conditions leads to a consideration of the effect of oscillating or pulsed gas flows on the evaporation of sprays. No references, other than that of Boucher (16), to spray drop systems are available but mention is made of the work by Krasuk and Smith (110) on mass-transfer in a packed, pulsed-column. They presented data for time-averaged mass-transfer coefficients. The coefficient was found to increase with an increase in the frequency of pulsation and decreased as the average flow rate through the column increased. This demonstration of an improved mass-transfer rate by pulsation of the liquid stream past a solid phase,

suggests a possible similar behaviour for a gas-liquid system.

9.2 SURFACTANT INFLUENCE.

It has been established that the presence of small quantities of surface-active impurities can have a profound influence on the rate of interphase mass-transfer (36, 140). The surfactant impurities reduce circulation inside drops by retarding interfacial flow and so depress the bulk phase transfer. As yet there are very few analytic equations relating transfer parameters to surfactant properties. One such analytic study is by Levich (125) who derives equations for the fall of drops in liquid media in the presence of surface-active substances. His derivation assumes that the surfactants are soluble in the liquid mediud, but not in the liquid of the drop. This is not the case for a liquid drop in a gaseous atmosphere and the results of this author must be interpreted accordingly.

Schechter and Farley (183) in their paper on interfacial phenomena refer to two types of mechanism of interaction. Both the "direct interaction" (as when the surfactant directly interferes with the transport of material across the phase boundary by some mechanism of molecular blocking), and the "indirect interaction" (as when the hydrodynamic behaviour of a multiphase system is changed due to the presence of surfactants and so the mass-transfer rate also changes) must appear as boundary conditions when solving the equations of transfer.

The simplest example of indirect interaction is

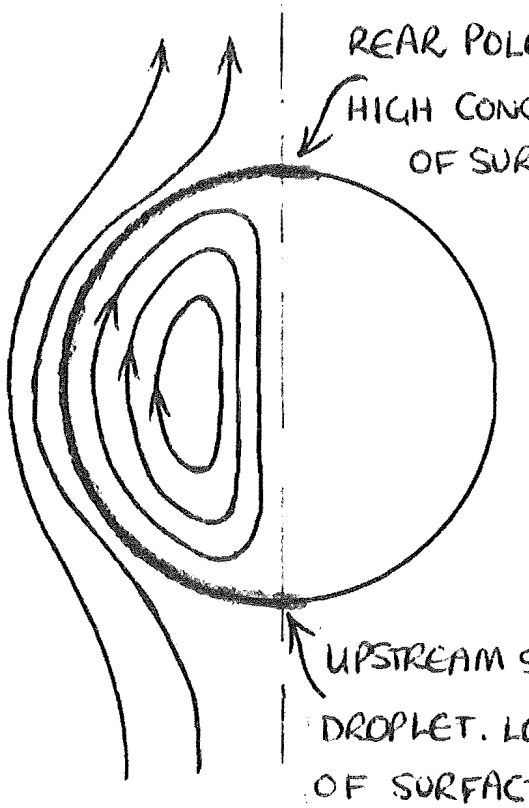

FIGURE 9.3 CONTAMINATED DROPLET BEHAVIOUR IN A FLOW FIELD (183).

the retardation of the droplet circulation in the presence of surface-active material. The mass-transfer rate is affected as the boundary layer increases with decreasing droplet circulation in a constant velocity flow field. Surfactants tend to be distributed non-uniformly over the surface of a droplet because of the motion of the fluid interface tends to convect the material toward the rear pole of the sphere, as shown in figure 9.3. The existence of concentration gradients over the interface gives rise to variations of the interfacial surface tension, which is strongly concentration-dependent and leads to interfacial turbulence as explained by the Marangoni effect referred to earlier. This variation in interfacial surface tension has the effect of counterbalancing part of the shearing stress exerted by the continuous phase on the surface of the droplet and so a sufficiently large concentration of surfactant could balance the viscous stress exerted by the external flow, resulting in complete stagnation of the discontinuous phase.

The rate of transfer for a slowly circulating drop contaminated with surfactant, whose relative velocity was small, was given by Lochiel (133) as

$$Sh = 0.99\left[\frac{\mu_d + 1.33\mu_c + B_1}{\mu_d + \mu_c + B_1}\right]Pe^{\frac{1}{3}} \quad . \qquad (9.1)$$

He reported this equation to hold for liquid drops in a gaseous medium when $\mu_d/\mu_c \gg 4$, whence $B_1 = 0$. In his discussion of the influence of surfactants on mass-transfer rates, Lochiel uses as the criterion for droplet sphericity that the Weber number be substantially less than unity. This follows Mugele's derivation of the Weber number (ref. section 7) where

$$We_{max} = \frac{8}{C_D} \quad .$$

For creeping flow ($Re < 1$), assuming Stokes' law to hold ($C_D = 24/Re$), then the Weber number is less than unity. Because the surface tension varied over the interface where there was no fluid flow was used to estimate We. Such a value generally gave a conservative estimate of the value of We_{max} at which a spherical drop can exist.

9.3 PRESSURE EFFECT.

To determine the rate of evaporation of a pure liquid from a spherical surface exposed to a gas stream of varying static pressure, Ingebo (88) used the heat balance equation,

$$\frac{dm}{d\theta} = \frac{h\ A\ \Delta T}{H_v} \qquad (9.2)$$

and assumed that the sensible heat transferred by the liquid to the sphere was negligible compared with the latent heat requirements.

From the experimental results obtained for the evaporation of four pure liquids over a static air stream pressure range from 450 ti 500 mm Hg, the following semi-empirical equation for predicting the evaporation rate was derived:

$$\frac{dm}{d\theta} = \frac{k_g \Delta T}{H_v} \cdot 2\pi D_p \left[1 + 1.29 \times 10^6 \left(\frac{Re.Sc.gl}{(c')^2}\right)^{0.6} \left(\frac{k_g}{k_v}\right)^{0.5}\right] \qquad (9.3)$$

where l = mean free path and c' = root-mean-square velocity of the gas molecules.

For single drops with a low value of upstream turbulence, the results indicated that the heat-transfer coefficient

was independent of the static pressure of the continuous system and that the effect of pressure on the evaporation rate could be determined directly from the pressure effect on the surface temperature of the drop.

Evaporation rates of droplets at very low pressures were reported by Sherwood and Cooke (189) in terms of the evaporation coefficient. Ideally, in the abscence of any gas-phase diffusional resistance, liquids would evaporate at a finite rate and at pressures of a few mm Hg this molecular resistance to diffusion would be expected to become significant. The concept of adding the diffusional and surface-escape resistances was used by the authors (as did Langmuir and others before them) to determine whether the evaporation coefficient changes as the drop becomes very small or the pressure of the gas very low. In their experiment where the rate of evaporation and the gas rate were very small, so that the evaporative cooling of the surface was negligible, they found that the evaporation coefficient was independent of pressure over the range of 0.1 to 3000μHg and that above this pressure the coefficient was dependent on the temperature of the gas and increased with increasing Reynolds number of the droplet. The results were for Reynolds numbers up to 1.37 and of the four gas atmospheres used as the continuous phase, the evaporation rates in Helium and Freon-12 gas were rather higher than the rates in air and Carbon dioxide for the same experimental conditions.

The effect of curvature on the vapour pressure of a drop can be estimated from the Thomson-Gibbs relationship

$$\log_e\left(\frac{p}{p_s}\right) = \frac{2M}{RT}\left[\frac{\sigma}{\rho_d r_p}\right] \quad , \qquad (9.4)$$

where p is the actual vapour pressure over the drop surface

and p_s is the normal vapour pressure of the liquid at the absolute temperature T. By substituting various values of r_p, the drop radius, in this equation it has been shown (113) that the vapour pressure over the drop is not increased more than 1 per cent until a drop diameter of the order of 0.2 micron is reached. The dependency of vapour pressure on the curvature of the drop then favours drop-size uniformity by the growth of larger drops in a spray at the expense of smaller ones.

10. DISCUSSION

Early work established that the evaporation rate of a drop was proportional to the drop diameter and that falling drops do not behave as though they were solid spheres. The equation by Frössling (53) which extended that of Fuchs (55) by allowing for the relative velocity effect between the droplet and the gas, has been well established and differs from the more commonly accepted equation by Ranz and Marshall (173) only in the value of the coefficient used. The results obtained when these two equations are used to correlate data for spray-driers are not very different.

The apparently simple relationship of the Ranz and Marshall correlation has been widely applied in chemical engineering problems and if accurate values of the physical constants and drag coefficientsfor the droplets are available, it will give a good estimate of the transfer rates to be expected in cases of evaporation from spherical interfaces. Although some workers assume a constant drop diameter for the design of spray-driers, most use the Ranz and Marshall equation and account for the changing relative velocity effect by assuming quasi-stationary conditions. The well established 'step' method is then employed to evaluate the drying requirements. Using modern computing methods the result may be as accurate as desired. Any true solution of the boundary-layer equations of the transfer processes would be extremely complex and require the evaluation of the thickness of the boundary layer as the evaporation proceeds. This is the result of the fact that the boundary layer is of the same size as the drop diameter. Hence, for a changing drop diameter as evaporation occurs, so a changing boundary layer thickness must be used in the calculations of the transfer rates. It should be remembered that the actual rates are more like those

shown in figure 3.6 and not like the averaged values given by the correlations for the heat- and mass-transfer rates around the drop. Nusselt number correlations which embody the free convection effect by incorporating a function of the Grashof number do not agree with experimental results so far reported or on the form of the equation itself.

The total lifetime of a droplet evaporating in still air conditions has been shown to be proportional to the square of the initial diameter of the droplet and evaporation under such conditions has been expressed by the use of the evaporation coefficient. This is an indication that the process of evaporation can be desribed by a fixed value of the Fourier number, since

$$Fo = \frac{k\,\theta}{C_p \rho_v D_p^2} \qquad (10.1)$$

and for a constant value of the number

$$D_p^2 = \frac{k\,\theta}{C_p \rho_v} \quad . \qquad (10.2)$$

Hence the expression,

$$D_p^2 = D_{p_o}^2 - \lambda\theta \quad , \qquad (10.3)$$

where

$$\lambda = \frac{k}{C_p \rho_v} \qquad (10.4)$$

and is termed the evaporation coefficient. The development of a similar expression involving an evaporation coefficient which incorporates the relative velocity effect would be of some considerable help in the design of spray-driers. The correlations available at present for the drying time of pure drops differ slightly, in that they are based on the different transfer correlations available and usually assume different boundary conditions as well.

Nusselt number correlations referred to in this survey

are mainly based on an average value of the thermal conductivity of the film about the drop, k_f. The one notable exception is that by Ingebo who had a separate factor of $(k_c/k_v)^{\frac{1}{2}}$ in his equation. If we are interested only in the heat- and mass-transfer rates occuring at the droplet surface then we could expect to use a value of the thermal conductivity of the continuous phase evaluated at the surface conditions. As becomes apparent for evaporation at high temperatures, the use of the average value of the conductivity of the film leads to incongruous results which in part, allow for the sensible heat transferred to the diffusing vapour. It should be established whether the Nusselt number reported is for the heat-transfer occuring at the droplet surface or for transfer occuring at some point within the vapour film. It should also be remembered that the original equations were derived based on the term $(Sc.p_{BM}/P)$ and it is assumed that the pressure ratio is nearly unity. In some cases this might not be so and the correct expression for the mass-transfer Nusselt number will then be

$$Sh = Sh\ Re(R_e, Sc.p_{BM}/P) \quad . \qquad (10.5)$$

Few studies have been made of the evaporation of drops containing solids either in suspension or in solution and most have been of a more general nature reporting on the operating variables of spray-driers. Work on the mechanism of the drying of solutions and on the behaviour of sprays of drops of solutions is then required, particularly on the growth and permeability of the skins formed on the surface of the evaporating drops. Differences, in the effective lowering of the vapour pressure for some salt solutions, need to be settled. This would be done by further studies of the drying of such solutions rather than by studying the thermodynamic properties. The question, as to how far held

droplet studies can be related to spray driers should also be considered. The main point seems to be, whether or not dynamic equilibrium as obtained for held droplet systems with relatively large drops is ever attained in any of the drying stages in actual spray driers.

Experimental studies on the evaporation of sprays in spray driers are not extensive and the need is apparent for further work in this field. The complete analytical solution of the complex heat- and mass-transfer phenomena occuring in the overall process of spray evaporation will only be possible when accurate data for the drag coefficients of liquid drops in all regions of the drying chamber become available. The investigation of spray evaporation should follow the two aspects of evaporation in the nozzle or the deceleration zone and the evaporation in the terminal velocity or free-falling region. A study of the evaporation which takes place from the unstable ligaments of liquid which exist for a length of the order of several droplet diameters immediately after the spray nozzle, should also be made. To obtain good results, the development of an easy and rapid size analysis technique must first be realised.

There are a number of proven correlations for the evaporation of sprays and although the total number of such is small they show the relative motion of the drop to be significant. The interaction effects of the dispersed spray droplets are apparently negligible and data obtained for single liquid drops can be used. The design of spray driers by employing the concept of transfer units will only be fully realised when proven correlations based on reliable data become available. Because the whole concept of the transfer unit is based on a number of simplifying assumptions which do not hold for the hydrodynamic conditions existing in spray drier chambers, the use of the transfer unit should

be restricted to providing only a quantative estimate of the requirements of the drying process. More recent attempts to evaluate the volumetric heat-transfer coefficient have yet to become established. At present, the engineering design of spray driers is usually based on the largest droplet to be formed by the atomiser and some of these designs are grossly over-sized. Atomisation is one of the most important aspects of spray drying and has been extensively reported. Opportunity still exists however, for the design of an atomiser which will produce a very small size range of droplets over a wide range of operating capacities. The recent development of the Jet-spray drier promises to be a valuable new tool in the drying of ultra heat-sensitive materials.

The few studies of the effect of turbulence on the evaporation of sprays of small drops have provided conflicting results. Some workers report no effect and suggest the use of a Nusselt number equal to two for the design of the drier. This assumption of no relative motion between the phases seems doubtful, as slip has been reported even for very small droplets. The possibility of the high molecular diffusivity, as compared to a liquid-liquid system, masking the transient effect should not be discounted though. Other reports show the intensity and scale to have separate effects on the transfer processes and the intensity effect to be more marked than that of scale. It has been suggested that the apparent increase in the transfer rates is in part due to a change in the value of the drag coefficient for the droplet in the turbulent flow region. A sorting out and explanation of the discrepancies and contradictions found in the literature is required. The development of a correlation like that by Zijnen, differentiating between the individual effects of scale and intensity would be preferred.

The extension of the equations for the drag coeffcicents of drops, to allow for drop circulation, drop acceleration, the fluid nature of the drop, the effect of the containing walls of the system and the continuous phase motion and turbulence, is needed. These effects are at present one of the major sources of disagreement between the reported values of the droplet drag coeffcicents and the behaviour of droplets in general. The need to study the effect of small amounts of solids or dust, on the shape and terminal velocity of the drop is of primary importance in investigating the evaporation of sprayed drops of solutions. It was long ago established that drops do not behave as solid spheres and the effect of the shape of the drop on the transfer processes has been reported though not necessarily correlated. The effect of acceleration or the motion of liquid drops in sprays has been overlooked as most studies have been with solid bodies. The criteria for the maximum stable drop size agree in principle but differ in the numerical value given to the limiting Weber number.

Studies of the evaporation process at high temperatures have shown that the sensible heat required to heat the diffusing vapour about the drop, is a significant part of the total heat transferred. Modified Nusselt numbers, some taking into account the heat transferred by radiation, appear to be satisfactory although none have apparently been put to any extensive experimental study. The use of the average film thermal conductivity results in the need to define real and apparent values of the heat-transfer coefficient and further emphasises the need to define the heat transferred as being a surface or film flux.

The resulting effect of the sonic energy in increasing the evaporation rate would seem to justify further investigation of the phenomena, firstly for held droplets and then

for the evaporation of whole sprays. It is also suggested that the effect of pulsed or oscillating airflow through the drying chamber could be investigated in a similar apparatus. The effects of turbulence, sonic energy and pulsating airflow on the evaporation rate all depend on the reduction of the film thickness about the drop and show a similar result but on a different scale.

The influence of surfactants on the transfer process has been well established for liquid-liquid systems but not for gas-liquid systems. The effect is apparently unpredictable and can result in an increased droplet stability or in the premature formation of the solid layer on the surface during the drying of droplets of solutions.

11. CONCLUSION.

There is a considerable scope for further work in the field of Spray Drying. The evaporation of single held drops of pure liquids has been studied extensively both theoretically and experimentally. All the correlations obtained by the workers in this field are substantially the same and take the form

$$Sh = 2.0 + C_1 (Re)^{\frac{1}{2}}(Sc)^{\frac{1}{3}}$$

and $$Nu = 2.0 + C_2 (Re)^{\frac{1}{2}}(Pr)^{\frac{1}{3}} \quad .$$

Exponents slightly different from the ones indicated have been obtained, but the above equations provide a good basis for design. The greater range of variation is in the values of the coefficients C_1 and C_2.

Studies of the mechanism of the drying of drops of solutions are limited and work on this aspect of droplet evaporation as related to the evaporation of whole sprays of either pure drops or drops of solutions, is needed. This important topic should be investigated as the evaporation occurring in the nozzle zone and in the free-falling region.

Turbulence effects on the evaporation of sprays must be reported as the separate effects of the scale and intensity of the continuous phase. No agreement between reported results will be possible until this is done. Since the evaluation of any effect on the evaporation rate, such as that of turbulence, can only be proven if reliable data for the drag coefficients of liquid drops is available, it is apparent that the effect of turbulence on the spray evaporation rate must

itself be related to the effect on the mechanics of the evaporating drops.

High temperature effects on the mass-transfer rates have led to a controversy over the definition of the Nusselt number. Clarification of the terminology used in heat- and mass-transfer equations for spray evaporation would be desirable and lead to an easier comparison of reported results, as the degree of turbulence, the drop shape, the liquid concentration, physical properties and mechanical dimensions of the system, to name but a few, all need to be detailed.

As a process for the drying of heat-sensitive materials, Spray Drying should be undergoing improvement as data is obtained on the operating characteristics of the systems at present employed. However, new designs for the basic process, such as the Jet-spray Drier, should also be contemplated and the design of different atomisers not neglected. The application of sonic energy or pulsed airstreams in the drying chamber for the drying of different types of heat-sensitive materials could easily be investigated. The study of the process of spray evaporation and spray drying is at present hampered by the limited operational and sampling techniques available and new and improved types of spray atomisers, spray driers, samplers and analysers are required.

It may be said that the work described here shows that spray drying still requires research into most aspects of the operating characteristics of the process and that with the exception perhaps of the evaporation of single, pure liquid drops, considerable scope for work in this field will exist for a long while.

12. NOTATION.

A	Area for heat- or mass-transfer, ft^2.
$\bar{A}$	Cross-sectional area of drying chamber, ft^2.
B_1	Factor defined in eq. (3.52).
B_2	Factor defined in eq. (3.57).
C_p	Heat capacity at constant pressure, Btu/lb^oF.
$\bar{c}$	Root-mean-square velocity of diffusing vapour molecules.
D	Diameter, ft or microns.
D_c	Diameter of cylinder, ft.
D_o	Diameter of nozzle orifice, ft.
D_{p_s}	Mean Sauter diameter, ft.
$D_{p_{vs}}$	Volume-surface mean diameter, ft.
D_v	Volumetric diffusivity, ft^2/hr.
D_1	Diameter of a finite spherical enclosure, ft.
d	Notation for differential operator.
E	Effective motive power as in eq.(5.15); also Eddy diffusivity, ft^2/hr.
E_1, E_2	Constants used in eq.(3,22).
e	Volume fraction or voidage, ft^3/ft^2.
F_A, F_e	Radiation view factors as in eq.(8.4).
f	Frequency of oscillation of drops, $secs^{-1}$.
$\mathfrak{f}$	Functional notation.
g	Acceleration of gravity, ft/sec^2.
H	Humidity, lb water vapour/lb dry air.
H_t	Height of a transfer unit, ft.
H_v	Latent heat of vapourisation, Btu/lb.
H_v'	Modified latent heat defined in eq.(8.10), Btu/lb.
h	Heat-transfer coefficient, Btu/ft^2hr^oF.
h_c	Convection heat-transfer coefficient, Btu/ft^2hr^oF.
h	Volumetric heat-transfer coefficient, Btu/ft^3hr^oF.
J	Air/liquid volumetric ratio for pneumatic nozzle.

K, K_1, K_2 Constant coefficients.

K_n Discharge coefficient of a pressure nozzle.

k Thermal conductivity, Btu-ft/ft^{2}hr$^{\circ}$F; also ratio of drop surface velocity to the velocity of potential flow of the continuous phase.

k_G Mass-transfer coefficient, lb moles/ft^{2}hr/mole fraction.

L Characteristic length dimension of particle, ft; also path length of evaporating drop, ft.

l Characteristic length in eq.(3.40).

$\bar{l}$ Mean free path of diffusing vapour molecules.

l_1 Langrangian scale of turbulence of gas phase.

M Molecular weight.

m Mass of particle.

N Mass-transfer flux, lb moles/hr.

N_t Number of transfer units as defined in eq.(5.16).

n Number of pseudo sections in drying process.

P Total static pressure, atmos.

P_n Hydraulic operating pressure of pressure nozzle, psi.

p Partial pressure of diffusing species, atmos.

p_{BM} Bulk mean partial pressure of non-diffusing species, atmos.

Q Volumetric flow rate, ft^3/hr.

q Evaporation constant in eq.(5.6); also heat-transfer rate, Btu/hr.

R Universal gas constant, ft lb force/lb mole $^{\circ}$R.

r Drop radius, ft.

S Specific surface area of spray as defined in eq. (5.12), ft^2/ft^3.

s Mean film thickness as defined in eq.(2.2), ft.

U Discharge velocity of atomised liquid, ft/sec; also velocity of drop as in eq.(5.5), ft/sec.

U_o Velocity of continuous phase, ft/sec.

u_1' Turbulent eddy velocity, ft/sec.

V Velocity of air relative to liquid at nozzle orifice, ft/sec.

V_t Terminal velocity, ft/sec.

V* Modified velocity as in eq.(3.42), ft/sec.

W Mass flow rate of spray, lb/hr.

W_c Critical moisture content, lb water/lb dry solid.

y Reduced droplet diameter, D_p/D_{p_o}.

z Height above solute surface, ft.

z Reduced relative velocity, $1-V/V_t$.

GREEK LETTERS.

γ Constant defined in eq.(3.62).

δ Constant indicating uniformity of spray drop-size distribution.

Δ Symbol designating potential difference or driving force such as Δ_p or ΔT.

ϵ Constant defined in eq.(3.61).

η_c Evaporative efficiency defined in eq.(5.23).

η_o Overall efficiency defined in eq.(5.22).

η_t Efficiency ratio of evaporation process defined in eq.(5.18).

θ Drying time, hrs.

θ_f Falling rate drying time, hrs.

θ^* Reduced time parameter defined in eq.(5.8).

λ Evaporation parameter defined in eq.(3.21), ft^2/hr.

Λ_f Longitudinal integral scale of turbulence.

μ Viscosity, lb/ft hr; also symbol for micron.

ν Kinematic viscosity, ft^2/hr.

ρ General notation for density of solid, liquid or gas phases, lb/ft^3.

ϱ_m Reciprocal of drift factor, p_{BM}/P.

σ Interfacial or surface tension, lb force/ft.

σ_r Stefan-Boltzmann constant, Btu/ft^{2}hr$^\circ$R^4.

τ Deforming force per unit area of drop surface as in eq.(7.4).

ψ Sphericity of drop.

DIMENSIONLESS GROUPS.

Ac Acceleration group, $(D_p dV/V^2 d\theta)$.

B Spaldings transfer number $(C_p \Delta T/H_v)$.

B' Spaldings transfer number $(C_p \Delta T/H_v')$.

C_D Drag coefficient $(2g F_d/u^2 \varrho A_p)$.

Fo Fourier number $(k\theta/C_p \varrho_v D_p^2)$.

Fr Froude number (u^2/gD_p).

Gr Grashof number $(D_p^3 \varrho^2 \beta g \Delta T/\mu^2)$.

Gr Grashof number $(L^3 \varrho^2 \beta g \Delta T/\mu^2)$.

j_D Heat-transfer number $(kp_{BM} Sc^{\frac{2}{3}}/UP)$.

Nu Nusselt number (hD_p/k).

Nu Nusselt number (hL/k).

Pe Peclet number $(D_p G C_p/k)$.

Pr Prandtl number $(C_p \mu/k)$.

Re Reynolds number $(VD_p \varrho/\mu)$.

Re_t Tube Reynolds number $(VD_t \varrho/\mu)$.

Re* Modified Reynolds number $(Re + \frac{1}{2}(Gr)^{\frac{1}{2}})$, as in eq.(3.40).

Sc Schimdt number $(D_v \varrho/\mu)$.

Sd Surface tension-size group (Su/Wt).

Sh Sherwood number (kD_p/D_v).

Su Surface tension group $(g\sigma D_p \varrho_c/\mu_d^2)$.

Tv Terminal velocity group (Re/Wt).

Vi Viscosity group defined in eq.(7.5).

We Weber number $(\varrho_d D_p V^2/\sigma)$.

Wt Gravitational group $(D_p[\frac{4}{3} g \varrho_c(\varrho_d - \varrho_c)/\mu_c^2]^{\frac{1}{3}})$.

SUBSCRIPTS.

A Actual value of the Nusselt number.

act. Actual value of the heat-transfer coefficient.

av. Average value.

c Continuous phase.

d Dispersed phase.

f Film value.

g Mean gas value.

h Heat-transfer process.

l Liquid phase.

m Mass-transfer process.

max Maximum value.

o Initial value.

p Particle or drop.

s Surface value.

T True value of the Nusselt number.

v Vapour phase.

x,y Planar coordinates.

SUPERSCRIPTS.

m,n Constant exponents for the Nusselt number and Sherwood

p,q number correlations.

* Modified definition values.

● Indicating transfer conditions as being dependent on the mass-transfer rate.

' Transfer in turbulent conditions.

13. BIBLIOGRAPHY.

1 Acrivos,A. Chemical Engineering Science,17,457,(1962).

2 Adler,C.R.,Mark,A.M.,Marshall,W.R. and Parent,R.J. Chem.Eng.Progr.,50,14,(1954).

3 Adler,C.R. and Marshall,W.R. Chem.Eng.Progr.,47,515, 601,(1951).

4 Ahloborn,F. Zt.Fur.Technsihe.Physik,12,10,(1931).

5 Albrecht,F. Physik.Z.,32,48,(1931).

6 Ashmus,D.H. "Momentum transport in Coaxial Jets in a high velocity Spray Drier." M.Sc.Thesis,Purdue Uni., (1954)

7 Baker,C.A.P. Appl.Sci.Res.,A10,241,(1961).

8 Basset,A.B. "Atreatise on Hydrodynamics".Cambridge, (1888).

9 Beek,W.J.and Kramers,H. Chemical Engineering Science, 17,909,(1962).

10 Belcher,D.W., Smith,D.A. and Cook,E.M. Chemical Engineering,70,83,201,(1963).

11 Bikerman,J.J. "Surface Chemistry". Academic Press, New York,(1958).

12 Binark,H. and Ranz,W.E. Ind.Eng.Chem.,51,(5).701,(1959).

13 Bird,R.B., Stewart,W.E. and Lightfoot,E.N. "Transport Phenomena".Wiley and Sons, New York,(1963).

14 Bond,W.N. and Newton,D,A. Phil.Mag.,5,794,(1928).

15 Bose,A.K. and Pei,D.C. Can.J.Chem.Eng.,42,(6),259, (1962).

16 Boucher,R.M.G. Chem.Eng.~~Progr~~.,66,(Sept.21),151,(1959).

17 Bouroutis,D.L. "An investigation of the equation Nu=f(Re,Pr) and the dimensionless numbers therein". Thesis,Tech.Uni.of Athens,(1962).

18 Boussinesq,J. J.Math.Pures.Appl.,1,285,(1905).

19 Bradford,P. and Briggs,S.W. Chem.Eng.Progr.,59,(3), 76,(1963).

20 Brown,R.A.,Sato,K. and Sage,B,H. Ind.Eng.Chem.,Chem. Eng.Data series,3,263,(1958).

21 Brown,R. and York,J.L. A.I,Ch.E.Journal,8,(2),149, (1962).

22 Buckham,J.A. and Moulton,R.W. Chem.Eng.Progr.,51,(3) 126,(1955).

23 Buikov,M.V. and Dukhin,S.S. International Chemical Engineering,2,399,(1962).

24 Chaloud,J.H. Martin,J.B, and Baker,J.S. Chem.Eng.Progr., 53,(12),593,(1957).

25 Charlesworth,D.H. and Marshall,W.R. A.I.Ch.E.Journal, 6,(1),9,(1960).

26 Chilton,T.H. and Colburn,A.P. Ind.Eng.Chem.,26,1183, (1935).

27 Colburn,A.P. Trans.A.I.Ch.E.,29,873,(1933).

28 Colburn,A.P. and Drew,T,B. Trans.A.I.Ch.E.,33,197,(1937).

29 Comings,E.W.,Clapp,J.T. and Taylor,J.F. Ind.Eng.Chem., 40,1096,(1948).

30 Comings,E.W. and Coldren,C.L. Chem.Eng.Progr.,53,(5), 231,(1957).

31, Conroy,E.H. and Johnstone,H.F. Ind.Eng.Chem.,41,2741, (1949).

32 Coslett,T.A. J.Imp.Coll.Chem.Eng.Soc.,5,68,(1949).

33 Crosby,E.J. and Marshall,W.R. Chem.Eng.Progr.,53,347, (1957).

34 Crosby,E.J. and Marshall,W.R. Chem.Eng.Progr.,54,(7), 57,(1958).

35 Dankwerts,P.V. Chemical Engineering Science,2,1,(1953).

36 Davidson,J.F.,Cullen,E.J.,Hanson,D. and Roberts,D. Trans. Instn Chem.Engrs,37,122,(1959).

37 Davies,C.N. Proc.Phys.Soc.(London),57,259,(1945).

38 Davies,J.T. and Rideal,E.K. "Interfacial Phenomena". Academic Press,(1961).

39 De Haas van Dorsser,A.H.,Lengier,H.A. and van Meel,D.A. De.Ingenieur,61,75,(1949).

40 Dloughy,J. and Gauvin,W.H. A.I.Ch.E.Journal,6,(1),29, (1960).

41 Dryden,H.I. Ind.Eng.Chem.,31,416,(1939).

42 Duffie,J.A. and Marshall,W.R. Chem.Eng.Progr.,49,(8), 417,480,(1953).

43 Durand,W.F. "Aerodynamic Theory". Vol.6. Julius Springer Co.,Berlin,(1935).

44 Edwards,A. and Fuber,B.N. Proc.Instn Mech. Engrs,170, 941,(1956).

45 Feder,A. Chemical Engineering, 66,(Sept.21),159,(1959).

46 Findlay,B.A. Ph.D. Thesis, Uni.of Birmingham,(1957).

47 Fogler,B.B. and Kleinschmidt,R.V. Ind.Eng.Chem.,30, 1373,(1938).

48 Fokin,A.P.,PLanovskii,A.N. and Akopyan,L.A. Inzhenero-fizicheskii Zhurnal,8,(1),116,(1965).

49 Fraser,R.P., Dombrwski,N. and Rowtley,J. Chemical Engineering Science,18,339,(1963).

50 Fraser,R.P. and Eisenklam,P. Trans.Instn Chem.Engrs, 34,294,(1956).

51 Fraser,R.P.,Eisenklam,P. and Dombrowski,N. Brit.Chem. Eng.,2,414,536,610,(1957).

52 Friedlander,S.K. A.I.Ch.E.Journal,3,381,(1957).

53 Frössling,N. Gerlands Beitri.Geophys.,52,170,(1938).

54 Frössling,N. Lunds Uni.Årsskr.,36,(4),(1940).

55 Fuchs,N. Phys.Z.Sowjet,6,244,(1934).

56 Garner,F.H. and Keey,R.B. Chemical Engineering Science, 9,119,(1958).

57 Garner,F.H. and Lane,J.J. Trans.Instn Chem.Engrs,37, 162,(1959).

58 Garner,F.H. and Skelland,A.H.P. Chemical Engineering Science,4,150,(1955).

59 Garner,F.H. and Suckling,R.D. A.I.Ch.E.Journal,4,114, (1958).

60 Geist,J.M.,York,J.L. and Brown,G.G. Ind.Eng.Chem.,43, 1371,(1951).

61 Gieske,J.A. and Mitchell,R.I. J.Chem.Eng.Data,10,(4), 350,(1965).

62 Glen,J.B. Ph.D. Thesis,Uni.of Canterbury,(1965).

63 Gluckert,F.A. A.I.Ch.E.Journal,8,460,(1962).

64 Godsave,G.A.E. "The burning of single drops of a fluid". Nat.Gas Turbine Est.,England,Report no.R88.

65 Goldstein,S. "Modern developments in Fluid Dynamics". Vol.2. Clarendon Press, Oxford,(1938).

66 Gunn,R.J. J.Geophys.Res.,54,383,(1949).

67 Guyton,A.C. J.Ind.Hyg.Toxicology,28,133,(1946).

68 Hadamard,J. C.R.Ass.Franc.Av.Science,152,1735,(1911).

69 Harmathy,T.Z. A.I.Ch.E.Journal,6,288,(1960).

70 Harriot,P. Can.J.Chem.Engng,40,60,(1962).

71 Hasson,D. and Mizrahi,T. Trans.Instn Chem.Engrs,39, 415,(1961).

72 Hausen,H. "Wärmeubertagung im Gegenström". Gleichström Kreuström,(1950).

73 Henrickson,F. "Mass-transfer to Drops". M.Sc. Thesis, M.I.T.,(1941).

74 Hillier,J. U.S.Patent 2,491,441.(1950).

75 Hinze,J.O. Appl.Sci.Res.,A1,263,(1949).

76 Hinze,J.O. A.I.Ch.E.Journal,1,(3),289,(1955).

77 Hinze,J.O. "Turbulence". McGraw-Hill Co.,New York,(1959).

78 Hodgins,J.W., Pei,D.C. and Hoffman,T.W. Can.J.Chem.Eng., 35,18,(1957).

79 Hoffman,T.W. and Gauvin,W.H. Can.J.Chem.Engng,38,(5), 129,(1960).

80 Hoffman,T.W. and Gauvin,W.H. Can.J.Chem.Engng,40,110, (1962).

81 Hottel,H.C.,Williams,G.C. and Simpson,H.C. "Combustion of droplets of heavy liquid fuels". Symposium on Combustion, Pittsburgh,(1954).

82 Houghton,H.G. Physics,4,419,(1933).

83 Hsu,N.T. and Sage,B.H. A.I.Ch.E.Journal,3,(3),405,(1957).

84 Hsu,N.T., Sato,K. and Sage,B.H. Ind.Eng.Chem.,46,870, (1954).

85 Hu,S. and Kintner,R.C. A.I.Ch.E.Journal,1,42,(1955).

86 Hughes,R.R. and Gilliland,E.R. Chem.Eng.Progr.,48,(10), 497,(1952).

87 Humphreys,B. "Physics of the Air". (1940).

88 Ingebo,R.D. Chem.Eng.Progr.,49,602,(1953).

89 Ingebo,R.D. N.A.C.A. TN.3672,(1956).

90 Jacob,M. "Heat-transfer". (1949).

91 Johnson,J.C. J.Appl.Phys.,21,22,(1950).

92 Johnstone,H.F. and Eads,D.K. Ind.Eng.Chem.,42,2293, (1950).

93 Johnstone,H.F.,Pigford,R.L. and Chapin,J.H. Trans.A. I.Ch.E.,37,95,(1941).

94 Johnstone,H.F. and Williams,G.C. Ind.Eng.Chem.,31,(8), 998,(1939).

95 Jones,S.R. and Smith,W. "Symposium on the interaction between fluids and particles". Instn Chem.Engrs,London, (1962).

96 Ju,Chin Chu, Stout,L.E. and Busche,R.M. Chem.Eng. Progr.,47,(1),29,(1951).

97 Kalinske,A.A. and Pien,C.L. Ind.Eng.Chem.,36,220, (1944).

98 Kay,J.M. "An introduction to Fluid Mechanics and Heat-Transfer". Cambridge Uni.Press,(1963).

99 Keey,R.B. and Glen,J.B. Trans.Instn Chem.Engrs,43,T221, (1965).

100 Kesseler,G.H. D.Sc. Thesis,M.I.T.,(1952).

102 Kessler,H.C. Chemi.Ing.Tech.,36,479,(1964).

103 Khrgian,A.K. "Physics of the Atmosphere". Gostekhizdat, (1953 and 1958).

104 Ki,Man Kim. International Chemical Engineering,6,(1), 57,(1966).

105 Kinard,G.E.,Manning,F.S. and Manning,W.P. Brit.Chem. Eng.,8,(5),326,(1963).

106 King,C. Mech,Eng.,54,190,(1932).

107 Kiraly,I.G. Brit.Chem.Eng.,5,791,(1961).

108 Kirshbaum,E. Chemi.Ing.Tech.,24,(1),4,(1952).

109 Kramers,J.H. Physica's Grav.,12,61,(1946).

110 Krasuk,J.H. and Smith,J.M. A.I.Ch.E.Journal,10,(5), 759,(1964).

111 Kronig,R and Bruijsten,J. J.Appl.Sci.Res.,A2,439,(1950).

112 Kudryashev,L.J. and Ipateako,A.Ya. Soviet Physic.Tech. Phys.,4,275,(1959).

113 La Mer and Gruen. Trans.Faraday Soc.,48,410,(1952).

114 La Mont,C.A. U.S.Patent 51,263.

115 Lamb,H. "Hydrodynamics". 4th Ed.,Cambridge Uni. Press, (1916).

116 Landahl,H.O. and Herrmann,R.G. J.Colloid.Sci.,4,103, (1949).

117 Lane,W.R. Ind.Eng.Chem.,43,1312,(1951).

118 Langmuir,I. Phys.Rev.,12,368,(1918).

119 Langstroth,G.O., Diehl,C.H.H. and Winhold,E.J. Can. J.Res.,A28,574,(1950).

120 Langstroth,G.O. and Luchak,G. Can.J.Res.,A28,580, (1950).

121 Lapple,C.E. and Shepherd,C.B. Ind.Eng.Chem.,35,(5), 605,(1940).

122 Laster,R. Food Technol.,7,264,(1953).

123 Laws,J.O. Agricultural Engineering,21,(1940).

124 Lenard,P. Meteor.Phys.,21,249,(1904).

125 Levich,V.G. "Physiochemical Hydroynamics". Prentice Hall, New York, (1962).

126 Lewis,H. Industrial Chemist, 10,439, 499,(1934);also 11,71,(1935).

127 Lewis,H.C. Ind.Eng.Chem., 40,67,(1948).

128 Lewis,H.C., Edwards,D.G., Gogla,H.J. Rice,R.I. and Smith,L.W. Ind.Eng.Chem.,40,67,(1948).

129 Lewis,J.B. Chemical Engineering Science,3,248,260,(1954).

130 Lewis,J.B. Chemical Engineering Science,8,295,(1958).

131 Lihou,D.A. Birmingham Uni.Chem.Engr,17,1,(1966).

132 Liu,v. Dept.U.S.A.F. Project no.2160,(1955).

133 Lochiel,A.C. Can.J.Chem.Engng,43,(1),40,(1965).

134 Loitiankii,L.G. and Schwab,B.A. Central Aero.and Dyn. Instn,U.S.S.R., Report no.329,(1935).

135 Longwell,J.P. Ph.D. Thesis,M.I.T.,(1943).

136 Longwell,J.P. "High speed Aerodynamics and Jet Propulsion". Combustion Processes,Vol.2,Princeton Uni.Press,(1956).

137 Longwell,J.P. and Weisse,M.A. Ind.Eng.Chem.,45,(3), 667,(1953).

138 Lorenz,L. Am.Phys.,13,422,582,(1881).

139 Luikov,M.V. Szuska Raspilenyijem,Mos.,Pischepromizdat. (1955).

140 Lynn,S., Straatemeier,J.R. and Kramers,H. Chemical Engineering Science,8, 81,(1958).

141 McAdams,W.H. "Heat-Transmission". McGraw-Hill, New York (1942).

142 McLain,H.A., Comings,E.W. and Meyers,J.E. Chem.Eng. Progr.,53,(6),282,(1957).

143 Maisel,D.S. and Sherwood,T.K. Chem.Eng.Progr.,46,(3), 131,(1950).

144 Manning,C. and Gauvin,W.H. A.I.Ch.E.Journal,6,184,(1960).

145 Marshall,W.R. "Atomisation and Spray drying". Chem. Eng.Progr.Monograph Series,50,(2),(1954).

146 Marshall,W.R. Trans.A.S.M.E.,77,1377,(1955).

147 Marshall,W.R. and Seltzer,E. Chem.Eng.Progr.,46,501, 575,(1950).

148 Martinelli,R.G. Trans.A.S.M.E.,69,947,(1947).

149 Masters,K. Birmingham Uni.Chem.Engr,17,18,(1966).

150 Maxwell,R.W. and Sterran,J.A. Chemical Engineering Science,6,204,(1957).

151 May,K.R. J.Sci.Instruments,27,128,(1950).

152 Meisse,C.C. Jet Propulsion,24,237,(1954).

153 Meisse,C.C. Franklin Institute,264,392,(1957).

154 Meyer,P. Trans.Instn Chem.Engrs,15,127,(1937).

155 Mikhailov,Y. International J.Heat- and Mas-Transfer, 1,37,(1960).

156 Möller,W.H. Phys.Zeits.,39,57,(1938).

157 Morse,H.W. Proc.Am.Acad.Arts and Sci.,45,363,(1910).

158 Mugele,R.A. A.I.Ch.E.Journal,6,(1),3,(1960).

159 Mugele,R.A. and Evans,H.D. Ind.Eng.Chem.,43,1317,(1951).

160 Nukiyama,S. and Tanasawa,Y. Trans.S.M.E.(Japan),4,86, 138,(1938); 5,63,68,(1939); 6,II-7,II-8,(1940).

161 Nusselt, Gesundheitsig,38,477,(1915).

162 Pasternak,I.S. and Gauvin,W.H. Can.J.Chem.Engng,38, 75,(1960).

163 Pasternak,I.S. and Gauvin,W.H. A.I.Ch.E.Journal,6,(2), 184,(1961).

164 Pei,D.C.T. Ph.D.Thesis, McGill Uni.,(1961).

165 Pei,D.C.T., Narasimhan,C. and Gauvin,W.H. "Symposium on the interaction between fluids and particles". Instn Chem.Engrs,London,(1962).

166 Perry,J.H. (editor). "Handbook of Chemical Engineers". 4th Ed.,McGraw-Hill, New York,(1963).

167 Pigford,R.L. Uni.of Delaware,Newark,Delaware,(1950).

168 Pilcher,J.M. and Thomas,R.E. "Literature on the Combustion of Petroleum". Am.Chem.Soc.,Washington D.C.,(1958).

169 Place,G., Ridgway,K. and Dankwerts,P.V. Trans.Instn, Chem.Engrs,37,268,(1959).

170 Probert,R.P. Phil.Mag.,37,94,(1946).

171 Ranz,W.E. Trans.A.S.M.E.,78,909,(1956).

172 Ranz,W.E. and Hofelt,B. Ind.Eng.Chem.,49,289,(1957).

173 Ranz,W.E. and Marshall,W.R. Chem.Eng.Progr.,48,141, 173,(1952).

174 Ranz,W.E. and Wong,J.B. Ind.Eng.Chem.,44,1371,(1952).

175 Rayliegh,Lord. Phil.Mag.,29,(1916).

176 Reynst,F.A. Chaleur et Industrie, 30, 304, (1949).

177 Rosin,P. and Rammler,E. Z.Ver.deut.Ing., 71, 1, (1927) and J.Inst.Feul, 7,29,(1933).

178 Rowe,P.N., Claxton,K.T. and Lewis,J. Trans.Instn Chem.Engrs, 43,T14,(1965).

179 Ruckenstein,E. Chemical Engineering Science,19, 131,(1964).

180 Rupe,J.H. "3rd Symposium on Combustion, Flame and Explosion Phenomena" Wilkins and Williams, Baltimore,(1949).

181 Saito,S. Sci.Rep.Tohoku Imp.Uni.,2,179,(1913).

182 Sano,Y. and Nishikawa,S. Chemical Engineering (Japan), 29,(5),294,(1965).

183 Schechter,R.S. and Farley,R.W. Brit.Chem.Eng., 8,(1),37,(1963).

184 Schlunder,E.U. International J.Heat- and Mass-Transfer, 7, 49, (1966).

185 Seban,R.A. and Shimazaki,T.T. Trans.A.S.M.E., 73, 808,(1951).

186 Sell,W. Forschungshaft, 347,(8),(1931).

187 Shapiro,A.H. and Erickson,A.J. Trans.A.S.M.E., 79, 775,(1957).

188 Sherwood,T.K. Trans.A.I.Ch.E., 36, 817,(1940).

189 Sherwood,T.K. and Cooke,N.E. A.I.Ch.E.Journal,3,(1), 37,(1957).

190 Sherwood,T.K. and Williams,G.C. Natl.Defence Res.Proj. no.P.B. 6538,(1941).

191 Sherwood,T.K. and Woertz,B.B. Trans.A.I.Ch.E.,35,517, (1937).

192 Sjenitzer,F. Chemical Engineering Science,1,101,(1952).

193 Sjenitzer,F. Chemical Engineering Science,17,(5),309, (1962).

194 Smith,D.A. Chem.Eng.Progr.,45,(12),703,(1949).

195 Soo,S.L. Chemical Engineering Science,5,(4),57,(1956).

196 Spalding,D.B. Proc.Roy.Soc.(London),A221,78,(1954).

197 Spilhaus,A.F. Journal Met.,5,108,(1948).

198 Stefan, Wien.Sitzb.Ber.,79,161,(1879).

199 Steinberger,R.L. and Treybal,R.E. A.I.Ch.E.Journal,6, (2),227,(1960).

200 Sternling,C.V and Scriven,L.E. A.I.Ch.E.Journal,5,514, (1959).

201 Suckling,R. Birmingham Uni.Chem.Engr.,11,(1),28,(1960).

202 Tate,R.W. A.I.Ch.E.Journal,7,(4),574,(1961).

203 Tate,R.W. and Marshall,W.R. Chem.Eng.Progr.,49,162, 226,(1953).

204 Taylor,E.H. and Harmon,D.B. Ind.Eng.Chem.,46,(7),1455, (1954).

205 Taylor,G.I. Proc.London Math.Soc.,20,196,(1921).

206 Taylor,G.I. Proc.Roy.Soc.(London),151A,421,(1935).

207 Tiubonchi,T. and Sato,S. Chem.Eng.Progr.Symposium Series, 56,(30),285,(1950).

208 Topley,B. and Whytlaw-Gray,R. Phil.Mag.,4,873,(1927).

209 Torobin,L.B. and Gauvin,W.H. Can.J.Chem.Engng,37,129, 167,224,(1959); 38,142,189,(1960); 39,113,(1961).

210 Torobin,L.B. and Gauvin,W.H. A.I.Ch.E.Journal,7,615, (1961).

211 Turba,J. and Németh,J. Brit.Chem.Eng.,9,(7),457,(1964).

212 Turner,G.M. and Moulton,R.W. Chem.Eng.Progr.,49,(4), 185,(1953).

213 Uhlher,P.H.T., Sinclair,G.C. and Baxter,B.A. Chemical Engineering Science,20,(12),997,(1965).

214 Uyehara,O.A. and Meyers,P.S. Trans.A.S.M.E.,78,909, (1956). (Discussion section).

215. van der Hegge Zijnen,B.G. Appl.Sci.Res.,7A,205,(1958).

216 Weiss,M.A. and Worsham,C.H. Chemical Engineering Science,16,(1),1,(1961).

217 White,R.R. and Churchill,S.W. A.I.Ch.E.Journal,5,354, (1959).

218 Whitman,W.G.,Long,L and Wang,H.W. Ind.Eng.Chem.,18, 363,(1926).

219 Whytlaw-Gray,R. and Patterson,B. "Smoke". Arnold and Son, London,(1932).

220 Williams,G.C. "Heat- and Mass-Transfer and Friction for Spheres". D.Sc. Thesis,M.I.T.,(1942).

221 Winny,H.F. Aero.Res.Council (London),Report no.1531, (1932).

222 York,J.L. and Stubbs,H.E. Trans,A.S.M.E.,74,1157, (1952).

223 Yuge,T. Trans.A.S.M.E.,82,(C),214,(1960).

APPENDIX 2

DESIGN OF A CYCLONE SEPARATOR

At the present time there is no generally accepted fundamental relationship for predicting the performance of a cyclone (A20). The most satisfactory expression of cyclone performance is still the empirical one by Rosin, Rammler and Intelmann (A21). They derived the following equation for the minimum diameter particle $D_{p_{min}}$, that should be completely separated from the gas stream in a cyclone:

$$D_{p_{min}} = \left[\frac{9\mu B}{\pi N v(\rho_s - \rho)}\right]^{\frac{1}{2}}$$

where μ =fluid viscosity (lb/ft sec), B=dimension of cyclone inlet, N=no. of turns made by gas stream in cyclone separator, ρ_s=true bulk density of material to be separated (lb/ft^3) and ρ =fluid density (lb/ft^3). Smaller particles are removed to an extent proportional to the initial distance of the particles from the wall. The derivation is based on Stokes' law, assuming the gas stream undergoes a fixed number of turns at constant spiral velocity without any mixing action or turbulence. For a cyclone separator of standard proportions (A22) re-entrainment is minor and based on a few plant and laboratory data, N has been found to be approximately 5. Cyclones are usually designed for an inlet velocity of 50 fps, though this need not be strictly adhered to as fan limitations generally dictate the maximum allowable pressure drop corresponding to a cyclone inlet velocity between 20

and 70 fps.

Considering an inlet velocity of 50 fps,

$$A = Q/V$$

and $A = D^2/8$ for a cyclone of standard proportions.

$$\therefore D = 2\sqrt{2Q/v}$$

For the maximum air flow rate of 250 c.f.m. then,

$$D = 2\sqrt{\frac{2 \times 250}{50 \times 60}} \backsim 10\text{" dia.}$$

With volume rates less than the maximum it would also be desirable to achieve reasonable separation so take D=9ins. The inlet area should then have the area A$\backsim$9 sq.in. Reasonable dimensions for a cyclone body diameter of 9ins would be a rectangular inlet area of 2"x3" = 6 sq.in. The cyclone inlet velocity would then be 100 fps for the maximum flow rate and 50 fps for half the maximum rate.

Assuming a value of $\rho_s = 160$ lb/ft^3 (ρ_g=negligible) then

$$D_{p_{min}} = \left[\frac{9 \times 0.013 \times 10^{-3} \times 2}{\pi \times N \times V \times 160 \times 9}\right]^{\frac{1}{2}} \text{ ft}$$

$$\backsim \frac{200}{(NV)^{\frac{1}{2}}} \text{ microns}$$

For N = 5 and inlet velocities of 50 or 100 fps, $D_{p_{min}}$ is less than 10 microns. For $D_{p_{min}}$ equal to 10 microns, N$\backsim$3.5. This suggests that the length of the cyclone body could then be shorter than

that recommended from the standard cyclone dimensions.

The remaining problem is the size of the pressure drop through the cyclone. For a cyclone of standard design dimensions

$$\Delta p = 0.024\ \rho_g v^2$$

For hot, moist air exit from the drying chamber, take $\rho_g \sim 0.07$ lb/ft^3. Then the pressure drop is ~ 17 or ~ 4 inches of water for inlet velocities of 100 and 50 fps, respectively. The former value of the pressure drop is rather excessive and the pressure drop can be halved by using a cyclone with a helical top. Such a design was selected and the final design dimensions of the cyclone separator (for particles down to 10 microns diameter) are given in figure A2.1. The cyclone has been successfully used to separate and collect spray-dried milk powder that was produced in the experimental spray drier.

... ...

References

A20 Perry, J.H. Chemical Engineers' Handbook, 4th ed. pg 20-71. McGraw-Hill Co., New York.

A21 Rosin, P., Rammler, E. and Intelmann, T. Z.Ver.deut. Ing., 76, 433 (1932).

A22 Lapple, C.E. and Shepherd, C.B. Ind.Eng.Chem., 31, 972 (1939); 32, 1246 (1940).

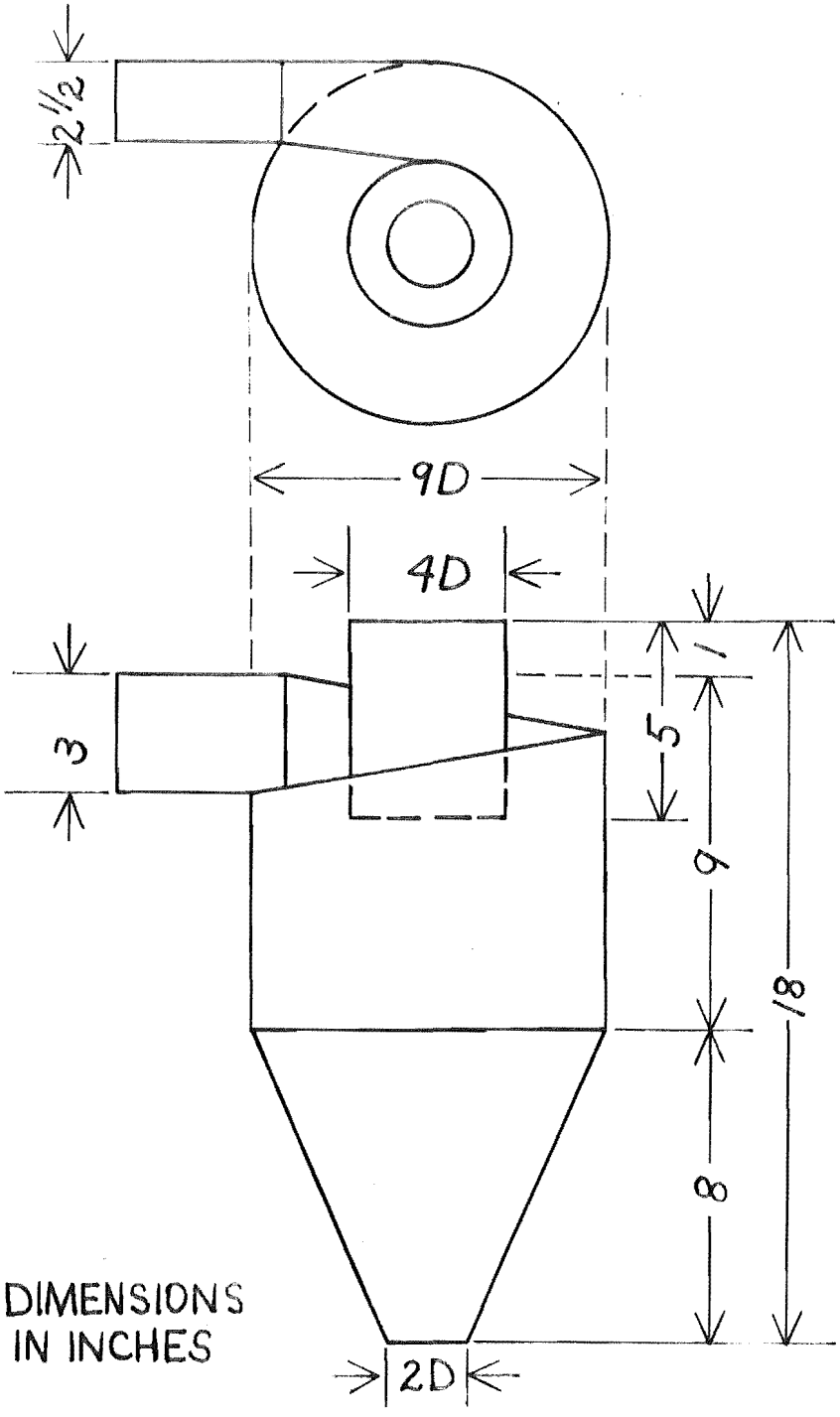

FIGUREA2.1 CYCLONE SEPARATOR DIMENSIONS

APPENDIX 3

RADIATION CORRECTIONS FOR UNSHIELDED WET-BULB THERMOMETERS

Data for evaluating the correction for the radiation effect on the unshielded wet-bulb thermocouple was taken from Carrier and Mackey's (A30) review of physchrometric data. The wet-bulb thermocouple was cemented to a standard wet-bulb thermometer (sling-hygrometer type) under the wick connected to the water supply reservoir. Calibration of the thermocouple (copper/constantan) gave the same temperature as indicated by the thermometer. The free cross-sectional area inside the chamber encasing the wet- and dry-bulb assembly was carefully measured and for a constant air flow through the chamber, as indicated by the rotameter (figure A3.1), the air velocity past the wet-bulb wick was calculated to be 10.3 fps.

The correction for the radiation effect E, is then calculated (figure A3.2) to be 1.7, 1.5, 1.3 and 1.15 per cent at wet-bulb temperatures of 50, 60, 70 and 80 F respectively (A30, A31)

... ...

References

A30 Carrier, W.H. and Mackey, C.O. Trans.A.S.M.E., 59, 33 (1937)

A31 Perry, J.H. Chemical Engineers' Handbook, 3rd ed. pg 776, McGraw-Hill Co., New York.

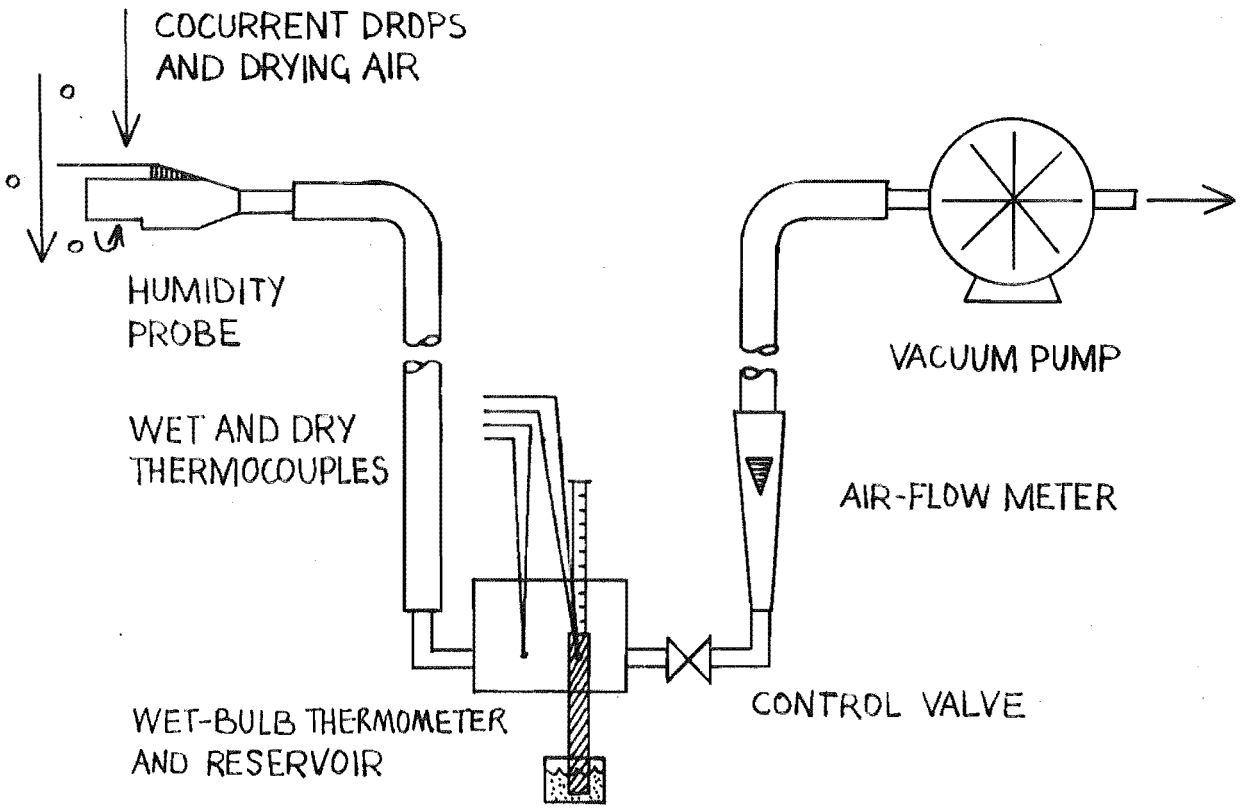

FIGURE A3.1 SCHEMATIC DIAGRAM OF HUMIDITY MEASURING APPARATUS

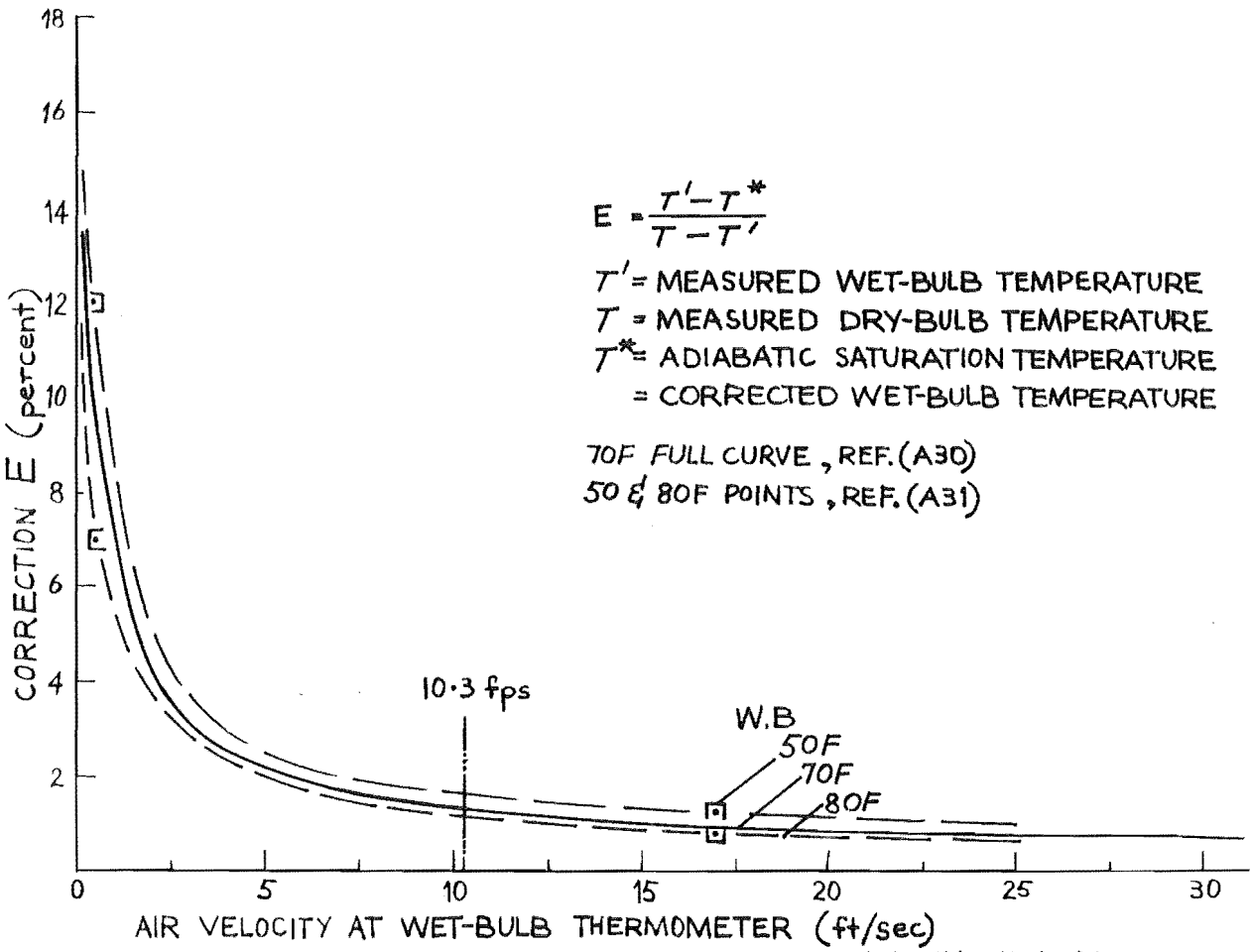

FIGURE A3·2 CORRECTION FOR RADIATION EFFECT ON AN UNSHIELDED WET-BULB THERMOMETER

APPENDIX 4

AMPLIFIER FOR TURBULENCE OUTPUT SIGNAL

The turbulence signal from the hot-wire anemometer could be as low as 5 millivolts (rms). Since the electronic pulse counter required an input signal of the order of 200 millivolts to successfully trigger the counting circuit, a small transistorised amplifier was made which had a good frequency response up to 100 kHz and was used to amplify the signal before the pulse counter. Figure A4.1 indicates the arrangement of amplifier with respect to the hot-wire anemometer and also shows the circuit of the amplifier.

The amplifier is a two-stage resistance-capacitive couples, common emitter transistor amplifier with a gain of approximately 50. A by-pass switch was provided to allow the anemometer signal to be directly coupled to the electronic counter should the signal be greater than 200 mV rms. The circuit was battery operated and enclosed in a small shielded metal case.

... ...

Reference

"Electronics for Scientists". Malmstadt, H.V. and Enke, C.G. by W.A. Benjamin Inc., N.Y. (1962)

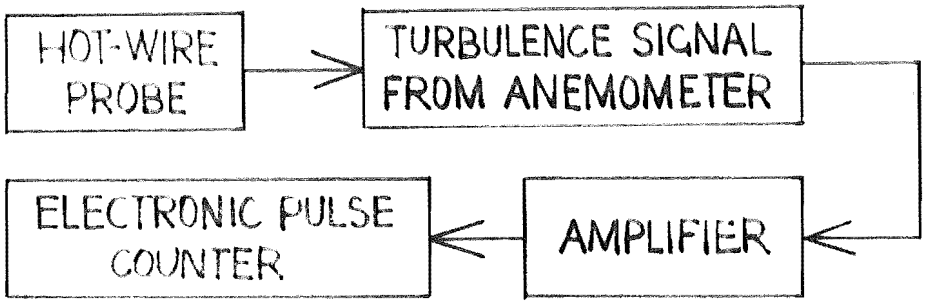

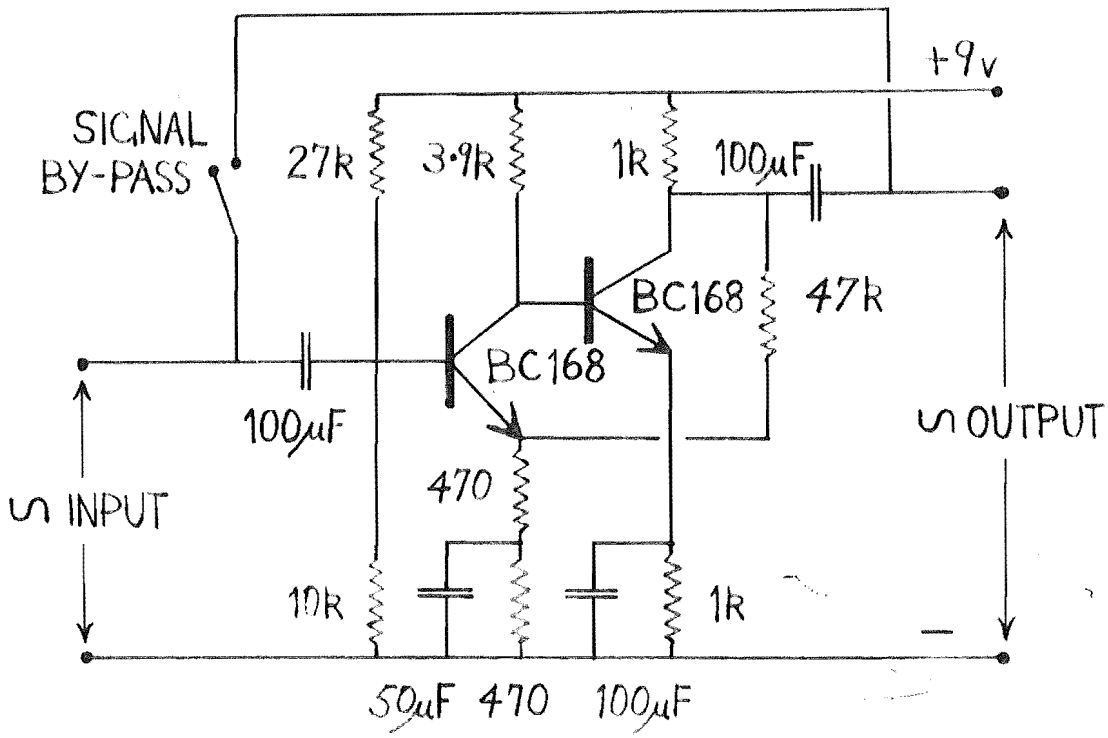

FIGURE A4.1 AMPLIFIER ARRANGEMENT AND CIRCUIT

APPENDIX 5

LAGRANGE INTERPOLATION FORMULA

The Lagrange Interpolation formula is similar to "Newton's fundamental interpolation formula", but is expressed explicitly in terms of the ordinates involved. The Lagrange interpolation polynomial degree n is

$$y(x) = \sum_{j=0}^{n} \frac{\Pi(x)}{(x-x_j)\,\Pi'(x_j)} \cdot f(x_j)$$

where $\Pi(x) = (x-x_o)(x-x_1) \ldots\ldots (x-x_n)$

$\Pi'(x) = (x_j-x_o)(x_j-x_1) \ldots\ldots (x_j-x_n)$

where (x_j-x_j) is the omitted factor. Thus

$$f(x) = y(x) + E_n(x)$$

where $E_n(x) = \text{error} = \frac{1}{(n+1)!}\,\Pi(n) f^{(n+1)}(\epsilon)$

for $\min.(x_0, \ldots, x) < \epsilon < \max.(x_o, x_1, \ldots, x_n, x)$

To find the value of the drop diameter D_{p1} at distance x_1 from the front pole of the drop, using the measured values D_{p0}, D_{p2}, D_{p4} and x_0, x_2, x_4, the interpolation polynomial of degree 2 is then

$$D_{p1} = \frac{(x_1-x_2)(x_1-x_4)}{(x_0-x_2)(x_0-x_4)} \cdot D_{p0} + \frac{(x_1-x_0)(x_1-x_4)}{(x_2-x_0)(x_2-x_4)} \cdot D_{p2}$$

$$+ \frac{(x_1-x_0)(x_1-x_2)}{(x_4-x_0)(x_4-x_2)} \cdot D_{p4}$$

As the rear pole of the drop is approached, the interpolation formula order is reversed so that the interpolated diameter sought is found between the measured diameters D_{p2} and D_{p4}.

... ...

Reference:

Chemical Engineers' Handbook. 4th Edition, J.H. Perry (ed.) McGraw-Hill Co., New York (1963).

APPENDIX 6

CONDUCTIVE HEAT-TRANSFER FROM A FINE GLASS ROD

The schematic diagram of a water droplet supported on the end of a fine glass rod is shown in figure A6.1. The method of analysis is that used to solve problems for heat-transfer from a fin.

For the real case: $T_g > T_L > T_o > T_d > T_s$ and $(dT/dx)_{x=L} \neq 0$; the temperature distribution along the rod is a function of both the radial and longitudinal distributions and the heat transfer coefficient along the rod is a function of position.

For the assumed model: $T_g \geq T_L > T_o = T_d = T_s$ and $(dT/dx)_{x=L} = 0$; the length of the rod is infinite ($L_{rod} \gg D_{rod}$); the temperature distribution of the rod in the radial direction is negligible; the heat-transfer coefficient between the rod and the air (h_{rod}) is constant and far smaller than the coefficient between the rod and the water (h_d) and the temperature of the air along the rod is constant.

For these assumptions, a heat balance along the rod combined with the Fourier conduction law, results in the differential equation of stationary heat conduction as follows:

$$\frac{d^2T}{dx^2} - \frac{h_{rod}\,P}{k_{rod}A_{rod}}(T_{rod}-T_g) = 0 \qquad (A6.1)$$

P is the perimeter of the glass rod. The boundary conditions for the equation solution are

$$T_{rod} = T_d \;;\quad x = 0$$
$$\text{and} \quad (dT/dx) = 0;\quad x = L \qquad (A6.2)$$

Putting $m = \sqrt{h_{rod}P/k_{rod}A_{rod}}$, the solution of equation 6.1 is

$$T_{rod} = T_g-(T_g-T_d)\left(\frac{e^{-m(L-x)}+e^{m(L-x)}}{2Cosh(mL)}\right) \qquad (A6.3)$$

then for x=0, $T_{rod}=T_d$ and for x=L

$$T_L = T_g-(T_g-T_d)/Cosh(mL)$$

The quantity of heat flowing to the supported drop at the end (x=0) of the glass rod is

$$Q_{rod} = k_{rod}A_{rod}(dT/dx)_{x=0} \qquad (A6.4)$$

Differentiating equation A6.3 and putting x=0 then

$$(dT/dx)_{x=0} = m(T_g-T_d)tanh(mL) \qquad (A6.5)$$

The solution of equation A6.4 then becomes

$$Q_{rod} = mk_{rod}A_{rod}(T_g-T_d)tanh(mL) \qquad (A6.6)$$

As $m = \sqrt{h_{rod}P/k_{rod}A_{rod}} = \sqrt{4h_{rod}/k_{rod}D_{rod}}$ then

$$Q_{rod} = \frac{\pi}{2}\sqrt{k_{rod}h_{rod}D_{rod}^3}\,.(T_g-T_d)tanh(mL) \qquad (A6.7)$$

Experimental values of the product mL were such that tanh(mL) was close to unity and cosh(mL) was very large. Equation A6.7 is the same as assuming an insulated tip for the glass rod at the end x=L, where $T_{rod} = T_L \backsim T_g$. Details of the construction, mounting and dimensions of the fine glass rods as given in section 4.4 shows the basis for the

assumed model to be acceptable and equation A6.7 can be expected to provide a measure of the heat transferred to the held droplet.

A more correct solution is obtained if equation A6.4 is written ($T_o \neq T_d$)

$$Q_{rod} = k_{rod}A_{rod}(dT/dx)_{x=0} = h_dA_{rod}(T_o-T_d) \qquad (A6.8)$$

where h_d is the convection coefficient for heat-transfer through the boundary-layer within the drop at the end of the glass fibre. The convection coefficient is due to droplet internal curvulation which also justifies the assumption of uniform temperature distribution within the drop. Equation A6.6 then takes the form

$$Q_{rod} = nmk_{rod}A_{rod}(T_o-T_d) \qquad (A6.9)$$

where $n = h_d/k_{rod}m$ and the expression for the temperature distribution along the glass fibre shows T_o to be a function of both h_{rod} and h_d. Equation A6.9 reduces to the last term of equation A6.8 and cannot be solved as values of h_d are at present not available, although droplet circulation studies may provide an answer as during the present study a supported droplet containing deliberate traces of dust particles showed quite clearly the circulation pattern within the droplet. A photographic study may provide some measure of the internal circulation velocities.

It will be noted that both equations A6.7 and A6.9 provide a solution for Q_{rod} which is dependent on the value of h_{rod}. The value of Q_{rod} assumes that h_{rod} is

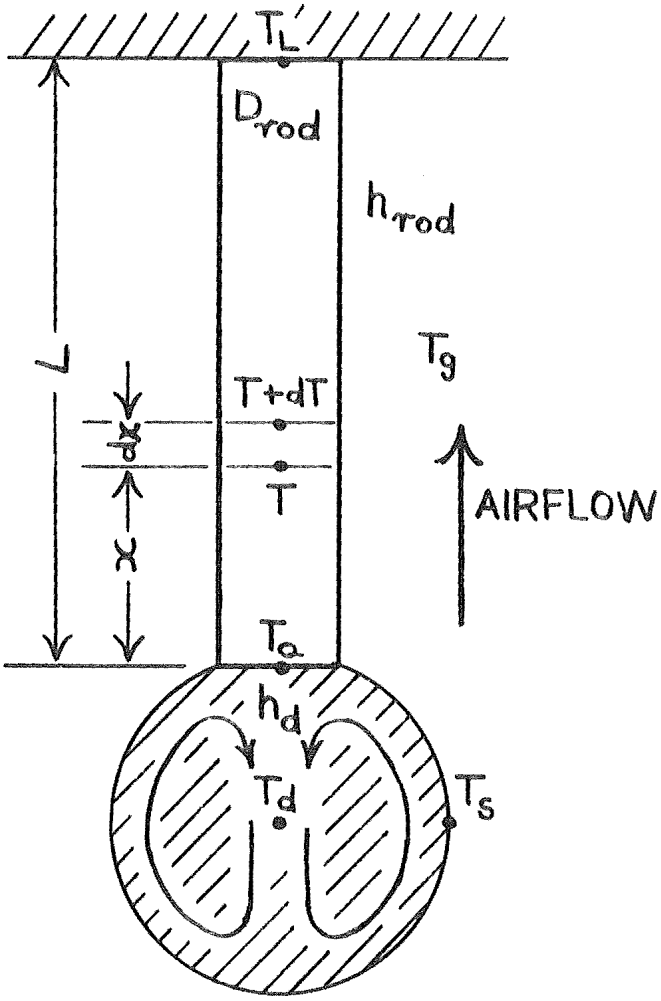

FIGURE A6·1 SCHEMATIC DIAGRAM OF A DROP SUPPORTED AT THE END OF A GLASS ROD.

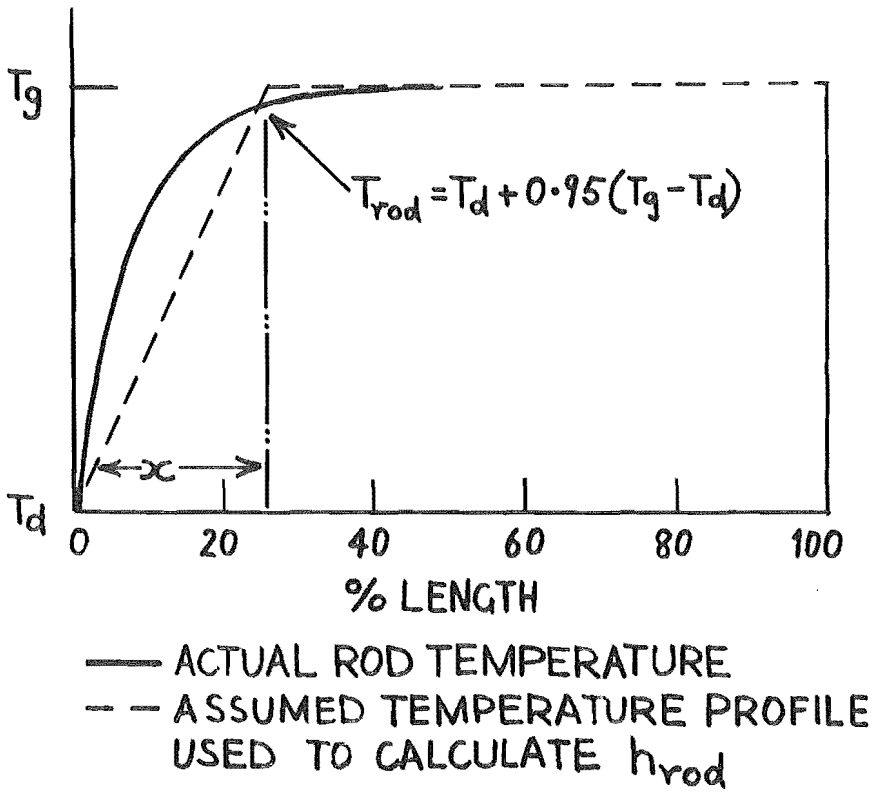

FIGURE A6·2 TEMPERATURE PROFILES ALONG A DROP-SUPPORTING GLASS ROD.

constant over the length of the glass fibre. Experimental values of the product mL were large and the temperature distribution along the glass rod then takes the form

$$T_{rod} = T_g-(T_g-T_d)e^{-mx} \qquad (A6.10)$$

As can be seen from the computer calculated temperature distributions (Appendix 7) and also figure A6.2, the temperature gradient (dT/dx) is significant only over that $\frac{1}{4}$ length of the rod at the end supporting the droplet. In view of this, and remembering that the droplet held on the end of the fine glass rod disturbs the air flow parallel to the rod, if h_{rod} is to be constant over the whole length then the coefficient must be considered as an average value for the whole length, combining both radiation and convection heat-transfer.

A literature search conducted to find suitable expressions describing h_{rod} resulted in a conclusion which agreed with that obtained by Fuchs (A60) in his booklet on evaporation and droplet growth. The conclusion is that by assuming sensible values of h_{rod}, the heat flowing along the glass fibre to the held drop is quite substantial, while the majority of workers in this field have unjustifiably neglected this effect. Frössling (A61) neglected the thermal conduction effect of his fine thermocouples used to measure the droplet temperature and well-known studies such as those of Ranz and Marshall (A62) and Hsu, Sato and Sage (A63) although making correction for the heat flow to the drop by the supporting fibre or thermocouple, do not report the method of calculation used. Many articles lack essential data about experimental

conditions, apparently considered irrelevant, but without them no real comparison of theory and experiment is possible.

Only one recent work by Ryozo Toei et al. (A64) reports the method of estimation of h_{rod} and refers to a paper by Sano and Nishikawa (A65). These latter workers calculated heat-transfer coefficients for fine wires in a parallel airflow. For forced convection, the heat-transfer coefficients for the wires were obtained from

$$Nu = 0.32 + 0.155Re^{\frac{1}{2}} \qquad (A6.11)$$

where the effects of the wire length and diameter on the Nusselt number were negligible. Values of h_{rod} calculated from this equation are approximately one-half of those calculated according to the recommended correlation by McAdams (A66) for cylinders in cross-flow. Equation A6.11 was experimentally obtained for very long wires (20 to 40 times the length of the glass fibres used to support the evaporating droplets) and a uniform temperature was assumed. These conditions do not approach those used in the present esperimental study and another solution for h_{rod} was sought.

The temperature profile along the glass rod is such that (dT/dx) is significant for only approximately $\frac{1}{4}$ length of the rod at the end supporting the drop (see figure A6.2). This profile can be approximated by using a linearly increasing temperature over this short length and putting the temperature for the remaining length of the rod equal to T_g. Then

$$T_{rod} = T_d + (T_g - T_d)x \qquad (A6.12)$$

To standardise the length over which the temperature gradient is significant (instead of assuming $x = L/4$), x is defined as the length where

$$T_{rod} = T_d + 0.95(T_g - T_d) \qquad (A6.13)$$

Equating equations A6.10 and A6.13, the solution for x is obtained as

$$x = 3.2958/m \qquad (A6.14)$$

To solve the problem of evaluating h_{rod}, the solution for heat-transfer to a semi-infinite flat plate is used. A constant free stream velocity along the rod is assumed and the specified surface temperature is of the form described by equation A6.12. In this case the solution will give an overestimate of h_x as the boundary-layer about the rod will be thicker than that over a flat plate (because of the high curvature of the rod). On the other hand, the heat-transfer region close to the supported drop will be in a region of possible vortex formation (according to the Reynolds number for the drop) which would reduce the thickness of the boundary-layer. The actual value of h_x calculated using the the flat plate solution may then not be too much in error.

For heat-transfer over a flat plate with a laminar boundary-layer and a surface temperature which increases linearly along the direction of flow, the <u>average</u> Nusselt number over the length x is given (A67) by

$$Nu_x = 1.070 Pr^{\frac{1}{3}} Re_x^{\frac{1}{2}} \qquad (A6.15)$$

Since h_{rod} is the average overall heat-transfer

coefficient for the rod and the temperature distribution along the rod (equation A6.10) is based on the total rod length, then h_{rod} is described by the equation

$$h_{rod} = x.h_x/L \qquad (A6.16)$$

Using equations A6.14, A6.15 and A6.16, a solution for h_{rod} can be obtained in the form

$$h_{rod} = \left[82.3Pr_g^{\frac{1}{3}}\left(\frac{\rho_g V_g}{u_g}\right)^{\frac{1}{2}} kg(D_{rod}k_{rod})^{\frac{1}{4}}/L\right]^{4/5} \qquad (A6.17)$$

h_{rod} is seen to depend not only on the diameter of the rod (A65), but also on the length of the rod. This is the difference between assuming a uniform temperature along the rod as against a linearly increasing temperature profile over the rod length near the supported droplet. The value of h_{rod} predicted is approximately $\frac{1}{3}$ that for a cylinder in crossflow (A66) and $\frac{2}{3}$ that for parallel flow along a cylinder of uniform temperature (A65).

Q_{rod} as calculated using h_{rod} from equation A6.17 was approximately 0.63 times the heat flow calculated using the heat-transfer correlation of equation A6.11. This is in reasonable agreement considering the basis of the derivation of h_{rod} as described by equation A6.17 and experimental values of Q_{rod} were 5 to 15% of Q_{total} so that h_{rod} values calculated from the Nusselt number correlation of Sano and Nushikawa (A65) would not significantly effect the final value of the overall Nusselt number calculated for the evaporating held droplet.

... ...

References

A60 Fuchs, N.A. "Evaporation and Droplet Growth in Gaseous Media" Permagon Press, London (1959).

A61 Frössling, N. Gerlands Beitri. Geophys., 52, 170 (1938)

A62 Ranz, N.E. and Marshall, W.R. Chem.Eng.Progr.,48, 141 (1952)

A63 Hsu, N.T., Sato, K. and Sage, B.H. Ind.Eng.Chem. 46, 870 (1954)

A64 Ryozo Toei, Morio Okazaki and Katsuyuki Kubota. Mem.Faculty of Engng, Kyoto University, 28, 413 (1966)

A65 Yuji Sano and Sinzo Nishikawa. Chem.Engng Japan, 2, 199 (1964)

A66 McAdams, W.H. "Heat transmission", 3rd Ed., 259 (1954) McGraw-Hill, New York.

A67 Kayes, W.M. "Convective Heat and Mass Transfer", 220 (1966), McGraw-Hill, New York.

APPENDIX 7

COMPUTER PROGRAM (HTCOEF)

The heat-transfer results from the evaporation studies of the supported droplets, were completely evaluated using the computer program (HTCOEF). The program was written in Fortran IV language for use in an IBM 360/44 computer. The program contains nearly 600 statements and is preceded by 5 small function programs. A listing of the program along with a sample of the computed results follows and the complete program can be considered to be the combination of 7 minor programs.

1: Cards 1 to 93 - (Statement numbers beginning with digit 1). This minor program calculates all relevant physical property data for the held evaporating droplet. The required input data are values of the humidity and vapour pressure of the drying air, the total pressure of the system, and the temperatures of the air, drop (wet-bulb temperature of air) and the column walls. The mean film properties are calculated at the volume mean m=0.60 (not 0.50 as for arithmetic mean) and the results are printed under the heading of Drops Physical Property Data. After the run number, the first line of the output is the measured values of the input data used to calculate the following lines of physical properties. The titles used are self explanatory and BFACT is the Mass Transfer number $B = C_p \Delta T/H_v$. The result shows the amount of sensible heat gained by the diffusing water vapour after evaporation to be about 0.5% of the total heat reaching

the drop surface and used as latent heat of vapourisation.

2: Cards 94 to 218 - (Statement numbers beginning with digit 2). This minor program calculates the air velocity and turbulence parameters as well as the turbulence energy spectrum. The input data required is the number of zeros (used to calculate λ_f by the zero count method), the dynamic velocity head as measured by the pitotstatic tube, and values of the anemometer bridge D.C. voltages V and V_o. This data is followed by values of the self noise and turbulence intensity spectrum as obtained by the gating method on the hot-wire anemometer. The calculated results are produced under the heading of Air Velocity and Turbulence Results and include the air velocity, longitudinal microscale λ_f and the turbulence intensity. The true mV signal for the turbulence spectrum is calculated and arranged in order of increasing frequency range. Using the relation $k = 2\pi f/U$, the frequency range is converted into a wavenumber range and the intensity (frequency) and energy spectra are computed from equations described in section 3. Dimensionless energy and wave number parameters were then calculated based on the mid-point wavenumber, estimates of the integral or macro-scale Λ_f of turbulence were obtained by solving the various equations describing the turbulence energy spectrum. The relative merit of the macroscale estimates is described in the next section.

3: Cards 219 to 319 - (Statement numbers beginning with digit 8). This minor program uses a simple plotting procedure to graphically display on a log-log plot the calculated intensity and energy spectra for midpoint wavenumbers. The program requires no input data as the plotting symbols are created within the program. The

first graph is for a high value of relative intensity (≈19%) and shows an energy peak. This allows an estimate of the wavenumber of the energy containing eddies (k_e). The spectra slope approximates the value of -5/3 only for a narrow range of wavenumbers and for this range the Liepmann estimate of the macro-scale is seen to be 1.35mm. The von Karman estimate (based on a value for k_e) records values of 1.6 to 1.3 mm for the same wavenumber range and the isotropic relation yields $\Lambda_f \approx 1.7$mm. These three solutions for Λ_f show reasonable agreement. The second graph is for a much lower value of relative intensity (≈ 5.5%) and no maximum energy peak is shown. As a consequence, a value of k_e cannot be obtained and the isotropic and von Karman macro-scale estimates are invalid. The liepmann correlation however, still produces two estimates in the -5/3 slope region (7.6 and 7.5 mm) and in practice values of Λ_f used to present the results were based on this latter correlation.

4: Cards 320 to 423 - (Statement numbers beginning with digit 3). This minor program calculated the supported droplet surface area and volume by the graphical integration method outlined in section 4.4. From each photograph of the held evaporating droplet, the time of evaporation, the length of the drop and cross-section diameters at equal distances from the front pole of the drop are used as input data. The data are used in the Lagrange interpolation formula (Appendix 5) to predict intermediate values of the drop diameter and all diameters (twice the measured number) are used in the formula for a frustum of a right cone which is used to approximte segments of the droplet. Summation of the surface areas

and volumes of these frustums provides a measure of the drop surface area and volume. These results are produced from each photograph of the evaporating droplet as shown under the heading Liquid Sphere Surface and volume Measures, and are self explanatory. Values of thedrop volume, surface area maximum diameter, equivalent diameter (of a sphere of the same volume) and length are stored along with the time of evaporation for use in the next section. The drop profile as printed out with the results is a valuable visual aid in checking that the input data and the Lagrange interpolated values were correct.

5: Cards 424 to 493 - (Statements beginning with digit 4). This minor program uses the University of Canterbury Computer Library subroutine POLFIT, to fit a polynomial to the evaporation curves of the time versus drop volume, area, diameter and length parameters. After fitting the curves for each variable, the equation descibing the change of the drop parameter with time was stored in the respective function programs which preceded the mainline program. This was done in every case except for the drop volume for which the equation obtained by POLFIT was analytically differentiated and the volume rate of change with time held as a function program. The results were printed as shown under the heading of Evaporation Rate curve Fitting and first and second order polynomials were fitted to the data. The degree of fit with the smallest error (XMSE) was chosen and test studies with higher order polynomials showed no significant further improvement. The terms COEF(1), COEF(2) etc are the coefficients of the equation

$$y = a_1 + a_2x + a_3x^2 + \ldots\ldots$$

6: Cards 494 to 545 - (Statements beginning with

digit 5). This minor program is used to compute preliminary heat-transfer results and also the Reynolds numbers at which the drop Nusselt numbers will be evaluated. The maximum and minimum Reynolds numbers found in the experiment are calculated and these are rounded up or down into whole multiples of 25. Intermediate Reynolds numbers as multiples of 25 are also found. The heat-transfer coefficient h_{rod} from the air to the glass fibre supporting the droplet is estimated and the total heat flow by conduction to the drop is then found. At the same time, the temperature profile along the supporting glass fibre is calculated. The results are shown beginning with the Experimental Reynolds number range and the significant part of the temperature profile along the supporting fibre is shown to be in that 1/4 length of the fibre nearest the drop.

7: Cards 546 to END - (Statements beginning with digit 6). This is the final section of the program and produces the heat-transfer results for the held evaporating droplets. For each selected Reynolds number (multiple of 25), the corresponding time of evaporation is sought from the function program for the maximum droplet diameter (on which the Reynolds number is based). On finding this diameter, which may be inside or outside of the actual experimental drop size range, the time of evaporation is then used to solve the other function programs for the drop evaporation rate (volume rate), surface area, equivalent sphere diameter and length. These solutions are used to calculate the net heat-transfer rate for the drop and so provide a value of the drop heat-transfer coefficient, which in turn is used to calculate the Nusselt number for the evaporating droplet. The Nusselt number according to

the Ranz and Marshall correlation (NUO) is also calculated along with the Frössling number for the evaporating droplet. The results are shown under the heading Heat Transfer Results (1) and are produced for each selected drop Reynolds number.

The program execution time was 4 to 5 minutes depending on the number of photographs to be analysed and the assistance of the staff of the Computer Centre of the University of Canterbury is gratefully acknowledged.

... ...

COMPUTER PROGRAM (HTCOEF)

```
0001              FUNCTION VOLRAT(R1,TYME,MR1)
0002              DIMENSION R1(5)
0003              VOLRAT=R1(2)
0004              DO 10 I=3,MR1
0005           10 VOLRAT=VOLRAT+(I-1)*R1(I)*TYME**(I-2)
0006              RETURN
0007              END

0001              FUNCTION AREAAA(R2,TYME,MR2)
0002              DIMENSION R2(5)
0003              AREAAA=R2(1)
0004              DO 10 I=2,MR2
0005           10 AREAAA=AREAAA+R2(I)*TYME**(I-1)
0006              RETURN
0007              END

0001              FUNCTION BIGDIA(R3,TYME,MR3)
0002              DIMENSION R3(5)
0003              BIGDIA=R3(1)
0004              DO 10 I=2,MR3
0005           10 BIGDIA=BIGDIA+R3(I)*TYME**(I-1)
0006              RETURN
0007              END

0001              FUNCTION AVDIAA(R4,TYME,MR4)
0002              DIMENSION R4(5)
0003              AVDIAA=R4(1)
0004              DO 10 I=2,MR4
0005           10 AVDIAA=AVDIAA+R4(I)*TYME**(I-1)
0006              RETURN
0007              END

0001              FUNCTION DROPLN(R5,TYME,MR5)
0002              DIMENSION R5(5)
0003              DROPLN=R5(1)
0004              DO 10 I=2,MR5
0005           10 DROPLN=DROPLN+R5(I)*TYME**(I-1)
0006              RETURN
0007              END

0001              DIMENSION DISTAN(90),DIAM(90),RAD(90),X(90),N(91)
0002              DIMENSION SELNO(10),TURVEL(10),TA(10),TB(10),TC(10),TD(10),TE(10)
0003              DIMENSION E10K(10),E1K(10),WAVEN(10),FREFUN(10),HAVEN(10)
0004              DIMENSION DIMENK(10),DIMERG(10),BLANK(120),D(2)
0005              DIMENSION VARIAB(100),TIME(20),RE(8),REQDIA(8)
0006              DIMENSION Y(20),COEF(5),ERROR(2),R1(5),R2(5),R3(5),R4(5),R5(5)
0007              INTEGER Z,ZZ,ZZZ
0008              REAL MTRATE
0009              REAL LATEHT,KGAS,KFILM,KVAPC,KVAPF,KGASC,KGASF,LENGTH,NU,NUO,LROD
0010         1001 READ(5,140) IRUNUM,HUMIDY,VAPRES,TOTPES,TEMGAS,TEMDOP,TWALL
0011          140 FORMAT(I10,6F10.5)
0012              WRITE(6,141)
0013          141 FORMAT('1',5X,' DROP NUSSELT NUMBER RESULTS')
0014              WRITE(6,120)
0015          120 FORMAT(//////////' DROPS PHYSICAL PROPERTY DATA')
0016              WRITE(6,130) IRUNUM
0017          130 FORMAT(//5X,'RUNUMBER=',I3)
0018              WRITE(6,150)
0019          150 FORMAT(//5X,'HUMIDY',4X,'VAPRES',4X,'TOTPES',4X,'TEMGAS',4X,'TEMDO
                 1P',4X,'TEMWALL')
0020              WRITE(6,160)HUMIDY,VAPRES,TOTPES,TEMGAS,TEMDOP,TWALL
0021          160 FORMAT(F11.5,5F10.2)
0022              TEMDIF=TEMGAS-TEMDOP
0023              TEMFLM=0.60*TEMDIF+TEMDOP
0024              PESDIF=TOTPES-VAPRES
0025              PESFLM=0.60*PESDIF+VAPRES
0026              YVAPFM=PESFLM/TOTPES
0027              YGASFM=1.000-YVAPFM
0028              WGTXVF=YVAPFM/(1.607-0.607*YVAPFM)
0029              WGTYCF=1.000-WGTXVF
0030              WGTXVC=HUMIDY/(HUMIDY+1.0)
0031              WGTYCC=1.000-WGTXVC
0032              XVC=0.0555*HUMIDY/(0.0345+0.0555*HUMIDY)
0033              YCC=1.000-XVC
0034              VISGC=0.0415+5.2E-5*TEMGAS
0035              VISGV=0.0198+5.0E-5*TEMGAS
0036              KGASC=0.013435+2.309E-5*TEMGAS
0037              KGASF=0.013435+2.389E-5*TEMFLM
0038              SPHTVC=0.43656+7.64E-5*TEMGAS
0039              SPHTVF=0.43656+7.64E-5*TEMFLM
0040              SPHTCC=0.23973+8.335E-6*TEMGAS
0041              SPHTCF=0.23973+8.335E-6*TEMFLM
0042              LATEHT=1090.3-0.5521*TEMDOP
0043              IF(TEMDOP-68.0)100,101,101
0044          100 RHODOP=(1.00133-4.56E-5*TEMDOP)*62.43
0045              GO TO 104
0046          101 IF(TEMDOP-104.0)102,103,103
0047          102 RHODOP=(1.00953-1.661E-4*TEMDOP)*62.43
0048              GO TO 104
0049          103 RHODOP=(1.01828-2.503E-4*TEMDOP)*62.43
0050          104 TEMPK=273.13+5.0*(TEMGAS-32.0)/9.0
0051              P=((TOTPES-1013.3)*65.1/86.7)+760.0
```

```
0052              RHOGAS=1.2929*(273.13/TEMPK)*(B-0.3783*VAPRES*0.75)*62.43/7.6E5
0053              IF(TEMGAS-114.3)105,106,106
0054          105 KVAPC=0.00902+3.46RE-5*TEMGAS
0055              GO TO 109
0056          106 IF(TEMGAS-212.0)107,108,108
0057          107 KVAPC=0.009992+1.748E-5*TEMGAS
0058              GO TO 109
0059          108 KVAPC=0.00782+2.778E-5*TEMGAS
0060          109 IF(TEMFLM-114.8)110,111,111
0061          110 KVAPF=0.00902+3.468E-5*TEMFLM
0062              GO TO 114
0063          111 IF(TEMFLM-212.0)112,113,113
0064          112 KVAPF=0.009992+1.748E-5*TEMFLM
0065              GO TO 114
0066          113 KVAPF=0.00782+2.778E-5*TEMFLM
0067          114 SPHTFM=WGTYCF*SPHTCF+WGTXVF*SPHTVF
0068              SPECHT=WGTYCC*SPHTCC+WGTXVC*SPHTVC
0069              AAA=YCC*3.071
0070              BBB=XVC*2.622
0071              KGAS=(AAA*KGASC+BBB*KVAPC)/(AAA+BBB)
0072              CCC=YGASFM*3.071
0073              DDD=YVAPFM*2.622
0074              KFILM=(CCC*KGASF+DDD*KVAPF)/(CCC+DDD)
0075              EEE=YCC*5.385
0076              FFF=XVC*4.245
0077              VISGAS=(EEE*VISGC+FFF*VISGV)/(EEE+FFF)
0078              PRGAS=SPECHT*VISGAS/KGAS
0079              BFACT=SPHTFM*TEMDIF/LATEHT
0080              TEMFFF=(TEMFLM-32.0)*5./9.+273.13
0081              DIFFUS=0.853*(TEMFFF/273.13)**2.*760./B
0082              WRITE(6,171)
0083          171 FORMAT(//5X,'RHOOOP',4X,'RHOGAS',4X,'LATEHT',4X,'TEMFLM',4X,'TEMDI
                  1F')
0084              WRITE(6,172)RHOOOP,RHOGAS,LATEHT,TEMFLM,TEMDIF
0085          172 FORMAT(F11.5,F10.5,3F10.2)
0086              WRITE(6,173)
0087          173 FORMAT(//7X,'KGAS',4X,'VISGAS',4X,'SPECHT',4X,'BFACT',5X,'PR.GAS')
0088              WRITE(6,174)KGAS,VISGAS,SPECHT,BFACT,PRGAS
0089          174 FORMAT(F11.5,4F10.5)
0090              WRITE(6,175)
0091          175 FORMAT(//6X,'KFILM',4X,'PESFLM',3X,'SPHTFLM',3X,'DIFUSTY')
0092              WRITE(6,176) KFILM,PESFLM,SPHTFM,DIFFUS
0093          176 FORMAT(F11.5,F10.2,2F10.5)
C
CCC           END OF DROPSAT
C
0094              WRITE(6,203)
0095          203 FORMAT(////////////' AIR VELOCITY AND TURBULENCE RESULTS')
0096              READ(5,204)ZERO,HEAD,VELNO,VEL,NUMBER
0097          204 FORMAT(F10.0,3F10.5,I10)
0098              AIRVEL=18.094*SQRT(HEAD/RHOGAS)
0099              WRITE(6,205)AIRVEL
0100          205 FORMAT(//5X,' AIR VELOCITY=',F5.2,'FT/SEC')
0101              SCALE=AIRVEL*2060./ZERO
0102              WRITE(6,206)SCALE
0103          206 FORMAT(//5X,' LONGITUDINAL MICROSCALE=',F6.3,'MM')
C
CC            CALCULATE MACROSCALE USING 'MACROSCALE=0.75/KE', (NOT FROM MICROSCALE)
C
0104              READ(5,207)(SELNO(I),I=1,9)
0105          207 FORMAT(8F10.5)
0106              READ(5,208)(TURVEL(I),I=1,9)
0107          208 FORMAT(8F10.5)
0108              TC(0)=0.0
0109              DO 209 I=1,9
0110              TA(I)=SELNO(I)*SELNO(I)
0111              TB(I)=TURVEL(I)*TURVEL(I)
0112              TC(I)=TB(I)-TA(I)
0113              TD(I)=TC(I)-TC(I-1)
0114              IF(TD(I).LT.0.0)TD(I)=0.0
0115          209 TE(I)=SQRT(TD(I))
0116              VRMS=SQRT(TC(9))
0117              TURB=0.4*VRMS*VEL/(VEL*VEL-VELNO*VELNO)
0118              TURB1=TURB/100.
0119              TURB2=TURB1*TURB1
0120              TURB4=TURB2*TURB2
0121              WRITE(6,210)TURB
0122          210 FORMAT(//5X,' TURBULENCE INTENSITY=',F5.2,'PERCENT')
0123              WAVEN(1)=31.416/AIRVEL
0124              WAVEN(2)=4.*WAVEN(1)
0125              WAVEN(3)=10.*WAVEN(1)
0126              WAVEN(4)=20.*WAVEN(1)
0127              DO 240 I=5,10
0128          240 WAVEN(I)=10.*WAVEN(I-3)
0129              DO 241 J=1,9
0130              I=10-J
0131              IF(J.GE.7)I=J-6
0132              HAVEN(J)=(WAVEN(J+1)+WAVEN(J))/2.
0133              DIMENK(J)=HAVEN(J)*2./3.
0134              XNTY=AIRVEL*0.004*VEL*TE(I)/(VEL*VEL-VELNO*VELNO)
0135              E1K(I)=XNTY*XNTY/(WAVEN(J+1)-WAVEN(J))
0136              E1OK(I)=E1K(I)*2.0*3.1416/AIRVEL
C
CC                E1OK(I)=INTENSITY FUNCTION OR E1(F)
CC                E1K(I)=ENERGY FUNCTION OR E1(K)
C
0137          241 DIMERG(I)=E1K(I)*3./(TURB2*AIRVEL*AIRVEL*2.)
0138              DO 211 I=1,9
0139          211 FREFUN(I)=TD(I)/TC(9)
0140              WRITE(6,212)
0141          212 FORMAT(//5X,' TURB. FREQ. RANGE   MV SIGNAL      FRAC. SIGNAL')
0142              WRITE(6,213)TE(9),FREFUN(9)
0143          213 FORMAT(/11X,' 5-20HZ',F14.2,F18.5)
0144              WRITE(6,214)TE(8),FREFUN(8)
0145          214 FORMAT(10X,' 20-50HZ',F14.2,F18.5)
```

```
0146              WRITE(6,215)TE(7),FREFUN(7)
0147          215 FORMAT(15X,' 50-100HZ',F13.2,F18.5)
0148              WRITE(6,216)TE(6),FREFUN(6)
0149          216 FORMAT(9X,' 100-200HZ',F13.2,F18.5)
0150              WRITE(6,217)TE(5),FREFUN(5)
0151          217 FORMAT(9X,' 200-500HZ',F13.2,F18.5)
0152              WRITE(6,218)TE(4),FREFUN(4)
0153          218 FORMAT(9X,' 500-1000HZ',F12.2,F18.5)
0154              WRITE(6,219)TE(1),FREFUN(1)
0155          219 FORMAT(8X,' 1000-2000HZ',F12.2,F18.5)
0156              WRITE(6,220)TE(2),FREFUN(2)
0157          220 FORMAT(8X,' 2000-5000HZ',F12.2,F18.5)
0158              WRITE(6,221)TE(3),FREFUN(3)
0159          221 FORMAT(8X,' 5000-10000HZ',F11.2,F18.5)
0160              WRITE(6,282)
0161          282 FORMAT(70X,' DIMENSIONLESS PARAMETERS')
0162              WRITE(6,222)
0163          222 FORMAT(/6X,' WAVE NUMBER (1/FT)  INTENSITY SPECTRA   ENERGY SPECTR
                 1A          K*D                    E1(KD)',/)
0164              DO 224 J=1,9
0165              K=J+1
0166              I=10-J
0167              IF(J.GE.7)I=J-6
0168              WRITE(6,223)WAVEN(J),WAVEN(K),E10K(I),E1K(I),DIMENK(J),DIMERG(I)
0169          223 FORMAT(7X,F7.1,' TO ',F7.1,5X,E10.4,9X,E10.4,9X,E10.4,9X,E10.4)
0170          224 CONTINUE
0171              WRITE(6,258)
0172          258 FORMAT(//32X,' MACROSCALE ESTIMATES (IN MMS)')
0173              WRITE(6,259)
0174          259 FORMAT(/5X,'    ISOTROPIC 0.75/K        LIEPMANN EMPIRICAL RELATIO
                 1N      VON KARMAN INTERPOLATION',/)
0175              DO 260 I=1,9
0176              J=10-I
0177              IF(I.GE.7)J=I-6
0178              IF(E10K(J).LE.0.0)GO TO 261
0179          280 ROOTB=(TURB4*(AIRVEL**4.))-(E1K(J)*E1K(J)*3.1416*3.1416*HAVEN(I)*H
                 1AVEN(I))
0180              IF(ROOTB.LT.0.0)GO TO 276
0181              ROOTB=SQRT(ROOTB)
0182              SCALE3=(TURB2*AIRVEL*AIRVEL+ROOTB)/(E1K(J)*3.1416*HAVEN(I)*HAVEN(I
                 1))*304.8
0183              SCALE4=(TURB2*AIRVEL*AIRVEL-ROOTB)/(E1K(J)*3.1416*HAVEN(I)*HAVEN(I
                 1))*304.8
0184              GO TO 281
0185          261 SCALE1=0.0
0186          276 SCALE3=0.0
0187              SCALE4=0.0
0188          281 SCALE5=SCALE/304.8
0189              IF(E1K(J).LE.0.0)GO TO 285
0190              DENOM=((4./3.)*HAVEN(I)*SCALE5)**2.0
0191              TEST1=DENOM/1.0
0192              TEST2=1.0/DENOM
0193              A=E1K(J)*3.1416/(2.0*TURB2*AIRVEL*AIRVEL)
0194              IF(TEST1.LT.0.001)GO TO 286
0195              IF(TEST2.LT.0.001)GO TO 287
0196              NN=1
0197              D(1)=1000.0
0198          298 SCALE5=SCALE5+2.E-4
0199              NN=NN+1
0200              B=(1.0+(16./9.)*HAVEN(I)*HAVEN(I)*SCALE5*SCALE5)**(5./6.)
0201              C=SCALE5/B
0202              D(NN)=ABS((A-C)/A)
0203              IF(D(NN).GE.D(NN-1))GO TO 292
0204              IF(D(NN).GE.0.15)SCALE5=SCALE5+8.E-4
0205              D(1)=D(NN)
0206              NN=NN-1
0207              GO TO 298
0208          285 SCALE5=0.0
0209              GO TO 283
0210          286 SCALE5=A*304.8
0211              GO TO 283
0212          287 SCALE5=304.8*((((4./3.)*HAVEN(I))**(5./3.)*A)**(-3./2.))
0213              GO TO 283
0214          292 SCALE5=SCALE5*304.8
0215          283 SCALE1= 0.75*304.8/HAVEN(I)
0216              WRITE(6,290)SCALE1,SCALE3,SCALE4,SCALE5
0217          290 FORMAT(14X,G10.4,12X,G10.4,3X,G10.4,15X,G10.4)
0218          260 CONTINUE
              C
              CC      END OF VELOCITY AND TURBULENCE RESULTS
              C
0219              WRITE(6,800)
0220          800 FORMAT(////////////' TURBULENCE INTENSITY AND ENERGY SPECTRA PLOTS
                 1     INTENSITY AND ENERGY ACROSS THE PAGE.   WAVE NO. DOWN.')
0221              WRITE(6,801)
0222          801 FORMAT(//21X,' INTENSITY=+  ENERGY=*       PLOT AXES ARE POWERS OF
                 1 TEN',/)
0223              WRITE(6,803)
0224          803 FORMAT(4X,'-10',10X,'-9',11X,'-8',11X,'-7',11X,'-6',11X,'-5',11X,'
                 1-4',11X,'-3',11X,'-2',11X,'-1')
0225              WRITE(6,804)
0226          804 FORMAT(3X,'0',1X,118('.'))
0227              INKY=0
0228              REWIND 1
0229              WRITE(1,861)
0230          861 FORMAT(' *+')
0231              REWIND 1
0232              READ(1,860) BLANK(1),STAR,NOUGHT
0233          860 FORMAT(3A1)
0234              DO 802 I=1,120
0235          802 BLANK(I)=BLANK(1)
0236              DO 890 I=1,9
0237              J=10-I
0238              IF(I.GE.7)J=I-6
0239              THING1=ALOG10(HAVEN(I))*13.0
0240              II=IFIX(THING1)
```

```
0241              DIF1=(THING1-I1)
0242              IF(DIF1.GE.0.5)I1=I1+1
0243          805 INKY=INKY+1
0244              IF(INKY.EQ.I1)GO TO 820
0245              IF(INKY.EQ.13)GO TO 807
0246              IF(INKY.EQ.26)GO TO 808
0247              IF(INKY.EQ.39)GO TO 809
0248              IF(INKY.EQ.52)GO TO 810
0249              WRITE(6,806)
0250          806 FORMAT(5X,'.',116X,'.')
0251              GO TO 805
0252          807 WRITE(6,811)
0253          811 FORMAT(3X,'1',1X,'.',116X,'.')
0254              GO TO 805
0255          808 WRITE(6,812)
0256          812 FORMAT(3X,'2',1X,'.',116X,'.')
0257              GO TO 805
0258          809 WRITE(6,813)
0259          813 FORMAT(3X,'3',1X,'.',116X,'.')
0260              GO TO 805
0261          810 WRITE(6,814)
0262          814 FORMAT(3X,'4',1X,'.',116X,'.')
0263              GO TO 805
0264          820 IF(I1.EQ.65)GO TO 895
0265              IF(E1OK(J).EQ.0.0)GO TO 823
0266              IF(E1K(J).EQ.E1OK(J)) GO TO 837
0267              GO TO 839
0268          837 E1OK(J)=0.085
0269              WRITE(6,838)
0270          838 FORMAT(7X,' INTENSITY AND ENERGY EQUAL')
0271          839 IF(E1K(J).GT.E1OK(J)) GO TO 840
0272              GO TO 843
0273          840 TEMP1=E1K(J)
0274              TEMP2=E1OK(J)
0275              E1OK(J)=TEMP1
0276              E1K(J)=TEMP2
0277              WRITE(6,842)
0278          842 FORMAT(7X,' INTENSITY AND ENERGY REVERSED')
0279          843 THING2=-(ALOG10(E1OK(J))+1.0)*13.0
0280              I2=IFIX(THING2)
0281              DIF2=(THING2-I2)
0282              IF(DIF2.GE.0.5)I2=I2+1
0283              I2=116-I2
0284              THING3=-(ALOG10(E1K(J))+1.0)*13.0
0285              I3=IFIX(THING3)
0286              DIF3=(THING3-I3)
0287              IF(DIF3.GE.0.5)I3=I3+1
0288              I3=116-I3
0289              I4=I2-I3-1
0290              I5=116-(I3+I4+2)
0291              IF(INKY.EQ.13)GO TO 862
0292              IF(INKY.EQ.26)GO TO 864
0293              IF(INKY.EQ.39)GO TO 866
0294              IF(INKY.EQ.52)GO TO 868
0295              GO TO 824
0296          823 I3=1
0297              WRITE(6,871)
0298          871 FORMAT(7X,' INTENSITY AND ENERGY=0.0')
0299              I4=113
0300          824 WRITE(6,825)(BLANK(K),K=1,I3),STAR,(BLANK(K),K=1,I4),NOUGHT,(BLANK
                 1(K),K=1,I5)
0301          825 FORMAT(5X,'.',116A1,'.')
0302              GO TO 870
0303          862 WRITE(6,863)(BLANK(K),K=1,I3),STAR,(BLANK(K),K=1,I4),NOUGHT,(BLANK
                 1(K),K=1,I5)
0304          863 FORMAT(3X,'1',1X,'.',116A1,'.')
0305              GO TO 870
0306          864 WRITE(6,865)(BLANK(K),K=1,I3),STAR,(BLANK(K),K=1,I4),NOUGHT,(BLANK
                 1(K),K=1,I5)
0307          865 FORMAT(3X,'2',1X,'.',116A1,'.')
0308              GO TO 870
0309          866 WRITE(6,867)(BLANK(K),K=1,I3),STAR,(BLANK(K),K=1,I4),NOUGHT,(BLANK
                1(K),K=1,I5)
0310          867 FORMAT(3X,'3',1X,'.',116A1,'.')
0311              GO TO 870
0312          868 WRITE(6,869)(BLANK(K),K=1,I3),STAR,(BLANK(K),K=1,I4),NOUGHT,(BLANK
                1(K),K=1,I5)
0313          869 FORMAT(3X,'4',1X,'.',116A1,'.')
0314          870 IF(I.EQ.9)GO TO 885
0315          890 CONTINUE
0316          885 I1=65
0317              GO TO 805
0318          895 WRITE(6,896)
0319          896 FORMAT(3X,'5',1X,118('.'))
                C
                C     END OF GRAPH PLOTTING OF TURBULENCE SPECTRA
                C
0320              WRITE(6,300)
0321          300 FORMAT(////////////' LIQUID SPHERE SURFACE AND VOLUME MEASURES')
0322              WRITE(6,394)
0323          394 FORMAT(//' X(**) IS THE DISTANCE FROM THE FRONT POLE OF THE SPHERE
                 1 AS MEASURED IN MMS'/' RAD(**) IS THE RADIUS OF THE SPHERE AT THAT
                 2 POSITION ALSO MEASURED IN MMS'/' (**)=ODD NO.=ORIGINAL DATA'/' (*
                 3*)=EVEN NO.=INTERPOLATED VALUES USING LAGRANGES FORMULA'///)
0324              READ(5,305)FACTOR,CONROD,DIAROD,LROD
0325          305 FORMAT(4F10.6)
0326              DO 367 M1=1,NUMBER
0327          301 READ(5,302)IRUNUM,Z,LENGTH,TIMED
0328          302 FORMAT(2I10,2F10.5)
0329              WRITE(6,303)IRUNUM
0330          303 FORMAT(//5X,' PHOTO NO.=',I2)
0331              READ(5,304)(DIAM(I),I=1,Z)
0332          304 FORMAT(8F10.5)
0333              TIME(M1)=TIMED
```

```
0334                M=Z-1
0335                DISTAN(1)=0.0
0336                DISTAN(Z)=LENGTH
0337                DO 355 I=2,M
0338           355  DISTAN(I)=DISTAN(I-1)+0.5
0339                DO 350 I=1,Z
0340                DISTAN(I)=DISTAN(I)/FACTOR
0341                DIAM(I)=DIAM(I)/FACTOR
0342                J=2*I-1
0343                ZZ=J-1
0344                ZZZ=J
0345                X(J)=DISTAN(I)
0346           350  RAD(J)=DIAM(I)/2.
0347                DO 390 J=2,ZZ,2
0348                IF(ZZ-2-J)307,307,306
0349           306  X(J)=(X(J+1)-X(J-1))/2.+X(J-1)
0350                GO TO 308
0351           307  X(J)=(X(J+1)-X(J-1))/2.+X(J-1)
0352                A=(X(J)-X(J-1))*(X(J)-X(J+1))*RAD(J-3)/((X(J-3)-X(J-1))*(X(J-3)-X(
                    1J+1)))
0353                B=(X(J)-X(J-3))*(X(J)-X(J+1))*RAD(J-1)/((X(J-1)-X(J-3))*(X(J-1)-X(
                    1J+1)))
0354                C=(X(J)-X(J-3))*(X(J)-X(J-1))*RAD(J+1)/((X(J+1)-X(J-3))*(X(J+1)-X(
                    1J-1)))
0355                GO TO 390
0356           308  A=(X(J)-X(J+1))*(X(J)-X(J+3))*RAD(J-1)/((X(J-1)-X(J+1))*(X(J-1)-X(
                    1J+3)))
0357                B=(X(J)-X(J-1))*(X(J)-X(J+3))*RAD(J+1)/((X(J+1)-X(J-1))*(X(J+1)-X(
                    1J+3)))
0358                C=(X(J)-X(J-1))*(X(J)-X(J+1))*RAD(J+3)/((X(J+3)-X(J-1))*(X(J+3)-X(
                    1J+1)))
0359           390  RAD(J)=A+B+C
0360                ACTA=0.0
0361                AREA=0.0
0362                VOL=0.0
0363                BIGR=RAD(1)
0364                DO 385 J=1,ZZZ
0365                IF(ZZZ-91)321,321,320
0366           320  GO TO 335
0367           321  IF(BIGR-RAD(J))323,324,324
0368           323  BIGR=RAD(J)
0369           324  CONTINUE
0370           385  CONTINUE
0371                DO 325 K=1,91
0372           325  N(K)=0
                C
                C       FOR 8 LINES PER INCH 'TOOTS'=1.233  ***********************************
                C       FOR 6 LINES PER INCH 'TOOTS'=1.603  ***********************************
                C
0373                TOOTS=1.603                                                          ***
0374                TOOTS=1.233                                                          ***
0375                DO 326 J=1,ZZZ
0376                M=IFIX(ZZZ*RAD(J)*TOOTS/(BIGR*2.))+1
0377                WRITE(6,327)(J,X(J),J,RAD(J),(N(K),K=1,M))
0378           327  FORMAT(5X,' X(',I2,')='F8.5,3X,'RAD(',I2,')='F8.5,3X,100(I1))
0379           326  CONTINUE
0380                DO 314 J=1,ZZ
0381                IF(BIGR-RAD(J))335,311,313
0382           335  WRITE(6,336)
0383           336  FORMAT(//' SOMETHING FUNNY SOMEWHERE')
0384                GO TO 367
0385           311  BIGD=2.0*BIGR
0386                AAA=AREA
0387                ACTB=ACTA
0388                VVV=VOL
0389                WRITE(6,312)BIGD,AAA,ACTB,VVV
0390           312  FORMAT(//5X,' MAX. CROSS SEC. DIA.='F8.5,'MMS',//5X,' VERT. CROSS
                    1SEC. AREA FRONT HALF='F8.5,'MMS*2',//5X,' SURFACE AREA FRONT HALF
                    2='F8.5,'MMS*2',//5X,' VOLUME FRONT HALF='F8.5,'MMS*3')
0391           313  H=X(J+1)-X(J)
0392                AREA=AREA+(RAD(J+1)+RAD(J))*H
0393                E=ABS(RAD(J+1)-RAD(J))
0394                F=SQRT(H*H+E*E)
0395                ACTA=ACTA+3.141593*(RAD(J+1)+RAD(J))*F
0396           314  VOL=VOL+3.141593*(RAD(J+1)*RAD(J+1)+RAD(J+1)*RAD(J)+RAD(J)*RAD(J))
                    1*H/3.0
0397                BAREA=AREA-AAA
0398                BACTB=ACTA-ACTB
0399                BVOL=VOL-VVV
0400                AVDIA=(6.0*VOL/3.141593)**(1./3.)
0401                WRITE(6,315)BAREA,BACTB,BVOL
0402           315  FORMAT(//5X,' VERT. CROSS SEC. AREA BACK HALF='F8.5,'MMS*2',//5X,'
                    1 SURFACE AREA BACK HALF='F8.5,'MMS*2',//5X,' VOLUME BACK HALF='F8.
                    25,'MMS*3')
0403                WRITE(6,316)AREA,ACTA,VOL
0404           316  FORMAT(//5X,' TOTAL VERT. CROSS SEC. AREA='F8.5,'MMS*2',//5X,' TOT
                    1AL SURFACE AREA OF  DROP='F8.5,'MMS*2',//5X,' TOTAL VOLUME OF  DRO
                    2P='F8.5,'MMS*3')
0405                RATIO1=ACTB/ACTA*100.
0406                RATIO2=VVV/VOL*100.
0407                RATIO3=3.1416*RAD(ZZZ)*RAD(ZZZ)/(ACTA+3.1416*RAD(ZZZ)*RAD(ZZZ))
0408                RATIO3=RATIO3*100.
0409                WRITE(6,365) RATIO1,RATIO2
0410           365  FORMAT(//5X,' FRONT HALF AREA AS PERCENTAGE OF TOTAL='F6.2,//5X,'
                    1FRONT HALF VOLUME AS PERCENTAGE OF TOTAL='F6.2)
0411                WRITE(6,364)RATIO3
0412           364  FORMAT(//5X,' SUPPORT ROD AREA AS PERCENTAGE OF TOTAL='F6.2)
0413                WRITE(6,366) AVDIA
0414           366  FORMAT(//5X,' DIAM. OF EQUIVALENT SPHERE='F8.5,'MMS')
0415                VARIAB(M1)=VOL
0416                M2=NUMBER+M1
0417                VARIAB(M2)=ACTA
0418                M3=NUMBER+M2
0419                VARIAB(M3)=BIGD
```

```
0420              M4=NUMBER+M3
0421              VARIAB(M4)=AVDIA
0422              M5=NUMBER+M4
0423          367 VARIAB(M5)=LENGTH
              C
              C       END OF SOLIDY JOB
              C
0424              WRITE(6,400)
0425          400 FORMAT(/////////5X,' EVAPORATION RATE CURVE FITTING')
0426              NN=NUMBER
0427              DO 481 J=1,5
0428              N1=(J-1)*NN
0429              MM=1
0430              DO 490 K=1,2
0431              MM=MM
0432              DO 480 I=1,NN
0433              Y(I)=VARIAB(I+N1)
0434          480 X(I)=TIME(I)
0435              WRITE(6,414)MM
0436          414 FORMAT(/5X,' DEGREE OF FIT=',I2)
0437              CALL POLFIT(X,Y,NN,MM,XMSE,COEF)
0438              MM=MM+1
0439              WRITE(6,415)(I,I=1,MM)
0440          415 FORMAT(/7X,'XMSE',8(3X,'COEF(',I1,')')/)
0441              WRITE(6,416)XMSE,(COEF(I),I=1,MM)
0442          416 FORMAT(E13.2,9G10.4)
0443          490 ERROR(K)=XMSE
0444              IF(ERROR(1)-ERROR(2))420,422,422
0445          420 DO 440 I=1,NN
0446              Y(I)=VARIAB(I+N1)
0447          440 X(I)=TIME(I)
0448              MM=1
0449              CALL POLFIT(X,Y,NN,MM,XMSE,COEF)
0450              MM=MM+1
0451          422 IF(N1.EQ.0)GO TO 461
0452              IF(N1.EQ.NN)GO TO 462
0453              NN2=NN*2
0454              NN3=NN*3
0455              NN4=NN*4
0456              IF(N1.EQ.NN2)GO TO 463
0457              IF(N1.EQ.NN3)GO TO 464
0458              IF(N1.EQ.NN4)GO TO 465
0459          461 DO 471 I=1,MM
0460          471 R1(I)=COEF(I)
0461              MR1=MM
0462              IFIT=MM-1
0463              WRITE(6,473)IFIT
0464          473 FORMAT(/////5X,' DEGREE OF FIT CHOSEN FOR VOLUME RATE=',I2,///)
0465              GO TO 481
0466          462 DO 472 I=1,MM
0467          472 R2(I)=COEF(I)
0468              MR2=MM
0469              IFIT=MM-1
0470              WRITE(6,474)IFIT
0471          474 FORMAT(/////5X,' DEGREE OF FIT CHOSEN FOR AREA RATE=',I2,///)
0472              GO TO 481
0473          463 DO 475 I=1,MM
0474          475 R3(I)=COEF(I)
0475              MR3=MM
0476              IFIT=MM-1
0477              WRITE(6,476)IFIT
0478          476 FORMAT(/////5X,' DEGREE OF FIT CHOSEN FOR BIG-DIA. RATE=',I2,///)
0479              GO TO 481
0480          464 DO 477 I=1,MM
0481          477 R4(I)=COEF(I)
0482              MR4=MM
0483              IFIT=MM-1
0484              WRITE(6,478)IFIT
0485          478 FORMAT(/////5X,' DEGREE OF FIT CHOSEN FOR AV-DIA. RATE=',I2,///)
0486              GO TO 481
0487          465 DO 466 I=1,MM
0488          466 R5(I)=COEF(I)
0489              MR5=MM
0490              IFIT=MM-1
0491              WRITE(6,467)IFIT
0492          467 FORMAT(/////5X,' DEGREE OF FIT CHOSEN FOR DROP LENGTH RATE=',I2,/)
0493          481 CONTINUE
              C
              C       END OF CURVE FITTING PROCEDURE
              C
0494              REMAX=RHOGAS*AIRVEL*3600.*VARIAB(NUMBER*2+1)*3.28E-3/VISGAS
0495              REMIN=REMAX*VARIAB(NUMBER*3)/VARIAB(NUMBER*2+1)
0496              WRITE(6,500)REMIN,REMAX
0497          500 FORMAT(//////////5X,' EXPTL REYNOLDS NO. RANGE=',F5.1,' TO 'F5.1)
0498              DIV1=REMAX/25.0
0499              DIV11=IFIX(DIV1)
0500              DIV111=DIV11
0501              REMR1=DIV1-DIV111
0502              IF(REMR1-0.5)501,502,502
0503          501 REMAX=DIV111*25.0
0504              GO TO 503
0505          502 REMAX=(DIV111+1)*25.0
0506          503 DIV2=REMIN/25.0
0507              DIV22=IFIX(DIV2)
0508              DIV222=DIV22
0509              REMR2=DIV2-DIV222
0510              IF(REMR2-0.5)504,505,505
0511          504 REMIN=DIV222*25.0
0512              GO TO 506
```

```
0513          505 PEMIN=(DIV222+1)*25.0
0514          506 NRE=(REMAX-REMIN)/25.0-1
0515              RE(1)=REMIN
0516              NREE=NRE+2
0517              DO 507 I=2,NREE
0518          507 RE(I)=RE(1)+25.0*(I-1)
0519              WRITE(6,508)(RE(I),I=1,NREE)
0520          508 FORMAT(//5X,' ASSUMED REYNOLDS NO.S ARE ',8(F5.1,','))
0521              DO 509 I=1,NREE
0522          509 REQDIA(I)=RE(I)*VISGAS/(RHOGAS*AIRVEL*3600.*3.28E-3)
0523              HROD=(82.3*(PRGAS**(1./3.))*((RHOGAS*AIRVEL/VISGAS)**(1./2.))*KGAS
                 1*((CONROD*DIAROD)**(1./4.))/LROD)**0.90
0524              XROD=3.2958*SQRT(CONROD*DIAROD/(4*HROD))
0525              HSTAR=LROD*HROD/XROD
0526              XRODY=XROD*100./LROD
0527              QROD=1.5708*SQRT(CONROD*HROD*DIAROD**3)*TEMDIF
0528              WRITE(6,521)HSTAR,XRODY,HROD
0529          521 FORMAT(//5X,' HSTAR=',F5.2,'BTU/SQ.FT HR DEG.F',//5X,' XSTAR=',F5.
                12,'PERCENT OF LROD',//5X,' HROD =',F5.2,'BTU/SQ.FT HR DEG.F')
0530              WRITE(6,530)
0531          530 FORMAT(//5X,' PERCENT LROD   TEMROD'/)
0532              FRAQX=LROD/50.0
0533              XL=-FRAQX
0534              AM=SQRT(4*HROD/(CONROD*DIAROD))
0535          522 XL=XL+FRAQX
0536              TROD=TEMGAS-TEMDIF*EXP(-AM*XL)
0537              XXL=XL*100./LROD
0538              WRITE(6,527)XXL,TROD
0539          527 FORMAT(F16.2,F11.2)
0540              IF(XL-XROD)522,522,523
0541          523 IF(XXL-99.0)524,525,525
0542          524 XL=XL+4*FRAQX
0543              IF(XL+FRAQX.GE.LROD)XL=LROD-FRAQX
0544              GO TO 522
0545          525 CONTINUE
              C
              CC    END OF REYNOLDS NUMBER SELECTION AND PRELIMINARY H.T. CALCULATIONS
              C
0546              TYME=2*TIME(NUMBER)-TIME(NUMBER-1)
0547          650 BIGDP=BIGDIA(R3,TYME,MR3)
0548              IF(BIGDP-REQDIA(1))651,652,652
0549          652 TYME=TYME+1.0
0550              GO TO 650
0551          651 CONTINUE
0552              DO 699 I=1,NREE
0553          640 TYME=(TYME*60.0-0.02)/60.0
0554              BIGD=BIGDIA(R3,TYME,MR3)
0555              IF(BIGD-REQDIA(I))641,642,642
0556          641 GO TO 640
0557          642 TYME=TYME
0558              MTRATE=VOLRAT(R1,TYME,MR1)*3.531E-8*60.*RHODOP
0559              DPAREA=AREAAA(R2,TYME,MR2)*1.0763E-5
0560              LENGTH=DROPLN(R5,TYME,MR5)
0561              SHAPE=LENGTH/(BIGD*FACTOR)
0562              BIGD=BIGD*3.28E-3
0563              EQDIA=AVDIAA(R4,TYME,MR4)*3.28E-3
0564              QRAD=0.1642*(((TWALL+459.4)/100.)**4-((TEMDOP+459.4)/100.)**4)*DPA
                 1REA
0565              QROD=QROD
0566              QTOT=ABS(MTRATE*LATEHT)
0567              QNET=QTOT-QROD-QRAD
0568              HTCOEF=QNET/(DPAREA*TEMDIF)
0569              NU=HTCOEF*EQDIA/KFILM
0570              RENO=RHOGAS*AIRVEL*3600.*BIGD/VISGAS
0571              NUO=2.0+0.60*PRGAS**(1./3.)*RENO**(1./2.)
0572              FROSNO=(NU-2.0)/((RENO**0.5)*(PRGAS**0.333))
0573              RATIO=NU/NUO
0574              BIGD1=BIGD/3.28E-3
0575              PERT1=QRAD*100./QTOT
0576              PERT2=QROD*100./QTOT
0577              PERT3=QNET*100./QTOT
0578              WRITE(6,689) I
0579          689 FORMAT(/////////5X,' HEAT TRANSFER RESULTS(',I1,')')
0580              WRITE(6,690)QTOT
0581          690 FORMAT(//5X,' QTOTAL=',G10.4,'BTU/HR')
0582              WRITE(6,693)QRAD,PERT1
0583          693 FORMAT(//5X,' QRADTN=',G10.4,'BTU/HR =',F5.2,'PERCENT OF QTOTAL')
0584              WRITE(6,694)QROD,PERT2
0585          694 FORMAT(//5X,' QROD  =',G10.4,'BTU/HR =',F5.2,'PERCENT OF QTOTAL')
0586              WRITE(6,695)QNET,PERT3
0587          695 FORMAT(//5X,' QNET  =',G10.4,'BTU/HR =',F5.2,'PERCENT OF QTOTAL')
0588              WRITE(6,691)HTCOEF,NUO,RATIO
0589          691 FORMAT(//5X,' HTCOEF=',F6.1,'BTU/SQ.FT HR DEG.F',//5X,' NU THEORY=
                 1'F5.2,//5X,' RATIO NU/NUO=',F6.3)
0590              WRITE(6,692)RENO,NU,TURB,SCALE,BIGD1
0591          692 FORMAT(//5X,'**** DROP REYNOLDS NUMBER=',F6.2,//5X,'**** DROP NUSS
                 1ELT NUMBER=',F6.2,//5X,'**** AIR TURBULENCE (PERCENT)=',F6.2,//5X,
                 2'**** AIR MICROSCALE(MMS)=',F6.3,//5X,'**** MAXIMUM DROP DIAMETER(
                 3MMS)=',F6.3)
0592              WRITE(6,696)SHAPE
0593          696 FORMAT(/5X,'**** DROP SPHERICITY(L/D)=',F4.2)
0594              WRITE(6,697)FROSNO
0595          697 FORMAT(/5X,'**** FROSSLING NUMBER=',F5.3)
0596          699 CONTINUE
0597              WRITE(6,700)
0598          700 FORMAT(/////5X,'END OF RESULTS FOR THIS RUNUMBER',///)
0599              GO TO 1001
0600              END
```

DROPS PHYSICAL PROPERTY DATA

RUNUMBER= 4

HUMIDY	VAPRES	TOTPES	TEMGAS	TEMDOP	TEMWALL
0.00639	10.20	997.50	72.00	56.80	67.40

RHODOP	RHOGAS	LATENT	TEMFLM	TEMDIF
62.35129	0.07319	1058.94	65.92	15.20

KGAS	VISGAS	SPECHT	REACT	PR.GAS
0.01512	0.04507	0.24161	0.00486	0.72001

KFILM	PESFLM	SPHTFLM	DIFUSTY
0.01291	602.58	0.33833	0.99022

AIR VELOCITY AND TURBULENCE RESULTS

AIR VELOCITY= 3.60FT/SEC

LONGITUDINAL MICROSCALE= 1.210MM

TURBULENCE INTENSITY=19.06PERCENT

TURB. FREQ. RANGE	MV SIGNAL	FRAC. SIGNAL
5-20HZ	15.56	0.06400
20-50HZ	27.62	0.20176
50-100HZ	30.33	0.24320
100-200HZ	30.35	0.24358
200-500HZ	25.70	0.17735
500-1000HZ	12.67	0.04246
1000-2000HZ	9.95	0.02617
2000-5000HZ	1.95	0.00101
5000-10000HZ	1.34	0.00048

WAVE NUMBER (1/FT)	INTENSITY SPECTRA	ENERGY SPECTRA	DIMENSIONLESS PARAMETERS K*D	E1(KD)
8.7 TO 34.9	0.2011E-02	0.1153E-02	0.1454E 02	0.3668E-02
34.9 TO 87.2	0.3170E-02	0.1817E-02	0.4071E 02	0.5783E-02
87.2 TO 174.5	0.2293E-02	0.1314E-02	0.8723E 02	0.4182E-02
174.5 TO 348.9	0.1148E-02	0.6582E-03	0.1746E 03	0.2094E-02
348.9 TO 872.3	0.2787E-03	0.1597E-03	0.4071E 03	0.5083E-03
872.3 TO 1744.5	0.4003E-04	0.2294E-04	0.8723E 03	0.7301E-04
1744.5 TO 3489.1	0.1234E-04	0.7071E-05	0.1745E 04	0.2250E-04
3489.1 TO 8722.7	0.1583E-06	0.9075E-07	0.4071E 04	0.2888E-06
8722.7 TO 17445.5	0.4488E-07	0.2572E-07	0.8723C 04	0.8185E-07

MACROSCALE ESTIMATES (IN MMS)

ISOTROPIC 0.75/K	LIEPMANN EMPIRICAL RELATION		VON KARMAN INTERPOLATION
10.48	165.7	1.179	1.332
3.744	11.29	2.206	2.551
1.747	0.0	0.0	2.490
0.8736	0.0	0.0	1.575
0.3744	1.351	0.1844	1.332
0.1747	2.305	0.2354E-01	3.648
0.8736E-01	1.882	0.7210E-02	3.770
0.3744E-01	27.04	0.1008E-03	306.5
0.1747E-01	20.77	0.3283E-04	302.1

TURBULENCE INTENSITY AND ENERGY SPECTRA PLOTS INTENSITY AND ENERGY ACROSS THE PAGE. WAVE NO. DOWN.

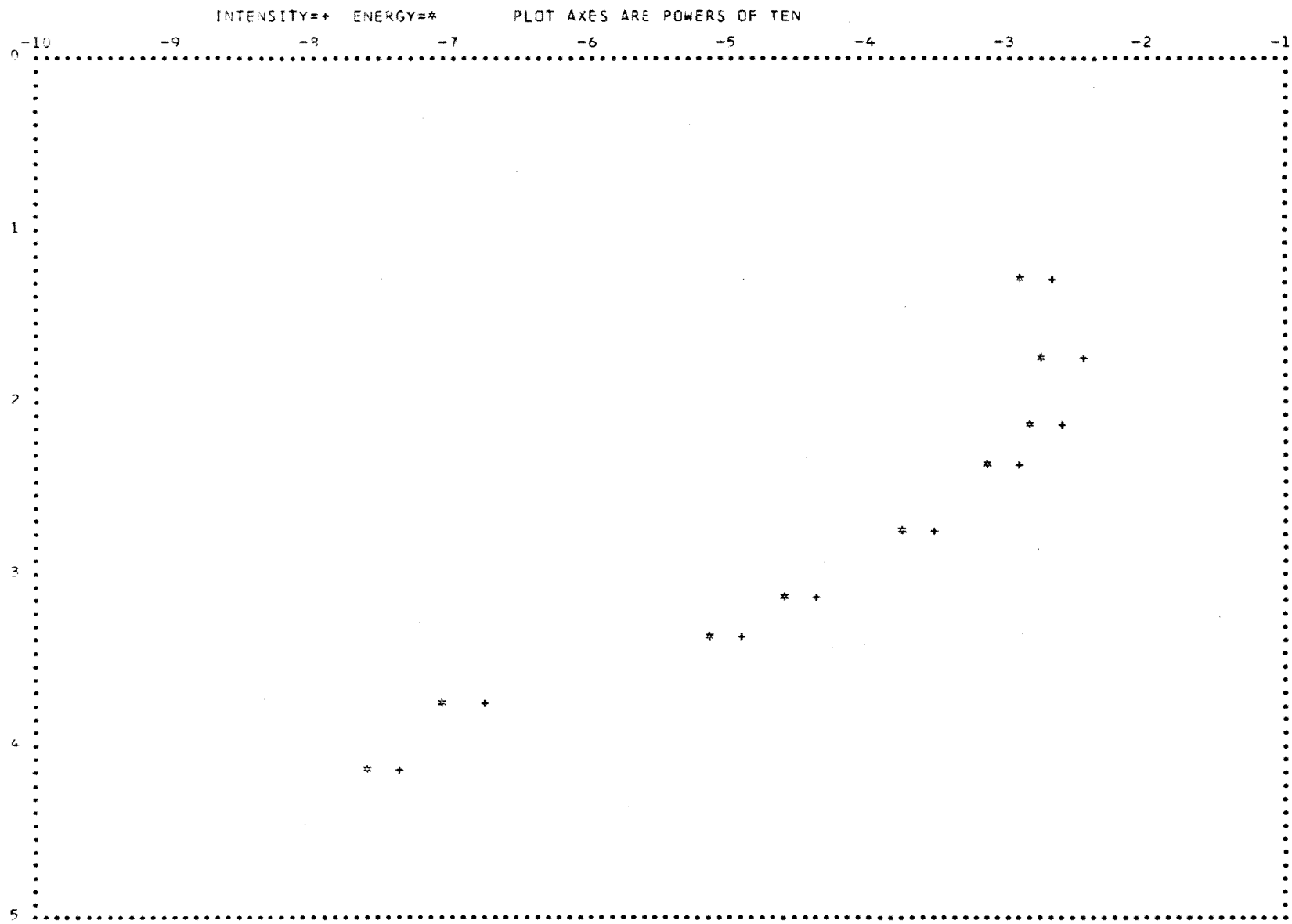

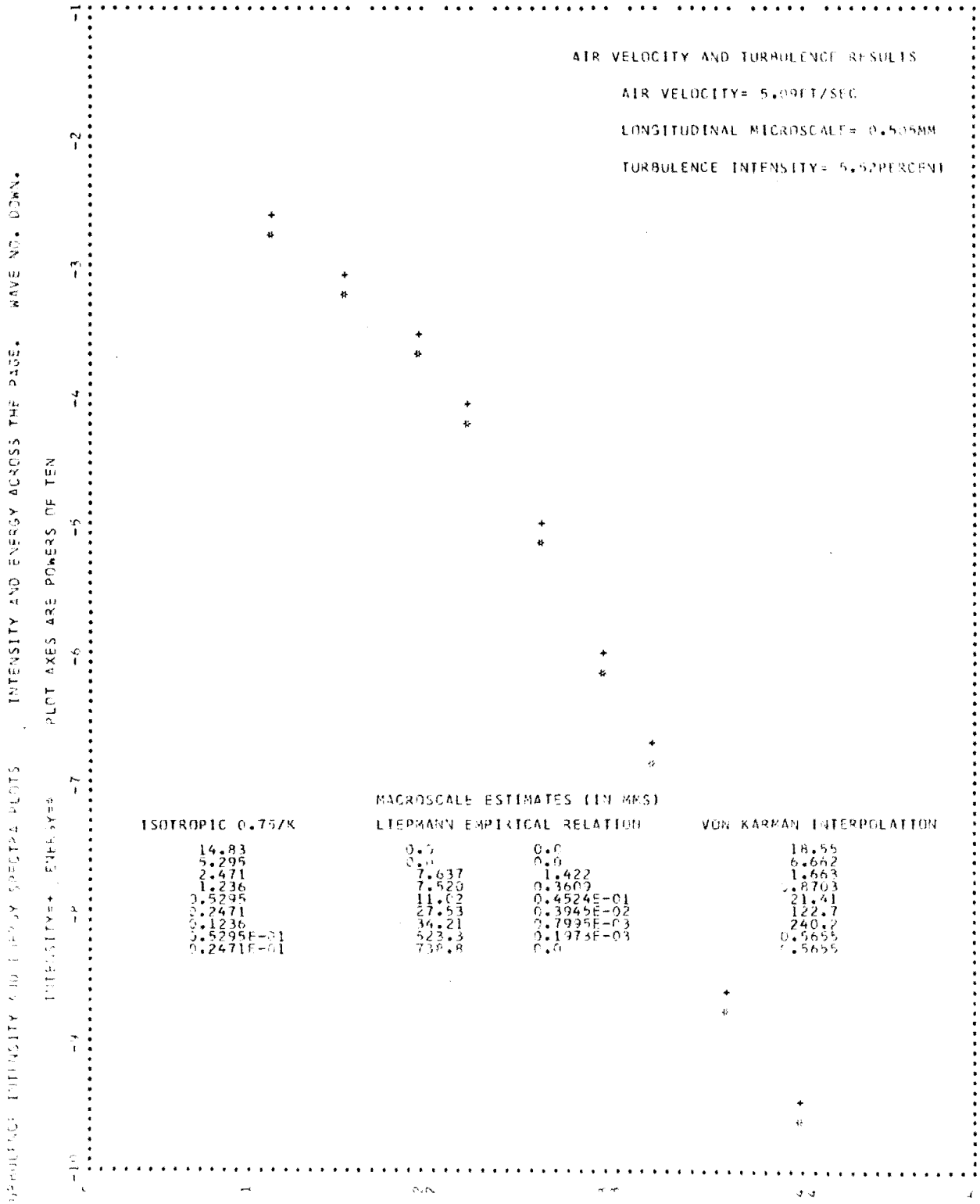
AIR VELOCITY AND TURBULENCE RESULTS
AIR VELOCITY= 5.09FT/SEC
LONGITUDINAL MICROSCALE= 0.505MM
TURBULENCE INTENSITY= 5.52PERCENT
INTENSITY AND ENERGY ACROSS THE PASS. WAVE NO. DOWN.
PLOT AXES ARE POWERS OF TEN
MACROSCALE ESTIMATES (IN MMS)
ISOTROPIC 0.75/K
LIEPMANN EMPIRICAL RELATION
VON KARMAN INTERPOLATION
14.83
5.295
2.471
1.236
0.5295
0.2471
0.1236
0.5295E-01
0.2471E-01
0.0
0.0
1.422
0.3609
0.4524E-01
0.3945E-02
0.7935E-03
0.1973E-03
0.0
18.55
6.662
1.663
0.8703
21.41
122.7
240.2
0.5655
0.5655

A206

LIQUID SPHERE SURFACE AND VOLUME MEASURES

X(**) IS THE DISTANCE FROM THE FRONT POLE OF THE SPHERE AS MEASURED IN MMS
RAD(**) IS THE RADIUS OF THE SPHERE AT THAT POSITION ALSO MEASURED IN MMS
(**)=ODD NO.=ORIGINAL DATA
(**)=EVEN NO.=INTERPOLATED VALUES USING LAGRANGES FORMULA

PHOTO NO.= 1

X(1)= 0.0	RAD(1)= 0.0	0
X(2)= 0.06024	RAD(2)= 0.29217	0000000
X(3)= 0.12048	RAD(3)= 0.50602	000000000000
X(4)= 0.18072	RAD(4)= 0.60964	0000000000000000
X(5)= 0.24096	RAD(5)= 0.69879	00000000000000000
X(6)= 0.30120	RAD(6)= 0.77093	000000000000000000
X(7)= 0.36145	RAD(7)= 0.83373	0000000000000000000000
X(8)= 0.42169	RAD(8)= 0.88539	00000000000000000000000
X(9)= 0.48193	RAD(9)= 0.93132	000000000000000000000000
X(10)= 0.54217	RAD(10)= 0.97078	0000000000000000000000000
X(11)= 0.60241	RAD(11)= 1.00602	00000000000000000000000000
X(12)= 0.66265	RAD(12)= 1.03735	000000000000000000000000000
X(13)= 0.72289	RAD(13)= 1.06386	0000000000000000000000000000
X(14)= 0.78313	RAD(14)= 1.08419	00000000000000000000000000000
X(15)= 0.84337	RAD(15)= 1.10241	000000000000000000000000000000
X(16)= 0.90361	RAD(16)= 1.11943	0000000000000000000000000000000
X(17)= 0.96386	RAD(17)= 1.13253	00000000000000000000000000000000
X(18)= 1.02410	RAD(18)= 1.14066	000000000000000000000000000000000
X(19)= 1.08434	RAD(19)= 1.14699	0000000000000000000000000000000000
X(20)= 1.14458	RAD(20)= 1.15196	00000000000000000000000000000000000
X(21)= 1.20482	RAD(21)= 1.15422	000000000000000000000000000000000000
X(22)= 1.26506	RAD(22)= 1.15376	0000000000000000000000000000000000000
X(23)= 1.32530	RAD(23)= 1.15060	00000000000000000000000000000000000000
X(24)= 1.38554	RAD(24)= 1.14427	000000000000000000000000000000000000000
X(25)= 1.44578	RAD(25)= 1.13614	0000000000000000000000000000000000000000
X(26)= 1.50602	RAD(26)= 1.12711	000000000000000000000000000000000000000000
X(27)= 1.56627	RAD(27)= 1.11446	0000000000000000000000000000000000000000000
X(28)= 1.62651	RAD(28)= 1.09819	00000000000000000000000000000000000000000000
X(29)= 1.68675	RAD(29)= 1.07831	000000000000000000000000000000000000000000000
X(30)= 1.74699	RAD(30)= 1.05542	0000000000000000000000000000000000000000000000
X(31)= 1.80723	RAD(31)= 1.02771	00000000000000000000000000000000000000000000000
X(32)= 1.86747	RAD(32)= 0.99337	000000000000000000000000000000000000000000000000
X(33)= 1.92771	RAD(33)= 0.95783	0000000000000000000000000000000000000000000000000
X(34)= 1.98795	RAD(34)= 0.92138	00000000000000000000000000000000000000000000000000
X(35)= 2.04819	RAD(35)= 0.88313	000000000000000000000000000000000000000000000000000
X(36)= 2.10843	RAD(36)= 0.84548	0000000000000000000000000000000000000000000000000000
X(37)= 2.16867	RAD(37)= 0.80120	00000000000000000000000000000000000000000000000000000
X(38)= 2.22892	RAD(38)= 0.75000	000000000000000000000000000000000000000000000000000000
X(39)= 2.28916	RAD(39)= 0.69277	0000000000000000000000000000000000000000000000000000000
X(40)= 2.34940	RAD(40)= 0.62952	00000000000000000000000000000000000000000000000000000000
X(41)= 2.40964	RAD(41)= 0.56024	000000000000000000000000000000000000000000000000000000000
X(42)= 2.45783	RAD(42)= 0.50489	0000000000000000000000000000000000000000000000000000000000
X(43)= 2.50602	RAD(43)= 0.44819	00000000000000000000000000000000000000000000000000000000000

MAX. CROSS SEC. DIA.= 2.30843MMS

VERT. CROSS SEC. AREA FRONT HALF= 2.17605MMS*2

SURFACE AREA FRONT HALF = 8.63822MMS*2

VOLUME FRONT HALF= 3.37106MMS*3

VERT. CROSS SEC. AREA BACK HALF= 2.43676MMS*2

SURFACE AREA BACK HALF= 8.74377MMS*2

VOLUME BACK HALF= 3.75909MMS*3

TOTAL VERT. CROSS SEC. AREA= 4.61281MMS*2

TOTAL SURFACE AREA OF DROP=17.38199MMS*2

TOTAL VOLUME OF DROP= 7.13015MMS*3

FRONT HALF AREA AS PERCENTAGE OF TOTAL= 49.70

FRONT HALF VOLUME AS PERCENTAGE OF TOTAL= 47.28

SUPPORT ROD AREA AS PERCENTAGE OF TOTAL= 3.50

DIAM. OF EQUIVALENT SPHERE= 2.38799MMS

```
 EVAPORATION RATE CURVE FITTING
 DEGREE OF FIT= 1
   XMSE    COEF(1)    COEF(2)    COEF(
0.26E 00 7.224     -.3347
 DEGREE OF FIT= 2
   XMSE    COEF(1)    COEF(2)    COEF(3)    COEF(
0.38E-02 7.587     -.4489     0.6170E-02


 DEGREE OF FIT CHOSEN FOR VOLUME RATE= 2


 DEGREE OF FIT= 1
   XMSE    COEF(1)    COEF(2)    COEF(
0.85E-01 17.94     -.6822
 DEGREE OF FIT= 2
   XMSE    COEF(1)    COEF(2)    COEF(3)    COEF(
0.72E-02 18.14     -.7452     0.3403E-02


 DEGREE OF FIT CHOSEN FOR AREA RATE= 2


 DEGREE OF FIT= 1
   XMSE    COEF(1)    COEF(2)    COEF(
0.37E-02 2.393     -.5079E-01
 DEGREE OF FIT= 2
   XMSE    COEF(1)    COEF(2)    COEF(3)    COEF(
0.16E-03 2.351     -.3749E-01-.7194E-03


 DEGREE OF FIT CHOSEN FOR BIG-DIA. RATE= 2


 DEGREE OF FIT= 1
   XMSE    COEF(1)    COEF(2)    COEF(
0.23E-02 2.467     -.5609E-01
 DEGREE OF FIT= 2
   XMSE    COEF(1)    COEF(2)    COEF(3)    COEF(
0.14E-03 2.434     -.4559E-01-.5679E-03


 DEGREE OF FIT CHOSEN FOR AV-DIA. RATE= 2


 DEGREE OF FIT= 1
   XMSE    COEF(1)    COEF(2)    COEF(
0.30E-01 10.71     -.2932
 DEGREE OF FIT= 2
   XMSE    COEF(1)    COEF(2)    COEF(3)    COEF(
0.14E-01 10.62     -.2042     -.1563E-02


 DEGREE OF FIT CHOSEN FOR DROP LENGTH RATE= 2
```

EXPTL REYNOLDS NO. RANGE=102.0 TO 159.4

ASSUMED REYNOLDS NO.S ARE 100.0,125.0,150.0,

HSTAR=12.33BTU/SQ.FT HR DEG.F
XSTAR=25.29PERCENT OF LROD
HROD = 3.12BTU/SQ.FT HR DEG.F

PERCENT LROD	TEMROD
0.0	56.80
2.00	60.29
4.00	62.98
6.00	65.05
8.00	66.64
10.00	67.87
12.00	68.82
14.00	69.55
16.00	70.11
18.00	70.54
20.00	70.88
22.00	71.14
24.00	71.33
26.00	71.49
36.00	71.86
46.00	71.96
56.00	71.99
66.00	72.00
76.00	72.00
86.00	72.00
96.00	72.00
100.00	72.00

HEAT TRANSFER RESULTS(1)

QTOTAL=0.3185E-01BTU/HR

QRADTN=0.6248E-03BTU/HR = 1.96PERCENT OF QTOTAL

QROD =0.5205E-02BTU/HR =16.34PERCENT OF QTOTAL

QNET =0.2602E-01BTU/HR =81.70PERCENT OF QTOTAL

HTCOEF= 27.1BTU/SQ.FT HR DEG.F
NU THEORY= 7.38
RATIO NU/NUO= 1.336

**** DROP REYNOLDS NUMBER=100.00
**** DROP NUSSELT NUMBER= 9.86
**** AIR TURBULENCE (PERCENT)= 19.06
**** AIR MICROSCALE(MMS)= 1.210
**** MAXIMUM DROP DIAMETER(MMS)= 1.448
**** DROP SPHERICITY(L/D)=0.90
**** FROSSLING NUMBER=0.876

APPENDIX 8

SUBLIMATION OF A NAPHTHALENE SPHERE

To assist in establishing the correct lighting and exposure conditions with which to photograph the held evaporating droplets, a solid naphthalene sphere was held in the column in place of the droplets. The opaqueness of the naphthalene and the absence of the internal reflection that occurs with pure water drops, made the trial photography studies a lot easier. When the correct photographic technique had been developed, a single test run for the sublimation of a naphthalene sphere was completed and is reported here because of the interesting result and the future work suggested from this result.

By successive dippings into pure naphthalne kept just above the melting point temperature, a 1 inch diameter sphere of uniform density was quickly made and then carefully trimmed until the sphericity was at least 0.997. The sphere to support-stem diameter ratio was 8:1 and the sphere sublimed in an air stream where the temperature was about 143F.

The result is presented as a relative rate of sublimation about the sphere for Re = 2,970 and with τ~5%. The change in the maximumdiameter of the sphere as exposed to the airstream was approximately 9% and the time taken was 3½hours. Figure A8.1 shows before and after photos of the naphthalene sphere and from enlarged copies of these, the relative rate of sublimation was calculated as a percentage of that occuring at the front pole of the sphere. This variation in local mass-transfer rate is shown in figure

A8.2. This figure shows two distict minima beyond the equator of the sphere and suggests the presence of two separation rings and the existence of two vortex rings.

The existence of this phenomenon has been know for some time and reported by a number of workers: for heat-transfer from cylinders (A80, A81, A82, A83); for mass-transfer from cylinders (A84, A85, A86); and for mass-transfer from spheres (A87, A88, A89, A90). It is noteworthy that of all these reports, only one (A87) has discussed this flow phenomenon in any length or detail.

From the forward stagnation point to the primary separation circle, the flow is well described by the boundary-layer equations. In this region the relative transport rate decreases due to the increasing thickness of the laminar boundary-layer. Beyond this separation circle though, external factors such as the method of support of the sphere, free-stream turbulence and the presence of the enclosure walls, can effect the flow. In general, vortices are shed at a frequency which increases with the sphere Reynolds number, but at high Re ($\sim 2\times10^{3}$(A87)) it has been found that the flow may rejoin the sphere and begin to build up another boundary-layer which subsequently separates (A88).

With this information about the flow pattern around a single sphere, the variation of the local transport rate can be considered. For lower Reynolds numbers, the rate of transfer decreases over the forward hemisphere and after separation increases gradually again. For higher Reynolds numbers, after separation the increase in the transfer rate is more pronounced and is due to the wake flow recontacting the surface of the sphere and then

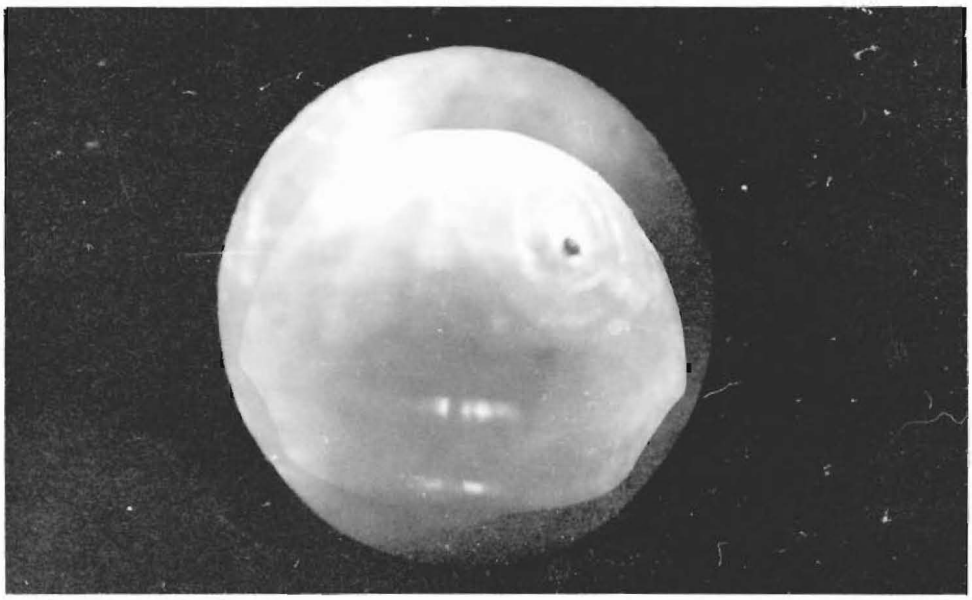

Figure A8.1 Before and after profiles of the subliming naphthalene sphere in a stream of warm air (T_g=143F).

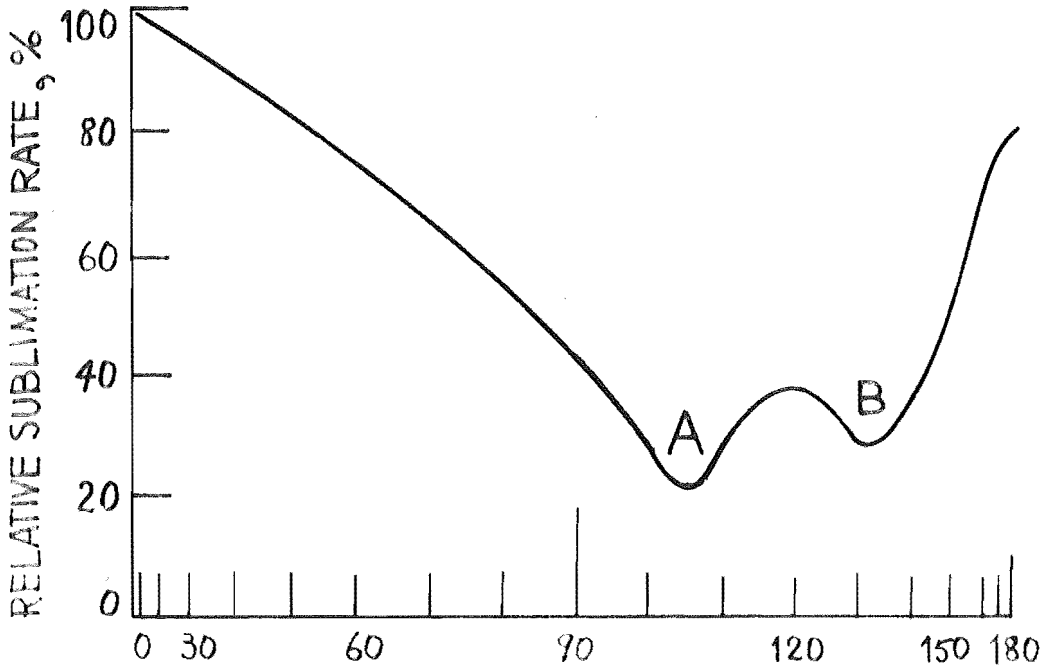

FIGURE A8.2 RELATIVE RATE OF SUBLIMATION OF A SOLID SPHERE OF NAPTHALENE (Re = 2,970)

rapidly separating again. After this second separation the variation of the transfer rate follows the behaviour for wake flow. This weaker maximum after the primary separation could be the result of a reaction of the wake against the stem supporting the sphere. However, the existence of such a second maximum has been reported for Reynolds numbers up to 2×10^5 (A85).

The phenomenon of two maxima for the variation of the local transport rate about a cylinder or a sphere has not been studied as a subject by itself, but is certainly worthy of a detailed investigation. Such a study should include the measuring of the delay in primary and secondary separation as caused by increasing the level of the air turbulence intensity (A85, A86).

... ...

References

A80 Zapp,G.M. M.Sc Thesis, Oregon State Coll (1960).

A81 Giedt,W,H. J.Aero.Sci., 18, 725 (1951).

A82 Seban.R.A. Trans.A.S.M.E., 826,101 (1960)

A83 Galloway,T.G. and Sage,B.H. A.I.Ch.E.Journal,13, 563 (1967)

A84 Windy,A and Cheney,G. I.E.C. 40, 1087 (1948)

A85 Sagin,H.H. and Subtamanian,V.S. Trams.A.S.M.E. 83C, 483 (1961)

A86 Moscow Institute of Chemical-Plant Design (1968). Priv. Comm. with Dr.R.B.Keey.

A87 Gillespie,B.M., Grandall,E.D. and Carberry,J.J. A.I.Ch.E.Journal 14, 483 (1968)

A88 Wadsworth,J. Nat'l Res. Counc. Canada Rept no.MT-41

(1960)

A89 Carey,J.R. Trans.A.S.M.E., 75, 483 (1953)

A90 Lee,K. and Barrow,H. Int.J.Heat and Mass Transfer 11, 1013 (1968)

APPENDIX 9

VARIABLE TIME DELAY

The "Bogus" variable delay unit was developed to provide a variable time delay from milliseconds up to seconds (A91). The electronic circuit for the delay unit is shown in figure A9.1 along with a block diagram for the complete double flash system.

The delay circuit consists of three micrologic components and a variable resistance-capacitive load. Light from the first electronic flash is sensed by the photo-diode (good response time up to 10kHz) and produces a positive 3.6 volt signal at the input to the circuit. The length of the output pulse from the first micrologic component depends on the value of the resistance-capacitive load of the circuit and there is provision for plugging in additional external capacitors if long delays (>12 millisecs) are required. the positive square wave of variable length is then sent to the second micrologic component which inverts the signal and clarifies the signal wave form. The capacitor-resistor network which follows then differentiates the signal and of the two voltage peaks that result the negative peak is chopped by the small diode. Only the remaining positive peak reaches the final micrologic component which simply amplifies the signal of the circuit and feeds it to the silicon-controlled-rectifier (high load capacity). The SCR then conducts because of the applied voltage bias and so triggers the second electronic flash unit.

The calibration curve for the "Bogus" variable delay unit is shown in figure A9.2. The vernier dial on the

variable resistor of the delay circuit facilitated easy reproduction of the time delay interval. Accurate to about 2%, the calibration was made by displaying the electrical pulses from the first and second electronic flah units on an oscilloscope screen and measuring the actual delay between flashes according to the time base of the oscilloscope. This was done in two ways: 1) by taking photographs of the moving trace on the oscilloscope screen using an oscilloscope camera, and 2) by using a storage oscilloscope which held the trace of the two pulses showing the delay on the screen and from which direct measurements could be made.

... ...

References

A91 Boag,I.F. M.E.Thesis, University of Canterbury, (1969). Mr Boag is thanked for constructing the variable delay and for assisting in the calibration.

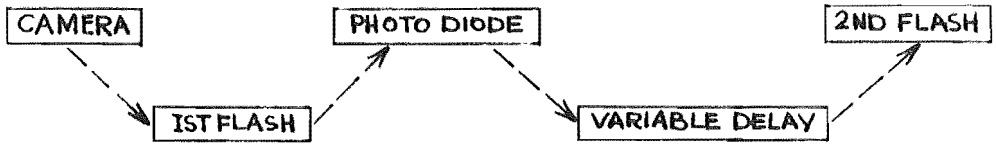

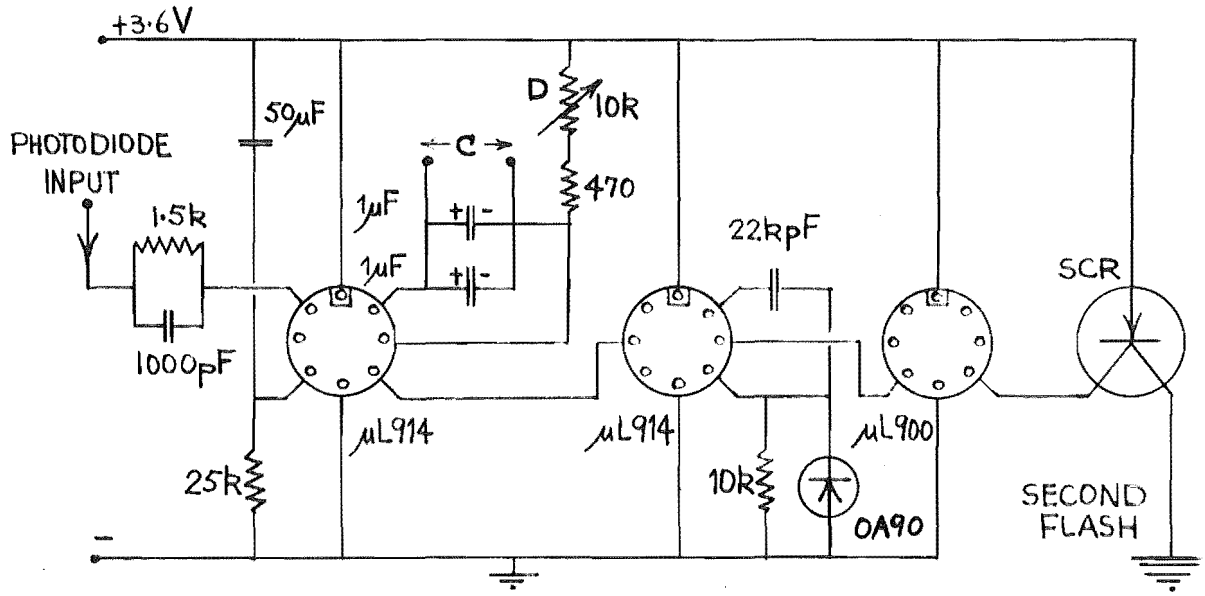

FIGURE A9.1 'BOGUS' VARIABLE TIME DELAY. C = EXTERNAL CAPACITOR CONNECTIONS. D = VERNIER DIAL FOR ACCURATE RESETTING OF TIME DELAY

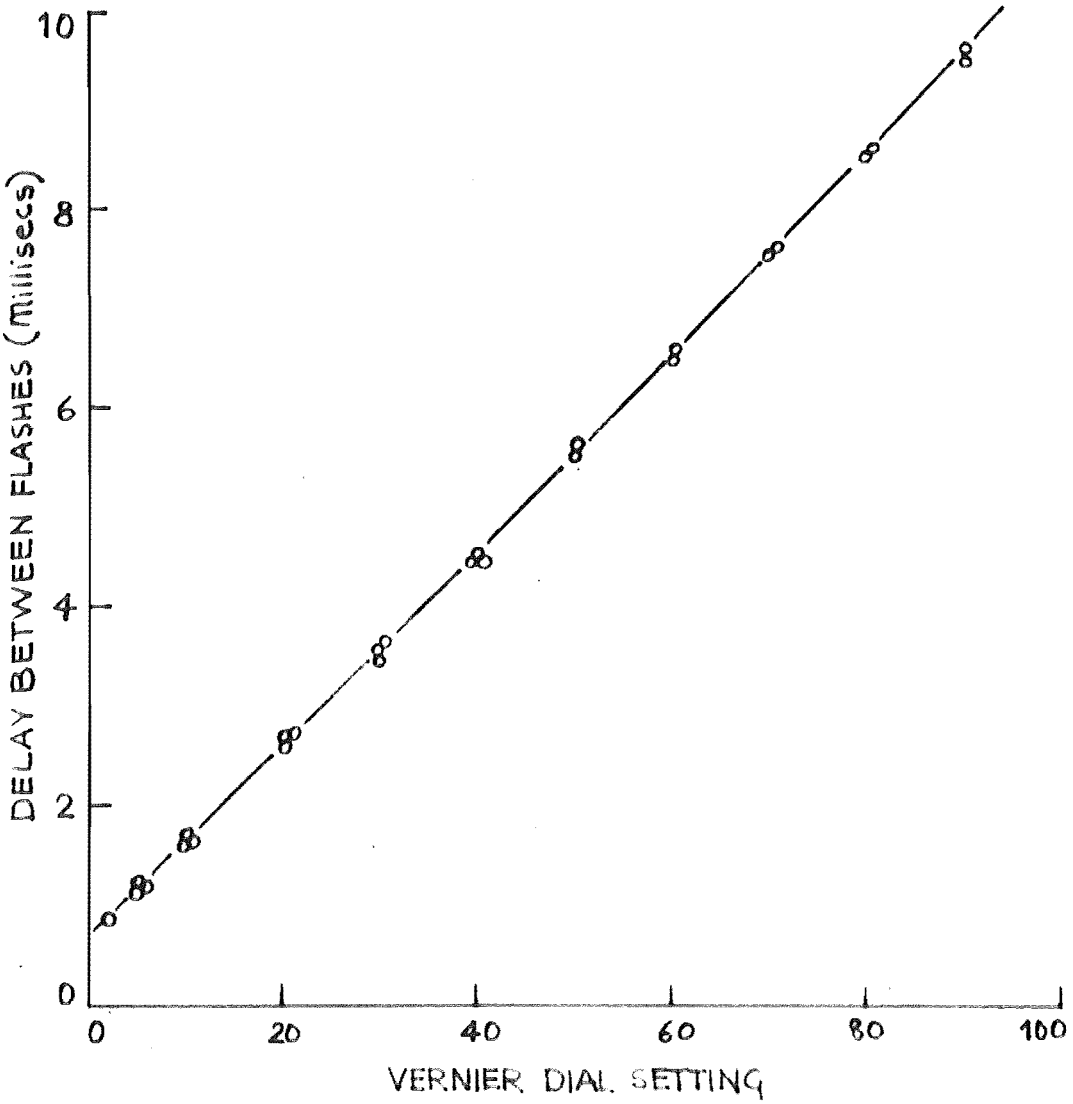

FIGURE A9.2 CALIBRATION CURVE FOR 'BOGUS' VARIABLE DELAY UNIT

APPENDIX 10

COMPUTER PROGRAM (DROPVEL)

The measured drop diameter/velocity data from the moving drop photographs was analysed by this program to provide a smooth curve equation describing the drop diameter/terminal velocity relation. The subroutine POLFIT is used to fit a polynomial to the experimental terminal velocity data and the smooth curve equation is then used to calculate values of the moving drop Reynolds number, the drag coefficients both corrected C_D^* and uncorrected C_D for intensive mass-transfer, and the drag coefficient group Π . The program was written in Fortran IV language for use with an IBM 360/44 computer and a listing and sample result output for the program follows.

The required input data are values of the velocity, density and viscosity of the entraining air, the density of the drop and the value of the Mass Transfer number, B (BFACT). (These properties were obtained using the minor program described in Appendix 7, which calculates all relevant physical property data for evaporating water drops). The number of pairs of drop diameter/absolute drop velocity data (NAA) is read before the data pairs (8 per card). The program rearranges the data into increasing drop diameter order and subtracts from each drop velocity the velocity of the cocurrent air (VELGAS), so obtaining the relative or terminal drop velocity (DROPTV). These drop terminal velocities were then printed out as shown in the program output.

The drop terminal velocity data were then fitted by 1st, 2nd, 3rd and 4th order polynomials and for each smooth

curve equation, the values of Re, C_D^*, C_D and π were calculated. The output example titled Drop Terminal Velocity Profile and Coefficients shows the result for the fitted 1st order polynomial. XMSE is the error of the polynomial fit and COEF(1), COEF(2), etc are the coeffcients of the equation

$$\text{Drop } U_t = a_1 + a_2 D_p + a_3 D_p^2 + a_4 D_p^3 + \ldots.$$

as generated by the small function program preceding the mainline program. In the same manner results for degrees of fit equal to 2, 3 and 4 were produced.

... ...

COMPUTER PROGRAM (DROPVEL)

```
C      **** THIS PROGRAM USES POLFIT TO FIND THE CURVE OF BEST FIT THROUGH
C      TERMINAL VELOCITY VS DROP DIAMETER RESULTS.   THE BEST FIT CURVE IS THEN
C      USED TO CALCULATE,FOR ANY DROP DIAMETER, SMOOTHED VALUES OF THE
C      DROP TERMINAL VELOCITY, REYNOLDS NO., DRAG COEFFICIENT BOTH CORRECTED
C      AND UNCORRECTED FOR INTENSIVE MASS-TRANSFER EFFECTS, AS WELL AS
C      EVALUATING *SMITHS* PHI.   ****************************************
C
C
0001          FUNCTION DOPVEL(COEF,DROPDD,MM)
0002          DIMENSION COEF(10)
0003          DOPVEL =COEF(1)
0004          DO 10 I=2,MM
0005       10  DOPVEL=DOPVEL+COEF(I)*DROPDD**(I-1)
0006          RETURN
0007          END

0001          DIMENSION DOPDIA(100),VELDOP(100),DROPTV(100)
0002          DIMENSION X(100),Y(100),COEF(9)
0003       100I WRITE(6,1)
0004           1 FORMAT(/////////' TERMINAL VELOCITY AND DRAG COEFFICIENT RESULTS')
0005             READ(5,2)IRUNUM
0006           2 FORMAT(I4)
0007             WRITE(6,3)IRUNUM
0008           3 FORMAT(//5X,' RUNUMBER=',I3)
0009             READ(5,4)NAA
0010           4 FORMAT(I4)
0011             READ(5,5)VELGAS,RHOGAS,VISGAS,RHODOP,BFACT
0012           5 FORMAT(5F10.5)
0013             READ(5,6)(DOPDIA(I),VELDOP(I),I=1,NAA)
0014           6 FORMAT(8F10.5)
0015             WRITE(6,65)VELGAS
0016          65 FORMAT(/5X,' VELGAS=',F5.2,'FT/SEC')
0017             BFACTA=BFACT*100.0
0018             WRITE(6,17)BFACTA
0019          17 FORMAT(//5X,'BFACT=',F6.3,'PERCENT')
0020             WRITE(6,7)
0021           7 FORMAT(//5X,'DROPDIA',3X,'VELDROP',3X,'DROPTV')
0022             NXA=NAA-1
0023             DO 9 I=1,NXA
0024             IP1=I+1
0025             DO 9 J=IP1,NAA
0026             IF(DOPDIA(I)-DOPDIA(J))9,9,8
0027           8 TEMP=DOPDIA(I)
0028             DOPDIA(I)=DOPDIA(J)
0029             DOPDIA(J)=TEMP
0030             TEMP=VELDOP(I)
0031             VELDOP(I)=VELDOP(J)
0032             VELDOP(J)=TEMP
0033           9 CONTINUE
0034             DO 10 I=1,NAA
0035          10 DROPTV(I)=VELDOP(I)-VELGAS
0036             WRITE(6,11)(DOPDIA(I),VELDOP(I),DROPTV(I),I=1,NAA)
0037          11 FORMAT(F11.1,2F10.2)
0038             RATIO1=RHOGAS*3.E-2/(2.54*VISGAS)
0039             RATIO2=3.575E-4*(RHODOP-RHOGAS)/(2.54*RHOGAS)
0040             NN=NAA
0041             MM=1
0042             WRITE(6,13)
0043          13 FORMAT(/////////' DROP TERMINAL VELOCITY PROFILE ERROR AND COEFS.')
0044             DO 20 K=1,4
0045             MM=MM
0046             DO 12 I=1,NAA
0047             Y(I)=DROPTV(I)
0048          12 X(I)=DOPDIA(I)
0049             WRITE(6,14)MM
0050          14 FORMAT(////5X,' DEGREE OF FIT=',I2)
0051             CALL POLFIT(X,Y,NN,MM,XMSE,COEF)
0052             MM=MM+1
0053             WRITE(6,15)(I,I=1,MM)
0054          15 FORMAT(/7X,'XMSE',8(3X,'COEF(',I1,')'))
0055             WRITE(6,16)XMSE,(COEF(I),I=1,MM)
0056          16 FORMAT(E13.2,9G10.4)
0057             WRITE(6,18)
0058          18 FORMAT(/6X,'DROPDIA',4X,'DROPTV',5X,'RE.NO',5X,'CD*',7X,'CD',7X,'P
             1HI')
0059             DROPDD=-50.0
0060             DO 20 J=1,16
0061             DROPDD=DROPDD+50.0
0062             TERMVL=DOPVEL(COEF,DROPDD,MM)
0063             RE=RATIO1*DROPDD*TERMVL
0064             CD1=(RATIO2*DROPDD)/(TERMVL*TERMVL)
0065             CD2=CD1*(1.0+BFACT)
0066             PHI=CD2*(RE/24.0)**2
0067             WRITE(6,19)DROPDD,TERMVL,RE,CD1,CD2,PHI
0068          19 FORMAT(F12.1,4F10.2,F10.3)
0069          20 CONTINUE
0070             WRITE(6,21)
0071          21 FORMAT(//5X,' END OF RESULTS FOR THIS RUNUMBER'//)
0072             GO TO 100I
0073             END
```

TERMINAL VELOCITY AND DRAG COEFFICIENT RESULTS

RUNUMBER= 3

VELGAS= 5.58FT/SEC

BFACT= 0.183PERCENT

DROPDIA	VELDROP	DROPTV
52.0	6.05	0.47
70.0	6.10	0.52
70.0	6.17	0.59
87.0	5.21	-0.37
113.0	7.13	1.55
131.0	6.80	1.22
139.0	6.63	1.05
139.0	7.28	1.70
148.0	6.43	0.85
148.0	7.49	1.91
160.0	8.11	2.53
174.0	8.24	2.66
174.0	7.35	1.77
177.0	7.96	2.38
177.0	7.21	1.63
177.0	7.02	1.44
195.0	7.54	1.96
195.0	7.25	1.67
209.0	8.27	2.69
213.0	8.33	2.75
213.0	7.47	1.89
213.0	8.09	2.51
213.0	7.88	2.30
220.0	8.33	2.75
244.0	8.80	3.22
248.0	8.37	2.79
248.0	8.48	2.90
248.0	8.97	3.39
248.0	7.99	2.41
248.0	8.93	3.35
248.0	8.86	3.28
248.0	8.59	3.01
255.0	8.93	3.35
284.0	8.82	3.24
284.0	8.82	3.24
284.0	9.16	3.58
284.0	9.19	3.61
301.0	9.72	4.14
308.0	9.91	4.33
337.0	9.61	4.03
408.0	11.78	6.20
443.0	11.94	6.36
496.0	12.95	7.37
496.0	12.20	6.62
567.0	13.87	8.29

DROP TERMINAL VELOCITY PROFILE ERROR AND COEFS.

DEGREE OF FIT= 1

XMSE	COEF(1)	COEF(2)	COEF(
0.74E 01	-.8308	0.1581E-01	

DROPDIA	DROPTV	RE.NO	CD*	CD	PHI
0.0	-0.83	0.0	0.0	0.0	0.0
50.0	-0.04	-0.04	3554.43	3560.93	0.010
100.0	0.75	1.49	20.64	20.68	0.080
150.0	1.54	4.60	7.34	7.35	0.270
200.0	2.33	9.28	4.27	4.28	0.640
250.0	3.12	15.53	2.98	2.98	1.250
300.0	3.91	23.36	2.28	2.28	2.161
350.0	4.70	32.76	1.84	1.84	3.431
400.0	5.49	43.74	1.54	1.54	5.122
450.0	6.28	56.28	1.32	1.33	7.292
500.0	7.07	70.40	1.16	1.16	10.003
550.0	7.86	86.10	1.03	1.03	13.314
600.0	8.65	103.37	0.93	0.93	17.286
650.0	9.44	122.21	0.85	0.85	21.977
700.0	10.23	142.62	0.78	0.78	27.449
750.0	11.02	164.61	0.72	0.72	33.761

APPENDIX 11

COMPUTER PROGRAM (DROPS)

This program consists of a mainline program of nearly 270 statements, preceded by two small function programs. The program calculates the corrected distributions from the measured drops in each sampling cell photograph. From the measured number and sizes of the drops in each cell, the radial location of each cell and the air velocity past each cell, the computer program scans all drops for sizes within the required size range and so calculates the corrected number that should have been collected in each cell, as well as the droplet concentration per unit area along the spray tower radius. From the corrected data, the spray mean diameters (number, surface-area, volume and Sauter) and the spray non-uniformity coefficient β are evaluated. From the radial droplet/area concentration profile, the total number of drops passing through the spray tower cross-section during the time of sampling is calculated using a graphical integation method. A listing of the program follows, written in Fortran IV language for use on an IBM 360/44 machine.

From the velocity dat first read in, the radial air velocity profile is computed. The subroutine POLFIT is then used to fit a polynomial to the air velocity profile and the resulting curve is integrated to find the total air volume flow in the column as well as the average air velocity. The average velocity (volume-mean value) is also computed at intermediate column radii. These results are shown in the program printout which follows the program listing. Note that the average velocity is quite high across the major

part of the column area (5.9 to 5.3 fps for column radii from 0 to 3.5 ins) and then decreases as the zero wall velocity term is included.

At card 70 of the mainline program, the water drop-size distribution calculations begin. Values are read for the Mass Transfer number B, the scale factor between the measured projected drop sizes and the actual drop sizes, the drop size scanning interval and the measured number of drops in each of the 11 collecting cells. The actual drop sizes measured for each cell are then read in and the corrected total number is computed considering the air velocity past each cell(from the velocity function program describing the fitted polynomial obtained earlier), the radial location of the cell and the sampler effectiveness for each drop size scanned. The corrected number of drops in each cell (NUMCELL) is then printed out and the drop number/area concentrations are calculated from these results. From the corrected number results, the biggest and smallest drops; the number, surface-mean, volume and Sauter mean drop diameters; and the spray non-uniformity coefficient are calculated. All these results are printed out as shown in the sample printout. Finally, a polynomial is fitted to the drop number/area concentration profile and this is integrated over the whole column cross-sectional area to produce an estimate of the total number of droplets in the spray passing the sampling level at the time of capture of the spray sample. The radial percentage distribution of the drops is also calculated to indicate the location of the major part of the spray.

... ...

COMPUTER PROGRAM (DROPS)

```
      C     PROGRAM TO CALCULATE THE FOLLOWING  ********************************
0001          FUNCTION AVL(COEF,COLRAD,MM)
0002          DIMENSION COEF(10)
0003          AVL=COEF(1)
0004          DO 10 I=2,MM
0005       10 AVL=AVL+COEF(I)*COLRAD**(I-1)
0006          RETURN
0007          END

0001          FUNCTION ENCONC(COEF,ACTRAD,MM)
0002          DIMENSION COEF(10)
0003          ENCONC=COEF(1)
0004          DO 10 I=2,MM
0005       10  ENCONC=ENCONC+COEF(I)*ACTRAD**(I-1)
0006          RETURN
0007          END

0001          REAL NUMCEL,NCONC,NUSUM,NUMBMN,NUMBR
0002          INTEGER TRURAD
0003          DIMENSION NCOL(11), NUMCEL(11), NCONC(11)
0004          DIMENSION D(2000)
0005          DIMENSION X(100),Y(100),COEF(9)
0006          DIMENSION RAD(4),AVHEAD(4),RHOGAS(4),AIRVEL(4)
0007       1001 WRITE(6,100)
0008        100 FORMAT(//' AIR VELOCITY PROFILE AND DROPSIZE DISTRIBUTION VALUES')
0009          READ(5,101) IRUNUM
0010        101 FORMAT(I4)
0011          WRITE(6,102)IRUNUM
0012        102 FORMAT(//5X,'RUNUMBER=',I3)
0013          READ(5,1045)(RAD(I),AVHEAD(I),RHOGAS(I),I=1,4)
0014       1045 FORMAT(F10.2,2F10.5)
0015          DO 106 I=1,4
0016          ABC=AVHEAD(I)/RHOGAS(I)
0017        106 AIRVEL(I)=18.1*SQRT(ABC)
0018          WRITE(6,111)
0019        111 FORMAT(/5X,'RADIUS',4X,'AIRVEL')
0020          WRITE(6,112)(RAD(I),AIRVEL(I),I=1,4)
0021        112 FORMAT(F10.2,F10.3)
0022          DO 113 I=1,4
0023          Y(I)=AIRVEL(I)
0024        113 X(I)=RAD(I)
0025          DO 1135 I=5,50
0026          Y(I)=0
0027       1135 X(I)=4
0028          READ(5,907) (NN,MM,XS,XI,J)
0029        907 FORMAT(I2,8X,I3,2F5.0,I5)
      C     FOR AIR VELOCITY PROFILE NN=50,MM=OPERATORS CHOICE
0030          CALL POLFIT(X,Y,NN,MM,XMSE,COEF)
0031          MM=MM+1
0032          WRITE(6,123)
0033        123 FORMAT(//'  AIR  VELOCITY  PROFILE ERROR  AND  COEFFS')
0034          WRITE(6,114) (I,I=1,MM)
0035        114 FORMAT(/7X,'XMSE',9(3X,'COEF(',I1,')'))
0036          WRITE(6,115) XMSE,(COEF(I),I=1,MM)
0037        115 FORMAT(E13.2,9G10.4)
      C     ***AIR VELOCITY(FT/SEC) PROFILE AND AVERAGE************************
      C     ***TOTAL AIR VOLUME FLOWRATE(FT**3/SEC)****************************
0038          WRITE(6,118)
0039        118 FORMAT(//5X,'COLRAD',5X,'QDFPS',4X,'FRACQF',5X,'AVFLO')
0040          DO 119 NRAD=1,9
0041          RADD=NRAD/2.+0.5
0042          COLRAD=ABS(RADD-5.0)
0043          N=COLRAD/0.05
0044          IF(N-1)1182,1182,1185
0045       1182 QDFPS=0.0
0046          FRACQF=0.0
0047          AVFLO=0.0
0048          GO TO 1219
0049       1185 QFLOW=0.0
0050          COLRAD=0.0
0051          DO 1195 I=1,N
0052          COLRAD =COLRAD
0053          RADA =COLRAD
0054          VELTOP = AVL(COEF,COLRAD,MM)
0055          COLRAD=COLRAD+0.05
0056          RADB= COLRAD
0057          VELBOT=AVL(COEF,COLRAD,MM)
0058       1195 QFLOW=QFLOW+3.1416/432*(VELTOP-VELBOT)*(RADA**2+RADA*RADB+RADB**2)
0059          QDFPS=QFLOW+3.1416/144*VELBOT*RADB**2
0060          IF(NRAD-1)121,120,121
0061        120 QDFTOT=QDFPS
0062          GO TO 1215
0063        121 QDFPS=QDFPS
0064       1215 FRACQF=QDFPS/QDFTOT
0065          AVFLO=144.*QDFPS/(3.1416*COLRAD**2)
0066       1219 WRITE(6,122) (COLRAD,QDFPS,FRACQF,AVFLO)
0067        122 FORMAT(F12.3,3F10.3)
0068        119 CONTINUE
0069          WRITE(6,1)
0070            1 FORMAT(//' WATER DROPSIZE DISTRIBUTION RESULTS')
0071          READ(5,3) REACT
0072          READ(5,4) FACTOR
```

```
0073            READ(5,5) DELTA
0074            READ(5,8) (NCOL(J),J=1,11)
0075            NTOT=0
0076            DO 9 J=1,11
0077          9 NTOT=NTOT+NCOL(J)
0078            READ(5,10) (D(I),I=1,NTOT)
0079          3 FORMAT(F10.4)
0080          4 FORMAT(F10.3)
0081          5 FORMAT(F10.1)
0082          8 FORMAT(8I10)
0083         10 FORMAT(16F5.2)
0084            WRITE(6,12) (I,I=1,11)
0085         12 FORMAT(//11(1X,'NUMCOL(',I2,')'))
0086            WRITE(6,805)(NCOL(J),J=1,11)
0087        805 FORMAT(1111)
0088            DO 13 I=1,NTOT
0089         13 D(I)=D(I)*FACTOR
0090            N=0
0091            L=1
0092            M=2
0093            BIGD=D(L)
0094            WEED=D(M)
0095            DO 14 J=1,11
0096            K=N+1
0097            N=N+NCOL(J)
0098            DO 15 I=K,N
0099            IF(D(L)-D(I)) 16,17,17
0100         16 TEMP=D(L)
0101            D(L)=D(I)
0102            D(I)=TEMP
0103         17 IF(D(M)-D(I)) 15,15,18
0104         18 TEMP=D(M)
0105            D(M)=D(I)
0106            D(I)=TEMP
0107         15 CONTINUE
0108            IF(D(L)-BIGD) 19,19,20
0109         20 BIGD=D(L)
0110         19 IF(D(M)-WEED) 21,22,22
0111         21 WEED=D(M)
0112         22 WEED=WEED
0113            L=N+1
0114         14 M=N+2
0115            DD=BIGD/DELTA
0116            ND=IFIX(DD)+1
0117            DAD=DELTA/2.0
0118            AVD=-DAD
0119            BUSTA=BFACT/0.688
0120            NUSUM=0.0
0121            SQSUM=0.0
0122            QDSUM=0.0
0123            BIGN=0.0
0124            DO 24 J=1,11
0125         24 NUMCEL(J)=0.0
0126            DO 25 I=1,ND
0127            AVD=AVD+DELTA
0128            AVD2=AVD*AVD
0129            AVD3=AVD*AVD2
0130            AVDM=AVD-DAD
0131            AVDP=AVD+DAD
0132            N=0
0133            SUMCEL=0.0
0134            DO 26 J=1,11
0135            M=N+NCOL(J)
0136            N=N+1
0137            SUM=0.0
0138            DO 27 K=N,M
0139            IF(D(K)-AVDM) 27,27,28
0140         28 IF(D(K)-AVDP) 29,29,27
0141         29 SUM=SUM+1.0
0142         27 CONTINUE
0143            N=M
0144            IF(SUM-0.5) 305,306,306
0145        305 GO TO 45
0146        306 IF(AVD-150.) 30,30,31
0147         30 DROPTV=(9.33E-3+8.E-4*BUSTA)*AVD
0148            GO TO 335
0149         31 IF(AVD-400.) 32,32,33
0150         32 DROPTV=(1.48E-2+6.E-4*BUSTA)*AVD+0.05*BUSTA-0.82
0151            GO TO 335
0152         33 DROPTV=(1.275E-2+1.E-3*BUSTA)*AVD-0.13*BUSTA
0153        335 RAD(J)=ABS((61.0/16.0)-FLOAT(J-1)*0.75)
0154            COLRAD=RAD(J)
0155            DROPVL=DROPTV+AVL(COEF,COLRAD,MM)
0156            IF(AVD-275.) 35,35,34
0157         34 COLEFF=3.5*AVD*1.E-5+0.965
0158            GO TO 42
0159         35 COLEFF=1.42E-2*AVD*SQRT(0.5*DROPVL)-0.25
0160            IF(COLEFF-0.75) 44,44,37
0161         37 IF(DROPVL-4.5) 38,38,39
0162         38 COLEFF=0.4503+0.575E-2*AVD-0.2306E-4*AVD2+0.3239E-7*AVD3
0163            GO TO 46
0164         39 IF(DROPVL-12.5) 40,40,41
0165         40 COLEFF=0.5622+0.6818E-2*AVD-0.3811E-4*AVD2+0.6989E-7*AVD3
0166            GO TO 46
0167         41 COLEFF=0.4498+0.138E-1*AVD-0.124E-3*AVD2+0.3677E-6*AVD3
0168            GO TO 46
0169         42 IF(COLEFF-1.0) 46,46,43
0170         43 COLEFF=1.0
0171         44 IF(COLEFF-0.01) 45,46,46
0172         45 COLEFF=0.005
0173         46 R=99.566*ABS(4.5625-0.75*J)
0174            WGSUM=SUM*R/COLEFF
0175            WGSUM=IFIX(WGSUM)
0176            NUMCEL(J)=NUMCEL(J)+WGSUM
```

```
0177            26 SUMCEL=SUMCEL+WGSUM
0178               NUSUM=NUSUM+AVD*SUMCEL
0179               SQSUM=SQSUM+AVD2*SUMCEL
0180               QDSUM=QDSUM+AVD3*SUMCEL
0181            25 BIGN=BIGN+SUMCEL
0182               DO 47 J=1,11
0183               A=0.50485*ABS(4.5625-0.75*J)
0184            47 NCONC(J)=NUMCEL(J)/A
0185               WRITE(6,48) (J,J=1,11)
0186            48 FORMAT(//11(1X,'NUMCEL(',I2,')'))
0187               WRITE(6,49) (NUMCEL(J),J=1,11)
0188            49 FORMAT(11G11.4)
0189               WRITE(6,50) (J,J=1,11)
0190            50 FORMAT(//11(1X,'NMCONC(',I2,')'))
0191               WRITE(6,51) (NCONC(J),J=1,11)
0192            51 FORMAT(11G11.4)
0193               NUMBMN=NUSUM/BIGN
0194               SURFMN=SQRT(SQSUM/BIGN)
0195               QDVLMN=QDSUM/BIGN
0196               QDVLMN=QDVLMN**(1./3.)
0197               SAUTMN=QDSUM/SQSUM
0198               BETA=QDSUM**2*BIGN/SQSUM**3
                C      ***SMALLEST AND BIGGEST DROPS OF THE SAMPLE COUNTED(MICRONS)******
0199               WRITE(6,52)
0200            52 FORMAT(/5X,'BIG(D)',5X,'WEE(D)',4X,'NTOT',6X,'BIGN',6X,'DELTA',8X,
                  1'ND')
0201               WRITE(6,53)  (BIGD,WEED,NTOT,BIGN,DELTA,ND)
0202            53 FORMAT(F10.1,F10.1,I10,2X,G10.4,F10.4,I10)
                C      ***NUMBER,SURFACE AREA,VOLUME AND SAUTER MEAN DROP DIAMETERS******
0203               WRITE(6,54)
0204            54 FORMAT(//5X,'NUMBMN',4X,'SURFMN',4X,'VOLUMN',4X,'SAUTMN',6X,'BETA'
                  1,5X,'BFACT')
0205               WRITE(6,55) NUMBMN,SURFMN,QDVLMN,SAUTMN,BETA,BFACT
0206            55 FORMAT(4F10.1,F12.3,F10.4)
0207               IF(SAUTMN-150.) 56,56,57
0208            56 SAUTVL=(9.33E-3+8.E-4*BUSTA)*SAUTMN
0209               GO TO 595
0210            57 IF(SAUTMN-400.) 58,58,59
0211            58 SAUTVL=(1.48E-2+6.E-4*BUSTA)*SAUTMN+0.05*BUSTA-0.82
0212               GO TO 595
0213            59 SAUTVL=(1.275E-2+1.E-3*BUSTA)*SAUTMN-0.13*BUSTA
0214           595 WRITE(6,60)
0215            60 FORMAT(//5X,'SAUTVL')
0216               WRITE(6,61) SAUTVL
0217            61 FORMAT(F10.2)
0218               DO 62 J=1,11
0219               Y(J)=NCONC(J)
0220            62 X(J)=RAD(J)
0221               DO 625 I=12,50
0222               Y(I)=0.0
0223           625 X(I)=4.0
0224               READ(5,7) (NN,MM,XS,XI,J)
0225             7 FORMAT(I2,8X,I3,2F5.0,I5)
                C      FOR DROP DISTRIBUTION PROFILE NN=50,MM=OPERATORS CHOICE
0226               CALL POLFIT(X,Y,NN,MM,XMSE,COEF)
0227               MM=MM+1
0228               WRITE(6,71)
0229            71 FORMAT(//' DROP DISTRIBUTION PROFILE ERROR AND COEFFS')
0230               WRITE(6,63) (I,I=1,MM)
0231            63 FORMAT(/7X,'XMSE',9(3X,'COEF(',I1,')'))
0232               WRITE(6,64) XMSE,(COEF(I),I=1,MM)
0233            64 FORMAT(E13.2,9G10.4)
                C      ***DROP CONCENTRATION PROFILE AND AVERAGE(NO./SQ.IN)**************
0234               WRITE(6,66)
0235            66 FORMAT(//5X,'ACTRAD',4X,'NUMBER',4X,'PERCENT')
0236               DO 70 TRURAD=1,9
0237               RADIUS=TRURAD/2.0+0.5
0238               ACTRAD=ABS(RADIUS-5.0)
0239               N=ACTRAD/0.05
0240               IF(N-1)661,661,662
0241           661  ACTRAD=0.0
0242               NUMBR=0.0
0243               PERCEN=0.0
0244               GO TO 686
0245           662  ACTRAD=0.0
0246               SUM=0.0
0247               DO 664 I=1,N
0248               ACTRAD=ACTRAD
0249               RADA=ACTRAD
0250               SUMTOP=ENCONC(COEF,ACTRAD,MM)
0251               ACTRAD=ACTRAD+0.05
0252               RADB=ACTRAD
0253               SUMBOT=ENCONC(COEF,ACTRAD,MM)
0254           664  SUM=SUM+((SUMTOP+SUMBOT)*3.1416*(RADB**2-RADA**2))/2.
0255               NUMBR=SUM
0256               IF(TRURAD-1)68,67,68
0257            67 GTOT=NUMBR
0258               GO TO 685
0259            68 NUMBR=NUMBR
0260           685 PERCEN=NUMBR*100./GTOT
                C      ***TOTAL NO. OF DROPS IN THE COLUMN AT THE LEVEL SAMPLED**********
0261           686  WRITE(6,69)ACTRAD,NUMBR,PERCEN
0262            69 FORMAT(F10.2,G12.4,F10.3)
0263            70 CONTINUE
0264               WRITE(6,700)
0265           700 FORMAT(//5X,'END OF RESULTS FOR THIS RUNUMBER',///)
0266               GO TO 1001
0267               END
```

AIR VELOCITY PROFILE AND DROPSIZE DISTRIBUTION VALUES

RUNUMBER= 11

RADIUS	AIRVEL
0.0	5.674
1.00	5.751
2.00	5.590
3.00	5.124

AIR VELOCITY PROFILE ERROR AND COEFFS

XMSE	COEF(1)	COEF(2)	COEF(3)	COEF(4)	COEF(5)	COEF(
-0.67E-03	5.674	1.244	-2.048	1.059	-.1784	

COLRAD	QDFPS	FRACQF	AVFLO
4.000	1.571	1.000	4.500
3.500	1.410	0.898	5.275
3.000	1.094	0.696	5.570
2.500	0.770	0.490	5.645
2.000	0.495	0.315	5.675
1.500	0.282	0.179	5.743
1.000	0.127	0.081	5.843
0.500	0.032	0.020	5.881
0.0	0.0	0.0	0.0

WATER DROPSIZE DISTRIBUTION RESULTS

← 8" COLUMN DIAMETER →

NUMCOL(1)	NUMCOL(2)	NUMCOL(3)	NUMCOL(4)	NUMCOL(5)	NUMCOL(6)	NUMCOL(7)	NUMCOL(8)	NUMCOL(9)	NUMCOL(10)	NUMCOL(11)
41	51	90	129	193	288	270	222	122	128	78

NUMCEL(1)	NUMCEL(2)	NUMCEL(3)	NUMCEL(4)	NUMCEL(5)	NUMCEL(6)	NUMCEL(7)	NUMCEL(8)	NUMCEL(9)	NUMCEL(10)	NUMCEL(11)
0.5620E 05	0.7999E 05	0.1226E 06	0.6563E 05	0.1775E 05	2259.	0.2382E 05	0.4556E 05	0.4321E 05	0.7953E 05	0.4093E 05

NMCONC(1)	NMCONC(2)	NMCONC(3)	NMCONC(4)	NMCONC(5)	NMCONC(6)	NMCONC(7)	NMCONC(8)	NMCONC(9)	NMCONC(10)	NMCONC(11)
0.2920E 05	0.5174E 05	0.1050E 06	0.8319E 05	0.4328E 05	0.7159E 05	0.6863E 05	0.6278E 05	0.3913E 05	0.5363E 05	0.2199E 05

BIG(D)	WEE(D)	NTOT	BIGN	DELTA	ND
188.9	6.7	1612	0.5775E 06	1.0000	189

NUMBMN	SUREMN	VOLUMN	SAUTMN	BETA	BFACT
39.7	52.4	62.1	87.3	2.776	0.8000

SAUTVL
0.90

DROP DISTRIBUTION PROFILE ERROR AND COEFFS

XMSE	COEF(1)	COEF(2)	COEF(3)	COEF(4)	COEF(5)	COEF(6)	COEF(7)	COEF(8)	COEF(
0.29E 10	0.5775E 05	0.2792E 06	-.9255E 06	0.1134E 07	-.6671E 06	0.2041E 06	-.3138E 05	1914.	

ACTRAD	NUMBER	PERCENT
4.00	0.2632E 07	100.000
3.50	0.2364E 07	89.801
3.00	0.1885E 07	71.608
2.50	0.1370E 07	52.038
2.00	0.8470E 06	32.176
1.50	0.4327E 06	16.436
1.00	0.1983E 06	7.534
0.50	0.6245E 05	2.373
0.0	0.0	0.0